frontiers | Research Topics

Novel immune markers and predictive models for immunotherapy and prognosis in breast and gynecological cancers

Edited by
Chao Liu, Feifei Teng, Alberto Traverso and Shicheng Guo

Published in
Frontiers in Immunology
Frontiers in Oncology

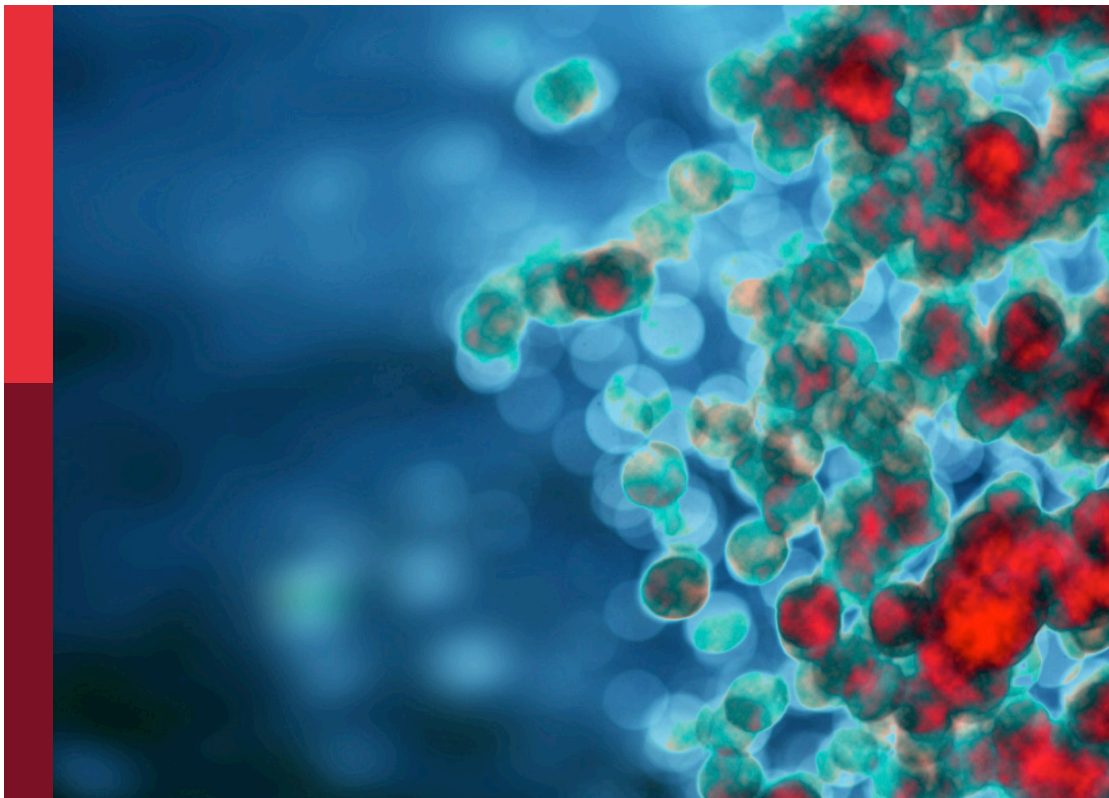

ISSN 1664-8714
ISBN 978-2-8325-4994-0
DOI 10.3389/978-2-8325-4994-0

About Frontiers

Frontiers is more than just an open access publisher of scholarly articles: it is a pioneering approach to the world of academia, radically improving the way scholarly research is managed. The grand vision of Frontiers is a world where all people have an equal opportunity to seek, share and generate knowledge. Frontiers provides immediate and permanent online open access to all its publications, but this alone is not enough to realize our grand goals.

Frontiers journal series

The Frontiers journal series is a multi-tier and interdisciplinary set of open-access, online journals, promising a paradigm shift from the current review, selection and dissemination processes in academic publishing. All Frontiers journals are driven by researchers for researchers; therefore, they constitute a service to the scholarly community. At the same time, the *Frontiers journal series* operates on a revolutionary invention, the tiered publishing system, initially addressing specific communities of scholars, and gradually climbing up to broader public understanding, thus serving the interests of the lay society, too.

Dedication to quality

Each Frontiers article is a landmark of the highest quality, thanks to genuinely collaborative interactions between authors and review editors, who include some of the world's best academicians. Research must be certified by peers before entering a stream of knowledge that may eventually reach the public - and shape society; therefore, Frontiers only applies the most rigorous and unbiased reviews. Frontiers revolutionizes research publishing by freely delivering the most outstanding research, evaluated with no bias from both the academic and social point of view. By applying the most advanced information technologies, Frontiers is catapulting scholarly publishing into a new generation.

What are Frontiers Research Topics?

Frontiers Research Topics are very popular trademarks of the *Frontiers journals series*: they are collections of at least ten articles, all centered on a particular subject. With their unique mix of varied contributions from Original Research to Review Articles, Frontiers Research Topics unify the most influential researchers, the latest key findings and historical advances in a hot research area.

Find out more on how to host your own Frontiers Research Topic or contribute to one as an author by contacting the Frontiers editorial office: frontiersin.org/about/contact

Novel immune markers and predictive models for immunotherapy and prognosis in breast and gynecological cancers

Topic editors

Chao Liu — Department of Radiation Oncology, Shandong Cancer Hospital, China
Feifei Teng — Shandong University Cancer Center, China
Alberto Traverso — Maastro Clinic, Netherlands
Shicheng Guo — Arrowhead Pharmaceuticals, United States

Citation

Liu, C., Teng, F., Traverso, A., Guo, S., eds. (2024). *Novel immune markers and predictive models for immunotherapy and prognosis in breast and gynecological cancers*. Lausanne: Frontiers Media SA. doi: 10.3389/978-2-8325-4994-0

Table of contents

frontiers | Frontiers in Immunology

TYPE Editorial
PUBLISHED 29 May 2024
DOI 10.3389/fimmu.2024.1431245

OPEN ACCESS

EDITED AND REVIEWED BY
Peter Brossart,
University of Bonn, Germany

*CORRESPONDENCE
Chao Liu
charles.liu@whu.edu.cn
Feifei Teng
tengfeifei16@126.com

†These authors have contributed equally to this work

RECEIVED 11 May 2024
ACCEPTED 20 May 2024
PUBLISHED 29 May 2024

CITATION
Wang F, Huang Q, Guo S, Traverso A, Teng F and Liu C (2024) Editorial: Novel immune markers and predictive models for immunotherapy and prognosis in breast and gynecological cancers.
Front. Immunol. 15:1431245.
doi: 10.3389/fimmu.2024.1431245

Editorial: Novel immune markers and predictive models for immunotherapy and prognosis in breast and gynecological cancers

Fuhao Wang[1†], Qingyu Huang[1†], Shicheng Guo[2], Alberto Traverso[3,4], Feifei Teng[1*] and Chao Liu[1*]

[1]Department of Radiation Oncology and Shandong Provincial Key Laboratory of Radiation Oncology, Shandong Cancer Hospital and Institute, Shandong First Medical University and Shandong Academy of Medical Sciences, Jinan, China, [2]Department of Medical Genetics, School of Medicine and Public Health, University of Wisconsin-Madison, Madison, WI, United States, [3]Department of Radiation Oncology (Maastro Clinic), School for Oncology and Reproduction (GROW), Maastricht University Medical Center, Maastricht, Netherlands, [4]School of Medicine, Libera Università Vita-Salute San Raffaele, Milan, Italy

KEYWORDS

gynecological cancers, breast cancer, immunotherapy, precision medicine, biomarkers, prognosis

Editorial on the Research Topic
Novel immune markers and predictive models for immunotherapy and prognosis in breast and gynecological cancers

In the evolving field of oncology, precision medicine is reshaping treatment paradigms for breast and gynecological cancers by leveraging individual patient profiles (1–3). Utilizing advanced high-throughput sequencing technologies, researchers are identifying predictive biomarkers that improve the selection and efficacy of immunotherapies (4, 5). Despite significant advancements, clinical integration of these markers remains a challenge, underscoring the need for robust predictive models that combine multiple biomarkers to improve treatment precision and patient outcomes (6).

For this special Research Topic, we have gathered a collection of 15 research studies that focus on the discovery and use of new immune markers and predictive models in breast and gynecological cancers. The studies conducted by Ma et al. unveiled potential links between alterations in mitochondrial DNA methylation and the proliferative capacity of breast cancer cells. Their work in developing a prognostic model based on these mitochondrial DNA methylation dynamics offers valuable insights for predicting response to immunotherapy, assessing patient prognosis, and identifying new therapeutic targets. The meta-analysis by Wang et al. examined the prognostic implications of various PD-L1 expression patterns and the presence of tumor-infiltrating lymphocytes in high-grade serous ovarian cancer. Zhao et al. utilized both single-cell and bulk RNA sequencing to develop a predictive model based on B-cell marker genes for patients with triple-negative breast cancer. Yang et al. reviewed the multiple roles of liquid biopsy in the context of breast cancer immunotherapy, highlighting its

utility in predicting and monitoring treatment outcomes, and identifying resistance mechanisms. The work by Zhang et al. highlighted the downregulation of *CYR61* in estrogen receptor-positive breast cancer and associated it with a poor prognosis. *CYR61*'s relationship with tumor suppressor pathways and its potential role in modulating the tumor immune microenvironment suggest its utility as a prognostic marker and therapeutic target. Zhou et al. identified reduced expression of *MSH6* as a marker potentially indicative of a favorable prognosis, and active immune landscape, and a better response to immune checkpoint inhibitors in endometrial cancer. Chen et al. proposed a prognostic model based on the expression of four genes (*RAD51AP1*, *HELLS*, *PLSCR4*, and *POLQ*) that could independently predict outcome and treatment response in breast cancer patients. Garcia-Torralba et al. suggest that a combination of immune biomarkers, genomic markers of proliferation (*AURKA* and *MYBL2*), and clinicopathological features can improve prognostic models for patients undergoing neoadjuvant therapy for breast cancer, potentially improving the management and stratification of early-stage disease. Yang et al. reported a case involving the use of an immunotherapy-based combination regimen to treat a patient with metastatic primary uterine sarcoma. Despite disease progression following multiple prior treatments, the patient experienced disease stabilization and partial remission after three rounds of combined immunotherapy, targeted therapy, and chemotherapy. The patient maintained a good quality of life, with prospects for long-term survival. Lv et al. found that serum levels of *BTNL8* may serve as a valuable prognostic tool for assessing outcomes in patients with high-risk human papillomavirus infection undergoing photodynamic therapy. This finding supports in the early screening and monitoring of disease progression in patients infected with high-risk human papillomavirus. Xiong et al. developed a prognostic model based on genes associated with programmed cell death. This model demonstrates excellent diagnostic performance and can predict clinical outcomes and levels of immune infiltration in high-risk endometrial cancer patients. Notably, *LRPPRC* is associated with poor prognosis, shows strong correlations with proliferative genes and several programmed cell death-related genes, and is highly expressed in patients with advanced clinical stages. Sammons et al. found that mutations in *B2M* and amplifications in *CD274* may help predict the therapeutic efficacy of immune checkpoint inhibitors in breast cancers with a high tumor mutational burden. This finding has implications for the targeted use of immune checkpoint inhibitors in the treatment of this subgroup of metastatic breast cancer patients. Zhao et al. demonstrated that detecting circulating tumor cells in breast cancer diagnosis is characterized by a sensitivity of 74% and a specificity of 98%. Furthermore, the presence of circulating tumor cell positivity is associated with worse overall survival and progression-free survival/disease-free survival in Asian populations. Zhang et al. provided a detailed review of the immunosuppressive tumor microenvironment in various molecular subtypes of endometrial cancer. They discussed the relationship between immune phenotypes and new immunotherapy strategies for advanced or recurrent EC, highlighting the potential for targeted therapeutic interventions based on molecular and immune classifications. Finally, Liu et al. developed and validated a nomogram that integrates ultrasonographic radiomic features, clinicopathological features, and ultrasound features. This model effectively predicts the likelihood of achieving a pathologic complete response in breast cancer patients undergoing neoadjuvant chemotherapy.

Through the papers included in this special Research Topic, we explore the importance and application of novel immune markers and predictive models in breast and gynecological cancers. These studies not only provide a deep understanding of the diversity of tumor immunology but also, through advanced sequencing technologies, reveal biomarkers for specific cancer subtypes and treatment responses, opening up new possibilities for personalized cancer treatment. While these studies highlight promising avenues, challenges remain. There is a need for larger and more diverse patient cohorts to validate the findings and improve the generalizability of the predictive models. Additionally, future research should focus on integrating multi-omics data with clinical information to develop robust and comprehensive predictive models. The integration of novel technologies, such as single-cell multi-omics, is likely to play a pivotal role in advancing our understanding of tumor biology and treatment response (7). We look forward to future research that will continue to make breakthroughs in this field and provide patients with more precise and effective treatment options.

Author contributions

FW: Writing – original draft. QH: Writing – review & editing. SG: Writing – review & editing. AT: Writing – review & editing. FT: Writing – review & editing. CL: Writing – review & editing.

Acknowledgments

We are grateful to all the authors for their valuable contributions to this research topic.

Conflict of interest

The authors declare that the research was conducted in the absence of any commercial or financial relationships that could be construed as a potential conflict of interest.

Publisher's note

References

1. Crimini E, Repetto M, Aftimos P, Botticelli A, Marchetti P, Curigliano G. Precision medicine in breast cancer: From clinical trials to clinical practice. *Cancer Treat Rev*. (2021) 98:102223. doi: 10.1016/j.ctrv.2021.102223

2. Garg P, Krishna M, Subbalakshmi AR, Ramisetty S, Mohanty A, Kulkarni P, et al. Emerging biomarkers and molecular targets for precision medicine in cervical cancer. *Biochim Biophys Acta Rev Cancer*. (2024) 1879(3):189106. doi: 10.1016/j.bbcan.2024.189106

3. Nolan E, Lindeman GJ, Visvader JE. Deciphering breast cancer: from biology to the clinic. *Cell*. (2023) 186:1708–28. doi: 10.1016/j.cell.2023.01.040

4. Akhoundova D, Rubin MA. Clinical application of advanced multi-omics tumor profiling: Shaping precision oncology of the future. *Cancer Cell*. (2022) 40:920–38. doi: 10.1016/j.ccell.2022.08.011

5. Donoghue MTA, Schram AM, Hyman DM, Taylor BS. Discovery through clinical sequencing in oncology. *Nat Cancer*. (2020) 1:774–83. doi: 10.1038/s43018-020-0100-0

6. Bai R, Lv Z, Xu D, Cui J. Predictive biomarkers for cancer immunotherapy with immune checkpoint inhibitors. *biomark Res*. (2020) 8:34. doi: 10.1186/s40364-020-00209-0

7. Baysoy A, Bai Z, Satija R, Fan R. The technological landscape and applications of single-cell multi-omics. *Nat Rev Mol Cell Biol*. (2023) 24:695–713. doi: 10.1038/s41580-023-00615-w

frontiers | Frontiers in Oncology

TYPE Original Research
PUBLISHED 29 May 2023
DOI 10.3389/fonc.2023.1182725

OPEN ACCESS

EDITED BY
Chao Liu,
Shandong Cancer Hospital, China

REVIEWED BY
Jingyi Xie,
University of Washington, United States
Xin Li,
Houston Methodist Research Institute, United States

*CORRESPONDENCE
Francisco Ayala de la Peña
frayala@um.es

RECEIVED 09 March 2023
ACCEPTED 17 May 2023
PUBLISHED 29 May 2023

CITATION
García-Torralba E, Navarro Manzano E, Luengo-Gil G, De la Morena Barrio P, Chaves Benito A, Pérez-Ramos M, Álvarez-Abril B, Ivars Rubio A, García-Garre E, Ayala de la Peña F and García-Martínez E (2023) A new prognostic model including immune biomarkers, genomic proliferation tumor markers (*AURKA* and *MYBL2*) and clinical-pathological features optimizes prognosis in neoadjuvant breast cancer patients. *Front. Oncol.* 13:1182725. doi: 10.3389/fonc.2023.1182725

A new prognostic model including immune biomarkers, genomic proliferation tumor markers (*AURKA* and *MYBL2*) and clinical-pathological features optimizes prognosis in neoadjuvant breast cancer patients

Esmeralda García-Torralba[1,2,3], Esther Navarro Manzano[2,3], Gines Luengo-Gil[1,2,3], Pilar De la Morena Barrio[1,2,3], Asunción Chaves Benito[4], Miguel Pérez-Ramos[4], Beatriz Álvarez-Abril[1,2,3], Alejandra Ivars Rubio[1,2,3], Elisa García-Garre[1,2,3], Francisco Ayala de la Peña[1,2,3]* and Elena García-Martínez[1,2,3,5]

[1]Department of Haematology and Medical Oncology, University Hospital Morales Meseguer, Murcia, Spain, [2]Department of Medicine, Medical School, University of Murcia, Murcia, Spain, [3]Instituto Murciano de Investigación Biosanitaria (IMIB), Murcia, Spain, [4]Department of Pathology, University Hospital Morales Meseguer, Murcia, Spain, [5]Medical School, Catholic University of Murcia, Murcia, Spain

Background: Up to 30% of breast cancer (BC) patients treated with neoadjuvant chemotherapy (NCT) will relapse. Our objective was to analyze the predictive capacity of several markers associated with immune response and cell proliferation combined with clinical parameters.

Methods: This was a single-center, retrospective cohort study of BC patients treated with NCT (2001-2010), in whom pretreatment biomarkers were analyzed: neutrophil-to-lymphocyte ratio (NLR) in peripheral blood, CD3+ tumor-infiltrating lymphocytes (TILs), and gene expression of AURKA, MYBL2 and MKI67 using qRT-PCR.

Results: A total of 121 patients were included. Median followup was 12 years. In a univariate analysis, NLR, TILs, AURKA, and MYBL2 showed prognostic value for overall survival. In multivariate analyses, including hormone receptor, HER2 status, and response to NCT, NLR (HR 1.23, 95% CI 1.01-1.75), TILs (HR 0.84, 95% CI 0.73-0.93), AURKA (HR 1.05, 95% CI 1.00-1.11) and MYBL2 (HR 1.19, 95% CI 1.05-1.35) remained as independent predictor variables.

Conclusion: Consecutive addition of these biomarkers to a regression model progressively increased its discriminatory capacity for survival. Should independent cohort studies validate these findings, management of early BC patients may well be changed.

KEYWORDS

Breast cancer, neoadjuvant chemotherapy, neutrophil-to-lymphocyte ratio, tumor-infiltrating lymphocytes, proliferation markers

1 Introduction

Neoadjuvant chemotherapy (NCT) is the first treatment option for locally advanced and inflammatory breast cancer (BC). It is also a standard treatment in HER2-positive (HER2+) and triple-negative (TNBC) early BC (1). NCT increases the rate of conservative surgery, enables treatment response monitoring and the selection of adjuvant treatment according to risk, and provides unique opportunities for developing novel and individualized therapeutic strategies (1, 2).

Risk stratification is critical in BC patients receiving NCT, as residual pathological disease can affect postoperative decision-making (3). Pathological complete response (pCR) has been classically considered a robust predictor of recurrence, disease-free survival (DFS), and overall survival (OS), especially in the context of the most aggressive subtypes, i. e., HER2+BC and TNBC (2, 4, 5). Despite curative intent, up to 30%-40% of these cases, including some who achieved pCR, will relapse in the first 5 years of follow-up (6). It is crucial that we identify other prognostic factors that can help distinguish individuals who will relapse despite having achieved pCR after NCT.

The adaptive and the innate immune response play a pivotal role in tumor immunosurveillance and can limit tumor development and growth, and determine response to new therapeutic approaches, such as immunotherapy. The role of the immune response in BC has not been fully elucidated. Nevertheless, there is growing evidence that the tumor immune microenvironment plays a key role in the response to different cancer treatments and in prognosis (7).

Several immunological parameters are being investigated or developed as intermediate biomarkers of cancer regression, progression, or recurrence. The most extensively studied marker to date is probably tumor lymphocytic infiltration (8). Tumor-infiltrating lymphocytes (TILs) have been proposed as a predictor of response and prognosis in HER2+ BC and TNBC subtypes, but their involvement in luminal BC is less clear (7). The characterization of the immune cell population in BC and its activation status is mandatory to improve prognosis and to predict treatment response (9).

The chronic inflammatory response is also closely linked to the development and prognosis of certain cancers (10). There is mounting evidence that the total leukocyte count and, most notably, the neutrophil-to-lymphocyte ratio (NLR) prior to embarking on anticancer treatment predict an adverse clinical outcome in several solid tumor (11, 12). This marker is particularly interesting since it integrates the subject's immune response capacity with their inflammatory status, which tends to correlate with tumor progression and poor prognosis (13). In BC patients, an elevated NLR has been implicated in decreased survival, above all in localized stages (14–16).

The expression of proliferation-related genes in BC is linked to more aggressive subtypes (luminal B and non-luminal subtypes) and forms the foundation for the recent inclusion of clinical KI67 determinations as a predictive and prognostic immunohistochemical (IHC) marker (17). Furthermore, proliferation gene expression is key to understanding biological diversity in luminal BC (18). In fact, gene testing to determine the risk of recurrence includes this information (18–20).

The aurora A kinase (*AURKA*) gene codifies a serine/threonine kinase with a key role in mitosis regulation that works as an oncogene promoting tumorigenesis (21, 22). Several signaling pathways have been related with *AURKA*, including PI3K-Akt, Wnt, Hippo, p53 and FOXO (21). Additionally, *AURKA* is a proliferation marker and its overexpression has also been linked to unfavorable prognosis in BC (23, 24). *AURKA* has been proposed as a possible biomarker and therapeutic target in chemotherapy and hormonotherapy resistance (25–31).

MYBL2 overexpression has been described as a robust marker of replicative instability (RIN) that can occur in multiple tumor and is a driver in progressive disease and treatment resistance (32). In BC patients, a high *MYBL2* proto-oncogene level may also be a biomarker of adverse prognosis (33, 34) and could promote tumor invasion by the induction of epithelial–mesenchymal transition (EMT) and modulation of immune microenvironment (35, 36). *In vitro* studies have demonstrated its role in tamoxifen resistance (37). Interestingly, Guarneri et al. in the ShortHER phase III trial found that HER2-enriched BC tumor with mutated *PIK3CA* had an upregulated expression of *MKI67*, *MYBL2*, *ESR1*, *PDCD1* and other genes, but only *MYBL2* and *PDCD1* were related with a better DFS (38).

A single perfect biomarker is unlikely to exist. Recent publications suggest that combined biomarker determination can potentially yield more complete and relevant information (39). Importantly, the predictive value of proliferative signatures and immune signatures are apparently independent, at least in TNBC (40). Combining two proliferation markers such as *AURKA* and *MYBL2*, with different biological meaning and with diverse impact on therapeutic resistance, might also improve prognostic

stratification. Hence, given the need to enhance currently available prognostic systems and to optimize therapeutic strategies, we have analyzed the prognostic contribution of several immune response-related markers, both in the tumor microenvironment and systemically, in combination with tumor proliferation and clinical-pathological features, in BC patients treated with NCT.

2 Materials and methods

2.1 Study cohort and clinical management

A series of patients consecutively diagnosed with stage II or III BC who received NCT in the Hematology and Medical Oncology Department of a single tertiary hospital (University Hospital Morales Meseguer, Murcia, Spain) between July 2001 and October 2010 was retrospectively analyzed. Clinical evaluation at diagnosis was conducted as per clinical practice criteria, including breast MRI and axillary ultrasound in all cases. Pre-NCT lymph node status was determined by ultrasound-guided fine needle aspiration or sentinel node biopsy. Treatment followed local protocols, in accordance with international recommendations applicable at the time of diagnosis (41). NCT included taxanes and anthracyclines, as well as trastuzumab in patients with HER2+ tumor. After surgery, hormone therapy was prescribed to all patients with hormone receptor (HR)-positive tumor and adjuvant trastuzumab in HER2+ tumor. Adjuvant radiotherapy was administered to all patients treated with conservative surgery, and to patients undergoing mastectomy with a high risk of relapse.

Written informed consent was obtained from all patients included in the study. The study was approved by the Clinical Research and Trials Committee of the University Hospital Morales Meseguer (Internal code: EST07/15) and was conducted in accordance with the ethical principles of the Declaration of Helsinki.

2.2 Clinical and laboratory variables and neutrophil-to-lymphocyte ratio estimation

Demographic and clinical-pathological variables and treatment and response data were obtained from participants' clinical records. Primary outcome variables included DFS, measured from the date of diagnosis to last follow-up or disease relapse, and OS, quantified as the date of diagnosis to the date of last follow-up or demise.

Routine laboratory parameters were collected from laboratory databases, using the closest blood count prior to the date NCT was initiated (maximum time: four weeks). Pretreatment NLR was calculated by dividing the absolute neutrophil count by the absolute lymphocyte count.

2.3 Histopathological evaluation of the tumor

Estrogen receptor (ER) and progesterone receptor (PR) status were assessed by IHC. Cases were considered negative when the percentage of immunoreactive tumor cells was <1%; the remaining cases (≥1% of stained tumor cells) were classified as positive. A validated IHC method (Herceptest, Dako North America, CA, USA) or fluorescent *in situ* hybridization (FISH) was used to determine HER2 status. Cases were positive if the Herceptest result was 3+ and/or FISH exhibited a HER2/CEP17 ratio ≥ 2; all others were coded as negative. pCR was defined as the absence of invasive carcinoma in the breast and axilla, regardless of the presence of carcinoma *in situ* (ypT0/Tis ypN0).

2.4 Tumor-infiltrating lymphocyte counts

CD3-positive TILs (TIL-CD3+) were quantified using IHC, as previously reported (9). In brief, after a pathologist (ACB) had selected tumor-predominant areas, a tissue microarray was constructed from 2 mm biopsies prior to initiating NCT treatment. Appropriate controls were included in each array. Sections measuring 4 µm were cut from the tissue microarray, deparaffinized, rehydrated, and processed by standard methods using an automated stainer (Autostainer Link 48, Dako, CA, USA). Secondary antibodies and visualization were performed using standard Dako Envision systems. All slides were simultaneously stained to avoid intersection variability. Positivity for human CD3 was tested using the polyclonal antibody IS503 (Dako, CA, USA).

After two independent observers had verified that staining was correct, each slide was scanned and digitized using an automated scanning system (Leica SCN400F). Digital images of pre-NCT samples were obtained for each tissue core and, after area quantification, adjusted morphometric analysis of the tumor area was performed with ImageJ software (National Institutes of Health, NIH, USA), including both stromal and intratumoral CD3+ cells. The results are expressed as TIL count/mm^2.

2.5 RNA purification and tumor gene expression assay

Total RNA from formalin-fixed paraffin-embedded (FFPE) biopsies was extracted using a RNeasy FFPE kit (QIAGEN, MD, USA) following the supplier's instructions. Total RNA from cells was extracted using RNAzol reagent (MRC Inc, OH, USA) and a Direct-zol RNA MiniPrep kit (ZYMO Research, CA, USA).

mRNA (with preamplification) was retrotranscribed and amplified using TaqMan® Gene Expression Assays (Applied Biosystems, CA, USA) on a LightCycler® 480 real-time PCR (qRT-PCR) system (Roche Diagnostics, Switzerland). Relative expression levels of each gene were calculated and quantified by 2-ΔΔCt using ACTB as the endogenous control.

2.6 Statistical analysis

Descriptive analyses of qualitative variables included proportions. Shapiro-Wilk tests were used to test continuous

variables for normality. Continuous variables with normal distribution were presented as means ± standard deviations (SD), whereas non-normally distributed variables were reported as median and interquartile ranges (IQR). Pearson's $\chi 2$ test was used to compare proportions or ordinal variables. Differences in means were studied with the Student's t-test (parametric) or the Mann-Whitney U test (non-parametric).

Survival analyses of DFS and OS outcome variables were calculated using the Kaplan-Meier method and log-rank tests. The predictive impact of the different clinical, biological, and genomic variables on the outcome variables was ascertained by uni- and multivariate Cox proportional hazards regression analyses. To overcome the possibility of collinearity, variables with strong ($|r| \geq 0.5$) or significant ($p < 0.05$) correlations were excluded. The predictive capacity of the regression models was appraised using the Akaike Information Criterion (AIC) index and Likelihood Ratio Test (LLRT). Biological and genomic variables were analyzed as continuous quantitative variables, although logarithmic or square root transformations of the TILs, *AURKA*, *MYBL2*, and *MKI67* variables were performed so that the data would comply more closely with the assumptions of the statistical procedures to be applied or to enhance interpretability. Assessment of mean calibration at 10 years was calculated for each model as observed/expected (O/E) survival ratio.

Statistical analyses were performed with STATA v.16 (StataCorp LLC, TX, USA); R version 4.2.3 and RStudio (version 2023.03.0) was also used for model assessment.

3 Results

3.1 Patients

A total of 121 NCT-treated BC patients were analyzed. Patients' baseline characteristics are shown in Table 1. Median age was 56 years and most tumors were diagnosed at stage IIB or IIIA-C.

TABLE 1 Patients' baseline characteristics.

Baseline characteristics	N = 121 (%)[a]	N = 47 (%)[b]	p*
Age (median, range)	56 (21-79) years	57 (21-73) years	0.711
Hormonal status			
Premenopausal	60 (49.6%)	21 (44.7%)	0.32
Postmenopausal	61 (50.4%)	26 (55.3%)	
Clinical stage			
IIA	19 (15.7%)	10 (21.3%)	0.11
IIB	34 (28.1%)	14 (29.8%)	
IIIA	40 (33.1%)	10 (21.3%)	
IIIB	8 (6.6%)	2 (4.3%)	
IIIC	20 (16.5%)	11 (24.3%)	
Pathological subtype			
Invasive ductal carcinoma	113 (93.4%)	44 (93.6%)	0.98
Invasive lobular carcinoma	5 (4.1%)	2 (4.3%)	
Other	3 (2.5%)	1 (2.1%)	
Histological grade			
Grade I	7 (5.8%)	3 (6.5%)	0.66
Grade II	39 (32.2%)	19 (41.3%)	
Grade III	61 (50.4%)	22 (47.8%)	
Not reported	14 (11.5%)	2 (4.3%)	
IHC subtype			
HR+/HER2-	61 (50.4%)	24 (51.1%)	0.09
HR+/HER2+	16 (13.2%)	7 (14.9%)	
HR-/HER2+	13 (10.7%)	9 (19.1%)	
TNBC	26 (21.5%)	7 (14.9%)	
N/A	5 (4.1%)	0 (0%)	
Clinical response			
CR/PR	102 (84.3%)	43 (91.5%)	0.16
SD/PD	14 (11.6%)	3 (6.4%)	
N/A	5 (4.1%)	1 (2.1%)	
Breast surgery			

(Continued)

TABLE 1 Continued

Baseline characteristics	N = 121 (%)[a]	N = 47 (%)[b]	p*
Mastectomy Conservative surgery	67 (55.3%) 53 (43.8%)	22 (46.8%) 25 (53.2%)	0.37
Nodal surgery			
SLN biopsy ALND	17 (14.0%) 104 (86.0%)	10 (21.3%) 37 (78.7%)	0.06
Radiotherapy			
Pre-NCT Post-NCT	0 (0%) 106 (87.6%)	0 (0%) 41(87.2%)	0.44
Follow-up (median, range) 10-year DFS (95% CI) 10-year OS (95% CI)	12.3 years (11.82-12.79) 73.3% (64.49-80.99) 75.83% (67.17-83.18)	11.6 years (11.30-11.93) 78.73% (64.34-89.30) 80.9% (66.74-90.85)	0.66 0.59 0.64

[a]Total number of patients included, N = 121.
[b]Nested cohort for the multivariate analysis, N = 47.
ALND, axillary lymph node dissection; CR, complete response; DFS, disease-free survival; HER2, human epidermal growth factor receptor 2; HR, hormone receptor; IHC, immunohistochemical; N/A, not available; NCT, neoadjuvant chemotherapy; OS, overall survival; PD, progression disease; PR, partial response; SD, stable disease; SLN, sentinel lymph node; TNBC, triple-negative breast cancer.
*The p value refers to the result of the comparison between proportions or means of both groups.

Infiltrating ductal carcinoma was the most common histological type and more than half of the tumors were poorly differentiated. ICH subtype distribution revealed 63.6% HR+ (13.2% HER2+), 10.7% HER2+/HR- tumors, and 21.5% TNBC.

Neoadjuvant treatment consisted primarily of sequential Adriamycin-cyclophosphamide for four cycles, followed by docetaxel for four cycles (NSABP-B27 scheme, 80.2%). The pCR rate was 17% (primary tumor pCR: 20.7%; axillary pCR: 36.4%). Median follow-up was 12.3 years, the 10-year DFS rate was 73.33%, and 10-year OS was 75.83%.

Of the total 121 participants, the full analysis of clinical variables (HR/HER2 status, response to NCT), immunological variables (NLR, TILs), and genomic markers (*AURKA*, *MYBL2*, and *MKI67*) were available for multivariate analysis in 47 patients (Supplementary Figure 1). Since the clinical and pathological characteristics of both groups were comparable and no statistically significant differences were found, this subgroup was representative of the total sample (Table 1).

3.2 Prognostic significance of clinical, biological, and genomic factors

We evaluated the prognostic significance of the clinical factors and the various biomarkers selected by Cox regression. NLR, TILs, and genomic markers were analyzed as continuous quantitative variables. Correlation analysis demonstrated association between genomic markers *MKI67*, and *MYBL2* (Supplementary Table 1). Notably, there was no correlation between pretreatment NLR and TILs in the pretreatment biopsy (|r|= 0.087, p = 0.503).

In a univariate analysis (Figure 1), pCR (N = 119) was a protective factor for DFS (HR 0.13, 95% CI 0.02-0.94) and OS

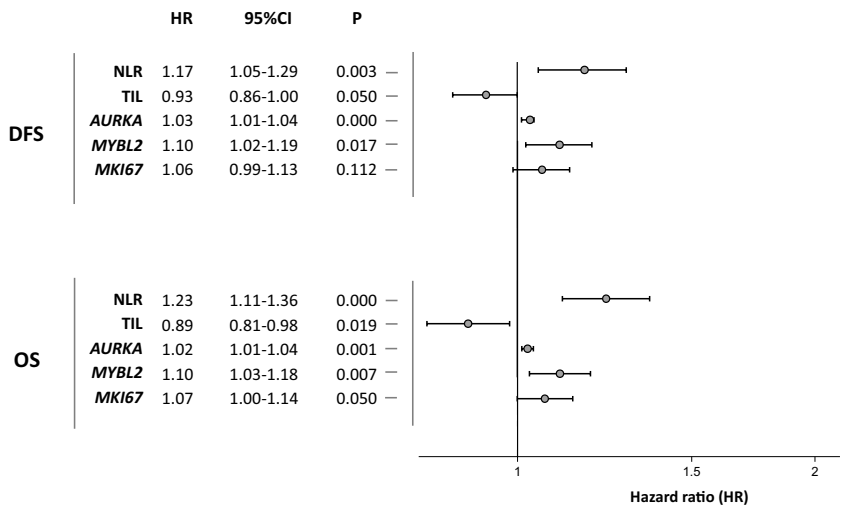

FIGURE 1
Univariate associations between immune response-related and proliferation markers and disease-free survival and overall survival.

(HR 0.30, 95% CI 0.07-1.27), albeit falling short of statistical significance. Results were similar for patients with HR+ and HER2+, in terms of DFS (HR 0.91, 95% CI 0.46-1.78 and HR 1.15, 95% CI 0.56-2.38, respectively) and OS (HR 0.97, 95% CI 0.46-2.06 and HR 0.76, 95% CI 0.31-1.85, respectively).

The NLR biomarker in peripheral blood (N = 101) was found to have prognostic implications. Increased NLR was associated with lower DFS (HR 1.17, 95% CI 1.05-1.29) and OS (HR 1.23, 95% CI 1.11-1.36). At the tumor level, the immunological marker TIL (N = 71) exhibited a statistically significant association in the opposite direction from NLR. Patients with higher tumor lymphocytic infiltration had a better prognosis in terms of DFS (HR 0.93, 95% CI 0.86-1.00) and OS (HR 0.89, 95% CI 0.81-0.98).

Genomic markers for tumor proliferation assessed were *AURKA*, *MYBL2*, and *MKI67*. *AURKA* (N = 79) demonstrated a significant prognostic impact on DFS (HR 1.03, 95% CI 1.01-1.04) and OS (HR 1.02, 95% CI 1.01-1.04). *MYBL2* expression (N = 79) also correlated with lower DFS (HR 1.10, 95% CI 1.02-1.19) and OS (HR 1.10, 95% CI 1.03-1.18). The proliferation marker *MKI67* (N = 79) only exhibited prognostic significance for OS (HR 1.07, 95% CI 1.00-1.14).

Clinically relevant variables and biomarkers that had previously exhibited prognostic significance were included to generate multivariate Cox models. *MKI67*, that showed significant correlation with *MYBL2*, was excluded to prevent collinearity (Supplementary Table 1). Thus, together with HR/HER2 status and response to NCT, the NLR, TILs, and *AURKA* and *MYBL2* expression remained as independent prognostic variables for both DFS and OS (Table 2).

3.3 Analysis of the prognostic capacity of the different models

We assessed the predictive performance of the biomarkers included in the multivariate Cox proportional hazards models using AIC and LLRT. We consecutively added the immune response biomarkers, NLR and TILs (model 2), and genomic markers, *AURKA* and *MYBL2* (model 3), to HR/HER2 status and NCT response (model 1). For both DFS and OS, we established that the consecutive addition of biomarkers generated a progressive increase in the models' predictive capacity (Table 3). This was reflected in a gradual decrease in AIC for both DFS (AIC model 3: 64 vs AIC model 1: 79) and OS (AIC model 3: 58 vs AIC model 1: 70), in addition to differences in LLRT for the different models that were statistically significant compared to the isolated clinical parameter (DFS: $p < 0.001$; OS: $p = 0.005$). A side-by-side comparison between this combinatorial model versus prediction using individual markers, is provided as Supplementary Table 2. Additionally, the 10 years mean calibration of the OS model also improved with the addition of proliferation and immune markers, while it remained virtually unchanged for the DFS models (Figure 2 and Supplementary Table 3).

The predictive value added by the biomarkers was also gauged by plotting cohort survival as a function of the predictions obtained with each model. Figure 3 depicts the Kaplan-Meier curves for DFS and OS obtained with the predictions of pCR and model 3 (pCR, HR and HER2 status, NLR, TILs, *AURKA*, and *MYBL2*), the latter divided into tertiles. This exploratory analysis showed that the incorporation of the immunological and proliferation parameters with the clinical variable (pCR) in model 3 allowed a better stratification of the risk of events in the cohort analyzed than model 1. In fact, while the log-rank test indicated no statistically significant differences for model 1, such differences were statistically significant for model 3, both for DFS ($p = 0.0014$) and OS ($p = 0.0054$).

4 Discussion

The expanding body of knowledge of the immune response to BC and the differences between the systemic and microenvironment response provides opportunities for identifying predictive and prognostic biomarkers (10, 42). In the challenging context of neoadjuvant BC treatment, it is likely that several biomarkers will need to be combined to improve prognostic stratification (39, 43). Although pCR has been considered a surrogate marker of survival in early BC patients treated with NCT, in the luminal subtype we should probably consider additional markers to achieve better survival prediction. Moreover, the selection of patients who may

TABLE 2 Multivariate analysis of immune response-related and proliferation markers for disease- free survival and overall survival.

Variables	DFS			OS		
	HR	95% CI	P	HR	95% CI	P
pCR	0.01	0.01 – 0.78	0.042	0.04	0.01 – 1.61	0.090
HR+	0.23	0.04 – 1.16	0.075	0.14	0.03 – 0.81	0.027
HER2+	0.15	0.14 – 1.74	0.131	0.25	0.03 – 2.10	0.204
NLR	1.80	1.12 – 2.88	0.014	1.37	1.03 – 1.83	0.033
TILs*	0.93	0.83 – 1.05	0.259	0.86	0.75 – 0.98	0.026
*AURKA**	1.04	1.00 – 1.08	0.069	1.04	1.00 – 1.09	0.090
*MYBL2**	1.13	1.01 – 1.27	0.037	1.19	1.05 – 1.35	0.007

AURKA, Aurora kinase A; DFS, disease-free survival; HER2+, human epidermal growth factor receptor 2 positive; HR, hazard ratio; HR+, hormone receptors positive; MYBL2, MYB Proto-Oncogene Like 2; NLR, neutrophil-to-lymphocyte ratio; OS, overall survival; pCR, pathological complete response; TILs, tumor-infiltrating lymphocytes; 95% CI, 95% confidence interval.
*Square root transformation of these variables was performed.

10.3389/fonc.2023.1182725

TABLE 3 Predictive capacity following the consecutive addition of biomarkers to clinical variables.

Models	DFS					OS				
	AIC	LLR†	P†	LLR‡	P‡	AIC	LLR†	P†	LLR‡	P‡
Model 1 pCR + HR/HER2 status	79	22.50	<0.001	15.46	<0.001	70	20.69	<0.001	10.71	0.005
Model 2 + NLR + TILs	68	7.04	0.030	ref	n/a	64	9.98	0.007	ref	n/a
Model 3 +*AURKA* + *MYBL2*	64	ref	n/a	n/a	n/a	58	ref	n/a	n/a	n/a

†Likelihood ratio test (LLRT) and p value for comparison of model 3 (reference category) and models 1 and 2 (nested models).
‡ Likelihood ratio test (LLRT) and p value for comparison of model 2 (reference category) and model 1 (nested model).
AIC, Akaike Information Criterion; AURKA, Aurora kinase A; DFS, disease-free survival; HER2, human epidermal growth factor receptor 2; HR, hormone receptor; NLR, neutrophil-to-lymphocyte ratio; MYBL2, MYB Proto-Oncogene Like 2; OS, overall survival; pCR, pathological complete response; TILs, tumor-infiltrating lymphocytes; Ref, reference; N/a, not applicable.

gain real benefit from chemotherapy and those who may not is a pressing issue in the investigation of new therapeutic strategies and the avoidance of unnecessary chemotherapy side effects.

To explore new combination prognostic biomarkers, we conducted this study in a cohort of NCT-treated BC patients and investigated the prognostic implications for both DFS and OS of immune biomarkers in peripheral blood, such as NLR, and at the tumor level (TILs), together with genomic proliferation markers (*AURKA*, *MYBL2*, and *MKI67*) and conventional parameters, and response to NCT. Integrating all of these factors in a prognostic model consisting of NLR, TIL, *AURKA* and *MYBL2*, as a complement to HR/HER2 status and response to NCT, displayed a remarkable capacity to predict relapse and death.

Individually, NLR and TILs reflect systemic and local immune status, respectively. Specifically, for NLR, the results we obtained in our cohort were consistent with most of the literature reported to date. Zhoe et al. confirmed in a recent meta-analysis with 5504 BC patients treated with NCT that an NLR < 2.3 was predictive of pCR independently of tumor stage or grade and KI67 expression level (44). They also identified NLR as a prognostic biomarker, with patients with higher NLR levels having worse DFS (44). A previous meta-analysis of 8563 patients reached similar conclusions, with a large NLR cut-off range (1.9 – 5) and a median of 3 (14). In our study, we evaluated NLR as a continuous quantitative variable, thus avoiding the selection of an arbitrary or data-driven cut-off point. To better understand the significance of the NLR, we should probably investigate the dynamic change of NLR associated with chemotherapy. It has been reported that a lower NLR after chemotherapy predicts better pCR (45), while another study demonstrated that this change could be a predictor of pCR beyond the third NCT cycle (46). This is consistent with previous data generated by our group, that evaluated the prognostic value of peripheral blood lymphocytes and changes associated with NCT in BC patients (47).

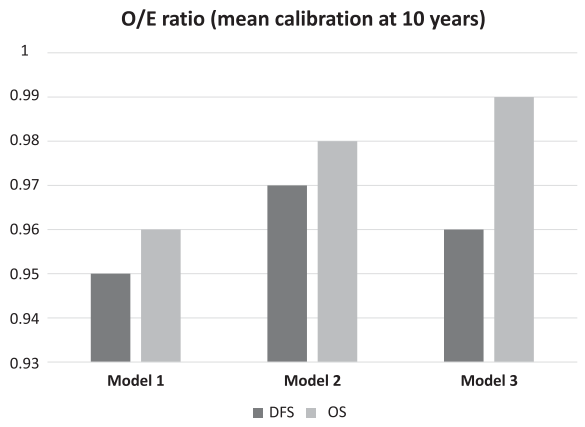

FIGURE 2
Mean calibration at 10 years. O/E (observed/expected) ratios for each model are shown, both for OS and DFS.

The prognostic implications of TILs were also in line with earlier works (7, 48). The 12-year follow-up of our series of BC patients who received NCT is one of the longest published. It is relevant that in this 12-year study, TILs predict the same good prognosis as we reported in our 5-year study (9). One strength of this analysis is that, since there is no valid cut-off point and the evidence available is extremely heterogeneous, we have evaluated TILs as a continuous quantitative variable, which is the recommended approach in these cases (49). The positive response and outcome of women with greater lymphocyte infiltration could be, at least in part, due to the activation of the antitumor immune response during NCT, induced after DNA damage and cell death (50). A meta-analysis of 18170 BC patients confirmed high TILs as a predictive and prognostic biomarker in HER2+ and TNBC. In luminal subtypes, high TILs were correlated with poor prognosis (51). Unfortunately, our series is small for BC subtype analyses. Luminal BC is characterized by low TIL infiltration with low HLA expression, so other immune cells such as tumor associated macrophages (TAM) could be more relevant than T cells (52) or even NK cells whose role has not yet been studied in depth in BC. In this line, it is essential to determine the infiltrating lymphocyte subtypes in BC (9, 53). The significance of defining the immune-infiltrating cell type has been studied by an immune risk score analyses using TGCA and other database genes. A low prognostic immune risk score with five cell subtypes (B cells, endothelial cells, macrophages, NK cells, other cells) has been correlated with better survival in BC (54).

The correlation between NLR and TILs and their combined predictive capacity for adverse events has yet to be fully elucidated. Our study confirms the lack of correlation between both variables,

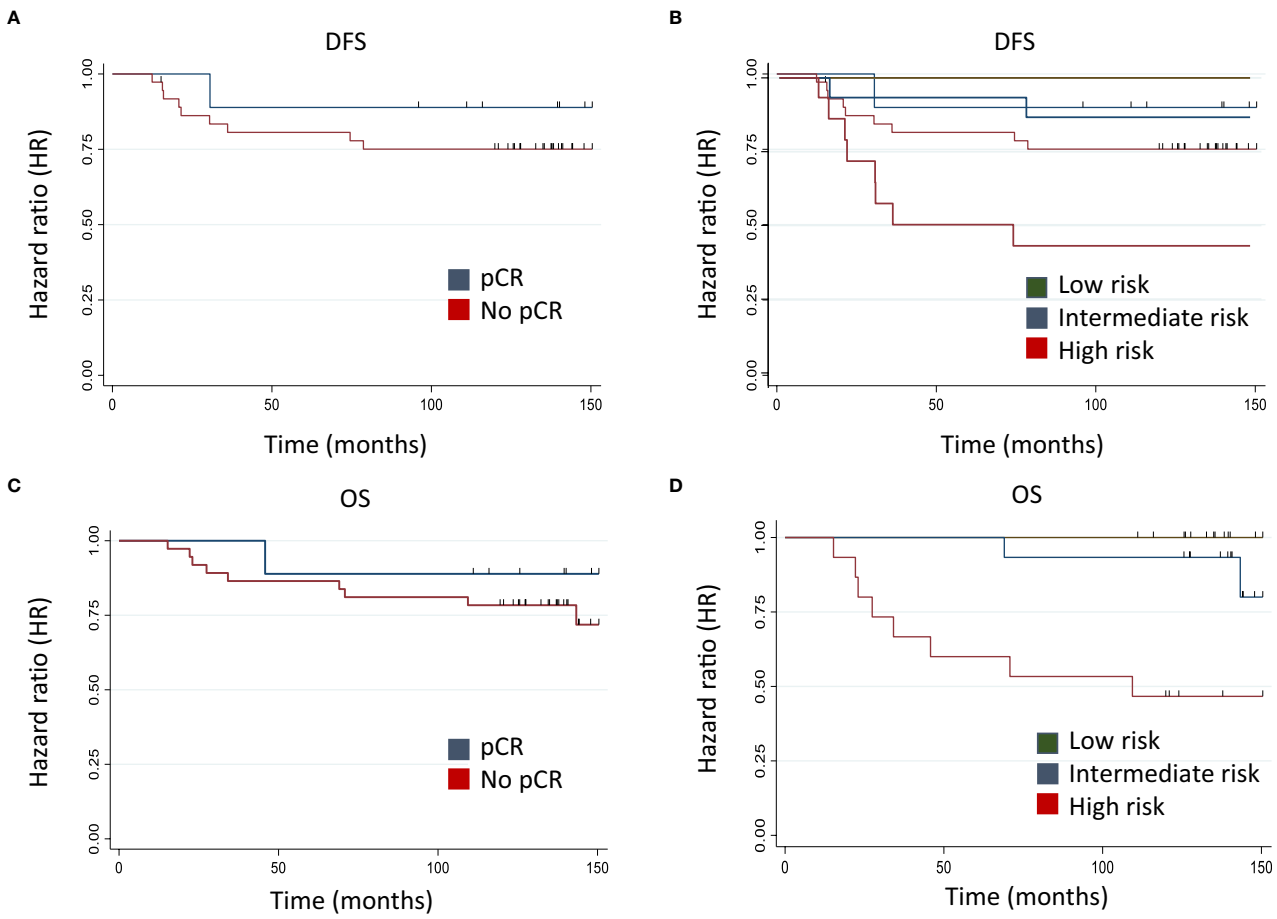

FIGURE 3
Model prediction with Kaplan-Meier curves for DFS and OS. Kaplan-Meier curves for DFS and OS obtained with predictions from clinical variable (pCR) **(A, C)** and model 3 (pCR, NLR, TILs *AURKA*, and *MYBL2*) **(B, D)**, the latter divided into tertiles. Model 1: PLR DFS: 0.34 - PLR OS: 0.41. Model 3: PLR DFS: 0.0014 - PLR OS: 0.0054.

suggesting that systemic and local immunities respond to different regulatory mechanisms (55); therefore, combined predictive models can offer a more comprehensive vision (39).This lack of correlation is consistent with previously published findings in TNBC and luminal BC (55–58). In our cohort, not only did both remain as independent prognostic variables in the multivariate analysis, but the combination of NLR and TILs improved the prognostic accuracy over pCR to NCT alone.

Genomics has improved our understanding of BC biology and revealed four intrinsic molecular subtypes with significant immunological differences, as previously mentioned (43). Immune-activated gene subsets, higher expression of proimmune factors and/or TILs have been associated with chemosensitivity, but also proliferation has been identified as a key factor in BC (59). Particularly, in the context of BC patients treated with NCT, proliferation markers correlate with oncologic progression and prognosis for the different IHC subtypes (60, 61). Therefore, the information they provide might complement what we learn from immunological biomarkers (61, 62). The choice of the optimal combination of proliferation markers was a difficult decision to make. Wirapati et al. published a meta-analysis of gene expression profiles with three gene modules (proliferation, ER signaling and *ERBB2* amplification) in 2833 breast tumor to better understand cancer subtyping and prognosis signatures (63). *AURKA* was chosen as a proliferation gene based on this study and others already discussed in the introduction (23, 24, 64). As we mentioned previously, *MYBL2* is one of the proliferation genes included in Oncotype, PAM50 and MammaPrint tests (19). Finally, *MKI67* was chosen since Ki67 is used in the clinical setting to identify luminal B cases and the correlation between Ki67 and *MKI67* has been previously established (65). One interesting finding is the statistically significant association observed between genomic markers *MKI67* and *MYBL2*. Previous reports have shown that the expression of MKI67 can be regulated by MYBL2, and this regulation is not specific to BC (66, 67). In our cohort, we did not observe a significant correlation between the proliferation markers *AURKA* and *MYBL2*, although previous work have noted a shared transcription between them (68).

Our study has demonstrated the independent prognostic value of the combination of systemic and microenvironmental immune biomarkers (NLR and TILs) with genomic proliferation markers (*AURKA* and *MYBL2*) and classical clinical factors (HR/HER status, pCR). Compellingly, the addition of proliferation biomarkers markedly increased the discriminatory capacity of the

model. The model combining all variables (HR/HER status, pCR, NLR, TILs, *AURKA*, and *MYBL2*) exhibited the greatest predictive ability for DFS and OS, both in terms of AIC and statistically significance (LLRT). To date, the factors associated with response to NCT have been obtained from clinical, pathological and molecular analyses. However, the majority of these studies include a limited sample size, combine data from patients with different therapeutic strategies and use profiles with isolated variables that fail to capture the complexity of the tumor ecosystem. As a result, empirical clinical risk stratification continues to be used for selecting patients who are candidates for neoadjuvant treatment (69).

Several studies have explored the combination of local immune biomarkers associated with classical clinical factors such as response to neoadjuvant treatment (39). In particular, TILs, PD-L1 and genomic signatures and their combinations have been extensively studied (39, 69). Prat et al. compared the three-gene model (SCMGENE) with *ESR1*, *ERBB2* and *AURKA* with that of the PAM50 test. They concluded that while both models were able to anticipate patient outcomes, PAM50 was the superior model and the only one with predictive value. This was because PAM50 reveals biological diversity better than the three-gene model (70). Interestingly, our results are consistent with the results obtained using the three-gene model.

In this context, it is important to remark the potential benefit of a model that combines multiple biomarkers, in which all variable contribute to provide comprehensive patient information. Such a novel approach can provide an integrated immuno-genetic-oncological biomarker for selecting the most accurate therapy strategy. Furthermore, the available evidence suggest the potential value of the systematic implementation of combined biomarkers to improve patient selection and safety (39). To identify the most appropriate combined model, it is necessary to start exploring some of the most extensively studied biomarkers, as we have done in our original research.

Our study has some limitations. First, the method used to quantify TILs was based on IHC for CD3, which includes both stromal and intra-tumor lymphocytic infiltration and differs from the currently accepted method (49). However, our group has previously shown good correlation for TILs measured by IHC for CD3 with HE-based assessment of lymphocyte infiltration (9). Second, the use of genomic markers of proliferation differs from the more recent routine use of KI67 (71), although genomic signatures of proliferation are the strongest factor for prognostic stratification in most predictive genomic tests in early luminal BC (60, 72) and also comprise a key prognostic marker in non-luminal subtypes (73, 74). Finally, this is a small, single-center, retrospective cohort, in which it was not possible to perform subgroup analyses according to tumor subtype with sufficient statistical power to draw conclusions.

Nonetheless, our series does have a number of strengths that make it compelling. Besides having one of the longest follow-up published in literature, it is highly homogeneous with respect to clinical management, including diagnosis, NCT, and response determination, which are key to obtain and interpret data within the context of early BC. NCT, surgery and radiation therapy were performed according to usual clinical procedures and following current clinical practice guidelines, which makes treatment bias unlikely for the final prognostic model. Furthermore, the inclusion in our model of clinical classical factors, local immunological factors, such as TILs, systemic immune status, such as NLR, and two of the most relevant proliferation markers, is a novel approach in the study of breast cancer prognosis. These results warrant prospective, multi-centre validation studies with a larger sample size.

5 Conclusions

In conclusion, our study reveals that combining systemic immune and proliferation biomarkers with clinical-pathological markers improved the predictive capacity for DFS and OS compared to treatment response alone in a cohort of BC patients treated with NCT. The real benefit and clinical usefulness of these biomarker-based models should be confirmed in broader series. The validation of these findings in independent cohorts could provide a new tool for improving prognostic stratification and therapeutic management in these patients.

Data availability statement

The data that support the findings of this study are available from the corresponding author upon reasonable request.

Ethics statement

The studies involving human participants were reviewed and approved by Clinical Research and Trials Comittee of the University Hospital Morales Meseguer. The patients/participants provided their written informed consent to participate in this study.

Author contributions

Concept, EG-T, EM, FP and EG-M. Data curation, EG-T, EM, EG-G, FP and EG-M. Formal analysis, EG-T, EM, FP and EG-M. Funding acquisition, FP. and EG-M. Investigation, EG-T, EM, GL-G, PB, MP-R, FP, and EG-M. Methodology, EG-T, EM, GL-G, MP-R, FP, and EG-M. Project administration, EG-T, EM, GL-G, FP and EG-M. Supervision, FP and EG-M. Writing—original draft, EG-T, FP and EG-M. Writing—review and editing, EG-T. EM, GL-G, PB., AB, MP-R, BA-A, AR, EG-G, FP, and EG-M. All authors contributed to the article and approved the submitted version.

Funding

This work was supported by the Ana Balil-GEICAM grant (Spanish Breast Cancer Research Group); the funding institution has not participated in collecting, analyzing, or interpreting the data, nor did it participate in drafting this manuscript. This work was also supported by Instituto de Salud Carlos III (PI12/02877), including FEDER funding by the European Union. ENM was funded by the

Ministerio de Educación, Cultura y Deporte [Ministry of Education, Culture, and Sports] (Spain) [FPU16/06537]. This work was also partially funded by two research-funding initiatives: "Calasparra se mueve", inspired by women from Calasparra (Murcia), Spain, and "Pulseras solidarias", Cieza (Murcia), Spain. The sponsors have in no way been involved in the study design, data collection, and analysis, decision to publish, or preparation of the manuscript. BIOBANC-MUR is supported by the Instituto de Salud Carlos III (project PT20/00109), by the Instituto Murciano de Investigación Biosanitaria, IMIB and by the Consejeria de Salud de la Comunidad Autónoma de la Región de Murcia [the regional healthcare authority for the Autonomous Community of Murcia].

Acknowledgments

The authors thank Dr Carlos Bravo-Pérez (Department of Haematology and Medical Oncology) for his contributions and critical review of the statistical analyses and writing style. We are particularly grateful for the generous contribution of the patients and the collaboration of the Biobank Network of the Region of Murcia, BIOBANC-MUR, registered with the National Registry of Biobanks with registration number B.0000859.

Conflict of interest

The authors declare that the research was conducted in the absence of any commercial or financial relationships that could be construed as a potential conflict of interest.

Publisher's note

Supplementary material

The Supplementary Material for this article can be found online at: https://www.frontiersin.org/articles/10.3389/fonc.2023.1182725/full#supplementary-material

References

1. Untch M, Konecny GE, Paepke S, von Minckwitz G. Current and future role of neoadjuvant therapy for breast cancer. *Breast* (2014) 23:526–37. doi: 10.1016/j.breast.2014.06.004

2. van Nes JGH, Putter H, Julien J-P, Tubiana-Hulin M, van de Vijver M, Bogaerts J, et al. Preoperative chemotherapy is safe in early breast cancer, even after 10 years of follow-up; clinical and translational results from the EORTC trial 10902. *Breast Cancer Res Treat* (2009) 115:101–13. doi: 10.1007/s10549-008-0050-1

3. Haque W, Verma V, Hatch S, Suzanne Klimberg V, Brian Butler E, Teh BS. Response rates and pathologic complete response by breast cancer molecular subtype following neoadjuvant chemotherapy. *Breast Cancer Res Treat* (2018) 170:559–67. doi: 10.1007/s10549-018-4801-3

4. Cortazar P, Zhang L, Untch M, Mehta K, Costantino JP, Wolmark N, et al. Pathological complete response and long-term clinical benefit in breast cancer: the CTNeoBC pooled analysis. *Lancet* (2014) 384:164–72. doi: 10.1016/S0140-6736(13)62422-8

5. Mamounas EP, Anderson SJ, Dignam JJ, Bear HD, Julian TB, Geyer CEJ, et al. Predictors of locoregional recurrence after neoadjuvant chemotherapy: results from combined analysis of national surgical adjuvant breast and bowel project b-18 and b-27. *J Clin Oncol* (2012) 30:3960–6. doi: 10.1200/JCO.2011.40.8369

6. LeVasseur N, Sun J, Gondara L, Diocee R, Speers C, Lohrisch C, et al. Impact of pathologic complete response on survival after neoadjuvant chemotherapy in early-stage breast cancer: a population-based analysis. *J Cancer Res Clin Oncol* (2020) 146:529–36. doi: 10.1007/s00432-019-03083-y

7. Denkert C, von Minckwitz G, Darb-Esfahani S, Lederer B, Heppner BI, Weber KE, et al. Tumour-infiltrating lymphocytes and prognosis in different subtypes of breast cancer: a pooled analysis of 3771 patients treated with neoadjuvant therapy. *Lancet Oncol* (2018) 19:40–50. doi: 10.1016/S1470-2045(17)30904-X

8. Dieci MV, Radosevic-Robin N, Fineberg S, van den Eynden G, Ternes N, Penault-Llorca F, et al. Update on tumor-infiltrating lymphocytes (TILs) in breast cancer, including recommendations to assess TILs in residual disease after neoadjuvant therapy and in carcinoma in situ: a report of the international immuno-oncology biomarker working group on breast cancer. *Semin Cancer Biol* (2018) 52:16–25. doi: 10.1016/j.semcancer.2017.10.003

9. García-Martínez E, Gil GL, Benito AC, González-Billalabeitia E, Conesa MAV, García García T, et al. Tumor-infiltrating immune cell profiles and their change after neoadjuvant chemotherapy predict response and prognosis of breast cancer. *Breast Cancer Res* (2014) 16:488. doi: 10.1186/s13058-014-0488-5

10. Hiam-Galvez KJ, Allen BM, Spitzer MH. Systemic immunity in cancer. *Nat Rev Cancer* (2021) 21:345–59. doi: 10.1038/s41568-021-00347-z

11. Templeton AJ, McNamara MG, Šeruga B, Vera-Badillo FE, Aneja P, Ocaña A, et al. Prognostic role of neutrophil-to-lymphocyte ratio in solid tumors: a systematic review and meta-analysis. *J Natl Cancer Inst* (2014) 106:dju124. doi: 10.1093/jnci/dju124

12. Cupp MA, Cariolou M, Tzoulaki I, Aune D, Evangelou E, Berlanga-Taylor AJ. Neutrophil to lymphocyte ratio and cancer prognosis: an umbrella review of systematic reviews and meta-analyses of observational studies. *BMC Med* (2020) 18:360. doi: 10.1186/s12916-020-01817-1

13. McAndrew NP, Bottalico L, Mesaros C, Blair IA, Tsao PY, Rosado JM, et al. Effects of systemic inflammation on relapse in early breast cancer. *NPJ Breast Cancer* (2021) 7:7. doi: 10.1038/s41523-020-00212-6

14. Ethier J-L, Desautels D, Templeton A, Shah PS, Amir E. Prognostic role of neutrophil-to-lymphocyte ratio in breast cancer: a systematic review and meta-analysis. *Breast Cancer Res* (2017) 19:2. doi: 10.1186/s13058-016-0794-1

15. Ivars Rubio A, Yufera JC, de la Morena P, Fernández Sánchez A, Navarro Manzano E, García Garre E, et al. Neutrophil-lymphocyte ratio in metastatic breast cancer is not an independent predictor of survival, but depends on other variables. *Sci Rep* (2019) 9:16979. doi: 10.1038/s41598-019-53606-3

16. Cullinane C, Creavin B, O'Leary DP, O'Sullivan MJ, Kelly L, Redmond HP, et al. Can the neutrophil to lymphocyte ratio predict complete pathologic response to neoadjuvant breast cancer treatment? a systematic review and meta-analysis. *Clin Breast Cancer* (2020) 20:e675–81. doi: 10.1016/j.clbc.2020.05.008

17. Yerushalmi R, Woods R, Ravdin PM, Hayes MM, Gelmon KA. Ki67 in breast cancer: prognostic and predictive potential. *Lancet Oncol* (2010) 11:174–83. doi: 10.1016/S1470-2045(09)70262-1

18. Paik S, Shak S, Tang G, Kim C, Baker J, Cronin M, et al. A multigene assay to predict recurrence of tamoxifen-treated, node-negative breast cancer. *N Engl J Med* (2004) 351:2817–26. doi: 10.1056/NEJMoa041588

19. Beňačka R, Szabóová D, Guľašová Z, Hertelyová Z, Radoňák J. Classic and new markers in diagnostics and classification of breast cancer. *Cancers (Basel)* (2022) 14(21):5444–5466. doi: 10.3390/cancers14215444

20. Kalinsky K, Barlow WE, Gralow JR, Meric-Bernstam F, Albain KS, Hayes DF, et al. 21-gene assay to inform chemotherapy benefit in node-positive breast cancer. *N Engl J Med* (2021) 385:2336–47. doi: 10.1056/NEJMoa2108873

21. Du R, Huang C, Liu K, Li X, Dong Z. Targeting AURKA in cancer: molecular mechanisms and opportunities for cancer therapy. *Mol Cancer* (2021) 20:15. doi: 10.1186/s12943-020-01305-3

22. Whately KM, Voronkova MA, Maskey A, Gandhi J, Loskutov J, Choi H, et al. Nuclear aurora-a kinase-induced hypoxia signaling drives early dissemination and

metastasis in breast cancer: implications for detection of metastatic tumors. *Oncogene* (2021) 40:5651–64. doi: 10.1038/s41388-021-01969-1

23. Xu J, Wu X, Zhou W, Liu A, Wu J, Deng J, et al. Aurora-a identifies early recurrence and poor prognosis and promises a potential therapeutic target in triple negative breast cancer. *PLoS One* (2013) 8:e56919. doi: 10.1371/journal.pone.0056919

24. Siggelkow W, Boehm D, Gebhard S, Battista M, Sicking I, Lebrecht A, et al. Expression of aurora kinase a is associated with metastasis-free survival in node-negative breast cancer patients. *BMC Cancer* (2012) 12:562. doi: 10.1186/1471-2407-12-562

25. Jalalirad M, Haddad TC, Salisbury JL, Radisky D, Zhang M, Schroeder M, et al. Aurora-a kinase oncogenic signaling mediates TGF-β-induced triple-negative breast cancer plasticity and chemoresistance. *Oncogene* (2021) 40:2509–23. doi: 10.1038/s41388-021-01711-x

26. Zhang Y, Wang Y, Xue J. Paclitaxel inhibits breast cancer metastasis via suppression of aurora kinase-mediated cofilin-1 activity. *Exp Ther Med* (2018) 15:1269–76. doi: 10.3892/etm.2017.5588

27. Zhou T, Zhang A, Kuang G, Gong X, Jiang R, Lin D, et al. Baicalin inhibits the metastasis of highly aggressive breast cancer cells by reversing epithelial-to-mesenchymal transition by targeting β-catenin signaling. *Oncol Rep* (2017) 38:3599–607. doi: 10.3892/or.2017.6011

28. Hole S, Pedersen AM, Lykkesfeldt AE, Yde CW. Aurora kinase a and b as new treatment targets in aromatase inhibitor-resistant breast cancer cells. *Breast Cancer Res Treat* (2015) 149:715–26. doi: 10.1007/s10549-015-3284-8

29. Lykkesfeldt AE, Iversen BR, Jensen M-B, Ejlertsen B, Giobbie-Hurder A, Reiter BE, et al. Aurora kinase a as a possible marker for endocrine resistance in early estrogen receptor positive breast cancer. *Acta Oncol* (2018) 57:67–73. doi: 10.1080/0284186X.2017.1404126

30. Donnella HJ, Webber JT, Levin RS, Camarda R, Momcilovic O, Bayani N, et al. Kinome rewiring reveals AURKA limits PI3K-pathway inhibitor efficacy in breast cancer. *Nat Chem Biol* (2018) 14:768–77. doi: 10.1038/s41589-018-0081-9

31. Wander SA, Cohen O, Gong X, Johnson GN, Buendia-Buendia JE, Lloyd MR, et al. The genomic landscape of intrinsic and acquired resistance to cyclin-dependent kinase 4/6 inhibitors in patients with hormone receptor-positive metastatic breast cancer. *Cancer Discovery* (2020) 10:1174–93. doi: 10.1158/2159-8290.CD-19-1390

32. Morris BB, Smith JP, Zhang Q, Jiang Z, Hampton OA, Churchman ML, et al. Replicative instability drives cancer progression. *Biomolecules* (2022) 12(11):1570–1592. doi: 10.3390/biom12111570

33. Shi H, Bevier M, Johansson R, Enquist-Olsson K, Henriksson R, Hemminki K, et al. Prognostic impact of polymorphisms in the MYBL2 interacting genes in breast cancer. *Breast Cancer Res Treat* (2012) 131:1039–47. doi: 10.1007/s10549-011-1826-2

34. Bayley R, Ward C, Garcia P. MYBL2 amplification in breast cancer: molecular mechanisms and therapeutic potential. *Biochim Biophys Acta Rev Cancer* (2020) 1874:188407. doi: 10.1016/j.bbcan.2020.188407

35. Tao D, Pan Y, Jiang G, Lu H, Zheng S, Lin H, et al. B-myb regulates snail expression to promote epithelial-to-mesenchymal transition and invasion of breast cancer cell. *Med Oncol* (2015) 32:412. doi: 10.1007/s12032-014-0412-y

36. Chen X, Lu Y, Yu H, Du K, Zhang Y, Nan Y, et al. Pan-cancer analysis indicates that MYBL2 is associated with the prognosis and immunotherapy of multiple cancers as an oncogene. *Cell Cycle* (2021) 20:2291–308. doi: 10.1080/15384101.2021.1982494

37. Li X, Zhang X, Wu C-C, Li P-P, Fu Y-M, Xie L-H, et al. The role of MYB proto-oncogene like 2 in tamoxifen resistance in breast cancer. *J Mol Histol* (2021) 52:21–30. doi: 10.1007/s10735-020-09920-6

38. Guarneri V, Dieci MV, Bisagni G, Brandes AA, Frassoldati A, Cavanna L, et al. PIK3CA mutation in the ShortHER randomized adjuvant trial for patients with early HER2(+) breast cancer: association with prognosis and integration with PAM50 subtype. *Clin Cancer Res* (2020) 26:5843–51. doi: 10.1158/1078-0432.CCR-20-1731

39. Gonzalez-Ericsson PI, Stovgaard ES, Sua LF, Reisenbichler E, Kos Z, Carter JM, et al. The path to a better biomarker: application of a risk management framework for the implementation of PD-L1 and TILs as immuno-oncology biomarkers in breast cancer clinical trials and daily practice. *J Pathol* (2020) 250:667–84. doi: 10.1002/path.5406

40. Filho OM, Stover DG, Asad S, Ansell PJ, Watson M, Loibl S, et al. Association of immunophenotype with pathologic complete response to neoadjuvant chemotherapy for triple-negative breast cancer: a secondary analysis of the BrighTNess phase 3 randomized clinical trial. *JAMA Oncol* (2021) 7:603–8. doi: 10.1001/jamaoncol.2020.7310

41. Carlson RW, Anderson BO, Burstein HJ, Carter WB, Edge SB, Farrar WB, et al. Invasive breast cancer. *J Natl Compr Canc Netw* (2007) 5:246–312. doi: 10.6004/jnccn.2007.0025

42. Dieci MV, Miglietta F, Guarneri V. Immune infiltrates in breast cancer: recent updates and clinical implications. *Cells* (2021) 10(2):223–250. doi: 10.3390/cells10020223

43. Hammerl D, Smid M, Timmermans AM, Sleijfer S, Martens JWM, Debets R. Breast cancer genomics and immuno-oncological markers to guide immune therapies. *Semin Cancer Biol* (2018) 52:178–88. doi: 10.1016/j.semcancer.2017.11.003

44. Zhou Q, Dong J, Sun Q, Lu N, Pan Y, Han X. Role of neutrophil-to-lymphocyte ratio as a prognostic biomarker in patients with breast cancer receiving neoadjuvant chemotherapy: a meta-analysis. *BMJ Open* (2021) 11:e047957. doi: 10.1136/bmjopen-2020-047957

45. Dan J, Tan J, Huang J, Zhang X, Guo Y, Huang Y, et al. The dynamic change of neutrophil to lymphocyte ratio is predictive of pathological complete response after neoadjuvant chemotherapy in breast cancer patients. *Breast Cancer* (2020) 27:982–8. doi: 10.1007/s12282-020-01096-x

46. Choi H, Noh H, Cho I-J, Lim S-T, Han A. Changes in neutrophil to lymphocyte ratio (NLR) during neoadjuvant treatment correlated with patients' survival. *Breast Cancer* (2020) 27:871–9. doi: 10.1007/s12282-020-01083-2

47. Vicente Conesa MA, Garcia-Martinez E, Gonzalez Billalabeitia E, Chaves Benito A, Garcia Garcia T, Vicente Garcia V, et al. Predictive value of peripheral blood lymphocyte count in breast cancer patients treated with primary chemotherapy. *Breast* (2012) 21:468–74. doi: 10.1016/j.breast.2011.11.002

48. Denkert C, Loibl S, Noske A, Roller M, Müller BM, Komor M, et al. Tumor-associated lymphocytes as an independent predictor of response to neoadjuvant chemotherapy in breast cancer. *J Clin Oncol* (2010) 28:105–13. doi: 10.1200/JCO.2009.23.7370

49. Salgado R, Denkert C, Demaria S, Sirtaine N, Klauschen F, Pruneri G, et al. The evaluation of tumor-infiltrating lymphocytes (TILs) in breast cancer: recommendations by an international TILs working group 2014. *Ann Oncol* (2015) 26:259–71. doi: 10.1093/annonc/mdu450

50. Chen DS, Mellman I. Oncology meets immunology: the cancer-immunity cycle. *Immunity* (2013) 39:1–10. doi: 10.1016/j.immuni.2013.07.012

51. Gao Z-H, Li C-X, Liu M, Jiang J-Y. Predictive and prognostic role of tumour-infiltrating lymphocytes in breast cancer patients with different molecular subtypes: a meta-analysis. *BMC Cancer* (2020) 20:1150. doi: 10.1186/s12885-020-07654-y

52. Goldberg J, Pastorello RG, Vallius T, Davis J, Cui YX, Agudo J, et al. The immunology of hormone receptor positive breast cancer. *Front Immunol* (2021) 12:674192. doi: 10.3389/fimmu.2021.674192

53. Mao P, Cohen O, Kowalski KJ, Kusiel JG, Buendia-Buendia JE, Cuoco MS, et al. Acquired FGFR and FGF alterations confer resistance to estrogen receptor (ER) targeted therapy in ER(+) metastatic breast cancer. *Clin Cancer Res* (2020) 26:5974–89. doi: 10.1158/1078-0432.CCR-19-3958

54. Sun Y, Zhang C. The types of tumor infiltrating lymphocytes are valuable for the diagnosis and prognosis of breast cancer. *Front Genet* (2022) 13:1019062. doi: 10.3389/fgene.2022.1019062

55. Pang J, Zhou H, Dong X, Wang S, Xiao Z. Relationship between the neutrophil to lymphocyte ratio, stromal tumor-infiltrating lymphocytes, and the prognosis and response to neoadjuvant chemotherapy in triple-negative breast cancer. *Clin Breast Cancer* (2021) 21:e681–7. doi: 10.1016/j.clbc.2021.04.004

56. Dong X, Liu C, Yuan J, Wang S, Ding N, Li Y, et al. Prognostic roles of neutrophil-to-Lymphocyte ratio and stromal tumor-infiltrating lymphocytes and their relationship in locally advanced triple-negative breast cancer treated with neoadjuvant chemotherapy. *Breast Care (Basel)* (2021) 16:328–34. doi: 10.1159/000509498

57. Lee J, Kim D-M, Lee A. Prognostic role and clinical association of tumor-infiltrating lymphocyte, programmed death ligand-1 expression with neutrophil-lymphocyte ratio in locally advanced triple-negative breast cancer. *Cancer Res Treat* (2019) 51:649–63. doi: 10.4143/crt.2018.270

58. Bun A, Fujimoto Y, Higuchi T, Sata A, Fukui R, Ozawa H, et al. Prognostic significance of neutrophil-to-lymphocyte ratio in luminal breast cancers with low levels of tumour-infiltrating lymphocytes. *Anticancer Res* (2020) 40:2871–80. doi: 10.21873/anticanres.14263

59. Denkert C, Loibl S, Müller BM, Eidtmann H, Schmitt WD, Eiermann W, et al. Ki67 levels as predictive and prognostic parameters in pretherapeutic breast cancer core biopsies: a translational investigation in the neoadjuvant GeparTrio trial. *Ann Oncol* (2013) 24:2786–93. doi: 10.1093/annonc/mdt350

60. Torrisi R, Marrazzo E, Agostinetto E, De Sanctis R, Losurdo A, Masci G, et al. Neoadjuvant chemotherapy in hormone receptor-positive/HER2-negative early breast cancer: when, why and what? *Crit Rev Oncol Hematol* (2021) 160:103280. doi: 10.1016/j.critrevonc.2021.103280

61. Sinn BV, Loibl S, Hanusch CA, Zahm D-M, Sinn H-P, Untch M, et al. Immune-related gene expression predicts response to neoadjuvant chemotherapy but not additional benefit from PD-L1 inhibition in women with early triple-negative breast cancer. *Clin Cancer Res* (2021) 27:2584–91. doi: 10.1158/1078-0432.CCR-20-3113

62. Wang K, Li H-L, Xiong Y-F, Shi Y, Li Z-Y, Li J, et al. Development and validation of nomograms integrating immune-related genomic signatures with clinicopathologic features to improve prognosis and predictive value of triple-negative breast cancer: a gene expression-based retrospective study. *Cancer Med* (2019) 8:686–700. doi: 10.1002/cam4.1880

63. Wirapati P, Sotiriou C, Kunkel S, Farmer P, Pradervand S, Haibe-Kains B, et al. Meta-analysis of gene expression profiles in breast cancer: toward a unified understanding of breast cancer subtyping and prognosis signatures. *Breast Cancer Res* (2008) 10:R65. doi: 10.1186/bcr2124

64. Fadaka AO, Sibuyi NRS, Madiehe AM, Meyer M. MicroRNA-based regulation of aurora a kinase in breast cancer. *Oncotarget* (2020) 11:4306–24. doi: 10.18632/oncotarget.27811

65. Chen L, Chen Y, Xie Z, Luo J, Wang Y, Zhou J, et al. Comparison of immunohistochemistry and RT-qPCR for assessing ER, PR, HER2, and Ki67 and

evaluating subtypes in patients with breast cancer. *Breast Cancer Res Treat* (2022) 194:517–29. doi: 10.1007/s10549-022-06649-6

66. Qin H, Li Y, Zhang H, Wang F, He H, Bai X, et al. Prognostic implications and oncogenic roles of MYBL2 protein expression in esophageal squamous-cell carcinoma. *Onco Targets Ther* (2019) 12:1917–27. doi: 10.2147/OTT.S190145

67. Luengo-Gil G, García-Martínez E, Chaves-Benito A, Conesa-Zamora P, Navarro-Manzano E, González-Billalabeitia E, et al. Clinical and biological impact of miR-18a expression in breast cancer after neoadjuvant chemotherapy. *Cell Oncol (Dordr)* (2019) 42:627–44. doi: 10.1007/s13402-019-00450-2

68. Musa J, Aynaud M-M, Mirabeau O, Delattre O, Grünewald TG. MYBL2 (B-myb): a central regulator of cell proliferation, cell survival and differentiation involved in tumorigenesis. *Cell Death Dis* (2017) 8:e2895. doi: 10.1038/cddis.2017.244

69. Sammut S-J, Crispin-Ortuzar M, Chin S-F, Provenzano E, Bardwell HA, Ma W, et al. Multi-omic machine learning predictor of breast cancer therapy response. *Nature* (2022) 601:623–9. doi: 10.1038/s41586-021-04278-5

70. Prat A, Parker JS, Fan C, Perou CM. PAM50 assay and the three-gene model for identifying the major and clinically relevant molecular subtypes of breast cancer. *Breast Cancer Res Treat* (2012) 135:301–6. doi: 10.1007/s10549-012-2143-0

71. Nielsen TO, Leung SCY, Rimm DL, Dodson A, Acs B, Badve S, et al. Assessment of Ki67 in breast cancer: updated recommendations from the international Ki67 in breast cancer working group. *J Natl Cancer Inst* (2021) 113:808–19. doi: 10.1093/jnci/djaa201

72. Buus R, Sestak I, Kronenwett R, Ferree S, Schnabel CA, Baehner FL, et al. Molecular drivers of oncotype DX, prosigna, EndoPredict, and the breast cancer index: a TransATAC study. *J Clin Oncol* (2021) 39:126–35. doi: 10.1200/JCO.20.00853

73. Stover DG, Coloff JL, Barry WT, Brugge JS, Winer EP, Selfors LM. The role of proliferation in determining response to neoadjuvant chemotherapy in breast cancer: a gene expression-based meta-analysis. *Clin Cancer Res* (2016) 22:6039–50. doi: 10.1158/1078-0432.CCR-16-0471

74. Zhang Y, Asad S, Weber Z, Tallman D, Nock W, Wyse M, et al. Genomic features of rapid versus late relapse in triple negative breast cancer. *BMC Cancer* (2021) 21:568. doi: 10.1186/s12885-021-08320-7

frontiers | Frontiers in Immunology

TYPE Original Research
PUBLISHED 29 June 2023
DOI 10.3389/fimmu.2023.1219652

OPEN ACCESS

EDITED BY
Alberto Traverso,
Maastro Clinic, Netherlands

REVIEWED BY
Leonard Maggi,
Washington University in St. Louis, United States
Cihui Yan,
Tianjin Medical University Cancer Institute and Hospital, China

*CORRESPONDENCE
Jumei Zhao
jmz2003.stu@163.com

†These authors have contributed equally to this work

RECEIVED 09 May 2023
ACCEPTED 14 June 2023
PUBLISHED 29 June 2023

CITATION
Ma Y, Du J, Chen M, Gao N, Wang S, Mi Z, Wei X and Zhao J (2023) Mitochondrial DNA methylation is a predictor of immunotherapy response and prognosis in breast cancer: scRNA-seq and bulk-seq data insights. *Front. Immunol.* 14:1219652. doi: 10.3389/fimmu.2023.1219652

Mitochondrial DNA methylation is a predictor of immunotherapy response and prognosis in breast cancer: scRNA-seq and bulk-seq data insights

Yixuan Ma†, Juan Du†, Meini Chen†, Ning Gao, Sijia Wang, Zhikuan Mi, Xiaoli Wei and Jumei Zhao*

Shaanbei Key Laboratory for Cancer Prevention of Yan'an, Medical College, Yan'an University, Yan'an, China

Background: Alterations in Mitochondrial DNA methylation (MTDM) exist in many tumors, but their role in breast cancer (BC) development remains unclear.

Methods: We analyzed BC patient data by combining scRNA-seq and bulk sequencing. Weighted co-expression network analysis (WGCNA) of TCGA data identified mitochondrial DNA methylation (MTDM)-associated genes in BC. COX regression and LASSO regression were used to build prognostic models. The biological function of MTDM was assessed using various methods, such as signaling pathway enrichment analysis, copynumber karyotyping analysis, and quantitative analysis of the cell proliferation rate. We also evaluated MTDM-mediated alterations in the immune microenvironment using immune microenvironment, microsatellite instability, mutation, unsupervised clustering, malignant cell subtype differentiation, immune cell subtype differentiation, and cell-communication signature analyses. Finally, we performed cellular experiments to validate the role of the MTDM-associated prognostic gene *NCAPD3* in BC.

Results: In this study, MTDM-associated prognostic models divided BC patients into high/low MTDM groups in TCGA/GEO datasets. The difference in survival time between the two groups was statistically significant (P<0.001). We found that high MTDM status was positively correlated with tumor cell proliferation. We analyzed the immune microenvironment and found that low-MTDM group had higher immune checkpoint gene expression/immune cell infiltration, which could lead to potential benefits from immunotherapy. In contrast, the high MTDM group had higher proliferation rates and levels of CD8+T cell exhaustion, which may be related to the secretion of GDF15 by malignant breast epithelial cells with a high MTDM status. Cellular experiments validated the role of the MTDM-associated prognostic gene NCAPD3 (the gene most positively correlated with epithelial malignant cell proliferation in the model) in BC. Knockdown of NCAPD3 significantly reduced the activity and proliferation of MDA-MB-231 and BCAP-37 cells, and significantly reduced their migration ability of BCAP-37 cell line.

Conclusion: This study presented a holistic evaluation of the multifaceted roles of MTDM in BC. The analysis of MTDM levels not only enables the prediction of response to immunotherapy but also serves as an accurate prognostic indicator for patients with BC. These insightful discoveries provide novel perspectives on tumor immunity and have the potentially to revolutionize the diagnosis and treatment of BC.

KEYWORDS

breast cancer, mitochondrial DNA methylation (MTDM), NCAPD3, immunotherapy, prognostic model

1 Introduction

Breast cancer (BC) is one of the most prevalent cancers that threatening women's lives and health. According to Global Cancer Statistics 2020 (1), BC has surpassed lung cancer as the most common type of tumors in women. According to statistical data, nearly 2.3 million new BC cases were reported in 2020, accounting for 11.7% of all cancer cases. Similarly, a study in 2022 showed that the mortality rate of BC in China will also increase dramatically, making it the most common cancer among Chinese women (2). BC is further classified into luminal (estrogen receptor [ER] positive), human epidermal growth factor receptor 2 (HER2) positive and ER-negative, and basal subtypes (3), and targeted therapies based on molecular typing have been applied clinically, changing the previous "one-size-fits-all" treatment approach (4). Over the past ten years, innovative healing methods, such as immunotherapy, have progressed remarkably. By utilizing the patient's immune system to detect and regulate tumors, immune checkpoint inhibitors (ICIs) such as PD-1, PD-L1, and CTLA-4 have effectively enhanced the prognosis of different types of cancers (5). However, recent clinical trials have shown that combined therapies are often more effective than single immunotherapy for BC (6), suggesting that more effective immunotherapy markers are needed to enable BC patients to benefit from immunotherapy. Currently, PDL1 may not be an ideal marker to identify patients sensitive to immunotherapy, as PD-L1 expression is dynamic and varies not only between individuals but also over time (7). Targeting mitochondria is a new option for tumor immunotherapy. Recent evidence suggests that using anti-cancer drugs to target the mitochondrial pathway can greatly enhance the ability of cancer cells to be recognized by immune cells, present tumor antigens, and enhance the anti-tumor function of immune cells, leading to the effective killing of cancer cells (8, 9). Thus, exploring the correlation between various biological pathways within mitochondria and the development of tumors, as well as the immune microenvironment, would be worthwhile. This will provide valuable insight into the mechanisms underlying tumorigenesis and facilitate the development of more effective therapies.

Mitochondria are essential organelles that control not only cellular energy metabolism but also the main site of energy metabolism; they are essential organelles for regulating reactions such as calcium homeostasis, apoptosis, and redox reactions, thus maintaining the homeostasis of the internal environment and playing a crucial role in cancer development. Mitochondrial DNA (mtDNA) is a double-stranded loop, divided into heavy (H) and light (L) strands, without histone involvement, and its circular DNA contains three promoter regions, located in the D-loop, transcribed as multiple cis-trans (10), which encode 13 oxidative phosphorylation (OXPHOS) subunits of proteins, as well as two ribosomal RNA genes and 22 tRNAs (11). These 13 proteins encoded by the mitochondria are components of the electron transport chain and are involved in regulating the oxidative respiratory chain and maintaining its functional integrity; alterations in their expression have been associated with cancer development (12–14). In addition, mitochondria play a key role in immune system functioning by regulating the development, activation, proliferation, differentiation, and death of immune cells. For example, mitochondria control immune cell differentiation by regulating metabolism and mtROS production (15, 16).

Recently, mitochondrial epigenetics has gained much attention, and the biological function of Mitochondrial DNA methylation (MTDM) has gradually been explored. Altered levels of mtDNA methylation and hydroxymethylation have been observed in various diseases, including BC, cardiovascular disease, diabetes, and neurodegenerative diseases (17). MTDM lacks CPG islands and methylates non-CPG sites such as CPA, CPC, and CPT (18), which may be associated with the development of various diseases. Initially, the role of MTDM was controversial, but as research progressed, the mitochondrial isoform of *DNMT1* (mtDNMT1) was identified in mitochondria which is homologous to nuclear *DNMT1*, confirming that *mtDNMT1* binds to the D-loop control region of mitochondria and forms a 5-mC that regulates mitochondrial gene expression (19, 20). Subsequently, *DNMT3A* and *DNMT3B* were found to be involved in MTDM (21, 22) which is associated with the active methyl donor SAM. Therefore the expression or absence of *SLC25A26*, the only channel for SAM entry into the mitochondria, also controls the level of MTDM (23). Despite significant attention in recent years, the precise role of MTDM in BC and its impact on the immune microenvironment remain unclear. To address this knowledge gap, our study employed both single-cell and bulk sequencing to investigate the biological function of MTDM in BC, as well as its potential as a prognostic indicator and

immunotherapeutic marker. By shedding light on the implications of MTDM, we hope to understand BC's development and progression better while offering new avenues for treatment and patient care.

2 Method

2.1 Transcriptome data download and processing

TCGA data of the training cohort was downloaded by using the "TCGAbiolinks" R package, with the TPM data type selected. Considering that more than 99% of BC patients were female, 13 male patients were excluded to maintain data integrity, and survival times ranged from 3 to 120 months for BC patients. Ultimately, 945 tumor samples were included in this study. The BC dataset GSE21653, downloaded from the GEO database (24) was used as the validation cohort. For subsequent analyses, all data were log2 transformed.

2.2 Single-cell sequencing data download and processing

The single-cell BC dataset GSE195861 (25) was downloaded from the GEO database, with samples of ductal carcinoma *in situ* (DCIS) and Invasive Ductal Carcinoma (IDC). The Seurat package was used for subsequent processing, and data quality control was performed by selecting cells with ribosomal genes ranging from 0 to 50, with a total number of genes greater than 200, and genes expressed in at least ten cells. The number of highly variable genes was set to 3000, and samples with a cell count greater than 500 were selected after filtering. They were then corrected and integrated by the IntegrateData function, followed by cells being clustered by setting the "DIMS" parameter to 20, reducing the data dimension using the UMAP method, and setting the resolution to 0.2 using the K-NearestNeighbor (KNN) method. Cell markers were then downloaded for annotation using the CellMarker 2.0, website (http://yikedaxue.slwshop.cn/), and each cell's percentage of MTDM genes was obtained by importing the MTDM-mediated genes through the PercentFeatureSet function.

2.3 Acquisition of mitochondrial DNA methylation -related genes

DNMT1, *DNMT3A*, *DNMT3B*, *SLC25A26*, *METTL4*, *NRF1*, *PPARGC1A* and *PRKAA1* were identified as MTDM-related genes according to the literatures (20–23, 26, 27)

2.4 Weighted co-expression network analysis and single sample gene set enrichment analysis

Co-expression network of all genes in MTDM and BC samples was constructed using the TCGA breast cancer patients' data cohort and the "WGCNA" R package. Genes in the top 90% were selected by variance screening and outlier sample filtering. The pickSoft Threshold function was used to calculate the optimal threshold of 10 and to set the minimum number of module genes to 80, which was then used to construct the WGCNA network. The R package GSVA (28) obtained scores associated with MTDM for each BC patient using the ssGSEA analysis module. Finally, the correlation between the modules and the MTDM scores in the WGCNA network was calculated.

2.5 Copynumber karyotyping analysis within tumors and mitochondrial DNA methylation differential biological pathway analysis

Subclonal structure analysis was performed using the Copykat package (29) to distinguish between normal and malignant cells, and the irGSEA package was used to score the high and low MTDM groups using AUCell, UCell, single-score, and ssGSEA enrichment methods. A heat map of the differentially enriched pathways between the two groups was generated.

2.6 Construction of mitochondrial DNA methylation -related prognostic model and external validation of the model

Univariate COX analysis was used to identify MTDM-related genes with prognostic value, which were further screened using least absolute shrinkage and selection operator (LASSO) regression to construct prognostic models. This approach allowed the calculation of MTDM scores for each BC sample by multiplying the coefficients by the expression and accumulating the results. Patients in the TCGA BC cohort were divided into high and low-risk groups based on the median value. Subsequently, the prognostic differences between the two groups were explored, and the accuracy of the model was assessed. The GSE21653 cohort in GEO was selected as the external validation cohort, MTDM scores for each sample were calculated according to the model formula and patients were divided into high-risk and low-risk groups based on the median. Survival analysis was then performed to determine whether the prognosis differed between the high- and low-risk groups in the validation cohort, with ROC curves used to assess the accuracy of the model. Principal component analysis (PCA) was used to explore whether the model could better group high and low MTDM, and a Nomogram was constructed through the rms package to assess the risk of death in patients with BC by combining clinical data with MTDM values. Finally, the accuracy of the nomogram for estimating patient outcomes was assessed using prognostic ROC curves.

2.7 Immune infiltration and the use of relevant scores

Immune infiltration analysis using the R package IOBR (30) was performed on BC samples using the CIBERSORT, EPIC, MCP-

counter, Quanti-seq, TIMER, xCell, and ESTIMATE methods, with the differences in immune cell infiltration between different MTDM subgroups explored in the form of heat maps that showed the immune cells at different infiltration levels. Additionally, differences in tumor mutation burden (TMB) and microsatellite instability (MSI) between the different MTDM subgroups were explored to investigate the sensitivity of patients in different subgroups to immunotherapy. TMB was analyzed using the maftools package (31), whereas MSI was analyzed using the PreMSIm package analysis (32), with the data normalized from 0 to 1.

2.8 Calculate the proliferation score

Proliferation scores were calculated using proliferation-related genes (*BIRC5*, *CCNB1*, *CDC2*, *NUF2*, *CEP55*, *NDC80*, *MKI67*, *PTTG1*, *RRM2*, *TYMS*, and *UBE2C*) (33) and grouped using scRNA-seq and bulk-seq.

2.9 Analysis of intercellular interactions

Cell-cell interaction analysis was performed using the R package CellChat (34), which models the probability of intercellular communication by combining gene expression with *a priori* knowledge of the interactions between signaling ligands, receptors, and their cofactors utilizing secretory signaling and cell-cell contact human databases. Circle and bubble plots were used to show the strength of cell-cell communication networks from target cell clusters to other cell clusters.

2.10 Cell culture and transfection

MDA-MB-231 and BCAP-37, were provided by the Medical Experiment Center of Yan'an University and cultured in RPMI-1640 (Biological Industries, Kibbutz Beit-Haemek, Israel) or DMEM (Biological Industries, Kibbutz Beit-Haemek, Israel) medium supplied with 10% fetal bovine serum (FBS) (Biological Industries, BI) at 37 °C, 5% CO_2. For small interference RNAs (siRNAs) transfection, jetPRIME reagent (polyplus-transfection, SA) was used according to the manufacturer's protocol. siRNAs of NCAPD3 were produced by GenePharma (Shanghai, China). The sequences of NCAP3 siRNAs is si-NCAPD3-1, forward 5′- GCAUUCAGACUCUAAAGAATT -3′, and reverse 5′- UUCUUUAGUCUGAAUGCTT -3′; si-NCAPD3-2, forward 5′-GAGAAGGAGAUAAGGUCAUTT-3′, and reverse 5′-AUGACCUUUAUCUCCUUCUCTT-3′.

2.11 Quantitative real-time PCR

Total RNA was extracted using TRIzol reagent (invitrogen, Carlsbad, CA, USA), followed by a reverse transcription using a reverse transcription kit (TaKaRa, RR036A) according to the manufacturer's instructions. Quantitative real-time PCR was performed using a qRT-PCR reagent (TaKaRa, RR820A) according to the manufacturer's instructions. *β-ACTIN*, was used as the interference gene. Relative expression changes of genes were calculated using the $2^{-\Delta\Delta Ct}$ method. Primer sequences used are *NCAPD3*, forward 5'- TGGAGCAAGAGTCGAATGGCG -3′ and reverse 5′- GGGGCGGTTTATCAGGCAGTG -3'; *β-ACTIN*, forward 5′- CATGTACGTTGCTATCCAGGC -3′, and reverse 5′-CTCCTTAATGTCACGCACGAT -3'.

2.12 Western blot analysis

Whole cell proteins were first extracted on ice using the RIPA lysis buffer with protein inhibitors. And then, the proteins extracted were quantified using a BCA protein assay kit (Beyotime, P0010S), 8% SDS-PAGE gels separated, and transferred to a PVDF membrane. For western bloting analysis, the PVDF membranes were then 5% skim milk blocked, primary antibody blotted, TBST washed, secondary antibody incubated, TBST washed and chemiluminescence detected. Primary antibodies of NCAPD3 antibody (Proteintect, Wuhan, China, 16828-1-AP) and *β*-Tubulin antibody (Proteintect, Wuhan, China, 10094-1-AP), and HRP tagged rabbit secondary antibody (Proteintect, Wuhan, China, SA00001-2) were all purchased from Proteintect (Wuhan, China)

2.13 CCK8

Cells in the logarithmic growth phase were seeded into 96-well plates. After transfection of siRNAs, the cells were then CCK-8 reagent (Topscience, Shanghai, China) incubated and 450 nm absorbance tested at the time of 24, 48, and 72 hours after trusfection according to the manufacturer's instructions.

2.14 Clone formation

Cells pre-transfected were counted and seeded into 12-well plates. After two weeks of culture, the cells were fixed with 4% paraformaldehyde, crystal violet stained, and photographed.

2.15 Scratch wound healing assay

Cells cultured in 6-well plates with a 60% confluency was NCAPD3 siRNAs or NC RNA transfected, scraped using a 100 µL sterile pipette tip, and gphotographed under a Nikon Ti-S fluorescence microscope at the time of 0, 12, 24, and 36 h after scrape (the same scratch area).

2.16 Statistical analysis

Statistical data analyses were performed using the SPSS 22.0 software. The ggplot2 package in the R programming language was used for the bioinformatic analyzing. The GraphPad Prism 9.0 software was employed to process the experimental data. The two-

tailed Student's t-test was performed to evaluate the difference between the two groups, $P < 0.05$ was considered to be statistically significant.

3 Results

3.1 Single-cell sequencing analysis depicts mitochondrial DNA methylation compartmentalization and breast cancer cell mapping

To investigate the modifications in mitochondrial DNA methylation (MTDM) in breast cancer (BC) cells, BC cell mapping was performed using single-cell data. After extracting and analyzing the GSE195861 dataset, 12 single-cell BC samples that were well integrated (Supplementary Figure 1A) and had no significant batch effect on subsequent analyses were selected. Using of "KNN" algorithm we divided the selected cells into 12 clusters (Figure 1A) and then annotated them according to the cell specific markers expression level (Supplementary Figure 1B). The annotation results showed that five cell types existed in the clusters: B cells, T cells, endothelial cells, epithelial cells, macrophages, and other cell types (Figures 1B, C), among which epithelial cells were mostly present, while endothelial cells were smallest (Figure 1C). To determine the MTDM levels in the screened cells, the annotated cells were divided into high and low MTDM groups based on the median MTDM-related gene expression (Figure 1D). As shown in Figures 1B, D, the high MTDM group was mainly concentrated in epithelial cells and macrophages. Thirteen mitochondria-encoded polypeptides are suppressed by mtDNA hypermethylation. We verified the accuracy of MTDM group division by detecting the MTDM-related genes expression. The results showed that all mitochondria-encoded polypeptides were significantly upregulated in the low-MTDM group (Figure 1E), consistent with the previous report. Thus, MTDM group division was reasonable. To determine the correlation between MTDM and BC malignancy, we differentiated annotated cells into ductal carcinoma *in situ* (DCIS) and invasive ductal carcinoma (IDC) cells (Figure 1F, Supplementary Figure 1C). The results showed that the epithelial cells of the more aggressive IDC group had a higher overlap with those of the high MTDM group than those of the DCIS group. Therefore, it is possible that high MTDM status contributes to BC progression.

3.2 BC cells with high mitochondrial DNA methylation are prone to be malignant

As 3.1 indicated that high MTDM status contributes to the malignant progression of BC, to further explore the malignant propensity of BC cells with a high MTDM status, biological pathway enrichment analysis (Figure 2A) and copynumber karyotyping analysis (Figure 2B) were conducted. The results showed that MTDM group gene alterations occurred not only in the proliferation-related E2F signaling pathway, MYC signaling pathway, G2M checkpoint, metastasis-related WNT signaling, and epithelial mesenchymal transformation-related biological pathways, but also in apoptosis, angiogenesis, inflammatory response, and metabolism-related pathways. Additionally, copynumber karyotyping analysis (Figure 2B) indicated that malignant BC cells were mainly concentrated in epithelial cells, and their distribution areas highly overlapped with high MTDM areas. Considering that patients with a higher rate of tumor proliferation usually have a poorer prognosis (35), relationship between MTDM status and proliferation was further examined by distinguishing single-cells using proliferation-related markers (Figure 2C). The results showed that the highly proliferative regions overlapped with the high MTDM regions, indicating a malignant tendency in high MTDM status. To explore the key genes affecting MTDM, gene modules associated with MTDM were analyzed using WGCNA (Supplementary Figures 2A–C), and seven non-gray modules were obtained. Among these seven non-grey modules, the turquoise and yellow modules had correlations of 0.68 and -0.53 with MDTM-score, respectively, and the genes contained in these two modules were closely related to MDTM-score (Figure 2D). Genes with a P-value <0.001 were selected for further analysis.

3.3 Status of mitochondrial DNA methylation is valuable for BC prognosis

Given the effect of changes in MTDM levels on a diverse range of biological processes, we investigated whether the genes associated with altered MTDM levels could serve as prognostic indicators in patients with BC. Thus, a total of 564 genes from the differential expression analysis of the high and low MTDM groups and WGCNA analysis of MTDM-associated genes were performed. Using univariate Cox analysis with a threshold of $P < 0.05$, 16 genes associated with patient prognosis were identified in the TCGA cohort. LASSO regression analysis stabilized gene contraction, and 11 genes were identified (Figures 3A, B and Supplementary Table 1). The LASSO regression results for these 11 genes are presented in Supplementary Table 1. Finally, we obtained a set of 11 genes, that are *ARID1B*, *B3GNT2*, *MPHOSPH10*, *NCAPD3*, *RABGAP1*, *RBM41*, *RBMXL1*, *SLBP*, *TMEM167A*, *TMEM67*, and *TUBGCP5*. To classify patients into high- and low-risk groups (i.e., high and low-MTDM groups), a prognostic model was constructed using the 11 genes and the median. Our findings revealed that the high MTDM group in the TCGA training cohort had a poorer prognosis than the low MTDM group ($P < 0.0001$, Figure 3C). The same trend was observed in the GSE21653 validation cohort ($P = 0.016$, Figure 3D). ROC curve analysis was performed in both the training and validation cohorts further evaluate the accuracy of MTDM in predicting the prognosis of patients with BC. The area under the curve (AUC) values were 0.734, 0.731, and 0.706 at 1, 2, and 5 years, respectively (Figure 3E) in the TCGA cohort, and 0.732, 0.686, and 0.673 at 1, 2, and 5 years, respectively (Figure 3F), in the validation cohort. These results indicate that the MTDM status could be used accurately to predict BC patient prognosis in both cohorts.

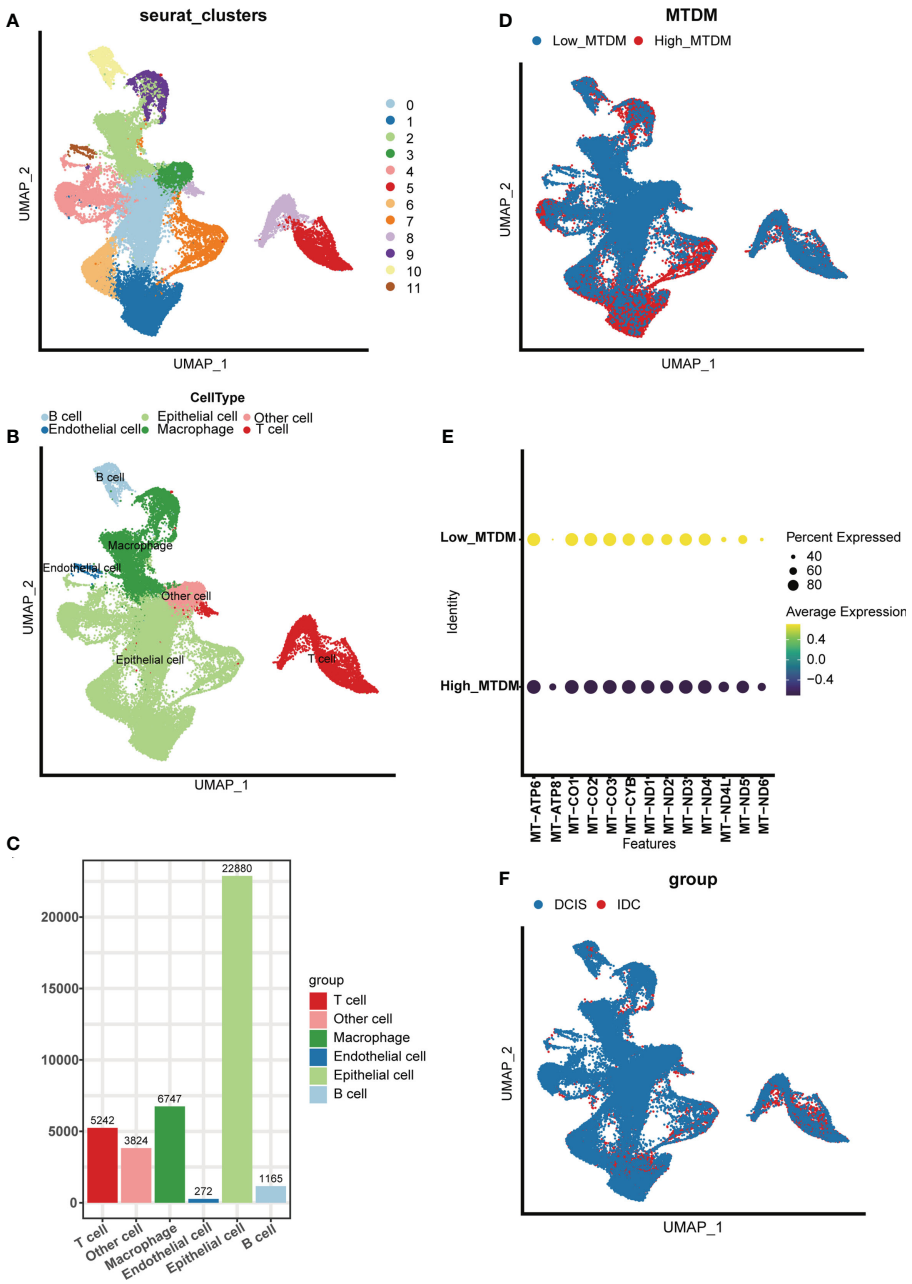

FIGURE 1
Single Cell Sequencing Data Analysis. **(A)** Dimensionality reduction and cluster analysis. All cells in 12 samples were clustered into 12 clusters. **(B)** According to the surface marker genes of different cell types, the cells are annotated as B cells, T cells, endothelial cells, epithelial cells, macrophages and other cells respectively. **(C)** Different cell types count. **(D)** The percentage of Mitochondrial DNA methylation genes in each cell. The cells were divided into high- and low-Mitochondrial DNA methylation cells. **(E)** Expression of mitochondrial coding peptides in high and low mitochondrial DNA methylation groups. **(F)** According to different cell types, breast cancer cells can be divided into Ductal carcinoma *in situ* and Invasive Ductal Carcinoma.

Additionally, we conducted a PCA of the 11 genes in both the training and validation set models, and the results showed that our constructed model could discriminate between high and low MTDM in both cohorts (Figures 3G, H). Hereafter, high and low MTDM distinguished by risk score was used to refer the high-risk score and low risk, respectively. To better assess the risk of BC patients, a nomogram combined clinical data and MTDM values was first constructed, based on the age, T-stage, total stage and MTDM score of patients "TCGA-A2-A0CY", our nomogram estimated a 0.0158, 0.113, and 0.216 mortality rate of patients at the year of 1, 3, and 5 years respectively (Figure 3I). ROC analysis was used to evaluate the accuracy of the nomogram, and the results showed that the AUC at 1, 2, 3, and 5 years were 0.85, 0.84, 0.8, and 0.8, respectively (Figure 3J). Thus, the constructed nomogram could effectively predict the patients with BC, and could be used to direct clinical decision-making.

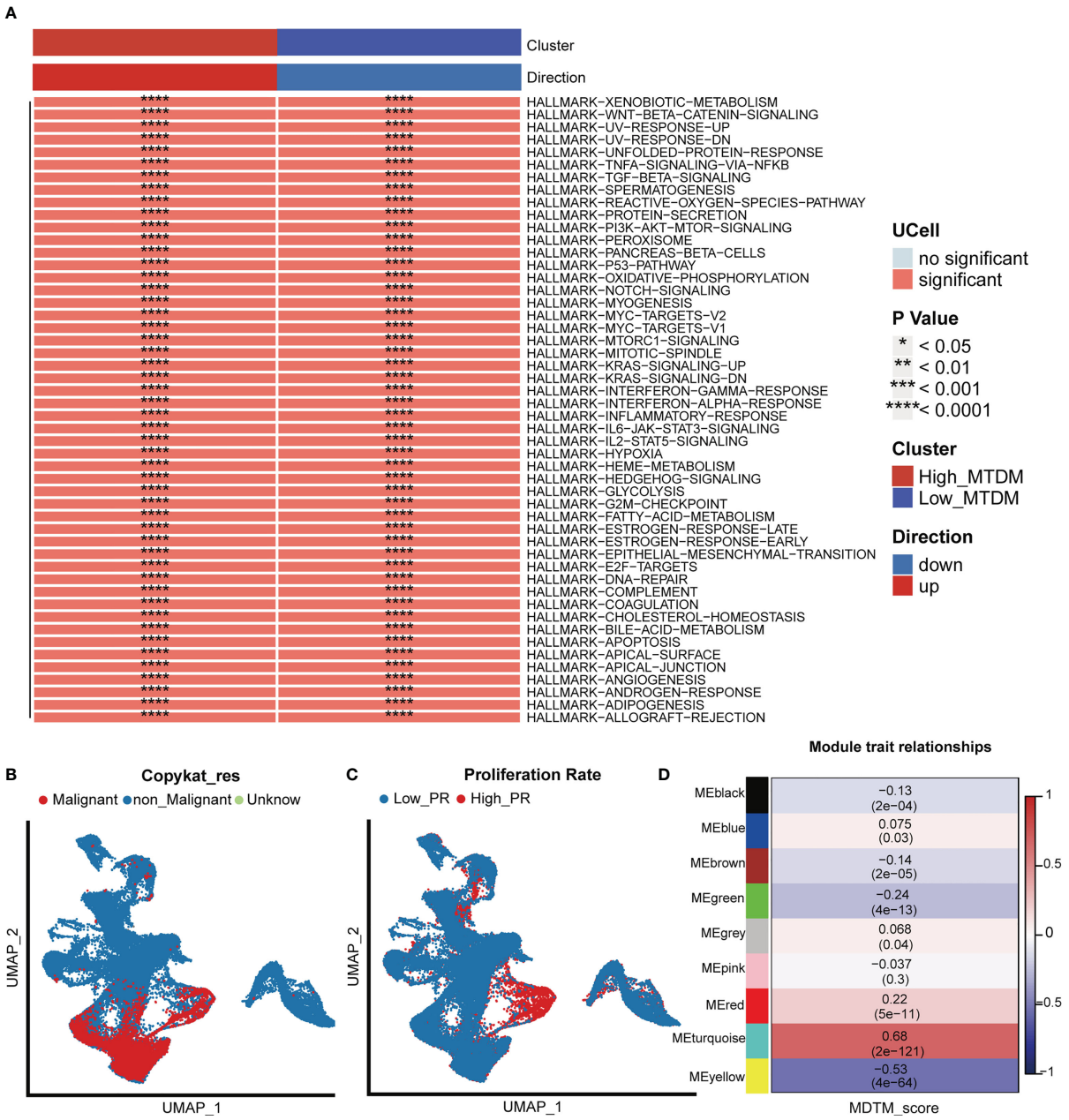

FIGURE 2
Biological differences in mitochondrial DNA methylation. **(A)** Differential biological pathway analysis showed that high and low mitochondrial DNA methylation groups were enriched in different signaling pathways. **(B)** Malignant cell identification, by chromosome integrity recognition, distinguish benign cells and malignant cells. **(C)** Cell proliferation rate was quantified by proliferation-related genes. **(D)** WGCNA found that MEturquoise, and MEyellow modules were closely related to the score of Mitochondrial DNA methylation.

3.4 Screen of mitochondrial DNA methylation-related prognostic genes that positively regulate breast cancer cells proliferation

As altered MTDM levels may affect BC cell proliferation, further screening of MTDM-related prognostic genes that positively regulate BC proliferation could potentially be used as therapeutic targets is required. Thus, we first explored the expression of MTDM-related prognostic genes in different cell types. The results showed that all MTDM-related genes were highly expressed in epithelial cells, except for *ARID1B* which was highly expressed in B cells (Figure 4A). Additionally, all MTDM-related prognostic genes were highly expressed in malignant cells and cells with a high MTDM status (Figures 4B–D). These results are consistent with our previous results described in Section 3.3, indicating that MTDM-associated prognostic gene expression correlates well with MTDM levels in cells.

Furthermore, we investigated the expression of MTDM prognosis-related genes in the high and low proliferation rate groups (Figure 5A) and found that all MTDM-related prognostic genes were highly expressed in the high proliferation rate group,

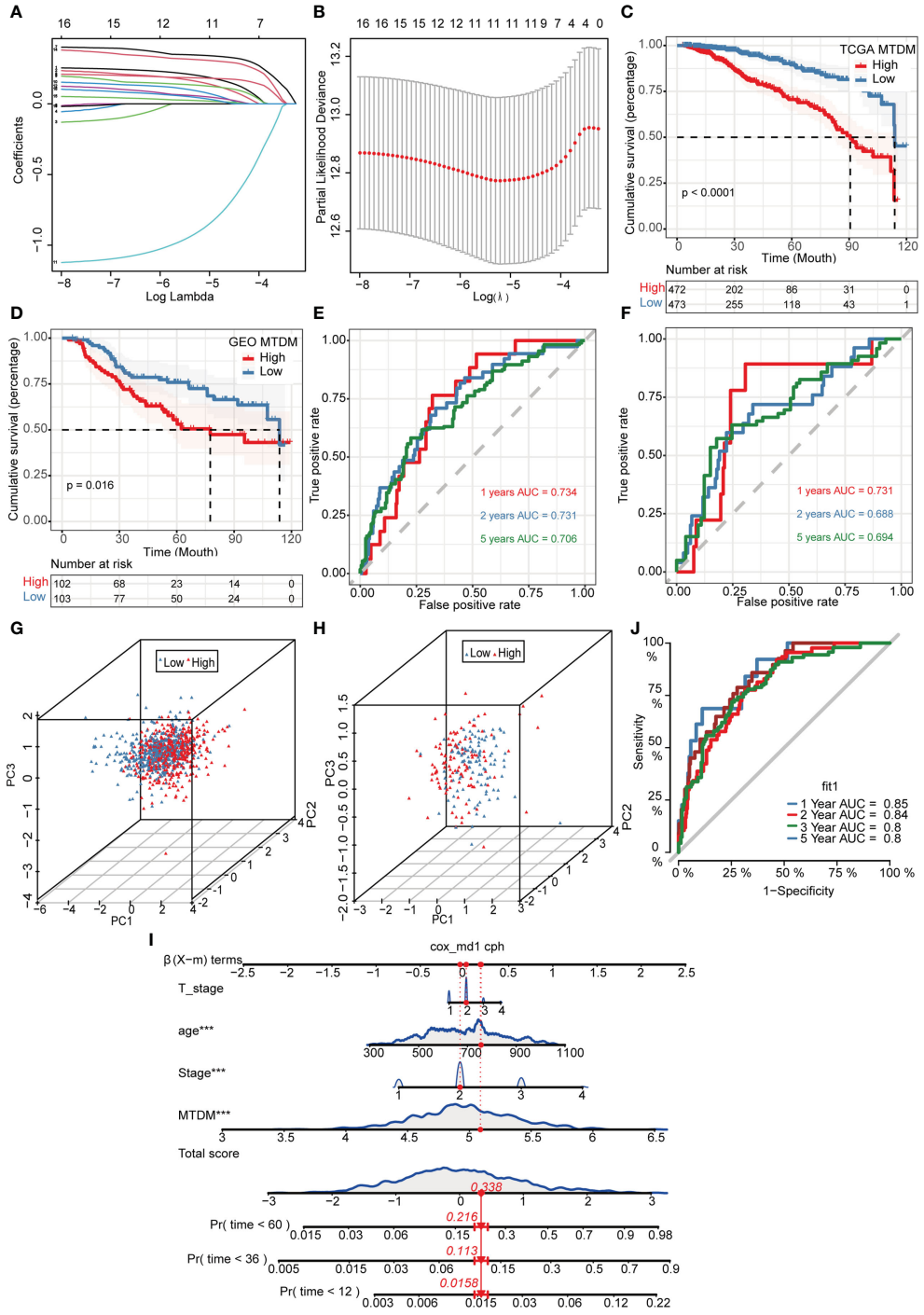

FIGURE 3
Construction and validation of Mitochondrial DNA methylation-related prognostic model. **(A, B)** sixteen genes were selected to construct the prognostic model by Lasso regression. **(C)** Survival analysis of TCGA cohort. The prognosis was significantly worse in the high-MTDM group (P<0.0001). **(D)** Survival analysis of GSE21653 Cohort. The prognosis was significantly worse in the high-MTDM group (P<0.016). **(E)** ROC curve of TCGA cohort. The AUC values of the model in 1, 2 and 5 years were 0.734, 0.731 and 0.706, respectively. **(F)** ROC curve of GSE21653 Cohort. The AUC values of the model in 1, 2 and 5 years were 0.731, 0.688 and 0.694, respectively. **(G, H)** PCA analysis of TCGA and GSE21653 queues. It was found that the model could well distinguish mitochondrial DNA methylation levels in both the training cohort and the validation cohort. **(I)** Nomogram of patient "TCGA-A2-A0CY". The mortality rate of the patient in 1, 3 and 5 years was estimated to be 0.0158, 0.113 and 0.216. **(J)** ROC curve of the nomogram. The area under the curve (AUC) in 1,2, 3 and 5 years were 0.85, 0.84, 0.8 and 0.8 respectively. ***P<0.001.

except for ARID1B which was highly expressed in the low proliferation rate group. Again, we generated scores for proliferation-related markers using ssGSEA in the TCGA BC patient cohort (Figure 5B). The high and low proliferation rate groups were distinguished by the median proliferation-related marker scores (Figure 5C). The results showed that MPHOSH10, NCAPD3 and SLBP were highly expressed at high proliferation rates, with the most significant difference observed in NCAPD3. The correlation heat map results also showed that NCAPD3 had a significant positive correlation with proliferation-related markers and correlated with MKI67 at 0.52 (Figure 5D). We further subdivided malignant cells to focus on the relationship between MTDM-related prognostic genes and malignant cells. We identified a total of six malignant cell clusters (Figure 5E) and compared the signature genes of each cluster and found that cluster 1 was highly expressed in proliferation-related markers, such as MKI67, CCNB1 and UBE2C (Figure 5F), and GSVA analysis also showed that cluster 1 was highly enriched in proliferation-related pathways, such as the MYC signaling pathway, DNA repair pathway, E2F signaling pathway, and G2M checkpoint signaling (Figure 5G). This suggests that Cluster 1 is a malignant cell in a proliferative state. Finally, we investigated the expression of MTDM-related prognostic genes in a subpopulation of malignant cells and consistent with the TCGA BC patient cohort, NCAPD3 was expressed at the highest level in malignant cells in the proliferative state (Figure 5H). These results also demonstrate that high MTDM status may promote malignant cell proliferation, and NCAPD3 in particular, may play a key role in this process.

3.5 The changes of immune microenvironment suggest that the mitochondrial DNA methylation status may respond to the sensitivity of breast cancer immunotherapy

Because a high MTDM state can affect the expression of mitochondria-encoded polypeptides, preventing them from effectively maintaining the integrity of the oxidative respiratory chain (12–14), this would cause alterations in the metabolic state of tumor cells. In turn, the metabolic reprogramming of tumor cells is also aimed at promoting the rapid proliferation of tumor cells by adjusting energy metabolism (36). Since high MTDM state would inhibit OXPHOS and promote malignant cell proliferation, we hypothesized that a high MTDM state could potentially drive tumor cells to shift from OXPHOS to aerobic glycolysis, and that the low PH microenvironment created by the metabolites of aerobic glycolysis is conducive to tumor immune escape and promotes tumor progression (37, 38). Therefore, we aimed to investigate changes in the tumor immune microenvironment under different states of MTDM and whether MTDM-related prognostic genes could respond to the sensitivity of BC immunotherapy. First, we explored the differences in immune cell infiltration levels between the high and low MTDM groups. The results showed increased immune cell infiltration, including B cells, NK cells, and T cells in the low-MTDM group (Figure 6A). The expression of immune checkpoint-related genes was analyzed, and the results showed that the immune checkpoint-related genes included in the study were highly expressed in the low-MTDM group (Figure 6B). This may have resulted in low immune cell responsiveness in the low-MTDM group owing to the high expression of immune checkpoint genes despite the high level of immune infiltration. To explore whether immunotherapy is more applicable to the low-MTDM group, we calculated the MSI and TMB scores to review their relationship with MTDM. Tumors with high MSI are usually sensitive to immune checkpoint blockade (39); therefore, we chose this score. Based on the results showing that the high MSI group had a lower MTDM score (Figure 6C), this evidence suggests that patients in the low-MTDM group may benefit more from immune checkpoint inhibitors. However, predicting TMB sensitivity to immune checkpoint inhibitors in BC is controversial (40–43). In our results, we found a higher TMB in the high MTDM group (Supplementary Figures 3A–C) and a negative correlation with the degree of immune infiltration, which is inconsistent with the positive correlation between TMB and immune infiltration in most studies. Therefore, we concluded that the TMB score is not suitable as a biomarker for BC immunotherapy. To further test our prediction, we used the cohort of immunotherapy-treated melanoma patients GSE91061 (44) (Figure 6D). As expected, the low-MTDM group had the largest proportion of patients who achieved a CR or PR. Meanwhile, unsupervised clustering showed that MTDM related prognostic genes were best classified into two groups in the TCGA dataset (Figures 6E, F). There was also a significant difference in the immune cells between the two groups (Figure 6G), with cluster B showing lower expression of MTDM related prognostic genes and higher levels of immune cell infiltration. Finally, we differentiated T cells among the single-cell data set, and the best binning was 12 according to the decision tree (Figure 6H, Supplementary Figure 3D). T cells were classified into CD8-positive T cells, Exhausted CD8 T cells, T follicular helper cells, effector memory T cells, naïve T cells, and Tregs according to the available markers (Figure 6I, Supplementary Figure 3E). The ratio of cells between the two groups showed that the high MTDM group had a higher proportion of Exhausted CD8 T cells, a marker of immune dysfunction (45), while the low MTDM group had a higher proportion of CD8-positive T cells (Figures 6J, K). These results suggested that the low-MTDM group may be more responsive to immunotherapy.

3.6 Cellular communication reveals a potential pathway for mitochondrial DNA methylation to mediate immunosuppression

We explored the cellular communication characteristics between malignant cells and T cell subpopulations in different MTDM states, and the intercellular communication characteristics can effectively identify the receptor-ligand relationships that exist between cell populations, and we used this approach to uncover possible ligand-receptor pairs between high MTDM/proliferation-associated malignant cells and immune cell

10.3389/fimmu.2023.1219652

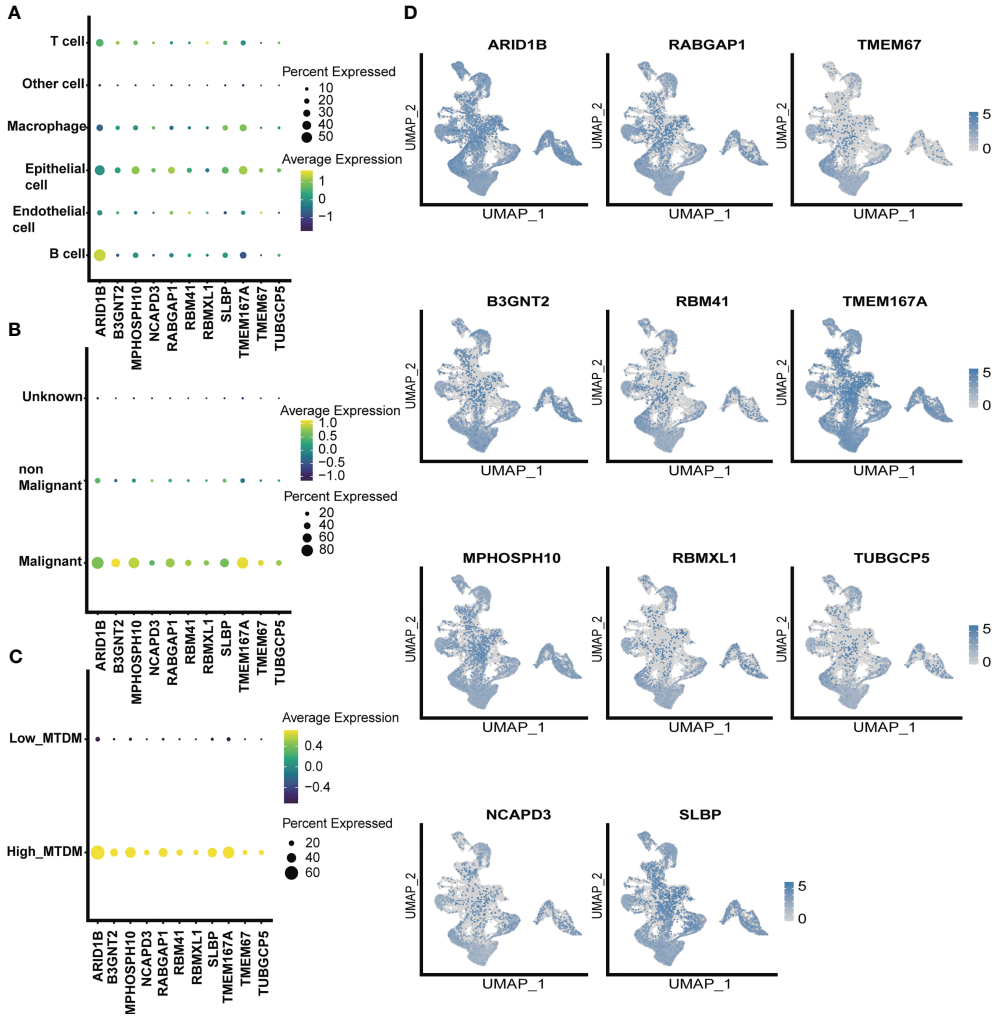

FIGURE 4
single-celled sequencing analysis, to explore the distribution of 11 modeling gene. **(A)** The expression levels of 11 modeling genes in different cell types. **(B)** The expression levels of 11 modeling genes in benign and malignant cells. **(C)** Expression levels of 11 modeling genes in high and low MTDM groups. **(D)** umap shows the expression distribution of model genes in the data set.

subpopulations as a response to the linkage between the two subpopulations and the potential mechanisms of action. Figure 7A shows the overall communication conditions between Exhausted CD8 T cells and high MTDM malignant cells. It was found that high MTDM malignant cells emit a *GDF15* signal. In contrast, Exhausted CD8 T cells relied on *TGFBR2*, the receptor of *GDF15*, to receive this signal (Figures 7B, C). In addition, the secretion of *GDF15* by high MTDM malignant cells and the expression of *TGFBR2* by Exhausted CD8 T cells were cell-specific (Figure 7D). *GDF15*, a member of the transforming growth factor β (TGF-β) family, inhibits the expression of co-stimulatory and major histocompatibility complex (MHC) class II molecules, it decreases IL-12 levels and increases TGF-β1 secretion (46). In hepatocellular carcinoma, *GDF15* acts as a critical promoter of Treg cells to promote Treg cell production thereby mediating immunosuppressive responses (47). Our results suggest that malignant cells with high MTDM status may cause exhaustion of CD8 T cells through the secretion of *GDF15*, leading to immunosuppression. Similarly, we explored the intercellular communication between proliferation-associated malignant cells (cluster1) and T cells. Figure 7E shows the overall communication between Exhausted CD8 T cells and high MTDM malignant cells. The same results showed that proliferation-associated malignant cells specifically secrete *GDF15*, and Exhausted CD8 T cells receive this signal (Figures 7F–H). This suggests that *GDF15* may be a key factor in the immunosuppressive response of malignant cells with a high MTDM status and proliferation rate.

3.7 *In vitro* experiments confirm that the MTDM-associated prognostic gene NCAPD3 does promote the proliferation of breast cancer cells

As *NCAPD3* is expressed at the highest level in proliferation-related malignant cells and is positively correlated with proliferation-related genes, we further explored the expression of

10.3389/fimmu.2023.1219652

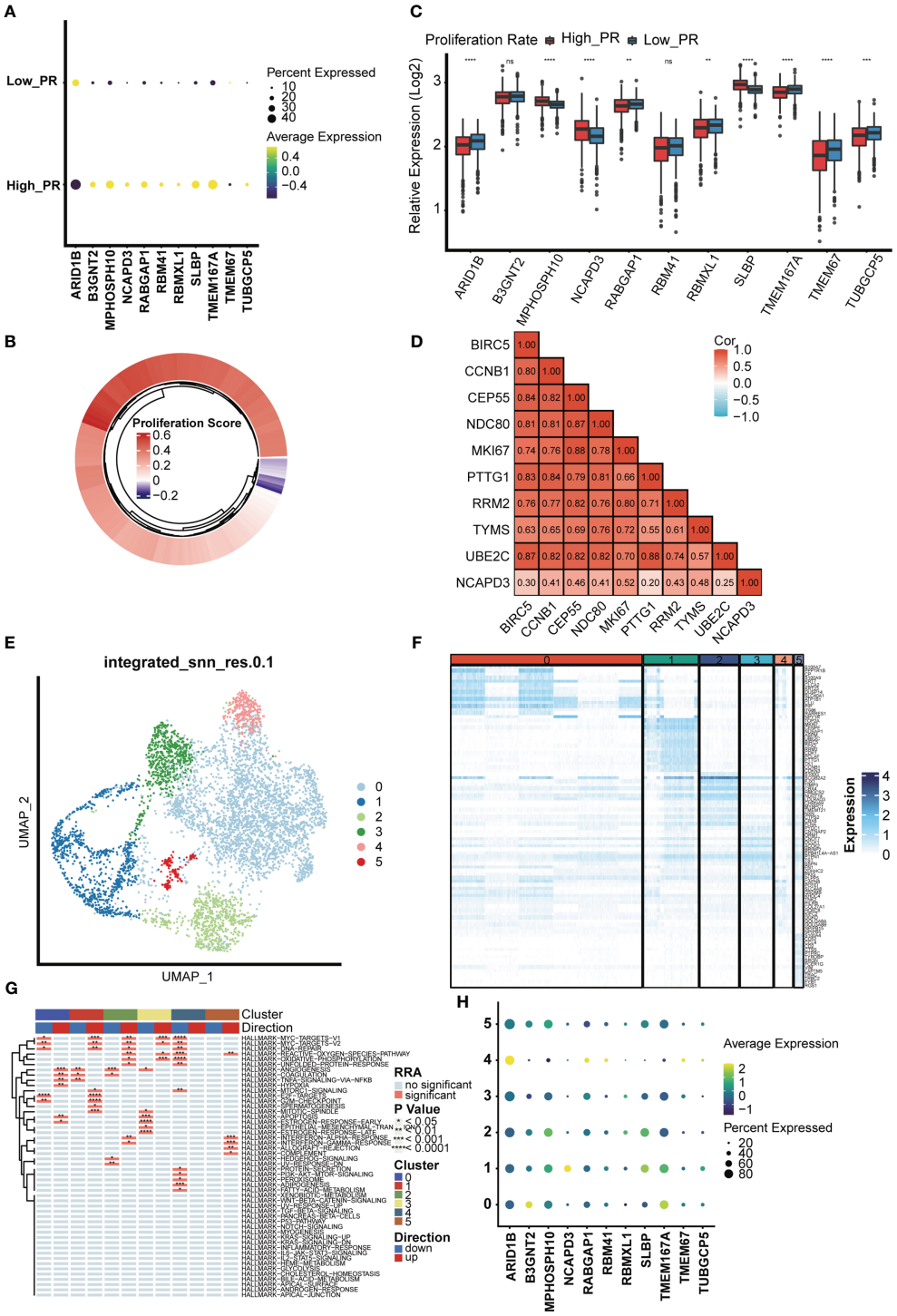

FIGURE 5
The relationship between the model gene and proliferation was analyzed in malignant cells. **(A)** Expression levels of 11 modeling genes in high and low proliferation rate groups. **(B)** The TCGA breast cancer data set was divided into high and low proliferation rate groups based on proliferation-related genes. **(C)** Expression levels of modeling genes in the high and low proliferation rate groups of the TCGA breast cancer data set. Results In the TCGA breast cancer data set, the difference in NCAPD3 was most significant between the high and low proliferation groups. ns, no significance; *p<0.05; **P<0.01; ***P<0.001. **(D)** Analysis of the correlation between NCAPD3 and proliferation-related genes showed that there was a strong correlation between NCAPD3 and proliferation-related genes. **(E)** Epithelial malignant cells were divided into 6 clusters. **(F)** Differential genes in 6 clusters showed specific expression of proliferation-related genes in cluster 1, which indicated that cluster 1 subgroup was proliferation-related epithelial malignant cells. **(G)** Differential biological pathway enrichment analysis shows the pathways enriched by different clusters. **(H)** The expression of 11 modeling genes in 6 epithelial malignant cell clusters showed that NCAPD3 had the highest expression level in cluster 1. *p<0.05; **P<0.01; ***P<0.001, ****P<0.0001.

10.3389/fimmu.2023.1219652

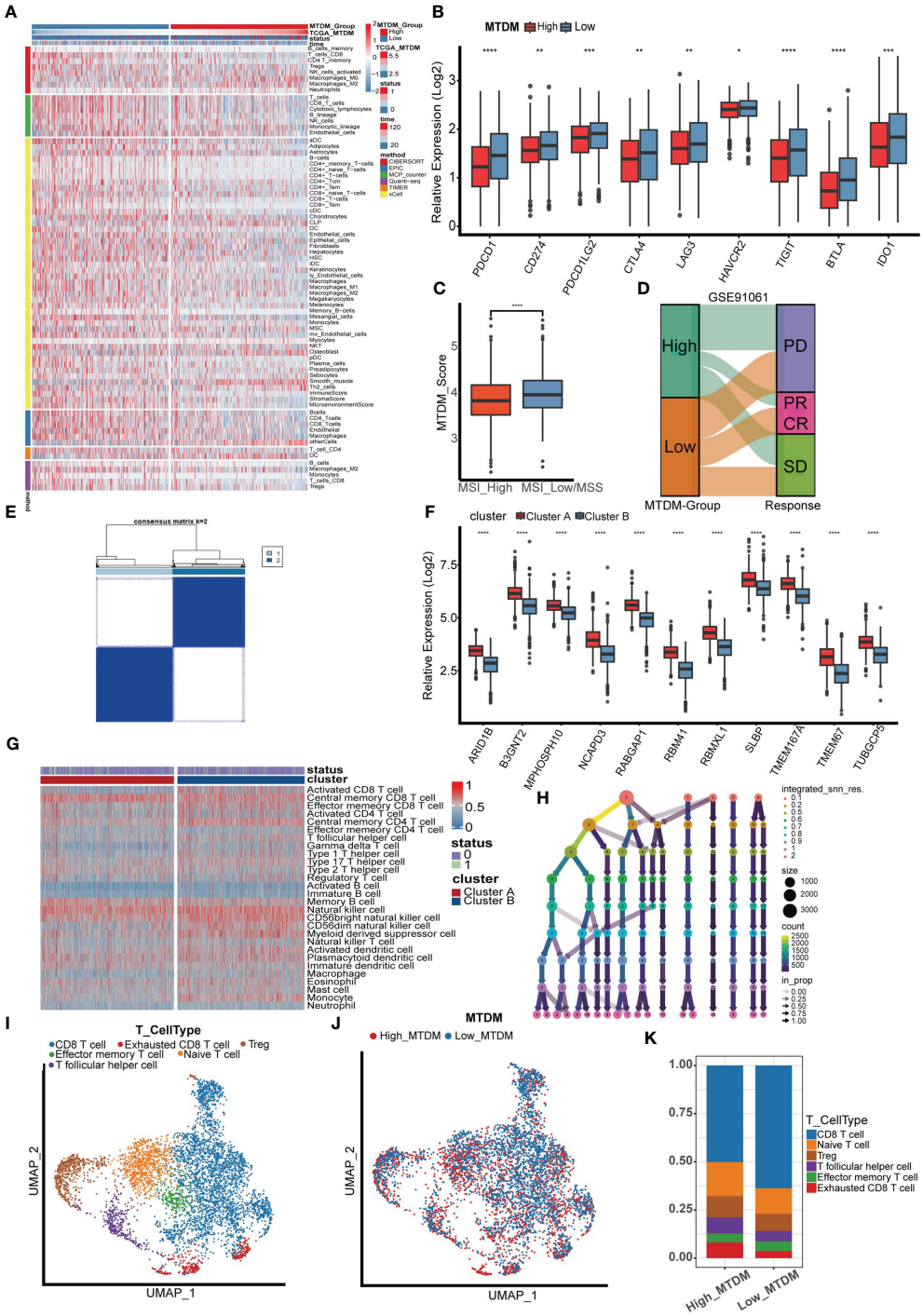

FIGURE 6
Immune infiltration analysis and immunotherapy sensitivity prediction. **(A)** Heat map of immune cell infiltration in high MTDM group and low MTDM group. **(B)** Expression of immune checkpoint related genes in high -MTDM group and low -MTDM group. **(C)** The results of microsatellite instability state analysis showed that the high MSI group had lower MTDM scores. *P < 0.05; **P < 0.01; ***P < 0.001; ****P < 0.0001. **(D)** The relationship between mitochondrial DNA methylation score and response to immunotherapy was evaluated using immunotherapy cohort GSE91061. **(E)** Unsupervised consistency cluster analysis. Patients can be divided into two clusters according to the expression of model genes. **(F)** The expression levels of model genes in different clusters. **(G)** Immune landscape of different clusters. **(H)** Decision tree analysis is used to determine the optimal clustering threshold. **(I)** According to the surface marker genes of different cell types, the cells are annotated as CD8 T cells, Exhausted CD8 T cells, T follicular helper cells, Treg cells, Effector memory T cells and Naive T cells respectively. **(J)** The percentage of Mitochondrial DNA methylation genes in T cells. The cells were divided into high- and low-MTDM cells. **(K)** Proportion of T cell types in high and low MTDM groups.

10.3389/fimmu.2023.1219652

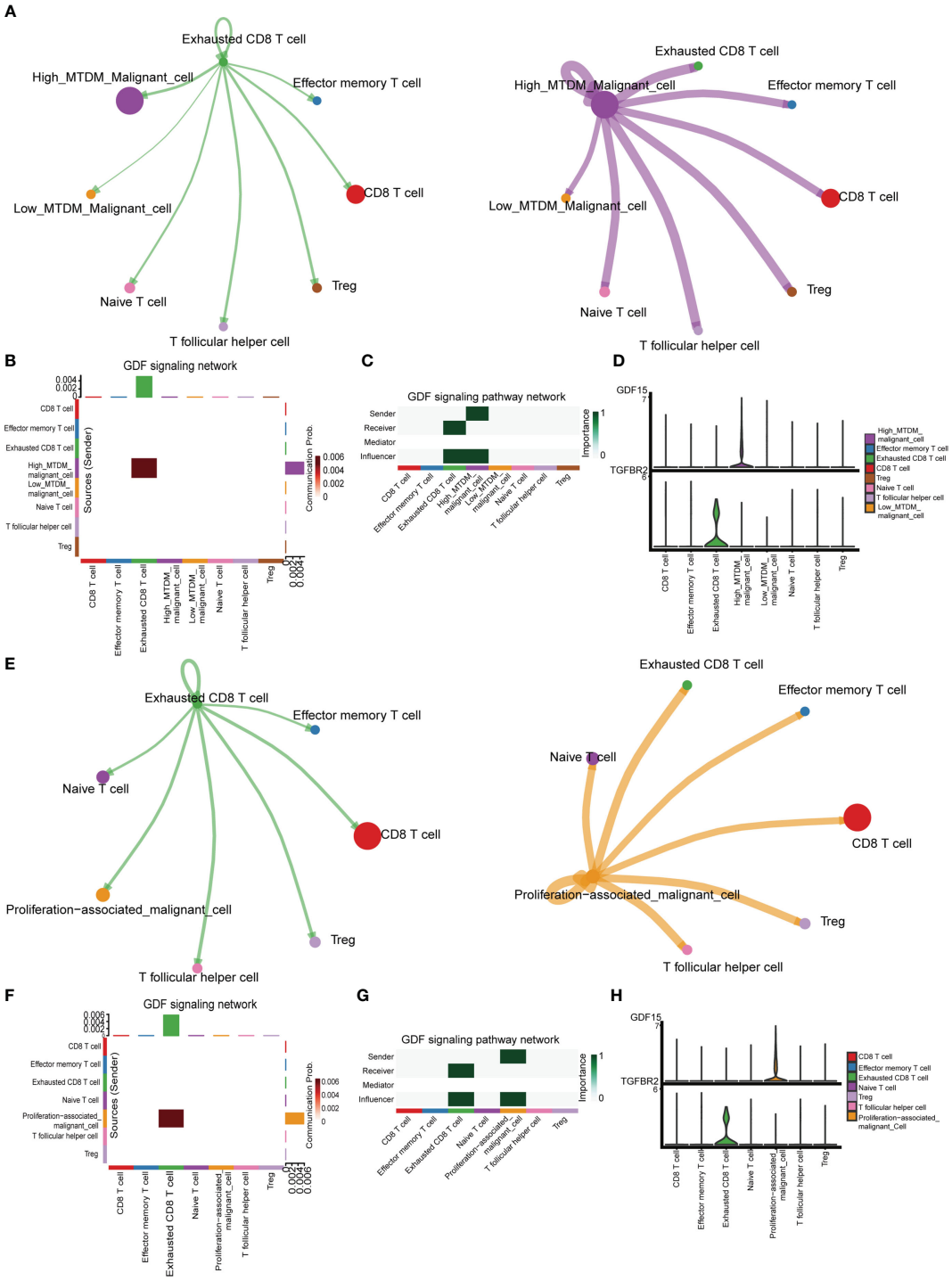

FIGURE 7
Cell communication analysis shows the interactions between different kinds of cells. **(A)** Overall communication condition of Exhausted CD8 T cells and High-MTDM Malignant cells. Circle sizes are proportional to the number of cells in each cell group and edge width represents the communication probability. **(B)** Overall activation of the GDF signaling pathway was observed in T cell subtypes and malignant cells with different MTDM levels. **(C)** The malignant cells in the high MTDM group were the only transmitters of GDF signal, and the Exhausted CD8 T cells were the only receivers of this signal. **(D)** Expression of GDF and its ligand, TGFBR2, in T cell subtypes and malignant cells with different MTDM levels. **(E)** Overall communication condition of Exhausted CD8 T cells and Proliferation-associated malignant cells. **(F)** Overall activation of the GDF signaling pathway was observed in T cell subtypes and Proliferation-associated malignant cells. **(G)** The Proliferation-associated malignant cells were the only transmitters of GDF signal, and the Exhausted CD8 T cells were the only receivers of this signal. **(H)** Expression of GDF and its ligand, TGFBR2, in T cell subtypes and Proliferation-associated malignant cells.

NCAPD3 in BC and its effect on the immune microenvironment. In the TCGA transcriptome, *NCAPD3* was also highly expressed in tumors (Figure 8A). We then evaluated the correlation between *NCAPD3* expression and the immune score and MSI separately and found that *NCAPD3* expression was negatively correlated with the immune score and MSI (Figures 8B–D). Next, we performed biological functional validation of NCAPD3 knockdown *in vitro* to test whether our model gene knockdown prevents the growth of breast cancer cell lines, which could indirectly respond to whether knockdown of NCAPD3 improves the prognosis of breast cancer patients. First, we verified the mRNA levels of *NCAPD3* in the MDA-MB-231 BC cell line 1 day after transfection using q-PCR (Figure 8E) and found that all siRNA interference resulted in a significant reduction in *NCAPD3* mRNA expression ($P< 0.05$). We also verified the protein levels of *NCAPD3* in MDA-MB-231 and BCAP-37 BC cell lines after 2 days of transfection by western blotting (Figures 8F, G) and again found that the siRNA sequences resulted in reduced protein levels of *NCAPD3* ($P< 0.01$). To assess the effect of *NCAPD3* on cell proliferation, we performed CCK8 and clone formation assays. CCK8 results showed that after *NCAPD3* knockdown, cell viability was significantly reduced in MDA-MB-231 and BCAP-37 BC cell lines compared to that in the siRNA negative control (NC) group ($P<0.05$) (Figures 8H, I). The results of the cloning assay showed that the number of colonies with reduced *NCAPD3* expression was significantly reduced in both the BC cell lines (Figures 8J, K, Supplementary Figure 3F). Finally, we performed scratch assays to test whether *NCAPD3* knockdown affected the migration ability of BCAP-37 BC cell lines. The results showed that scratch healing was significantly slower in the *NCAPD3* knockdown group than in the siRNA negative control (NC) group (Figure 8L, Supplementary Figure 3G), indicating that *NCAPD3* knockdown may be an effective strategy to inhibit the proliferation and migration of BC cells. These results suggest that NCAPD3 targeting may be a desirable outcome for BC treatment and may improve patient prognosis.

4 Discussion

In this study, we found that altered MTDM levels play a key role in BC progression and influence the prognosis and immunotherapy outcomes of BC patients. We constructed a BC cell profile by using GSE195861 single cell data and distinguished between high and low MTDM groups, while high MTDM cells were mainly present in cells derived from IDC patients, with high proliferation rates and higher malignancy, suggesting that high levels of MTDM may be associated with the malignant trend of BC. Further investigation revealed that MTDM levels also had an impact on BC progression and patient prognostic key gene expression and were influenced by these genes regulating downstream signaling pathways. The high MTDM group showed a lower level of immune infiltration, a higher proportion of Exhausted CD8 T cells and a higher proliferation rate compared to the low MTDM group, which also had a poorer prognosis. In addition, the findings revealed that cells with low MTDM levels had a higher percentage of immune cell infiltration and a higher percentage of CD8-active T cells adapted for immunotherapy. Finally, we also analyzed the cell-to-cell communication characteristics of T cell fractions and high MTDM malignancy/proliferation-associated malignancy cells. The results showed that high MTDM malignancy/proliferation-associated malignancy cells secreted GDF15 and Exhausted CD8 T cells expressed TGFBR2, the receptor for GDF15, leading to tumor cell immunosuppression. In conclusion, our study highlights the non-negligible role of MTDM in BC progression and its impact on a wide range of biological functions. Therefore, this is an area worth exploring in BC therapy.

In the article, we identified MTDM-related molecules representative of patient prognosis and immunotherapy sensitivity to construct a portfolio of markers for predicting BC patient prognosis and immunotherapy sensitivity. These include *ARID1B*, *B3GNT2*, *MPHOSPH10*, *NCAPD3*, *RABGAP1*, *RBM41*, *RBMXL1*, *SLBP*, *TMEM167A*, *TMEM67*, and *TUBGCP5*. AT-Rich Interaction Domain 1B (ARID1B) is a component of the SWI/SNF chromatin remodeling complex. In a zebrafish model, deletion of ARID1B results in reduced body length due to dysregulation of the Wnt/β-catenin signaling pathway (48), which reveals an association between ARID1B and the Wnt/β-catenin signaling pathway. In a recent study, loss of ARID1B in ARID1A-deficient tumors destabilized SWI/SNF and impaired cancer cell proliferation (49). Meanwhile, ARID1B was identified as a potential therapeutic target in ARID1A mutant neuroblastoma (50). BetaGal Beta-1,3-N-Acetylglucosaminyltransferase 2 (B3GNT2) encodes a poly-N-acetyl lactosamine synthase that targets multiple ligands and receptors to disrupt tumor-T cell interactions and reduces T cell activation (51). M-Phase Phosphoprotein 10 (MPHOSPH10) encodes a protein that is phosphorylated during mitosis and may be involved in rRNA preprocessing (52). For fast-growing cancer cells, an active translational machinery is required to meet the needs of protein production, in which robust ribosome biogenesis plays a key role (53). Recent studies have shown that UTP11 facilitates pre-rRNA processing by binding to MPHOSPH10. When this process is blocked, it triggers nuclear stress and leads to p53 activation and cancer cell growth arrest (54). RAB GTPase Activating Protein 1 (RABGAP1) is a GTPase activating protein of RAB6A that plays a key role as a master regulator in cellular compartment localization and vesicle transport (55). Many Rab proteins are involved in cancer progression and in recent studies, RABGAP1 was shown to be regulated by Tuftelin 1 (TUFT1), promoting perinuclear lysosome accumulation and intracellular vesicle transport, which in turn is involved in tumor development (56). RNA Binding Motif Protein 41 (RBM41) is predicted to be a target gene for hsa-miR-136 (57), which has been shown to possess oncogenic effects (58), and RBM41 may also be involved in this process. RNA Binding Motif protein, X-linked Like 1 (RBMXL1) is an RNA-binding protein that may be involved in pre-mRNA splicing, and it has been reported that melanomas with RBMXL1 mutations may have correspondingly extensive Studies of Alternative RNA Splicing (ARS) (59), which may provide novel antigenic epitopes (60). stem-loop binding protein (SLBP) is a protein that binds to the histone mRNA stem-loop sequence and regulates the 3' processing

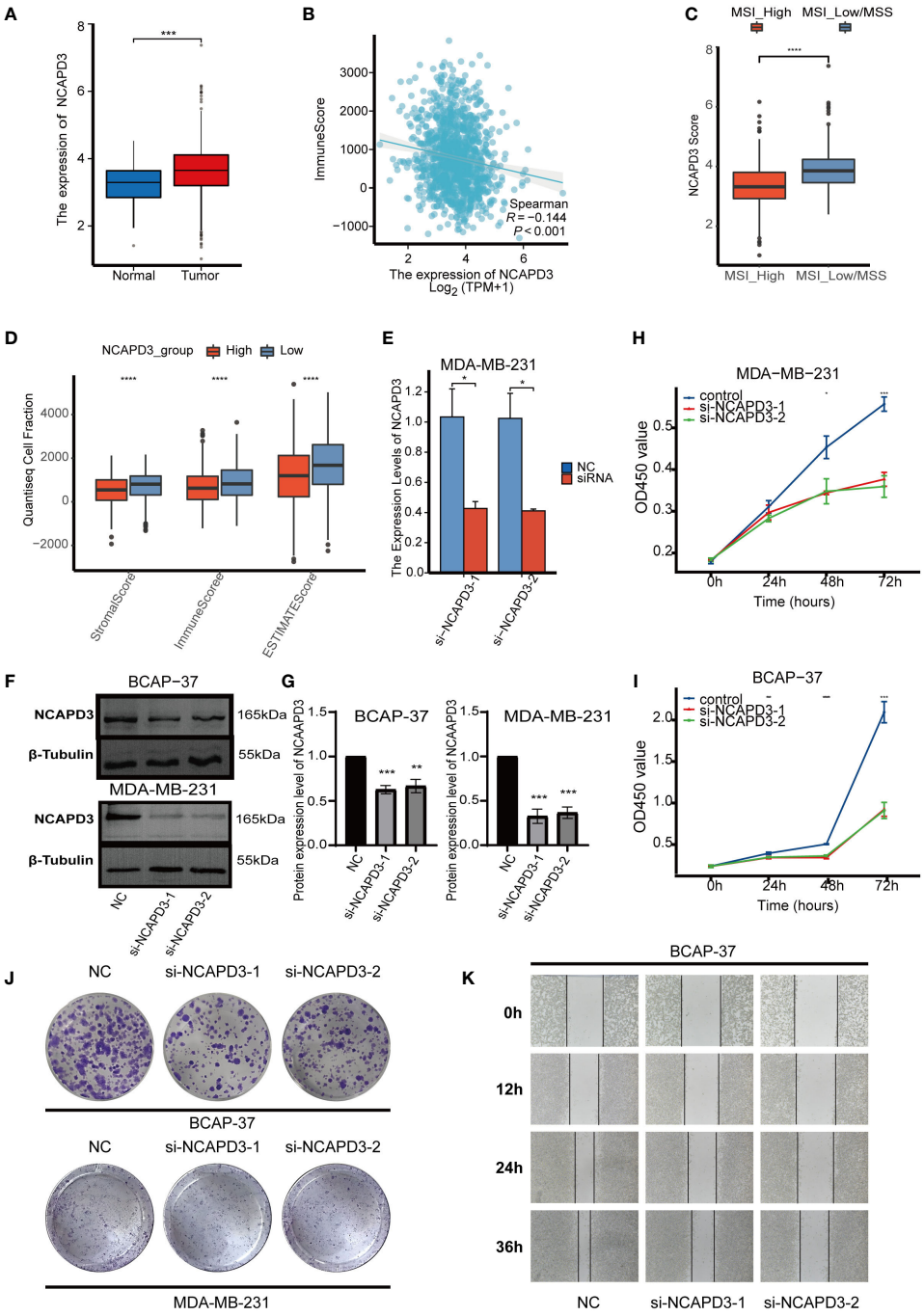

FIGURE 8
In vitro biofunctional validation of the MTDM-associated prognostic molecule NCAPD3. **(A)** Expression of NCAPD3 in cancer and peritumoral samples in the TCGA breast cancer dataset. **(B)** Analysis of correlation between NCAPD3 and immune score. **(C)** The results of microsatellite instability analysis showed that the high MSI group had lower NCAPD3 expression. **(D)** The estimate analysis showed the relationship between the expression level of NCAPD3 and stromal score, immune score and estimate score. **(E)** qRT-PCR to evaluate the level of NCAPD3 mRNA 1 days after transfection. All siRNA sequences could result in significant decrease in NCAPD3 mRNA expression (P<0.05). **(F-G)** Western Blot to evaluate the level of NCAPD3 proteins 2 days after transfection. All siRNA sequences could result in significant decrease in NCAPD3 proteins expression (P<0.01). **(H-I)** CCK8 assay. After NCAPD3 knockdown, the cells showed significant reduction in viability. **(J)** Colony formation assay. Cells with a reduced NCAPD3 expression exhibited a significant decrease in the numbers of colonies, compared with the siRNA negative control (NC) group. **(K)** Scratch-wound healing assay. A significantly slower wound healing rate was observed in cells with a decreased expression of NCAPD3 gene. All data were presented as the means ± SD of three independent experiments. *P < 0.05, **P < 0.01, ***P < 0.001, ****P < 0.0001.

of histone mRNA (61), SLBP is required for histone biosynthesis and also for rapid cell proliferation (62), as RNAi downregulation of SLBP expression inhibits DNA synthesis and thus inhibits cycle progression (63). A recent study showed that SLBP is indeed involved in breast cancer development and that inhibition of SLBP expression would be a promising therapeutic target for breast cancer (64). Transmembrane Protein 167A (TMEM167A) is a protein associated with vesicle transport and secretion that regulates the transport of newly synthesized proteins from the ER-Golgi to the cell membrane or other organelles and is also required for glioma growth in human cell xenografts and Drosophila models, and interference with TMEM167A expression impedes a variety of tumor cell proliferation (65, 66). Transmembrane Protein 67 (TMEM67) plays a role in the migration of centrioles to the apical membrane and the formation of primary cilia (67). TMEM67 was identified as a candidate therapeutic target for triple negative breast cancer (TNBC) in a recent study, which revealed TMEM67 amplification in TNBC and proliferation inhibition of TNBC cell lines by interference with TMEM67 expression (68). Gamma-Tubulin Complex Component 5 (TUBGCP5, also known as GCP5), is involved in microtubule binding activity and microtubule nucleation (69). Recent studies have reported that TUBGCP5 can be regulated by the Long non-coding RNA Hotair, which in turn promotes the proliferation, migration and invasion of gastric cancer cells, and the regulation of the Hotair/TUBGCP5 axis may be a potential therapeutic target for gastric cancer (70). Non-SMC Condensin II Complex Subunit D3 (NCAPD3) is a subunit of the cohesin II complex, a complex of mitotic chromosomal structures involved in the physical rigidity of the chromosome spindle (71). Recent studies have shown that NCAPD3 plays a key role in CRC progression by upregulating various transcription factors, such as E2F1 and c-Myc and regulating glycolytic function in multiple ways to mediate tumorigenesis and progression (72). In prostate cancer, NCAPD3 has also been shown to activate E2F1 and STAT3 and drive prostate cancer progression (73). In addition, NCAPD3 is present in the outer mitochondrial membrane and regulates oxidative stress in the mitochondria, which is not dependent on glycolysis and does not affect the number of mitochondria (74). Ultimately, *in vitro* experiments also confirmed that the knockdown of NCAPD3 resulted in a significant decrease in cell viability and colony number in BC cell lines MDA-MB-231 and BCAP-37 and a significant slowdown in scratch healing in MDA-MB-231 cells. Thus, our results suggest that NCAPD3 is a promising therapeutic target for BC and further studies are needed to explore its potential.

In BC, it is commonly observed that BC possesses lower mtDNA content compared to standard breast specimens (75, 76), and it has also been shown that the reduction of mtDNA in BC cell lines may be associated with the conversion to a mesenchymal phenotype (77). Furthermore, MTDM largely determines the mtDNA expression. The role of MTDM in BC is almost unknown; therefore, it is necessary to analyze the specific role of MTDM in BC, and further research is needed to understand the role of MTDM and its potential as a therapeutic target.

In previous studies, the exploration of MTDM focused on its presence and alteration in different diseases (17),leading to a lack of clarity on the one hand as to why this alteration occurs, and on the other, as to what impact this alteration will have on the development of the disease. Recently, through methodological and functional studies, the academic community established MTDM as an important research direction in mammalian mitochondrial physiology (78). Previous methodologies have been dedicated to the more precise identification of MTDM modification sites (22), and thus to determining the overall level of MTDM. We quantified the overall level of MTDM by collecting genes that positively regulate MTDM and quantifying the overall level of MTDM based on their expression levels, and the expression of mitochondria-encoded peptides similarly confirmed the validity of our approach. The accuracy of this method needs to be validated in combination with other MTDM sequencing methods.

In this study, we present the first systematic demonstration of the role of MTDM in breast cancer and explore its relationship with immunity and prognosis. This study provided new insights into the use of BC immunotherapy. We found that MTDM-related prognostic molecules, particularly *NCAPD3*, were strongly positively correlated with proliferation. *In vitro* knockdown of *NCAPD3* interfered with cell viability, clonogenic capacity, and migration ability of BC cell lines, suggesting that *NCAPD3* may be a promising target for BC therapy. This demonstrates that interference with the MTDM pathway has great potential for cancer therapy. In particular, the understanding of the importance of MTDM in mammalian mitochondrial physiology has strengthened research in this direction. Thus, intervention of the MTDM pathway is a novel cancer treatment strategy that will lead to better patient outcomes. Our findings provide a potential target for BC therapy; however, further studies are needed to explore this potential.

Data availability statement

Publicly available datasets were analyzed in this study. This data can be found in TCGA database, GEO database, GSE195861, GSE21653, and GSE91061.

Author contributions

Conception and design: JZ, YM, JD, MC, and XW. Acquisition of data: YM, MC, and NG. Data analysis and interpretation: YM, JD, and SW. Draft and manuscript: YM, JD, and ZM. All authors contributed to the article and approved the submitted version.

Funding

This work was supported by the Pecial Branch Plan of Shaanxi, Development Talents of Shaanxi Province, Cancer development

and anti-cancer drug Innovation Research Team and Shaanxi Province Natural Science Foundation (2018JQ3073).

Acknowledgments

We would like to thank the sample donors and research teams for the TCGA, GSE195861, GSE21653, and GSE91061 cohorts, which provided data for this study.

Conflict of interest

The authors declare that the research was conducted in the absence of any commercial or financial relationships that could be construed as a potential conflict of interest.

Publisher's note

Supplementary material

The Supplementary Material for this article can be found online at: https://www.frontiersin.org/articles/10.3389/fimmu.2023.1219652/full#supplementary-material

SUPPLEMENTARY FIGURE 1
Single cell sequencing analysis of GSE195861. **(A)** The integration effect of 12 samples is good. **(B)** Cell numbers in ductal carcinoma *in situ* and invasive ductal carcinoma samples. **(C)** Annotated markers of different kinds of cells.

SUPPLEMENTARY FIGURE 2
WGCNA analysis. **(A)** Cluster tree of TCGA breast cancer samples to exclude outliers. **(B)** Find the optimal soft threshold. **(C)** Cluster Dendrogram, used to find correlations between modules and samples.

SUPPLEMENTARY FIGURE 3
TMB analysis and T cell isotype annotation. **(A)** Mutation landscape of high-MTDM group. **(B)** Mutation landscape of low-MTDM group. **(C)** TPM scores of high and low MTDM groups. **(D)** Dimensionality reduction and cluster analysis. All T cells were clustered into 12 clusters. **(E)** Annotated markers of different kinds of T cells. **(F)** Quantitative diagram of clone formation experiments. **(G)** Experimental quantified graph of scratch healing ability.

References

1. Sung H, Ferlay J, Siegel RL, Laversanne M, Soerjomataram I, Jemal A, et al. Global cancer statistics 2020: GLOBOCAN estimates of incidence and mortality worldwide for 36 cancers in 185 countries. *CA Cancer J Clin* (2021) 71(3):209–49. doi: 10.3322/caac.21660

2. Xia C, Dong X, Li H, Cao M, Sun D, He S, et al. Cancer statistics in China and the united states, 2022: profiles, trends, and determinants. *Chin Med J (Engl)* (2022) 135 (5):584–90. doi: 10.1097/CM9.0000000000002108

3. Perou CM, Sørlie T, Eisen MB, van de Rijn M, Jeffrey SS, Rees CA, et al. Molecular portraits of human breast tumours. *Nature* (2000) 406(6797):747–52.

4. McDonald ES, Clark AS, Tchou J, Zhang P, Freedman GM. Clinical diagnosis and management of breast cancer. *J Nucl Med* (2016) 57 Suppl 1:9S–16S. doi: 10.2967/jnumed.115.157834

5. Ribas A, Wolchok JD. Cancer immunotherapy using checkpoint blockade. *science* (2018) 359(6382):1350–5. doi: 10.1126/science.Aar4060

6. Emens LA. Breast cancer immunotherapy: facts and hopes. *Clin Cancer Res* (2018) 24(3):511–20. doi: 10.1158/1078-0432.CCR-16-3001

7. Schmidt C. Immunology: another shot at cancer. *nature* (2015) 527:S105–7. doi: 10.1038/527S105a

8. Han X, Song Z, Zhou Y, Zhang Y, Deng Y, Qin J, et al. Mitochondria-targeted high-load sound-sensitive micelles for sonodynamic therapy to treat triple-negative breast cancer and inhibit metastasis. *Mater Sci Eng C Mater Biol Appl* (2021) 124:112054. doi: 10.1016/j.msec.2021.112054

9. Bai R, Cui J. Mitochondrial immune regulation and anti-tumor immunotherapy strategies targeting mitochondria. *Cancer Lett* (2023) 564:216223. doi: 10.1016/j.canlet.2023.216223

10. Mposhi A, van der Wijst MGP, Faber KN, Rots MG. Regulation of mitochondrial gene expression, the epigenetic enigma. *Front Biosci (Landmark Ed)* (2017) 22(7):1099–113. doi: 10.2741/4535

11. Anderson S, Bankier AT, Barrell BG, de Bruijn MH, Coulson AR, Drouin J, et al. Sequence and organization of the human mitochondrial genome. *Nature* (1981) 290 (5806):457–65. doi: 10.1038/290457a0

12. Singh RK, Saini SK, Prakasam G, Kalairasan P, Bamezai RNK. Role of ectopically expressed mtDNA encoded cytochrome c oxidase subunit I (MT-COI) in tumorigenesis. *mitochondrion* (2019) 49:56–65. doi: 10.1016/j.mito.2019.07.002

13. Wallace L, Mehrabi S, Bacanamwo M, Yao X, Aikhionbare FO. Expression of mitochondrial genes MT-ND1, MT-ND6, MT-CYB, MT-COI, MT-ATP6, and 12S/MT- RNR1 in colorectal adenopolyps. *Tumour Biol* (2016) 37(9):12465–75. doi: 10.1007/s13277-016-5101-3

14. Grzybowska-Szatkowska L, Slaska B, Rzymowska J, Brzozowska A, Floriańczyk B. Novel mitochondrial mutations in the ATP6 and ATP8 genes in patients with breast cancer. *Mol Med Rep* (2014) 10(4):1772–8. doi: 10.3892/mmr.2014.2471

15. Angajala A, Lim S, Phillips JB, Kim JH, Yates C, You Z, et al. Diverse roles of mitochondria in immune responses: novel insights into immuno-metabolism. *Front Immunol* (2018) 9:1605. doi: 10.3389/fimmu.2018.01605

16. Breda CNS, Davanzo GG, Basso PJ, Saraiva Câmara NO, Moraes-Vieira PMM. Mitochondria as central hub of the immune system. *Redox Biol* (2019) 26:101255. doi: 10.1016/j.redox.2019.101255

17. Stoccoro A, Coppedè F. Mitochondrial DNA methylation and human diseases. *Int J Mol Sci* (2021) 22(9):4594. doi: 10.3390/ijms22094594

18. Sharma N, Pasala MS, Prakash A. Mitochondrial DNA: epigenetics and environment. *Environ Mol Mutagen* (2019) 60(8):668–82.

19. Tajima S, Suetake I, Takeshita K, Nakagawa A, Kimura H. Domain structure of the Dnmt1, Dnmt3a, and Dnmt3b DNA methyltransferases. *Adv Exp Med Biol* (2016) 945:63–86. doi: 10.1007/978-3-319-43624-1_4

20. Shock LS, Thakkar PV, Peterson EJ, Moran RG, Taylor SM. DNA Methyltransferase 1, cytosine methylation, and cytosine hydroxymethylation in mammalian mitochondria. *Proc Natl Acad Sci U S A* (2011) 108(9):3630–5. doi: 10.1073/pnas.1012311108

21. Dou X, Boyd-Kirkup JD, McDermott J, Zhang X, Li F, Rong B, et al. The strand-biased mitochondrial DNA methylome and its regulation by DNMT3A. *Genome Res* (2019) 29(10):1622–34. doi: 10.1101/gr.234021.117

22. Patil V, Cuenin C, Chung F, Aguilera JRR, Fernandez-Jimenez N, Romero-Garmendia I, et al. Human mitochondrial DNA is extensively methylated in a non-CpG context. *Nucleic Acids Res* (2019) 47(19):10072–85. doi: 10.1093/nar/gkz762

23. Menga A, Palmieri EM, Cianciulli A, Infantino V, Mazzone M, Scilimati A, et al. SLC25A26 overexpression impairs cell function *via* mtDNA hypermethylation and rewiring of methyl metabolism. *FEBS J* (2017) 284(6):967–84. doi: 10.1111/febs.14028

24. Sabatier R, Finetti P, Cervera N, Lambaudie E, Esterni B, Mamessier E, et al. A gene expression signature identifies two prognostic subgroups of basal breast cancer. *Breast Cancer Res Treat* (2011) 126(2):407–20. doi: 10.1007/s10549-010-0897-9

25. Tokura M, Nakayama J, Prieto-Vila M, Shiino S, Yoshida M, Yamamoto T, et al. Single-cell transcriptome profiling reveals intratumoral heterogeneity and molecular features of ductal carcinoma in situ. *Cancer Res* (2022) 82(18):3236–48. doi: 10.1158/0008-5472

26. Cao K, Lv W, Wang X, Dong S, Liu X, Yang T, et al. Hypermethylation of hepatic mitochondrial ND6 provokes systemic insulin resistance. *Adv Sci (Weinh)* (2021) 8(11):2004507. doi: 10.1002/advs.202004507

27. Hao Z, Wu T, Cui X, Zhu P, Tan C, Dou X, et al. N6 -deoxyadenosine methylation in mammalian mitochondrial DNA. *Mol Cell* (2020) 78(3):382–395.e8. doi: 10.1016/j.molcel.2020.02.018

28. Hänzelmann S, Castelo R, Guinney J. GSVA: gene set variation analysis for microarray and RNA-seq data. *BMC Bioinf* (2013) 14:7. doi: 10.1186/1471-2105-14-7

29. Gao R, Bai S, Henderson YC, Lin Y, Schalck A, Yan Y, et al. Delineating copy number and clonal substructure in human tumors from single-cell transcriptomes. *Nat Biotechnol* (2021) 39(5):599–608. doi: 10.1038/s41587-020-00795-2

30. Zeng D, Ye Z, Shen R, Yu G, Wu J, Xiong Y, et al. IOBR: multi-omics immuno-oncology biological research to decode tumor microenvironment and signatures. *Front Immunol* (2021) 12:687975. doi: 10.3389/fimmu.2021.687975

31. Mayakonda A, Lin DC, Assenov Y, Plass C, Koeffler HP. Maftools: efficient and comprehensive analysis of somatic variants in cancer. *Genome Res* (2018) 28(11):1747–56. doi: 10.1101/gr.239244.118

32. Li L, Feng Q, Wang X. PreMSIm: an r package for predicting microsatellite instability from the expression profiling of a gene panel in cancer. *Comput Struct Biotechnol J* (2020) 18:668–75. doi: 10.1016/j.csbj.2020.03.007

33. Wu SZ, Al-Eryani G, Roden DL, Junankar S, Harvey K, Andersson A, et al. A single-cell and spatially resolved atlas of human breast cancers. *Nat Genet* (2021) 53 (9):1334–47. doi: 10.1038/s41588-021-00911-1

34. Jin S, Guerrero-Juarez CF, Zhang L, Chang I, Ramos R, Kuan CH, et al. Inference and analysis of cell-cell communication using CellChat. *Nat Commun* (2021) 12(1):1088. doi: 10.1038/s41467-021-21246-9

35. Luen SJ, Asher R, Lee CK, Savas P, Kammler R, Dell'Orto P, et al. Association of somatic driver alterations with prognosis in postmenopausal, hormone receptor-positive, HER2-negative early breast cancer: a secondary analysis of the BIG 1-98 randomized clinical trial. *JAMA Oncol* (2018) 4(10):1335–43. doi: 10.1001/jamaoncol.2018.1778

36. Wang X, Yang K, Wu Q, Kim LJY, Morton AR, Gimple RC, et al. Targeting pyrimidine synthesis accentuates molecular therapy response in glioblastoma stem cells. *Sci Transl Med* (2019) 11(504):eaau4972. doi: 10.1126/scitranslmed.aau4972

37. Harmon C, O'Farrelly C, Robinson MW. The immune consequences of lactate in the tumor microenvironment. *Adv Exp Med Biol* (2020) 1259:113–24. doi: 10.1007/978-3-030-43093-1_7

38. Huang Z, Gan J, Long Z, Guo G, Shi X, Wang C, et al. Targeted delivery of let-7b to reprogramme tumor-associated macrophages and tumor infiltrating dendritic cells for tumor rejection. *Biomaterials* (2016) 90:72–84. doi: 10.1016/j.biomaterials.2016.03.009

39. Marcus L, Lemery SJ, Keegan P, Pazdur R. FDA Approval summary: pembrolizumab for the treatment of microsatellite instability-high solid tumors. *Clin Cancer Res* (2019) 25(13):3753–8. doi: 10.1158/1078-0432.CCR-18-4070

40. Subbiah V, Solit DB, Chan TA, Kurzrock R. The FDA approval of pembrolizumab for adult and pediatric patients with tumor mutational burden (TMB) ≥10: a decision centered on empowering patients and their physicians. *Ann Oncol* (2020) 31(9):1115–8. doi: 10.1016/j.annonc.2020.07.002

41. McGrail DJ, Pilié PG, Rashid NU, Voorwerk L, Slagter M, Kok M, et al. High tumor mutation burden fails to predict immune checkpoint blockade response across all cancer types. *Ann Oncol* (2021) 32(5):661–72. doi: 10.1016/j.annonc.2021.02.006

42. Zhu Y, Zhu X, Tang C, Guan X, Zhang W. Progress and challenges of immunotherapy in triple-negative breast cancer. *Biochim Biophys Acta Rev Cancer* (2021) 1876(2):188593. doi: 10.1016/j.bbcan.2021.188593

43. Loibl S, Untch M, Burchardi N, Huober J, Sinn BV, Blohmer JU, et al. A randomised phase II study investigating durvalumab in addition to an anthracycline taxane-based neoadjuvant therapy in early triple-negative breast cancer: clinical results and biomarker analysis of GeparNuevo study. *Ann Oncol* (2019) 30(8):1279–88. doi: 10.1093/annonc/mdz158

44. Riaz N, Havel JJ, Makarov V, Desrichard A, Urba WJ, Sims JS, et al. Tumor and microenvironment evolution during immunotherapy with nivolumab. *cell* (2017) 171 (4):934–949.e16. doi: 10.1016/j.cell.2017.09.028

45. Sakuishi K, Apetoh L, Sullivan JM, Blazar BR, Kuchroo VK, Anderson AC. Targeting Tim-3 and PD-1 pathways to reverse T cell exhaustion and restore anti. *J Exp Med* (2010) 207(10):2187–94. doi: 10.1084/jem.20100643

46. Wischhusen J, Melero I, Fridman WH. Growth/Differentiation factor-15 (GDF-15): from biomarker to novel targetable immune checkpoint. *Front Immunol* (2020) 11:951. doi: 10.3389/fimmu.2020.00951

47. Wang Z, He L, Li W, Xu C, Zhang J, Wang D, et al. GDF15 induces immunosuppression *via* CD48 on regulatory T cells in hepatocellular carcinoma. GDF15 induces immunosuppression *via* CD48 on regulatory T cells in hepatocellular carcinoma. *J Immunother Cancer* (2021) 9(9):e002787. doi: 10.1136/jitc-2021-002787

48. Liu X, Hu G, Ye J, Ye B, Shen N, Tao Y, et al. *De novo* ARID1B mutations cause growth delay associated with aberrant wnt/β-catenin signaling. *Hum Mutat* (2020) 41 (5):1012–24. doi: 10.1002/humu.23990

49. Helming KC, Wang X, Wilson BG, Vazquez F, Haswell JR, Manchester HE, et al. ARID1B is a specific vulnerability in ARID1A-mutant cancers. *Nat Med* (2014) 20 (3):251–4. doi: 10.1038/nm.3480

50. Shi H, Tao T, Abraham BJ, Durbin AD, Zimmerman MW, Kadoch C, et al. ARID1A loss in neuroblastoma promotes the adrenergic-to-mesenchymal transition by regulating enhancer-mediated gene expression. *Sci Adv* (2020) 6(29):eaaz3440. doi: 10.1126/sciadv.aaz3440

51. Joung J, Kirchgatterer PC, Singh A, Cho JH, Nety SP, Larson RC, et al. CRISPR activation screen identifies BCL-2 proteins and B3GNT2 as drivers of cancer resistance to T cell-mediated cytotoxicity. *Nat Commun* (2022) 13(1):1606. doi: 10.1038/s41467-022-29205-8

52. Granneman S, Gallagher JE, Vogelzangs J, Horstman W, van Venrooij WJ, Baserga SJ, et al. The human Imp3 and Imp4 proteins form a ternary complex with hMpp10, which only interacts with the U3 snoRNA in 60-80S ribonucleoprotein complexes. *Nucleic Acids Res* (2003) 31(7):1877–87. doi: 10.1093/nar/gkg300

53. Pelletier J, Thomas G, Volarević S. Ribosome biogenesis in cancer: new players and therapeutic avenues. *Nat Rev Cancer* (2018) 18(1):51–63. doi: 10.1038/nrc.2017.104

54. Gan Y, Deng J, Hao Q, Huang Y, Han T, Xu JG, et al. UTP11 deficiency suppresses cancer development *via* nucleolar stress and ferroptosis. *Redox Biol* (2023) 62:102705. doi: 10.1016/j.redox.2023.102705

55. Stenmark H. Rab GTPases as coordinators of vesicle traffic. *Nat Rev Mol Cell Biol* (2009) 10(8):513–25. doi: 10.1038/nrm2728

56. Kawasaki N, Isogaya K, Dan S, Yamori T, Takano H, Yao R, et al. TUFT1 interacts with RABGAP1 and regulates mTORC1 signaling. *Cell Discovery* (2018) 4:1. doi: 10.1038/s41421-017-0001-2

57. Huang J, Chen J, Huang Q. The profile analysis of circular RNAs in cervical cancer. *Med (Baltimore)* (2021) 100(39):e27404. doi: 10.1097/MD.0000000000027404

58. Zheng J, Ge P, Liu X, Wei J, Wu G, Li X. MiR-136 inhibits gastric cancer-specific peritoneal metastasis by targeting HOXC10. *Tumour Biol* (2017) 39 (6):1010428317706207. doi: 10.1177/1010428317706207

59. Cifola I, Pietrelli A, Consolandi C, Severgnini M, Mangano E, Russo V, et al. Comprehensive genomic characterization of cutaneous malignant melanoma cell lines derived from metastatic lesions by whole-exome sequencing and SNP array profiling. *PloS One* (2013) 8(5):e63597. doi: 10.1371/journal.pone.0063597

60. Robinson TJ, Freedman JA, Al Abo M, Deveaux AE, LaCroix B, Patierno BM, et al. Alternative RNA splicing as a potential major source of untapped molecular targets in precision oncology and cancer disparities. *Clin Cancer Res* (2019) 25 (10):2963–8. doi: 10.1158/1078-0432.CCR-18-2445

61. Hanson RJ, Sun J, Willis DG, Marzluff WF. Efficient extraction and partial purification of the polyribosome-associated stem-loop binding protein bound to the 3' end of histone mRNA. *Biochemistry* (1996) 35(7):2146–56. doi: 10.1021/bi9521856

62. Marzluff WF, Wagner EJ, Duronio RJ. Metabolism and regulation of canonical histone mRNAs: life without a poly(A) tail. *Nat Rev Genet* (2008) 9(11):843–54. doi: 10.1038/nrg2438

63. Zhao X, McKillop-Smith S, Müller B. The human histone gene expression regulator HBP/SLBP is required for histone and DNA synthesis, cell cycle progression and cell proliferation in mitotic cells. *J Cell Sci* (2004) 117(Pt 25):6043-51. doi: 10.1242/jcs.01523

64. Li S, Jia H, Zhang Z, Wu D. DRAIC promotes growth of breast cancer by sponging miR-432-5p to upregulate SLBP. *Cancer Gene Ther* (2022) 29(7):951–60. doi: 10.1038/s41417-021-00388-4

65. Portela M, Segura-Collar B, Argudo I, Sáiz A, Gargini R, Sánchez-Gómez P, et al. Oncogenic dependence of glioma cells on kish/TMEM167A regulation of vesicular trafficking. *Glia* (2019) 67(2):404–17. doi: 10.1002/glia.23551

66. Bond KH, Sims-Lucas S, Oxburgh L. Targets for renal carcinoma growth control identified by screening FOXD1 cell proliferation pathways. *Cancers (Basel)* (2022) 14 (16):3958. doi: 10.3390/cancers14163958

67. Yinsheng Z, Miyoshi K, Qin Y, Fujiwara Y, Yoshimura T, Katayama T. TMEM67 is required for the gating function of the transition zone that controls entry of membrane-associated proteins ARL13B and INPP5E into primary cilia. *Biochem Biophys Res Commun* (2022) 636(Pt 1):162–9. doi: 10.1016/j.bbrc.2022.10.078

68. He J, McLaughlin RP, van der Beek L, Canisius S, Wessels L, Smid M, et al. Integrative analysis of genomic amplification-dependent expression and loss-of-function screen identifies ASAP1 as a driver gene in triple-negative breast cancer progression. *Oncogene* (2020) 39(20):4118–31. doi: 10.1038/s41388-020-1279-3

69. Murphy SM, Preble AM, Patel UK, O'Connell KL, Dias DP, Moritz M, et al. GCP5 and GCP6: two new members of the human gamma-tubulin complex. *Mol Biol Cell* (2001) 12(11):3340–52. doi: 10.1091/mbc.12.11.3340

70. Dong X, He X, Guan A, Huang W, Jia H, Huang Y, et al. Long non-coding RNA hotair promotes gastric cancer progression *via* miR-217-GPC5 axis. *Life Sci* (2019) 217:271–82. doi: 10.1016/j.lfs.2018.12.024

71. Ono T, Losada A, Hirano M, Myers MP, Neuwald AF, Hirano T. Differential contributions of condensin I and condensin II to mitotic chromosome architecture in vertebrate cells. *Cell* (2003) 115(1):109–21. doi: 10.1016/s0092-8674(03)00724-4

72. Jing Z, Liu Q, He X, Jia Z, Xu Z, Yang B, et al. NCAPD3 enhances warburg effect through c-myc and E2F1 and promotes the occurrence and progression of colorectal cancer. *J Exp Clin Cancer Res* (2022) 41(1):198. doi: 10.1186/s13046-022-02412-3

73. Jing Z, Liu Q, Xie W, Wei Y, Liu J, Zhang Y, et al. NCAPD3 promotes prostate cancer progression by upregulating EZH2 and MALAT1 through STAT3 and E2F1. *Cell Signal* (2022) 92:110265. doi: 10.1016/j.cellsig.2022.110265

74. Deutschman E, Ward JR, Kumar A, Ray G, Welch N, Lemieux ME, et al. Condensin II protein dysfunction impacts mitochondrial respiration and mitochondrial oxidative stress responses. *J Cell Sci* (2019) 132(22):jcs233783. doi: 10.1242/jcs.233783

75. Bai RK, Chang J, Yeh KT, Lou MA, Lu JF, Tan DJ, et al. Mitochondrial DNA content varies with pathological characteristics of breast cancer. *J Oncol* (2011) 2011:496189. doi: 10.1155/2011/496189

76. Fan AX, Radpour R, Haghighi MM, Kohler C, Xia P, Hahn S, et al. Mitochondrial DNA content in paired normal and cancerous breast tissue samples from patients with breast cancer. *J Cancer Res Clin Oncol* (2009) 135(8):983–9. doi: 10.1007/s00432-008-0533-9

77. Weerts MJ, Sieuwerts AM, Smid M, Look MP, Foekens JA, Sleijfer S, et al. Mitochondrial DNA content in breast cancer: impact on *in vitro* and *in vivo* phenotype and patient prognosis. *oncotarget* (2016) 7(20):29166–76. doi: 10.18632/oncotarget.8688

78. Iacobazzi V, Castegna A, Infantino V, Andria G. Mitochondrial DNA methylation as a next-generation biomarker and diagnostic tool. *Mol Genet Metab* (2013) 110(1-2):25–34. doi: 10.1016/j.ymgme.2013.07.012

frontiers | Frontiers in Oncology

TYPE Original Research
PUBLISHED 29 June 2023
DOI 10.3389/fonc.2023.1218808

OPEN ACCESS

EDITED BY
Chao Liu,
Shandong Cancer Hospital, China

REVIEWED BY
Qinyong Hu,
Renmin Hospital of Wuhan University, China
Cong Wang,
Shandong Cancer Hospital and Institute, China

*CORRESPONDENCE
Ying Yang
gfyangying@sina.com
Meilan Chen
18257968343@139.com
Pan Chen
lychenpan@126.com

†These authors have contributed equally to this work

RECEIVED 08 May 2023
ACCEPTED 09 June 2023
PUBLISHED 29 June 2023

CITATION
Lv H, Lou S, Zhang L, Cui D, Li Y, Yang Y, Chen M and Chen P (2023) Evaluation of the impacts of photodynamic therapy on the prognosis of patients with hrHPV infection based on BTNL8 expression. *Front. Oncol.* 13:1218808. doi: 10.3389/fonc.2023.1218808

Evaluation of the impacts of photodynamic therapy on the prognosis of patients with hrHPV infection based on BTNL8 expression

Hongqing Lv[1†], Shuai Lou[1†], Lin Zhang[1], Dawei Cui[1], Yao Li[1], Ying Yang[1*], Meilan Chen[2*] and Pan Chen[1*]

[1]Department of Gynecology, Jinhua Municipal Central Hospital, Jinhua, Zhejiang, China, [2]Department of Gynecology, Jinhua Maternal and Child Health Hospital, Jinhua, Zhejiang, China

Objective: The aim of this study was to evaluate the prognostic value of Butyrophilin-like protein 8 (BTNL8) expression in high-risk HPV (hrHPV) infection treated with photodynamic therapy.

Methods: A total of 93 patients with hrHPV infection were enrolled as research study subjects, along with 69 healthy women who served as controls. Serum samples were obtained from each participant, and BTNL8 levels were quantified. The patients were divided into high- and low-expression groups (n = 45 and n = 48, respectively), and both groups underwent photodynamic therapy. We recorded the following data: BTNL8 expression pre-treatment and at 3/6 months post-treatment, HPV negative conversion ratio, regression rate of low-grade squamous intraepithelial lesions (LSIL), incidence of adverse reactions, complication rate, serum inflammatory factors, persistence of HPV positivity, LSIL residue or recurrence, and incidence of high-grade cervical intraepithelial lesions (HCIL).

Results: Patients with HPV infection exhibited higher BTNL8 expression than healthy individuals. Compared to the low-expression group, the high-expression group showed increased HPV negative conversion ratios, LSIL regression rates, and levels of IL-17 and IL-23. This group also demonstrated decreased total complication rate, HPV positivity persistence, LSIL residue or recurrence, and IL-10 levels. Additionally, there was no significant difference between the two groups in terms of the number of adverse reactions and cases with LSIL residue/recurrence.

Conclusion: Serum BTNL8 expression may serve as a valuable tool for early screening and prognosis monitoring of patients with hrHPV infection.

KEYWORDS

high-risk HPV infection, photodynamic therapy, BTNL8, prognosis evaluation, HPV

1 Introduction

Cervical cancer (CC) is the fourth most commonly diagnosed cancer in women. In 2020, approximately 604,127 new cases were reported globally, accounting for 3.1% of all cancer diagnoses, making it the ninth most common type of cancer (1). China, in particular, faces a significant challenge due to its high incidence rate. As per recent statistics, 106,000 confirmed cases of CC and 48,000 related deaths were reported in China in 2018 (2). Notably, high-risk human papillomavirus (hrHPV) infection is associated with up to 90% of all CC cases.

HPV, a small double-stranded DNA virus, circumvents the host's innate immunity and integrates its genome into the host cell (3). When hrHPV infection persists, it causes its structural oncoproteins E6 and E7 to contribute to the inactivation of the tumor suppressor proteins p53 and pRB, thereby disrupting the normal functioning of DNA repair and apoptosis and triggering abnormal proliferation of normal cervical epithelial squamous cells, known as cervical intraepithelial neoplasia (CIN) (4–6). If left untreated, unresolved CIN1 will continue to progress into high-grade squamous intraepithelial lesions (HSIL), with massive genomic alterations that induce CC occurrence (7).

The treatment options for hrHPV infection include circumcision, cryotherapy, conization, therapeutic vaccine, and photodynamic therapy (8). Traditional treatment methods, which mainly encompass circumcision, cryotherapy, and conization, present some shortcomings, such as high recurrence rate, serious tissue damage, and potential structural destruction of cervical if improperly applied (9). Photodynamic therapy, a novel cancer treatment modality, involves the activation of photosensitive molecules by lasers of a specific wavelength. The activated photosensitive molecules prompt the production of reactive oxygen species (ROS) leading to irreversible cell apoptosis and necrosis, and consequently inhibiting the proliferation and invasion of cancer cells (10, 11). Photodynamic therapy offers advantages in fostering good tissue healing and the convenient utilization of light (12). Cang et al. (13) pointed out the potential of photodynamic therapy to effectively eliminate hrHPV infection, particularly HPV16 and HPV18. Gu et al. (14) propose that 5-aminolevulinic acid-mediated photodynamic therapy, an effective treatment for hrHPV infection co-occurring with cervical squamous intraepithelial lesions, is less likely to cause cervical injury. Therefore, photodynamic therapy emerges as a promising, effective therapy for hrHPV infection.

During the course of hrHPV infection, genes such as p16 and galectin-3 may demonstrate aberrant expression, which could serve as biomarkers of HPV infection for early screening for cervical lesions (15, 16). Thus, incorporating gene expression into the prognostic evaluation of hrHPV infections can facilitate dynamic detection post-therapy and expedite the investigation and treatment of recurrent cases. Butyrophilin-like protein 8 (BTNL8) is implicated in adaptive immune process and thus serves as a crucial regulatory factor of tumor immunity (17–19). Yang et al. (20) observed a significant correlation of BTNL8 expression with patients' survival rate according to the relatively low survival rate in CC patients with high BTNL8 expression (<40%) and the over 60% of survival rate in CC patients with low expression. The results suggest BTNL8 as one possible biomarker for the prognosis of CC and its potential for postoperative evaluation of hrHPV infection.

As of now, the potential evaluative significance of BTNL8 in HPV infection has not been reported. Therefore, this study aims to assess the clinical efficacy and postoperative recurrence of photodynamic therapy in hrHPV infection through the lens of BTNL8, hoping to provide a reliable basis for the clinical dynamic monitoring of hrHPV infection.

2 Methods

2.1 General data

A total of 93 women diagnosed with hrHPV infection at Jinhua Central Hospital from January 2020 to March 2022 were included in this study. The inclusion criteria were as follows: patients confirmed with hrHPV infection according to the PCR method (21) and cervical cytology (22), patients with detailed clinical data, patients not in pregnancy and lactation period, and those who were willing to participate in the research. The exclusion criteria were as follows: patients who had received HPV infection therapy; patients who had received immunosuppressive agents or glucocorticoids recently; patients with comorbid CC or other malignant tumors of the reproductive system; patients with comorbid dysfunction of the heart, lung, liver, or kidney; patients with comorbid mental disorder; and those allergic to photodynamic therapy. A total of 69 healthy women were enrolled as controls. All participants of the study offered signed informed consent forms after understanding the whole process of the study, and approval was obtained for the study from the ethics committee of our hospital.

2.2 Photodynamic therapy

5-Aminolevulinic acid-mediated photodynamic therapy was adopted for treating patients with hrHPV infection in this study. Specifically, each patient was given photodynamic therapy at 7 days after the menstrual period. Before therapy, the patient was required to empty his/her bladder to avoid interference. Start with a surface shave, the lesions were cleaned *via* normal saline and then given ultra-expensive disinfection, followed by even application of 20% 5-aminolevulinic acid (Shanghai Fudan-Zhangjiang Bio-Pharmaceutical Co., Ltd, 118 mg/piece) with cotton swabs (23). After 3 h, the lesions were irradiated with a Y-HN300 He-Ne laser therapy machine (Wuhan Yage Laser Equipment Co., Ltd.) (output wavelength: 632.8 nm; rated power: 300 mW) at 20 min each time, once every 7 days, for four consecutive treatments, and the observation course was 6 months.

2.3 Outcome measures

(1) Clinical efficacy: Patients are asked to visit the hospital for regular follow-up at 3 months and 6 months after surgery.

The negative convention of HPV and inversion of low-grade squamous intraepithelial lesions (LSIL) in patients at 3 months and 6 months after surgery were recorded. The LSIL residue/recurrence of LSIL lesions (the cervicovaginal part and the cervicovaginal part + cervical canal) at 6 months after surgery was evaluated and recorded.

(2) Serum BTNL8 expression: Serum was sampled from each patient with hrHPV infection before admission, and serum was also acquired from healthy women as controls. Serum was sampled from every patient before therapy and at 3 and 6 months after therapy. All blood specimens were acquired on an empty stomach. Total RNA of sampled serum was acquired *via* a plasma/serum RNA extraction kit (NORGEN, Canada), followed by fluorescent quantitation *via* a qPCR instrument. The design and synthesis of BTNL8 primers were completed by Shanghai Sangon Biotech Co., Ltd. The $2^{-\Delta\Delta Ct}$ method was adopted for standardizing the gene expression.

(3) Serum inflammatory factor levels: Serum inflammatory factors were quantified *via* ELISA kits of IL-17 (ab100556), IL-23 (ab221837), and IL-10 (ab185986) (Abcam, Shanghai) at 3 months after surgery.

(4) Adverse reactions and complications: The adverse reactions and complications of patients within 3 months after surgery were recorded. Adverse reactions included colporrhagia, menstrual abdominal pain, and colpitis. Postoperative complications included bleeding, infection, menstrual disorder, prolonged menstrual period, and cervical duct adhesion.

(5) Prognostic indexes: Prognostic indexes at 6 months after surgery were recorded, including persistence in positive HPV, LSIL residue/recurrence, and progression to high-grade cervical intraepithelial lesions (HCIL).

2.4 Statistical analyses

This study adopted SPSS 20.0 for statistical analyses of data. Counting data were presented by *n* (%), and measurement data were presented by mean ± SD, all of which were analyzed *via* the normality test. The independent-samples *t*-test was utilized for inter-group comparison and the chi-square test was used for inter-group comparison of counting data, and the repeated measures analysis of variance was used for intra-group comparison. 95% CI was adopted. $p < 0.05$ implies a notable difference.

3 Results

3.1 Aberrant serum BTNL8 expression in cases with hrHPV infection

A total of 93 patients with hrHPV infection and 69 healthy women were enrolled, and compared in serum BTNL8 expression (Figure 1). The patients showed notably downregulated serum BTNL8 than the healthy women ($p < 0.05$). In contract to serum BTNL8 expression before therapy, the HPV infection group showed notably up-regulated BTNL8 expression at 3 and 6 months after photodynamic therapy ($p < 0.05$). ROC curves revealed the potential value of serum BTNL8 in screening hrHPV infection (AUC = 0.835, $p < 0.05$).

3.2 Correlation of serum BTNL8 expression with clinical efficacy of photodynamic therapy for HPV infection

Patients were assigned to the high- and low-expression groups (n = 45 and 48, respectively) based on the median relative expression level of serum BTNL8 obtained prior to admission (1.02). The relative expression levels of BTNL8 in the two groups were 1.11 ± 0.06 and 0.93 ± 0.08, respectively. The former group consisted of patients at 35.69 ± 6.73 years old, with a course of disease of 15.76 ± 5.20 months and body mass index (BMI) of 20.72 ± 1.76 kg/m^2, including 33 cases of cervicovaginal attacks and 12 cases of attacks in the cervicovaginal part + cervical canal. The latter group consisted of patients at 36.24 ± 6.20 years old, with a course

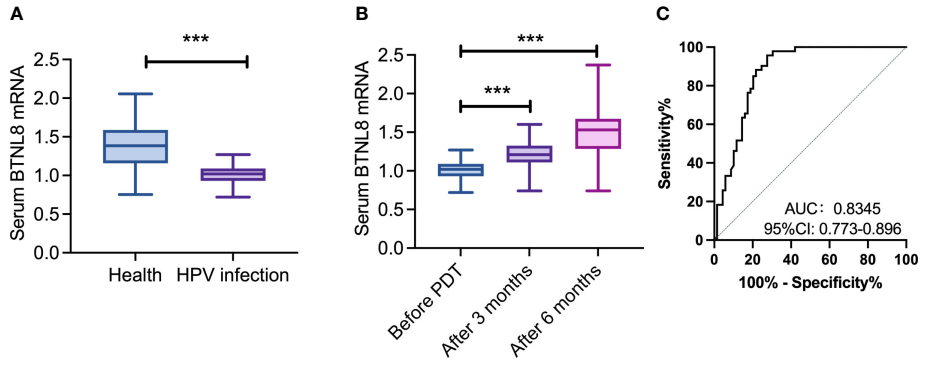

FIGURE 1
Aberrant serum BTNL8 expression in cases with hrHPV infection. **(A)** Comparison of serum BTNL8 expression levels between patients and healthy women. **(B)** Comparison of serum BTNL8 expression between patients after photodynamic therapy 3 months and before. **(C)** Comparison of serum BTNL8 expression levels between patients before and after photodynamic therapy for 6 months. *** vs. $p < 0.001$.

of disease of 13.84 ± 4.54 months and a body mass index (BMI) of 20.99 ± 1.70 kg/m^2, including 37 cases of cervicovaginal attacks and 11 cases of attacks in the cervicovaginal part + cervical canal. The two groups were similar in general data (Table 1).

The clinical efficacy at 3 and 6 months after photodynamic therapy were counted (Tables 2, 3). At 3 and 6 months after therapy, the high-expression group presented notably higher negative conversion ratio of HPV and inversion rate of LISL than the other (both $p < 0.05$). The quantification results of serum inflammatory factors in postoperative patients revealed notably higher IL-17 and IL-23 levels and a notably lower IL-10 level in the high-expression group than in the other group (all $p < 0.04$, Figure 2).

3.3 Associations of serum BTNL8 expression with postoperative adverse reactions and complications

The postoperative adverse reactions (colporrhagia, menstrual abdominal pain, and colpitis) and complications in patients were counted. The low-expression group presented a total incidence of adverse reactions of 10.42%, with two cases of colporrhagia, two cases of menstrual abdominal pain, and one case of colpitis, while the other group presented a total incidence of adverse reactions of 9.76%, with two cases of colporrhagia, one case of menstrual abdominal pain, and one case of colpitis (Figure 3). The two groups were similar in the incidence of adverse reactions ($p > 0.05$).

The associations of serum BTNL8 with postoperative complications (bleeding, infection, menstrual disorder, prolonged menstrual period, and cervical duct adhesion) were analyzed (Table 4). The low-expression group presented a total incidence of complications of 29.17%, with one case of bleeding, two cases of infection, four cases of menstrual disorder, five cases of prolonged menstruation, and two cases of cervical duct adhesion, while the other group presented a total incidence of complications of 11.11%, with one case of bleeding, one case of infection, two cases of menstrual disorder, no case of prolonged menstruation, and one case of cervical duct adhesion. The latter group presented a notably lower incidence than the former group.

3.4 Association of serum BTNL8 with postoperative survival outcome

The associations of BTNL8 expression with persistence in positive HPV, LSIL residue/recurrence, and HCIL were analyzed, and the results revealed 4 cases of persistent positive HPV (8.89%), 6 cases of LSIL residue/recurrence (12.50%), and 0 cases of progression to HCIL in the high-expression group and 12 cases of persistent positive HPV (25.00%), 15 cases of LSIL residue/recurrence (31.25%), and 0 cases of progression to HCIL in the other group (Table 5). The two groups were notably different in persistence in positive HPV and LSIL residue/recurrence (both $p < 0.05$).

The associations of BTNL8 expression with residual/recurrent sites of LSIL were also analyzed, and the results revealed two cases in the cervicovaginal part (4.44%) and four cases in the cervical part (8.89%) in the high-expression group, and six cases in the cervicovaginal part (12.50%) and nine cases in the cervicovaginal part + cervical canal (18.75%) in the other group (Table 6). The two groups were similar in the incidence rate in the cervicovaginal part and cervicovaginal part + cervical canal ($p > 0.05$).

4 Discussion

Screening for hrHPV infection is a crucial link to prevent CC. At the current stage, hrHPV infection is mainly detected *via* membrane liquid-based ultrathin cytology, HPV-DNA detection, and colposcopy biopsy. With features of convenient and simple operation, serum marker-based detection can be adopted as one auxiliary means of the above methods, which is helpful for postoperative dynamic monitoring of patients. Troja et al. (24) believe a strong association of serum vitamin D with hrHPV infection. BTNL8 has been verified to be bound up with the survival of CC (20). Thus, we adopted it for evaluating clinical significance of photodynamic therapy for hrHPV infection. Our results imply the positive role of serum BTNL8 for the evaluation.

Firstly, we found downregulated BTNL8 in serum samples of patients with hrHPV infection and the induction of photodynamic therapy to BTNL8 expression, which may be attributed to the regulatory influence of BTNL8 on the immune system. In principle, photodynamic therapy triggers DNA damage,

TABLE 1 General data.

	High-expression group (n = 45)	Low-expression group (n = 48)	χ^2/t	p
Age (years)	35.69 ± 6.73	36.24 ± 6.20	0.421	0.675
Course of disease (months)	15.76 ± 5.20	13.84 ± 4.54	1.851	0.067
Body mass index (kg m^{-2}	20.72 ± 1.76	20.99 ± 1.70	0.764	0.447
Lesion site			0.176	0.675
Cervicovaginal part	33 (73.33)	37 (77.08)		
Cervicovaginal part + cervical canal	12 (26.67)	11 (22.92)		

10.3389/fonc.2023.1218808

TABLE 2 Association of BTNL8 expression with negative conversion ratio of HPV.

	At 3 months after treatment	At 6 months after treatment
High-expression group (n = 45)	35 (77.78)	37 (82.22)
Low-expression group (n = 48)	28 (58.33)	30 (62.50)
χ^2	4.019	4.485
p-value	0.045	0.034

TABLE 3 Association of BTNL8 expression with inversion of LSIL.

	At 3 months after treatment	At 6 months after treatment
High-expression group (n = 45)	34 (75.56)	36 (80.00)
Low-expression group (n = 48)	26 (54.17)	27 (56.25)
χ^2	4.641	5.995
p-value	0.031	0.014

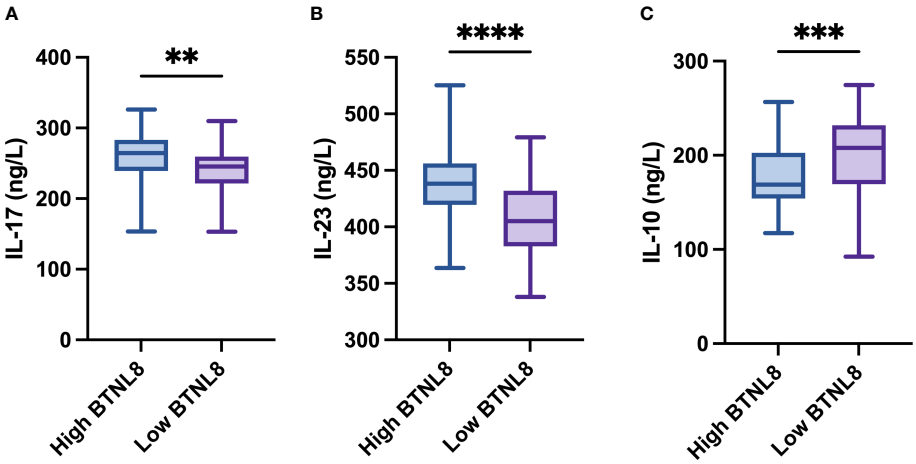

FIGURE 2
Comparison of BTNL8 expression with postoperative serum inflammatory factors. Comparison of BTNL8 expression with postoperative serum **(A)** IL-17 levels; **(B)** IL-23; **(C)** IL-10 levels. ** vs. $p < 0.01$; *** vs. $p < 0.001$; **** vs. $p < 0.0001$.

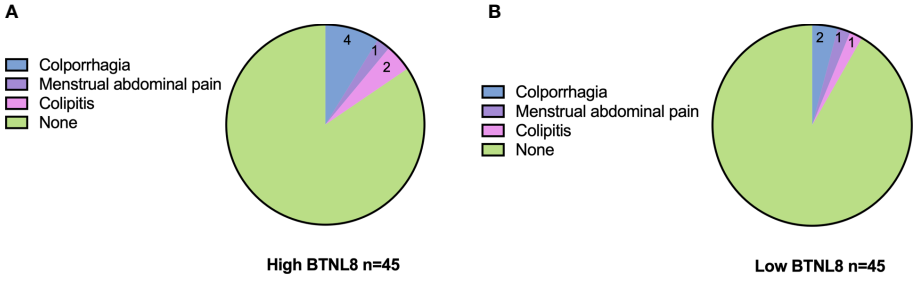

FIGURE 3
Associations of serum BTNL8 expression with postoperative adverse reactions. Distribution of postoperative adverse effects in patients in the **(A)** high BTNL8 expression group versus those in the **(B)** low BTNL8 expression group.

TABLE 4 Association of BTNL8 expression with postoperative complications.

	Bleeding	Infection	Menstrual disorder	Prolonged menstruation	Cervical duct adhesion	Total incidence of complications
High-expression group (n = 45)	1 (2.22)	1 (2.22)	2 (4.44)	0	1 (2.22)	5 (11.11)
Low-expression group (n = 48)	1 (2.08)	2 (4.17)	4 (8.33)	5 (10.42)	2 (4.17)	14 (29.17)
χ^2						4.658
p-value						0.031

TABLE 5 Association of serum BTNL8 with postoperative survival outcome.

	Persistent HPV positive	LSIL residue/recurrence	Progression to HCIL
High-expression group (n = 45)	4(8.89)	6 (12.50)	0
Low-expression group (n = 48)	12 (25.00)	15 (31.25)	0
χ^2	4.232	4.265	–
p-value	0.040	0.039	–

apoptosis, and necrosis through the production of ROS, during which it also stimulates a series of immune responses to clear cells (25, 26). BTNL8 happens to be one crucial factor associated with immune system, which mediates the dependent selection of T-cell receptors such as Vγ4+/Vδ1+ intraepithelial lymphocytes and γδT cells (27, 28). Thus, under the influence of photodynamic therapy on immune response in the tumor microenvironment, BTNL8 expression changes and acts as a key factor to regulate the proliferation of associated immune cells, which is probably the reason for the increase of BTNL8 under photodynamic forces. Furthermore, the high efficacy accompanied by high BTNL8 expression and the association of the high expression with serum inflammatory factors also verify the possible involvement of BTNL8 in the immune mechanism under photodynamic therapy for hrHPV infection. The specific function of BTNL8 will be discussed in future research. According to ROC-based analysis, BTNL8 facilitates distinguishing hrHPV infection. The results imply that serum BTNL8 is promising in the triage and management of HPV-positive patients to lower unnecessary colposcopy referrals and other related injuries (29).

In our investigation, we did not discern a significant correlation between BTNL8 expression and the occurrence of postoperative adverse events. However, the limited sample size of our study might obscure more nuanced impacts, potentially introducing selection bias and limiting the validity of these findings. In future investigations, we plan to enlarge our sample size, which will enable a more comprehensive and reliable analysis of the potential association between BTNL8 expression and postoperative adverse reactions in the context of hrHPV infection. Interestingly, our data pointed towards an inverse relationship between BTNL8 expression and complication incidence. Recurrence symptoms following photodynamic therapy in hrHPV-infected patients can manifest as persistent HPV positivity, residual or recurrent LSIL, or progression to HCIL (30–33).

Within our study cohort, no patients advanced to HCIL post-photodynamic therapy. Nonetheless, a higher BTNL8 expression was associated with significantly reduced instances of LSIL recurrence and persistent HPV positivity. It should be noted that we have not accounted for potential confounding factors that could impact BTNL8 expression within this study. Furthermore, we did not identify a correlation between serum BTNL8 expression and the location of LSIL residue or recurrence. This suggests that while serum BTNL8 levels may serve as an indicator of residual or recurrent LSIL, it does not appear to facilitate identification of the specific site of these conditions. This aspect warrants further exploration in future research.

To sum up, this study suggests the associations of serum BTNL8 expression with the clinical efficacy, complications, persistent

TABLE 6 Association of serum BTNL8 with LSIL residue/recurrence.

	Cervicovaginal part	Cervicovaginal part + cervical canal
High-expression group (n = 45)	2(4.44)	4 (8.89)
Low-expression group (n = 48)	6 (12.50)	9 (18.75)
χ^2	1.917	1.878
p	0.166	0.171

positive HPV, and LSIL residue/recurrence in the therapy of HPV infection by photodynamic therapy, which is helpful to dynamically monitor the prognosis of patients, timely screen patients with recurrence risk, and potentially facilitate biomarker-based triage and management of HPV-positive patients.

Data availability statement

The original contributions presented in the study are included in the article/supplementary material. Further inquiries can be directed to the corresponding authors.

Ethics statement

The studies involving human participants were reviewed and approved by Ethics Committee of Jinhua Central Hospital. The patients/participants provided their written informed consent to participate in this study.

Author contributions

HL, SL, and LZ contributed to conception and design of the study. HL organized the data. DC performed the statistical analysis. YL wrote the first draft of the manuscript. YY, MC, and PC wrote sections of the manuscript. All authors contributed to the article and approved the submitted version.

Funding

This work was supported by Jinhua Municipal Science and Technology Project, approval number: No. 2020-4-019.

Conflict of interest

The authors declare that the research was conducted in the absence of any commercial or financial relationships that could be construed as a potential conflict of interest.

Publisher's note

References

1. Arbyn M, Weiderpass E, Bruni L, de Sanjosé S, Saraiya M, Ferlay J, et al. Estimates of incidence and mortality of cervical cancer in 2018: a worldwide analysis. *Lancet Global Health* (2020) 8(2):e191–203. doi: 10.1016/S2214-109X(19)30482-6

2. Sung H, Ferlay J, Siegel RL, Laversanne M, Soerjomataram I, Jemal A, et al. Global cancer statistics 2020: GLOBOCAN estimates of incidence and mortality worldwide for 36 cancers in 185 countries. *CA: Cancer J Clin* (2021) 71(3):209–49. doi: 10.3322/caac.21660

3. de Sanjose S, Brotons M, Pavon MA. The natural history of human papillomavirus infection. *Best Pract Res Clin Obstetr Gynaecol* (2018) 47:2–13. doi: 10.1016/j.bpobgyn.2017.08.015

4. Balasubramaniam SD, Balakrishnan V, Oon CE, Kaur G. Key molecular events in cervical cancer development. *Med (Kaunas)* (2019) 55(7):384. doi: 10.3390/medicina55070384

5. Liu C, Zhang M, Yan X, Ni Y, Gong Y, Wang C, et al. Single-cell dissection of cellular and molecular features underlying human cervical squamous cell carcinoma initiation and progression. *Sci Adv* (2023) 9(4):eadd8977. doi: 10.1126/sciadv.add8977

6. Moscicki A-B, Schiffman M, Burchell A, Albero G, Giuliano AR, Goodman MT, et al. Updating the natural history of human papillomavirus and anogenital cancers. *Vaccine* (2012) 30:F24–33. doi: 10.1016/j.vaccine.2012.05.089

7. Schiffman M, Castle PE, Jeronimo J, Rodriguez AC, Wacholder S. Human papillomavirus and cervical cancer. *Lancet* (2007) 370(9590):890–907. doi: 10.1016/S0140-6736(07)61416-0

8. Hoffman SR, Le T, Lockhart A, Sanusi A, Dal Santo L, Davis M, et al. Patterns of persistent HPV infection after treatment for cervical intraepithelial neoplasia (CIN): a systematic review. *Int J Cancer* (2017) 141(1):8–23. doi: 10.1002/ijc.30623

9. Wittmaack A, Dudley D, Boyle A. Maternal history of cervical surgery and preterm delivery: a retrospective cohort study. *J Women's Health* (2019) 28(11):1538–42. doi: 10.1089/jwh.2018.7457

10. Raizada K, Naik M. Photodynamic therapy for the eye. In *StatPearls* (StatPearls Publishing) (2020).

11. Donohoe C, Senge MO, Arnaut LG, Gomes-da-Silva LC. Cell death in photodynamic therapy: from oxidative stress to anti-tumor immunity. *Biochimica et biophysica Acta. Reviews on cancer* (2019) 1872(2):188308. doi: 10.1016/j.bbcan.2019.07.003

12. Dobson J, de Queiroz GF, Golding JP. Photodynamic therapy and diagnosis: principles and comparative aspects. *Vet J* (2018) 233:8–18. doi: 10.1016/j.tvjl.2017.11.012

13. Cang W, Gu L, Hong Z, Wu A, Di W, Qiu L. Effectiveness of photodynamic therapy with 5-aminolevulinic acid on HPV clearance in women without cervical lesions. *Photodiagnosis Photodyn Ther* (2021) 34:102293. doi: 10.1016/j.pdpdt.2021.102293

14. Gu L, Cheng M, Hong Z, Di W, Qiu L. The effect of local photodynamic therapy with 5-aminolevulinic acid for the treatment of cervical low-grade squamous intraepithelial lesions with high-risk HPV infection: a retrospective study. *Photodiagnosis Photodyn Ther* (2021) 33:102172. doi: 10.1016/j.pdpdt.2020.102172

15. Kumar R, Mandal S, Arora P, Mala Y, Khurana N. The expression of p16 and galectin-3 in cervical intraepithelial neoplasia (CIN) and squamous cell carcinoma (SCC) uterine cervix. *J Obstetr Gynaecol* (2021) 41(5):785–90. doi: 10.1080/01443615.2020.1803235

16. Curty G, Menezes AN, Brant AC, de Mulder Rougvie M, Moreira MÂM, Soares MA. Expression of retroelements in cervical cancer and their interplay with HPV infection and host gene expression. *Cancers* (2021) 13(14):3513. doi: 10.3390/cancers13143513

17. Riquelme P, Hutchinson JA. Novel molecules mediate specialized functions of human regulatory macrophages. *Curr Opin Organ Transplant* (2018) 23(5):533–7. doi: 10.1097/MOT.0000000000000560

18. Blazquez J-L, Benyamine A, Pasero C, Olive D. New insights into the regulation of γδ T cells by BTN3A and other BTN/BTNL in tumor immunity. *Front Immunol* (2018) 9:1601. doi: 10.3389/fimmu.2018.01601

19. Chapoval AI, Smithson G, Brunick L, Mesri M, Boldog FL, Andrew D, et al. BTNL8, a butyrophilin-like molecule that costimulates the primary immune response. *Mol Immunol* (2013) 56(4):819–28. doi: 10.1016/j.molimm.2013.08.003

20. Yang L, Yang Y, Meng M, Wang W, He S, Zhao Y, et al. Identification of prognosis-related genes in the cervical cancer immune microenvironment. *Gene* (2021) 766:145119. doi: 10.1016/j.gene.2020.145119

21. Zeng Z, Yang H, Li Z, He X, Griffith CC, Chen X, et al. Prevalence and genotype distribution of HPV infection in China: analysis of 51,345 HPV genotyping results from china's largest CAP certified laboratory. *J Cancer* (2016) 7(9):1037–43. doi: 10.7150/jca.14971

22. Wang J, Tang D, Wang J, Zhang Z, Chen Y, Wang K, et al. Genotype distribution and prevalence of human papillomavirus among women with cervical cytological abnormalities in xinjiang, China. *Hum Vaccines Immunotherapeutics* (2019) 15(7-8):1889–96. doi: 10.1080/21645515.2019.1578598

23. Zhao S, Liu D, Shi W, Kang Y, Li Q, Liu Q, et al. Efficacy of a new therapeutic option for vulvar intraepithelial neoplasia: superficial shaving combined with photodynamic therapy. *Lasers Surg Med* (2020) 52(6):488–95. doi: 10.1002/lsm.23185

24. Troja C, Hoofnagle AN, Szpiro A, Stern JE, Lin J, Winer RL. Serum concentrations of emerging vitamin d biomarkers and detection of prevalent high-risk HPV infection in mid-adult women. *Cancer Epidemiol Biomarkers Prev* (2020) 29 (7):1468–74. doi: 10.1158/1055-9965.EPI-20-0126

25. Doix B, Trempolec N, Riant O, Feron O. Low photosensitizer dose and early radiotherapy enhance antitumor immune response of photodynamic therapy-based dendritic cell vaccination. *Front Oncol* (2019) 9:811. doi: 10.3389/fonc.2019.00811

26. Hou Y-j, Yang X-x, Liu R-q, Zhao D, Guo C-x, Zhu A-c, et al. Pathological mechanism of photodynamic therapy and photothermal therapy based on nanoparticles. *Int J Nanomed* (2020) 15:6827–38. doi: 10.2147/IJN.S269321

27. Vantourout P, Laing A, Woodward MJ, Zlatareva I, Apolonia L, Jones AW, et al. Heteromeric interactions regulate butyrophilin (BTN) and BTN-like molecules governing γδ T cell biology. *Proc Natl Acad Sci* (2018) 115(5):1039–44. doi: 10.1073/pnas.1701237115

28. Mayassi T, Ladell K, Gudjonson H, McLaren JE, Shaw DG, Tran MT, et al. Chronic inflammation permanently reshapes tissue-resident immunity in celiac disease. *Cell* (2019) 176(5):967–81. e19. doi: 10.1016/j.cell.2018.12.039

29. Clarke MA, Cheung LC, Castle PE, Schiffman M, Tokugawa D, Poitras N, et al. Five-year risk of cervical precancer following p16/Ki-67 dual-stain triage of HPV-positive women. *JAMA Oncol* (2019) 5(2):181–6. doi: 10.1001/jamaoncol.2018.4270

30. Pandey D, Solleti V, Jain G, Das A, Shama Prasada K, Acharya S, et al. Human papillomavirus (HPV) infection in early pregnancy: prevalence and implications. *Infect Dis Obstetr Gynecol* (2019) 2019:4376902. doi: 10.1155/2019/4376902

31. Abdulaziz AM, You X, Liu L, Sun Y, Zhang J, Sun S, et al. Management of high-grade squamous intraepithelial lesion patients with positive margin after LEEP conization: a retrospective study. *Medicine* (2021) 100(20):e26030. doi: 10.1097/MD.0000000000026030

32. Chen J-y, Wang Z-l, Wang Z-y, Yang X-s. The risk factors of residual lesions and recurrence of the high-grade cervical intraepithelial lesions (HSIL) patients with positive-margin after conization. *Medicine* (2018) 97(41):e12792. doi: 10.1097/MD.0000000000012792

33. Lee H, Lee EJ. HPV infection and p16 promoter methylation as predictors of ASC-US/LSIL progression. *Cancer Cytopathol* (2016) 124(1):58–65. doi: 10.1002/cncy.21615

frontiers | Frontiers in Oncology

TYPE Case Report
PUBLISHED 04 July 2023
DOI 10.3389/fonc.2023.1198765

OPEN ACCESS

EDITED BY
Chao Liu,
Shandong Cancer Hospital, China

REVIEWED BY
Bo Tian,
Shanghai University, China
Shihao Hu,
Janssen Pharmaceuticals, Inc.,
United States
Yuting Liu,
Akoya Biosciences, Inc., United States

*CORRESPONDENCE
Yufang Zuo
yufangzuo0102@163.com
Yuzhou Wang
yuzhouwang17@126.com
Sihai Liao
liaosihai163@163.com

†These authors share first authorship

RECEIVED 06 April 2023
ACCEPTED 01 June 2023
PUBLISHED 04 July 2023

CITATION
Yang J, Chen X, Li X, Liu W, Liao S, Wang Y and Zuo Y (2023) Case Report: Clinical application of immunotherapy-based combination regimen in primary osteosarcoma of the uterus.
Front. Oncol. 13:1198765.
doi: 10.3389/fonc.2023.1198765

Case Report: Clinical application of immunotherapy-based combination regimen in primary osteosarcoma of the uterus

Jing Yang[1†], Xiaowen Chen[1†], Xiaofang Li[2], Wenci Liu[3], Sihai Liao[1*], Yuzhou Wang[1*] and Yufang Zuo[1*]

[1]Department of Gynecological Oncology, Cancer Center, Affiliated Hospital of Guangdong Medical University, Zhanjiang, China, [2]Department of Pathology, Affiliated Hospital of Guangdong Medical University, Zhanjiang, China, [3]Department of Imaging, Affiliated Hospital of Guangdong Medical University, Zhanjiang, China

Primary osteosarcoma of the uterus is an extremely rare pure heterologous sarcoma of the uterus. The relevant available information is limited to case reports. To date, only 31 cases of this type of cancer have been reported. Here, we report the first clinical experience with the administration of an immunotherapy-based combination regimen for multiple metastatic primary osteosarcomas of the uterus. The patient had undergone multiple treatments prior to this regimen, but her condition continued to progress. However, after 3 cycles of immunotherapy combined with targeted therapy and chemotherapy, a review showed that the disease was stable and even in partial remission. The patient has a good quality of life, and long-term survival is expected.

KEYWORDS

sarcomas, osteosarcoma, immunotherapy, targeted therapy, chemotherapy

Introduction

Uterine sarcomas are unusual, accounting for less than 1% of all gynecologic tumors and 3-7% of all uterine tumors. Uterine sarcomas can be classified as homologous (composed of intrinsic uterine components) or heterologous (composed of foreign components such as cartilage and bone). Most uterine sarcomas are homologous, and heterologous uterine osteosarcomas are extremely rare (1). The majority of heterologous uterine tumors are classified as malignant mixed mullerian tumors (MMMTs). Heterologous MMMTs include carcinomas, heterologous sarcomas, and usually homologous mesenchymal components, such as those in leiomyosarcomas or stromal sarcomas. Most uterine sarcomas have been identified as rhabdomyosarcomas or chondrosarcomas, and heterogenous sarcomas have rarely been reported to produce bone and osteophytes (2). In general, the clinical course of osteosarcoma of the uterus is short, probably because it is difficult to detect a pelvic mass until symptoms appear. In addition, osteosarcoma of the uterus has an unusually malignant nature compared to osteosarcomas of other sites (3). The average age of the previously reported patients was 64

years. The majority of patients were perimenopausal or postmenopausal at the time of diagnosis (4). Due to the rarity of primary uterine osteosarcoma, there are currently no effective treatment options for this disease. In recent years, with the rise of immunotherapy and targeted therapy, we have tried to use immunotherapy combined with targeted therapy and chemotherapy to treat this disease. Herein, we report a case of primary uterine osteosarcoma and review the available literature.

Case report

A 60-year-old female patient presented to a local hospital in February 2021 with irregular vaginal bleeding. At the first visit, vaginal ultrasound showed a heterogeneous hypoechoic mass in the pelvic cavity, with a size of 9.0×7.4 cm. The results of other tests were unknown. An extensive total hysterectomy was subsequently performed.

The postoperative pathological diagnosis was a malignant mesenchymal tumor of the uterus, and the morphology was consistent with a malignant giant cell tumor, accompanied by a large amount of bleeding and necrosis. There was no tumor cell involvement in the bilateral adnexa. No metastasis was found in the lymph nodes examined.

Initial staining showed that the tumor was positive for EMA, CylinD1, Vim, SMA, and CD10, while it was negative for PAX8, ER, PR and S100. Keratin staining did not support the diagnosis of carcinosarcoma, which exhibits neither cartilage formation nor cancerous components. Ultimately, the pathological diagnosis was consistent with high-grade uterine sarcoma with heterologous differentiation (osteosarcoma).

According to the National Comprehensive Cancer Network (NCCN) guidelines for uterine sarcoma, the patient was treated with epirubicin combined with ifosfamide. After 2 cycles of chemotherapy, abdominal magnetic resonance imaging (MRI) showed that the pelvic lesions were smaller than before. Subsequently, chemotherapy was continued for 4 cycles according to the original regimen. A total dosage of 6000 rads of volumetric intensity-modulated radiation therapy was delivered to the pelvic region. Two months later, the patient found a palpable mass of approximately 6.0×6.0 cm in the surgical scar in the lower abdominal wall. Positron emission tomography/computed tomography (PET/CT) showed multiple metastases in the anterior abdominal wall incision, omentum, pelvic mesentery and lungs. After tumor progression, the patient was treated with gemcitabine and docetaxel combined with bevacizumab. After 2 cycles of treatment, abdominal MRI showed that the original mass was significantly larger than before, at approximately 9.7×9.0 cm in size. At that time, the patient was advised to undergo palliative tumor reduction surgery. One month later, preoperative examination was performed, and abdominal CT showed liver metastasis. Considering the risk of surgery and complications, the patient refused to undergo surgical treatment.

For further treatment, the patient visited our hospital. Abdominal CT showed large metastases in the anterior abdominal wall and multiple metastases in the liver (Figures 1A, I). Chest CT showed multiple metastatic tumors in both lungs (Figure 1E). Treatment with tislelizumab and anlotinib was then considered. After 3 cycles of treatment, chest CT showed that the metastatic tumors in both lungs had increased in size, and disease progression was considered. Therefore, paclitaxel injection was added to the original treatment regimen. After 2 cycles of treatment, chest CT and abdominal MRI showed that the metastatic tumors in both lungs, anterior abdominal wall mass and liver metastases were larger than before (Figures 1B, F, J). As the disease progressed, the patient gradually developed abdominal pain and bloating.

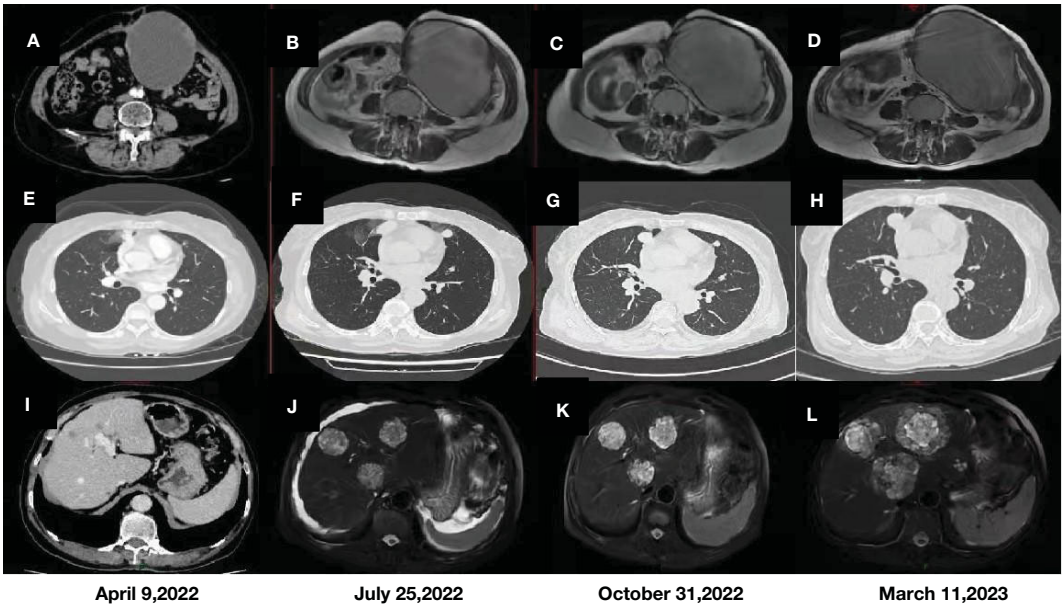

FIGURE 1
CT and MRI images of the anterior abdominal wall mass **(A, B)** and liver metastases **(I, J)** before immunotherapy. MRI images of the anterior abdominal wall mass **(C, D)** and liver metastases **(K, L)** after immunotherapy. Comparison of CT images of metastatic tumors in both lungs before **(E, F)** and after immunotherapy **(G, H)**.

Given the advantages of current immunotherapy, we tested the patient for programmed cell death-1 (PD-1) and programmed cell death-ligand 1 (PD-L1), but the results were negative (tumor cell (TC) <1%). Eventually, however, we changed the treatment to tislelizumab, liposomal doxorubicin and lenvatinib. After three cycles of treatment, reexamination by abdominal MRI showed no significant changes in the anterior abdominal wall mass and liver metastases (Figures 1C, K), but chest CT showed that multiple metastases in both lungs were smaller than before (Figure 1G). In addition, the patient's abdominal pain and bloating symptoms were significantly less than before. Reexamination after 3 cycles of treatment indicated that some of the lung lesions were smaller and some were larger than before (Figure 1H), and the anterior abdominal wall masses were the same as before (Figure 1D), but the liver metastases were significantly larger (Figure 1L). On March 20, 2023, transhepatic arterial chemoembolization and puncture biopsy of the liver mass were performed. The pathological findings after puncture biopsy showed necrotic tissue in some areas, a few heterotrophic cells in some tissues, and pathological mitosis, which were considered to indicate a malignant tumor. Immunohistochemical and genetic analyses were not available because of the small amount of tissue collected. Although the patient's condition progressed with the previous treatment regimen, her disease was moderately controlled through immunotherapy combined with chemotherapy and targeted therapy, and her survival was expected to be prolonged.

Discussion

Primary osteosarcoma of the uterus is distinctly rare, and the detailed mechanism of its carcinogenic process remains unclear (5). The available literature contains little information on its relative incidence, clinical behavior, and treatment outcomes (4). A review of the available literature (Table 1) showed that the previously reported patients ranged in age from 41 to 82 years, and all but 3 patients were perimenopausal or menopausal at the time of diagnosis. The clinical manifestations of most patients were vaginal bleeding and abdominal pain (1–19). In our case, the patient presented with vaginal bleeding in the early stage and mainly abdominal distension in the later stage.

Microscopically, uterine malignancy was associated with extensive necrosis, neoplastic osteogenesis in most areas, diffuse

TABLE 1 Primary uterine osteosarcoma literature review.

Author	Age	Symptoms	Extension of tumor, size	Treatment	Prognosis
Stier and Lyman (1936) (4)	53	Lower abdominal pain,12 months	Uterus and omentum,6cm	Subtotal hysterectomy, BSO	Died at 2 months (recurrence and pulmonary metastasis)
Bickel et al. (1956) (4)	73	Vaginal bleeding,3 months	Uterus	Intracavitary radium,TAH	Died at 20 months (osseous metastasis)
Scheffey et al. (1956) (4)	67	Abdominal discomfort,vaginal bleeding,3 months	Uterus with intraoperative rupture, 4 cm	TAH,BSO	Died at 6 months with spread to abdominal wall
Radman and Korman (1960) (4)	60	Vaginal bleeding, 3-4 weeks	Uterus	TAH,BSO	Died soon after discharge
Carleton and Williamson (1961) (4)	82	Vaginal bleeding and discharge, 8 months	Uterus, extending to base of the bladder, metastasizing to lungs (autopsy)	Intracavitary radium	Died at 8 months (lung metastases at autopsy)
Amromin and Gildenhorn (1962) (4)	72	Vaginal bleeding, weight loss	Uterus, peritoneum, small bowel,40cm	Intracavitary radium	Died at 2 months (intraabdominal metastases)
Karpas and Merendino (1964) (4)	62	Vaginal bleeding	Uterus, small bowel, bladder,8cm	TAH,BSO	Lost to follow-up
Crum et al. (1980) (2)	41	Vaginal bleeding, 1 month	Uterine cervix, 9cm	TAH, BSO, RT, CHT	Alive at 4 months
Vakiani et al. (1982) (4)	53	Vaginal bleeding	Uterus, 13 cm	TAH, BSO, CHT	Alive at 1 year
Piscioli et al. (1985) (6)	56	Vaginal bleeding	Uterus, 12 cm	TAH, BSO, RT	Died at 37 months (lung metastases)
Jotkowitz and Valentine (1985) (7)	51	Backache, abdominal pain, weight loss	Uterus, pelvis, omentum, peritoneum	None	Died at 20 days
Basolo et al. (1988) (4)	60	Abdominal pain, vaginal bleeding	Uterus	Radical Wertheim hysterectomy	Lost to follow-up
Caputo et al. (1990) (8)	58	Vaginal bleeding	Uterus, urinary bladder, rectum, uterine cervix, vagina (autopsy), 18 cm	None	Died at 2 weeks (regional lymph nodes, liver and lung metastases at autopsy)

(Continued)

TABLE 1 Continued

Author	Age	Symptoms	Extension of tumor, size	Treatment	Prognosis
De Young et al. (1992) (9)	63	Uterine bleeding	Uterus, 7 cm	TAH, BSO	Died at 20 days after surgery due to myocardial infarction
Emoto et al. (1994) (10)	67	Abdominal pain	Uterus; lung metastases, 16 cm	TAH, BSO	Died at 4 months (local recurrence and distant metastases)
Akiba et al. (1994) (11)	73	NA	Uterus,10cm	TAH, BSO	Alive at 20 months; lung metastases
Hardisson et al. (2001) (4)	41	Vaginal bleeding	Uterus, 8 cm	TAH, BSO, CHT, RT	Alive at 8 months; tumor recurrence
Su et al. (2002) (3)	62	Abdominal pain	Uterus, 20 cm	Biopsy of mass	Died at 4 months (Lung, thyroid, and Peritoneum metastases)
Lin et al. (2002) (12)	67	Lower abdominal pain for a month	Uterus, peritoneum	OMT, CHT	Alive at 6 months
Kostopoulou et al. (2002) (13)	56	abdominal distention and lower abdominal pain	Uterus, the right adnexum and the cecum	TAH, BSO	Died at 6 months
Ribeiro-Silva et al. (2004) (14)	60	abdominal pain, 2 years	Uterus	hysterectomy	NA
Wang et al. (2011) (15)	53	Vaginal bleeding	Uterus, 8 cm	RH,OMT,CHT	Died at 5 months
Kefeli et al. (2012) (15)	53	Vaginal bleeding	Uterus, 19 cm	TAH, BSO	NA
Powell et al. (2014) (16)	60	Vaginal bleeding	Uterus, 12 cm	TAH, BSO	Died at 7 months (local recurrence and lung metastases)
Abraham et al. (2015) (1)	47	Abdominal pain, vaginal bleeding, early satiety, chronic cough	Uterus, 14 cm	TAH, BSO, CHT	Died at 6 months (cardiac and lung metastases)
Tsukasaki et al. (2016) (15)	57	Abdominal pain	Uterus, 12 cm	TAH, BSO, appendectomy,CHT	Alive at 13 months (local recurrence and lung metastases)
Zheng et al. (2019) (5)	74	postmenopausal bleeding, bloating, and weight loss	Uterus	TAH, BSO,CHT, palliative radiation therapy	Died at 7 months with multiple distant metastases
Yang et al. (2020) (17)	50	None	Uterus, 12cm	TAH, BSO, CHT	Died at 8 months (lung and brain metastases)
Effah et al. (2021) (18)	60	postmenopausal bleeding, weight loss	Uterus	TAH, BSO	Died at 14 months after surgery
Effah et al. (2021) (18)	42	lower abdominal pain	Uterus,sigmoid colon, the upper rectum	TAH, BSO,resection of the sigmoid colon and upper rectum with the construction of colostomy, radiotherapy	Died at 4 months after surgery
Ruhotina et al. (2022) (19)	57	Abdominal pain	Uterus, 15cm	TAH, BSO, CHT	Alive at 12 months (Peritoneal metastasis)
This case	60	Vaginal bleeding	Uterus, 9 cm	Extensive total hysterectomy, CHT, RT, antiangiogenic therapy, targeted therapy, immunotherapy	Alive at 25 months (multiple distant metastases)

TAH, total abdominal hysterectomy; BSO, bilateral salpingo-oophorectomy; CHT, chemotherapy; RT, external radiotherapy; RH, radical hysterectomy; OMT, omentectomy; NA, not available/reported.

distribution of giant cells, local spindle-shaped tumor cells, rich red cytoplasm, severe nuclear atypia, and clear mitosis (Figure 2). According to the description published by Piscioli et al., primary uterine osteosarcoma must meet the following three criteria: exclusion of a primary source of bone, presence of neoplastic osteoids, and absence of epithelial components and other specific homologous or heterologous components after confirmation of the presence of sufficient tissue samples (1, 6). Accordingly, the histological findings of this patient fully met the above criteria.

This tumor is highly aggressive with a poor prognosis, and the mean survival time is 8.1 months (15). As shown in the Table 1, hysterectomy was performed in 24 patients, and bilateral salpingo-oophorectomy was also performed in 21 of these patients. Seven patients were treated with radiation therapy, including luminal radium therapy and external radiation therapy. Eleven patients received chemotherapy. The table shows that even after a combination of surgery, radiotherapy and chemotherapy, the treatment outcome is still unsatisfactory. Survival ranged from 2 weeks to 20 months, except for one patient who had survived for 37 months. In comparison, our patient has now survived for 25 months, and the survival time is expected to be extended. The results of tracking indicate that this cancer has a high probability of recurrence and distant metastasis, as well as a mortality rate. Regardless of treatment, most patients develop local or pulmonary metastases early after surgery and die within one year of starting treatment (15). Due to the rarity of uterine osteosarcoma, there is currently no standard for treatment. In this patient, previous first- and second-line treatments for uterine sarcoma failed. Her third-line therapy was challenging, and we referred to the NCCN guidelines for soft tissue sarcoma to recommend the application of pembrolizumab in third-line therapy (20). Due to the patient's financial situation, we chose domestic tislelizumab as an alternative. Moreover, because our hospital only has SP263 antibody to detect the expression of PD-L1, although the result showed TC < 1%, this result may not necessarily reflect the real immune microenvironment of the patient. Sarcomas are cold tumors, and the effect of immunotherapy alone is poor. Existing studies have shown that the immune microenvironment can be changed by using targeted drugs to turn cold tumors into hot tumors (21, 22), and anlotinib is recommended in the domestic guidelines for soft tissue sarcoma (23); thus, we chose tislelizumab in combination with anlotinib. However, after treatment with this regimen, the patient's disease progressed. We reviewed the NCCN guidelines for endometrial cancer and found that lenvatinib in combination with pembrolizumab has been approved for advanced endometrial cancer with pMMR (24). Therefore, we replaced anlotinib with lenvatinib. Considering the poor effect of tislelizumab in combination with anlotinib in the treatment of this patient, we referred to the NCCN guidelines for uterine sarcoma and added liposomal doxorubicin (25). As a combined result of the above analysis, we chose a regimen of lenvatinib in combination with tislelizumab and liposomal doxorubicin to treat this patient. As a result, the patient's condition remained stable, with no obvious adverse reactions, and the symptoms of abdominal pain and abdominal distension were relieved. The patient has survived for nearly 25 months since treatment began and is in good condition (Figure 3). This is the first clinical experience with using a combination regimen based on immunotherapy to treat this disease. This treatment regimen may serve as a new option for controlling this tumor.

Since this study is a case report, there are not sufficient data to support the efficacy of this treatment regimen. As the incidence of primary uterine osteosarcoma is extremely low, there are few

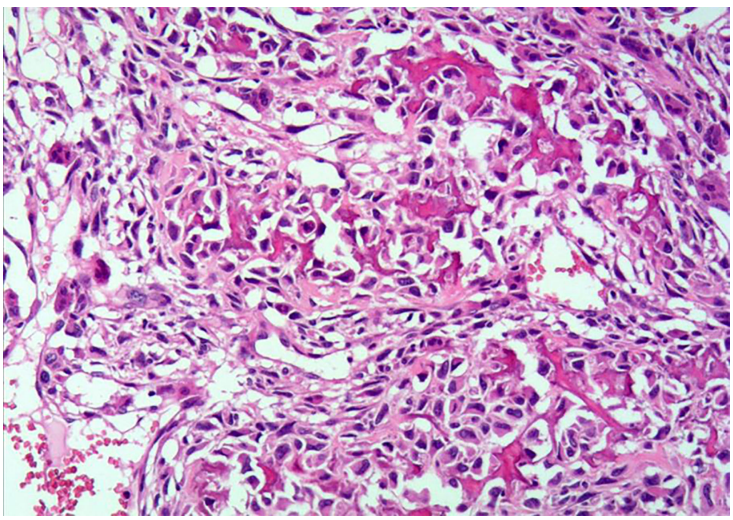

FIGURE 2
Hematoxylin and eosin staining of primary uterine osteosarcoma tissue sample (under 200× magnification).

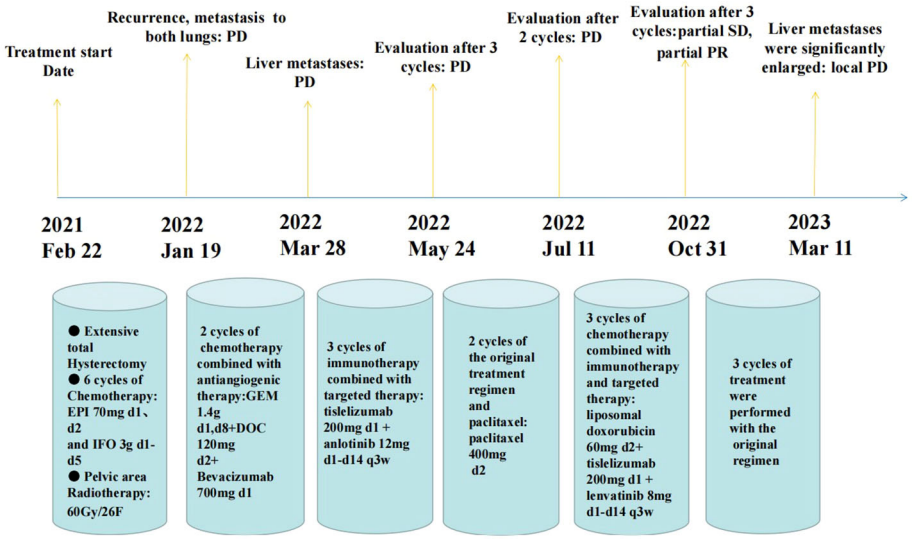

FIGURE 3
A nearly 25-month treatment history of the patient with primary uterine osteosarcoma. (PD, progressive disease; SD, stable disease; PR, partial remission).

relevant studies, all of which are case reports. There are not enough patients to conduct a large randomized controlled clinical trial, which is a limitation for the future treatment of this tumor. For this rare disease, a global multicenter collaboration is needed to conduct analyses of larger cohorts.

Data availability statement

The original contributions presented in the study are included in the article/supplementary material. Further inquiries can be directed to the corresponding authors.

Ethics statement

Written informed consent was obtained from the individual(s) for the publication of any potentially identifiable images or data included in this article.

Author contributions

Data collection and article writing: JY, XC. Pathological picture analysis: XL. Image analysis: WL. Clinical data analysis: SL, YW. Subject design and article revision: YZ. All authors contributed to the article and approved the submitted version.

Funding

This study was supported by Medical Research Foundation of Guangdong Province (No. B2021114), Guangdong Medical College Doctoral Initiation Program (XB1228) and Natural Science Foundation of Guangdong province (No.2014A020212299).

Conflict of interest

The authors declare that the research was conducted in the absence of any commercial or financial relationships that could be construed as a potential conflict of interest.

Publisher's note

References

1. Abraham C, O'Cearbhaill R, Soslow R. Primary osteosarcoma of the uterus with cardiac and pulmonary metastases. *Gynecol Oncol Rep* (2015) 11:4–6. doi: 10.1016/j.gore.2014.07.002

2. Crum CP, Rogers BH, Andersen W. Osteosarcoma of the uterus: case report and review of the literature. *Gynecol Oncol* (1980) 9:256–68. doi: 10.1016/0090-8258(80)90036-0

3. Su M, Tokairin T, Nishikawa Y, Yoshioka T, Takahashi O, Watanabe H, et al. Primary osteosarcoma of the uterine corpus: case report and review of the literature. *Pathol Int* (2002) 52:158–63. doi: 10.1046/j.1440-1827.2002.01325.x

4. Hardisson D, Simón RS, Burgos E. Primary osteosarcoma of the uterine corpus: report of a case with immunohistochemical and ultrastructural study. *Gynecol Oncol* (2001) 82:181–6. doi: 10.1006/gyno.2001.6262

5. Zheng G, Richmond A, Liu C, Berrebi A, Pallavajjala A, Haley L, et al. Clinicopathologic features and genetic alterations of a primary osteosarcoma of the uterine corpus. *Int J Gynecol Pathol* (2019) 38:414–9. doi: 10.1097/PGP.0000000000000511

6. Piscioli F, Govoni E, Polla E, Pusiol T, Dalri P, Antolini M. Primary osteosarcoma of the uterine corpus. report of a case and critical review of the literature. *Int J Gynecol Obstet* (1985) 23:377–85. doi: 10.1016/0020-7292(85)90146-8

7. Jotkowitz MW, Valentine R. A rare pelvic mass: osteosarcoma of the body of the uterus. *Aust N Z J Obstet Gynaecol* (1985) 25:132–6. doi: 10.1111/j.1479-828X.1985.tb00627.x

8. Caputo MG, Reuter KL, Reale F. Primary osteosarcoma of the uterus. *Br J Radiol* (1990) 63:578–80. doi: 10.1259/0007-1285-63-751-578

9. De Young B, Bitterman P, Lack EE. Primary osteosarcoma of the uterus: report of a case with immunohistochemical study. *Mod Pathol Off J U S Can Acad Pathol Inc* (1992) 5:212–5.

10. Emoto M, Iwasaki H, Kawarabayashi T, Egami D, Yoshitake H, Kikuchi M, et al. Primary osteosarcoma of the uterus: report of a case with immunohistochemical analysis. *Gynecol Oncol* (1994) 54:385–8. doi: 10.1006/gyno.1994.1229

11. Akiba T, Ujiie H, Takasaki N, Ohki T, Kurihara H, Endo Y, et al. Endobronchial metastasis from a primary uterine osteosarcoma in a patient with multiple myeloma: report of a case. *Surg Today* (1994) 24:179–82. doi: 10.1007/BF02473406

12. Lin J-W, Ko S-F, Ng S-H, Eng H-L, Changchien C-C. Primary osteosarcoma of the uterus with peritoneal osteosarcomatosis: CT features. *Br J Radiol* (2002) 75 (897):772–4. doi: 10.1259/bjr.75.897.750772

13. Kostopoulou E, Dragoumis K, Zafrakas M, Myronidou Z, Agelidou S, Bontis I. Primary osteosarcoma of the uterus with immunohistochemical study: case report. *Acta Obstet Gynecol Scand* (2002) 81:678–80. doi: 10.1034/j.1600-0412.2002.810716.x

14. Ribeiro-Silva A, Ximenes L. Pathologic quiz case: a 60-Year-Old woman with diffuse uterine enlargement. *Arch Pathol Lab Med* (2004) 128:e172–4. doi: 10.5858/2004-128-e172-PQCAYW

15. Tsukasaki N, Mori T, Yasukawa S, Konishi E, Kokabu T, Kitawaki J. Primary osteosarcoma of the uterine corpus: a case report: osteosarcoma arising from the uterus. *J Obstet Gynaecol Res* (2016) 42:1604–8. doi: 10.1111/jog.13079

16. Powell G, Barth L, Todd R, Ganesan R. Primary uterine osteosarcoma presenting synchronously with bilateral breast carcinomas. *Case Rep* (2014) 2014: bcr2013201502–bcr2013201502. doi: 10.1136/bcr-2013-201502

17. Yang VS, Lim JQ, Tay TKY, Selvarajan S, Ng CC-Y, Farid M, et al. Clinicopathologic features and whole genome sequencing of a primary osteosarcoma of the uterus. *J Immunother Precis Oncol* (2020) 3:90–5. doi: 10.36401/JIPO-19-34

18. Effah K, Hiadzi E, Osabutey A, K. Boateng A, B. Akosa A, T. Anim J. Primary osteosarcoma of the uterus: a report of two cases. *Ghana Med J* (2021) 55:232–5. doi: 10.4314/gmj.v55i3.10

19. Ruhotina M, Kukla J, Wilcox A, Murphy C, Menderes G. Primary uterine osteosarcoma arising in a leiomyoma with rapid local recurrence: a case report. *Gynecol Oncol Rep* (2022) 44:101102. doi: 10.1016/j.gore.2022.101102

20. von Mehren M, Kane JM, Agulnik M, Bui MM, Carr-Ascher J, Choy E, et al. Soft tissue sarcoma, version 2.2022, NCCN clinical practice guidelines in oncology. *J Natl Compr Cancer Netw JNCCN* (2022) 20:815–33. doi: 10.6004/jnccn.2022.0035

21. Galon J, Bruni D. Approaches to treat immune hot, altered and cold tumours with combination immunotherapies. *Nat Rev Drug Discovery* (2019) 18:197–218. doi: 10.1038/s41573-018-0007-y

22. Zhang J, Huang D, Saw PE, Song E. Turning cold tumors hot: from molecular mechanisms to clinical applications. *Trends Immunol* (2022) 43:523–45. doi: 10.1016/j.it.2022.04.010

23. Chi Y, Fang Z, Hong X, Yao Y, Sun P, Wang G, et al. Safety and efficacy of anlotinib, a multikinase angiogenesis inhibitor, in patients with refractory metastatic soft-tissue sarcoma. *Clin Cancer Res Off J Am Assoc Cancer Res* (2018) 24:5233–8. doi: 10.1158/1078-0432.CCR-17-3766

24. Makker V, Rasco D, Vogelzang NJ, Brose MS, Cohn AL, Mier J, et al. Lenvatinib plus pembrolizumab in patients with advanced endometrial cancer: an interim analysis of a multicentre, open-label, single-arm, phase 2 trial. *Lancet Oncol* (2019) 20:711–8. doi: 10.1016/S1470-2045(19)30020-8

25. Judson I, Radford JA, Harris M, Blay JY, van Hoesel Q, le Cesne A, et al. Randomised phase II trial of pegylated liposomal doxorubicin (DOXIL/CAELYX) versus doxorubicin in the treatment of advanced or metastatic soft tissue sarcoma: a study by the EORTC soft tissue and bone sarcoma group. *Eur J Cancer Oxf Engl 1990* (2001) 37:870–7. doi: 10.1016/s0959-8049(01)00050-8

frontiers | Frontiers in Oncology

TYPE Original Research
PUBLISHED 18 July 2023
DOI 10.3389/fonc.2023.1224071

OPEN ACCESS

EDITED BY
Feifei Teng,
Shandong University Cancer Center, China

REVIEWED BY
Yidong Xie,
Sichuan University, China
Siyu Yao,
The Ohio State University, United States
Hao Huang,
Central South University, China
Shuai Guo,
University of Texas MD Anderson Cancer Center Houston, United States, in collaboration with reviewer HH

*CORRESPONDENCE
Li Yuan
lizzyklarck@126.com
Kefei Gao
gaokefei_fezx@yeah.net

†These authors have contributed equally to this work

RECEIVED 17 May 2023
ACCEPTED 29 June 2023
PUBLISHED 18 July 2023

CITATION
Xiong J, Chen J, Guo Z, Zhang C, Yuan L and Gao K (2023) A novel machine learning-based programmed cell death-related clinical diagnostic and prognostic model associated with immune infiltration in endometrial cancer.
Front. Oncol. 13:1224071.
doi: 10.3389/fonc.2023.1224071

A novel machine learning-based programmed cell death-related clinical diagnostic and prognostic model associated with immune infiltration in endometrial cancer

Jian Xiong[1†], Junyuan Chen[2†], Zhongming Guo[3], Chaoyue Zhang[2], Li Yuan[3*] and Kefei Gao[1*]

[1]Department of Obstetrics and Gynaecology, Guangzhou Women and Children's Medical Center, Guangzhou Medical University, Guangzhou, China, [2]China Medical University, Shenyang, China, [3]Department of Pathology, Guangzhou Women and Children's Medical Center, Guangzhou Medical University, Guangzhou, China

Background: To explore the underlying mechanism of programmed cell death (PCD)-related genes in patients with endometrial cancer (EC) and establish a prognostic model.

Methods: The RNA sequencing data (RNAseq), single nucleotide variation (SNV) data, and corresponding clinical data were downloaded from TCGA. The prognostic PCD-related genes were screened and subjected to consensus clustering analysis. The two clusters were compared by weighted correlation network analysis (WGCNA), immune infiltration analysis, and other analyses. The least absolute shrinkage and selection operator (LASSO) algorithm was used to construct the PCD-related prognostic model. The biological significance of the PCD-related gene signature was evaluated through various bioinformatics methods.

Results: We identified 43 PCD-related genes that were significantly related to prognoses of EC patients, and classified them into two clusters *via* consistent clustering analysis. Patients in cluster B had higher tumor purity, higher T stage, and worse prognoses compared to those in cluster A. The latter generally showed higher immune infiltration. A prognostic model was constructed using 11 genes (GZMA, ASNS, GLS, PRKAA2, VLDLR, PRDX6, PSAT1, CDKN2A, SIRT3, TNFRSF1A, LRPPRC), and exhibited good diagnostic performance. Patients with high-risk scores were older, and had higher stage and grade tumors, along with worse prognoses. The frequency of mutations in PCD-related genes was correlated with the risk score. LRPPRC, an adverse prognostic gene in EC, was strongly correlated with proliferation-related genes and multiple PCD-related genes. LRPPRC expression was higher in patients with higher clinical staging and

in the deceased patients. In addition, a positive correlation was observed between LRPPRC and infiltration of multiple immune cell types.

Conclusion: We identified a PCD-related gene signature that can predict the prognosis of EC patients and offer potential targets for therapeutic interventions.

KEYWORDS

LASSO, cell death, endometrial cancer, signature, cell assay, immune infiltration

1 Introduction

Endometrial cancer (EC) was the sixth most common cancer diagnosed in women in 2020, with a total of 417,000 new cases documented worldwide. The median age of diagnosis of EC patients is 61 years, and the lifetime risk of EC is around 3% (1). EC is associated with a high mortality rate, and over 76,000 women die annually as a result of EC (2). The mortality rate due to EC further increases with advanced tumor stage, invasive histology, and metastasis (3). There is currently a paucity of biomarkers or models that can effectively predict the prognosis and survival of EC patients (4). Therefore, it is crucial to elucidate the molecular mechanisms underlying EC occurrence and progression in order to identify novel prognostic markers and therapeutic targets.

Cell death plays a crucial role in several biological processes, and can be classified as programmed cell death (PCD) and accidental cell death (ACD) (5). PCD is the culmination of ordered, gene-controlled pathways following the spontaneous loss of cellular function, whereas ACD is an uncontrolled process that is triggered in response to certain harmful stimuli. PCD is primarily responsible for maintaining intracellular homeostasis (6). Various types of PCD have been documented so far, including autophagy-dependent cell death, necroptosis, apoptosis, ferroptosis, pyroptosis, entosis, parthanatos, NETosis, alkaliptosis, lysosome-dependent cell death (LCD), and oxeiptosis (7).

Lysosomal degradation during autophagy-mediated cell death facilitates metabolic adaptation and nutrient recycling (8). Necrosis has long been considered an involuntary form of cell death, although recent evidence indicates that necrosis can be initiated and sustained, resulting in necroptosis that centers around the formation of necrosomes (9, 10). Apoptosis is an intrinsic mechanism for eliminating damaged cells and involves a series of events including condensation, nucleolysis, and nuclear fragmentation, which culminate in the engulfment of apoptotic vesicles by macrophages (11). Ferroptosis is characterized by the accumulation of lipid hydroperoxides in an iron-dependent manner that ultimately reaches a lethal threshold (12, 13). Cuproptosis is a recently identified mode of PCD that is triggered by copper imbalance and is closely associated with disease progression (14). Pyroptosis is an inflammatory form of PCD that is typified by the creation of membrane pores that compromise cellular integrity, eventually leading to cell rupture (15). Entosis is a form of cell "cannibalism" wherein one live cell is engulfed and lysed by another cell without the activation of the apoptotic pathway (16). Parthanatos is induced by excessive activation of the nuclease PARP-1 (17), an RNA polymerase (RP) that interacts with and activates DNA or RNA, leading to replication or repair of damaged DNA and proteins. NETosis is initiated by the release of neutrophil extracellular traps (NETs), i.e., interconnected structures that cells release in response to infection or injury (18). Alkaliptosis, a newly recognized type of PCD, heavily relies on the intracellular alkalization process (19). LCD is dependent on hydrolase, which facilitates lysosomal transport to the cytoplasm by means of membrane penetration. This process is regulated by intracellular signaling systems and membrane proteins (20). KEAP1, a detector of reactive oxygen species (ROS), has recently been shown to be involved in a unique type of cell death known as oxygen apoptosis (21).

Mutations in the PCD pathways have been detected in the early stages of cancer, which endow the tumor cells with resistance to anti-cancer treatments (7). Therefore, targeted interventions that activate PCD pathways using single or combined therapies are an effective anti-cancer strategy. For instance, the FDA-approved BCL-2 inhibitor triggers apoptosis in lymphoma cells (22). In addition, activation of GSDME-mediated pyroptosis has proved to be highly effective against many cancers (23). Cancer cells can resist PD-1/PD-L1 checkpoint inhibition by blocking ferroptosis through the regulation of ferritin and other proteins (24), indicating that activation of the ferroptosis pathway in these cells can sensitize them to PD-1/PD-L1 blockers.

In this study, we used bioinformatic approaches to establish a PCD-related prognostic gene signature for EC and found that higher risk scores were associated with a worse prognosis. Our findings provide new insights into the molecular basis of EC progression. Furthermore, the genes associated with PCD have significant potential as prognostic biomarkers and therapeutic targets for EC.

2 Materials and methods

2.1 Data acquisition and preprocessing

The RNA sequencing (RNAseq), single nucleotide variation (SNV), and relevant clinical data of 544 tumor samples and 35 normal samples from TCGA-UCEC (Uterine Corpus Endometrial

Carcinoma) were downloaded through the UCSC XENA website (https://xenabrowser.net/datapages/) and Sangerbox website (http://www.sangerbox.com/). TCGA-CESC (168 tumor samples) and TCGA-BRCA (1057 tumor samples) were downloaded from the UCSC XENA website (https://xenabrowser.net/datapages/) for external validation. The RNAseq data was transformed into fragments per kilobase of exon model per million mapped fragments (FPKM) format. In addition, the curated transcriptome data, SNV data, and corresponding clinical data of 12,591 patients across 32 cancer types were also retrieved from the UCSC XENA website (http://xena.ucsc.edu/). All transcriptomic data were transformed to the FPKM format for downstream analysis.

2.2 Screening of prognostic PCD-related genes, consensus clustering, and immune infiltration

A list of PCD-related genes (Supplementary Table S1) was obtained through literature review and manual searching (7), and these genes were extracted from the TCGA-UCEC cohort. The prognostically relevant genes were screened through univariate Cox regression analysis using the "survival" package, and subjected to consensus clustering using the "ConsensusClusterPlus" package. The patients were accordingly divided into two clusters. The "limma" and "estimate" packages were used for scoring immune filtration, and the results were visualized using the "ComplexHeatmap", "gplots", "ggplot2", "RColorBrewer" and "oompaBase" packages. The immune cell populations were characterized on the basis of classical markers, including immunoglobulin G (IgG), hematopoietic cell kinase (HCK), major histocompatibility complex class II (MHC-II), lymphocyte-specific kinase (LCK), activation transcription 1 (STAT1), interferons, TNF and B7-CD28 (CD28) (25). The scores of the immune cell subsets in both clusters were evaluated by ssGSEA. Weighted correlation network analysis (WGCNA) was performed using the "WGCNA" and "limma" packages, with cluster, age, stage, grade, and tumor mutation burden (TMB) as the factors. The gene modules with the strongest correlations with each factor were screened using abline=60 and soft threshold=4 as the criteria. Finally, the PCD-related genes were functionally annotated by GO analysis.

2.3 Construction and validation of PCD-related genes signature

The "glmnet" package was used for LASSO analysis to select the PCD-related genes for the prognostic model. Although overfit potential generally exists in machine learning-based models, feature selection can effectively solve the overfitting problem because it can select the most relevant features from the original feature set, thus reducing the complexity and noise interference of the model. Common feature selection methods include Filter method, Wrapper method, and Embedded method. Among them, the Filter method sorts and filters according to the correlation between features and target variables. The wrapper method, by constantly trying different feature subsets, uses the model itself to evaluate and select the optimal subset. Embedded methods use feature selection as part of the model training process, such as LASSO and ridge regression. As our model is exactly based on the LASSO algorithm, the overfit potential could be avoided to some extent. The risk score was calculated by multiplying the expression of each gene with its respective coefficient:

$$\text{Riskscore} = \sum_{i=1}^{n}[\exp ression \quad value \quad of \quad gene_i * \beta_i] \quad (1)$$

The variable "n" represents the number of genes included in the signature, and the variable "β" denotes the coefficient assigned to each gene obtained from LASSO regression.

Risk score= [expression value of GZMA × (-0.116286998)] + [expression value of ASNS × (0.127252486)] + [expression value of GLS × (0.042654301)] + [expression value of PRKAA2 × (0.1310519)] + [expression value of VLDLR × (-0.114179696)] + [expression value of PRDX6 × (0.016522634)] + [expression value of PSAT1 × (0.016313951)] + [expression value of CDKN2A × (0.116960742)] + [expression value of SIRT3 × (-0.180170396)] + [expression value of TNFRSF1A × (-0.026584716)] +[expression value of LRPPRC × (0.055918364)]

According to the median risk score, patients were divided into high-risk and low-risk groups. The "survival" package was used to perform proportional hazards assumption testing and survival regression, and the "survminer" and "ggplot2" packages were used to plot the graphs. The diagnostic capability of PCD-related gene signature in the TCGA-UCEC cohort was evaluated by receiver operational characteristic (ROC) analysis using the "timeROC" package, and the results were visualized with the "ggplot2" package. All the samples with survival information were included in the ROC analysis. The number of samples was 544. The area under the curve (AUC) was calculated, and 0.7 was the cut-off for satisfactory diagnostic performance. The "ggplot2" package was used to visualize the risk factor plot. The prognostic model was tested on 32 types of cancer (Supplementary Table S2) using the "ggplot2", "data.table", "survival", "cowplot" and "ggpub" packages. The prognostic endpoints of the patients included disease-specific survival (DSS), overall survival (OS), and progression-free interval (PFI).

2.4 Analysis of single-nucleotide variations of PCD-related genes

Pan-cancer analysis on the top 10 mutated genes in the signature using the "ggplot2", "data.table", "cowplot", "ggpubr", "GSVA", "SimDesign" and "tidyr" packages. The mutation frequencies of the PCD-related genes in the different organs were also calculated.

2.5 Comparison of risk groups

The "ComplexHeatmap" package was used to create a heatmap showing the relationship between the risk score and the clinical factors like age, grade, and stage. Gene set enrichment analysis

(GSEA) was performed on the high-risk and low-risk groups, and the top 5 pathways in each group were identified. The "RColorBrewer" package was used to visualize the results. The "oncoPredict" package was used for drug sensitivity analysis.

2.6 Construction and validation of a prognostic nomogram

The "survival" package was used to perform proportional hazards assumption testing and Cox regression analysis, and a nomogram consisting of age, stage, grade, and the PCD risk score was constructed using the "rms" package. The 1-, 3- and 5-year survival were predicted using the nomogram. Calibration curves for 1-, 3- and 5-year survival were plotted using the "rms" package. All the samples with survival information were included in the ROC analysis. The number of samples was 544.

2.7 Correlation between PCD-related genes, proliferation genes, and immune cell phenotypes

The correlation between the PCD-related genes and proliferation-related genes (*WNT5A, PCNA, MKI67, CTNNB1*, and *CDH1*) was analyzed using the "ggplot2" package. *LRPPRC* was identified as the gene of interest. The "survival" and "survminer" packages were used to evaluate the prognostic relevance of *LRPPRC*, and analyze its expression across different clinical stages and OS events. The "igraph" and "ggraph" packages were used to analyze the pairwise correlation of genes within the PCD-related gene signature. Finally, the "ggplot2" package was used to visualize the association between LRPPRC and the infiltration of 24 immune cell types infiltration through Spearman correlation analysis.

2.8 Statistical analysis

R software (4.1.3) was used for statistical analyses. T-test was used to compare the data between the two groups. P value< 0.05 was considered statistically significant.

3 Results

3.1 Identification and clustering of prognostic PCD-related genes

The workflow of our study is illustrated in Figure 1. We identified 43 PCD-related genes that were significantly correlated to the prognosis of EC patients (Supplementary Table S3), and the Forest plot of the genes with p<0.01 is shown in Figure 2A. Consensus clustering analysis of these 43 genes with 2-9 clusters showed that dividing the samples into two clusters resulted in better distinction (Figures 2B, C). Patients in Cluster B had higher tumor purity, more advanced T stage, and worse prognosis compared to those in Cluster A. The latter generally had higher ESTIMATEScore, ImmuneScore, and StromalScore (Supplementary Table S4). Furthermore, Cluster A was associated with high expression levels of *IgG, HCK, MHC-II,*

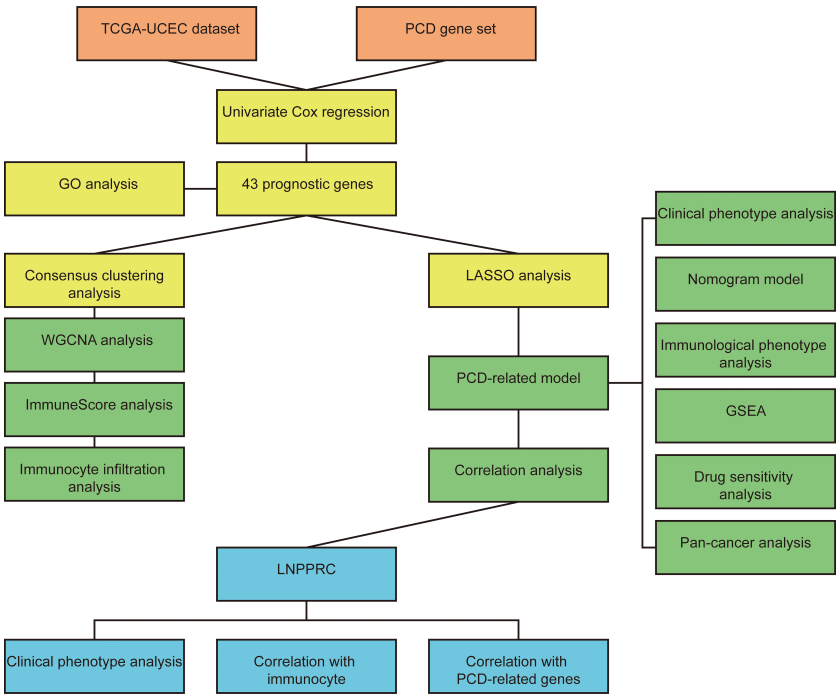

FIGURE 1
The workflow chart of the study.

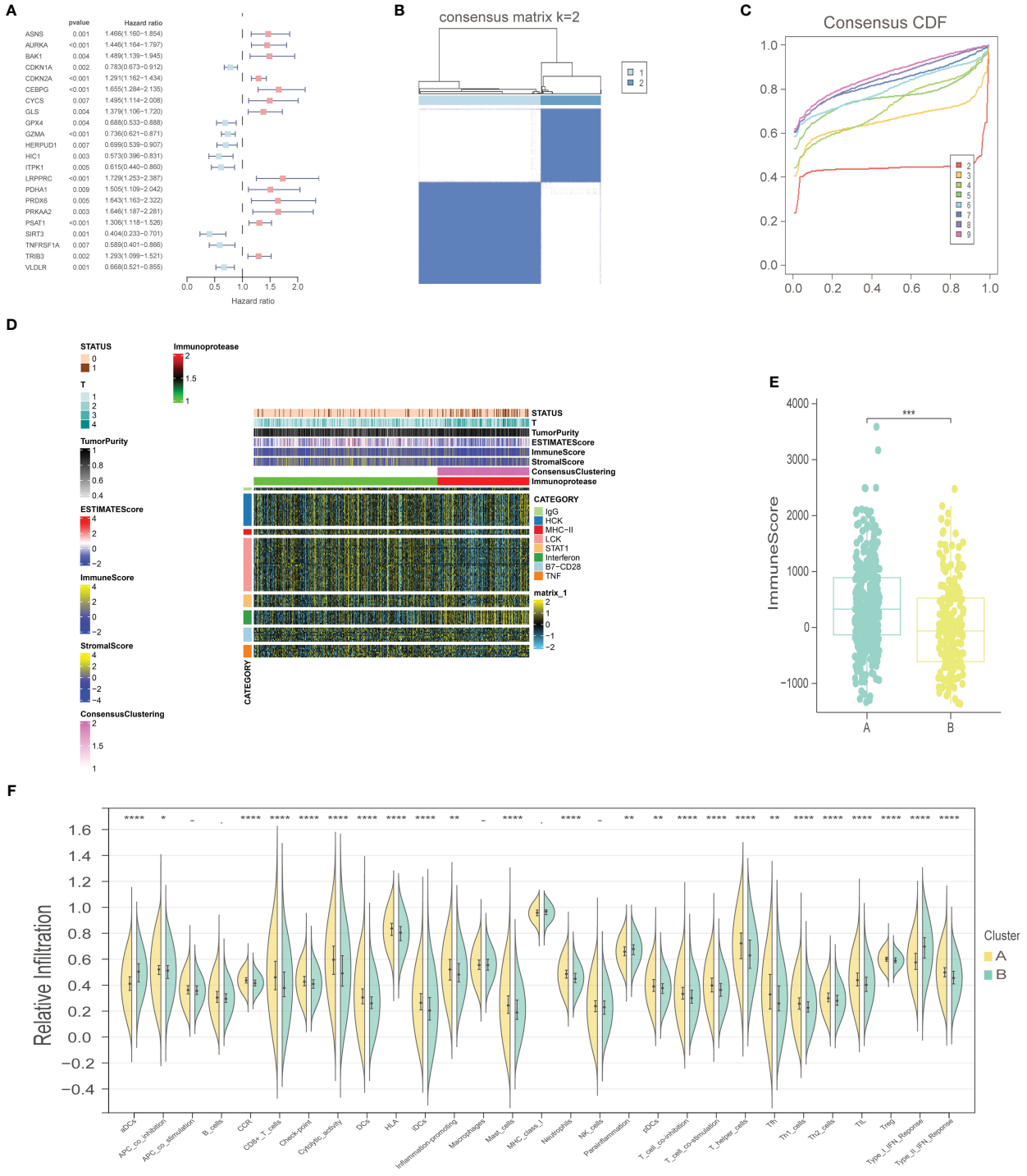

FIGURE 2
Selection of prognostic-related PCD-related genes, consensus clustering analysis, and immune-related analysis. **(A)** Forest plot of PCD-related genes with prognostic significance at p<0.01. **(B)** Consensus matrix, k=2. **(C)** Consensus CDF. **(D)** Heat map of immune scores. **(E)** ImmuneScore boxplot of two clusters. **(F)** Violin plot of immune infiltration analysis for two clusters. "*" represents p < 0.05; "**" represents p < 0.01; "***" represents p < 0.001; "****" represents p < 0.0001.

LCK, *B7-CD28*, and *TNF*, whereas *STAT1* and *IFN* were overexpressed in Cluster B (Figures 2D, E). Subsequently, ssGSEA showed distinct immune cell infiltration patterns of Cluster A and Cluster B (p<0.05). For instance, $CD8^+$ T cells, cytolytic activity, inflammation-promoting, T-cell co-stimulation, etc. were significantly higher in Cluster A compared with Cluster B, whereas the latter had higher levels of aDCs, para inflammation, and Type I IFN response (Figure 2F). The results of WGCNA indicated that the brown module had a high degree of positive correlation with both Cluster and Grade, with correlation coefficients of 0.49 (p<0.05). You could see that the brown module had a high degree of positive correlation (0.49) with both Cluster and Grade. In the meanwhile,

other modules were almost poorly or negatively correlated with Cluster and Grade. That is to say, the brown module shows high specificity for Cluster and Grade. Although the royal blue module had the strongest correlation with Cluster (with a related coefficient of 0.56, p<0.05), the low number of genes in the module was not representative. Therefore, we selected the brown module for further analysis (Figure 3A). The correlation scatter plot of Module Membership in the brown module (MM) and Gene significance for Cluster (GS) showed a highly positive correlation (with a correlation coefficient of 0.45, $p=7.8*10^{-28}$), which suggested that the brown module genes were upregulated in Cluster B (Figure 3B). GO analysis indicated that the 43 prognosis-related PCD-related genes were significantly downregulated in the "lipid and atherosclerosis" pathway (Figure 3C; Table 1).

3.2 Construction and validation of PCD-related genes signature

A total of 200 PCD-related genes were incorporated in the LASSO algorithm and 11 genes (*GZMA, ASNS, GLS, PRKAA2, VLDLR, PRDX6, PSAT1, CDKN2A, SIRT3, TNFRSF1A, LRPPRC*) were finally selected to construct the prognostic gene signature (Figures 4A, B). The detailed information and coefficients of these genes are shown in Supplementary Table S5. The risk scores of the individual patients in the TCGA-UCEC cohort were calculated (see methods), and the patients were divided into high-risk and low-risk groups based on the median PCD risk score. As shown in Figure 4C, higher risk scores correlated with shorter OS and higher mortality rates (p<0.001). In addition, the PCD signature showed strong predictive performance for 1-, 3- and 5-year OS, with respective AUC values of 0.678, 0.776, and 0.77 (Figure 4D). *LRPPRC, CDKN2A, PSAT1, PRDX6, PRKAA2, GLS*, and *ASNS* were overexpressed in the high-risk group, whereas *TNFRSF1A, SIRT3, VLDLR*, and *GZMA* were highly expressed in the low-risk group (Figure 4E). We also tested the risk score across 32 types of cancer and found that uterine carcinosarcoma, brain lower-grade glioma, and ovarian serous cystadenocarcinoma had higher risk scores, while uveal melanoma, mesothelioma, and skin cutaneous melanoma typically had lower risk scores. The PCD risk score distribution for other cancers is shown in Figure 4F.

The PCD-related genes signature was further validated in TCGA-CESC and TCGA-BRCA cohorts. The risk scores of the individual patients in the TCGA-BRCA cohort were calculated, and the patients were divided into high-risk and low-risk groups based on the median PCD risk score. As shown in Figure S1A, higher risk scores correlated with shorter OS and higher mortality rates (p<0.001). In addition, the PCD signature showed strong predictive performance for 1-, 3- and 5-year OS, with respective AUC values of 0.661, 0.647, and 0.632 (Figure S1B). The calibration curves for 1-, 3- and 5-year OS showed good consistency between observed survival and predicted survival (Figure S1C). The risk scores of the individual patients in the TCGA-CESC cohort were also calculated, and the patients were divided into high-risk and low-risk groups based on the median PCD risk score. As shown in Figure S1D, higher risk scores correlated with shorter OS and higher mortality rates (p<0.01). In addition, the PCD signature showed strong predictive performance for 1-, 3- and 5-year OS, with respective AUC values of 0.765, 0.816, and 0.849 (Figure S1E). The calibration curves for 1-, 3- and 5-year OS showed good consistency between observed survival and predicted survival (Figure S1F).

3.3 Pan-cancer variations in PCD-related genes

The pan-cancer SNV profiles of the top 10 mutated genes of the PCD risk model were also analyzed. *CDKN2A* displayed higher mutation rates across multiple cancer types (31%), and other frequently mutated genes included *LRPPRC* (13%), *PRKAA2* (11%), *VLDLR* (9%), *ASNS* (8%), *GZMA* (7%), *GLS* (7%), *TNFRSF1A* (6%), *PSAT1* (5%), and *PRDX6* (4%). A missense mutation was the most frequently observed mutation type. However, the mutation types in *CDKN2A* were predominantly nonsense mutation, splice site, frameshift deletion, and multi-hit (Figure 5A). Furthermore, *CDKN2A* displayed higher mutation frequency in head and neck squamous cell carcinoma (104%), lung squamous cell carcinoma (73%), skin cutaneous melanoma (61%), pancreatic adenocarcinoma (36%), bladder urothelial carcinoma (27%), and lung adenocarcinoma (24%). The SNV frequency of *PRKAA2* in skin cutaneous melanoma was 42%.

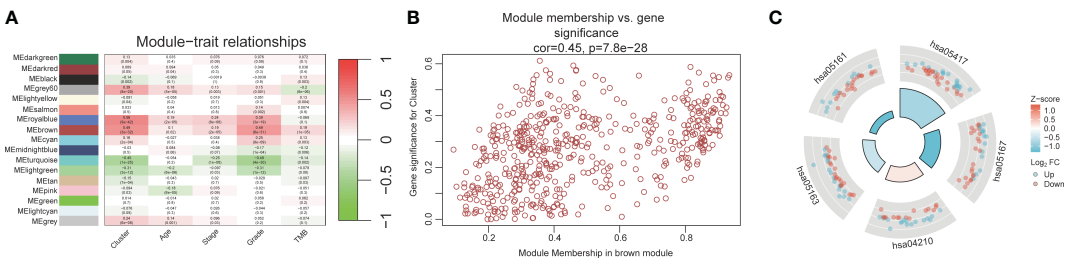

FIGURE 3
WGCNA and GO analysis. **(A)** Heat map of module-trait relationships. **(B)** Scatter plot of module membership versus gene significance. **(C)** GO analysis for 43 prognostic PCD-related genes.

10.3389/fonc.2023.1224071

TABLE 1 Description of ID in GO analysis.

ID	Description
hsa05417	Lipid and atherosclerosis
hsa05167	Kaposi sarcoma-associated herpesvirus infection
hsa04210	Apoptosis
hsa05163	Human cytomegalovirus infection
hsa05161	Hepatitis B

Also, several PCD-related genes exhibited high mutation frequency in uterine corpus endometrial carcinoma and skin cutaneous melanoma (Figure 5B).

3.4 Comprehensive analysis of two risk groups

As shown in Figure 6A, patients in the high-risk group were older ($p<0.001$) and had more advanced tumor grade and stage ($p<0.001$),

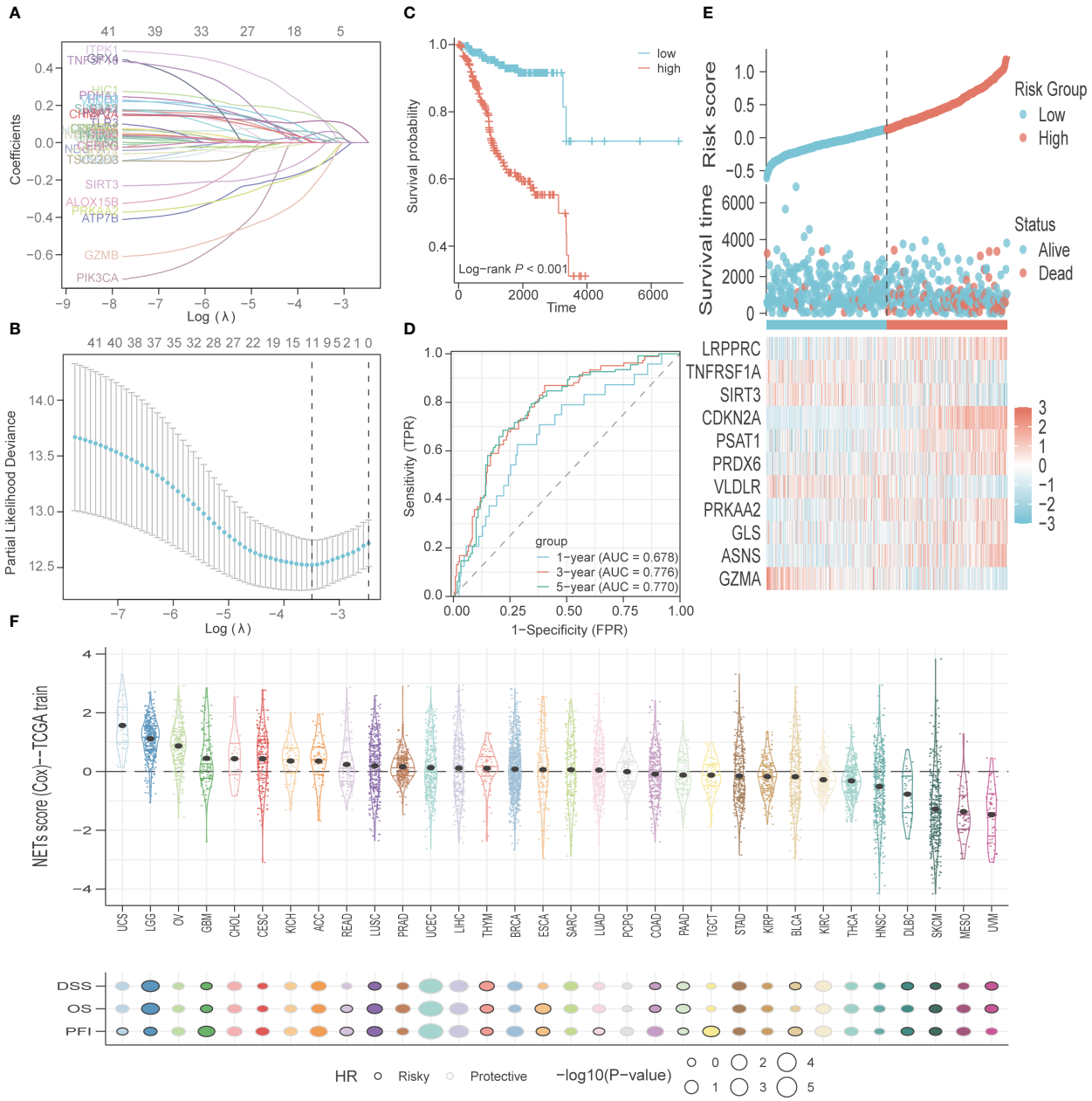

FIGURE 4
Construction and validation of PCD-related genes signature. **(A)** The variable coefficient values, logarithmic lambda values, and L1 regularization values obtained through LASSO analysis were visualized. **(B)** Lambda values, maximum likelihood numbers, and C-Index obtained from LASSO analysis were visualized. **(C)** K-M curves for OS in high-risk and low-risk patient groups. **(D)** ROC analysis to evaluate the performance of signature in 1-year, 3-year, and 5-year prognoses. **(E)** Visualization of risk factors. **(F)** The PCD risk score in other types of cancer, with patients' prognostic endpoints including DSS, OS, and PFI.

10.3389/fonc.2023.1224071

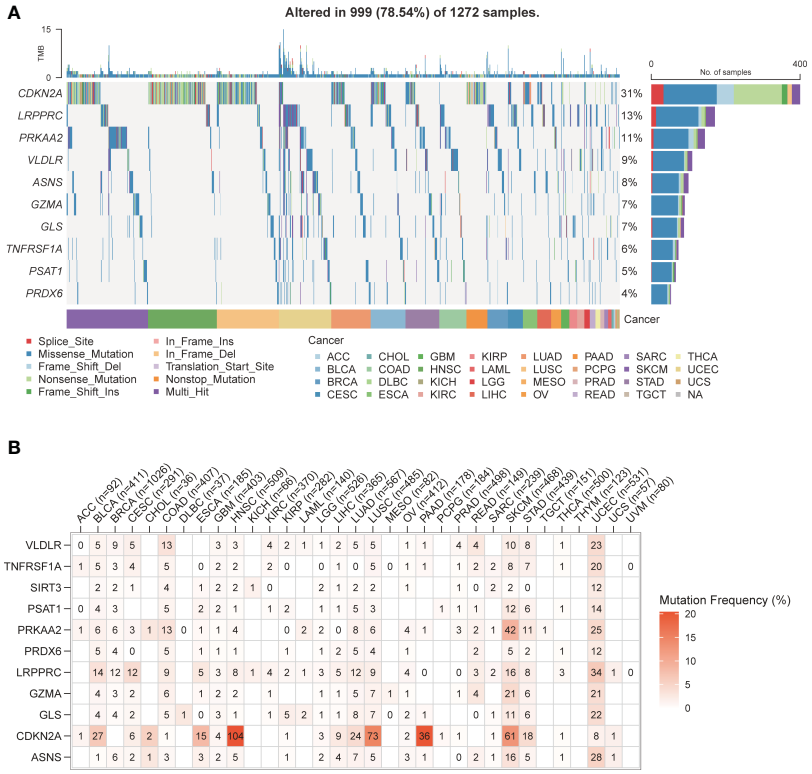

FIGURE 5
PCD-related genes SNV patterns. **(A)** Waterfall plot of PCD-related genes SNV pattern in various types of cancer. **(B)** Mutation frequency of PCD-related genes in various types of cancer.

which was indicative of poor prognosis. GSEA on the two risk groups revealed significant enrichment of "KEGG_CELL_CYCLE" and "KEGG_DNA_REPLICATION" in the high-risk group, and that of "KEGG_CHEMOKINE_SIGNALING_PATHWAY" and "KEGG_CYTOKINE_CYTOKINE_RECEPTOR_INTERACTION" in the low-risk group (Figure 6B; Supplementary Table S6). Four subgroups were identified through immune typing analysis. The proportion of high-risk patients was higher in the c2 subgroup, while the opposite trend was observed in the other subgroups. The sample distribution of the high-risk and low-risk groups differed significantly ($p<0.001$) across the four subgroups (Figure 6C). Drug sensitivity analysis also showed significant differences between the high-risk and low-risk groups (Supplementary Table S7). As shown in Figure 6D, patients in the high-risk group showed greater sensitivity to AT3148, Elephantin, I-BET-762, and Niraparib ($p<0.001$).

3.5 Construction and validation of a prognostic nomogram

A nomogram was constructed using age, staging, grading, and the PCD risk score to predict patient survival at 1, 3, and 5 years (Supplementary Table S8). The scores for each risk factor were calculated, and the total score was plotted (Figure 7A). On this basis, this study intends to establish a correction curve to verify the applicability of the model at the PCD gene level. Our prognostic indicators predicted favorable 1,3 and 5-year survival rates (Figure 7B).

3.6 Correlation between PCD-related genes, proliferation genes, and immune cell phenotypes

The correlation between the expression of the PCD-related genes and five proliferation-related genes, including *WNT5A, PCNA, MKI67, CTNNB1*, and *CDH1*, was also evaluated. *LRPPRC* showed a significant positive correlation with *PCNA, MKI67, CTNNB1*, and *CDH1* ($p< 0.001$), which indicated that LRPPRC may promote the proliferation of EC cells. *CDKN2A* was correlated to all five proliferation-related genes, with a positive correlation with MKI67 and PCNA ($p<0.05$), and a negative correlation with *WNT5A, CTNNB1*, and *CDH1* ($p<0.01$). PSAT1 was positively correlated with *PCNA, MKI67, CTNNB1* and *CDH1* ($p<0.05$; Figure 8A). High expression levels of *LRPPRC*, *CDKN2A*, and *PSAT1* were associated with poor patient prognosis (Figure 8B). Furthermore, *LRPPRC* was expressed at higher levels in the deceased patients compared to the surviving patients ($p< 0.01$; Figure 8C). Furthermore, *LRPPRC* was also significantly upregulated in stage IV tumors compared to stage I/II tumors ($p< 0.05$; Figure 8D). *LRPPRC* also showed a significant positive correlation with some genes of the prognostic signature, including *GLS*, *PRKAA2*, and *PSAT1*, and this correlation was stronger compared to that among the other genes (Figure 8E). Finally, the relationship between *LRPPRC* and the infiltration of 24 immune cells was analyzed. *LRPPRC* showed a highly positive correlation with Th2 cells (R=0.433), Tcm cells (R=0.391), and T helper cells

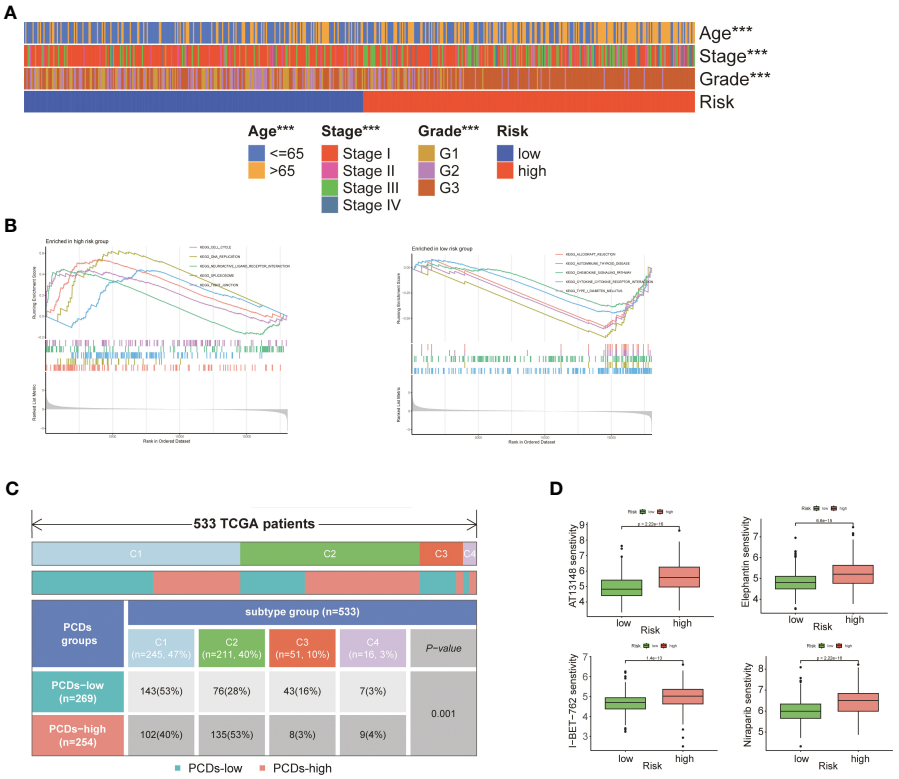

FIGURE 6
Comprehensive analysis of two risk groups. **(A)** Heat map of the correlation between risk groups and clinical characteristics. **(B)** GSEA analysis of two risk groups. **(C)** Immunotyping analysis. **(D)** Boxplot of the difference in drug sensitivity between high-risk and low-risk groups. "***" represents p < 0.001.

(R=0.316) (p<0.001), and a negative correlation with NK CD56^{bright} cells (R=-0.540), pDCs (R=-0.487), and NK cells (R=-0.43) (Figures 8F, G).

4 Discussion

Since irregular vaginal bleeding is an early symptom of EC, most patients are diagnosed at an early stage. Although early diagnosis confers some survival advantage, the annual mortality rate due to EC is still high (4, 26), which warrants the identification of novel prognostic biomarkers. The aim of this study was to identify the prognostic PCD-associated genes in EC in order to construct a predictive model to guide clinical decision-making. A total of 43 PCD-related genes were associated with the prognosis of EC patients, and two distinct clusters were identified.

The patients in Cluster B generally had higher tumor purity, higher T stage, and worse prognosis, while Cluster A was associated with higher ESTIMATE scores, ImmuneScore, and StromalScore. The ImmuneScore is a measure of the percentage of cytotoxic and

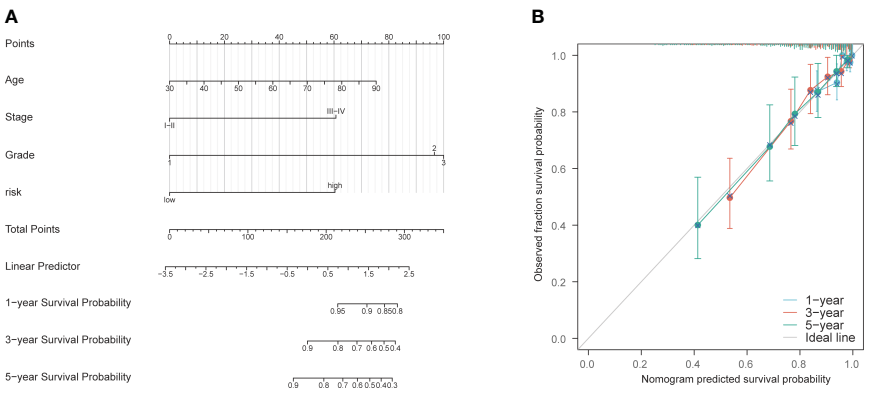

FIGURE 7
Construction and validation of nomogram model. **(A)** Nomogram prognostic model. **(B)** 1-year, 3-year, and 5-year calibration curves.

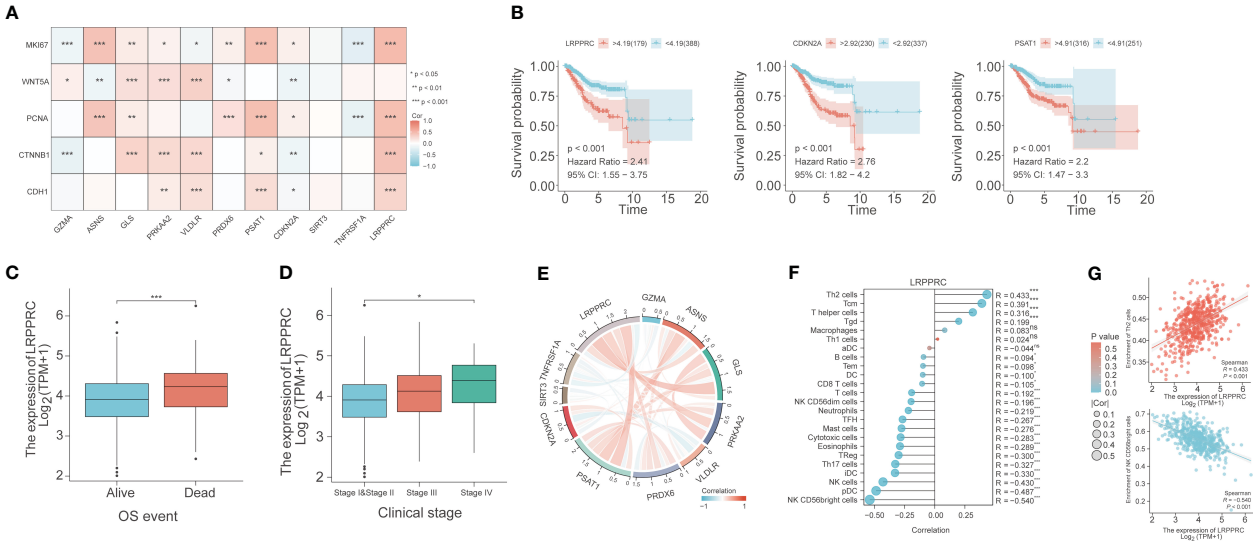

FIGURE 8
Bioinformatics analysis reveals the correlation between PCD-related genes, proliferation genes, and immune cell phenotypes. **(A)** Correlation heat map depicting the relationship between genes in the PCD-related gene signature and genes associated with cell proliferation. **(B)** Survival curves for LRPPRC, CDKN2A, and PSAT1. **(C)** Box plot of the relationship between LRPPRC and OS event. **(D)** Box plot of the relationship between LRPPRC and clinical stage. **(E)** Co-expression network within PCD-related genes. **(F)** The lollipop graph depicts the correlation between LRPPRC and immune phenotype. **(G)** Scatter plot of the correlation between LRPPRC expression and Th2 cells and CD56bright cells, respectively. "*" represents $p < 0.05$; "**" represents $p < 0.01$; "***" represents $p < 0.001$.

memory T cells at the tumor core and tumor margin (27), and the StromalScore is indicative of the ratio of stromal cells in the tumor microenvironment (TME) (28). A higher ImmuneScore or StromalScore suggests the presence of more immune substances or matrix components in the TME. Thus, Cluster B was associated with a general decrease in stromal and immune cells and an overall increase in tumor purity compared to Cluster A, indicating that immune infiltration and tumor purity are determinants of EC development and that enhancing the degree of immune infiltration may slow tumor growth. Furthermore, patients in Cluster A generally expressed genes characteristic of immune cell subsets, while patients in Cluster B showed high expression levels of STAT1 and interferon genes, which suggests an immune active state corresponding to favorable prognosis in Cluster A. Consistent with this, Cluster A showed a significant increase in the infiltration of T cells (such as $CD8^+$ T cells, cytolytic activity, inflammation-promoting, and T cell co-stimulation) compared to Cluster B. On the other hand, Cluster B showed a significant increase in aDCs, para-inflammation, and type I IFN response compared to Cluster A. Furthermore, WGCNA indicated that the brown module has the strongest correlation with the clusters, and the genes in the brown module are upregulated in Cluster B. The WGCNA algorithm is a powerful tool for identifying co-expressed gene modules and their relationships with phenotypic traits. One of the main advantages of WGCNA is that it can handle large-scale gene expression data sets and identify biologically meaningful gene modules that are associated with specific traits or conditions. Additionally, WGCNA can be used to identify key hub genes that play important roles in regulating gene expression networks. Overall, WGCNA is a valuable tool for understanding the complex relationships between genes and phenotypes. Thus, the brown module was thought to be reliable. In addition, GO analysis showed that the 43 prognostic PCD-related genes were negatively regulated in the pathway of "lipids and atherosclerosis". Based on these findings, we hypothesize overexpression of PCD-related genes may allow cancer cells to proliferate rapidly by accelerating lipid metabolism.

A LASSO-based PCD-related gene signature comprising 11 genes, including *GZMA, ASNS, GLS, PRKAA2, VLDLR, PRDX6, PSAT1, CDKN2A, SIRT3, TNFRSF1A*, and *LRPPRC*, was developed to predict the OS of EC patients. The LASSO algorithm is a type of linear regression that is used for feature selection and regularization. One of the main advantages of the LASSO algorithm is that it can help prevent overfitting by shrinking the coefficients of less important variables to zero. This can lead to a more parsimonious model that is easier to interpret and less prone to errors. Additionally, the LASSO algorithm can handle high-dimensional data sets with many variables, which can be useful in fields like genetics and finance. The PCD-related gene signature showed good performance in the TCGA-UCEC cohort and two external validation cohorts, TCGA-CESC and TCGA-BRCA. This finding strongly supported the accuracy, sensitivity, and specificity of the PCD-related gene signature in predicting prognosis. GZMA is predominantly expressed in the cytosolic granules of NK cells and cytotoxic T-cells. It cleaves gasdermin-B (GSDMB), which releases the pore-forming moiety of *GSDMB* and triggers pyroptosis (29–31). Asparagine synthetase (ASNS) catalyzes the *de novo* synthesis of asparagine by transferring amino groups from glutamine to aspartic acid. Inhibiting ASNS expression in cancer cells impairs nutrient uptake and promotes apoptosis (32). GLS hydrolyzes glutamine to produce glutamate (33), and its inhibition can induce apoptosis in tumor cells (34). PRKAA2 encodes the

catalytic subunit of AMPK, a key enzyme that senses cellular energy status (35). VLDLR is a cell surface receptor with multiple functions, such as binding to very low-density lipoprotein and facilitating its endocytosis, which contributes to energy metabolism (36). PRDX6 is a mercaptan-specific peroxidase that reduces hydrogen peroxide and organic hydroperoxide to water and alcohol respectively (37, 38), and can attenuate apoptosis induced by oxygen-glucose deprivation/reoxygenation (39). PSAT1 is a member of the V-class pyridoxal phosphate ester-dependent transaminase family that fuels tumor cells by generating serine. Inhibition of PSAT1 expression can suppress serine synthesis in tumors, thereby inhibiting their growth (40). CDKN2A prevents MDM2-induced degradation of p53, and promotes p53-dependent apoptosis (41). SIRT3 is an exclusive mitochondrial member of the Sirtuin family of class III histone deacetylases, similar to the yeast Sir2 protein. It can eliminate reactive oxygen species, prevent malignant transformation, and inhibit apoptosis (42). TNFRSF1A belongs to the TNF receptor superfamily of proteins that plays a role in TNFα-mediated cell apoptosis and necrosis (7). LRPPRC is a mitochondrial protein that regulates RNA metabolism and transcription. Loss of LRPPRC affects the electron transport chain in the mitochondria, which increases mitochondrial permeability and generation of reactive oxygen species (43). LRPPRC, CDKN2A, PSAT1, PRDX6, PRKAA2, GLS, and ASNS were highly expressed in the high-risk group, while TNFRSF1A, SIRT3, VLDLR, and GZMA showed high expression in the low-risk group. Consistent with our findings, Tian et al. reported high expression of LRPPRC in EC tissues (44). Upregulation of CDKN2A in the extracellular matrix can promote EC progression by releasing cytokines and proteases in the TME (45, 46). Roh et al. demonstrated that silencing EZH2 in EC cells inhibited PRDX6, leading to the activation of the exogenous homocysteine pathway and eventually cell death (47). Zhou et al. found that estrogen activates Grn metabolism in estrogen-sensitive EC, depending on the up-regulation of GLS (48). However, the functions of LRPPRC, PSAT1, PRKAA2, ASNS, TNFRSF1A, SIRT3, VLDLR, and GZMA in EC progression, and the underlying mechanisms, remain to be elucidated.

The PCD risk score was also calculated across 32 types of cancer and showed marked organ specificity. For instance, uterine carcinosarcoma, brain lower-grade glioma, and ovarian serous cystadenocarcinoma had higher PCD risk scores, while uveal melanoma, mesothelioma, and skin cutaneous melanoma usually had lower PCD risk scores. The PCD risk scores of other cancers were similarly distributed. The PCD-related genes are likely overexpressed in the cancers with higher risk scores, and relatively lowly expressed in cancers with lower scores. We found that cancers with higher mutation frequencies in PCD-related genes tended to have lower PCD risk scores. The mutations may affect the normal expression of PCD-related genes, thereby affecting the level of the risk score. Furthermore, mutations in PCD-related genes may reduce their expression in some cancers, leading to dysregulation of cell death pathways and malignant development. CDKN2A was the most frequently mutated PCD gene across all cancer types, and exhibited the most diverse mutation profile, indicating that SNVs in CDKN2A are ubiquitous in multiple cancers.

The EC patients in the high-risk group were older and have more advanced-stage tumors, which corresponded to a worse prognosis. The PCD gene signature exhibited good predictive performance for 1-, 3- and 5-year survival. Furthermore, the prognosis of high-risk patients worsened with age and tumor grade. GSEA results showed that signaling pathways related to DNA replication were abundant in the high-risk group, while the low-risk group was enriched in pathways related to chemotaxis. This indicated that the tumor cells in the high-risk population proliferate actively, while an active immune response characterizes the tumors in the low-risk population. There were remarkable discrepancies in the distribution of specimens between high-risk and low-risk groups for the four different types of immunization. The patients in the high-risk group were sensitive to AT3148, elephantirin, I-BET-762, and Niraparib, suggesting their potential clinical applicability in EC patients. We also established a nomogram consisting of age, stage, grade, and risk score, which predicted the 1-, 3- and 5-year survival rates with high accuracy.

The PCD genes also showed a significant correlation with several proliferation-related genes. WNT5A is known to regulate the proliferation, invasion, and metastasis of tumor cells. In a previous study, we found that low expression of WNT5A in gastric cancer tissues was significantly associated with the invasion and metastasis of tumor cells, and poor prognosis (49, 50). MKI67 is a typical marker of cell proliferation that remains on the single mitotic chromosome after the breakdown of the nuclear membrane. It is expressed at low levels in EC tissues (51). Mutations in the CTNNB1 gene promote the development of esophageal cancer by upregulating the Wnt/beta-catenin pathway and the downstream target genes (52). CDH1 encodes E-cadherin, an epithelial marker that regulates cell adhesion, migration, and proliferation. It is downregulated during epithelial-mesenchymal transformation (EMT), which is the driver of tumor cell metastasis (53). Low expression of E-cadherin is linked to worse prognosis and survival (54). No study so far has reported any interaction between LRPPRC and these proliferation-related genes in EC. Based on the expression patterns and clinical association of LRPPRC, this gene is likely a risk factor in EC patients and therefore a potential therapeutic target. LRPPRC showed a strong positive correlation with GLS, PRKAA2, and PSAT1. There is a possibility of a synergistic interaction between these genes in EC development, which warrants further research. Wang et al. have identified biomarkers in different tumors by combining computational biology methods such as WGCNA, opening up more possibilities for researching tumorigenesis mechanisms (55, 56). LRPPRC expression showed a positive correlation with Th2 cells and a negative correlation with NK $CD56^{bright}$ cells, which may accelerate tumor progression. High expression of LRPPRC may inhibit NK cell activity, thereby suppressing the immune response and promoting cancer progression. Further studies are needed to assess the role of LRPPRC in tumorigenesis and development, and the underlying molecular mechanisms involved in programmed cell death. Single-cell sequencing (scRNA-seq) has been widely used to explore the mechanisms and biomarkers of gynecological tumors (57, 58). In our subsequent study, we will focus on the mechanism of LRPPRC in EC development through the scRNA-seq approach.

5 Conclusion

PCD-related genes are involved in the development of EC and can predict patient prognosis. We developed a PCD-related cluster system for discriminating EC patients with different prognoses. We also constructed an 11-gene PCD-related signature with high predictive performance in prognosis, mutation, and drug response. LRPPRC, an adverse prognostic gene in EC and a member of the model genes, could predict the clinical status and immune infiltration level of EC patients. Our findings provide new insights into the mechanisms underlying EC development and highlight potential therapeutic targets.

Data availability statement

The original contributions presented in the study are included in the article/Supplementary Material. Further inquiries can be directed to the corresponding authors.

Ethics statement

The studies involving human participants were reviewed and approved by Department of Obstetrics and Gynaecology, Guangzhou Women and Children's Medical Center, Guangzhou Medical University. The patients/participants provided their written informed consent to participate in this study.

Author contributions

KG contribute to the method and the results, JX wrote the manuscript. Other authors confirmed their contribution to this research. All authors contributed to the article and approved the submitted version.

Funding

This study was funded by the Research Foundation of Guangzhou Women and Children's Medical Center for Clinical Doctor (2020RC003, 2021BS044), the Science and Technology Program of Guangzhou, China (2023A04J1244), the Plan on enhancing scientific research in GMU (02-410-2302169XM), and the Administration of Traditional Chinese Medicine of Guangdong Province (20201299).

Acknowledgments

We thank the TCGA database for its open source.

Conflict of interest

The authors declare that the research was conducted in the absence of any commercial or financial relationships that could be construed as a potential conflict of interest.

Publisher's note

Supplementary material

The Supplementary Material for this article can be found online at: https://www.frontiersin.org/articles/10.3389/fonc.2023.1224071/full#supplementary-material

SUPPLEMENTARY FIGURE 1
External validation of PCD-related genes signature. **(A)** K-M curves for OS in high-risk and low-risk patient groups. **(B)** ROC analysis to evaluate the performance of signature in 1-year, 3-year, and 5-year prognoses. **(C)** Calibration curves to evaluate the performance of signature in 1-year, 3-year, and 5-year prognoses. **(D)** K-M curves for OS in high-risk and low-risk patient groups. **(E)** ROC analysis to evaluate the performance of signature in 1-year, 3-year, and 5-year prognoses. **(F)** Calibration curves to evaluate the performance of signature in 1-year, 3-year, and 5-year prognoses.

References

1. Crosbie EJ, Kitson SJ, McAlpine JN, Mukhopadhyay A, Powell ME, Singh N. Endometrial cancer. *Lancet (London England)* (2022) 399(10333):1412–28. doi: 10.1016/S0140-6736(22)00323-3

2. Urick ME, Bell DW. Clinical actionability of molecular targets in endometrial cancer. *Nat Rev Cancer* (2019) 19(9):510–21. doi: 10.1038/s41568-019-0177-x

3. Sud S, Holmes J, Eblan M, Chen R, Jones E. Clinical characteristics associated with racial disparities in endometrial cancer outcomes: a surveillance, epidemiology and end results analysis. *Gynecol Oncol* (2018) 148(2):349–56. doi: 10.1016/j.ygyno.2017.12.021

4. Lai J, Xu T, Yang H. Protein-based prognostic signature for predicting the survival and immunotherapeutic efficiency of endometrial carcinoma. *BMC Cancer* (2022) 22(1):325. doi: 10.1186/s12885-022-09402-w

5. Galluzzi L, Vitale I, Aaronson SA, Abrams JM, Adam D, Agostinis P, et al. Molecular mechanisms of cell death: recommendations of the nomenclature committee on cell death 2018. *Cell Death Differ* (2018) 25(3):486–541. doi: 10.1038/s41418-017-0012-4

6. Christgen S, Tweedell RE, Kanneganti TD. Programming inflammatory cell death for therapy. *Pharmacol Ther* (2022) 232:108010. doi: 10.1016/j.pharmthera.2021.108010

7. Peng F, Liao M, Qin R, Zhu S, Peng C, Fu L, et al. Regulated cell death (RCD) in cancer: key pathways and targeted therapies. *Signal Transduct Target Ther* (2022) 7(1):286. doi: 10.1038/s41392-022-01110-y

8. Amaravadi RK, Kimmelman AC, Debnath J. Targeting autophagy in cancer: recent advances and future directions. *Cancer Discov* (2019) 9(9):1167–81. doi: 10.1158/2159-8290.CD-19-0292

9. Su Z, Yang Z, Xu Y, Chen Y, Yu Q. Apoptosis, autophagy, necroptosis, and cancer metastasis. *Mol Cancer* (2015) 14:48. doi: 10.1186/s12943-015-0321-5

10. Xie J, Tian W, Tang Y, Zou Y, Zheng S, Wu L, et al. Establishment of a cell necroptosis index to predict prognosis and drug sensitivity for patients with triple-negative breast cancer. *Front Mol Biosci* (2022) 9:834593. doi: 10.3389/fmolb.2022.834593

11. Zhao R, Kaakati R, Lee AK, Liu X, Li F, Li CY. Novel roles of apoptotic caspases in tumor repopulation, epigenetic reprogramming, carcinogenesis, and beyond. *Cancer Metastasis Rev* (2018) 37(2-3):227–36. doi: 10.1007/s10555-018-9736-y

12. Stockwell BR, Friedmann Angeli JP, Bayir H, Bush AI, Conrad M, Dixon SJ, et al. Ferroptosis: a regulated cell death nexus linking metabolism, redox biology, and disease. *Cell* (2017) 171(2):273–85. doi: 10.1016/j.cell.2017.09.021

13. Zou Y, Zheng S, Xie X, Ye F, Hu X, Tian Z, et al. N6-methyladenosine regulated FGFR4 attenuates ferroptotic cell death in recalcitrant HER2-positive breast cancer. *Nat Commun* (2022) 13(1):2672. doi: 10.1038/s41467-022-30217-7

14. Tsvetkov P, Coy S, Petrova B, Dreishpoon M, Verma A, Abdusamad M, et al. Copper induces cell death by targeting lipoylated TCA cycle proteins. *Sci (New York NY)* (2022) 375(6586):1254–61. doi: 10.1126/science.abf0529

15. Tang R, Xu J, Zhang B, Liu J, Liang C, Hua J, et al. Ferroptosis, necroptosis, and pyroptosis in anticancer immunity. *J Hematol Oncol* (2020) 13(1):110. doi: 10.1186/s13045-020-00946-7

16. Wen S, Niu Y, Lee SO, Chang C. Androgen receptor (AR) positive vs negative roles in prostate cancer cell deaths including apoptosis, anoikis, entosis, necrosis and autophagic cell death. *Cancer Treat Rev* (2014) 40(1):31–40. doi: 10.1016/j.ctrv.2013.07.008

17. Fatokun AA, Dawson VL, Dawson TM. Parthanatos: mitochondrial-linked mechanisms and therapeutic opportunities. *Br J Pharmacol* (2014) 171(8):2000–16. doi: 10.1111/bph.12416

18. Brinkmann V, Reichard U, Goosmann C, Fauler B, Uhlemann Y, Weiss DS, et al. Neutrophil extracellular traps kill bacteria. *Sci (New York NY)* (2004) 303 (5663):1532–5. doi: 10.1126/science.1092385

19. Song X, Zhu S, Xie Y, Liu J, Sun L, Zeng D, et al. JTC801 induces pH-dependent death specifically in cancer cells and slows growth of tumors in mice. *Gastroenterology* (2018) 154(5):1480–93. doi: 10.1053/j.gastro.2017.12.004

20. Aits S, Jäättelä M. Lysosomal cell death at a glance. *J Cell Sci* (2013) 126(Pt 9):1905–12. doi: 10.1242/jcs.091181

21. Scaturro P, Pichlmair A. Oxeiptosis: a discreet way to respond to radicals. *Curr Opin Immunol* (2019) 56:37–43. doi: 10.1016/j.coi.2018.10.006

22. Carneiro BA, El-Deiry WS. Targeting apoptosis in cancer therapy. *Nat Rev Clin Oncol* (2020) 17(7):395–417. doi: 10.1038/s41571-020-0341-y

23. Zhang Z, Zhang Y, Xia S, Kong Q, Li S, Liu X, et al. Gasdermin e suppresses tumour growth by activating anti-tumour immunity. *Nature* (2020) 579(7799):415–20. doi: 10.1038/s41586-020-2071-9

24. Jiang Z, Lim SO, Yan M, Hsu JL, Yao J, Wei Y, et al. TYRO3 induces anti-PD-1/PD-L1 therapy resistance by limiting innate immunity and tumoral ferroptosis. *J Clin Invest* (2021) 131(8). doi: 10.1172/JCI139434

25. Rody A, Holtrich U, Pusztai L, Liedtke C, Gaetje R, Ruckhaeberle E, et al. T-Cell metagene predicts a favorable prognosis in estrogen receptor-negative and HER2-positive breast cancers. *Breast Cancer Res BCR* (2009) 11(2):R15. doi: 10.1186/bcr2234

26. Bell DW, Ellenson LH. Molecular genetics of endometrial carcinoma. *Annu Rev Pathol* (2019) 14:339–67. doi: 10.1146/annurev-pathol-020117-043609

27. Galon J, Pagès F, Marincola FM, Angell HK, Thurin M, Lugli A, et al. Cancer classification using the immunoscore: a worldwide task force. *J Trans Med* (2012) 10:205. doi: 10.1186/1479-5876-10-205

28. Xue YN, Xue YN, Wang ZC, Mo YZ, Wang PY, Tan WQ. A novel signature of 23 immunity-related gene pairs is prognostic of cutaneous melanoma. *Front Immunol* (2020) 11:576914. doi: 10.3389/fimmu.2020.576914

29. Zhou Z, He H, Wang K, Shi X, Wang Y, Su Y, et al. Granzyme a from cytotoxic lymphocytes cleaves GSDMB to trigger pyroptosis in target cells. *Sci (New York NY)* (2020) 368(6494). doi: 10.1126/science.aaz7548

30. Hansen JM, de Jong MF, Wu Q, Zhang LS, Heisler DB, Alto LT, et al. Pathogenic ubiquitination of GSDMB inhibits NK cell bactericidal functions. *Cell* (2021) 184 (12):3178–91.e18. doi: 10.1016/j.cell.2021.04.036

31. Gong W, Liu P, Liu J, Li Y, Zheng T, Wu X, et al. GSDMB n-terminal assembles in plasma membrane to execute pyroptotic cell death. *Genes Dis* (2022) 9(6):1405–7. doi: 10.1016/j.gendis.2021.12.022

32. Gwinn DM, Lee AG, Briones-Martin-Del-Campo M, Conn CS, Simpson DR, Scott AI, et al. Oncogenic KRAS regulates amino acid homeostasis and asparagine biosynthesis *via* ATF4 and alters sensitivity to l-asparaginase. *Cancer Cell* (2018) 33 (1):91–107.e6. doi: 10.1016/j.ccell.2017.12.003

33. Song M, Kim SH, Im CY, Hwang HJ. Recent development of small molecule glutaminase inhibitors. *Curr Topics Med Chem* (2018) 18(6):432–43. doi: 10.2174/1568026618666180525100830

34. Zhang J, Mao S, Guo Y, Wu Y, Yao X, Huang Y. Inhibition of GLS suppresses proliferation and promotes apoptosis in prostate cancer. *Bioscience Rep* (2019) 39(6). doi: 10.1042/BSR20181826

35. Weijiao Y, Fuchun L, Mengjie C, Xiaoqing Q, Hao L, Yuan L, et al. Immune infiltration and a ferroptosis-associated gene signature for predicting the prognosis of patients with endometrial cancer. *Aging* (2021) 13(12):16713–32. doi: 10.18632/aging.203190

36. Dlugosz P, Tresky R, Nimpf J. Differential action of reelin on oligomerization of ApoER2 and VLDL receptor in HEK293 cells assessed by time-resolved anisotropy and fluorescence lifetime imaging microscopy. *Front Mol Neurosci* (2019) 12:53. doi: 10.3389/fnmol.2019.00053

37. Kang SW, Baines IC, Rhee SG. Characterization of a mammalian peroxiredoxin that contains one conserved cysteine. *J Biol Chem* (1998) 273(11):6303–11. doi: 10.1074/jbc.273.11.6303

38. Chen JW, Dodia C, Feinstein SI, Jain MK, Fisher AB. 1-cys peroxiredoxin, a bifunctional enzyme with glutathione peroxidase and phospholipase A2 activities. *J Biol Chem* (2000) 275(37):28421–7. doi: 10.1074/jbc.M005073200

39. Kim JE, Lee DS, Kang TC. Sp1-mediated Prdx6 upregulation leads to clasmatodendrosis by increasing its aiPLA2 activity in the CA1 astrocytes in chronic epilepsy rats. *Antioxidants (Basel Switzerland)* (2022) 11(10). doi: 10.3390/antiox11101883

40. Montrose DC, Saha S, Foronda M, McNally EM, Chen J, Zhou XK, et al. Exogenous and endogenous sources of serine contribute to colon cancer metabolism, growth, and resistance to 5-fluorouracil. *Cancer Res* (2021) 81(9):2275–88. doi: 10.1158/0008-5472.CAN-20-1541

41. Han M, Yamaguchi S, Onishi M, Fujii T, Hosoya M, Wen X, et al. The MDM2 and CDKN2A copy-number-variation influence the TP53-signature-score in wild-type TP53 luminal type breast cancer. *Anticancer Res* (2022) 42(5):2277–88. doi: 10.21873/anticanres.15707

42. Zu Y, Chen XF, Li Q, Zhang ST, Si LN. PGC-1α activates SIRT3 to modulate cell proliferation and glycolytic metabolism in breast cancer. *Neoplasma* (2021) 68(2):352–61. doi: 10.4149/neo_2020_200530N584

43. Hu S, Sechi M, Singh PK, Dai L, McCann S, Sun D, et al. A novel redox modulator induces a GPX4-mediated cell death that is dependent on iron and reactive oxygen species. *J Med Chem* (2020) 63(17):9838–55. doi: 10.1021/acs.jmedchem.0c01016

44. Tian T, Ikeda J, Wang Y, Mamat S, Luo W, Aozasa K, et al. Role of leucine-rich pentatricopeptide repeat motif-containing protein (LRPPRC) for anti-apoptosis and tumourigenesis in cancers. *Eur J Cancer (Oxford Engl 1990)* (2012) 48(15):2462–73. doi: 10.1016/j.ejca.2012.01.018

45. Davalos AR, Coppe JP, Campisi J, Desprez PY. Senescent cells as a source of inflammatory factors for tumor progression. *Cancer Metastasis Rev* (2010) 29(2):273–83. doi: 10.1007/s10555-010-9220-9

46. Coppé JP, Desprez PY, Krtolica A, Campisi J. The senescence-associated secretory phenotype: the dark side of tumor suppression. *Annu Rev Pathol* (2010) 5:99–118. doi: 10.1146/annurev-pathol-121808-102144

47. Roh JW, Choi JE, Han HD, Hu W, Matsuo K, Nishimura M, et al. Clinical and biological significance of EZH2 expression in endometrial cancer. *Cancer Biol Ther* (2020) 21(2):147–56. doi: 10.1080/15384047.2019.1672455

48. Zhou WJ, Zhang J, Yang HL, Wu K, Xie F, Wu JN, et al. Estrogen inhibits autophagy and promotes growth of endometrial cancer by promoting glutamine metabolism. *Cell Commun Signal CCS* (2019) 17(1):99. doi: 10.1186/s12964-019-0412-9

49. Opławski M, Nowakowski R, Średnicka A, Ochnik D, Grabarek BO, Boroń D. Molecular landscape of the epithelial-mesenchymal transition in endometrioid endometrial cancer. *J Clin Med* (2021) 10(7). doi: 10.3390/jcm10071520

50. Cao M, Chan RWS, Cheng FHC, Li J, Li T, Pang RTK, et al. Myometrial cells stimulate self-renewal of endometrial mesenchymal stem-like cells through WNT5A/β-catenin signaling. *Stem Cells (Dayton Ohio)* (2019) 37(11):1455–66. doi: 10.1002/stem.3070

51. Lax SF. Pathology of endometrial carcinoma. *Adv Exp Med Biol* (2017) 943:75–96. doi: 10.1007/978-3-319-43139-0_3

52. Ledinek Ž, Sobočan M, Knez J. The role of CTNNB1 in endometrial cancer. *Dis Markers* (2022) 2022:1442441. doi: 10.1155/2022/1442441

53. González-Rodilla I, Aller L, Llorca J, Muñoz AB, Verna V, Estévez J, et al. The e-cadherin expression vs. tumor cell proliferation paradox in endometrial cancer. *Anticancer Res* (2013) 33(11):5091–5. doi: 10.1093/annonc/mdt460.34

54. Stefansson IM, Salvesen HB, Akslen LA. Prognostic impact of alterations in p-cadherin expression and related cell adhesion markers in endometrial cancer. *J Clin Oncol* (2004) 22(7):1242–52. doi: 10.1200/JCO.2004.09.034

55. Wang Y, Wang J, Yan K, Lin J, Zheng Z, Bi J. Identification of core genes associated with prostate cancer progression and outcome *via* bioinformatics analysis in multiple databases. *PeerJ* (2020) 8:e8786. doi: 10.7717/peerj.8786

56. Wang Y, Yan K, Lin J, Liu Y, Wang J, Li X, et al. CD8+ T cell Co-expressed genes correlate with clinical phenotype and microenvironments of urothelial cancer. *Front Oncol* (2020) 10:553399. doi: 10.3389/fonc.2020.553399

57. Liu C, Li X, Huang Q, Zhang M, Lei T, Wang F, et al. Single-cell RNA-sequencing reveals radiochemotherapy-induced innate immune activation and MHC-II upregulation in cervical cancer. *Signal Transduct Target Ther* (2023) 8(1):44. doi: 10.1038/s41392-022-01264-9

58. Liu C, Zhang M, Yan X, Ni Y, Gong Y, Wang C, et al. Single-cell dissection of cellular and molecular features underlying human cervical squamous cell carcinoma initiation and progression. *Sci Adv* (2023) 9(4):eadd8977. doi: 10.1126/sciadv.add8977

frontiers | Frontiers in Oncology

TYPE Original Research
PUBLISHED 11 August 2023
DOI 10.3389/fonc.2023.1235902

OPEN ACCESS

EDITED BY
Tiziana Triulzi,
Fondazione IRCCS Istituto Nazionale dei Tumori, Italy

REVIEWED BY
Takeo Fujii,
National Institutes of Health (NIH), United States
Valentina Zavala,
University of California, Davis, United States

*CORRESPONDENCE
Sarah Sammons
sarahl_sammons@dfci.harvard.edu

†These authors have contributed equally to this work and share first authorship

RECEIVED 06 June 2023
ACCEPTED 17 July 2023
PUBLISHED 11 August 2023

CITATION
Sammons S, Elliott A, Barroso-Sousa R, Chumsri S, Tan AR, Sledge GW Jr, Tolaney SM and Torres ETR (2023) Concurrent predictors of an immune responsive tumor microenvironment within tumor mutational burden-high breast cancer.
Front. Oncol. 13:1235902.
doi: 10.3389/fonc.2023.1235902

Concurrent predictors of an immune responsive tumor microenvironment within tumor mutational burden-high breast cancer

Sarah Sammons[1,2,3*†], Andrew Elliott[4†], Romualdo Barroso-Sousa[5,6], Saranya Chumsri[7], Antoinette R. Tan[8], George W. Sledge Jr.[4], Sara M. Tolaney[1,2,3] and Evanthia T. Roussos Torres[9]

[1]Department of Medical Oncology, Dana-Farber Cancer Institute, Boston, MA, United States, [2]Breast Oncology Program, Dana-Farber Brigham Cancer Center, Boston, MA, United States, [3]Harvard Medical School, Boston, MA, United States, [4]Clinical and Translational Research, Caris Life Sciences, Phoenix, AZ, United States, [5]Department of Oncology, Dasa Institute for Education and Research (IEPD), Brasilia, Brazil, [6]Dasa Oncology/Hospital Brasilia, Brasilia, Brazil, [7]Department of Hematology Oncology and Department of Cancer Biology, Mayo Clinic, Jacksonville, FL, United States, [8]Levine Cancer Institute, Atrium Health, Charlotte, NC, United States, [9]Division of Oncology, Department of Medicine, Keck School of Medicine, Norris Comprehensive Cancer Center, University of Southern California, Los Angeles, CA, United States

Background: Data supporting high tumor mutational burden (TMB-H) as a lone biomarker for an immune-responsive tumor microenvironment (TME) in metastatic breast cancer (MBC) are weak, yet tumor agnostic approval in TMB-H advanced tumors provides immune checkpoint inhibition (ICI) as a clinical option. We evaluated concurrent predictors of immune-responsive and non-responsive TME within MBC.

Methods: Tumor samples from patients with MBC (N=5621) were analyzed by next-generation sequencing of DNA (592-gene panel or whole exome) and RNA (whole transcriptome) at Caris Life Sciences (Phoenix, AZ). TMB-H threshold was set to ≥ 10 muts/Mb. PDL-1 was evaluated using SP142 antibody. Gene expression profiling and RNA deconvolution were used to estimate immune and stromal cell population abundance in the TME, and transcriptomic signature of immunotherapy response (T cell-inflamed score).

Results: 461 (8.2%) TMB-H MBC samples were identified. Consistent with prior studies, TMB-H tumors exhibited significant dMMR/MSI-H enrichment (7 vs. 0%, p<0.0001) and PD-L1+ expression (36 vs. 28%, p<0.05) compared to TMB-L. Across all samples, T cell-inflamed scores were weakly correlated with TMB. TMB-H was not associated with significantly increased immune responsive cell types (CD8+ T-cells, NK cells, or B cells) or immune response gene signatures (e.g. antigen presentation), yet positive trends were observed, while immunosuppressive fibroblasts were significantly decreased in TMB-H tumors (0.84-fold change compared to TMB-L, P<0.05). HR+/HER2- breast cancer was

the only subtype in which TMB-H tumors exhibited increased T cell-inflamed scores vs. TMB-L. Concurrent PD-L1+ or dMMR/MSI-H with TMB-H was associated with high T cell-inflamed scores in both HR+/HER2- and TNBC. Among several associated biomarkers, *B2M* mutations and *CD274* amplifications were positively associated with T-cell inflamed scores in TMB-H tumors; *CDH1* and *ERBB2* mutations were negatively associated.

Conclusion: High TMB alone does not strongly correlate with immune infiltrate or immune-related gene signatures in MBC. TMB-H predicts T-cell inflamed signature compared to TMB-L in HR+/HER2- tumors only. Along with MSI-H and PD-L1+, several biomarkers, including *B2M* mutation and *CD274* amplification, may help predict ICI benefit amongst TMB-H tumors. Co-occurring biomarkers within TMB-H breast cancer warrant evaluation in larger cohorts for response or resistance to ICI to develop composite predictive biomarkers in MBC.

KEYWORDS

breast cancer, tumor mutational burden, genetic profiling, microenvironment, immune checkpoint inhibitors

Introduction

Data supporting high tumor mutational burden (TMB-H) as a lone biomarker for an immune-responsive tumor microenvironment (TME) in metastatic breast cancer (MBC) is weak, yet the tumor agnostic approval of immune checkpoint inhibitors (ICI) in TMB-H advanced tumors makes this an option in the clinic. The U.S. Food and Drug Administration (FDA) approved pembrolizumab on June 16, 2020, for the advanced TMB-H (≥10 mutations/megabase (mut/Mb), as determined by an FDA-approved test) solid tumors that have progressed following prior treatment with no satisfactory alternative treatment options. This approval was based on an overall response rate of 29% (95% CI, 21-39) in the subset of patients with TMB-H solid tumors (n = 102) spanning nine different tumor types enrolled in a multicenter single-arm trial KEYNOTE-158 (1). There were no MBC patients in this trial, making extrapolation to this population impossible. In pooled meta-analyses, TMB does not predict survival in MBC (2).

The TAPUR clinical trial included a TMB-H MBC cohort that enrolled 28 patients with TMB ranging from 9-37 mut/Mb by Foundation Medicine CDX, who were enrolled to receive pembrolizumab monotherapy every 3 weeks (3). The overall response rate (ORR) was 21% (95% confidence interval (CI), 8 to 41), and the median progression-free survival (PFS) was 10.6 weeks (95% CI, 7.7 to 21.1). Though this is a respectable ORR in heavily pretreated MBC for therapy with tolerable safety, most TMB-H patients will not derive benefit from ICI monotherapy, and further biomarkers within TMB-H MBC to predict an immune hot TME are needed.

We sought to further evaluate concurrent predictors of an immune-responsive or non-responsive TME within TMB-H MBC.

Materials and methods

Patient samples/study cohort

Formalin-fixed paraffin-embedded (FFPE) samples from patients with breast cancer (n=5621) were submitted by various academic and community cancer institutes, predominately in the United States, to a commercial CLIA-certified laboratory for molecular profiling (Caris Life Sciences, Phoenix, AZ). The present study was conducted in accordance with the guidelines of the Declaration of Helsinki, Belmont Report, and U.S. Common Rule. In compliance with policy 45 CFR 46.101(b), this study was conducted using retrospective, de-identified clinical data, patient consent was not required, and the study was considered IRB exempt.

Next-generation sequencing (NGS)

NGS of 592 cancer-relevant genes was performed on genomic DNA isolated from formalin-fixed paraffin-embedded (FFPE) tumor samples using the NextSeq platform (Illumina, Inc., San Diego, CA, USA). Matched normal tissue or germline DNA was not sequenced. A custom-designed SureSelect XT assay was used to enrich exonic regions of 592 whole-gene targets (Agilent Technologies, Santa Clara, CA, USA). All variants were detected with >99% confidence based on allele frequency and amplicon coverage, with an average sequencing depth of coverage of >500 and an analytic sensitivity threshold established of 5% for variant calling. Prior to molecular testing, tumor enrichment was achieved by harvesting targeted tissue using manual microdissection techniques. Genomic variants were classified by board-certified

molecular geneticists according to criteria established by the American College of Medical Genetics and Genomics (ACMG). When assessing mutation frequencies of individual genes, 'pathogenic' and 'likely pathogenic' were counted as mutations, while 'benign', 'likely benign' variants, and 'variants of unknown significance' were excluded.

RNA Whole Transcriptome Sequencing (WTS) uses a hybrid-capture method to pull down the full transcriptome from FFPE tumor samples (using the Agilent SureSelect Human All Exon V7 bait panel (Agilent Technologies, Santa Clara, CA, USA) and the Illumina NovaSeq platform (Illumina, Inc., San Diego, CA, USA). FFPE specimens underwent pathology review to discern the percent tumor content and tumor size; a minimum of 20% tumor content in the area for microdissection was required to enable enrichment and extraction of tumor-specific RNA. A Qiagen RNA FFPE tissue extraction kit was used for extraction, and the RNA quality and quantity were determined using the Agilent TapeStation. Biotinylated RNA baits were hybridized to the synthesized and purified cDNA targets, and the bait-target complexes were amplified in a post-capture PCR reaction. The resultant libraries were quantified and normalized, and the pooled libraries were denatured, diluted, and sequenced. Raw data were demultiplexed using the Illumina DRAGEN FFPE accelerator. FASTQ files were aligned with STAR aligner (Alex Dobin, release 2.7.4a GitHub). A full 22,948-gene dataset of expression data was produced by the Salmon, which provided fast and bias-aware quantification of transcript expression BAM files from STAR aligner (4), and were further processed for RNA variants using a proprietary custom detection pipeline. The reference genome used was GRCh37/hg19, and analytical validation of this test demonstrated ≥97% Positive Percent Agreement (PPA), ≥99% Negative Percent Agreement (NPA), and ≥99% Overall Percent Agreement (OPA) with a validated comparator method.

RNA signatures

T cell-inflamed scores were defined by an 18-gene signature, with scores calculated as the weighted sum of log2-transformed gene expression values using previously reported coefficients (5). The Microenvironment Cell Populations (MCP)-counter tool was used to assess the relative abundance of immune and stromal cells in the tumor microenvironment (6, 7).

Immunohistochemistry (IHC)

IHC was performed on FFPE sections of glass slides. Slides were stained using the Agilent DAKO Link 48 (Santa Clara, CA, USA) automated platform and staining techniques, per the manufacturer's instructions, and were optimized and validated per CLIA/CAP and ISO requirements. Staining was scored for intensity (0 = no staining; 1+ = weak staining; 2+ = moderate staining; 3+ = strong staining) and staining percentage (0–100%). Positive expression of immune cell (IC) PD-L1 (SP142), tumor cell ESTROGEN RECEPTOR (ER), and tumor cell PROGESTERONE RECEPTOR (PR) was defined as ≥1+ stain intensity and ≥1% of cells stained. Positive HER2 expression was determined according to the 2018 ASCO-CAP guidelines (8).

Tumor mutational burden (TMB)

TMB was measured by counting all non-synonymous missense, nonsense, in-frame insertion/deletion, and frameshift mutations found per tumor that had not been previously described as germline alterations in dbSNP151, Genome Aggregation Database (gnomAD) databases, or benign variants identified by Caris's geneticists. TMB-H was defined by a threshold of ≥10 mutations per megabase (mut/MB) based on the KEYNOTE-158 pembrolizumab trial (1).

Mismatch repair/microsatellite instability

Deficient mismatch repair/microsatellite instability-high (dMMR/MSI-H) was determined by a combination of IHC (MLH1, M1 antibody; MSH2, G2191129 antibody; MSH6, 44 anti-body; and PMS2, EPR3947 antibody (Ventana Medical Systems, Inc., Tucson, AZ) and NGS (>2800 target microsatellite loci were examined and compared to the reference genome hg19 from the University of California, Santa Cruz (UCSC) Genome Browser database). The platforms generated highly concordant results as previously reported (9) and in the rare cases of discordant results, the status was determined by IHC.

Statistical analyses

All statistical analyses were performed with JMP V13.2.1 (SAS Institute, Cary, NC, USA). Continuous data were assessed using a Mann-Whitney U test, and categorical data were evaluated using Chi-square or Fisher's exact test, where appropriate. P-values were adjusted for multiple hypothesis testing using the Benjamini-Hochberg procedure, unless noted as exploratory (not adjusted).

Results

Clinical and molecular characteristics associated with TMB-H breast cancer

Comprehensive molecular profiles of breast cancer patient samples (N=5621) were analyzed from various cancer institutes, predominantly within the United States. Samples were stratified into TMB-H (N=461, 8.2%) and TMB-Low cohorts based on a threshold of ≥10 mut/MB (Table 1). Utilizing different cut-offs, 4% of patients had a TMB ≥ 14 and 1.81% had TMB ≥ 20. Compared to TMB-Low tumors, the TMB-H cohort had an increased median age (64 vs. 60 years, $p<0.0001$) and a greater proportion of distant metastatic tumor biopsy sites compared to breast biopsy specimens (78.3% vs. 60.3%, $p<0.0001$). As previously described, TMB-H

TABLE 1 Overall cohort characteristics and of TMB-H and TMB-L cohorts.

Characteristic	Overall	TMB-H	TMB-L	P-value
Samples, N (%)	5621 (100%)	461 (8.2%)	5160 (91.8%)	————————
Median Age, years - Range	60 19-90+	64 26-90+	60 19-90+	< 0.0001
Gender, N (%) - Female - Male	 5572 (99.1%) 49 (0.9%)	 458 (99.3%) 3 (0.7%)	 5114 (99.1%) 46 (0.9%)	0.59
Biopsy site - Primary - Metastatic	 2115 (37.6%) 3506 (62.4%)	 100 (21.7%) 361 (78.3%)	 2015 (39.1%) 3145 (60.9%)	< 0.0001
Histology, N (%) - Ductal - Lobular - Metaplastic - Mixed - [NOS]	 2273 (40.4%) 349 (6.2%) 85 (1.5%) 58 (1.0%) [2856]	 116 (65.9%) 56 (31.8%) 2 (1.1%) 2 (1.1%) [285]	 2157 (83.3%) 293 (11.3%) 83 (3.2%) 56 (2.2%) [2571]	< 0.0001
Receptor Subtypes, N (%) - HR+/HER2+ - HR+/HER2- - HR-/HER2+ - Triple Negative - [Unclear]	 266 (5.3%) 3087 (61.6%) 179 (3.6%) 1476 (29.5%) [613]	 22 (5.4%) 242 (59.7%) 14 (3.5%) 127 (31.4%) [56]	 244 (5.3%) 2845 (61.8%) 165 (3.6%) 1349 (29.3%) [557]	0.85

TMB-H, high tumor mutational burden; TMB-L, low tumor mutational burden; NOS, not otherwise specified; HR, hormone receptor; HER2, human epidermal growth factor receptor 2.

tumors were more likely to be invasive lobular than invasive ductal carcinoma (31.8% vs. 11.3%, p<0.0001) (10). The distribution of receptor subtypes (HR+/HER2-, HR-/HER2-, HR+/HER2+, HR-/HER2+) was similar between TMB-H and TMB-low cohorts.

TMB-H is a poor predictor of inflamed tumor microenvironments (TMEs) in breast cancer

Despite the FDA approval of pembrolizumab for the treatment of adult and pediatric patients with unresectable or metastatic TMB-H solid tumors, not all TMB-H tumors will respond to therapy, suggesting additional predictive biomarkers are needed. We estimated immune and stromal cell population abundance in breast cancer TMEs using the MCP-Counter tool and observed similar distributions in TMB-H and TMB-L tumors for most cell populations (Figure 1A). While TMB-H tumors have slightly increased median abundance of pro-immune cell types (e.g. T cells, not significant), presumably immunosuppressive fibroblasts were significantly decreased in TMB-H tumors (0.84-fold change compared to TMB-L, P<0.05).

A transcriptional 'T cell-inflamed' score, which was previously demonstrated to predict response to ICI therapy in all tumor types (5), was significantly increased in TMB-H tumors compared to TMB-Low (4.15 vs. 4.02, P<0.01), though the score distributions largely overlapped (Figure 1B), and correlated with immune and stromal cell population abundance in both TMB-H and TMB-L tumors (Figure 1C). Similar to individual TME cell populations, the T cell-inflamed score was weakly correlated with the number of muts/Mb. Tumors with very high TMB > 20 were very limited in our population making true assessments of the immune TME in these patients challenging.

PD-L1 positivity and Microsatellite instability are enriched in TMB-H tumors and further predict an inflamed tumor microenvironment

PD-L1 expression on tumor immune cells is a consistent biomarker of ICI response in advanced/metastatic first-line triple-negative breast cancer (TNBC) (11–13). PD-L1 expression on immune cells (PD-L1+ IC [SP142]) was more common in TMB-H versus TMB-Low tumors (35.7% vs. 27.9%, p<0.001) (Figure 2A). PD-L1 evaluation by Dako 22C3 combined positive score was not available in this dataset. dMMR/MSI-High, a known mechanism of tumor hypermutation, is another tumor agnostic FDA-approved biomarker for ICI. In the entire cohort, dMMR/MSI-High status was rare with an overall frequency of 0.8% (46/5570) of all breast tumors. dMMR/MSI-High status (7.2% vs. 0.3%, p<0.001) was almost exclusively found in TMB-H tumors. The median TMB of TMB-H/MSI-High was 24 mut/Mb versus 13 mut/Mb TMB-H/MSI stable. Greater differences in median T cell-inflamed scores were observed when samples were further stratified by PD-L1+ IC and dMMR/MSI-High status (Figures 2B, C). Tumors that were TMB-H and PD-L1+ had significantly higher T-cell inflamed scores than TMB-H PD-L1- tumors. Interestingly, this was true in both TMB-H and TMB-L cohorts suggesting that immune responsive TME's exist in TMB-L tumors with PD-L1+.

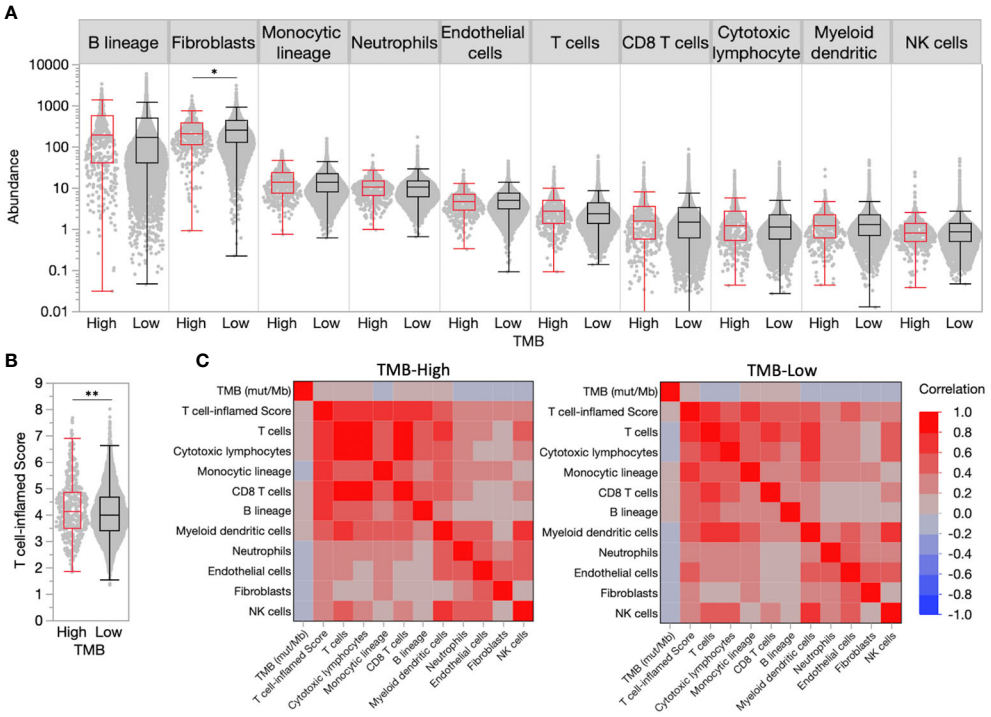

FIGURE 1
High tumor mutational burden (TMB-H) is a poor predictor of inflamed tumor microenvironments (TMEs) in breast cancer. **(A)** TME immune and stromal cell population abundance in TMB-H and low tumor mutational burden (TMB-L) tumors. **(B)** Distribution of T cell-inflamed scores in TMB-H and TMB-L tumors. **(C)** Correlation matrix for TMB, T cell-inflamed scores, and immune/stromal cell population abundance in TMB-H and TMB-L tumors. *P<0.05, **P<0.01.

TMEs vary across breast cancer receptor subtypes and histologies

Among breast cancer receptor subtypes, median T cell-inflamed scores were highest among TNBC samples, which were significantly increased compared to HR+/HER2- samples that exhibited the lowest median score (4.17 vs. 3.96, P<0.001) (Figure 3A). While TMB-H HR+/HER2- samples had significantly increased T cell-inflamed scores compared to TMB-L, scores in other receptor subtypes were not significantly different when stratified by TMB status (Figure 3B). Similar to the overall trend, T cell-inflamed scores were increased HR+/HER2- and TNBC samples further stratified by PD-L1+ IC status in both TMB-H and TMB-L subgroups, while scores associated with dMMR/MSI-High status varied by receptor subtype (Figures 3C, D).

Comparison of histological subtypes found significantly increased T cell-inflamed scores in ductal vs. lobular tumors (4.14 vs. 3.90, P<0.001) (Figure 4A). TMB-H ductal tumors had

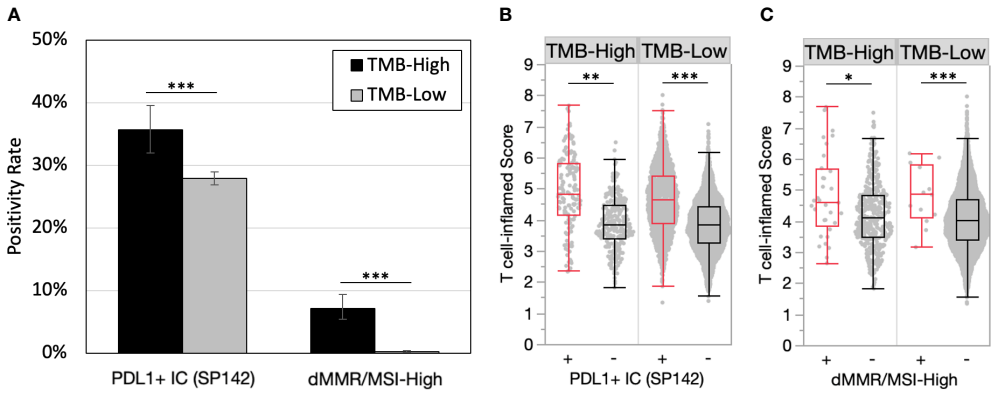

FIGURE 2
PD-L1 positivity and microsatellite instability are enriched in TMB-H tumors and predict inflamed TMEs. **(A)** PD-L1+ immune cells **(IC)** (SP142) and dMMR/MSI-High positivity rates in TMB-H and TMB-L tumors. **(B-C)** T cell-inflamed scores in by PD-L1+ IC (SP142) **(B)** and dMMR/MSI-High status **(C)**. *P<0.05, **P<0.01, ***P<0.001.

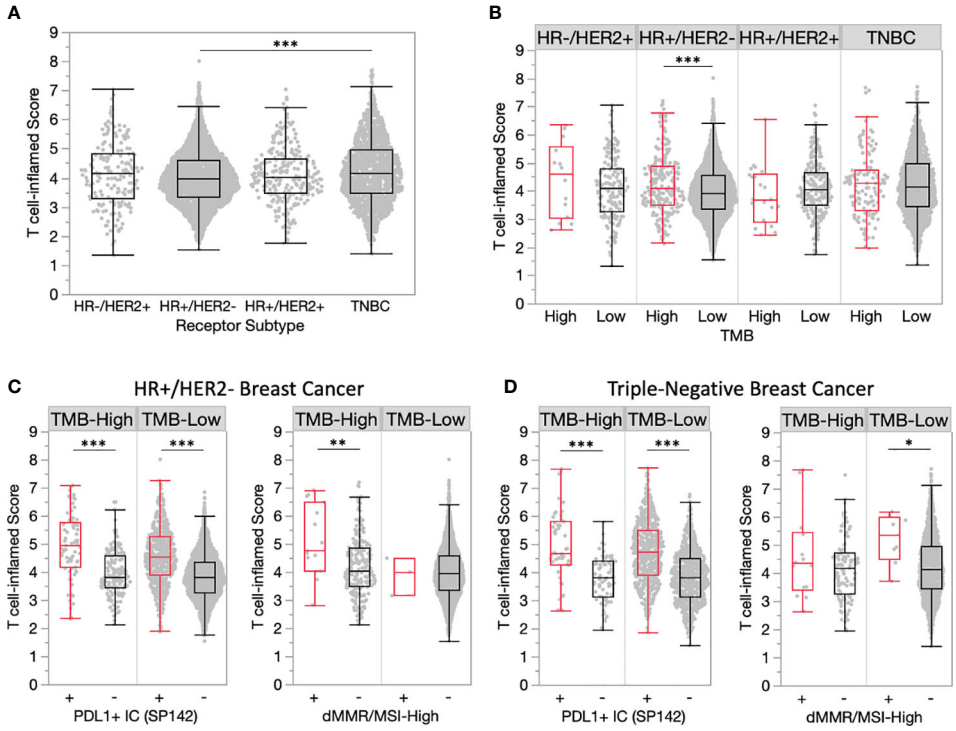

FIGURE 3
TMEs vary across breast cancer receptor subtypes. **(A)** T cell-inflamed scores in receptor subtype subgroups. **(B)** T cell-inflamed scores in TMB-H and TMB-L tumors by receptor subtype. **(C-D)** T cell-inflamed scores in TMB-H and TMB-L HR+/HER2- **(C)** and triple-negative **(D)** subgroups further stratified by PD-L1+ immune cells **(IC)** (SP142) and dMMR/MSI-High status. *P<0.05, **P<0.01, ***P<0.001.

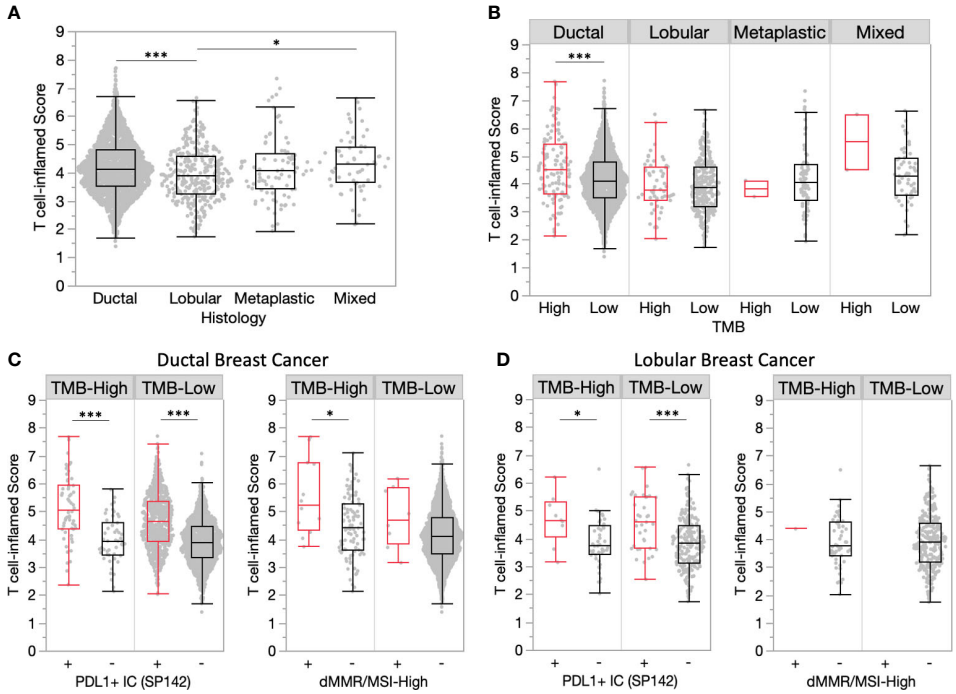

FIGURE 4
Ductal tumors have more inflamed TMEs compared to lobular tumors. **(A)** T cell-inflamed scores in ductal and lobular subgroups. **(B)** T cell-inflamed scores in TMB-H and TMB-L tumors by histology. **(C-D)** T cell-inflamed scores in TMB-H and TMB-L ductal **(C)** and lobular **(D)** subgroups further stratified by PD-L1+ immune cells **(IC)** (SP142) and dMMR/MSI-High status. *P<0.05, ***P<0.001.

significantly increased T cell-inflamed scores compared to TMB-L, yet this was not observed in other histological subtypes (Figure 4B). PDL1+ immune cells within ductal and lobular tumors were consistently associated with significantly increased T cell-inflamed scores regardless of TMB status (Figures 4C, D). A similar trend was observed for dMMR/MSI-High ductal tumors, while lobular tumors were rarely dMMR/MSI-High.

Biomarker association with inflamed tumor microenvironments

To identify new predictive biomarkers of inflamed tumor microenvironments, we compared T cell-inflamed scores in TMB-H and TMB-L cohorts stratified by biomarker status (mutation, amplification, fusion, etc). Consistent with our initial analysis, PD-L1+ IC was associated with higher T cell-inflamed scores in TMB-H tumors, while scores associated with many of the most commonly altered biomarkers were much more variable (Figure 5A). However, several other biomarkers were associated with significantly higher or lower scores, including mutations in *CDH1* and *ERBB2* that associated with lower T cell-inflamed scores in TMB-H tumors (Figure 5B). This is of interest as *CDH1* mutations are strongly present in lobular breast cancer and is consistent with lower scores in lobular compared to ductal tumors. *ZNF703* and *ADGRA2* copy number amplifications were associated with lower T cell-inflamed scores, regardless of TMB status (Figures 5B, C). Several alterations were associated with differences in T cell-inflamed scores only in TMB-H or TMB-Low cohorts. Interestingly, in TMB-H tumors, increased T cell-inflamed scores were associated with mutations in *B2M (Beta-2 microglobulin)*, a scaffolding protein essential for MHC-I complex formation and peptide presentation. *CD274* (PDL-1) amplification was also associated with T cell-inflamed score in TMB-H tumors.

We further evaluated TMB-H vs TMB-L T cell-inflamed scores in HR+/HER2- (Figures 5D, E) and TNBC subgroups (Figures 5F, G). Many biomarkers were significantly associated with higher or lower T cell-inflamed scores in a receptor subtype-dependent manner. For example, while dMMR/MSI-High and *SETD2* mutations were associated with higher scores and *CDH1* mutations were associated with lower scores in TMB-H HR +/HER2- samples, *EP300* mutations and *CD247* amplifications were associated with higher scores and *LZTR1* mutations were associated with lower scores in TMB-H TNBC samples.

Discussion

Tumor mutational burden is an overall poor predictor of ICI response in metastatic breast cancer. The TAPUR clinical trial is the largest series to evaluate single agent immunotherapy in TMB-H MBC defined as ≥ 9 mut/Mb by Foundation Medicine CDX. The ORR to single agent pembrolizumab was 21% (95% CI, 8 to 41) and the median PFS was 10.6 weeks (95% CI, 7.7 to 21.1) (3). However, TMB as a continuous variable did not predict response. More recently, the NIMBUS clinical trial evaluated the efficacy of immunotherapy combination, ipilimumab and nivolumab, in TMB-H (defined as ≥ 9 mut/Mb) HER2-negative MBC (14). After a median follow-up of 10 months, the ORR was 16.7%, though the median duration of response has not been reached

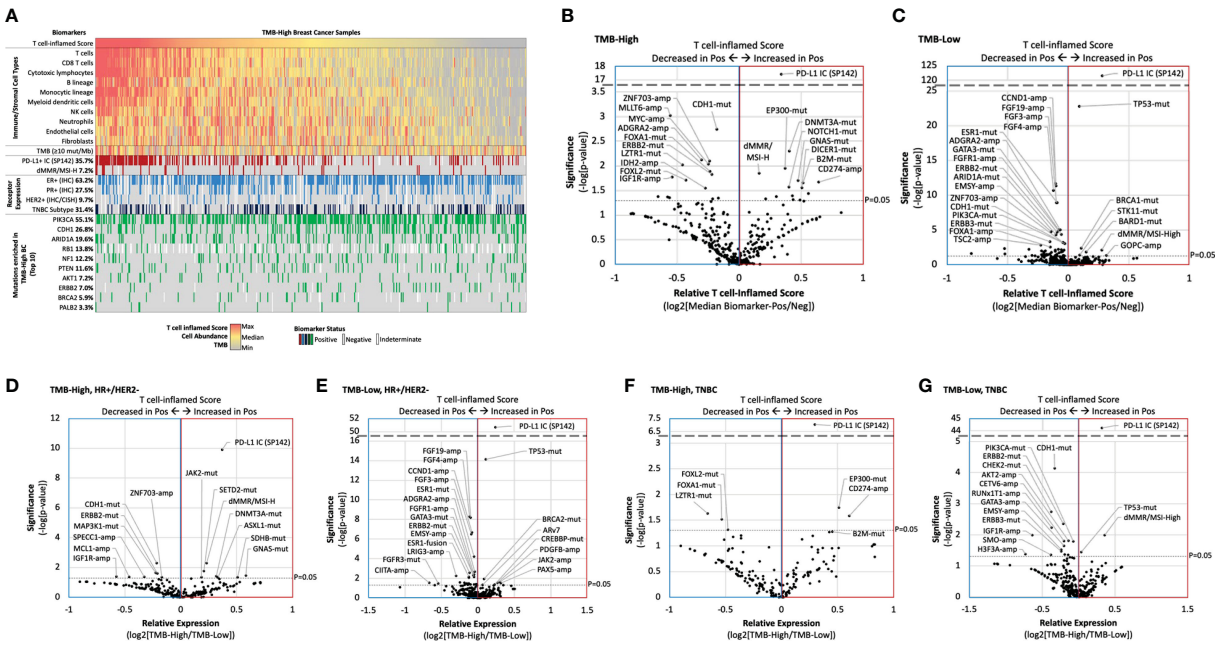

FIGURE 5
Biomarker association with inflamed tumor microenvironments. **(A)** Oncoprint of TMB-H breast cancer T cell-inflamed score immune/stromal cell population abundance, and key biomarkers. **(B-G)** Relative T cell-inflamed score according to biomarker status (ratio of median biomarker-positive [Pos]/negative [Neg]) in TMB-H **(B, D, F)** and TMB-L samples **(C, E, G)** for the overall cohort (B,C), HR+/HER2- samples **(D, E)**, and TNBC samples **(F, G)**.

and 3 patients were progression-free for at least 15 months. The median PFS and overall survival (OS) was respectively 1.4 (95% CI 1.3 - 9.5) months and 8.8 (95% CI 4.2 - not reached). Response rate in patients with TMB ≥ 14 muts/Mb was 60%, suggesting the ultra-high TMB patients may have an immune responsive TME. Given the known toxicities of ICI, identification of biomarkers within TMB-H tumors to predict ICI response and immune responsive TME would be of particular importance.

In a large cohort of 5621 breast cancer tumors, we identified 461 (8.2%) TMB-H tumors and examined concurrent predictive biomarkers of an immune-inflamed TME to assess predictors of immune checkpoint blockade (ICB) response. RNA signatures hold promise as biomarkers of immunotherapy response across solid tumor malignancies. We used a well validated T cell-inflamed scores defined by an 18-gene signature to select tumors with an immune responsive TME within this cohort (5). This immune signature has correlated strongly with response to ICI in solid tumors. The T-cell inflamed score was significantly increased in TMB-H tumors compared to TMB-Low (4.15 vs. 4.02, P<0.01), though the score distributions largely overlapped (Figure 1B) indicating weak association. TMB-H was a biomarker of T-cell inflamed score within the HR+, HER2- negative subtype but not in HER2+ or triple negative tumors. This is of particular interest as nearly ¾ of all breast cancers are HR+, HER2-. In unselected HR+/HER2- breast cancer, immune checkpoint inhibition has not been effective (15, 16). Our data support the use of TMB as a biomarker of ICI response in future prospective clinical trials of HR+, HER2- MBC.

We then assessed the impact of known biomarkers of immune response in breast cancer and solid tumors within TMB-H breast cancer and found that PD-L1 positivity and microsatellite instability were enriched in TMB-H tumors and predicted inflamed TMEs. This finding was true regardless of tumor subtype (HR+ and TNBC) and histology (ductal and lobular). These findings are particularly clinically relevant as commercially available next generation sequencing tests routinely report PD-L1 and dMMR/MSI-H status along with TMB. A logical next step to this analysis would be to assess ICI responses in patients with TMB-H and PDL-1+ tumors in prospective or retrospective cohorts. One limitation of this study is the use of PD-L1 testing using the Ventana SP142 assay on tumor immune cells, which is no longer used in United States clinical practice. These findings should be repeated using diverse PD-L1 assays.

Lobular breast cancer encompasses about 10% of all breast tumors with increasing incidence in recent decades (17). Several studies have shown that TMB-H lobular tumors have higher TMB than ductal tumors, making immunotherapy an appealing strategy (18). Inactivating *CDH1* mutations are found in 53% of lobular breast cancers in the literature (19) and have higher median TMB than ductal tumors (18). In this analysis, lobular tumors had significantly lower T-cell inflamed scores than ductal tumors. Furthermore, *CDH1* mutations were associated with lower T-cell inflamed score within TMB-H tumors. T-cell inflamed scores in lobular tumors were similar between TMB-H and TMB-L. These data suggest that neither lobular histology nor the composite of lobular and TMB-H will be strong enough predictors of an immune responsive tumor microenvironment. PD-L1 positivity did still enrich for a higher immune TME within lobular tumors, suggesting PD-L1+ lobular BC could be a better predictor of ICI response. The multicenter GELATO-trial (NCT03147040) evaluated patients with metastatic lobular breast cancer treated with induction carboplatin followed by atezolizumab (PD-L1 inhibitor). Four (4/21) patients with triple negative disease had a partial response to treatment (20) without any responses reported in the HR+ patients, suggesting ICI is not a promising strategy in unselected lobular tumors.

Lastly, our analysis showed that *B2M* mutations and *CD274* amplifications were associated with a strong T-cell inflamed score within TMB-H tumors and not TMB-Low tumors, which was also observed in TNBC but not HR+/HER2- subgroups. Recent data suggest that somatic *B2M* mutations are associated with a higher load of neoantigens for MHC-I presentation (21), which could lead to T cell recognition in the setting of ICI. Programmed death ligand-1 (PD-L1) is encoded by the *CD274* gene is a target for both PDL-1 and PD-1 inhibitors. Although PDL-1/CD274 amplification in solid tumors is rare, it has been linked to ICI response in small series (22). Furthermore, in the randomized phase II SAFIR02-BREAST IMMUNO trial, durvalumab was studied as maintenance therapy after chemotherapy induction in MBC patients, and in an exploratory analyses of TNBC patients, durvalumab efficacy was limited to those with CD274 gain/amplification (23).

There are several limitations of this analysis. The lack of matched treatment and response data limits our ability to determine potential therapy-induced effects on the TME signatures evaluated, as well as limiting the evaluation of immune-related signatures and co-alterations as predictive biomarkers of response to therapy. Additionally, as bulk tumor sequencing approaches do not allow for robust characterization of cell type-specific molecular features or signals, future studies utilizing single-cell sequencing may provide novel insights of breast cancer TMEs.

In conclusion, high TMB alone does not strongly correlate with immune infiltrate or immune-related gene signatures in further unselected MBC. In our dataset, TMB-H predicted a more immune responsive microenvironment compared to TMB-L in HR+, HER2- tumors which could further be enhanced when selecting PD-L1+ tumors. This subset of patients would be relatively rare, though a small prospective trial assessing immunotherapy strategies in this population would be warranted. *B2M* mutation and *CD274* amplification may help predict benefit to ICI within TMB-H MBC. Co-occurring biomarkers within TMB-H breast cancer warrant further evaluation in larger cohorts for response or resistance to ICI to help develop composite predictive biomarkers in MBC.

Data availability statement

The datasets presented in this article are not readily available because the raw data is protected proprietary information. Requests to access the datasets should be directed to aelliott@carisls.com of Caris Life Sciences.

Ethics statement

Ethical review and approval was not required for the study on human participants in accordance with the local legislation and institutional requirements. Written informed consent for participation was not required for this study in accordance with the national legislation and the institutional requirements.

Author contributions

SS and ET: Conception, design, data analysis, manuscript writing and editing. AE: Conception, design, data analysis, biostatistical analysis. RB-S and ST: data analysis, manuscript editing. SC, AT, and GS: data analysis, manuscript editing. All authors contributed to the article and approved the submitted version.

Acknowledgments

The authors would like to thank Valerie Hope Goldstein for her assistance with editing and manuscript submission.

Conflict of interest

SS declares research funding to their institution from Astra Zeneca, Eli Lilly, SEAGEN and Sermonix; and consulting fees from Foundation Medicine, Astra Zeneca, Daiichi-Sankyo, Eli Lilly, Pfizer, SEAGEN, Sermonix and Novartis. RB-S reports receiving speaker bureau fees from AstraZeneca, Daiichi-Sankyo, Eli Lilly, Pfizer, Novartis, Merck, and Roche. He has also served as a consultant/advisor for AstraZeneca, Daiichi-Sankyo, Eli Lilly, Libbs, Merck, Roche and has received support for attending medical conferences from Astrazeneca, Roche, Eli Lilly, Daiichi-Sankyo, and Merck. ST reports serving in consulting or advisory roles for Novartis, Pfizer, Merck, Eli Lilly, AstraZeneca, Genentech/Roche, Eisai, Sanofi, Bristol Myers Squibb, Seattle Genetics, CytomX Therapeutics, Daiichi-Sankyo, Gilead, Ellipses Pharma, 4D Pharma, OncoSec Medical Inc., BeyondSpring Pharmaceuticals, OncXerna, Zymeworks, Zentalis, Blueprint Medicines, Reveal Genomics, ARC Therapeutics, Infinity Therapeutics, Myovant, Zetagen, Umoja Biopharma, Artios Pharma, Menarini/Stemline, Aadi Biopharma, Bayer, and Incyte Corp.; and research funding from Genentech/Roche, Merck, Exelixis, Pfizer, Lilly, Novartis, Bristol Myers Squibb, Eisai, AstraZeneca, Gilead, NanoString Technologies, Gilead, Seattle Genetics, and OncoPep.

The remaining authors declare that the research was conducted in the absence of any commercial or financial relationships that could be construed as a potential conflict of interest.

Publisher's note

References

1. Marabelle A, Fakih M, Lopez J, Shah M, Shapira-Frommer R, Nakagawa K, et al. Association of tumour mutational burden with outcomes in patients with advanced solid tumours treated with pembrolizumab: prospective biomarker analysis of the multicohort, open-label, phase 2 KEYNOTE-158 study. *Lancet Oncol* (2020) 21 (10):1353–65. doi: 10.1016/S1470-2045(20)30445-9

2. Ke L, Li S, Cui H. The prognostic role of tumor mutation burden on survival of breast cancer: a systematic review and meta-analysis. *BMC Cancer* (2022) 22(1):1185. doi: 10.1186/s12885-022-10284-1

3. Alva AS, Mangat PK, Garrett-Mayer E, Halabi S, Hansra D, Calfa CJ, et al. Pembrolizumab in patients with metastatic breast cancer with high tumor mutational burden: results from the targeted agent and profiling utilization registry (TAPUR) study. *J Clin Oncol* (2021) 39(22):2443–51. doi: 10.1200/JCO.20.02923

4. Patro R, Duggal G, Love MI, Irizarry RA, Kingsford C. Salmon provides fast and bias-aware quantification of transcript expression. *Nat Methods* (2017) 14(4):417–9. doi: 10.1038/nmeth.4197

5. Cristescu R, Mogg R, Ayers M, Albright A, Murphy E, Yearley J, et al. Pan-tumor genomic biomarkers for PD-1 checkpoint blockade-based immunotherapy. *Science* (2018) 362(6411):eaar3593. doi: 10.1126/science.aar3593

6. Becht E, Giraldo NA, Lacroix L, Buttard B, Elarouci N, Petitprez F, et al. Estimating the population abundance of tissue-infiltrating immune and stromal cell populations using gene expression. *Genome Biol* (2016) 17(1):218. doi: 10.1186/s13059-016-1070-5

7. Becht E, Giraldo NA, Lacroix L, Buttard B, Elarouci N, Petitprez F, et al. Erratum to: Estimating the population abundance of tissue-infiltrating immune and stromal cell populations using gene expression. *Genome Biol* (2016) 17(1):249. doi: 10.1186/s13059-016-1113-y

8. Wolff AC, Hammond MEH, Allison KH, Harvey BE, Mangu PB, Bartlett JMS, et al. Human epidermal growth factor receptor 2 testing in breast cancer: American society of clinical oncology/college of American pathologists clinical practice guideline focused update. *J Clin Oncol* (2018) 36(20):2105–22. doi: 10.1200/JCO.2018.77.8738

9. Vanderwalde A, Spetzler D, Xiao N, Gatalica Z, Marshall J. Microsatellite instability status determined by next-generation sequencing and compared with PD-L1 and tumor mutational burden in 11,348 patients. *Cancer Med* (2018) 7(3):746–56. doi: 10.1002/cam4.1372

10. Barroso-Sousa R, Jain E, Cohen O, Kim D, Buendia-Buendia J, Winer E, et al. Prevalence and mutational determinants of high tumor mutation burden in breast cancer. *Ann Oncol* (2020) 31(3):387–94. doi: 10.1016/j.annonc.2019.11.010

11. Schmid P, Adams S, Rugo HS, Schneeweiss A, Barrios CH, Iwata H, et al. Atezolizumab and nab-paclitaxel in advanced triple-negative breast cancer. *New Engl J Med* (2018) 379(22):2108–21. doi: 10.1056/NEJMoa1809615

12. Emens LA. Immunotherapy in triple-negative breast cancer. *Cancer J* (2021) 27 (1):59–66. doi: 10.1097/PPO.0000000000000497

13. Cortes J, Cescon DW, Rugo HS, Nowecki Z, Im SA, Yusof MM, et al. Pembrolizumab plus chemotherapy versus placebo plus chemotherapy for previously untreated locally recurrent inoperable or metastatic triple-negative breast cancer (KEYNOTE-355): a randomised, placebo-controlled, double-blind, phase 3 clinical trial. *Lancet* (2020) 396(10265):1817–28. doi: 10.1016/S0140-6736(20)32531-9

14. Barroso-Sousa R, Trippa L, Lange P, Andrews C, McArthur HL, Haley BB, et al. Nimbus: A phase II study of nivolumab plus ipilimumab in metastatic hypermutated HER2-negative breast cancer. *J Clin Oncol* (2019) 37(15_suppl):TPS1115–TPS. doi: 10.1200/JCO.2019.37.15_suppl.TPS1115

15. Tolaney SM, Barroso-Sousa R, Keenan T, Li T, Trippa L, Vaz-Luis I, et al. Effect of eribulin with or without pembrolizumab on progression-free survival for patients with hormone receptor-positive, ERBB2-negative metastatic breast cancer: A randomized clinical trial. *JAMA Oncol* (2020) 6(10):1598–605. doi: 10.1001/jamaoncol.2020.3524

16. Dirix LY, Takacs I, Jerusalem G, Nikolinakos P, Arkenau HT, Forero-Torres A, et al. Avelumab, an anti-PD-L1 antibody, in patients with locally advanced or metastatic breast cancer: a phase 1b JAVELIN Solid Tumor study. *Breast Cancer Res Treat* (2018) 167(3):671–86. doi: 10.1007/s10549-017-4537-5

17. Li CI, Anderson BO, Daling JR, Moe RE. Trends in incidence rates of invasive lobular and ductal breast carcinoma. *Jama* (2003) 289(11):1421–4. doi: 10.1001/jama.289.11.1421

18. Sammons S, Elliott A, Force JM, DeVito NC, Marcom PK, Swain SM, et al. Genomic evaluation of tumor mutational burden-high (TMB-H) versus TMB-low (TMB-L) metastatic breast cancer to reveal unique mutational features. *J Clin Oncol* (2021) 39(15_suppl):1091–. doi: 10.1200/JCO.2021.39.15_suppl.1091

19. Pereira B, Chin S-F, Rueda OM, Vollan H-KM, Provenzano E, Bardwell HA, et al. The somatic mutation profiles of 2,433 breast cancers refine their genomic and transcriptomic landscapes. *Nat Commun* (2016) 7(1):11479. doi: 10.1038/ncomms11479

20. Voorwerk L, Horlings H, Van Dongen M, Sikorska K, Kemper I, Mandjes I, et al. LBA3 Atezolizumab with carboplatin as immune induction in metastatic lobular breast cancer: First results of the GELATO-trial. *Ann Oncol* (2021) 32:S58. doi: 10.1016/j.annonc.2021.03.212

21. Castro A, Ozturk K, Pyke RM, Xian S, Zanetti M, Carter H. Elevated neoantigen levels in tumors with somatic mutations in the HLA-A, HLA-B, HLA-C and B2M genes. *BMC Med Genomics* (2019) 12(6):107. doi: 10.1186/s12920-019-0544-1

22. Goodman AM, Piccioni D, Kato S, Boichard A, Wang H-Y, Frampton G, et al. Prevalence of PDL1 amplification and preliminary response to immune checkpoint blockade in solid tumors. *JAMA Oncol* (2018) 4(9):1237–44. doi: 10.1001/jamaoncol.2018.1701

23. Bachelot T, Filleron T, Bieche I, Arnedos M, Campone M, Dalenc F, et al. Durvalumab compared to maintenance chemotherapy in metastatic breast cancer: the randomized phase II SAFIR02-BREAST IMMUNO trial. *Nat Med* (2021) 27(2):250–5. doi: 10.1038/s41591-020-01189-2

frontiers | Frontiers in Immunology

TYPE Systematic Review
PUBLISHED 15 August 2023
DOI 10.3389/fimmu.2023.1234894

OPEN ACCESS

EDITED BY
Chao Liu,
Shandong Cancer Hospital, China

REVIEWED BY
Dongjiao Zhao,
Messiah College, United States
Zhongkun Zhang,
Dana–Farber Cancer Institute, United States
Yile Dai,
Yale University, United States

*CORRESPONDENCE
Huan Deng
beandeng@ncu.edu.cn

RECEIVED 05 June 2023
ACCEPTED 31 July 2023
PUBLISHED 15 August 2023

CITATION
Wang Y-M, Cai W, Xue Q-M, Zhang J-Y, Zhou L, Xiong S-Y and Deng H (2023) Prognostic role of different PD-L1 expression patterns and tumor-infiltrating lymphocytes in high-grade serous ovarian cancer: a systematic review and meta-analysis.
Front. Immunol. 14:1234894.
doi: 10.3389/fimmu.2023.1234894

Prognostic role of different PD-L1 expression patterns and tumor-infiltrating lymphocytes in high-grade serous ovarian cancer: a systematic review and meta-analysis

Ye-Min Wang[1], Wei Cai[1], Qing-Ming Xue[2], Jin-Yao Zhang[1], Lv Zhou[1], Su-Yi Xiong[1] and Huan Deng[1]*

[1]Department of Pathology, the Fourth Affiliated Hospital of Nanchang University, Nanchang, Jiangxi, China, [2]Medical College, Nanchang University, Nanchang, Jiangxi, China

Background: The prognostic value of programmed cell death ligand 1 (PD-L1) expression and tumor-infiltrating lymphocytes (TILs) in high-grade serous ovarian cancer (HGSOC) remains a controversial topic in the research field. To comprehensively assess the importance of PD-L1 and TILs in this particular subtype of ovarian cancer, we performed a meta-analysis.

Methods: We conducted a comprehensive search of PubMed, Embase, Scopus, Web of Science, and Cochrane Library databases up to December 25, 2022. The association between PD-L1, TILs, and survival outcomes was evaluated using the combined hazard ratios (HRs) and their corresponding 95% confidence intervals (CIs).

Results: This meta-analysis comprised 11 trials involving a total of 1746 cases. The results revealed no significant association between PD-L1 expression in tumor cells (TCs) and overall survival (OS, HR = 0.76, 95% CI: 0.52-1.09, p = 0.136) or progression-free survival (PFS, HR = 0.71, 95% CI: 0.4 -1.24, p = 0.230). Nevertheless, a correlation was observed between PD-L1 expression in immune cells (ICs) and OS (HR = 0.73, 95% CI: 0.55-0.97, p = 0.031). Furthermore, the presence of $CD8^+$ and $PD\text{-}1^+$ TILs was found to significantly enhance OS (HR = 0.70, 95% CI = 0.55-0.87, p = 0.002; HR = 0.57, 95% CI = 0.40-0.80, p = 0.001, respectively) and PFS (HR = 0.62, 95% CI = 0.41-0.92, p = 0.019; HR = 0.52, 95% CI = 0.35-0.78, p = 0.002, respectively), whereas the presence of $CD3^+$ and $CD4^+$ TILs was positively associated with OS (HR = 0.50, 95% CI = 0.29-0.87, p = 0.014; HR = 0.55, 95% CI = 0.34-0.91, p = 0.020, respectively).

Conclusion: This study indicates a positive correlation between ICs-derived PD-L1 and survival, while no significant correlation was observed between TCs-derived PD-L1 and prognosis. These results highlight the importance of studying PD-L1 expression in ICs as a prognostic predictor. In addition, the presence of

TILs was found to significantly improve patient survival, suggesting that TILs may be a valuable prognostic biomarker.

Systematic review registration: https://www.crd.york.ac.uk/prospero/, identifier CRD42022366411.

KEYWORDS

high-grade serous ovarian cancer, PD-L1, tumor-infiltrating lymphocytes, prognosis, meta-analysis

1 Introduction

High-grade serous ovarian cancer (HGSOC) accounts for up to 85% of ovarian cancer and represents the most aggressive histologic type (1). Due to the lack of specific signs and reliable screening tools, this tumor is often diagnosed at an advanced stage (FIGO stage III-IV) with an unacceptable five-year survival rate. Despite surgery and platinum-based chemotherapy regimens, more than 70% of patients develop recurrence, metastasis, and drug resistance (2). The establishment of prognostic factors is crucial in determining the clinical management and treatment strategies for HGSOC. It has been proposed that chemotherapy sensitivity, tumor stage, and cytoreductive surgery are associated with the prognosis of HGSOC (3), but these factors still lack considerable accuracy and specificity in predicting the survival of individual patients. Therefore, there is an urgent need to unveil more novel and reliable biomarkers to guide the tailored treatment and predict survival outcomes of HGSOC patients.

Cancer research has been long hampered by the variation of intrinsic tumor factors. With the development of genomic and molecular techniques, accumulating evidence provides more insights into the central role of the tumor microenvironment (TME). Tumor-infiltrating lymphocytes (TILs), an important component of the TME, exert bidirectional effects on the antitumor immune response. TILs represent a heterogeneous population of T cells, generally localized in the tumor stroma or epithelium, and are capable of recognizing tumor antigens and killing malignant cells (4, 5). Unfortunately, cancer cells can skillfully utilize multiple pathways to create an immunosuppressive microenvironment and evade anti-tumor immune responses. The programmed death ligand 1 (PD-L1)/programmed cell death-1 (PD-1) axis is considered a crucial pathway for this. PD-1, belonging to the CD28 receptor family, is prominently found in activated TILs and possesses the capability to impede T cell proliferation and cytokine secretion, thereby culminating in T cell exhaustion (6). PD-L1, the main ligand of PD-1, belongs to the B7 family and is mainly expressed in tumor cells (TCs) and immune cells (ICs), but the regulatory mechanisms of the two are different (Figure 1) (7). In TCs, PD-L1 expression is primarily governed by tumor intrinsic mechanisms (8–10), while in ICs, it depends on an adaptive immune mechanism (11). The upregulation of PD-L1 leads to its specific binding to PD-1 on the surface of T cells, thereby inhibiting the function of local effector T cells and enabling TCs to successfully evade immune surveillance (12, 13). In recent years, PD-L1 blockade therapies have shown unprecedented efficacy against a variety of tumors. There is growing evidence that TILs and PD-L1 are strongly associated with the prognosis of cancer patients, including breast cancer, non-small cell lung cancer, colorectal cancer, and melanoma (14–17). However, studies on the prognostic impact of TILs and PD-L1 on HGSOC are scarce and often contradictory (18–20).

Our objective was to evaluate the potential prognostic significance of PD-L1 and TILs in HGSOC by conducting a thorough analysis of all scientific studies that met our eligibility criteria. It is worth highlighting that recent research indicates that the expression of PD-L1 in ICs is directly associated with the response of patients with solid tumors to PD-L1 targeting antibody MPDL3280A, whereas such a correlation is not observed in TCs (21). Consequently, we examined the prognostic value of PD-L1 in two distinct expression patterns, specifically TCs and ICs. In contrast to previous meta-analyses (22, 23), our focus was solely on HGSOC, as it exhibits a more prevalent immune infiltration phenomenon and distinctive immunological features when compared to other histological subtypes (24). In addition, the interactions between PD-L1, TILs, and survival appears to be found only in HGSOC (25), suggesting the possibility that patients with this subtype may benefit more from immunotherapy. To our knowledge, this is the first meta-analysis to comprehensively explore the relationship between TILs, PD-L1, and prognosis in patients with HGSOC.

2 Materials and methods

2.1 Protocol and eligibility criteria

This systematic review and meta-analysis has been registered in PROSPERO (CRD42022366411) and its reporting adheres to the guidelines outlined in the Preferred Reporting Items for Systematic Reviews and Meta-Analyses (PRISMA) 2020 statement (26) (Supplementary Table 1).

The selection of studies was based on the following criteria: (1) patients were diagnosed with primary HGSOC by histopathology; (2) the immunohistochemistry technique was employed to

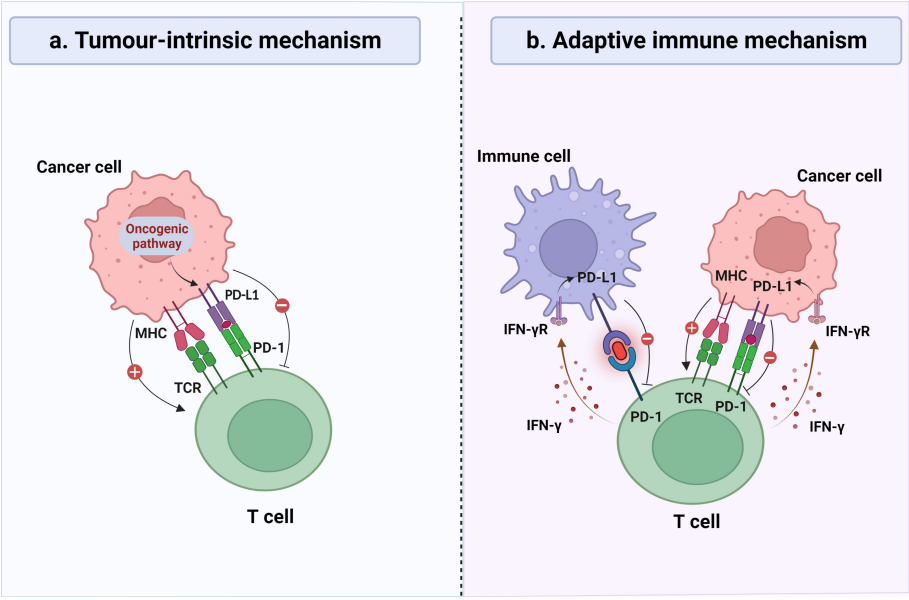

FIGURE 1
General mechanisms of PD-L1 expression on tumor cells (TCs) and immune cells (ICs). **(A)** In certain types of cancer, continuous activation of the oncogenic signaling cascades may lead to overexpression of PD-L1 on the surface of TCs, thereby inhibiting the recognition and elimination of TCs by cytotoxic T lymphocytes, regardless of the inflammatory signaling status in the tumor microenvironment. **(B)** In certain types of cancer, the expression of PD-L1 was observed on both TCs and ICs, which is induced by inflammatory signaling generated in response to a robust antitumor immune response, representing an adaptive immune response mechanism. IFN-γ, interferon-γ; MHC, major histocompatibility complex; TCR, T-cell receptor.

determine the levels of PD-L1 expression and the density of TILs in HGSOC; (3) studies assessed the correlation among PD-L1, TILs, and survival outcomes, including overall survival (OS), progression-free survival (PFS), disease-free survival (DFS), and disease-specific survival (DSS); (4) articles were published in English. Conversely, we excluded studies that met the following requirements: (1) duplicate publications; (2) studies that had inadequate data to calculate Hazard Ratios (HRs) and 95% confidence intervals (CIs); (3) reviews, annals, conference abstracts, or letters.

2.2 Information sources and search criteria

We searched five databases: PubMed, Web of Science, Embase, the Cochrane Library and Scopus. There were no constraints on time, gender, or age. This review's coverage dates began with the creation of each database and ended on December 25, 2022. The keywords were searched as follows: ("PD-L1" OR "B7-H1" OR "CD274" OR "programmed death ligand 1" OR "programmed cell death ligand 1" OR "PD L1 Protein" OR "B7-H1 antigen" OR "CD274 antigen") AND ("Ovarian Neoplasms" OR "Ovarian Cancer" OR "Ovary Neoplasm" OR "Ovary Cancers" OR "Cancer of Ovary") AND ("Tumor-Infiltrating Lymphocytes" OR "Tumor Infiltrating Lymphocyte" OR "Tumor-Derived Activated Cells" OR "Tumor Derived Activated Cells" OR "TILs") (Supplementary Table 2). Moreover, we reviewed the reference lists of the studies ultimately included to identify potential studies.

2.3 Study selection

We imported the retrieved studies into EndNote (version X9) and removed duplicates. Two researchers (LZ and WC) independently reviewed the title and abstract of each study, after excluding unrelated studies, two more researchers (QMX and JYZ) independently reviewed the full text of the remaining studies according to the same criteria, and a third researcher (YMW) ruled on any differing points of view.

2.4 Data collection process and data items

We pre-prepared and tested a standardized form for data extraction. Two investigators (QMX and JYZ) independently extracted the first author's name, year of publication, country, sample size, age, method of assessing PD-L1 and TILs, cut-off values, location of PD-L1 and TILs, TILs subtypes, median follow-up, and survival outcomes from each study. Any disagreements that arose were discussed and a consensus was reached.

2.5 Quality assessment

YMW and WC conducted a rigorous quality evaluation of each included study through the implementation of the Newcastle-Ottawa Scale (NOS) assessment tool (27). Specifically, the assessment focused on three critical dimensions, namely selection

(0-4 points), comparability (0-2 points), and outcome (0-3 points), resulting in the assignment of a predetermined number of stars (≥6 stars were deemed high quality). If any disputes arise, a third reviewer, SYX, will be consulted to settle the matter.

2.6 Statistical analysis

We assessed the prognostic impacts of PD-L1 expression and TILs on HGSOC by pooling the HRs and 95% CIs of all included studies. The Cochrane Q test (χ^2 test) and the I^2 statistic were used to determine whether there was heterogeneity among studies. $I^2 > 50\%$ and $p < 0.05$ were considered to be heterogeneous and the combined effect was calculated using a random-effects model (REM); otherwise, a fixed-effects model was used (FEM).

The publication bias was assessed using Egger's linear regression test (28) and Begg's funnel plot (29). The method of leave-one-out was employed to assess the sensitivity analysis of the results. We used STATA version 12.0 (Stata Corp LP, Texas, USA) for all the statistical analyses described above. The statistical significance level was set at a two-sided p value of 0.05.

3 Results

3.1 Literature search

Our team retrieved a total of 828 records from five different databases. Upon further examination, 297 duplicate records were excluded from our analysis. The remaining 531 studies were screened based on their titles and abstracts, and 490 were deemed irrelevant and removed from our investigation. After conducting a full analysis of the remaining 41 studies, 11 were deemed suitable for inclusion in our quantitative and qualitative analyses. A detailed overview of the search process, including the specific reasons for study exclusion, can be found in Figure 2.

3.2 Study characteristics

Table 1 contains a comprehensive overview of the 11 studies that were included. Collectively, these studies encapsulate a patient

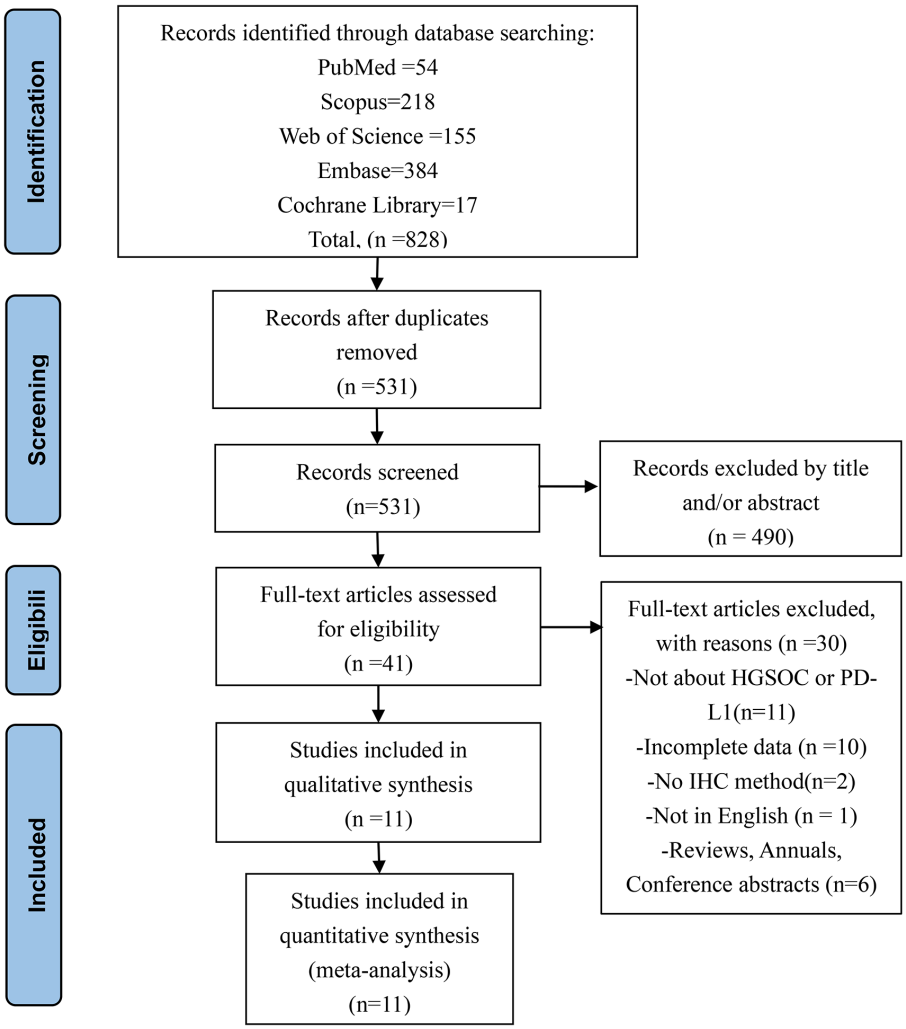

FIGURE 2
Flowchart of the study selection process.

TABLE 1 Basic characteristics of included studies.

Author/ Year	Country	Number of Patients	Age Median (range)	Detection method	Cut-Off value of PD-L1 Positive	Cut-Off value of TILs Positive	Location of PD-L1	Location of TILs	TILs subtype	Median follow-up (m)	Outcome	NOS score
Chen 2020	USA	100	53 (37-72)	IHC	TPS≥1%; CPS≥1	density for each marker	TC	IT	CD8	NR	OS, PFS	7
Darb-Esfahani 2016	Germany	215	60	IHC	IRS>0	density for each marker	TC	IT	PD-1, CD3	NR	OS, PFS	6
Henriksen 2020	Denmark	283	63	IHC	≥1%	≥80 cells/mm^2	TC	IT	CD8	156	OS	8
Kim 2018	Korea	131	58 (32-79)	IHC	TC≥25%; IC≥5%	ST ≥50%; IT ≥10%	TC, IC	IT, ST	CD8, PD-1, FOXP3	30	OS, PFS	8
Martin de la Fuente 2020	Sweden	130	67 (43-86)	IHC	≥1%	≥1%	IC	IT	CD3, PD-1	39	OS	8
Mills 2019	US	112	59.7 (69.7-49.7)	IHC	≥1%	≥12.95 cells/HPF	TC, IC	IT	CD8, FOXP3	NR	OS	8
Pinto 2018	Chile	128	57 (29-83)	IHC	score≥2	≥10 cells/HPF	TC	IT, ST	CD3, CD4, CD8	NR	OS, PFS	7
Strickland 2016	US	245	NR	IHC	TC≥5%; IC≥1 cell/HPF	≥13 cells/HPF	TC, IC	IT	CD3, CD8, PD-1	NR	OS, DFS	6
Wang 2017	China	107	57 (29–82)	IHC	≥5%	score > 2 or 3	TC, IC	IT, ST	CD3, CD4, CD8	NR	OS	7
Webb 2016	Canada	195	NR	IHC	≥1 cell/HPF	≥5 cells/HPF	IC	IT	CD3, CD8, PD-1, FOXP3	NR	DSS	6
Bansal 2021	India	100	50.8 (31.5-82)	IHC	≥ 10%	score > 1	TC, IC	IT, ST	CD4, CD8	NR	OS, DFS	6

US, United States; NR, not reported; IHC, immunohistochemistry; HPF, high power field; CPS, combined positive score; TPS, tumor proportion score; IRS, immuno-reactivity score; TC, tumor cell; IC, immune cell; IT, intraepithelial; ST, stromal; OS, overall survival; PFS, progression-free survival; DFS, disease-free survival; DSS, disease-specific survival; NOS, Newcastle-Ottawa scale.

10.3389/fimmu.2023.1234894

cohort of 1746 individuals. The sample sizes from which these studies were conducted ranged from 100 to 283. The median age of the patients ranged from 50.8 to 67 years, and the median follow-up time extended from 30 to 156 months. There were four European studies, three Asian studies, three North American studies, and one South American study. Various studies employed immunohistochemical methodologies to evaluate PD-L1 and TILs, applying distinct cut-off values and scoring systems. Seven studies examined the correlation between TCs PD-L1 expression and associated prognoses, while five studies investigated the prognostic relevance of PD-L1 expression in ICs. Moreover, five studies concentrated solely on the relationship between intraepithelial TILs and survival. Finally, three studies probed the prognostic ramifications of intraepithelial and stromal TILs. According to NOS scores, all included studies scored ≥6, indicating the high methodological quality of these studies. Specific scoring details are shown in Table 2.

3.3 PD-L1 and prognosis

3.3.1 TCs PD-L1 expression and prognosis

The association between TCs PD-L1 expression and OS has been investigated in seven studies. The

combined data analysis revealed that there was no significant correlation (HR = 0.76, 95% CI: 0.52-1.09, p = 0.136), which was further confirmed using REM due to the presence of heterogeneity (I^2 = 64.8%, p = 0.009) (Figure 3A). Additionally, data from four studies were analyzed to determine the relationship between TCs PD-L1 expression and PFS. Pooled results showed that TCs PD-L1 expression was not significantly correlated with prognosis (HR = 0.71, 95% CI: 0.41-1.24, p = 0.230). Given the slight heterogeneity among the four studies (I^2 = 67.0%, p = 0.028), REM was employed (Figure 3B).

3.3.2 ICs PD-L1 expression and prognosis

Due to the limited availability of PFS data, our study specifically focused on the relationship between PD-L1expression in ICs and OS. A total of five studies were included in our analysis, and the combined results showed that PD-L1 expression in ICs was positively correlated with OS (HR = 0.73, 95% CI: 0.57-0.94, p = 0.013). FEM was used in view of the absence of significant heterogeneity (I^2 = 4.5%, p = 0.381) (Figure 4).

3.4 TILs subtypes and prognosis

3.4.1 $CD8^+$ T lymphocyte subset

Intraepithelial TILs were subjected to analysis in this study. The pooled HRs and 95% CIs indicated that $CD8^+$ TILs had a positive impact on OS in patients (HR = 0.70, 95% CI = 0.55-0.87, p = 0.002). Given the absence of heterogeneity, FEM was deemed appropriate for analysis (I^2 = 0.0%, p = 0.687) (Figure 5A).

TABLE 2 The NOS quality assessment of the enrolled studies.

Study	Selection				Comparability	Outcome			Total Score
	Representativeness of exposed cohort	Selection of non-exposed cohort	Exposure ascertainment	Outcome not present prior to exposure	Control for factor	Assessment of outcome	Follow-up long enough	Adequacy of follow-up of cohorts	0-9
Chen 2020	★	★	★	★	★★	★	☆	☆	7
Darb-Esfahani 2016	★	★	☆	★	★★	★	☆	☆	6
Henriksen 2020	★	★	★	★	★★	★	★	☆	8
Martin de la Fuente 2020	★	★	☆	★	★★	★	★	★	8
Mills 2019	★	★	★	★	★★	★	★	☆	8
Pinto 2018	★	★	☆	★	★★	★	☆	★	7
Strickland 2016	★	★	☆	★	★★	☆	☆	★	6
Wang 2017	★	★	★	★	★★	★	☆	☆	7
Webb 2016	★	★	☆	★	★★	★	☆	☆	6
Bansal 2021	★	★	☆	★	★★	☆	☆	★	6
Kim 2018	★	★	☆	★	★★	★	★	★	8

NOS, Newcastle-Ottawa scale.
☆, zero score; ★, one score.

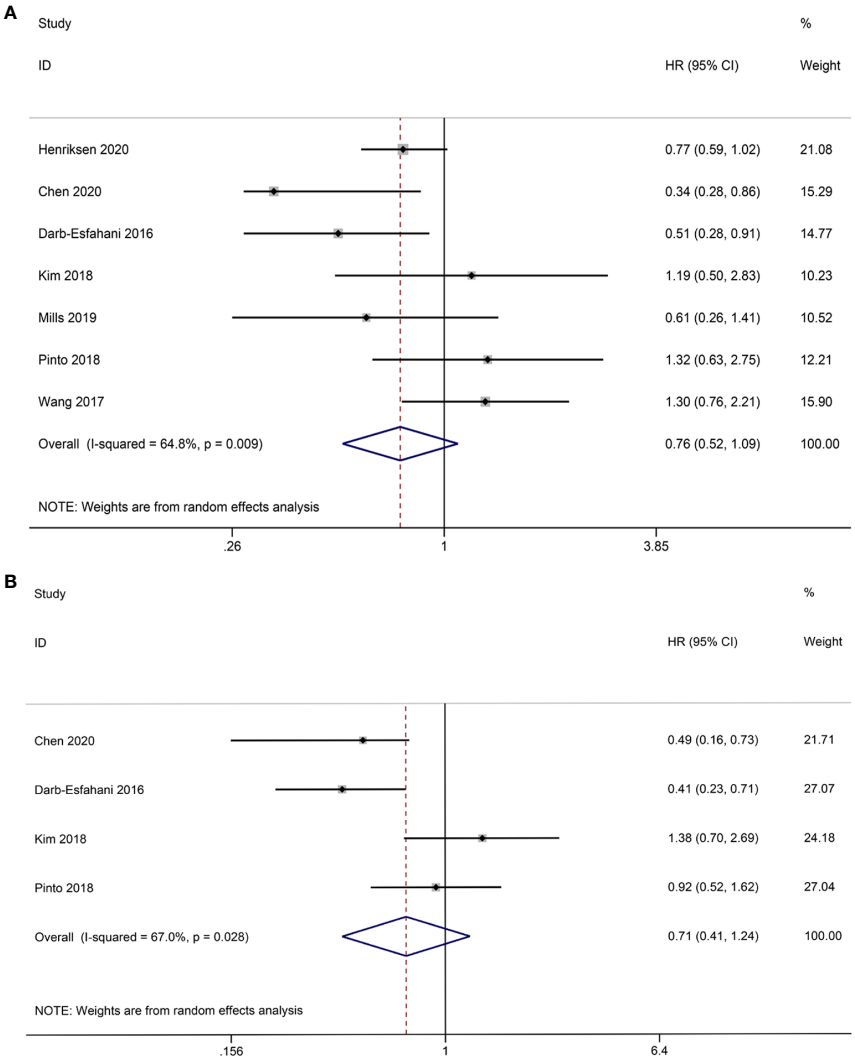

FIGURE 3
Forest plot of the relationship between TCs PD-L1 expression and survival outcomes in HGSOC. **(A)** Forest plots of overall survival (OS); **(B)** Forest plots of progression-free survival (PFS).

Although only two studies provided data on $CD8^+$ TILs and PFS, the combined results demonstrated a significant enhancement in patients' PFS (HR = 0.62; 95% CI= 0.41-0.92, p = 0.019). Importantly, no heterogeneity was observed, thus warranting the use of FEM for analysis (I^2 = 0.0%, p = 0.563) (Figure 5B).

3.4.2 PD-1^+ T lymphocyte subset

Only two studies have investigated the potential correlation between PD-1^+ TILs and OS. The aggregated findings imply that PD-1^+ TILs have the potential to serve as a beneficial prognostic factor for OS (HR = 0.57; 95% CI = 0.40-0.80, p = 0.001) (Figure 6A). As for PFS, our analysis was limited to two eligible studies. Our results suggest that PD-1^+ TILs are associated with improved PFS in patients (HR = 0.52; 95% CI = 0.35-0.78, p = 0.002) (Figure 6B). Heterogeneity was not observed in either the OS (I^2 = 0.0%, p = 0.882) or PFS (I^2 = 0.0%, p = 0.415) analyses, therefore, the FEM was utilized.

3.4.3 $CD3^+$ T lymphocyte subset

Four studies investigated the prognostic significance of $CD3^+$ TILs. The pooled analysis revealed the following results: HR = 0.54, 95% CI = 0.41-0.72, p = 0.000, suggesting a positive correlation between $CD3^+$ TILs and OS. No notable heterogeneity is observed among the studies, thus justifying the use of the FEM (I^2 = 36.3%, p = 0.194) (Figure 7A).

3.4.4 $CD4^+$ T lymphocyte subset

Two studies provided data on the relationship between $CD4^+$ TILs and OS. The pooled HRs and 95% CIs showed that $CD4^+$ TILs were associated with better OS (HR = 0.55, 95% CI = 0.34-0.91, p =

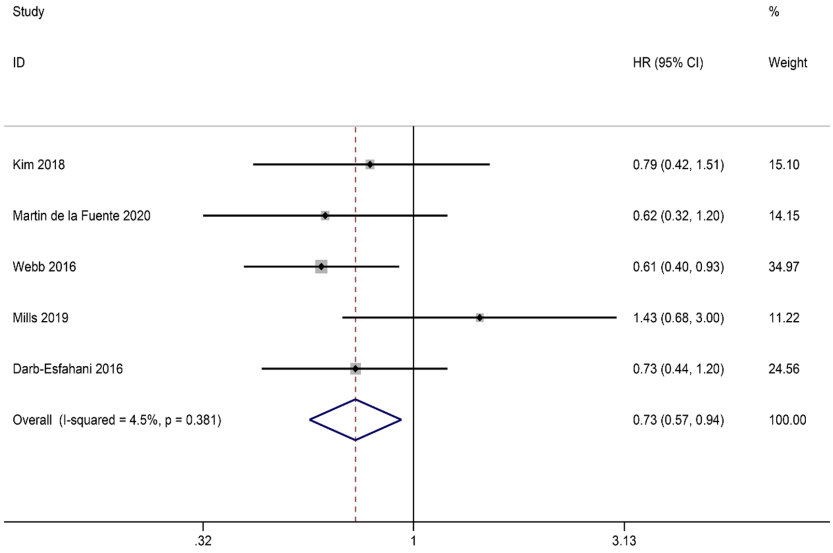

FIGURE 4
Forest plot of the relationship between ICs PD-L1 expression and overall survival (OS) in HGSOC.

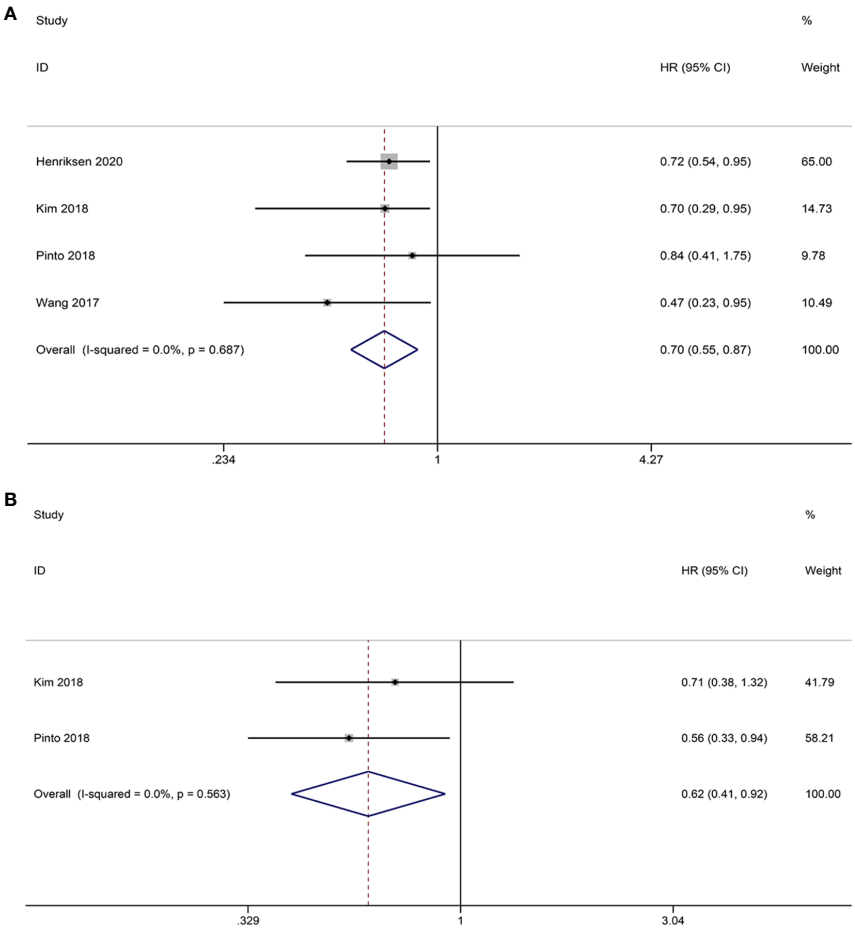

FIGURE 5
Forest plots of the relationship between $CD8^+$ TILs and survival outcomes in HGSOC. **(A)** Forest plots of overall survival (OS); **(B)** Forest plots of progression-free survival (PFS).

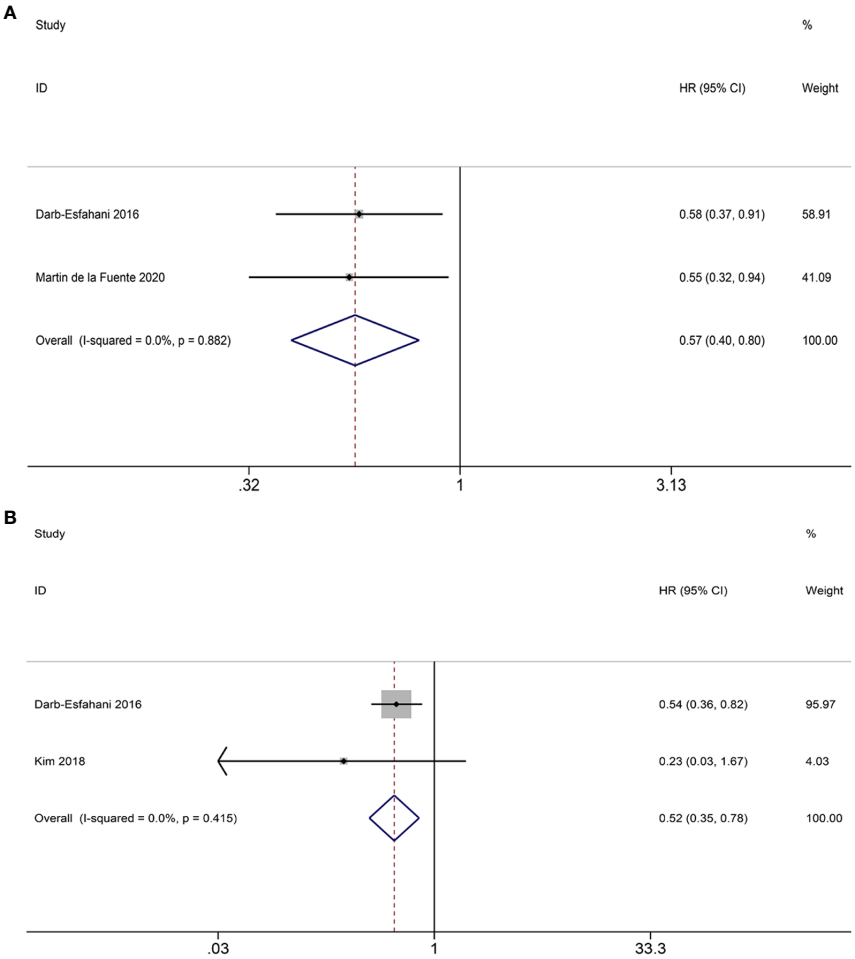

FIGURE 6
Forest plots of the relationship between PD-1$^+$ TILs and survival outcomes in HGSOC. **(A)** Forest plots of overall survival (OS); **(B)** Forest plots of progression-free survival (PFS).

0.020). No heterogeneity was observed between studies the two studies, so FEM was used (I^2 = 0.0%, p = 0.348) (Figure 7B).

3.5 Publication bias and sensitivity analysis

To assess publication bias for included studies, we used Begg's funnel plot and Egger's linear regression test. For TCs, Begg's funnel plot presents nearly symmetric features. Begg's test (OS: p = 1.000; PFS: p = 0.734) and Egger's test (OS: p = 0.926; PFS: p = 0.909) showed no significant publication bias (Figures 8A–D). For ICs, publication bias was also not observed (Begg's test: p = 0.308; Egger's test: p = 0.276) (Figures 8E, F). In addition, we performed a sensitivity analysis to assess the impact of each study on the overall outcome. Excluding each study individually did not significantly affect the pooled HR (Figure 9). This finding highlights the robustness of our pooled results.

4 Discussion

Our study demonstrates that PD-L1 expression in TCs is not significantly associated with the prognosis of patients with HGSOC. However, PD-L1 expression derived from ICs is linked to better survival outcomes. These findings indicate that PD-L1 exhibits distinct prognostic values through two different patterns. Importantly, our observation that PD-L1 expression in TCs does not contribute to the development of HGSOC is consistent with previous investigations (30, 31). Accumulating evidence suggests that PD-L1 in TCs does not promote primary tumor formation and progression. However, it may facilitate the metastasis of malignant tumors through the interacting with myeloid cell-derived PD-L1, hindering the infiltration of cytotoxic T cells into the affected area (32). These findings may further support our results, as metastatic lesions were excluded from this study. Numerous studies utilizing mouse models have indicated that PD-L1 expression in ICs is a crucial risk factor for the impairment of T cell-mediated antitumor response (33). However, our results proposed that PD-L1 in ICs correlates with an improved OS of HGSOC patients. These observations are in good agreement with previous research on esophageal cancer (7), which demonstrated that PD-L1 expression in ICs serves as an independent prognostic factor that significantly prolongs patient survival. Furthermore, Kowanetz et al. (34) also reported a positive association between PD-L1 expression in ICs

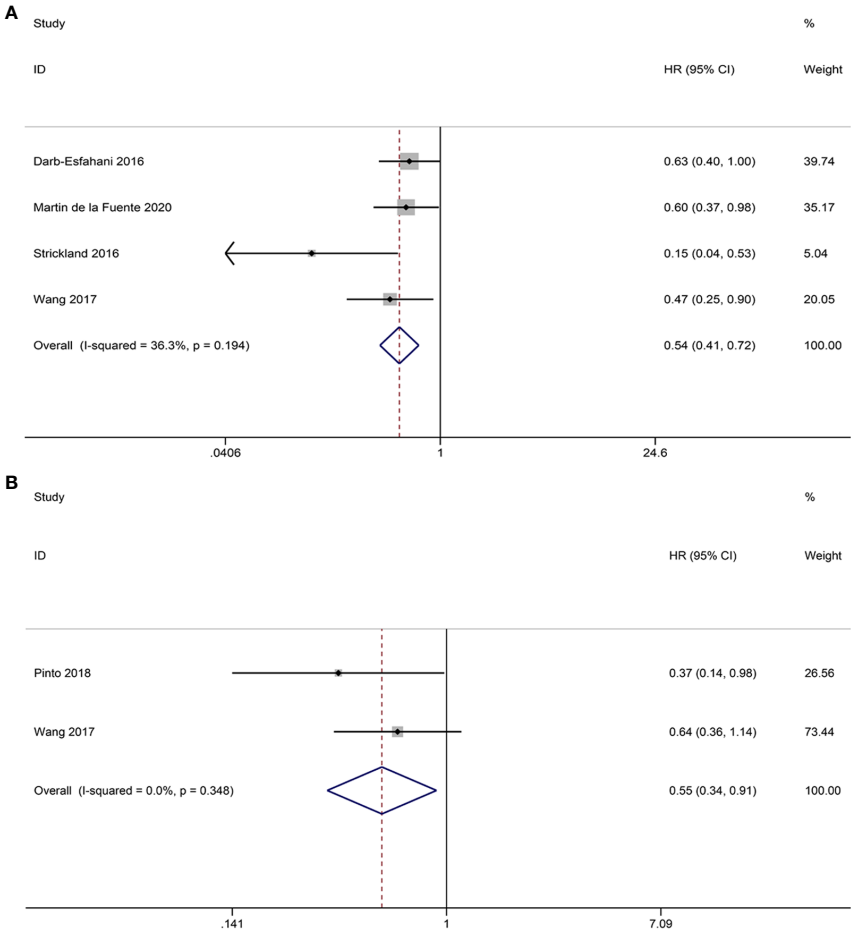

FIGURE 7
Forest plots of the relationship between $CD3^+$, $CD4^+$ TILs and overall survival (OS) in HGSOC. **(A)** Forest plot of $CD3^+$ TILs; **(B)** Forest plot of $CD4^+$ TILs.

and improved outcomes in patients with non-small cell lung cancer. These data reveal an interesting idea that PD-L1 expression not only plays a positive role in immunosuppression, but also plays a crucial role in endogenous anti-tumor immune responses, leading to inconsistencies in PD-L1 as a prognostic indicator. This inconsistency may not only be related to individual patient differences and tumor heterogeneity, but also be affected by the complex TME.

In fact, PD-L1 expression in the TME is influenced by a variety of interrelated regulatory factors, which makes it dynamic and complex. A variety of ICs exist in the TME, including tumor-associated macrophages, dendritic cells, NK cells, T cells, etc. (35). These ICs and their secreted cytokines play an important role in regulating PD-L1 expression. In general, interferon γ (IFN-γ) produced by activated T cells and NK cells is the main stimulator, which can up-regulate PD-L1 expression by activating the JAK/STAT and PI3K-AKT signaling pathways (36). Recent studies have shown that, in addition to the direct effects on TCs, tumor necrosis factor-α (TNF-α) also induces the expression of PD-L1, thus participating in the escape of TCs from host immune surveillance (37). Other cytokines such as interleukin 6 (IL-6), interleukin 17 (IL-17), and epidermal growth factor (EGF) also directly or indirectly influence PD-L1 behaviors (38, 39). In the setting of pathological conditions, including hypoxia, low nutrients, and stress, an abundant PD-L1 was found in TME (40–42). Barsoum et al. (40) showed that hypoxia-inducing factors can increase the expression of PD-L1 in cancer cells, which, in turn, impedes the effects of cytotoxic T lymphocytes on TCs. At the same time, the expression level of PD-L1 was also interfered by various signaling pathways. Kim et al. (43) found that the activation of PI3K-AKT signaling could lead to an increased expression of PD-L1 in gastric cancer. The administration of PI3K inhibitor (LY294002) significantly decrease the secretion of PD-L1. In addition, Stutvoet et al. (44) confirmed that the activation of EGF-MAPK pathway leads to the upregulation of PD-L1 mRNA and protein in lung adenocarcinoma cells. In conclusion, the expression of PD-L1 in TME represent the result regulated by the combination of multiple exogenous and endogenous factors. This complex regulatory mechanism makes it necessary to take the spatial and temporal dynamic differences into consideration when PD-L1 is served as a prognostic indicator.

It is important to note that different groups arrived at different conclusions about the prognostic value of PD-L1. The regulatory effects of chemotherapy on tumor immune parameters should also be considered. Peng et al. (45) showed that chemotherapy can upregulate PD-L1 expression through the activation of NF–κB

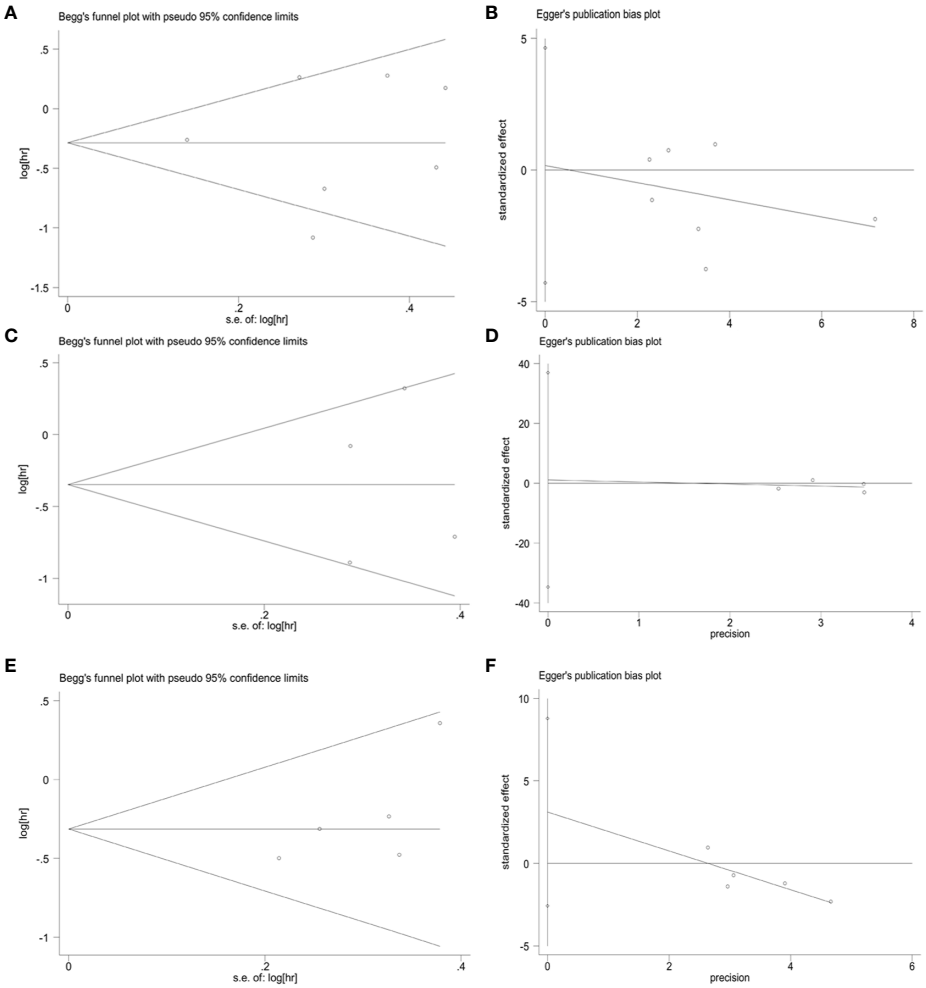

FIGURE 8
Publication bias. **(A)** Begg's test for OS in TCs (p = 1.000), **(B)** Egger's test for OS in TCs (p = 0.926), **(C)** Begg's test for PFS in TCs (p = 0.734), **(D)** Egger's test for PFS in TCs (p = 0.909), **(E)** Begg's test for OS in ICs (p = 0.308), **(F)** Egger's test for OS in ICs (p = 0.276).

signaling pathway in a mouse model of ovarian cancer, leading to local immunosuppression. Meanwhile, Researchers also found that the combination of paclitaxel and anti-PD-L1 drugs significantly increased the survival of murine models with aggressive tumors. Message et al. (46) observed immune cell infiltration and up-regulated PD-L1 expression in the majority of ovarian cancer patients received neoadjuvant chemotherapy (NACT). Consistently, Lee et al. (47) found a NACT-induced increase in PD-L1 expression and TILs density from HGSOC samples. However, these parameters did not result in a survival advantage, which may be partly explained by an increase in the proportion of Foxp3$^+$-regulatory T cells. These studies suggest that chemotherapy plays an important and complex role in immune regulation and has a non-negligible impact on PD-L1 expression and prognosis. Due to the limited data provided by the included literature, our study was unable to conduct a comprehensive analysis of the treatment of all patients. In order to better understand the function of PD-L1 and provide tailored treatments, these factors should be taken into account when predicting PD-L1 expression patterns and its impact on prognosis.

TIL refers to a population of lymphocytes that leave the vascular system and infiltrate tumor tissue. Based on molecular markers on the cell surface, such as CD3, CD4, CD8, and PD-1, TILs can be further subdivided into multiple subgroups. The differentiation antigen CD3 is prevalent in mature T cells (48). CD3$^+$ TILs represent the level of total T lymphocytes and reflect the status of the host immune function. In keeping with the majority of previous reports (49–51), our findings indicated that the high infiltration of CD3$^+$ TILs is significantly associated with better OS of cancer patients and can be served as a reliable biomarker for predicting survival outcomes in HGSOC.

Unlike CD3$^+$ TILs, the prognostic value of CD4$^+$ TILs has been controversial. Several studies demonstrated that there was no significant correlation between CD4$^+$ TILs and prognosis in patients with hepatocellular carcinoma, esophagus cancer, and colorectal cancer (52–54). Conversely, in pancreatic, nasopharyngeal, lung, and bile duct cancers, elevated levels of CD4$^+$ TILs have been shown to improve patient survival (50, 55–57). Our findings support the hypothesis that the presence of CD4$^+$ TILs in patients with HGSOC can serve as a predictor for an improved survival. The intricate differentiation

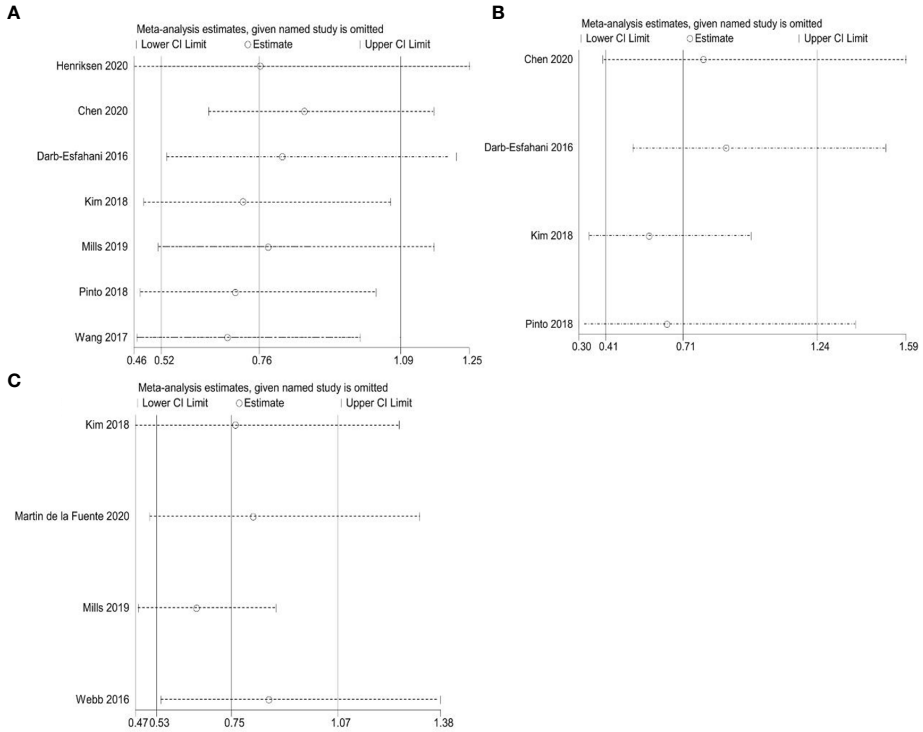

FIGURE 9
Sensitivity analyses. **(A)** Correlation between PD-L1 expression and overall survival (OS) in TCs; **(B)** Correlation between PD-L1 expression and progression-free survival (PFS) in TCs; **(C)** Correlation between PD-L1 expression and overall survival (OS) in ICs.

characteristics of $CD4^+$ TILs may contribute to the apparent paradox of behaviors. They can differentiate into multiple T helper (Th) subgroups, thereby effectively enhancing immune responses. Another daughter cell of $CD4^+$ TILs is regulatory T cells (Tregs), which are capable of establishing an immunosuppressive microenvironment (58). Because of the acknowledged technical limitations, it is currently unclear if the prognostic significance of $CD4^+$ TILs is influenced by the type of cancer, $CD4^+$ TILs subgroups, or both. Therefore, further comprehensive investigations and validation of functional subtypes are warranted to explore and confirm the association between $CD4^+$ TILs and the prognosis of HGSOC patients.

Another key effector cell involved in the anti-tumor immune response is $CD8^+$ TILs, which are able to bind to major histocompatibility complex type I (MHC-I) molecules and directly kill cancer cells through the secretion of granzymes, interferons and other cytokines (59). The favorable prognostic value of $CD8^+$ TILs has been extensively studied in various cancers, including head and neck squamous cell carcinoma (49), non-small cell lung cancer (60) and nasopharyngeal carcinoma (50). Consequently, $CD8^+$ TILs have emerged as a promising target for novel immunotherapeutic approaches. Our systematic review and meta-analysis provide further support for the notion that increased levels of $CD8^+$ TILs significantly improve clinical outcomes in patients with HGSOC. Notably, recent clinical trials utilizing adoptive TILs therapy against melanoma have shown promising results. In these trials, infused $CD8^+$ TILs were able to migrate, infiltrate, and eliminate cancer cells, leading to sustained tumor regression in patients (61). Our findings contribute additional evidence supporting the role of $CD8^+$ TILs as a reliable prognostic indicator for tumors and their significant potential for augmenting the efficacy of immunotherapy against HGSOC.

The inhibitory molecule PD-1 has attracted much attention as a target for cancer immunomodulation. However, there are still many unveiled areas regarding the relationship between PD-1 expression and patient prognosis. $PD\text{-}1^+$ TILs numbers increase in direct proportion to disease severity of breast cancer, kidney cancer, nasopharyngeal cancer, and Hodgkin's lymphoma (62–65). Our results support that $PD\text{-}1^+$ TILs are more heterogeneous than traditionally thought and may inhibit the progression of HGSOC. Recent studies generally encourage this view that PD-1-expressing TILs convey important anti-tumor effects in follicular lymphoma, head and neck cancer, and colorectal cancer (66–68). These findings have triggered a rethinking of the significance of $PD\text{-}1^+$ TILs in the battle against cancer. In some cases, PD-1 may serve as an indicator of T cell activation rather than a marker of impaired T cell function (69). Furthermore, given the small amount of literature integrated in this study, a definitive explanation for this discrepancy requires further research in the future to obtain more accurate conclusions.

Our meta-analysis may have some limitations. First, the limited number of included studies may raise concerns about the conclusions. This situation may partly be explained by two reasons. First, the research areas we focused on may be relatively new, resulting in limited available literature resources. Second, to ensure the high quality of the studies, we have developed a strict set

of inclusion and exclusion criteria. All literature without reliable methods, high quality, and consistent objects and questions were excluded to improve the scientific rigor and accuracy of our research. Due to the small number of studies included, this study only analyzed the predictive value of intraepithelial TILs and did not investigate stromal TILs in depth. Therefore, it is necessary to further study the infiltration of TILs at different sites to identify possible candidates for immunotherapy. In addition, inconsistencies in the antibodies, assessment methods, and positive thresholds used in the studies may also lead to potential heterogeneity. Future studies should further improve the scoring system and harmonize the cut-off points to obtain more reliable results. Finally, it is important to note that the data extracted from the studies that met the criteria were abstract data rather than individual patient data, which may affect the accuracy of the combined results.

5 Conclusions

We found that PD-L1 expression in TCs did not significantly affect long-term survival, but ICs PD-L1 expression was correlated with better OS. Meanwhile, the infiltration of $CD8^+$, $CD4^+$, $CD3^+$, and PD-1^+ TILs is associated with improved survival. Our results suggest that PD-L1 and TILs may serve as potential biomarkers for personalizing treatment and predicting prognosis in HGSOC patients. However, further well-designed prospective studies are necessary to verify our findings.

Data availability statement

The original contributions presented in the study are included in the article/Supplementary Material. Further inquiries can be directed to the corresponding author.

Author contributions

Y-MW and WC designed the study. LZ and J-YZ screened the studies and extracted data. The quality of the evidence was assessed using Y-MW, S-YX and WC. Q-MX and J-YZ analyzed and interpreted the data. Y-MW and HD prepared figures and drafted the manuscript. HD contributed to reviewing and editing the manuscript. All authors have approved the final version of the article, including the authorship list. All authors contributed to the article.

Funding

This work was supported by the National Science Foundation of China, No.82160546; the Science Foundation of Jiangxi Province, No. 20202BBG73027, No.20192BAB205015 and No.20202ACBL206017; the Foundation of Jiangxi Province for Distinguished Scholars, No. JXSQ2023201020.

Acknowledgments

Figure 1 was created with BioRender software (https://biorender.com).

Conflict of interest

The authors declare that the research was conducted in the absence of any commercial or financial relationships that could be construed as a potential conflict of interest.

Publisher's note

All claims expressed in this article are solely those of the authors and do not necessarily represent those of their affiliated organizations, or those of the publisher, the editors and the reviewers. Any product that may be evaluated in this article, or claim that may be made by its manufacturer, is not guaranteed or endorsed by the publisher.

Supplementary material

The Supplementary Material for this article can be found online at: https://www.frontiersin.org/articles/10.3389/fimmu.2023.1234894/full#supplementary-material

References

1. Seidman JD, Horkayne-Szakaly I, Haiba M, Boice CR, Kurman RJ, Ronnett BM. The histologic type and stage distribution of ovarian carcinomas of surface epithelial origin. *Int J gynecological Pathol* (2004) 23(1):41–4. doi: 10.1097/01.pgp.0000101080.35393.16

2. Naumann RW, Coleman RL. Management strategies for recurrent platinum-resistant ovarian cancer. *Drugs* (2011) 71(11):1397–412. doi: 10.2165/11591720-000000000-00000

3. Ezzati M, Abdullah A, Shariftabrizi A, Hou J, Kopf M, Stedman JK, et al. Recent advancements in prognostic factors of epithelial ovarian carcinoma. *Int scholarly Res notices* (2014) 2014:953509. doi: 10.1155/2014/953509

4. Anderson KG, Stromnes IM, Greenberg PD. Obstacles posed by the tumor microenvironment to T cell activity: A case for synergistic therapies. *Cancer Cell* (2017) 31(3):311–25. doi: 10.1016/j.ccell.2017.02.008

5. Hodi FS, Dranoff G. The biologic importance of tumor-infiltrating lymphocytes. *J cutaneous Pathol* (2010) 37 Suppl 1(0 1):48–53. doi: 10.1111/j.1600-0560.2010.01506.x

6. Bardhan K, Anagnostou T, Boussiotis VA. The PD1:PD-L1/2 pathway from discovery to clinical implementation. *Front Immunol* (2016) 7:550. doi: 10.3389/fimmu.2016.00550

7. Zhang W, Pang Q, Zhang X, Yan C, Wang Q, Yang J, et al. Programmed death-ligand 1 is prognostic factor in esophageal squamous cell carcinoma and is associated

with epidermal growth factor receptor. *Cancer Sci* (2017) 108(4):590–7. doi: 10.1111/cas.13197

8. Parsa AT, Waldron JS, Panner A, Crane CA, Parney IF, Barry JJ, et al. Loss of tumor suppressor PTEN function increases B7-H1 expression and immunoresistance in glioma. *Nat Med* (2007) 13(1):84–8. doi: 10.1038/nm1517

9. Atefi M, Avramis E, Lassen A, Wong DJ, Robert L, Foulad D, et al. Effects of MAPK and PI3K pathways on PD-L1 expression in melanoma. *Clin Cancer Res* (2014) 20(13):3446–57. doi: 10.1158/1078-0432.CCR-13-2797

10. NOman MZ, Desantis G, Janji B, Hasmim M, Karray S, Dessen P, et al. PD-L1 is a novel direct target of HIF-1α, and its blockade under hypoxia enhanced MDSC-mediated T cell activation. *J Exp Med* (2014) 211(5):781–90. doi: 10.1084/jem.20131916

11. Kim HR, Ha SJ, Hong MH, Heo SJ, Koh YW, Choi EC, et al. PD-L1 expression on immune cells, but not on tumor cells, is a favorable prognostic factor for head and neck cancer patients. *Sci Rep* (2016) 6:36956. doi: 10.1038/srep36956

12. Teng MW, Ngiow SF, Ribas A, Smyth MJ. Classifying cancers based on T-cell infiltration and PD-L1. *Cancer Res* (2015) 75(11):2139–45. doi: 10.1158/0008-5472.CAN-15-0255

13. Marincola FM, Jaffee EM, Hicklin DJ, Ferrone S. Escape of human solid tumors from T-cell recognition: molecular mechanisms and functional significance. *Adv Immunol* (2000) 74:181–273. doi: 10.1016/S0065-2776(08)60911-6

14. Tsang JY, Au WL, Lo KY, Ni YB, Hlaing T, Hu J, et al. PD-L1 expression and tumor infiltrating PD-1+ lymphocytes associated with outcome in HER2+ breast cancer patients. *Breast Cancer Res Treat* (2017) 162(1):19–30. doi: 10.1007/s10549-016-4095-2

15. Rashed HE, Abdelrahman AE, Abdelgawad M, Balata S, Shabrawy ME. Prognostic significance of programmed cell death ligand 1 (PD-L1), CD8+ Tumor-infiltrating lymphocytes and p53 in non-small cell lung cancer: an immunohistochemical study. *Turk patoloji dergisi* (2017) 1(1):211–22. doi: 10.5146/tjpath.2017.01398

16. Li Y, Liang L, Dai W, Cai G, Xu Y, Li X, et al. Prognostic impact of programed cell death-1 (PD-1) and PD-ligand 1 (PD-L1) expression in cancer cells and tumor infiltrating lymphocytes in colorectal cancer. *Mol Cancer* (2016) 15(1):55. doi: 10.1186/s12943-016-0539-x

17. Bence C, Hofman V, Chamorey E, Long-Mira E, Lassalle S, Albertini AF, et al. Association of combined PD-L1 expression and tumour-infiltrating lymphocyte features with survival and treatment outcomes in patients with metastatic melanoma. *J Eur Acad Dermatol Venereol JEADV* (2020) 34(5):984–94. doi: 10.1111/jdv.16016

18. Chen H, Molberg K, Strickland AL, Castrillon DH, Carrick K, Jiang Q, et al. PD-L1 expression and CD8+ Tumor-infiltrating lymphocytes in different types of tubo-ovarian carcinoma and their prognostic value in high-grade serous carcinoma. *Am J Surg Pathol* (2020) 44(8):1050–60. doi: 10.1097/PAS.0000000000001503

19. Kim HS, Kim JY, Lee YJ, Kim SH, Lee JY, Nam EJ, et al. Expression of programmed cell death ligand 1 and immune checkpoint markers in residual tumors after neoadjuvant chemotherapy for advanced high-grade serous ovarian cancer. *Gynecologic Oncol* (2018) 151(3):414–21. doi: 10.1016/j.ygyno.2018.08.023

20. Henriksen JR, Donskov F, Waldstrøm M, Jakobsen A, Hjortkjaer M, Petersen CB, et al. Favorable prognostic impact of Natural Killer cells and T cells in high-grade serous ovarian carcinoma. *Acta Oncol (Stockholm Sweden)* (2020) 59(6):652–9. doi: 10.1080/0284186X.2019.1711173

21. Herbst RS, Soria JC, Kowanetz M, Fine GD, Hamid O, Gordon MS, et al. Predictive correlates of response to the anti-PD-L1 antibody MPDL3280A in cancer patients. *Nature* (2014) 515(7528):563–7. doi: 10.1038/nature14011

22. Wang L. Prognostic effect of programmed death-ligand 1 (PD-L1) in ovarian cancer: a systematic review, meta-analysis and bioinformatics study. *J Ovarian Res* (2019) 12(1):37. doi: 10.1186/s13048-019-0512-6

23. Huang LJ, Deng XF, Chang F, Wu XL, Wu Y, Diao QZ. Prognostic significance of programmed cell death ligand 1 expression in patients with ovarian carcinoma: A systematic review and meta-analysis. *Med (Baltimore)* (2018) 97(43):e12858. doi: 10.1097/MD.0000000000012858

24. Milne K, Köbel M, Kalloger SE, Barnes RO, Gao D, Gilks CB, et al. Systematic analysis of immune infiltrates in high-grade serous ovarian cancer reveals CD20, FoxP3 and TIA-1 as positive prognostic factors. *PloS One* (2009) 4(7):e6412. doi: 10.1371/journal.pone.0006412

25. Webb JR, Milne K, Kroeger DR, Nelson BH. PD-L1 expression is associated with tumor-infiltrating T cells and favorable prognosis in high-grade serous ovarian cancer. *Gynecol Oncol* (2016) 141(2):293–302. doi: 10.1016/j.ygyno.2016.03.008

26. Page MJ, McKenzie JE, Bossuyt PM, Boutron I, Hoffmann TC, Mulrow CD, et al. The PRISMA 2020 statement: an updated guideline for reporting systematic reviews. *BMJ (Clinical Res ed)* (2021) 372:n71. doi: 10.1136/bmj.n71

27. Stang A. Critical evaluation of the Newcastle-Ottawa scale for the assessment of the quality of nonrandomized studies in meta-analyses. *Eur J Epidemiol* (2010) 25(9):603–5. doi: 10.1007/s10654-010-9491-z

28. Egger M, Davey Smith G, Schneider M, Minder C. Bias in meta-analysis detected by a simple, graphical test. *BMJ (Clinical Res ed)* (1997) 315(7109):629–34. doi: 10.1136/bmj.315.7109.629

29. Begg CB, Mazumdar M. Operating characteristics of a rank correlation test for publication bias. *Biometrics* (1994) 50(4):1088–101. doi: 10.2307/2533446

30. Mamat Yusof MN, Chew KT, Kampan N, Abd Aziz NH, Md Zin RR, Tan GC, et al. PD-L1 expression in endometrial cancer and its association with clinicopathological features: A systematic review and meta-analysis. *Cancers* (2022) 14(16):3911. doi: 10.3390/cancers14163911

31. Tokito T, Azuma K, Kawahara A, Ishii H, Yamada K, Matsuo N, et al. Predictive relevance of PD-L1 expression combined with CD8+ TIL density in stage III non-small cell lung cancer patients receiving concurrent chemoradiotherapy. *Eur J Cancer (Oxford Engl 1990)* (2016) 55:7–14. doi: 10.1016/j.ejca.2015.11.020

32. Klement JD, Redd PS, Lu C, Merting AD, Poschel DB, Yang D, et al. Tumor PD-L1 engages myeloid PD-1 to suppress type I interferon to impair cytotoxic T lymphocyte recruitment. *Cancer Cell* (2023) 41(3):620–36.e9. doi: 10.1016/j.ccell.2023.02.005

33. Oh SA, Wu DC, Cheung J, Navarro A, Xiong H, Cubas R, et al. PD-L1 expression by dendritic cells is a key regulator of T-cell immunity in cancer. *Nat Cancer* (2020) 1(7):681–91. doi: 10.1038/s43018-020-0075-x

34. Kowanetz M, Zou W, Gettinger SN, Koeppen H, Kockx M, Schmid P, et al. Differential regulation of PD-L1 expression by immune and tumor cells in NSCLC and the response to treatment with atezolizumab (anti-PD-L1). *Proc Natl Acad Sci U.S.A.* (2018) 115(43):E10119–e26. doi: 10.1073/pnas.1802166115

35. Quail DF, Joyce JA. Microenvironmental regulation of tumor progression and metastasis. *Nat Med* (2013) 19(11):1423–37. doi: 10.1038/nm.3394

36. Zhang X, Zeng Y, Qu Q, Zhu J, Liu Z, Ning W, et al. PD-L1 induced by IFN-γ from tumor-associated macrophages via the JAK/STAT3 and PI3K/AKT signaling pathways promoted progression of lung cancer. *Int J Clin Oncol* (2017) 22(6):1026–33. doi: 10.1007/s10147-017-1161-7

37. Wang X, Yang L, Huang F, Zhang Q, Liu S, Ma L, et al. Inflammatory cytokines IL-17 and TNF-α up-regulate PD-L1 expression in human prostate and colon cancer cells. *Immunol Lett* (2017) 184:7–14. doi: 10.1016/j.imlet.2017.02.006

38. Zhang N, Zeng Y, Du W, Zhu J, Shen D, Liu Z, et al. The EGFR pathway is involved in the regulation of PD-L1 expression via the IL-6/JAK/STAT3 signaling pathway in EGFR-mutated non-small cell lung cancer. *Int J Oncol* (2016) 49(4):1360–8. doi: 10.3892/ijo.2016.3632

39. Concha-Benavente F, Srivastava RM, Trivedi S, Lei Y, Chandran U, Seethala RR, et al. Identification of the cell-intrinsic and -extrinsic pathways downstream of EGFR and IFNγ That induce PD-L1 expression in head and neck cancer. *Cancer Res* (2016) 76(5):1031–43. doi: 10.1158/0008-5472.CAN-15-2001

40. Barsoum IB, Smallwood CA, Siemens DR, Graham CH. A mechanism of hypoxia-mediated escape from adaptive immunity in cancer cells. *Cancer Res* (2014) 74(3):665–74. doi: 10.1158/0008-5472.CAN-13-0992

41. Yao X, Tu Y, Xu Y, Guo Y, Yao F, Zhang X. Endoplasmic reticulum stress-induced exosomal miR-27a-3p promotes immune escape in breast cancer via regulating PD-L1 expression in macrophages. *J Cell Mol Med* (2020) 24(17):9560–73. doi: 10.1111/jcmm.15367

42. Yu Y, Liang Y, Li D, Wang L, Liang Z, Chen Y, et al. Glucose metabolism involved in PD-L1-mediated immune escape in the Malignant kidney tumour microenvironment. *Cell Death Discovery* (2021) 7(1):15. doi: 10.1038/s41420-021-00401-7

43. Kim YB, Ahn JM, Bae WJ, Sung CO, Lee D. Functional loss of ARID1A is tightly associated with high PD-L1 expression in gastric cancer. *Int J Cancer* (2019) 145(4):916–26. doi: 10.1002/ijc.32140

44. Stutvoet TS, Kol A, de Vries EG, de Bruyn M, Fehrmann RS, Terwisscha van Scheltinga AG, et al. MAPK pathway activity plays a key role in PD-L1 expression of lung adenocarcinoma cells. *J Pathol* (2019) 249(1):52–64. doi: 10.1002/path.5280

45. Peng J, Hamanishi J, Matsumura N, Abiko K, Murat K, Baba T, et al. Chemotherapy induces programmed cell death-ligand 1 overexpression via the nuclear factor-κB to foster an immunosuppressive tumor microenvironment in ovarian cancer. *Cancer Res* (2015) 75(23):5034–45. doi: 10.1158/0008-5472.CAN-14-3098

46. Mesnage SJL, Auguste A, Genestie C, Dunant A, Pain E, Drusch F, et al. Neoadjuvant chemotherapy (NACT) increases immune infiltration and programmed death-ligand 1 (PD-L1) expression in epithelial ovarian cancer (EOC). *Ann Oncol* (2017) 28(3):651–7. doi: 10.1093/annonc/mdw625

47. Lee YJ, Woo HY, Kim YN, Park J, Nam EJ, Kim SW, et al. Dynamics of the tumor immune microenvironment during neoadjuvant chemotherapy of high-grade serous ovarian cancer. *Cancers* (2022) 14(9):2308. doi: 10.3390/cancers14092308

48. Wagner P, Koch M, Nummer D, Palm S, Galindo L, Autenrieth D, et al. Detection and functional analysis of tumor infiltrating T-lymphocytes (TIL) in liver metastases from colorectal cancer. *Ann Surg Oncol* (2008) 15(8):2310–7. doi: 10.1245/s10434-008-9971-5

49. de Ruiter EJ, Ooft ML, Devriese LA, Willems SM. The prognostic role of tumor infiltrating T-lymphocytes in squamous cell carcinoma of the head and neck: A systematic review and meta-analysis. *Oncoimmunology* (2017) 6(11):e1356148. doi: 10.1080/2162402X.2017.1356148

50. Berele BA, Cai Y, Yang G. Prognostic value of tumor infiltrating lymphocytes in nasopharyngeal carcinoma patients: meta-analysis. *Technol Cancer Res Treat* (2021) 20:15330338211034265. doi: 10.1177/15330338211034265

51. Kong JC, Guerra GR, Pham T, Mitchell C, Lynch AC, Warrier SK, et al. Prognostic impact of tumor-infiltrating lymphocytes in primary and metastatic

colorectal cancer: A systematic review and meta-analysis. *Dis colon rectum* (2019) 62 (4):498–508. doi: 10.1097/DCR.0000000000001332

52. Yao W, He JC, Yang Y, Wang JM, Qian YW, Yang T, et al. The prognostic value of tumor-infiltrating lymphocytes in hepatocellular carcinoma: a systematic review and meta-analysis. *Sci Rep* (2017) 7(1):7525. doi: 10.1038/s41598-017-08128-1

53. Zheng X, Song X, Shao Y, Xu B, Hu W, Zhou Q, et al. Prognostic role of tumor-infiltrating lymphocytes in esophagus cancer: a meta-analysis. *Cell Physiol Biochem* (2018) 45(2):720–32. doi: 10.1159/000487164

54. Toor SM, Murshed K, Al-Dhaheri M, Khawar M, Abu Nada M, Elkord E. Immune checkpoints in circulating and tumor-infiltrating CD4(+) T cell subsets in colorectal cancer patients. *Front Immunol* (2019) 10:2936. doi: 10.3389/fimmu.2019.02936

55. Orhan A, Vogelsang RP, Andersen MB, Madsen MT, Hölmich ER, Raskov H, et al. The prognostic value of tumour-infiltrating lymphocytes in pancreatic cancer: a systematic review and meta-analysis. *Eur J Cancer (Oxford Engl 1990)* (2020) 132:71–84. doi: 10.1016/j.ejca.2020.03.013

56. Geng Y, Shao Y, He W, Hu W, Xu Y, Chen J, et al. Prognostic role of tumor-infiltrating lymphocytes in lung cancer: a meta-analysis. *Cell Physiol Biochem* (2015) 37 (4):1560–71. doi: 10.1159/000438523

57. Liu D, Heij LR, Czigany Z, Dahl E, Lang SA, Ulmer TF, et al. The role of tumor-infiltrating lymphocytes in cholangiocarcinoma. *J Exp Clin Cancer Res CR* (2022) 41 (1):127. doi: 10.1186/s13046-022-02340-2

58. Kim HJ, Cantor H. CD4 T-cell subsets and tumor immunity: the helpful and the not-so-helpful. *Cancer Immunol Res* (2014) 2(2):91–8. doi: 10.1158/2326-6066.CIR-13-0216

59. Turner TB, Buchsbaum DJ, Straughn JM Jr., Randall TD, Arend RC. Ovarian cancer and the immune system - The role of targeted therapies. *Gynecol Oncol* (2016) 142(2):349–56. doi: 10.1016/j.ygyno.2016.05.007

60. Schalper KA, Brown J, Carvajal-Hausdorf D, McLaughlin J, Velcheti V, Syrigos KN, et al. Objective measurement and clinical significance of TILs in non-small cell lung cancer. *J Natl Cancer Institute* (2015) 107(3):dju435. doi: 10.1093/jnci/dju435

61. Dudley ME, Wunderlich JR, Robbins PF, Yang JC, Hwu P, Schwartzentruber DJ, et al. Cancer regression and autoimmunity in patients after clonal repopulation with antitumor lymphocytes. *Science* (2002) 298(5594):850–4. doi: 10.1126/science.1076514

62. Muenst S, Soysal SD, Gao F, Obermann EC, Oertli D, Gillanders WE. The presence of programmed death 1 (PD-1)-positive tumor-infiltrating lymphocytes is associated with poor prognosis in human breast cancer. *Breast Cancer Res Treat* (2013) 139(3):667–76. doi: 10.1007/s10549-013-2581-3

63. Thompson RH, Dong H, Lohse CM, Leibovich BC, Blute ML, Cheville JC, et al. PD-1 is expressed by tumor-infiltrating immune cells and is associated with poor outcome for patients with renal cell carcinoma. *Clin Cancer Res* (2007) 13(6):1757–61. doi: 10.1158/1078-0432.CCR-06-2599

64. Hsu MC, Hsiao JR, Chang KC, Wu YH, Su IJ, Jin YT, et al. Increase of programmed death-1-expressing intratumoral CD8 T cells predicts a poor prognosis for nasopharyngeal carcinoma. *Modern Pathol* (2010) 23(10):1393–403. doi: 10.1038/modpathol.2010.130

65. Muenst S, Hoeller S, Dirnhofer S, Tzankov A. Increased programmed death-1+ tumor-infiltrating lymphocytes in classical Hodgkin lymphoma substantiate reduced overall survival. *Hum Pathol* (2009) 40(12):1715–22. doi: 10.1016/j.humpath.2009.03.025

66. Carreras J, Lopez-Guillermo A, Fox BC, Colomo L, Martinez A, Roncador G, et al. High numbers of tumor-infiltrating FOXP3-positive regulatory T cells are associated with improved overall survival in follicular lymphoma. *Blood* (2006) 108 (9):2957–64. doi: 10.1182/blood-2006-04-018218

67. Badoual C, Hans S, Merillon N, Van Ryswick C, Ravel P, Benhamouda N, et al. PD-1-expressing tumor-infiltrating T cells are a favorable prognostic biomarker in HPV-associated head and neck cancer. *Cancer Res* (2013) 73(1):128–38. doi: 10.1158/0008-5472.CAN-12-2606

68. Salama P, Phillips M, Grieu F, Morris M, Zeps N, Joseph D, et al. Tumor-infiltrating FOXP3+ T regulatory cells show strong prognostic significance in colorectal cancer. *J Clin Oncol* (2009) 27(2):186–92. doi: 10.1200/JCO.2008.18.7229

69. Legat A, Speiser DE, Pircher H, Zehn D, Fuertes Marraco SA. Inhibitory receptor expression depends more dominantly on differentiation and activation than "Exhaustion" of human CD8 T cells. *Front Immunol* (2013) 4:455. doi: 10.3389/fimmu.2013.00455

frontiers | Frontiers in Oncology

TYPE Review
PUBLISHED 20 October 2023
DOI 10.3389/fonc.2023.1278863

OPEN ACCESS

EDITED BY
Chao Liu,
Shandong Cancer Hospital, China

REVIEWED BY
Nayara Tessarollo,
ICESP, Brazil
Zhongkun Zhang,
Dana–Farber Cancer Institute,
United States
Xiaohui Li,
Shandong University, China

*CORRESPONDENCE
Yumei Wu
wym597118@ccmu.edu.cn

RECEIVED 17 August 2023
ACCEPTED 09 October 2023
PUBLISHED 20 October 2023

CITATION
Zhang C, Wang M and Wu Y (2023) Features of the immunosuppressive tumor microenvironment in endometrial cancer based on molecular subtype.
Front. Oncol. 13:1278863.
doi: 10.3389/fonc.2023.1278863

Features of the immunosuppressive tumor microenvironment in endometrial cancer based on molecular subtype

Chong Zhang[1], Ming Wang[2] and Yumei Wu[2]*

[1]Departments of Obstetrics, Beijing You'an Hospital of Capital Medical University, Beijing, China, [2]Department of Gynecologic Oncology, Beijing Obstetrics and Gynecology Hospital, Capital Medical University, Beijing Maternal and Child Health Care Hospital, Beijing, China

Endometrial cancer (EC) is one of the three most prevalent gynecological tumors affecting women and is the most prevalent gynecological malignancy in the developed world. Its incidence is rapidly increasing worldwide, mostly affecting postmenopausal women, whereas recently its prevalence has increased in younger people. EC is an immune gene disease and many studies have shown that the tumor-immunosuppressive microenvironment plays an important role in cancer progression. In recent years, findings regarding the immunosuppressive tumor microenvironment (ITME) of EC have included immune evasion mechanisms and immunotherapy, which are mostly immune checkpoint inhibitors (ICI) for EC. Recently studies on the ITME of different molecular types of EC have found that different molecular types may have different ITME. With the research on the immune microenvironment of EC, a new immunophenotype classification based on the immune microenvironment has been carried out in recent years. However, the impact of the ITME on EC remains unclear, and the immunophenotype of EC remains limited to the research stage. Our review describes recent findings regarding the ITME features of different EC molecular types. The advent of immunotherapy has brought hope for improved efficacy and prognosis in patients with advanced or recurrent EC. The efficacy and safety of ICIs combination therapy remains the focus of future research.

KEYWORDS

endometrial cancer, immunosuppressive tumor microenvironment, immunophenotype, molecular subtypes, immunotherapy

1 Introduction

Endometrial cancer (EC) is an immune gene disease, and many studies have suggested that the immunosuppressive tumor microenvironment (ITME) plays an important role in cancer progression (1–3). EC is commonly diagnosed at an early stage because abnormal bleeding is a common clinical symptom with a favorable prognosis (five-year overall

survival: 71-80%) (4). For patients with advanced disease before symptoms appear, the prognosis is worse and they respond poorly to conventional therapies (5). Therefore, in recent years, immunotherapy has attracted attention, and researchers have conducted studies on the ITME of EC. Since 2014, the Food and Drug Administration (FDA) has approved several immune checkpoint inhibitors (ICI) in clinical practice, mainly for patients with late-stage or recurrent cancers for whom routine treatment has failed. However, the relatively low response rate limits its application in clinical practice, and the efficacy of immunotherapy is unsatisfactory (6). Therefore, screening populations for therapeutic advantages when using ICIs is crucial. Classification methods for EC are constantly improving, gradually shifting from traditional clinical and pathological classifications to molecular classifications. Therefore, studying the ITME of different molecular subtypes is important. Recently studies on the ITME of different molecular types of EC have revealed that different molecular types may have different ITME (7, 8). However impact of the ITME on EC remains unclear. Our review describes recent findings regarding the ITME features of different EC molecular types.

2 Main body

2.1 Molecular types of EC

EC has been broadly divided into two groups based on histomorphology since 1983. Type I is endometrioid tumors, which are the most common subtype, and most of the tumors express the estrogen receptor (ER) and have a favorable prognosis. In contrast, type II is estrogen-independent and mainly represents a serous carcinoma with a poor outcome (9, 10). However, the classification based on tumor histopathology is subjective, has reproducibility challenges, and high-level EC cannot be reliably based on histological criteria. Misdiagnosis is possible due to the presence of mixed high-grade histological components. Biological information to enhance diagnosis is urgently required in this situation.

To overcome these limitations, the Cancer Genome Atlas (TCGA) Research Network, based on mutational burden and somatic copy-number variations, revealed four molecular subtypes of EC with distinct prognoses: DNA polymerase epsilon (POLE) ultramutated (POLEmut) with an excellent prognosis, microsatellite instability hypermutated (MSI-H) with an intermediate prognosis, copy number high (CNH) with the worst prognosis, and copy number low (CNL) with an intermediate prognosis (11). However, the TCGA studies only include endometrioid and serous EC, and the additional cost of entire genome sequencing greatly limits its practical application. Subsequent studies have found cheaper and easier surrogates. To broaden the utility of TCGA classification, Talhouk proposed a practical molecular POLE mutation-based classification model, the Proactive Molecular Risk Classifier for Endometrial Cance (ProMisE) (12). In this study, immunohistochemistry (IHC) for mismatch repair (MMR) proteins and immunohistochemical staining for p53 were used instead of molecular assessments of mutational burden and copy number variations. Therefore, the ProMisE model classified four subgroups: mismatch repair deficient (MMRd), POLE-ultramutated (POLEmut), p53-wild type (p53wt), and p53-abnormal (p53abn) (13, 14). In 2016, Stelloo et al. validated a more pragmatic, cost-effective, and clinically applicable molecular classification system called the Translational Research in Post-Operative Radiation Therapy in EC (TransPORTEC) system. Therefore, EC can be subdivided into four subgroups: the POLE-mutated, MMRd, p53abn, and no specific molecular profile (NSMP) (15, 16). POLE-mutant ECs have a highly favorable prognosis and do not require adjuvant treatment. MMRd ECs have an intermediate prognosis. Numerous recent studies have focused on the immunotherapy for EC (17, 18). And reports have demonstrated these two groups may benefit from immunotherapy (19, 20). P53-mutant ECs are typically associated with more advanced stages, higher rates of lymphatic vascular space infiltration (LVSI), and diverse pathological types. Most P53-mutant ECs are serous adenocarcinomas and have a poor prognosis. The NSMP group was the most frequent, and its prognosis was uncertain (16), as shown in Figure 1.

In view of the important prognostic and therapeutic implications of the European Society of Gynecological Oncology (ESGO), European Society of Pathology (ESP), and European Society for Radiotherapy and Oncology (ESTRO) guidelines, new prognostic risk groups were defined of adopting the molecular classification for EC treatment in 2020 (21). ECs with POLE-mutant confined to the uterus are regarded as low-risk, whereas p53-abnormal ECs are regarded as “high-risk” in the presence of invasion (22).

2.2 Tumor immunosuppressive microenvironment in EC

The tumor microenvironment plays a crucial role in the occurrence and development of malignant tumors, and has a significant impact on the clinical outcomes of EC (23). Immune cells in a normal endometrium are vital for protection against external pathogens. The immune cells, mesenchymal cells, endothelial cells, inflammatory mediators, and extracellular matrix (ECM) molecules are components of the ITME. Infiltrating stromal and immune cells are the major components of the ITME and play a significant role in the biological behavior of cancer (24). Related studies have shown that many immune cells and cytokines are found in EC tissues and can stimulate an endogenous anti-tumor immune response. Therefore, these patients may benefit from immunotherapy (25–27).

Tumor-infiltrating immune cells can exert an anti-tumor killing effect through a specific cellular immune-mediated immune response. Some subsets can control the growth and progression of tumors, whereas others can promote immune suppression and help tumor cells escape the immune system. Finally, the body reaches a balance between the tumor immune response and tumor immune escape (28, 29). Tumor-infiltrating immune cells include T cells, tumor-associated macrophages (TAMs), natural killer (NK) cells,

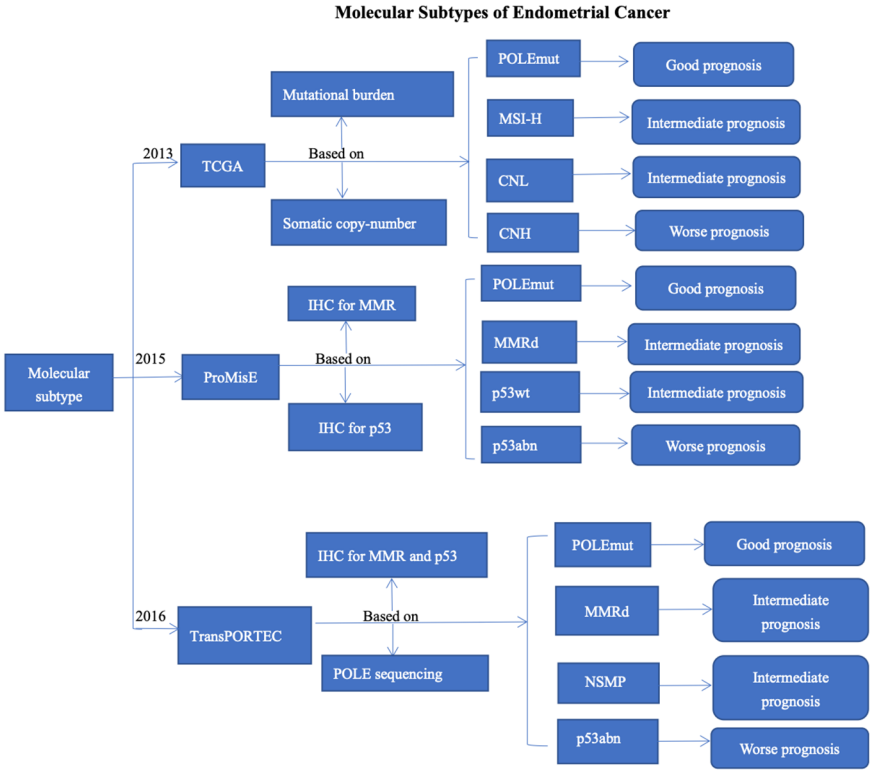

FIGURE 1
Molecular Subtypes of Endometrial Cancer.

dendritic cells (DCs), and B cells. (Table 1) T cells can be divided into two subgroups: $CD4^+$ and $CD8^+$. In terms of immune function, $CD4^+$ T cells are mainly regulatory T cells (Tregs), which assist humoral and cellular immunity by secreting various lymphokines. $CD8^+$ T cells mainly include inhibitory and cytotoxic T cells. $CD8^+$ inhibitory T cells can inhibit humoral immunity. $CD8^+$ cytotoxic T lymphocytes (CTLs) can lead to the apoptosis of target cells by releasing perforin, granzyme killer cells, or through the Fas/FasL pathway (30, 31). Cytokines are immune checkpoint molecules and inflammatory factors. The immune checkpoint molecules include members of the B7 family, human leukocyte antigen 1(HLA 1) and lymphocyte activation gene-3 (LAG-3) are shown in. Table 2 (61–64). Inflammatory factors includes interleukin−6 (IL−6), IL-11, tumor necrosis factor a (TNF-α), Cox-2 and interferon.

2.3 Tumor-infiltrating immune cells

2.3.1 $CD8^+$ CTLs

$CD8^+$ CTLs can induce the apoptosis of target cells (30, 31). $CD8^+$ CTLs have been isolated from the peripheral blood or tumor tissues of patients with a variety of cancers, such as melanoma and lung cancer. This may have potential value in the early diagnosis of tumors (65). In terms of EC, reports have demonstrated that the number of $CD8^+$ CTLs is lower in the endometrium of EC patients than in the normal endometrium (32). Studies have found that tumors with fewer somatic mutations produced lower levels of immunogenic antigens (66). Therefore, $CD8^+$ CTLs generally indicate a good prognosis and a lower T-cell density has been found in advanced-stage ECs (26). Furthermore, Suemori (33) analyzed 123 cases of EC tissues using immunohistochemistry (IHC) and found that $CD8^+$ CTLs can be used as an independent predictors of the overall survival rate (OS) of EC. Dai et al. (7) conducted a retrospective study of 26 patients with EC and observed relatively high percentages of $CD8^+$ CTLs in TMB-high EC samples, which were considered to have a good survival outcome. Kondratiev et al. (67) studied 90 patients with EC and found that an increased number of $CD8^+$ CTLs in the epithelial cells at the tumor-invasive border was a favorable prognostic factor for EC patients. Compared to patients with a lower number of $CD8^+$ CTLs in the epithelium at the infiltrating boundary of tumors, patients with a higher number of $CD8^+$ CTLs showed an improvement in overall survival (OS) time. The study showed that tumor stage, tumor grade, vascular invasion, and the number of $CD8^+$ CTLs in ITME were independent predictors of OS (67). All the above studies illustrate the value of $CD8^+$ CTLs in the prognostic evaluation of EC. Dynamic monitoring of changes in $CD8^+$ CTLs in patients EC has great clinical reference value for

TABLE 1 Tumor-infiltrating immune cells in immunosuppressive tumor microenvironment.

Regulatory function	Immune cell	Role	Clinical studies and findings
Down-regulation	CD8+CTL	Induce the apoptosis of target cells (30, 31).	The number of $CD8^+$ CTLs is lower in the endometrium of EC patients than in the normal endometrium (32). $CD8^+$ CTLs generally indicate a good prognosis and a lower T-cell density has been found in advanced-stage ECs (26). CD8+ CTLs can be used as an independent predictor of OS (33).
	DC	Identify tumor antigen presentation signals, induce the generation of $CD8^+$ CTLs, and secrete cytokines (34).	The reduction of DC activity was associated with EC progression (35). There are morphological differences in the DCs of the endometrium between patients with EC and healthy humans, and the endometrium in patients had lower levels of CD80, CD86, and CD40, which are expressed on DCs (36).
	NK	Be activated by various cytokines and have cell-killing functions (37).	Mean values of NK cell activity were significantly lower in patients with stages I and II of EC when compared with healthy controls (38). NK cell activity in stage I EC patients was negatively associated with nuclear grading, myometrial invasion, and immunoreactivity of proliferating cell nuclear antigen (39).
Up-regulation	TAM	Express many anti-inflammatory factors, such as IL-10 and TGF-β (40).	Most studies reported a positive correlation between the expression of TAMs and advanced stage, RFS and OS in patients with EC (41–43).
	Treg	Mediate the immune escape of tumor cells and promote tumor metastasis and progression (44).	Tregs expression was significantly increased in the tumor groups of all grades compared to the normal endometrial group (44). The upregulation of CD4 expression in T cells in the ITME was positively associated with high cancer grade, cancer stage, and myometrium invasion (45).

$CD8^+$CTL, $CD8^+$ T lymphocytes; DC, dendritic cells; NK, Natural killer cells; TAM, tumor associated macrophages; Treg, regulatory T cells; OS, overall survival; RFS, recurrence-free survival.

TABLE 2 Immune checkpoint molecules in immunosuppressive tumor microenvironment.

Regulatory function	Immune checkpoint molecules	Mechanism	Clinical studies and findings
Up-regulation	PD-1/PD-L1	PD-1 combined with PD-L1 can inhibit the proliferation and differentiation of T cells (46).	The expression levels of PD-1 and PD-L1 are related to a poor prognosis (47). The expression levels of PD-1 and PD-L1 are related to the degree of T lymphocyte infiltration in POLEmut and MSI-H EC (48, 49). Both POLEmut and MSI-H type EC patients are more sensitive to immunotherapy based on PD-1/PD-L1 inhibitors (48, 49).
	CTLA-4	Inhibit CTL activation by preventing the binding of B7 ligand to CD28 (50).	The combined blockade of CTLA-4 and PD-1 amplifies anti-tumor T cell responses and provides synergistic activity (51).
	B7-H3	A negative regulatory factor for T-cell activation and may protect tumor cells from immune system surveillance (52).	B7-H3 is expressed in most EC, and its high expression is closely associated with high-risk tumors (52). The expression of B7–H3 in EC cells positively correlated with the frequency of $CD8^+$ TILs and the overexpression of B7–H3 in EC cells was associated with short OS time (52).
	B7-H4	Inhibit T lymphocyte proliferation and cytokine secretion (53).	B7–H4 was upregulated in malignant EC and was more common in advanced subgroups (54). The expression of B7–H4 was an independent factor of EC grade, histological type, and infiltrating–immune cell type (55).
	HLA	Present immunogenic peptides to CTL (56).	HLA class I molecules were downregulated on the surface of the EC (56). HLA was associated with high grade of EC (57). The HLA level in patients with early stages of EC was high (58).
	LAG-3	Iinhibit immune cell proliferation and cytokine release (59).	LAG-3 expression in immune cells was more common in high-grade, high-intermediate risk, high-risk, and advanced/metastatic subgroups and was relevant to lymphovascular space invasion (60). LAG-3 expression was more prevalent in POLEmut and MMRd EC than in p53abn and p53wt EC in tumor cells Positive LAG-3 expression may be a predictor of improved RFS (60).

PD–1, programmed cell death 1; PD–L1, programmed cell death 1 ligand 1; CTLA-4, cytotoxic T-lymphocyte-associated protein 4; B7-H3, B7 homolog 3; TILs, tumor-infiltrating lymphocytes; B7-H4, B7 homolog 4; HLA, human leukocyte antigen; LAG-3, lymphocyte activation gene-3; EC, endometrial cancer; POLEmut, DNA polymerase epsilon ultramutated; MMRd, mismatch repair deficient; MSI-H, microsatellite instability hypermutated; RFS, recurrence-free survival.

judging prognosis, guiding treatment, and follow-up management (26, 33, 68).

2.3.2 TAMs

TAMs are important factors that affect the tumor microenvironment and can lead to drug resistance by promoting tumor invasion, metastasis, and blood vessel formation (69). TAMs are a diverse subset of tumor-infiltrating immune cells derived from monocytes that exhibit traditional cytotoxicity and phagocytic properties (70). Macrophages can be induced to form two major phenotypes: classically activated macrophages (M1) and selectively activated macrophages (M2). M1 type macrophages express a range of pro-inflammatory cytokines, chemokines and effector molecules, such as IL-12, IL-23, TNF-α and MHC I/II. In contrast, the M2 type macrophages express many anti-inflammatory factors, such as IL-10 and TGF-β. TAMs are classified as M2 type macrophages (40). Wang et al. (68) found that TAMs are the most abundant TME-infiltrating cells, followed by $CD8^+$ CTLs. Currently, whether measuring TAM density in EC has clinical or prognostic significance is controversial. Hannah (26) reported no correlation between TAM density and cancer progression. Kübler et al. (41) reported a positive correlation between the expression of TAMs and advanced stage, recurrence-free survival (RFS), and OS in patients with EC. Dun et al. (42) reported that compared with normal endometrial cells, $CD68^+$ macrophages were more abundant in the epithelial and stromal cells of type I and type II EC. Furthermore, Soeda et al. (43) compared patients with low $CD68^+$ TAM density with EC patients who had higher $CD68^+$ macrophage counts in ITME and found that they had worse progression–free survival (PFS) and OS time.

2.3.3 Tregs

Tregs are immunosuppressive regulatory cells that are incapable of preventing excessive immune responses in a various tumor tissues. Studies have shown that Tregs mediate the immune escape of tumor cells and promote tumor metastasis and progression. A balance exists between the numbers of Tregs and $CD8^+$ CTLs, which is crucial for the establishment of an effective immune monitoring system. The increase in the Tregs/$CD8^+$ CTLs ratio indicated a poor anti-tumor effect. In addition, Julie et al. (44) reported that Tregs expression was significantly increased in the tumor groups of all grades compared to the normal endometrial group. In a study involving 57 patients with stage I–IV EC, Chang et al. (45) found that the number of $CD4^+$ T cells was higher in the infiltrating lymphocytes of tumors than in the peripheral blood lymphocytes. Furthermore, they showed that the upregulation of CD4 expression in T cells in the ITME was positively associated with high cancer grade, cancer stage, and myometrium invasion (45). Another study reported that the infiltration of $CD4^+$ Tregs into the ITME is relevant to the prognosis of patients with EC (71). All evidence suggests that Tregs are indicators of poor prognosis in patients with EC (72).

2.3.4 DCs

DCs are the most powerful antigen presenting cells in the human body. They can identify tumor antigen presentation signals, induce the generation of $CD8^+$ CTLs, and secrete cytokines during anti-tumor immune processes. Tumor cells cannot be recognized or presented by DCs owing to their low antigenicity. Therefore, $CD8^+$ CTLs cannot be activated, leading to tumor cell escape and continued tumor growth. Effective identification of tumor cells is the first step in immunotherapy (34). Li et al. reported that DCs are significantly associated with survival patients with EC (73). Chen et al. (35) suggested that a reduction in DC activity is associated with EC progression. Studies have also shown that there are morphological differences in the DCs of the endometrium between patients with EC and healthy humans, and the endometrium in patients had lower levels of CD80, CD86, and CD40, which are expressed on DCs (36). This evidence reflected that the function of tumor–infiltrating DCs in tumor microenvironment was downregulated which affected antigen presentation, and promoted immune escape of tumor. In 2010, the FDA approved the peptide DC vaccine Sipuleucel-T for the treatment of refractory prostate cancer (74). Currently many DC vaccines are in different stages of clinical trials. Studies on DC vaccine applications in EC treatment have found that activated DC have an obvious killing effect on EC cells (75).

2.3.5 NK cells

NK cells are a class of innate immune cells with cytotoxicity similar to that of $CD8^+$ CTLs and both of are anti-tumor effector cells. The activation and cytotoxicity of NK cells depend on the balance between the inhibitory and activation signals. NK cells are activated by various cytokines and have cell-killing functions (37). Although NK cells kill tumor cells, if this balance is disrupted, they can promote tumor growth and tissue infiltration during the immune escape of EC tumors. Human leukocytes antigens (HLA), co-inhibitory molecules, and inhibitory cytokines can also activate NK cells, but the inhibitory signals provided by them impairs the cytotoxic function of NK cells. The abundance of immunosuppressive molecules present in the EC tumor microenvironment is involved in EC progression by affecting NK cell function (76). Garzetti et al. (38) reported that the mean values of NK cell activity were significantly lower in patients with stages I and II of EC when compared with healthy controls. The authors suggested that a decrease in NK cell activity was associated with the depth of myometrial invasion (38). In the following research, Garzetti et al. (39) made further studies about the activity of NK cells and found that NK cell activity in stage I EC patients was negatively associated with nuclear grading, myometrial invasion, and immunoreactivity of proliferating cell nuclear antigen.

2.4 Immune checkpoint molecules

2.4.1 B7 family

The B7 family of immune checkpoint molecules is divided into three subgroups. Group I comprises B7-1, B7-2, CD28, Cytotoxic T-lymphocyte-associated protein 4 (CTLA-4), and B7H. Group II comprises programmed cell death 1 (PD−1)/programmed cell death 1 ligand 1(PD−L1). Group III comprises B7 homolog 3 (B7−H3), B7

homolog 4(B7-H4), HERV–H LTR–associating 2, and transmembrane and immunoglobulin domain-containing protein 2. Members of the B7 family play a critical role in the immune response and immune escape (77).

2.4.1.1 PD-1/PD-L1

PD-1 is an important inhibitory co-stimulatory molecule and is expressed on the surface of activated T cells. Combined with its ligand, PD-L1 can inhibit the proliferation and differentiation of T cells, cause T cells to be in an inhibitory state, reduce their lethality to tumor cells, and lead to the immune escape of tumor cells. PD-1/PD-L1 inhibitors can relieve the negative immune regulatory effect of PD 1/PD L1 on T cells, promote effector T cell-specific recognition, and kill tumor cells (46). To escape the immune system, EC cells can stimulate immune checkpoints to activate negative feedback mechanisms and establish a local ITME. PD-1/PD -L1 inhibitors cause an excessive immune response and tissue damage. Liu et al. (78) found that the positive expression rates of PD-L1 in primary, recurrent, and metastatic endometrial cancers were 83%, 68%, and 100%, respectively by immunohistochemistry. Previous studies showed that PD-1 and PD-L1 are expressed in most EC tissues. The higher the level of PD-L1 expression, the worse is the differentiation of the tissue. Vanderstraeten et al. (79) found that the expression rate of PD-L1 in primary and metastatic EC tumor cells were 83% and 100%, respectively. In type II EC, the expression rates of PD-1 in the tumor tissue and the tumor microenvironment were 42% and 53%, respectively. And the expression rate of PD-L1 in the tumor tissue and tumor microenvironment were 15% and 28%, respectively. All the evidence indicates that the expression levels of PD-1 and PD-L1 are associated with a poor prognosis (47). Eggink (48) and Howitt (49) confirmed that the expression levels of PD-1 and PD-L1 are related to the degree of T lymphocyte infiltration in POLEmut and MSI-H EC. The higher the number of T lymphocytes, the stronger the local immune response and the better the prognosis. Therefore, patients with both POLEmut and MSI-H-type EC are more sensitive to immunotherapies based on PD-1/PD-L1 inhibitors.

2.4.1.2 CTLA-4

CTLA-4, also called CD152, is regarded as a negative immune regulator and is a leukocyte differentiation antigen and a transmembrane receptor on T cells. CTLA-4 shares CD28 with the B7 molecular ligand, which inhibits CTL activation by preventing the binding of the B7 ligand to CD28 (50). CTLA-4 is usually expressed in activated T cells to downregulate or terminate T cell activation and participates in negative immune regulation (80). CTLA-4 inhibitors have significant killing effects on solid tumors and are currently approved for of breast cancer treatment. However, their application in patients with EC remains in clinical trials (81). According to previous reports, the combined blockade of CTLA-4 and PD-1 amplifies anti-tumor T cell responses and provides synergistic activity (51). This combination therapy has been investigated in Phase III clinical trials (82). In 2018, the FDA approved the combination of ipilimumab and nivolumab for the treatment of MSI-H or MMRd metastatic colorectal cancer based on the CHECKMATE 142 study. This combination therapy has also been studied for gynecological cancer and has shown good clinical efficacy in patients with EC (83). Taylor et al. (84) reported that the efficacy rate of this combination therapy could reach 50%.

2.4.1.3 B7-H3

B7-H3 is often overexpressed in tumors. This is related to tumor immune escape. As is shown in Brunner's study, B7-H3 is expressed in most EC, and its high expression is closely associated with high-risk tumors. Therefore, EC B7-H3 is regarded as a negative regulatory factor for T-cell activation and may protect tumor cells from immune system surveillance (52). In addition, the expression of B7–H3 in EC cells positively correlated with the frequency of $CD8^+$ tumor-infiltrating lymphocytes (TILs) and the overexpression of B7–H3 in EC cells was associated with short OS time (52).

2.4.1.4 B7-H4

B7-H4, discovered in 2003, is a co-inhibitory molecule that negatively modulates T cell immune responses and promotes immune evasion by inhibiting T lymphocyte proliferation and cytokine secretion (53). However, increasing evidence suggests that B7-H4 in tumor cells is related to the inhibitory microenvironment of T lymphocytes and can limit tumor growth in animal models (85). Similar to the results of this study, Rahbar et al. (86) found that high expression of B7-H4 protein in breast cancer tissues was associated with a favorable prognosis for patients. Miyatake et al. (54) reported that B7–H4 was upregulated in malignant EC and was more common in advanced subgroups. Additionally, Bregar et al. suggested that the expression of B7–H4 was an independent factor of EC grade, histological type, and infiltrating–immune cell type (55).

2.4.2 HLA

Because various tumor cells lack the expression of HLA class I molecules, they are unable to present immunogenic peptides to CTL that cannot be activated, leading to the immune escape of tumors. Researchers studied 486 patients with sporadic EC and found that HLA class I molecules were downregulated on the surface of the EC (56). Compared with patients with normal HLA expression, these patients had a significantly decreased number of CD8+ CTL in the tumor microenvironment. These patients have decreased disease-free survival rates. This suggests that EC escape the immune system by downregulating the expression of HLA class I molecules in the cell membrane (57, 87, 88). A previous study which involving 486 EC patients showed that the loss of HLA was 41.3% and that HLA was associated with high grade of EC (57). Furthermore Ben et al. (58) reported that the HLA level in patients with early stages of EC was high, which is consistent with a previous study.

2.4.3 LAG-3

LAG-3, also known to as CD223, is primarily expressed in activated T and NK cells. LAG-3 can inhibit immune cell proliferation and cytokine release when activated by the major histocompatibility complex II (MHC II) (59). Studies have reported

that binding to its ligand LAG-3 can induce the suppression of T-cell and thus causing tumor evasion (89). Preclinical studies have shown that various solid tumors, including colorectal, ovarian, and renal cancers, are associated with LAG-3, suggesting that LAG-3 is a promising immune checkpoint for the development of immunotherapies. Therefore, several clinical trials of ICIs targeting LAG-3 are currently associated with advanced solid tumors [NCT03743766, NCT02519322, NCT03662659, NCT03610711, NCT03459222, NCT03499899] (90). Recently, Zhang et al. (60) conducted a retrospective study of 421 patients with EC and found that LAG-3 expression in immune cells was more common in high-grade, high-intermediate risk, high-risk, and advanced/metastatic subgroups and was relevant to lymphovascular space invasion. Furthermore, LAG-3 expression was more prevalent in POLEmut and MMRd EC than in p53abn and p53wt EC in tumor cells (34.4% and 66.3% in POLEmut and MMRd versus 28.6% and 19.5% in p53abn and p53wt, $P < 0.001$). The positive expression of LAG-3 in tumor cells is associated with high levels of CD8+ T cell immune infiltration. In addition, positive LAG-3 expression may be a predictor of improved RFS (60).

Other novel immune checkpoint molecules that are not yet in clinical use include moiety 2,3-dioxygenase inhibitors (IDO), and T-cell immunoglobulin and mucin domain-containing protein 3 (TIM-3), and T-cell immunoglobulin and ITIM domain protein (TIGIT).

2.5 Inflammatory factors

Inflammatory cells can release IL-6 and TNF-α cytokines to affect cell proliferation signals. Cytokines can promote rapid cell proliferation and differentiation and increase the probability of abnormal mutations. For example, TNF-α at high concentrations can kill EC tumor cells. Meanwhile, EC tumor cells can release TNF-α causing DNA damage and abnormal cell repair (91). TNF-α can enhance tumor invasion by affecting angiogenic factors. Inflammatory cells can also promote the production of cyclooxygenase 2 (COX-2), which participates in tumor generation and invasion by affecting IL-6 and IL-11. Furthermore, inflammatory cells can produce local active nitrogen clusters and reactive oxygen clusters, which can cause cell DNA damage, and easily form abnormal mutations that can promote growth and tumor invasion (92). Che et al. (93) suggested that IL-6 promotes autosynthesis and EC growth via autocrine feedback mediated by the ERK-NF-κB signaling pathway. High expression rates of colony stimulation factor-1 (CSF-1), TNF-α and IL-6 were associated with poor prognosis in EC patients. Lay et al. (92) suggested that IL-11 promotes EC progression by activating STAT. These cytokines may be involved in the immune escape in EC.

2.6 ITME in EC revealed by single-cell RNA sequencing

ScRNA-seq is a method to measure the expression levels of all genes from individual cells, and reveals heterogeneity at cell level (94, 95). Liu et al. (96–99) applied ScRNA-seq to tumor tissues from patients of cervical cancer to explore the ITME. With the aid of scRNA-seq, the understanding of the ITME in gynecological tumors is improved. Several studies have been studied on EC using scRNA seq. Huang et al. (100) revealed that the small GTPase 3 (RAC3) was specifically distributed in EC tumor cells compared to normal tissues. High levels of RAC3 in EC tissues were reversely associated with $CD8^+$ T cell infiltration. Furthermore, RAC3 accelerated tumor cell proliferation and inhibited its apoptosis, without impacting cell cycle stages. Importantly, silencing RAC3 improved the sensitivity of EC cells to chemotherapeutic drugs (100). Yu et al. (101) suggested EC cells can confer malignant phenotype to endothelial cells by Midkine (MDK)-nucleolin (NCL) signal and NCL is associated with suppressed immune activity. EC cells may shape ITME by inhibiting immune cells via MDK-NCL signal. Guo et al. (102) suggested the percentage composition of monocytes, DC and mast cells were higher in paratumor than in tumor. On the other hand, the percentage composition of macrophages was higher in tumor than in paratumor. They found that tumor infiltrating macrophages were associated with increased OS. Wu et al. (103) identified three macrophage subsets, and two of them showed tissue-specific distribution. The tumor-enriched macrophage subset was found to predict immunotherapy responses in EC. Furthermore, six genes were selected from macrophage subset markers that could predict the survival of EC patients, SCL8A1, TXN, ANXA5, CST3, CD74 and NANS, and a prognostic signature was constructed. Further research is needed to study ITME through scRNA-seq.

2.7 ITME in different subtypes of EC

To date, studies on ITME in EC have mostly focused on POLE mutations and the MMRd subtype. According to the TCGA data, patients with POLE mutations showed the highest tumor mutation burden (TMB), followed by those with the MSI-H subtype. Reports have illuminated that TMB is highly associated with tumor-infiltrating immune cells, PD-L1 expression and patients' prognosis in EC (104–106). Meanwhile, studies have also reported that POLEmut and MMRd EC have a high number of CD8+ CTLs expressing PD-1 (29). This is the key mechanism of immune tolerance in POLEmut and MMRd EC, as PD-1 binds to PD-L1 to restricts CD8+ CTLs function. Furthermore, previous studies have shown that $CD8^+$ CTLs generally indicate good prognosis (26). These results are consistent with each other, as in clinical practice, POLEmut and MMRd have relatively favorable prognoses and can benefit from immunotherapy. Fusco et al. (107) revealed that a possible hypothesis supporting these results is that tumors with more somatic mutations produce higher levels of immunogenic antigens. Consequently, these tumors can be detected by CD8+ CTLs and are less likely to progress to a late stage. Guo et al. (20) explored 123 MSI EC and found that MSI tumors were enriched with CD8+ CTLs, Treg cells, fewer M2 macrophages, activated DCs, and a higher trend of $CD20^+$ B cells infiltration. Patients with MSI EC were identified more often in the early stages, had a lower age, and better survival. Julie et al. (44) found CTLA4, PD-1, PD-L1,

TIM-3 and IL-6 expression significantly increased in all EC grades. The number of $CD4^+$ T cells was similarly increased in all EC grades, whereas the number of $CD8^+$ CTL was only increased in the grade 1 ECs and decreased or remained unchanged in others grades. Daniel (108) studied the POLEmut type and found similar results to those of the prominent $CD8^+$ CTL present in POLE-mutant. Mohammad (109) performed a retrospective study and found that a combination of PD-L1 positivity and MMR deficiency may be associated with aggressive features such as LVSI. Dai et al. (7) conducted a retrospective study to comprehensively analyze the ITME of four molecular subtypes in EC comprehensively for the first time. They combined the POLE mutant and MSI-H subtypes into the TMB high (TMB-H) subtype owing to their small sample size. They analyzed the ITME features of 30 EC cases, including TMB, infiltration of anti-tumor-related immune cells and negatively regulatory immune cells, and expression of immune checkpoint molecules. Similar results were found in previous studies, which showed that POLE mutations showed the highest level of TMB, followed by the MSI-H subtype, NSMP, and TP53 mutant subtypes. The TMB-H subtype showed a high degree of infiltration of $CD8^+$ T cells and relatively high levels of PD-L1 expression in tumor cells. Although TMB levels were low in the TP53 mutant subtype, the proportions of Treg, M2 macrophages, $PD\text{-}L1^+$ $CD68^+$ macrophages, and $CD8^+$ $PD\text{-}1^+$ T cells were relatively high, indicating a strong immunosuppressive microenvironment in this subtype. In the NSMP subtype, the TMB, proportions of multiple tumor-infiltrating immune cells, and expression levels of immune checkpoint molecules were low, indicating a lack of effective anti-tumor immune responses. Based on the immune microenvironmental features, they summarized the immune phenotype of the three molecular subtypes as normal immune response, absence of immune infiltration, and suppressed immune response. Due to the relatively small sample size, further studies with larger sample sizes are required to confirm these findings. The ITME in different subtypes of EC is shown in Table 3.

2.8 Immunotherapy in EC

Immunotherapeutic strategies for EC are widely used and can be divided into three categories: anticancer vaccines, ICI, and immunomodulators. In recent years, with the development of tumor cells and the tumor immune microenvironment, immunotherapy, especially ICI, has been applied for the treatment of a variety of malignancies. Immune checkpoints regulate co-stimulation signaling to maintain immune self-tolerance in the body and prevent immune damage caused by the excessive activation of T cells. This is the mechanism by which tumor cells escape immune surveillance and death. By suppressing immune checkpoint activity, ICI activate the tumors recognition and killing functions of immune cells. At present PD-1/PD-L1 and CTLA-4 antibodies were widely used (110). These immunotherapies are most effective for POLEmut and MMRd tumors because of their high TMB and increased immunogenic antigens (111). The higher TMB and PD-L1 expression in MSI-H and MMRd endometrial tumors support the clinical efficacy of PD-1 inhibitors in treating solid tumors with MMRd (112). Moreover, as mentioned earlier, PD-L1 expression increased with TIL abundance in the EC ITME, indicating that PD-1 inhibitors can induce an effective anti-tumor immune response in EC with high PD-L1 expression (104–106). In 2017, the FDA approved pabolizumab for the treatment of solid tumors with unresectable or metastatic MSI-H or MMRd. In 2021, the FDA approved dostarlimab-gxly for adult patients with MMRd solid tumors (113). Furthermore the National Comprehensive Cancer Network (UCCN) and ESGO/ESTRO/ESP guidelines in 2020 recommended anti-PD-1 targeted therapy for patients with advanced MMRd EC (21). Multiple clinical trials are currently underway regarding the treatment of EC with PD-1 antibody. KEYNOTE-016 study, a phase II clinical study in the United States evaluated the efficacy and safety of pabolizumab in 41 cases of metastatic colorectal cancer. The objective response rate (ORR) of tumors with MMRd and proficient MMR (pMMR) were 40% and 0%, respectively (19). KEYNOTE-

TABLE 3 Main Findings in The immunosuppressive tumor microenvironment of different EC subtypes.

Molecular subtype	Main findings
POLEmut	Have a high rate of $CD8^+$CTLs with PD-1 (7, 26, 29). (104–106, 108) Have relatively favorable prognosis and can benefit from immunotherapy (26, 107).
MMRd/ MSI-H	Have a high rate of $CD8^+$CTLs with PD-1 (7, 26, 29). (104–106) Have relatively favorable prognosis and can benefit from immunotherapy (26, 107). Enriched with $CD8^+$ CTLs, Treg cells, fewer M2 macrophages, activated DCs, and a higher trend of $CD20^+$ B cells infiltration (20). CTLA4, PD-1, PD-L1and IL-6 expression significantly increased in all EC grades. The number of $CD4^+$ T cells was similarly increased in all EC grades, whereas the number of $CD8^+$ CTL was only increased in the grade 1 ECs (44). a combination of PD-L1 positivity and MMR deficiency may be associated with aggressive features such as LVSI (109).
TP53abn	the proportions of Treg, M2 macrophages, $PD\text{-}L1^+$ $CD68^+$ macrophages, and $CD8^+$ $PD\text{-}1^+$ T cells were relatively high, indicating a strong immunosuppressive microenvironment in this subtype (7).
NSMP	proportions of multiple tumor-infiltrating immune cells, and expression levels of immune checkpoint molecules were low, indicating a lack of effective anti-tumor immune responses (7).

POLEmut, DNA polymerase epsilon ultramutated; MMRd, mismatch repair deficient; MSI-H, microsatellite instability hypermutated; p53abn, p53-abnormal; NSMP, no specific molecular profile; EC, endometrial cancer; PD–1, programmed cell death 1; PD–L1, programmed cell death 1 ligand 1; LVSI, lymphatic vascular space infiltration; CTLA-4, cytotoxic T-lymphocyte-associated protein 4.

158 multicenter phase II clinical study further evaluated the efficacy and safety of pabolizumab in patients with MSI-H/MMRd endometrial cancer (114). GARNET Study, a phase I/IIb clinical study conducted in 117 centers in 9 countries, had the largest sample size of monotherapy with PD-1 antibody for advanced or recurrent EC. A total of 271 patients were enrolled in this subgroup, and dostarlimab (TSR-042) was administered to patients with MMRd and pMMR. The ORR for MMRd and pMMR patients were 44.7% and 13.4%, respectively (115). Based on the GARNET study, dostarlimab was approved by the FDA for monotherapy in adult patients with recurrent or advanced EC with MMRd after chemotherapy with previous platinum-containing drugs. ICI therapy can relieve the symptoms of some patients and improve their prognosis; however, many patients show primary or acquired resistance. Therefore, immunocombination therapy is necessary to improve the efficacy and mainly includes combined chemotherapy, immunotherapy, and targeted therapy. Several clinical studies have investigated the efficacy and safety of the combination of PD-1/PD-L1 and CTLA-4 antibodies in patients with advanced/recurrent EC (NCT03015129, NCT03508570, and NCT02982486). With the expansion of clinical research on PD-1/PD-L1 antibodies, the management of their adverse reactions is particularly important. The anti-tumor mechanisms of PD-1/PD-L1 antibody and classical chemotherapy are different, so the adverse reaction profile is also quite different. The molecular mechanism is not yet clear and is mostly considered to affect immune homeostasis.

2.9 New subtypes of EC based on ITME—Immunophenotype

In 2020, Liu et al. (116) selected a series of immune-related genes between EC and normal endometria, and used Cox regression model analysis to select the genes related to prognosis, and obtained 15 immune-related genes to calculate the risk score. Patients were then divided into high and low-risk groups according to their risk scores. Li and Wen (73) also used immune-related genes in TCGA database to define four immune types: Immunosuppressive (type C1), Interferon γ-dominant (type C2), Inflammatory (type C3), and Immune balance (type C4) respectively. Bagaey et al. (117) performed tumor microenvironment typing based on the expression of immune-related genes in the ITME and identified four immune types: immune-enhanced fibrosis (type IE/F), immune-enhanced non-fibrosis (type IE), fibrosis (type F), and immune depletion (type D). Type E is the most effective immunotherapy and has the best prognosis. Thorsson et al. (118) used immune-related genes to obtain six immune-related types: tissue-based type (type 1), interferon γ-dominant (type 2), inflammatory (type 3), lymphocyte depletion (type 4), immune silent type (type 5), and transforming growth factor (type 6). Types 4 and 6 are mainly giant cells in the tumor microenvironment with less lymphocyte infiltration and the worst prognosis, whereas types 2 and 3 have the best prognosis.

Some investigators have performed immunotyping based on the infiltration of immune cells into the tumor tissue. Cai et al. (119) clustered samples according to immune cell infiltration in tumor tissues and obtained three subsets, CI, CII, and CIII, whose immune cell infiltration was high, medium, and low, respectively. Most specific gene mutations were detected in CI and CII, whereas a higher frequency of TP53 gene mutation and copy number variations were found in CIII. Wang et al. (120) combined the degree of immune cell infiltration with gene expression levels to calculate the tumor microenvironment score and divided EC into high- and low-risk groups. Immune activation and immune checkpoint related genes were frequently expressed in low-risk groups. The high-risk group had a higher frequency of PTEN, CSE 1 L, ITGB3 mutations. These studies indicate that immune features in the EC tumor microenvironment are related to prognosis and can be used as a new basis for EC classification.

3 Conclusion

EC is an immune gene disease. Patients with early stage of EC have a favorable prognosis, whereas those with advanced EC have a worse prognosis and respond poorly to treatment. Therefore, immunotherapy has attracted attention, and researchers have focused on the ITME of EC in recent years. Since 2014, the FDA has approved several ICIs in clinical practice, mainly for patients with advanced or recurrent cancer who have failed conventional treatment. However, the relatively low response rate limits their application in clinical practice, and the efficacy of immunotherapy is not satisfactory (121). Therefore, screening the dominant therapeutic population when using ICIs is crucial. The classification method for EC has been continuously improved, gradually changing from traditional clinical and pathological classification to molecular classification. Research on the microenvironment of EC based on molecular typing remains unclear. Most studies have focused on POLEmut and MMRd types, and their results were consistent in that the two types have a high rate of $CD8^+$ CTLs with PD-1, a relatively favorable prognosis, and can benefit from immunotherapy. Dai et al. (7) comprehensively studied the ITME of four different EC molecular subtypes for the first time and found that the TP53 mutant subtype had a relatively high proportions of Treg cells, M2 macrophages, $PD\text{-}L1^+$ $CD68^+$ macrophages, and $CD8^+$ $PD\text{-}1^+$ T cells, indicating that the TP53 mutant subtype could benefit from immunotherapy to some extent. Furthermore, in the NSMP subtype, which accounted for 31.5% according to the data published by TransPORTEC-3, the TMB, the proportions of multiple tumor-infiltrating immune cells and the expression levels of immune checkpoint molecules were low. It is important to investigate whether these patients could benefit from immunotherapy, as the P53abn and NSMP subtypes were enriched with immune cells to some extent. This suggests that the P53abn and NSMP subtypes may also be suitable candidates for immune checkpoint-blocking

therapy. However, few relevant studies on ITME have been reported, and most are retrospective studies with small sample sizes. To clarify the microenvironment of various types of EC and identify biomarkers that can accurately predict the response to immunotherapy, prospective studies with large samples sizes are needed in the future.

With research on the immune microenvironment of EC, a new immunophenotype classification based on the immune microenvironment has been carried out in recent years. However, the immunophenotype of EC is still limited to the research stage and there are many limitations. First, owing to intratumor heterogeneity, the samples used for testing may hardly represent the overall immune environment of the tumor, resulting in inaccurate immunophenotyping. Second, most current studies have only analyzed the gene level and have not verified the actual infiltration of immune cells using methods such as immunohistochemistry. Third, some studies lack validation of independent cohorts and immunotyping models in clinical trials. Currently, molecular typing based on tumor cells is gradually being incorporated into clinical practice, providing a basis for the selection of adjuvant and immunotherapies for patients. However, immunotyping methods based on immune characteristics are still under study, and more clinical practice is needed to evaluate their benefits.

Therefore, further studies are required to promote the use of these immunotypes in clinical practice.

In conclusion, the advent of immunotherapy has brought hope for improved efficacy and prognosis in patients with advanced or recurrent EC. The efficacy and safety of ICIs combination therapy remains the focus of future research. In the future, additional potential molecular markers should be explored through molecular pathways and immune resistance mechanisms in the tumor microenvironment. In future research, the results may change the current limited treatment patterns, believing that more cancer patients will benefit from them.

Author contributions

CZ: Writing – original draft, Writing – review & editing. MW: Supervision, Writing – review & editing. YW: Conceptualization, Writing – review & editing.

Funding

The author(s) declare that no financial support was received for the research, authorship, and/or publication of this article.

Acknowledgments

The authors express their gratitude to Dr. Hongliang Zhang for providing valuable assistance in revising the manuscript.

Conflict of interest

The authors declare that the research was conducted in the absence of any commercial or financial relationships that could be construed as a potential conflict of interest.

Publisher's note

References

1. Sung H, Ferlay J, Siegel RL, Laversanne M, Soerjomataram I, Jemal A, et al. Global cancer statistics 2020: GLOBOCAN estimates of incidence and mortality worldwide for 36 cancers in 185 countries. *CA Cancer J Clin* (2021) 71:209–49. doi: 10.3322/caac.21660

2. Siegel RL, Miller KD, Jemal A. Cancer statistics, 2018. *CA Cancer J Clin* (2018) 68:7–30. doi: 10.3322/caac.21442

3. Zheng R, Zhang S, Zeng H, Wang S, Sun K, Chen R, et al. Cancer incidence and mortality in China, 2016. *J Natl Cancer Center* (2022) 2:1–9. doi: 10.1016/j.jncc.2022.02.002

4. Colombo N, Creutzberg C, Amant F, Bosse T, Gonzalez-Martin A, Ledermann J, et al. ESMO-ESGO-ESTRO consensus conference on endometrial cancer: diagnosis, treatment and follow-up. *Int J Gynecol Cancer* (2016) 26:2–30. doi: 10.1097/IGC.0000000000000609

5. Wilkinson-Ryan I, Binder PS, Pourabolghasem S, Al-Hammadi N, Fuh K, Hagemann A, et al. Concomitant chemotherapy and radiation for the treatment of advanced-stage endometrial cancer. *Gynecol Oncol* (2014) 134:24–8. doi: 10.1016/j.ygyno.2014.05.002

6. Cao W, Ma X, Fischer JV, Sun C, Kong B, Zhang Q. Immunotherapy in endometrial cancer: rationale, practice and perspectives. *biomark Res* (2021) 9:49. doi: 10.1186/s40364-021-00301-z

7. Dai Y, Zhao L, Hua D, Cui L, Zhang X, Kang N, et al. Tumor immune microenvironment in endometrial cancer of different molecular subtypes: evidence from a retrospective observational study. *Front Immunol* (2022) 13:1035616. doi: 10.3389/fimmu.2022.1035616

8. Jiang F, Jiang S, Cao D, Mao M, Xiang Y. Immunologic signatures across molecular subtypes and potential biomarkers for sub-stratification in endometrial cancer. *Int J Mol Sci* (2023) 24. doi: 10.3390/ijms24021791

9. Brooks RA, Fleming GF, Lastra RR, Lee NK, Moroney JW, Son CH, et al. Current recommendations and recent progress in endometrial cancer. *CA Cancer J Clin* (2019) 69:258–79. doi: 10.3322/caac.21561

10. Bokhman JV. Two pathogenetic types of endometrial carcinoma. *Gynecol Oncol* (1983) 15:10–7. doi: 10.1016/0090-8258(83)90111-7

11. Cancer Genome Atlas Research N, Kandoth C, Schultz N, Cherniack AD, Akbani R, Liu Y, et al. Integrated genomic characterization of endometrial carcinoma. *Nature* (2013) 497:67–73. doi: 10.1038/nature12113

12. Talhouk A, McConechy MK, Leung S, Li-Chang HH, Kwon JS, Melnyk N, et al. A clinically applicable molecular-based classification for endometrial cancers. *Br J Cancer* (2015) 113:299–310. doi: 10.1038/bjc.2015.190

13. Talhouk A, McConechy MK, Leung S, Yang W, Lum A, Senz J, et al. Confirmation of ProMisE: A simple, genomics-based clinical classifier for endometrial cancer. *Cancer* (2017) 123:802–13. doi: 10.1002/cncr.30496

14. Kommoss S, McConechy MK, Kommoss F, Leung S, Bunz A, Magrill J, et al. Final validation of the ProMisE molecular classifier for endometrial carcinoma in a

large population-based case series. *Ann Oncol* (2018) 29:1180–8. doi: 10.1093/annonc/mdy058

15. Stelloo E, Nout RA, Osse EM, Jurgenliemk-Schulz IJ, Jobsen JJ, Lutgens LC, et al. Improved risk assessment by integrating molecular and clinicopathological factors in early-stage endometrial cancer-combined analysis of the PORTEC cohorts. *Clin Cancer Res* (2016) 22:4215–24. doi: 10.1158/1078-0432.CCR-15-2878

16. Bayramoglu D, Secilmis Kerimoglu O, Bayramoglu Z, Cintesun E, Sahin G, Karabagli P, et al. Classification of high-grade endometrium carcinomas using molecular and immunohistochemical methods. *Ginekol Pol* (2023) 94:3–11. doi: 10.5603/GP.a2021.0177

17. Arciuolo D, Travaglino A, Raffone A, Raimondo D, Santoro A, Russo D, et al. TCGA molecular prognostic groups of endometrial carcinoma: current knowledge and future perspectives. *Int J Mol Sci* (2022) 23. doi: 10.3390/ijms231911684

18. Mimura K, Shimomura A, Gota T, Ando K, Kawamura Y, Taniyama T, et al. Response to lenvatinib and pembrolizumab combination therapy in pembrolizumab-pretreated relapsed endometrial cancer. *Gynecol Oncol Rep* (2022) 44:101084. doi: 10.1016/j.gore.2022.101084

19. Le DT, Durham JN, Smith KN, Wang H, Bartlett BR, Aulakh LK, et al. Mismatch repair deficiency predicts response of solid tumors to PD-1 blockade. *Science* (2017) 357:409–13. doi: 10.1126/science.aan6733

20. Guo YE, Liu Y, Zhang W, Luo H, Shu P, Chen G, et al. The clinicopathological characteristics, prognosis and immune microenvironment mapping in MSI-H/MMR-D endometrial carcinomas. *Discovery Oncol* (2022) 13:12. doi: 10.1007/s12672-022-00466-5

21. Concin N, Matias-Guiu X, Vergote I, Cibula D, Mirza MR, Marnitz S, et al. ESGO/ESTRO/ESP guidelines for the management of patients with endometrial carcinoma. *Int J Gynecol Cancer* (2021) 31:12–39. doi: 10.1136/ijgc-2020-002230

22. Santoro A, Angelico G, Travaglino A, Inzani F, Arciuolo D, Valente M, et al. New pathological and clinical insights in endometrial cancer in view of the updated ESGO/ESTRO/ESP guidelines. *Cancers (Basel)* (2021) 13. doi: 10.3390/cancers13112623

23. Vanderstraeten A, Tuyaerts S, Amant F. The immune system in the normal endometrium and implications for endometrial cancer development. *J Reprod Immunol* (2015) 109:7–16. doi: 10.1016/j.jri.2014.12.006

24. Chen P, Yang Y, Zhang Y, Jiang S, Li X, Wan J. Identification of prognostic immune-related genes in the tumor microenvironment of endometrial cancer. *Aging (Albany NY)* (2020) 12:3371–87. doi: 10.18632/aging.102817

25. Dyck L, Prendeville H, Raverdeau M, Wilk MM, Loftus RM, Douglas A, et al. Suppressive effects of the obese tumor microenvironment on CD8 T cell infiltration and effector function. *J Exp Med* (2022) 219. doi: 10.1084/jem.20210042

26. Hannah van der Woude H, Hally KE, Currie MJ, Gasser O, Henry CE. Importance of the endometrial immune environment in endometrial cancer and associated therapies. *Front Oncol* (2022) 12:975201. doi: 10.3389/fonc.2022.975201

27. Mendiola M, Pellinen T, Ramon-Patino JL, Berjon A, Bruck O, Heredia-Soto V, et al. Prognostic implications of tumor-infiltrating T cells in early-stage endometrial cancer. *Mod Pathol* (2022) 35:256–65. doi: 10.1038/s41379-021-00930-7

28. Hendry S, Salgado R, Gevaert T, Russell PA, John T, Thapa B, et al. Assessing tumor-infiltrating lymphocytes in solid tumors: A practical review for pathologists and proposal for a standardized method from the international immunooncology biomarkers working group: part 1: assessing the host immune response, TILs in invasive breast carcinoma and ductal carcinoma in situ, metastatic tumor deposits and areas for further research. *Adv Anat Pathol* (2017) 24:235–51. doi: 10.1097/PAP.0000000000000162

29. Talhouk A, Derocher H, Schmidt P, Leung S, Milne K, Gilks CB, et al. Molecular subtype not immune response drives outcomes in endometrial carcinoma. *Clin Cancer Res* (2019) 25:2537–48. doi: 10.1158/1078-0432.CCR-18-3241

30. Chraa D, Naim A, Olive D, Badou A. T lymphocyte subsets in cancer immunity: Friends or foes. *J Leukoc Biol* (2019) 105:243–55. doi: 10.1002/JLB.MR0318-097R

31. Mousset CM, Hobo W, Woestenenk R, Preijers F, Dolstra H, van der Waart AB. Comprehensive phenotyping of T cells using flow cytometry. *Cytometry A.* (2019) 95:647–54. doi: 10.1002/cyto.a.23724

32. Pascual-Garcia M, Bertolo C, Nieto JC, Serrat N, Espinosa I, D'Angelo E, et al. CD8 down-regulation on cytotoxic T lymphocytes of patients with endometrioid endometrial carcinomas. *Hum Pathol* (2016) 56:180–8. doi: 10.1016/j.humpath.2016.05.025

33. Suemori T, Susumu N, Iwata T, Banno K, Yamagami W, Hirasawa A, et al. Intratumoral CD8+ Lymphocyte infiltration as a prognostic factor and its relationship with cyclooxygenase 2 expression and microsatellite instability in endometrial cancer. *Int J Gynecol Cancer* (2015) 25:1165–72. doi: 10.1097/IGC.0000000000000482

34. Jung NC, Lee JH, Chung KH, Kwak YS, Lim DS. Dendritic cell-based immunotherapy for solid tumors. *Transl Oncol* (2018) 11:686–90. doi: 10.1016/j.tranon.2018.03.007

35. Chen C, Zhu YB, Qu QX, Ge Y, Huang JA, Wang Y, et al. CD40-activated apoptotic tumor cell-pulsed dendritic cell could potentially elicit antitumor immune response: Involvement of up−regulation of B7−H3 expression. *J Immunother* (2009) 32:29–35. doi: 10.1097/CJI.0b013e31818c8816

36. Lijun Z, Xin Z, Danhua S, Xiaoping L, Jianliu W, Huilan W, et al. Tumor −infiltrating dendritic cells may be used as clinicopathologic prognostic factors in endometrial carcinoma. *Int J Gynecol Cancer* (2012) 22:836–841. doi: 10.1097/IGC.0b013e31825401c6

37. Tarazona R, Lopez-Sejas N, Guerrero B, Hassouneh F, Valhondo I, Pera A, et al. Current progress in NK cell biology and NK cell-based cancer immunotherapy. *Cancer Immunol Immunother* (2020) 69:879–99. doi: 10.1007/s00262-020-02532-9

38. Garzetti GG, Ciavattini A, Muzzioli M, Goteri G, Fabris N, Valensise H, et al. The relationship of clinical−pathologic status and adjuvant treatment with natural killer cell activity in stage I and II endometrial carcinoma. *Acta Obstet Gynecol Scand* (1994) 73:652–657. doi: 10.3109/00016349409013461

39. Garzetti GG, Ciavattini A, Goteri G, Tranquilli AL, Muzzioli M, Fabris N, et al. Natural killer cell activity in stage I endometrial carcinoma: Correlation with nuclear grading, myometrial invasion, and immunoreactivity of proliferating cell nuclear antigen. *Gynecol Oncol* (1994) 55:111–4. doi: 10.1006/gyno.1994.1258

40. Hao NB, Lu MH, Fan YH, Cao YL, Zhang ZR, Yang SM. Macrophages in tumor microenvironments and the progression of tumors. *Clin Dev Immunol* (2012) 2012:948098. doi: 10.1155/2012/948098

41. Kübler K, Ayub TH, Weber SK, Zivanovic O, Abramian A, Keyver−Paik MD, et al. Prognostic significance of tumor-associated macrophages in endometrial adenocarcinoma. *Gynecol Oncol* (2014) 135:176–183. doi: 10.1016/j.ygyno.2014.08.028

42. Dun EC, Hanley K, Wieser F, Bohman S, Yu J, Taylor RN. Infiltration of tumor −associated macrophages is increased in the epithelial and stromal compartments of endometrial carcinomas. *Int J Gynecol Pathol* (2013) 32:576–584. doi: 10.1097/PGP.0b013e318284e198

43. Soeda S, Nakamura N, Ozeki T, Nishiyama H, Hojo H, Yamada H, et al. Tumor −associated macrophages correlate with vascular space invasion and myometrial invasion in endometrial carcinoma. *Gynecol Oncol* (2008) 109:122–128. doi: 10.1016/j.ygyno.2007.12.033

44. Antomarchi J, Ambrosetti D, Cohen C, Delotte J, Chevallier A, Karimdjee-Soilihi B, et al. Immunosuppressive tumor microenvironment status and histological grading of endometrial carcinoma. *Cancer Microenviron* (2019) 12:169–79. doi: 10.1007/s12307-019-00225-1

45. Chang WC, Li CH, Huang SC, Chang DY, Chou LY, Sheu BC. Clinical significance of regulatory T cells and CD8+ effector populations in patients with human endometrial carcinoma. *Cancer* (2010) 116:5777–5788. doi: 10.1002/cncr.25371

46. Sharpe AH, Pauken KE. The diverse functions of the PD1 inhibitory pathway. *Nat Rev Immunol* (2018) 18:153–67. doi: 10.1038/nri.2017.108

47. Vanderstraeten A, Luyten C, Verbist G, Tuyaerts S, Amant F. Mapping the immunosuppressive environment in uterine tumors :implications for immunotherapy. *Cancer Immunol Immunother* (2014) 63(6):545–57. doi: 10.1007/s00262-014-1537-8

48. Eggink FA, Van Gool IC, Leary A, Pollock PM, Crosbie EJ, Mileshkin L, et al. Immunological profiling of molecularly classified high-risk endometrial cancers identifies POLE-mutant and microsatellite unstable carcinomas as candidates for checkpoint inhibition. *Oncoimmunology* (2017) 6(2):e1264565. doi: 10.1080/2162402X.2016.1264565

49. Howitt BE, Shukla SA, Sholl LM, Ritterhouse LL, Watkins JC, Rodig S, et al. Association of polymerase-mutated and microsatellite -instable endometrial cancers with neoantigen load, number of tumor-infiltrating lymphocytes, and expression of PD-1 and PD-L1. *JAMA Oncol* (2015) 1(9):1319–23. doi: 10.1001/jamaoncol.2015.2151

50. Heong V, Ngoi N, Tan DS. Update on immune checkpoint inhibitors in gynecological cancers. *J Gynecol Oncol* (2017) 28:e20. doi: 10.3802/jgo.2017.28.e20

51. Rizvi NA, Cho BC, Reinmuth N, Lee KH, Luft A, Ahn MJ, et al. Durvalumab with or without Tremelimumab vs standard chemotherapy in first-line treatment of metastatic non−small cell lung cancer: the MYSTIC phase 3 randomized clinical trial. *JAMA Oncol* (2020) 6:661–74. doi: 10.1001/jamaoncol.2020.0237

52. Brunner A, Hinterholzer S, Riss P, Heinze G, Brustmann H. Immunoexpression of B7-H3 in endometrial cancer: relation to tumor T-cell infiltration and prognosis. *Gynecol Oncol* (2012) 124:105–11. doi: 10.1016/j.ygyno.2011.09.012

53. Kaur G, Janakiram M. B7x-from bench to bedside. *ESMO Open* (2019) 4:e000554. doi: 10.1136/esmoopen-2019-000554

54. Miyatake T, Tringler B, Liu W, Liu SH, Papkoff J, Enomoto T, et al. B7−H4 (DD-O110) is overexpressed in high risk uterine endometrioid adenocarcinomas and inversely correlated with tumor T−cell infiltration. *Gynecol Oncol* (2007) 106:119−127. doi: 10.1016/j.ygyno.2007.03.039

55. Bregar A, Deshpande A, Grange C, Zi T, Stall J, Hirsch H, et al. Characterization of immune regulatory molecules B7−H4 and PD−L1 in low and high grade endometrial tumors. *Gynecol Oncol* (2017) 145:446–452. doi: 10.1016/j.ygyno.2017.03.006

56. Thor Straten P, Garrido F. Targetless T cells in cancer immunotherapy. *J Immunother Cancer* (2016) 4:23. doi: 10.1186/s40425-016-0127-z

57. de Jong RA, Boerma A, Boezen HM, Mourits MJ, Hollema H, Nijman HW. Loss of HLA class I and mismatch repair protein expression in sporadic endometrioid endometrial carcinomas. *Int J Cancer* (2012) 131:1828–36. doi: 10.1002/ijc.27449

58. Ben Yahia H, Babay W, Bortolotti D, Boujelbene N, Laaribi AB, Zidi N, et al. Increased plasmatic soluble HLA−G levels in endometrial cancer. *Mol Immunol* (2018) 99:82–86. doi: 10.1016/j.molimm.2018.04.007

59. He Y, Rivard CJ, Rozeboom L, Yu H, Ellison K, Kowalewski A, et al. Lymphocyte-activation gene-3, an important immune checkpoint in cancer. *Cancer Sci* (2016) 107:1193–7. doi: 10.1111/cas.12986

60. Zhang Y, Yang R, Xu C, Zhang Y, Deng M, Wu D, et al. Analysis of the immune checkpoint lymphocyte activation gene-3 (LAG-3) in endometrial cancer: An emerging target for immunotherapy. *Pathology - Res Pract* (2022) 236:153990. doi: 10.1016/j.prp.2022.153990

61. Wu T, Qiao Q, Qin X, Zhang D, Zhang Z. Immunostimulatory cytokine and doxorubicin co-loaded nanovesicles for cancer immunochemotherapy. *Nanomedicine* (2019) 18:66–77. doi: 10.1016/j.nano.2019.02.008

62. Zhan L, Liu X, Zhang J, Cao Y, Wei B. Immune disorder in endometrial cancer: Immunosuppressive microenvironment, mechanisms of immune evasion and immunotherapy. *Oncol Lett* (2020) 20:2075–90. doi: 10.3892/ol.2020.11774

63. Buchbinder EI, Desai A. CTLA-4 and PD-1 pathways: similarities, differences, and implications of their inhibition. *Am J Clin Oncol* (2016) 39:98–106. doi: 10.1097/COC.0000000000000239

64. Wei SC, Levine JH, Cogdill AP, Zhao Y, Anang NAS, Andrews MC, et al. Distinct cellular mechanisms underlie anti-CTLA-4 and anti-PD-1 checkpoint blockade. *Cell* (2017) 170:1120–33.e1117. doi: 10.1016/j.cell.2017.07.024

65. Durgeau A, Virk Y, Corgnac S, Mami-Chouaib F. Recent advances in targeting CD8 T-cell immunity for more effective cancer immunotherapy. *Front Immunol* (2018) 9:14. doi: 10.3389/fimmu.2018.00014

66. Workel HH, Komdeur FL, Wouters MC, Plat A, Klip HG, Eggink FA, et al. CD103 defines intraepithelial CD8+ PD1+ tumour-infiltrating lymphocytes of prognostic significance in endometrial adenocarcinoma. *Eur J Cancer* (2016) 60:1–11. doi: 10.1016/j.ejca.2016.02.026

67. Kondratiev S, Sabo E, Yakirevich E, Lavie O, Resnick MB. Intratumoral CD8+ T lymphocytes as a prognostic factorof survival in endometrial carcinoma. *Clin Cancer Res* (2004) 10:4450–4456. doi: 10.1158/1078-0432.CCR-0732-3

68. Wang Y, Zhang J, Zhou Y, Li Z, Lv D, Liu Q. Construction of a microenvironment immune gene model for predicting the prognosis of endometrial cancer. *BMC Cancer* (2021) 21:1203. doi: 10.1186/s12885-021-08935-w

69. Mantovani A, Sica A. Macrophages, innate immunity and cancer: balance, tolerance, and diversity. *Curr Opin Immunol* (2010) 22:231–7. doi: 10.1016/j.coi.2010.01.009

70. Lin Y, Xu J, Lan H. Tumor-associated macrophages in tumor metastasis: biological roles and clinical therapeutic applications. *J Hematol Oncol* (2019) 12:76. doi: 10.1186/s13045-019-0760-3

71. Yamagami W, Susumu N, Tanaka H, Hirasawa A, Banno K, Suzuki N, et al. Immunofluorescence-detected infiltration of CD4+FOXP3+ regulatory T cells is relevant to the prognosis of patients with endometrial cancer. *Int J Gynecol Cancer* (2011) 21:1628–1634. doi: 10.1097/IGC.0b013e31822c271f

72. Li L, Li Y, Yin Z, Zhu J, Yan D, Lou H. Increased frequency of regulatory T cells in the peripheral blood of patients with endometrioid adenocarcinoma. *Oncol Lett* (2019) 18:1424–30. doi: 10.3892/ol.2019.10452

73. Li BL, Wan XP. Prognostic significance of immune landscape in tumour microenvironment of endometrial cancer. *J Cell Mol Med* (2020) 24:7767–77. doi: 10.1111/jcmm.15408

74. Kantoff PW, Higano CS, Shore ND, Berger ER, Small EJ, Penson DF, et al. Sipuleucel-T immunotherapy for castration-resistant prostate cancer. *N Engl J Med* (2010) 363:411–22. doi: 10.1056/NEJMoa1001294

75. Coosemans A, Wolfl M, Berneman ZN, Van Tendeloo V, Vergote I, Amant F, et al. Immunological response after therapeutic vaccination with WT1 mRNA-loaded dendritic cells in end-stage endometrial carcinoma. *Anticancer Res* (2010) 30:3709–14.

76. Shreeve N, Depierreux D, Hawkes D, Traherne JA, Sovio U, Huhn O, et al. The CD94/NKG2A inhibitory receptor educates uterine NK cells to optimize pregnancy outcomes in humans and mice. *Immunity* (2021) 54:1231–44.e1234. doi: 10.1016/j.immuni.2021.03.021

77. Ni L, Dong C. New checkpoints in cancer immunotherapy. *Immunol Rev* (2017) 276:52–65. doi: 10.1111/imr.12524

78. Liu J, Liu Y, Wang W, Wang C, Che Y. Expression of immune checkpoint molecules in endometrial carcinoma. *Exp Ther Med* (2015) 10:1947–52. doi: 10.3892/etm.2015.2714

79. Mo Z, Liu J, Zhang Q, Chen Z, Mei J, Liu L, et al. Expression of PD-1,PD-L1 and PD-L2 is associated with differentiation status and histological type of endometrial cancer. *Oncol Lett* (2016) 12(2):944–50. doi: 10.3892/ol.2016.4744

80. Arce Vargas F, Furness AJS, Litchfield K, Joshi K, Rosenthal R, Ghorani E, et al. Fc effector function contributes to the activity of human anti-CTLA-4 antibodies. *Cancer Cell* (2018) 33:649–63.e644. doi: 10.1016/j.ccell.2018.02.010

81. Mittica G, Ghisoni E, Giannone G, Aglietta M, Genta S, Valabrega G. Checkpoint inhibitors in endometrial cancer: preclinical rationale and clinical activity. *Oncotarget* (2017) 8:90532–44. doi: 10.18632/oncotarget.20042

82. Morse MA, Overman MJ, Hartman L, Khoukaz T, Brutcher E, Lenz HJ, et al. Safety of nivolumab plus low-dose ipilimumab in previously treated microsatellite instabilityhigh/mismatch repair-deficient metastatic colorectal cancer. *Oncologist* (2019) 24:1453–61. doi: 10.1634/theoncologist.2019-0129

83. Peng Hongling, He X, Wang Q. Immune checkpoint blockades in gynecological cancers: A review of clinical trials. *Acta Obstet Gynecol Scand* (2022) 101:941–51. doi: 10.1111/aogs.14412

84. Taylor MH, Lee CH, Makker V, Rasco D, Dutcus CE, Wu J, et al. Phase IB/II trial of lenvatinib plus pembrolizumab in patients with advanced renal cell carcinoma, endometrial cancer, and other selected advanced solid tumors. *J Clin Oncol* (2020) 38:1154–63. doi: 10.1200/JCO.19.01598

85. MacGregor HL, Garcia-Batres C, Sayad A, Elia A, Berman HK, Toker A, et al. Tumor cell expression of B7-H4 correlates with higher frequencies of tumor-infiltrating APCs and higher CXCL17 expression in human epithelial ovarian cancer. *Oncoimmunology* (2019) 8:e1665460. doi: 10.1080/2162402X.2019.1665460

86. Rahbar R, Lin A, Ghazarian M, Yau HL, Paramathas S, Lang PA, et al. B7-H4 expression by nonhematopoietic cells in the tumor microenvironment promotes antitumor immunity. *Cancer Immunol Res* (2015) 3:184–95. doi: 10.1158/2326-6066.CIR-14-0113

87. Liepe J, Marino F, Sidney J, Jeko A, Bunting DE, Sette A, et al. A large fraction of HLA class I ligands are proteasome-generated spliced peptides. *Science* (2016) 354:354–8. doi: 10.1126/science.aaf4384

88. Chowell D, Morris LGT, Grigg CM, Weber JK, Samstein RM, Makarov V, et al. Patient HLA class I genotype influences cancer response to checkpoint blockade immunotherapy. *Science* (2018) 359:582–7. doi: 10.1126/science.aao4572

89. Wang J, Sanmamed MF, Datar I, Su TT, Ji L, Sun J, et al. Fibrinogen-like protein 1 is a major immune inhibitory ligand of LAG-3. *Cell* (2019) 176:334–47.e312. doi: 10.1016/j.cell.2018.11.010

90. Calabrese LH, Caporali R, Blank CU, Kirk AD. Modulating the wayward T cell: new horizons with immune checkpoint inhibitor treatments in autoimmunity, transplant, and cancer. *J Autoimmun* (2020) 115:102546. doi: 10.1016/j.jaut.2020.102546

91. Wang T, Rohan TE, Gunter MJ, Xue X, Wactawski-Wende J, Rajpathak SN, et al. A prospective study of inflammation markers and endometrial cancer risk in postmenopausal hormone nonusers. *Cancer Epidemiol Biomarkers Prev* (2011) 20:971–7. doi: 10.1158/1055-9965.EPI-10-1222

92. Lay V, Yap J, Sonderegger S, Dimitriadis E. Interleukin 11 regulates endometrial cancer cell adhesion and migration via STAT3. *Int J Oncol* (2012) 41:759–64. doi: 10.3892/ijo.2012.1486

93. Che Q, Liu BY, Wang FY, He YY, Lu W, Liao Y, et al. Interleukin 6 promotes endometrial cancer growth through an autocrine feedback loop involving ERK-NF-kappaB signaling pathway. *Biochem Biophys Res Commun* (2014) 446:167–72. doi: 10.1016/j.bbrc.2014.02.080

94. Wang Z, Ding H, Zou Q. Identifying cell types to interpret scRNA-seq data: How, why and more possibilities. *Brief Funct Genomics* (2020) 19:286–91. doi: 10.1093/bfgp/elaa003

95. Zhao J, Jaffe A, Li H, Lindenbaum O, Sefik E, Jackson R, et al. Detection of differentially abundant cell subpopulations in scRNA-seq data. *Proc Natl Acad Sci USA* (2021) 118. doi: 10.1073/pnas.2100293118

96. Liu C, Li X, Huang Q, Zhang M, Lei T, Wang F, et al. Single-cell RNA-sequencing reveals radiochemotherapy-induced innate immune activation and MHC-II upregulation in cervical cancer. *Signal Transduct Target Ther* (2023) 8(1):44. doi: 10.1038/s41392-022-01264-9

97. Liu C, Zhang M, Yan X, Ni Y, Gong Y, Wang C, et al. Single-cell dissection of cellular and molecular features underlying human cervical squamous cell carcinoma initiation and progression. *Sci Adv* (2023) 9(4):eadd8977. doi: 10.1126/sciadv.add8977

98. Yue S, Wang Q, Zhang J, Hu Q, Liu C. Understanding cervical cancer at single-cell resolution. *Cancer Lett* (2023) 576:216408. doi: 10.1016/j.canlet.2023.216408

99. Li X, Zhang M, Lei T, Zou W, Huang R, Wang F, et al. Single-cell RNA-sequencing dissects cellular heterogeneity and identifies two tumor-suppressing immune cell subclusters in HPV-related cervical adenosquamous carcinoma. *J Med Virol* (2022) 94(12):6047–59. doi: 10.1002/jmv.28084

100. Huang Pu, Qian Y, Xia Yu, Wang S. Integrated analysis identifies RAC3 as an immune-related prognostic biomarker associated with chemotherapy sensitivity in endometrial cancer. *J Cell Mol Med* (2023) 00:1–13. doi: 10.1111/jcmm.17824

101. Yu X, Xie L, Ge J, Li H, Zhong S, Liu X. Integrating single-cell RNA-seq and spatial transcriptomics reveals MDK-NCL dependent immunosuppressive environment in endometrial carcinoma. *Front Immunol* (2023) 14. doi: 10.3389/fimmu.2023.1145300

102. Guo Y-e, Li Y, Cai B, He Q, Chen G, Wang M, et al. Phenotyping of immune and endometrial epithelial cells in endometrial carcinomas revealed by single-cell RNA sequencing. *Aging (Albany NY)* (2021) 13(5):6565–6591. doi: 10.18632/aging.202288

103. Wu Q, Jiang G, Sun Y, Li B. Reanalysis of single-cell data reveals macrophage subsets associated with the immunotherapy response and prognosis of patients with endometrial cancer. *Exp Cell Res* (2023) 430. doi: 10.1016/j.yexcr.2023.113736

104. Zhang J, An L, Zhou X, Shi R, Wang H. Analysis of tumor mutation burden combined with immune infiltrates in endometrial cancer. *Ann Transl Med* (2021) 9:551. doi: 10.21037/atm-20-6049

105. Picard E, Verschoor CP, Ma GW, Pawelec G. Relationships between immune landscapes, genetic subtypes and responses to immunotherapy in colorectal cancer. *Front Immunol* (2020) 11:369. doi: 10.3389/fimmu.2020.00369

106. Huang RSP, Haberberger J, Severson E, Duncan DL, Hemmerich A, Edgerly C, et al. A pan-cancer analysis of PD-L1 immunohistochemistry and gene amplification, tumor mutation burden and microsatellite instability in 48,782 cases. *Mod Pathol* (2021) 34:252–63. doi: 10.1038/s41379-020-00664-y

107. Fusco MJ, West HJ, Walko CM. Tumor mutation burden and cancer treatment. *JAMA Oncol* (2021) 7:316. doi: 10.1001/jamaoncol.2020.6371

108. Temko D, Van Gool IC, Rayner E, Glaire M, Makino S, Brown M, et al. Somatic POLE exonuclease domain mutations are early events in sporadic endometrial and colorectal carcinogenesis, determining driver mutational landscape, clonal neoantigen burden and immune response. *J Pathol* (2018) 245:283–96. doi: 10.1002/path.5081

109. Arafa M, Shebl AM, Salama A, ElZahaf E, Ashamallah SA, Foda AA, et al. Correlation of PD-L1 immunohistochemical expression with microsatellite instability and p53 status in endometrial carcinoma. *Eur J Obstet Gynecol Reprod Biol X* (2022) 16:100172. doi: 10.1016/j.eurox.2022.100172

110. Maciejko L, Smalley M, Goldman A. Cancer immunotherapy and personalized medicine: emerging technologies and biomarker-based approaches. *J Mol biomark Diagn* (2017) 8. doi: 10.4172/2155-9929.1000350

111. Perumal D, Imai N, Lagana A, Finnigan J, Melnekoff D, Leshchenko VV, et al. Mutation-derived neoantigen-specific T-cell responses in multiple myeloma. *Clin Cancer Res* (2020) 26:450–64. doi: 10.1158/1078-0432.CCR-19-2309

112. Song Y, Gu Y, Hu X, Wang M, He Q, Li Y. Endometrial tumors with MSI-H and dMMR share a similar tumor immune microenvironment. *Onco Targets Ther* (2021) 14:4485–97. doi: 10.2147/OTT.S324641

113. Green AK, Feinberg J, Makker V. A review of immune checkpoint blockade therapy in endometrial cancer. *Am Soc Clin Oncol Educ Book*. (2020) 40:1–7. doi: 10.1200/EDBK_280503

114. O'Malley DM, Bariani GM, Cassier PA, Marabelle A, Hansen AR, De Jesus Acosta A, et al. Pembrolizumab in patients with microsatellite instability-high advanced endometrial cancer: results from the KEYNOTE-158 study. *J Clin Oncol* (2022) 40:752–61. doi: 10.1200/JCO.21.01874

115. Oaknin A, Gilbert L, Tinker AV, Brown J, Mathews C, Press J, et al. Safety and antitumor activity of dostarlimab in patients with advanced or recurrent DNA mismatch repair deficient/microsatellite instability-high (dMMR/MSI-H) or proficient/stable (MMRp/MSS) endometrial cancer: interim results from GARNET-a phase I, single-arm study. *J Immunother Cancer* (2022) 10. doi: 10.1136/jitc-2021-003777

116. Liu J, Chen X, Jiang Y, Cheng W. Development of an immune gene prognostic classifier for survival prediction and respond to immunocheckpoint inhibitor therapy/chemotherapy in endometrial cancer. *Int Immunopharmacol* (2020) 86:106735. doi: 10.1016/j.intimp.2020.106735

117. Bagaev A, Kotlov N, Nomie K, Svekolkin V, Gafurov A, Isaeva O, et al. Conserved pan-cancer microenvironment subtypes predict response to immunotherapy. *Cancer Cell* (2021) 39:845–65.e847. doi: 10.1016/j.ccell.2021.04.014

118. Thorsson V, Gibbs DL, Brown SD, Wolf D, Bortone DS, Ou Yang TH, et al. The immune landscape of cancer. *Immunity* (2018) 48:812–30.e814. doi: 10.1016/j.immuni.2018.03.023

119. Cai Y, Chang Y, Liu Y. Multi-omics profiling reveals distinct microenvironment characterization of endometrial cancer. *BioMed Pharmacother* (2019) 118:109244. doi: 10.1016/j.biopha.2019.109244

120. Wang G, Wang D, Sun M, Liu X, Yang Q. Identification of prognostic and immune-related gene signatures in the tumor microenvironment of endometrial cancer. *Int Immunopharmacol* (2020) 88:106931. doi: 10.1016/j.intimp.2020.106931

121. Carlson JW, Nastic D. High-grade endometrial carcinomas: classification with molecular insights. *Surg Pathol Clin* (2019) 12:343–62. doi: 10.1016/j.path.2019.02.003

frontiers | Frontiers in Immunology

TYPE Review
PUBLISHED 23 November 2023
DOI 10.3389/fimmu.2023.1303491

OPEN ACCESS

EDITED BY
Chao Liu,
Shandong Cancer Hospital, China

REVIEWED BY
Yuchen Li,
Fudan University, China
Bo Cheng,
Shandong University, China

*CORRESPONDENCE
Qiang Wen
wq890425@126.com

†These authors have contributed equally to this work

RECEIVED 28 September 2023
ACCEPTED 07 November 2023
PUBLISHED 23 November 2023

CITATION
Yang J, Qiu L, Wang X, Chen X, Cao P, Yang Z and Wen Q (2023) Liquid biopsy biomarkers to guide immunotherapy in breast cancer. *Front. Immunol.* 14:1303491. doi: 10.3389/fimmu.2023.1303491

Liquid biopsy biomarkers to guide immunotherapy in breast cancer

Jinghan Yang[1†], Liang Qiu[2†], Xi Wang[3], Xi Chen[4], Pingdong Cao[5], Zhe Yang[5] and Qiang Wen[5*]

[1]Department of Biological Science, Vanderbilt University, Nashville, TN, United States, [2]Department of Radiation Oncology, Stanford University, Palo Alto, CA, United States, [3]Department of Computer Science and Engineering, The Chinese University of Hong Kong, Hong Kong, Hong Kong SAR, China, [4]Department of Human Resource, Shandong Provincial Hospital Affiliated to Shandong First Medical University, Jinan, China, [5]Department of Radiation Oncology, Shandong Provincial Hospital Affiliated to Shandong First Medical University, Jinan, China

Immune checkpoint inhibitors (ICIs) therapy has emerged as a promising treatment strategy for breast cancer (BC). However, current reliance on immunohistochemical (IHC) detection of PD-L1 expression alone has limited predictive capability, resulting in suboptimal efficacy of ICIs for some BC patients. Hence, developing novel predictive biomarkers is indispensable to enhance patient selection for immunotherapy. In this context, utilizing liquid biopsy (LB) can provide supplementary or alternative value to PD-L1 IHC testing for identifying patients most likely to benefit from immunotherapy and exhibit favorable responses. This review discusses the predictive and prognostic value of LB in breast cancer immunotherapy, as well as its limitations and future directions. We aim to promote the individualization and precision of immunotherapy in BC by elucidating the role of LB in clinical practice.

KEYWORDS

liquid biopsy, breast cancer, immunotherapy, immune checkpoint inhibitors, biomarkers

1 Introduction

Over the past decade, cancer immunotherapy has emerged as an effective anti-tumor therapeutic approach on par with traditional modalities like chemotherapy, radiotherapy, and surgery. In particular, immune checkpoint inhibitors (ICIs) that target the programmed death-ligand 1 (PD-L1), programmed death 1 (PD-1), and cytotoxic T-lymphocyte-associated protein 4 (CTLA-4) pathways can restore T-cell functionality and promote anti-tumor immunity (1). As a result, ICIs including the anti-PD-L1 antibody atezolizumab (2), the anti-PD-1 antibody pembrolizumab (3), and the anti-CTLA-4 antibody ipilimumab (4), have been approved by the Food and Drug Administration (FDA) and European Medicines Agency (EMA) for various cancer types (5).

Breast cancer (BC) represents the leading cause of cancer-related mortality and most frequently diagnosed malignancy among women worldwide (6). Historically characterized as a 'cold' tumor type, BC exhibits a less inflammatory tumor microenvironment compared to 'hot' tumors with heightened immunogenicity and abundant tumor-infiltrating lymphocytes (TILs) (7). However, remarkable progress has been made with PD-1/PD-L1 agents in triple-negative breast cancer (TNBC), resulting in promising outcomes in both early (8, 9) and metastatic cases (10, 11). Moreover, ongoing research is actively investigating their potential in human epidermal growth factor receptor 2 (HER-2) positive and high-risk hormone receptor (HR)+ BC (12). Notable clinical trials, including Impassion 130 and Keynote 355, have demonstrated substantial benefits of ICIs for BC treatment (11, 13). A comprehensive overview of key studies evaluating ICIs efficacy in BC is summarized in Table 1 (14–25).

Currently, identifying appropriate first-line immunotherapy candidates within BC and predicting individual patient treatment responses primarily relies on immunohistochemistry (IHC) testing to evaluate PD-L1 expression levels. However, the utilization of PD-L1 as a sole biomarker and predictor encounters certain limitations and challenges. First, numerous different PD-L1 antibodies are currently employed for IHC-based tumor PD-L1 expression assessment, including Dako 28-8 rabbit monoclonal, Dako 22C3 mouse monoclonal, Roche Ventana SP142 rabbit monoclonal, and Roche Ventana SP263 rabbit monoclonal antibodies, introducing inherent variability into the PD-L1 results obtained from different studies and clinical settings (26). Second, the heterogeneity in IHC cutoff values for defining PD-L1 positivity across clinical trials utilizing different assay platforms leads to discrepancies in PD-L1 designation. Moreover, intratumoral heterogeneity of PD-L1 expression potentially underestimates overall PD-L1 status in the context of small tumor biopsy samples, which may not fully and accurately represent the entire heterogeneous PD-L1 expression profile within the tumor as a whole (27). Lastly, the predictive value of IHC-based PD-L1 expression for immunotherapy response is not definitive, due in part to practical challenges obtaining adequately sized and preserved tumor tissue samples and isolating sufficient quantities of viable tumor cells from limited biopsy specimens (28). Consequently, a subset of patients with PD-L1 positive tumors still lack significantly favorable clinical immunotherapy responses, necessitating the development and validation of additional robust predictive biomarkers to more precisely select candidates likely to derive maximal therapeutic benefit from ICIs.

Liquid biopsy (LB) has recently emerged as a promising minimally invasive surrogate biomarker to guide immunotherapy decisions in BC. LB allows assessment of various tumor components in the peripheral blood, including circulating tumor cells (CTCs), circulating tumor DNA (ctDNA), exosomes, and proteins (Figure 1). Compared with traditional tissue biopsy, LB offers advantages such as minimal invasiveness, reproducibility, and rapid turnaround (Figure 2) (29). This review provides an updated overview of LB applications for ICIs therapy in BC, highlighting current research and future directions. We discuss the strengths and limitations of LB as a biomarker for BC immunotherapy, including its potential to identify responders, detect resistance mechanisms, and predict clinical outcomes. Ongoing studies will help validate the clinical utility of LB-based biomarkers to optimize patient selection and management for ICIs treatment in BC.

2 CTCs

CTCs present in the peripheral blood can be identified through analytical methods based on biological (e.g. epithelial markers and absent hematopoietic markers) and physical (e.g. size, density, invasiveness) characteristics (30–33). The CellSearch™ system remains the only FDA-approved platform for CTCs detection in metastatic breast cancer to date (34). This system isolates EpCAM+ CTCs using antibody-coated magnetic beads, followed by immunofluorescent staining for cytokeratins and cluster of differentiation 45 (CD45) to distinguish CTCs from leukocytes (34).

Multiple studies have explored associations between CTCs and the tumor immune microenvironment (TIM) in breast cancer. For instance, patients with detectable CTCs were found to exhibit increased regulatory T cell infiltration in tumor tissues compared to those without CTCs, indicating an immunosuppressive phenotype (35). Mego et al. revealed an inverse correlation between CD8+ cytotoxic T cell levels and CTC counts in breast cancer tissues through immunohistochemical analysis. They also observed reduced dendritic cell infiltration into bone marrow metastatic niches accompanied by high CTC numbers in inflammatory breast cancer patients (36). Most recently, the same group demonstrated a positive correlation between mesenchymal-like CTCs undergoing epithelial-to-mesenchymal transition (EMT) and PD-L1 positive stromal cells in the tumor microenvironment (37). Together, these findings position CTCs as promising indicators of anti-tumor immune activity and immunosuppression within tumor tissues.

Recent technological advances have enabled comprehensive functional profiling of CTCs, providing powerful tools to identify predictive biomarkers for ICIs therapy in breast cancer. Specifically, single-cell proteomic, transcriptomic and metabolomic analyses of CTCs can elucidate multidimensional molecular characteristics associated with therapeutic response. For instance, proteomic profiling may reveal specific CTC subpopulations correlated with immunotherapeutic sensitivity or resistance. Transcriptomic sequencing could uncover distinct CTC gene signatures related to immune evasion mechanisms. Metabolomic analyses of CTCs may also provide insights into immunometabolic phenotypes influencing immunotherapy efficacy. Furthermore, the C-X-C chemokine receptor type 4 (CXCR-4) was found to be upregulated on breast cancer CTCs, suggesting a potential role in regulating immune cell recruitment and function in the tumor microenvironment during treatment (38). Assessing dynamic changes in CXCR4 expression on CTCs by single-cell assays may thus help monitor immune modulation effects. In summary, technological progress has enabled in-depth interrogation of CTCs as a valuable biomarker source to predict and monitor immunotherapy outcomes in breast cancer patients.

TABLE 1 Summary of immunotherapy trails in breast cancer.

Trail	Subtype	Experimental vs. Control	Antibody/Cut-off	ORR	PFS	OS
Metastasis BC with ICI + Chemo						
IMpassion-130 (11)	TNBC	Atezolizumab + Nab-pac vs. PBO+ Nab-pac	VENTANA PD-L1 IHC SP142 IC:1%	58.9 vs. 42.6	7.5 vs 5.0	25.4 vs. 17.9
KEYNOTE-355 (13)	TNBC	Pembrolizumab + Nab-pac (Pac or Gem-Carbo) vs. PBO + Nab-pac (Pac or Gem-Carbo)	Agilent PD-L1 IHC 22C3 CPS:1	53.2 vs. 39.8	9.7 vs. 5.6	23.0 vs. 16.1
IMpassion-131 (14)	TNBC	Atezolizumab + Pac vs. PBO + Pac	VENTANA PD-L1 IHC SP142 IC:1%	63.4 vs. 55.4	6.0 vs. 5.7	22.1 vs. 28.3
ENHANCE 1 (15)	HR+HER2+	Pembrolizumab + Eribulin vs. Eribulin	Agilent PD-L1 IHC 22C3 CPS:1	27.0 vs. 34.0	4.1 vs. 4.2	13.4 vs. 12.5
KELLY (16)	HR+HER2+	Pembrolizumab + Eribulin	Agilent PD-L1 IHC 22C3 CPS:1	40.9	6.0	59.1% for 1-year OS
Metastasis BC with ICI						
KEYNOTE-086 Cohort A (17)	TNBC	Pembrolizumab	Agilent PD-L1 IHC 22C3 CPS:1	5.3	2	9
KEYNOTE-086 Cohort B (17)	TNBC	Pembrolizumab	Agilent PD-L1 IHC 22C3 CPS:1	21.4	2.1	18
KEYNOTE-119 (18)	TNBC	Pembrolizumab vs. TPC	Agilent PD-L1 IHC 22C3 CPS:1	9.6 vs. 10.6	2.1 vs. 3.3	9.9 vs. 10.8
KEYNOTE-028 (19)	HR+HER2+	Pembrolizumab	Agilent PD-L1 IHC 22C3 CPS:1	12	1.8	8.6
JAVELIN (20)	TNBC	Avelumab	Dako PD-L1 IHC 73-10 pharmDx; tumor cell: 1,5,25%; tumor associated cell:10%	5.2	1.5	9.2
JAVELIN (20)	HR+HER2+	Avelumab	Dako PD-L1 IHC 73-10 pharmDx; tumor cell: 1,5,25%; tumor associated cell:10%	2.8	NA	NA
NCT01375842 (21)	TNBC	Atezolizumab	VENTANA PD-L1 IHC SP142 IC:1%	10	1.4	8.9
Early Stage BC						
KEYNOTE-522 (22)	TNBC	Pembrolizumab + Cab + Pac vs. PBO+ Cab + Pac	Agilent PD-L1 IHC 22C3 CPS:1	64.8 VS.51.2	NA	NA
I-SPY 2 (23)	TNBC	Pembrolizumab + Cab vs. Pac	NA	60 vs 20	NA	NA
I-SPY 2 (23)	HR+ HER2+	Pembrolizumab + Cab vs. Pac	NA	30 vs. 13	NA	NA
IMpassion-031 (24)	TNBC	Atezolizumab + Nab-pac (AC) vs. PBO + Nab-pac (AC)	VENTANA PD-L1 IHC SP142 IC:1%	57.6 vs 41.1	NA	NA
GeparNuevo (9)	TNBC	Durvalumab+ Nab-pac vs. PBO+ Nab-pac	VENTANA PD-L1 IHC SP263 IC:1%	53.4 vs. 44.2	NA	NA
NeoTRIP (25)	TNBC	Atezolizumab + Carbo + Nab-pac vs. Carbo + Nab-pac	VENTANA PD-L1 IHC SP142 IC:1%	43.5 vs. 40.8	NA	NA

3 ctDNA

ctDNA is released into the bloodstream by tumor cells, distinguishing it from cell-free DNA (cfDNA) derived from normal apoptotic or necrotic cells. Compared to CTCs, ctDNA is present at higher concentrations in plasma, making it an attractive noninvasive liquid biopsy target (39). Somatic genomic alterations specific to cancer cells enable the differentiation of tumor-derived ctDNA from normal cfDNA in blood (40). ctDNA holds promise as a biomarker for early detection of metastasis and disease recurrence post-

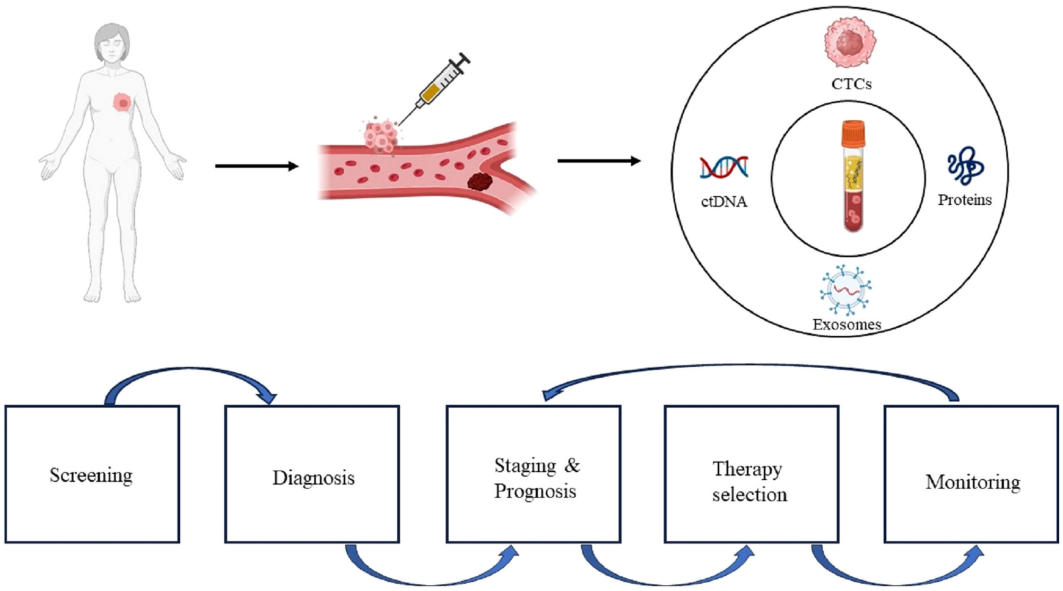

FIGURE 1
Clinical applications of liquid biopsy. The immunology information extracted from liquid biopsy can be used for continuous monitoring, from early stage disease screening, assistance diagnosis, personalized therapy selection, to recurrence monitoring. CTCs, circulating tumor cells; ctDNA, circulating tumor DNA.

treatment (41, 42). However, clinical data on the utility of ctDNA to predict immunotherapy outcomes remains limited thus far.

A study by Magbanua et al. analyzed 511 plasma samples from 138 high-risk HR+/HER2- breast cancer patients who received pembrolizumab with neoadjuvant chemotherapy in the I-SPY2 trial (43). ctDNA levels declined over time in both the pembrolizumab and control arms. All patients achieving pathological complete response (pCR) cleared ctDNA prior to

Liquid Biopsy Component	Circulating Tumor Cells (CTCs)	Circulating Tumor DNA (ctDNA)	Exosomes	Proteins and Cytokines
				
Main Function	Diagnosis and prognosis	Diagnosis and treatment evaluation	Diagnosis, Prognosis, Prediction of response	Prediction of response and treatment evaluation
Advantages	• Accessible for RNA/DNA/proteins • Early detection of recurrence or progression • Provide tumor-specific information	• Higher concentrations • Higher stability • Capture tumor heterogeneity • Mature method • Well-established procedure • Detection of bTMB	• Genomic contents protected from degradation • Accessible and variable source of tumor component	• Easily isolation • Sensitive • Standardized methods
Limitation	• Low counts in early stage • Difficulty differentiating CTCs from other cells	• Low concentration in early stage • Difficulty differentiating cfDNA from ctDNA	• Lack of standardized isolation methods for clinical application	• Lack of stability • Not specific for BC

FIGURE 2
Comparison of four liquid biopsy components and the main advantages, disadvantages, and future directions of their clinical application in breast cancer management. RNA, ribonucleic acid; DNA, deoxyribonucleic acid; CTCs, circulating tumor cells; ctDNA, circulating tumor DNA; bTMB, blood-based tumor mutational burden; cfDNA, cell-free DNA; BC, breast cancer.

surgery. Among non-pCR patients, those ctDNA-negative after neoadjuvant treatment exhibited markedly higher distant recurrence-free survival compared to ctDNA-positive patients, with a hazard ratio (HR) of 0.13. This supports the potential of longitudinal ctDNA monitoring to guide clinical decision-making in breast cancer immunotherapy. Additionally, the INSPIRE trial by Bratman et al. prospectively assessed ctDNA dynamics as a biomarker of tumor burden in diverse cancer patients on pembrolizumab (44). Cohorts included head and neck squamous cell carcinoma (HNSCC), TNBC, ovarian cancer, melanoma, and mixed solid tumors (MST). Patients with decreased ctDNA after 3 treatment cycles had improved clinical benefit rate (CBR), overall survival (OS), and progression-free survival(PFS); whereas increased ctDNA indicated disease progression and poorer survival (median OS 13.7 months). Undetectable ctDNA levels strongly correlated with therapeutic response. Importantly, ctDNA changes provided complementary data to the Response Evaluation Criteria in Solid Tumors (RECIST) criteria for predicting immunotherapy survival benefit. Overall, detecting ctDNA dynamics noninvasively predicts immunotherapy outcomes and has implications for guiding breast cancer treatment.

In addition to tumor burden monitoring, ctDNA analysis can provide insight into immunotherapy response mechanisms. Somatic mutation profiling of ctDNA may reveal neoantigen loss associated with acquired resistance. Integrated genomic and transcriptomic ctDNA data may elucidate immune evasion pathways in breast cancer immunotherapy. Emerging techniques like low-pass whole genome sequencing help overcome technical hurdles in detecting scarce ctDNA.

4 Exosomes

Extracellular vesicles (EVs) are an integral intercellular communication strategy utilized by both pathogenic and non-pathogenic cells (45). Considerable evidence indicates EVs play a key role in the interaction between tumor cells and immune cells (46). Tumor-derived EVs predominantly demonstrate immunosuppressive capabilities, thereby promoting immune evasion of tumors (47). Such immunosuppression involves EVs downregulating major histocompatibility complex II (MHC II) expression in dendritic cells (48), activating cGAS-STING signaling in dendritic cells (49), inducing STAT3-mediated M2 polarization in monocytes (50), reducing interferon-gamma (IFN-γ) production in natural killer cells (51), and triggering apoptosis in T cells (52). Presentation of PD-L1 on EVs surfaces, as described above, induces T cell exhaustion and dampens anti-tumor immune responses.

Conversely, tumor-derived EVs have been shown to elicit immune activation by stimulating natural killer cells, macrophages, and B and T lymphocytes. Robust tumor clearance associated with EVs affecting the Hippo pathway has been linked to immune activation. EVs from antigen-presenting cells frequently exhibit immunostimulatory properties by carrying MHC complexes that activate T cells, although T cell stimulation by EVs is less potent (53).

Regarding the potential of EVs as biomarkers in immuno-oncology, increased vesicular PD-L1 in melanoma patients undergoing ICIs signifies adaptive immune responses and distinguishes clinical responders from non-responders (53). Elevated vesicular PD-L1 and CD28 correlate with improved PFS and OS in patients receiving anti-CTLA-4 therapy (54). Moreover, specific vesicular RNA profiles have been found to correlate with responses to anti-CTLA-4 treatment. In summary, EVs are integral immune modulators and profiling circulating EVs exhibits tremendous promise as a marker of immunogenicity. While profiling EVs in the blood of breast cancer patients is commonplace, major hurdles remain regarding validated, standardized isolation techniques. Resolving these issues is an imperative first step toward clinically implementing EV analysis.

5 Proteins

5.1 PD-L1

The immune checkpoint protein PD-L1, also termed CD247 or B7-H1, is expressed on antigen presenting and tumor cells. Ligation of PD-L1 with its cognate receptor PD-1 found on T lymphocytes leads to inhibition of T-cell activation, resulting in impaired anti-cancer immunity. Monoclonal antibodies blocking the PD-1/PD-L1 axis have exhibited clinical activity in patients with elevated PD-L1 levels quantified through IHC staining of tumor biopsies. However, some individuals with low tumoral PD-L1 expression have also shown benefits from immune checkpoint blockade (55). This discrepancy is attributed to the dynamic features of immune regulation that cannot be fully captured in static IHC-based assessments. Moreover, PD-L1 expression on both malignant cells and infiltrating leukocytes creates challenges in interpreting PD-L1 levels in tumor tissues. Variations in PD-L1 detection antibodies remain an unresolved issue precluding standardization of PD-L1 IHC methodology. Finally, heterogeneous PD-L1 expression among primary and metastatic lesions restricts the utility of tissue-based approaches. Blood-based profiling of PD-L1 status through analyses of circulating markers like CTCs, EVs, peripheral blood mononuclear cells (PBMCs) could help overcome certain limitations inherent to tissue biopsies (Table 2).

5.2 PD-L1 on CTCs

Expression of PD-L1 on tumor cells can be readily influenced by inflammatory, microenvironmental, and treatment-associated factor (56). Since CTCs arise from multiple tumor sites, they may better capture the heterogeneity of PD-L1 expression compared to localized tissue samples. Initial studies have established CTCs analysis as a platform to evaluate PD-L1 status in cancer patients. Mazel et al. performed the first study enumerating PD-L1-positive CTCs in metastatic breast carcinoma, revealing substantial variability with positivity ranging from 0.2-100% among 11/16 PD-L1-positive cases (57). This seminal study provided the foundation for subsequent research on PD-L1 expression in

TABLE 2 Studies on PD-L1 in breast cancer patients receiving immunotherapy.

Research	Subtype	Location	Sample size	Results
Mazel et al. (56)	HR+,HER2- metastatic BC	CTC	16	A strong heterogeneity in PD-L1 CTC expression, ranging from 0.2 to 100
Schott et al. (57)	Metastatic and early stage BC	CTC	72	More PD-L1+CTC in metastatic patients than patients without metastatic (75% vs. 61.1%)
Jacot et al. (58)	Metastatic BC	CTC	72	PD-L1+ CTCs was associated with PDS while tissue PD-L1 was not
Agelaki et al. (59)	Metastatic BC	CTC	98	PD-L1+ CTC was associated with shorter PFS(5.8 vs. 13.3m)and reduced OS(23.8 vs 35.7m)
Yang et al. (60)	TNBC cell line	EV	NA	Exosomes enhance anti-tumor immunity in PD-L1 downregulated tumor microenvironment; exosomes transfer PD-L1 from the positive cells to negative cells.
Li et al. (61)	TNBC	Soluble	66	sPD-1 was elevated in TNBC; a decrease in sPD-L1 levels were detected in patients with CR and PR

CTCs. Additional investigations have confirmed detection of PD-L1-positive CTCs in breast cancer and elucidated clinical implications. Schott et al. examined 72 breast cancer patients, identifying PD-L1-positive CTCs in 94.5% (57). Metastatic patients exhibited significantly higher CTC counts versus non-metastatic cases. (75% vs. 61.1%; $p<0.05$). Moreover, declining PD-L1-positive CTCs associated with treatment responses, indicating CTCs may serve as pharmacodynamic markers of immunotherapy efficacy. Interestingly, PD-L1-positive CTCs increased even after discontinuing ICIs, implying the ability of these inhibitors to reduce the quantity of PD-L1-positive CTCs in BC patients. Hence, PD-L1-positive CTCs presence associated with poorer prognosis and could be utilized to monitor immunotherapy efficacy while also reflecting potential resistance mechanisms.

In a prospective study, Jacot et al. detected CTCs and PD-L1-positive CTCs and PD-L1-positive CTCs pre-treatment in 79.2% and 36.1% of metastatic BC patients, respectively (59). Compared to tissue PD-L1 expression, PD-L1-positive CTCs were associated with shorter progression-free survival, although this was not confirmed on multivariate analysis. Compared to tissue PD-L1 expression, PD-L1-positive CTCs were associated with shorter progression-free survival, although this was not confirmed on multivariate analysis. Moreover, Compared to tissue PD-L1 expression, PD-L1-positive CTCs were associated with shorter progression-free survival, although this was not confirmed on multivariate analysis (62). High PD-L1 expression occurred in approximately 11.6% of patients and was associated with poorer median survival (23.8 vs 35.7 months, $p=0.043$). The study also demonstrated a significant correlation between PD-L1-positive CTCs and increased recurrence risk (HR = 4.8; $p=0.011$). These findings suggest that subgroups of BC patients with PD-L1-positive CTCs may derive greater benefit from anti-PD-L1 immunotherapy.

PD-L1-positive CTCs have also been confirmed in other malignancies, including non-small cell lung cancer (NSCLC) (63), head and neck cancer (64), colon cancer (65), prostate cancer (66), and pancreatic cancer (67). Recent comprehensive analysis of CTCs in breast cancer confirms similar patterns of PD-L1 and CD47 expression as seen in lung cancer. Papadaki et al. examined PBMCs from early stage and metastatic BC patients using triple immunofluorescence staining (68). PD-L1 enables immune evasion while CD47 signals “do not eat me” to macrophages. A lower concordance in PD-L1 and CD47 labeling between CTCs and tumor tissue as well as between PBMCs and TILs. Approximately 11-30% of CTCs were PD-L1/CD47 positive, increasing with disease progression. Critically, metastatic patients with high CD47/PD-L1 CTCs showed associations with poorer outcomes including shorter progression-free survival and greater risk of relapse and death. These data strengthen the biological rationale for dual PD-L1/CD47 inhibition in BC.

Liquid biopsy represents an advanced method for dynamically and continuously monitoring PD-L1 expression in breast cancer patients receiving immune checkpoint inhibitors. Further research is warranted on utilizing PD-L1-positive circulating tumor cells during immunotherapy and correlating their expression with tumor tissue. Before employing liquid biopsy for treatment decision-making, several issues must be addressed. These include the substantial evidence linking epithelial-mesenchymal transition and PD-L1 expression (69, 70), and the need to mitigate false-positive results since PD-L1 is also expressed on suppressor cells from the bone marrow (71, 72).

5.3 PD-L1 on exosomes

The clinical prognostic value of PD-L1 expression on exosomes has been validated in several solid tumor types (60, 73, 74) However, further studies are still needed to evaluate the clinical utility of exosomal PD-L1 specifically in breast cancer. Experimental findings have proposed that PD-L1 bound to the surface of exosomes can effectively interact with PD-1 receptors, resulting in inhibition of T cell activation, suppression of apoptosis in breast cancer cells, and facilitation of tumor immune evasion (61). Additionally, exosomes were able to transfer PD-L1 from PD-L1-positive cancer cells to PD-L1-negative cancer cells, elucidating

the underlying mechanisms of immune evasion employed by breast cancer cells.

5.4 PD-L1 in plasma

Plasma represents another important specimen for liquid biopsy to detect PD-1, PD-L1, and PD-L2 (75). A notable study in 66 patients with TNBC revealed significantly higher plasma PD-L1 levels compared to healthy controls (76). Furthermore, serum PD-L1 levels correlated with tumor stage (p=0.030). Patients who achieved complete or partial response after neoadjuvant chemotherapy (NAC) exhibited decreased plasma PD-L1 levels, whereas patients with stable disease or disease progression displayed increased plasma PD-L1 levels. These findings demonstrate the potential clinical utility of measuring PD-L1 in plasma as a liquid biopsy approach for prognostication, predicting response to chemotherapy, and monitoring disease status in TNBC.

5.5 PD-L1 in PBMCs

Analysis of PBMCs from BC patients showed PD-L1 promoter hypomethylation may explain increased PD-L1 expression in PBMCs versus matched tumor tissue. Additionally, the PD-1 promoter was hypermethylated in PBMCs compared to tumor (77). Methylation profiling in cell-free DNA could thus serve as a molecular correlate for PD-L1 expression. Another study found significantly more PD-1 high CD8+ exhausted T cells in tumor versus matched blood of triple negative BC patients (78). These data demonstrate differential tumor immune interactions in circulation versus tissue.

6 Genomic biomarkers

6.1 Tumor mutational burden

Although the FDA and EMA no longer endorse tumor mutational burden (TMB) as a standard treatment selection biomarker, TMB remains a potential indicator of T-cell activation that may help predict response to ICIs therapy (79). While tumor tissue biopsies were previously the primary TMB sample source (80), alternative liquid biopsy samples like ctDNA and CTCs represent promising substitutes for TMB quantification in patients with limited tumor tissue.

Assessment of TMB from ctDNA represents a promising advancement that expands its application to patients with limited biopsy samples or difficulties obtaining high-quality tissue samples for TMB assays (81). Previous studies have demonstrated a correlation between blood-based TMB and tissue-based TMB (82, 83).

In one study of 30 patients, detectable mutations ranging from 1 to 53 were identified in ctDNA. Furthermore, decreased variant allele frequencies of ctDNA mutations were observed in 3 patients who had objective responses to treatment, suggesting ctDNA may enable early prediction of treatment efficacy. Gandara et al. analyzed two large retrospective randomized trials and showed a blood-based TMB threshold ≥16 was predictive of efficacy for ICIs therapy (84). These results indicated blood-based TMB (bTMB) could independently predict clinical benefit in terms of progression-free survival associated with atezolizumab. Use of plasma, rather than tissue, as a DNA source for assessing bTMB provides an attractive alternative for patients with metastatic non-small cell lung cancer who may not be suitable candidates for biopsy or lack sufficient tumor tissue.

In metastatic TNBC, the median value of biopsy-based TMB has been associated with breast tumor subtype and sample type. Higher TMB detected in tumor tissue was correlated with longer PFS, compared to bTMB (85, 86). Therefore, there are still certain challenges that need to be addressed and clarified regarding discordance between tissue and blood TMB. The establishment of standardized processes and meaningful thresholds would facilitate accurate assessment, taking into account the specific panel of genes that contribute significantly to the precise evaluation of bTMB (87). While a close correlation between tissue-based TMB and bTMB exists, bTMB is a relatively independent predictive factor (88–90). While a close correlation between tissue-based TMB and bTMB exists, bTMB is a relatively independent predictive factor.

6.2 dMMR/MSI

DNA mismatch repair (MMR) plays a vital role in maintaining DNA integrity by correcting errors during replication, recombination, and repair (91). MMR deficiencies can result in microsatellite instability (MSI), observed across cancer types. In colorectal cancer, increased mutational burden from deficient MMR (dMMR) and MSI associates with improved response to PD-1/PD-L1 blockade (92), leading to FDA approval of pembrolizumab for any dMMR/MSI tumor (93).

Despite the relatively low 1-2% incidence, current evidence remains insufficient regarding MSI/dMMR predictive value in breast cancer (94, 95). However, data indicate MSI presence across breast cancer subtypes, particularly in high grade, low progesterone receptor tumors (96). Cases showed metastatic breast cancer patients exhibited favorable immune checkpoint inhibitor responses, including nivolumab in dMMR/MSI triple negative breast cancer and pembrolizumab in dMMR/MSI luminal (97) or HER2+ disease with high tumor mutational burden and dMMR (98). Thus, utilizing dMMR as a predictive biomarker may improve outcomes and guide appropriate immune therapy selection.

Similarly, MSI evaluation can be performed via circulating tumor DNA analysis (99). Notably, MSI is effectively detected even at low coverage (100). Previous studies show high MSI levels in ctDNA correlate with improved immune checkpoint inhibitor responses (101). Detecting ctDNA somatic mutations may identify non-responders, since such mutations regulate tumor immunity. In anti-PD-1 treated pan-cancer cohorts, high pretreatment plasma MSI and tumor mutational burden strongly predicted progression-free survival (p=0.001 and 0.003, respectively) (102).

6.3 TCR repertoire

The clinical efficacy of ICIs relies on the recognition of neoantigens by T cells. These neoantigens are presented to T cells through interaction with MHC molecules (103). Appropriate T cell receptors (TCRs) recognize these neoantigens, triggering an immune response as they are perceived as foreign rather than self-antigens (104). Analysis of the TCR repertoire by sequencing the TCR CD3 region provides valuable insight, as the CD3 region is unique to each TCR, and its diversity can serve as a predictive biomarker for ICIs response (105).

One study reported the circulating CD8+ T cell TCR repertoire in the blood of breast cancer patients changed following chemotherapy (106). There was an association between increased TCR repertoire diversity and improved treatment outcomes. Gao et al. performed TCR sequencing on PBMCs from metastatic inflammatory and triple-negative breast cancer patients (107). Therefore, TCR sequencing from blood not only reflects the diversity of the TCR repertoire, but also serves as a surrogate indicator for evaluating the effectiveness of breast cancer immunotherapy.

7 Novel liquid biopsy approaches

CTCs and cfDNA in blood represent emerging liquid biomarkers with potential clinical utility for cancer management. In addition to detecting mutations in ctDNA, other novel cfDNA analysis approaches that go beyond mutation profiling are being developed and show promise.

One such approach is evaluation of genome-wide fragmentation patterns of cfDNA, termed "fragmentomics" (108). By combining fragmentation pattern analysis with mutation profiling, this approach can accurately discriminate between cancer patients and healthy individuals based on differences in cfDNA fragmentation profiles. Another emerging technique is methylation sequencing of cfDNA (109). For example, detailed evaluation of methylation patterns across more than 900 CpG sites in cfDNA has been shown to enable detection of cancer presence as well as identification of cancer type in patients with advanced cancers.

Chromatin state analysis and nucleosome footprinting of cfDNA are other approaches under development (110). Nucleosome positions on DNA determine chromatin structure, which in turn affects gene expression. These techniques involve generating genome-wide maps showing nucleosome occupancy and transcription factor binding patterns in cfDNA fragments. Analysis of such nucleosome footprints has revealed patient- and tumor-specific patterns that allow accurate prediction of cancer subtypes (111).

A key challenge is that tumor-derived DNA represents only a small fraction of total cfDNA. Tumors with low mutational burden like breast cancer are especially difficult to detect. However, these emerging cfDNA analysis platforms allow interrogation of significantly more genomic loci compared to targeted mutation panels. For example, low-coverage genome sequencing of cfDNA to measure copy number changes can monitor immunotherapy response (112). Such whole-genome analysis approaches complement mutation profiling and may provide clinically actionable information beyond what can be achieved with ctDNA analysis alone. Further validation of the ability of these novel platforms to guide immunotherapy decisions in cancers including breast cancer is warranted.

8 Challenge and future

Liquid biopsy shows promise for improving management of breast cancer and enhancing patient survival, with increasing evidence supporting its potential. Over the past decade, advancements in molecular analysis techniques have enabled widespread application of liquid biopsy for diagnosis, prognosis and predicting treatment response in breast cancer. However, realizing the full potential of liquid biopsy faces several challenges that need to be addressed. Figure 3 provides a detailed summary of the clinical applications of liquid biopsy components, along with their advantages and disadvantages.

A major challenge with CTCs is their rarity, requiring highly sensitive equipment for detection. The enumeration of CTCs relies on specialized reagents like immunomagnetic beads and automated fluorescence microscopes. However, these techniques have limited sensitivity and accuracy. CTCs analysis is more effective in

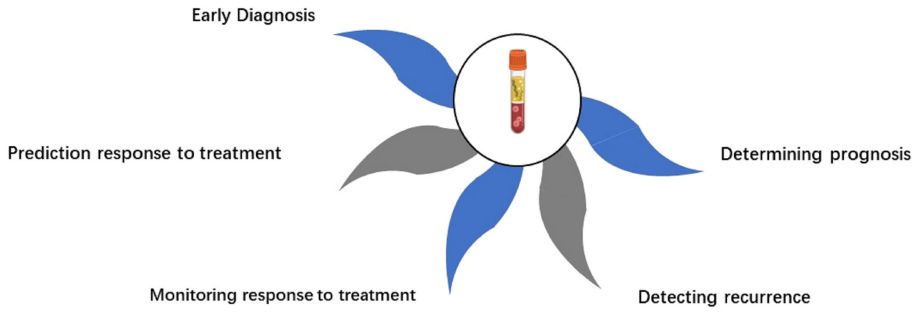

FIGURE 3
Overview of the five major clinical applications of liquid biopsy in breast cancer.

metastatic patients with higher CTC counts, yet only around half of these patients exhibit positive CTCs (113, 114). Even in metastatic disease, CTCs can comprise less than one cell per billion blood cells. More robust methods are urgently needed to reliably capture, amplify and detect scarce CTCs. Emerging microfluidic and imaging technologies hold promise if challenges with throughput, purity and clinical validation can be overcome. Machine learning methods like deep learning could help improve detection and classification accuracy.

The current challenge with using ctDNA as a biomarker is its low quantity compared to normal cell-free DNA, especially with smaller tumors. CtDNA levels can be as low as 0.01% of total cfDNA. CtDNA is predominantly released from necrotic tumor cells, resulting in longer fragments versus healthy individuals. In contrast, ctDNA from apoptotic cells is shorter at around 133-144bp (115). Size-based isolation can enrich for ctDNA by leveraging its short length. However, this approach may miss longer ctDNA fragments carrying crucial genomic information. Optimized isolation and amplification techniques are needed to comprehensively capture ctDNA diversity. Ultra-deep sequencing could enable detection of rare mutations missed by shallow sequencing. However, this is expensive and bioinformatically challenging currently. Tailored gene panels may provide a balanced approach.

ctDNA analysis could be enhanced by profiling additional hallmark features of cfDNA using integrative approaches. Assessing cfDNA fragmentation patterns, tumor-derived epigenetic signatures, and nucleosome footprints associated with active genes may provide supplementary information to optimize liquid biopsies. This could improve utility for patient selection, risk stratification, and immunotherapy response monitoring. Multiparameter liquid biopsy testing combining circulating biomarkers with cfDNA analysis has shown promise for early cancer detection (116). Similarly, incorporating diverse noninvasive measures, including baseline ctDNA, longitudinal ctDNA changes, and immune cell dynamics, may leverage tumor and immune components to better define molecular response to immunotherapy.

Assessing structural and fragmentation patterns of cfDNA (117, 118), along with tumor-derived epigenetic marks and nucleosome footprints associated with active genes (119), could provide additional features to optimize liquid biopsies. This may improve their utility for patient selection, risk stratification, and monitoring immunotherapy response. Circulating microbiome DNA fragments have also been detected in the blood of melanoma, prostate and lung cancer patients (120). This reveals potential for liquid biopsies to characterize changes in the bacterial microbiome associated with immunotherapy outcomes.

A key limitation is that liquid biopsy may not fully recapitulate tumor heterogeneity, since it samples only some subgroups (121). Multidimensional analysis integrating liquid biopsy data with clinical and radiomic features can help mitigate this. Combining liquid and tissue biopsy may also improve heterogeneity assessment. However, tissue biopsy also has limitations in capturing spatial and temporal heterogeneity. New techniques that can assess tumor evolution are required. Repeated liquid biopsies could help track changes in biomarkers over time. However, standardizing the timing and frequency of longitudinal sampling remains an open question. Mathematical modeling approaches could help optimize longitudinal sampling strategies.

Currently, standardization procedures and calibration methods for liquid biopsy lack consistency. Variations exist in operational workflows and quality control standards employed across different laboratories and studies, resulting in inconsistent results and reduced reproducibility. To address this issue, it is crucial to improve standardization of liquid biopsy practices. One approach is developing consensus guidelines that establish clear protocols and quality control measures for various aspects of liquid biopsy, including sample collection, processing, analysis, and reporting. Such guidelines would provide a standardized framework ensuring consistency and reliability across different laboratories and research settings. Furthermore, implementing external quality assessment (EQA) programs can significantly enhance standardization. EQA programs involve external evaluation and proficiency testing of laboratories, enabling identification of potential errors or variations in testing procedures. By participating in these programs, laboratories can identify areas for improvement and align their practices with established standards.

Collaboration among laboratories is essential to promote standardization in the field of liquid biopsy. Fostering partnerships and sharing best practices allow laboratories to learn from each other's experiences and work toward harmonizing their approaches. Potential collaborations can include joint research projects, data sharing, and establishing common quality control measures. Through such collaborative efforts, laboratories can shape consensus guidelines and EQA programs that facilitate the standardization of liquid biopsy practices.

Standardization is critical for enhancing the reliability and reproducibility of liquid biopsy results. By improving standardization through laboratory collaborations, consensus guidelines, and EQA programs, liquid biopsy can be implemented consistently in clinical practice. The widespread and uniform utilization of liquid biopsy will only be achieved through improving result consistency. Standardization relies on open collaboration and communication between laboratories to share knowledge and align approaches. By working together, laboratories can promote the standardization needed to move liquid biopsy into routine clinical use.

Conclusions

Immunotherapy is an highly effective treatment strategy for breast cancer, while there are substantial variations in treatment response among patients. Therefore, it is imperative to identify patient subgroups and enable precision treatment through the use of biomarkers. Liquid biopsies provide a valuable source for assessing various immune-related biomarkers in breast cancer. In this review, we have comprehensively listed and detailed the applications of these immune-related biomarkers. The analysis of PD-L1 on CTCs and exosomes is currently under investigation, while the detection of cfDNA and ctDNA is being utilized with

advanced technologies. The value of TMB as an immunotherapy biomarker still requires validation in prospective clinical trials. Currently, there is compelling evidence demonstrating the correlation between genomic markers such as MSI and TCR analysis in the blood of breast cancer patients receiving ICIs therapy, which is associated with treatment efficacy and prognosis.

LB offers several advantages in the context of guiding immunotherapy for breast cancer. One of its key benefits is the ability to obtain multiple and repetitive samples throughout the treatment process, which facilitates effective follow-up and evaluation of treatment response. LB is characterized by its simplicity, rapidity, and minimally invasive nature, making it a convenient tool for monitoring disease progression and therapeutic efficacy.

Immunotherapy, particularly ICIs therapy, can induce distinct alterations in breast cancer. This highlights the importance of determining the optimal timing for extracting biomarkers from LB. By capturing biomarkers at the right time points, clinicians can gain valuable insights into treatment response and tailor therapeutic strategies accordingly. Additionally, different ICIs targeted therapies may require the assessment of specific individual biomarkers or a combination of multiple biomarkers to effectively guide treatment decisions.

While liquid biopsy biomarkers for guiding immunotherapy in breast cancer have not yet been formally recommended in treatment guidelines, current evidence suggests that the non-invasive and feasible nature of LB allows for continuous sampling and longitudinal monitoring. This opens up possibilities for utilizing LB as a valuable tool in guiding the selection of appropriate immunotherapeutic approaches for breast cancer patients.

Author contributions

JY: Writing – original draft. LQ: Formal Analysis, Writing – original draft. XW: Methodology, Writing – review & editing. XC: Conceptualization, Writing – review & editing. PC: Writing – review & editing. ZY: Writing – review & editing, Supervision. QW: Writing – original draft, Writing – review & editing.

Funding

The author(s) declare financial support was received for the research, authorship, and/or publication of this article. This study was supported by Radiation Oncology Translational Medicine Foundation for Scientific Research of Bethune (grant number flzh202123), Shandong Medical Association Clinical Research Fund–Qilu Special Project (grant number YXH2022ZX02196) and Jinan Science and Technology Clinical Medicine Innovation Plan (grant number 20225011 and 20238073). The funding sources had no role in the study design, data collection, analysis of interpretation, or writing of this manuscript.

Conflict of interest

The authors declare that the research was conducted in the absence of any commercial or financial relationships that could be construed as a potential conflict of interest.

The handling editor CL declared a shared parent affiliation with the authors XC, PC, ZY, and QW at the time of review.

Publisher's note

References

1. Pritzker KP. Predictive and prognostic cancer biomarkers revisited. *Expert Rev Mol Diagnostics* (2015) 15:971–4. doi: 10.1586/14737159.2015.1063421

2. Reddy SM, Carroll E, Nanda R. Atezolizumab for the treatment of breast cancer. *Expert Rev Anticancer Ther* (2020) 20:151–8. doi: 10.1080/14737140.2020.1732211

3. Garon EB, Rizvi NA, Hui R, Leighl N, Balmanoukian AS, Eder JP, et al. Pembrolizumab for the treatment of non–small-cell lung cancer. *New Engl J Med* (2015) 372:2018–28. doi: 10.1056/NEJMoa1501824

4. Hodi FS, O'day SJ, McDermott DF, Weber RW, Sosman JA, Haanen JB, et al. Improved survival with ipilimumab in patients with metastatic melanoma. *New Engl J Med* (2010) 363:711–23. doi: 10.1056/NEJMoa1003466

5. Hofman P, Heeke S, Alix-Panabières C, Pantel K. Liquid biopsy in the era of immuno-oncology: is it ready for prime-time use for cancer patients? *Ann Oncol* (2019) 30:1448–59. doi: 10.1093/annonc/mdz196

6. Sung H, Ferlay J, Siegel RL, Laversanne M, Soerjomataram I, Jemal A, et al. Global cancer statistics 2020: GLOBOCAN estimates of incidence and mortality worldwide for 36 cancers in 185 countries. *CA: Cancer J Clin* (2021) 71:209–49. doi: 10.3322/caac.21660

7. Mina LA, Lim S, Bahadur SW, Firoz AT. Immunotherapy for the treatment of breast cancer: emerging new data. *Breast Cancer: Targets Ther* (2019) 11:321–8. doi: 10.2147/BCTT.S184710

8. Schmid P, Cortes J, Pusztai L, McArthur H, Kümmel S, Bergh J, et al. Pembrolizumab for early triple-negative breast cancer. *New Engl J Med* (2020) 382:810–21. doi: 10.1056/NEJMoa1910549

9. Loibl S, Untch M, Burchardi N, Huober J, Sinn B, Blohmer J-U, et al. A randomised phase II study investigating durvalumab in addition to an anthracycline taxane-based neoadjuvant therapy in early triple-negative breast cancer: clinical results and biomarker analysis of GeparNuevo study. *Ann Oncol* (2019) 30:1279–88. doi: 10.1093/annonc/mdz158

10. Schmid P, Adams S, Rugo HS, Schneeweiss A, Barrios CH, Iwata H, et al. Atezolizumab and nab-paclitaxel in advanced triple-negative breast cancer. *New Engl J Med* (2018) 379:2108–21. doi: 10.1056/NEJMoa1809615

11. Schmid P, Adams S, Rugo HS, Schneeweiss A, Barrios CH, Iwata H, et al. IMpassion130: updated overall survival (OS) from a global, randomized, double-blind, placebo-controlled, Phase III study of atezolizumab (atezo)+ nab-paclitaxel (nP) in previously untreated locally advanced or metastatic triple-negative breast cancer (mTNBC). *Am Soc Clin Oncol* (2019) 37(15_suppl):1003. doi: 10.1200/JCO.2019.37.15_suppl.1003

12. Denkert C, von Minckwitz G, Darb-Esfahani S, Lederer B, Heppner BI, Weber KE, et al. Tumour-infiltrating lymphocytes and prognosis in different subtypes of breast cancer: a pooled analysis of 3771 patients treated with neoadjuvant therapy. *Lancet Oncol* (2018) 19:40–50. doi: 10.1016/S1470-2045(17)30904-X

13. Cortes J, Cescon DW, Rugo HS, Nowecki Z, Im S-A, Yusof MM, et al. KEYNOTE-355: Randomized, double-blind, phase III study of pembrolizumab+ chemotherapy versus placebo+ chemotherapy for previously untreated locally recurrent inoperable or metastatic triple-negative breast cancer. *Am Soc Clin Oncol* (2020) 38(15_suppl):1000. doi: 10.1200/JCO.2020.38.15_suppl.1000

14. Miles D, Gligorov J, André F, Cameron D, Schneeweiss A, Barrios C, et al. Primary results from IMpassion131, a double-blind, placebo-controlled, randomised phase III trial of first-line paclitaxel with or without atezolizumab for unresectable locally advanced/metastatic triple-negative breast cancer. *Ann Oncol* (2021) 32:994–1004. doi: 10.1016/j.annonc.2021.05.801

15. Tolaney SM, Kalinsky K, Kaklamani VG, D'Adamo DR, Aktan G, Tsai ML, et al. Eribulin plus pembrolizumab in patients with metastatic triple-negative breast cancer (ENHANCE 1): a phase Ib/II study. *Clin Cancer Res* (2021) 27:3061–8. doi: 10.1158/1078-0432.CCR-20-4726

16. Pérez-García JM, Llombart-Cussac A, Gion M, Curigliano G, López-Miranda E, Alonso JL, et al. Pembrolizumab plus eribulin in hormone-receptor–positive, HER2-negative, locally recurrent or metastatic breast cancer (KELLY): An open-label, multicentre, single-arm, phase II trial. *Eur J Cancer* (2021) 148:382–94. doi: 10.1016/j.ejca.2021.02.028

17. Adams S, Schmid P, Rugo H, Winer E, Loirat D, Awada A, et al. Pembrolizumab monotherapy for previously treated metastatic triple-negative breast cancer: cohort A of the phase II KEYNOTE-086 study. *Ann Oncol* (2019) 30:397–404. doi: 10.1093/annonc/mdy517

18. Winer EP, Lipatov O, Im S-A, Goncalves A, Muñoz-Couselo E, Lee KS, et al. Pembrolizumab versus investigator-choice chemotherapy for metastatic triple-negative breast cancer (KEYNOTE-119): a randomised, open-label, phase 3 trial. *Lancet Oncol* (2021) 22:499–511. doi: 10.1016/S1470-2045(20)30754-3

19. Ott PA, Elez E, Hiret S, Kim D-W, Morosky A, Saraf S, et al. Pembrolizumab in patients with extensive-stage small-cell lung cancer: results from the phase Ib KEYNOTE-028 study. *J Clin Oncol* (2017) 35:3823–9. doi: 10.1200/JCO.2017.72.5069

20. Dirix LY, Takacs I, Jerusalem G, Nikolinakos P, Arkenau H-T, Forero-Torres A, et al. Avelumab, an anti-PD-L1 antibody, in patients with locally advanced or metastatic breast cancer: a phase 1b JAVELIN Solid Tumor study. *Breast Cancer Res Treat* (2018) 167:671–86. doi: 10.1007/s10549-017-4537-5

21. Molinero L, Li Y, Chang C-W, Maund S, Berg M, Harrison J, et al. Tumor immune microenvironment and genomic evolution in a patient with metastatic triple negative breast cancer and a complete response to atezolizumab. *J immunotherapy Cancer* (2019) 7:1–9. doi: 10.1186/s40425-019-0740-8

22. Schmid P, Cortés J, Dent R, Pusztai L, McArthur H, Kuemmel S, et al. KEYNOTE-522: Phase III study of pembrolizumab (pembro)+ chemotherapy (chemo) vs placebo (pbo)+ chemo as neoadjuvant treatment, followed by pembro vs pbo as adjuvant treatment for early triple-negative breast cancer (TNBC). *Ann Oncol* (2019) 30:v853–v4. doi: 10.1093/annonc/mdz394.003

23. Nanda R, Liu MC, Yau C, Asare S, Hylton N, Veer LVt, et al. Pembrolizumab plus standard neoadjuvant therapy for high-risk breast cancer (BC): results from I-SPY 2. *Am Soc Clin Oncol* (2017) 35(15_suppl):506. doi: 10.1200/JCO.2017.35.15_suppl.506

24. Mittendorf EA, Zhang H, Barrios CH, Saji S, Jung KH, Hegg R, et al. Neoadjuvant atezolizumab in combination with sequential nab-paclitaxel and anthracycline-based chemotherapy versus placebo and chemotherapy in patients with early-stage triple-negative breast cancer (IMpassion031): a randomised, double-blind, phase 3 trial. *Lancet* (2020) 396:1090–100. doi: 10.1016/S0140-6736(20)31953-X

25. Gianni L, Huang C-S, Egle D, Bermejo B, Zamagni C, Thill M, et al. Pathologic complete response (pCR) to neoadjuvant treatment with or without atezolizumab in triple-negative, early high-risk and locally advanced breast cancer: NeoTRIP Michelangelo randomized study. *Ann Oncol* (2022) 33:534–43. doi: 10.1016/j.annonc.2022.02.004

26. Brahmer JR, Tykodi SS, Chow LQ, Hwu W-J, Topalian SL, Hwu P, et al. Safety and activity of anti–PD-L1 antibody in patients with advanced cancer. *New Engl J Med* (2012) 366:2455–65. doi: 10.1056/NEJMoa1200694

27. Ilie M, Long-Mira E, Bence C, Butori C, Lassalle S, Bouhlel L, et al. Comparative study of the PD-L1 status between surgically resected specimens and matched biopsies of NSCLC patients reveal major discordances: a potential issue for anti-PD-L1 therapeutic strategies. *Ann Oncol* (2016) 27:147–53. doi: 10.1093/annonc/mdv489

28. Ilie M, Benzaquen J, Hofman V, Lassalle S, Yazbeck N, Leroy S, et al. Immunotherapy in non-small cell lung cancer: biological principles and future opportunities. *Curr Mol Med* (2017) 17:527–40. doi: 10.2174/1566524018666180222114038

29. Martins I, Ribeiro IP, Jorge J, Gonçalves AC, Sarmento-Ribeiro AB, Melo JB, et al. Liquid biopsies: applications for cancer diagnosis and monitoring. *Genes* (2021) 12:349. doi: 10.3390/genes12030349

30. Ramos-Medina R, López-Tarruella S, del Monte-Millán M, Massarrah T, Martín M. Technical challenges for CTC implementation in breast cancer. *Cancers* (2021) 13:4619. doi: 10.3390/cancers13184619

31. Galletti G, Sung MS, Vahdat LT, Shah MA, Santana SM, Altavilla G, et al. Isolation of breast cancer and gastric cancer circulating tumor cells by use of an anti HER2-based microfluidic device. *Lab Chip* (2014) 14:147–56. doi: 10.1039/C3LC51039E

32. Magbanua MJM, Sosa EV, Roy R, Eisenbud LE, Scott JH, Olshen A, et al. Genomic profiling of isolated circulating tumor cells from metastatic breast cancer patients. *Cancer Res* (2013) 73:30–40. doi: 10.1158/0008-5472.CAN-11-3017

33. Lianidou ES, Markou A. Circulating tumor cells in breast cancer: detection systems, molecular characterization, and future challenges. *Clin Chem* (2011) 57:1242–55. doi: 10.1373/clinchem.2011.165068

34. Cristofanilli M, Budd GT, Ellis MJ, Stopeck A, Matera J, Miller MC, et al. Circulating tumor cells, disease progression, and survival in metastatic breast cancer. *New Engl J Med* (2004) 351:781–91. doi: 10.1056/NEJMoa040766

35. Xue D, Xia T, Wang J, Chong M, Wang S, Zhang C. Role of regulatory T cells and CD8+ T lymphocytes in the dissemination of circulating tumor cells in primary invasive breast cancer. *Oncol Lett* (2018) 16:3045–53. doi: 10.3892/ol.2018.8993

36. Mego M, Kalavska K, Karaba M, Minarik G, Benca J, Sedlackova T, et al. Abstract P4-01-15: CTC with EMT phenotype are associated with PD-L1 expression in tumor associated stroma in primary breast cancer patients. *Cancer Res* (2020) 80:P4–01-15-P4-01-15. doi: 10.1158/1538-7445.SABCS19-P4-01-15

37. Mego M, Gao H, Cohen EN, Anfossi S, Giordano A, Tin S, et al. Circulating tumor cells (CTCs) are associated with abnormalities in peripheral blood dendritic cells in patients with inflammatory breast cancer. *Oncotarget* (2017) 8:35656. doi: 10.18632/oncotarget.10290

38. Kallergi G, Tsintari V, Sfakianakis S, Bei E, Lagoudaki E, Koutsopoulos A, et al. The prognostic value of JUNB-positive CTCs in metastatic breast cancer: from bioinformatics to phenotypic characterization. *Breast Cancer Res* (2019) 21:1–13. doi: 10.1186/s13058-019-1166-4

39. Haber DA, Velculescu VE. Blood-based analyses of cancer: circulating tumor cells and circulating tumor DNA. *Cancer Discovery* (2014) 4:650–61. doi: 10.1158/2159-8290.CD-13-1014

40. Siravegna G, Marsoni S, Siena S, Bardelli A. Integrating liquid biopsies into the management of cancer. *Nat Rev Clin Oncol* (2017) 14:531–48. doi: 10.1038/nrclinonc.2017.14

41. Bettegowda C, Sausen M, Leary RJ, Kinde I, Wang Y, Agrawal N, et al. Detection of circulating tumor DNA in early-and late-stage human Malignancies. *Sci Trans Med* (2014) 6:224ra24–ra24. doi: 10.1126/scitranslmed.3007094

42. Bardelli A, Pantel K. Liquid biopsies, what we do not know (yet). *Cancer Cell* (2017) 31:172–9. doi: 10.1016/j.ccell.2017.01.002

43. Magbanua MJM, Wolf D, Renner D, Shchegrova S, Swigart LB, Yau C, et al. Abstract PD9-02: Personalized ctDNA as a predictive biomarker in high-risk early stage breast cancer (EBC) treated with neoadjuvant chemotherapy (NAC) with or without pembrolizumab (P). *Cancer Res* (2021) 81:PD9–02-PD9-. doi: 10.1158/1538-7445.SABCS20-PD9-02

44. Bratman SV, Yang SC, Iafolla MA, Liu Z, Hansen AR, Bedard PL, et al. Personalized circulating tumor DNA analysis as a predictive biomarker in solid tumor patients treated with pembrolizumab. *Nat Cancer* (2020) 1:873–81. doi: 10.1038/s43018-020-0096-5

45. Eguchi A, Kostallari E, Feldstein AE, Shah VH. Extracellular vesicles, the liquid biopsy of the future. *J Hepatol* (2019) 70:1292–4. doi: 10.1016/j.jhep.2019.01.030

46. Yu Dd, Wu Y, Shen Hy, Lv MM, Chen WX, Zhang XH , et al. Exosomes in development, metastasis and drug resistance of breast cancer. *Cancer Sci* (2015) 106:959–64. doi: 10.1111/cas.12715

47. Gobbo J, Marcion G, Cordonnier M, Dias AM, Pernet N, Hammann A, et al. Restoring anticancer immune response by targeting tumor-derived exosomes with a HSP70 peptide aptamer. *J Natl Cancer Institute* (2016) 108:djv330. doi: 10.1093/jnci/djv330

48. Ding G, Zhou L, Qian Y, Fu M, Chen J, Chen J, et al. Pancreatic cancer-derived exosomes transfer miRNAs to dendritic cells and inhibit RFXAP expression via miR-212-3p. *Oncotarget* (2015) 6:29877. doi: 10.18632/oncotarget.4924

49. Kitai Y, Kawasaki T, Sueyoshi T, Kobiyama K, Ishii KJ, Zou J, et al. DNA-containing exosomes derived from cancer cells treated with topotecan activate a STING-dependent pathway and reinforce antitumor immunity. *J Immunol* (2017) 198:1649–59. doi: 10.4049/jimmunol.1601694

50. Gabrusiewicz K, Li X, Wei J, Hashimoto Y, Marisetty AL, Ott M, et al. Glioblastoma stem cell-derived exosomes induce M2 macrophages and PD-L1 expression on human monocytes. *Oncoimmunology* (2018) 7:e1412909. doi: 10.1080/2162402X.2017.1412909

51. Zhao J, Schlößer HA, Wang Z, Qin J, Li J, Popp F, et al. Tumor-derived extracellular vesicles inhibit natural killer cell function in pancreatic cancer. *Cancers* (2019) 11:874. doi: 10.3390/cancers11060874

52. Andreola G, Rivoltini L, Castelli C, Huber V, Perego P, Deho P, et al. Induction of lymphocyte apoptosis by tumor cell secretion of FasL-bearing microvesicles. *J Exp Med* (2002) 195:1303–16. doi: 10.1084/jem.20011624

53. Chen G, Huang AC, Zhang W, Zhang G, Wu M, Xu W, et al. Exosomal PD-L1 contributes to immunosuppression and is associated with anti-PD-1 response. *Nature* (2018) 560:382–6. doi: 10.1038/s41586-018-0392-8

54. Tucci M, Passarelli A, Mannavola F, Stucci LS, Ascierto PA, Capone M, et al. Serum exosomes as predictors of clinical response to ipilimumab in metastatic melanoma. *Oncoimmunology* (2018) 7:e1387706. doi: 10.1080/2162402X.2017.1387706

55. Wen Q, Yang Z, Zhu J, Qiu Q, Dai H, Feng A, et al. Pretreatment CT-based radiomics signature as a potential imaging biomarker for predicting the expression of PD-L1 and CD8+ TILs in ESCC. *OncoTargets Ther* (2020) 13:12003–13. doi: 10.2147/OTT.S261068

56. Cogdill AP, Andrews MC, Wargo JA. Hallmarks of response to immune checkpoint blockade. *Br J Cancer* (2017) 117:1–7. doi: 10.1038/bjc.2017.136

57. Mazel M, Jacot W, Pantel K, Bartkowiak K, Topart D, Cayrefourcq L, et al. Frequent expression of PD-L1 on circulating breast cancer cells. *Mol Oncol* (2015) 9:1773–82. doi: 10.1016/j.molonc.2015.05.009

58. Schott DS, Pizon M, Pachmann U, Pachmann K. Sensitive detection of PD-L1 expression on circulating epithelial tumor cells (CETCs) could be a potential biomarker to select patients for treatment with PD-1/PD-L1 inhibitors in early and metastatic solid tumors. *Oncotarget* (2017) 8:72755. doi: 10.18632/oncotarget.20346

59. Jacot W, Mazel M, Mollevi C, Pouderoux S, D'Hondt V, Cayrefourcq L, et al. Clinical correlations of programmed cell death ligand 1 status in liquid and standard biopsies in breast cancer. *Clin Chem* (2020) 66:1093–101. doi: 10.1093/clinchem/hvaa121

60. Xie F, Xu M, Lu J, Mao L, Wang S. The role of exosomal PD-L1 in tumor progression and immunotherapy. *Mol Cancer* (2019) 18:1–10. doi: 10.1186/s12943-019-1074-3

61. Yang Y, Li C-W, Chan L-C, Wei Y, Hsu J-M, Xia W, et al. Exosomal PD-L1 harbors active defense function to suppress T cell killing of breast cancer cells and promote tumor growth. *Cell Res* (2018) 28:862–4. doi: 10.1038/s41422-018-0060-4

62. Agelaki S, Papadaki MA, Tsoulfas PG, Aggouraki D, Monastirioti AA, Merodoulaki KA, et al. Role of the expression of PD-L1 and CD47 on circulating tumor cells (CTCs) in the prediction of outcome in metastatic breast cancer (mBC) patients. *Am Soc Clin Oncol* (2019) 37(15_suppl):e14045. doi: 10.1200/JCO.2019.37.15_suppl.e14045

63. Nicolazzo C, Raimondi C, Mancini M, Caponnetto S, Gradilone A, Gandini O, et al. Monitoring PD-L1 positive circulating tumor cells in non-small cell lung cancer patients treated with the PD-1 inhibitor Nivolumab. *Sci Rep* (2016) 6:31726. doi: 10.1038/srep31726

64. Strati A, Koutsodontis G, Papaxoinis G, Angelidis I, Zavridou M, Economopoulou P, et al. Prognostic significance of PD-L1 expression on circulating tumor cells in patients with head and neck squamous cell carcinoma. *Ann Oncol* (2017) 28:1923–33. doi: 10.1093/annonc/mdx206

65. Raimondi L, Raimondi FM, Di Benedetto L, Cimino G, Spinelli GP. PD-L1 expression on circulating tumour cells may be predictive of response to regorafenib in patients diagnosed with chemorefractory metastatic colorectal cancer. *Int J Mol Sci* (2020) 21:6907. doi: 10.3390/ijms21186907

66. Xu Y, Song G, Xie S, Jiang W, Chen X, Chu M, et al. The roles of PD-1/PD-L1 in the prognosis and immunotherapy of prostate cancer. *Mol Ther* (2021) 29:1958–69. doi: 10.1016/j.ymthe.2021.04.029

67. Wang Y, Xu Y, Feng A, Wen Q, Shi X, Zhang S, et al. Comprehensive analysis and potential clinical applications of immunotherapy-related biomarkers in Chinese patients with pancreatic adenocarcinoma. *Cancer Res* (2022) 82:5753–. doi: 10.1158/1538-7445.AM2022-5753

68. Papadaki MA, Koutsopoulos AV, Tsoulfas PG, Lagoudaki E, Aggouraki D, Monastirioti A, et al. Clinical relevance of immune checkpoints on circulating tumor cells in breast cancer. *Cancers* (2020) 12:376. doi: 10.3390/cancers12020376

69. Raimondi C, Carpino G, Nicolazzo C, Gradilone A, Gianni W, Gelibter A, et al. PD-L1 and epithelial-mesenchymal transition in circulating tumor cells from non-small cell lung cancer patients: a molecular shield to evade immune system? *Oncoimmunology* (2017) 6:e1315488. doi: 10.1080/2162402X.2017.1315488

70. Asgarova A, Asgarov K, Godet Y, Peixoto P, Nadaradjane A, Boyer-Guittaut M, et al. PD-L1 expression is regulated by both DNA methylation and NF-kB during EMT signaling in non-small cell lung carcinoma. *Oncoimmunology* (2018) 7:e1423170. doi: 10.1080/2162402X.2017.1423170

71. Qu Q-X, Huang Q, Shen Y, Zhu Y-B, Zhang X-G. The increase of circulating PD-L1-expressing CD68+ macrophage in ovarian cancer. *Tumor Biol* (2016) 37:5031–7. doi: 10.1007/s13277-015-4066-y

72. Adams DL, Adams DK, He J, Kalhor N, Zhang M, Xu T, et al. Sequential tracking of PD-L1 expression and RAD50 induction in circulating tumor and stromal cells of lung cancer patients undergoing radiotherapy. *Clin Cancer Res* (2017) 23:5948–58. doi: 10.1158/1078-0432.CCR-17-0802

73. Lux A, Kahlert C, Grützmann R, Pilarsky C. c-Met and PD-L1 on circulating exosomes as diagnostic and prognostic markers for pancreatic cancer. *Int J Mol Sci* (2019) 20:3305. doi: 10.3390/ijms20133305

74. Li C, Li C, Zhi C, Liang W, Wang X, Chen X, et al. Clinical significance of PD-L1 expression in serum-derived exosomes in NSCLC patients. *J Trans Med* (2019) 17:1–10. doi: 10.1186/s12967-019-2101-2

75. Krueger K, Mayer Z, Gerckens M, Boeck S, Luppa P, Holdenrieder S. High quality performance of novel immunoassays for the sensitive quantification of soluble PD-1, PD-L1 and PD-L2 in blood. *Biomedicines* (2022) 10:2405. doi: 10.3390/biomedicines10102405

76. Li Y, Cui X, Yang Y-J, Chen Q-Q, Zhong L, Zhang T, et al. Serum sPD-1 and sPD-L1 as biomarkers for evaluating the efficacy of neoadjuvant chemotherapy in triple-negative breast cancer patients. *Clin Breast Cancer* (2019) 19:326–32. e1. doi: 10.1016/j.clbc.2019.03.008

77. Elashi AA, Sasidharan Nair V, Taha RZ, Shaath H, Elkord E. DNA methylation of immune checkpoints in the peripheral blood of breast and colorectal cancer patients. *Oncoimmunology* (2019) 8:e1542918. doi: 10.1080/2162402X.2018.1542918

78. Guo L, Cao C, Goswami S, Huang X, Ma L, Guo Y, et al. Tumoral PD-1hiCD8+ T cells are partially exhausted and predict favorable outcome in triple-negative breast cancer. *Clin Sci* (2020) 134:711–26. doi: 10.1042/CS20191261

79. Jardim DL, Goodman A, de Melo Gagliato D, Kurzrock R. The challenges of tumor mutational burden as an immunotherapy biomarker. *Cancer Cell* (2021) 39:154–73. doi: 10.1016/j.ccell.2020.10.001

80. Nguyen A, Garner C, Reddy SK, Sanborn JZ, Benz SC, Seery TE, et al. Three-fold overestimation of tumor mutation burden using 248 gene panel versus whole exome. *Am Soc Clin Oncol* (2018) 36(15_suppl):12117. doi: 10.1200/JCO.2018.36.15_suppl.12117

81. Thompson JR, Menon SP. Liquid biopsies and cancer immunotherapy. *Cancer J* (2018) 24:78–83. doi: 10.1097/PPO.0000000000000307

82. Koeppel F, Blanchard S, Jovelet C, Genin B, Marcaillou C, Martin E, et al. Whole exome sequencing for determination of tumor mutation load in liquid biopsy from advanced cancer patients. *PloS One* (2017) 12:e0188174. doi: 10.1371/journal.pone.0188174

83. Wen Q, Yang Z, Dai H, Feng A, Li Q. Radiomics study for predicting the expression of PD-L1 and tumor mutation burden in non-small cell lung cancer based on CT images and clinicopathological features. *Front Oncol* (2021) 11:620246. doi: 10.3389/fonc.2021.620246

84. Gandara DR, Paul SM, Kowanetz M, Schleifman E, Zou W, Li Y, et al. Blood-based tumor mutational burden as a predictor of clinical benefit in non-small-cell lung cancer patients treated with atezolizumab. *Nat Med* (2018) 24:1441–8. doi: 10.1038/s41591-018-0134-3

85. Barroso-Sousa R, Jain E, Cohen O, Kim D, Buendia-Buendia J, Winer E, et al. Prevalence and mutational determinants of high tumor mutation burden in breast cancer. *Ann Oncol* (2020) 31:387–94. doi: 10.1016/j.annonc.2019.11.010

86. Barroso-Sousa R, Keenan TE, Pernas S, Exman P, Jain E, Garrido-Castro AC, et al. Tumor mutational burden and PTEN alterations as molecular correlates of response to PD-1/L1 blockade in metastatic triple-negative breast cancer. *Clin Cancer Res* (2020) 26:2565–72. doi: 10.1158/1078-0432.CCR-19-3507

87. Ke L, Li S, Cui H. The prognostic role of tumor mutation burden on survival of breast cancer: a systematic review and meta-analysis. *BMC Cancer* (2022) 22:1–12. doi: 10.1186/s12885-022-10284-1

88. Ravaioli S, Limarzi F, Tumedei MM, Palleschi M, Maltoni R, Bravaccini S. Are we ready to use TMB in breast cancer clinical practice? *Cancer Immunology Immunotherapy* (2020) 69:1943–5. doi: 10.1007/s00262-020-02682-w

89. Xu J, Guo X, Jing M, Sun T. Prediction of tumor mutation burden in breast cancer based on the expression of ER, PR, HER-2, and Ki-67. *OncoTargets Ther* (2018) 11:2269–75. doi: 10.2147/OTT.S159830

90. Fridland S, Choi J, Nam M, Schellenberg SJ, Kim E, Lee G, et al. Assessing tumor heterogeneity: integrating tissue and circulating tumor DNA (ctDNA) analysis in the era of immuno-oncology-blood TMB is not the same as tissue TMB. *J immunotherapy Cancer* (2021) 9:002551–9. doi: 10.1136/jitc-2021-002551

91. Jiricny J. The multifaceted mismatch-repair system. *Nat Rev Mol Cell Biol* (2006) 7:335–46. doi: 10.1038/nrm1907

92. Le DT, Uram JN, Wang H, Bartlett BR, Kemberling H, Eyring AD, et al. PD-1 blockade in tumors with mismatch-repair deficiency. *New Engl J Med* (2015) 372:2509–20. doi: 10.1056/NEJMoa1500596

93. Prasad V, Kaestner V, Mailankody S. Cancer drugs approved based on biomarkers and not tumor type—FDA approval of pembrolizumab for mismatch repair-deficient solid cancers. *JAMA Oncol* (2018) 4:157–8. doi: 10.1001/jamaoncol.2017.4182

94. Bonneville R, Krook MA, Kautto EA, Miya J, Wing MR, Chen H-Z, et al. Landscape of microsatellite instability across 39 cancer types. *JCO Precis Oncol* (2017) 1:1–15. doi: 10.1200/PO.17.00073

95. Cheng AS, Leung SC, Gao D, Burugu S, Anurag M, Ellis MJ, et al. Mismatch repair protein loss in breast cancer: clinicopathological associations in a large British Columbia cohort. *Breast Cancer Res Treat* (2020) 179:3–10. doi: 10.1007/s10549-019-05438-y

96. Haricharan S, Bainbridge MN, Scheet P, Brown PH. Somatic mutation load of estrogen receptor-positive breast tumors predicts overall survival: an analysis of genome sequence data. *Breast Cancer Res Treat* (2014) 146:211–20. doi: 10.1007/s10549-014-2991-x

97. Fremd C, Hlevnjak M, Zapatka M, Zoernig I, Halama N, Fejzibegovic N, et al. Mismatch repair deficiency drives durable complete remission by targeting programmed death receptor 1 in a metastatic luminal breast cancer patient. *Breast Care* (2019) 14:53–9. doi: 10.1159/000492580

98. Dinan MA, Lyman GH, Schilsky RL, Hayes DF. Proposal for value-based, tiered reimbursement for tumor biomarker tests to promote innovation and evidence generation. *JCO Precis Oncol* (2019) 3:1–10. doi: 10.1200/PO.19.00210

99. Mayrhofer M, De Laere B, Whitington T, Van Oyen P, Ghysel C, Ampe J, et al. Cell-free DNA profiling of metastatic prostate cancer reveals microsatellite instability, structural rearrangements and clonal hematopoiesis. *Genome Med* (2018) 10:1–13. doi: 10.1186/s13073-018-0595-5

100. Jensen TJ, Goodman AM, Kato S, Ellison CK, Daniels GA, Kim L, et al. Genome-wide sequencing of cell-free DNA identifies copy-number alterations that can be used for monitoring response to immunotherapy in cancer patients. *Mol Cancer Ther* (2019) 18:448–58. doi: 10.1158/1535-7163.MCT-18-0535

101. Weiss GJ, Beck J, Braun DP, Bornemann-Kolatzki K, Barilla H, Cubello R, et al. Tumor cell–free DNA copy number instability predicts therapeutic response to

immunotherapy. *Clin Cancer Res* (2017) 23:5074–81. doi: 10.1158/1078-0432.CCR-17-0231

102. Georgiadis A, Durham JN, Keefer LA, Bartlett BR, Zielonka M, Murphy D, et al. Noninvasive detection of microsatellite instability and high tumor mutation burden in cancer patients treated with PD-1 blockade. *Clin Cancer Res* (2019) 25:7024–34. doi: 10.1158/1078-0432.CCR-19-1372

103. Schumacher TN, Schreiber RD. Neoantigens in cancer immunotherapy. *Science* (2015) 348:69–74. doi: 10.1126/science.aaa4971

104. Rosati E, Dowds CM, Liaskou E, Henriksen EKK, Karlsen TH, Franke A. Overview of methodologies for T-cell receptor repertoire analysis. *BMC Biotechnol* (2017) 17:1–16. doi: 10.1186/s12896-017-0379-9

105. Gibney GT, Weiner LM, Atkins MB. Predictive biomarkers for checkpoint inhibitor-based immunotherapy. *Lancet Oncol* (2016) 17:e542–e51. doi: 10.1016/S1470-2045(16)30406-5

106. Lin K-R, Pang D-M, Jin Y-B, Hu Q, Pan Y-M, Cui J-H, et al. Circulating CD8+ T-cell repertoires reveal the biological characteristics of tumors and clinical responses to chemotherapy in breast cancer patients. *Cancer Immunology Immunotherapy* (2018) 67:1743–52. doi: 10.1007/s00262-018-2213-1

107. Gao H, Kida K, Cohen EN, Alexander A, Lim B, Parker , et al. Abstract P3-09-12: Peripheral T cell clonality and exhaustion as novel biomarkers for anti-PD-1 (pembrolizumab) maintenance therapy in patients with metastatic inflammatory breast cancer (mIBC) and non-IBC triple negative breast cancer (mTNBC). *Cancer Res* (2020) 80:P3–09-12-P3-09-12. doi: 10.1158/1538-7445.SABCS19-P3-09-12

108. Cristiano S, Leal A, Phallen J, Fiksel J, Adleff V, Bruhm DC, et al. Genome-wide cell-free DNA fragmentation in patients with cancer. *Nature* (2019) 570:385–9. doi: 10.1038/s41586-019-1272-6

109. Liu MC, Oxnard G, Klein E, Swanton C, Seiden M, Liu MC, et al. Sensitive and specific multi-cancer detection and localization using methylation signatures in cell-free DNA. *Ann Oncol* (2020) 31:745–59. doi: 10.1016/j.annonc.2020.02.011

110. Snyder MW, Kircher M, Hill AJ, Daza RM, Shendure J, et al. Cell-free DNA comprises an in *vivo* nucleosome footprint that informs its tissues-of-origin. *Cell* (2016) 164:57–68. doi: 10.1016/j.cell.2015.11.050

111. Ulz P, Perakis S, Zhou Q, Moser T, Belic J, Lazzeri I, et al. Inference of transcription factor binding from cell-free DNA enables tumor subtype prediction and early detection. *Nat Commun* (2019) 10:4666. doi: 10.1038/s41467-019-12714-4

112. Goodman AM, Holden KA, Jeong A-R, Kim L, Fitzgerald KD, Almasri E, et al. Assessing CAR T-cell therapy response using genome-wide sequencing of cell-free DNA in patients with B-cell lymphomas. *Transplant Cell Ther* (2022) 28:30. e1–. e7. doi: 10.1016/j.jtct.2021.10.007

113. Bidard F-C, Peeters DJ, Fehm T, Nolé F, Gisbert-Criado R, Mavroudis D, et al. Clinical validity of circulating tumour cells in patients with metastatic breast cancer: a pooled analysis of individual patient data. *Lancet Oncol* (2014) 15:406–14. doi: 10.1016/S1470-2045(14)70069-5

114. Magbanua MJM, Hendrix LH, Hyslop T, Barry WT, Winer EP, Hudis C, et al. Serial analysis of circulating tumor cells in metastatic breast cancer receiving first-line chemotherapy. *JNCI: J Natl Cancer Institute* (2021) 113:443–52. doi: 10.1093/jnci/djaa113

115. Underhill HR, Kitzman JO, Hellwig S, Welker NC, Daza R, Baker DN, et al. Fragment length of circulating tumor DNA. *PloS Genet* (2016) 12:e1006162. doi: 10.1371/journal.pgen.1006162

116. Cohen JD, Li L, Wang Y, Thoburn C, Afsari B, Danilova L, et al. Detection and localization of surgically resectable cancers with a multi-analyte blood test. *Science* (2018) 359:926–30. doi: 10.1126/science.aar3247

117. Douville C, Springer S, Kinde I, Cohen JD, Hruban RH, Lennon AM, et al. Detection of aneuploidy in patients with cancer through amplification of long interspersed nucleotide elements (LINEs). *Proc Natl Acad Sci* (2018) 115:1871–6. doi: 10.1073/pnas.1717846115

118. Kirkizlar E, Zimmermann B, Constantin T, Swenerton R, Hoang B, Wayham N, et al. Detection of clonal and subclonal copy-number variants in cell-free DNA from patients with breast cancer using a massively multiplexed PCR methodology. *Trans Oncol* (2015) 8:407–16. doi: 10.1016/j.tranon.2015.08.004

119. Shen SY, Singhania R, Fehringer G, Chakravarthy A, Roehrl MH, Chadwick D, et al. Sensitive tumour detection and classification using plasma cell-free DNA methylomes. *Nature* (2018) 563:579–83. doi: 10.1038/s41586-018-0703-0

120. Poore GD, Kopylova E, Zhu Q, Carpenter C, Fraraccio S, Wandro S, et al. Microbiome analyses of blood and tissues suggest cancer diagnostic approach. *Nature* (2020) 579:567–74. doi: 10.1038/s41586-020-2095-1

121. Guo L, Kong D, Liu J, Zhan L, Luo L, Zheng W, et al. Breast cancer heterogeneity and its implication in personalized precision therapy. *Exp Hematol Oncol* (2023) 12:1–27. doi: 10.1186/s40164-022-00363-1

frontiers | Frontiers in Oncology

TYPE Review
PUBLISHED 27 November 2023
DOI 10.3389/fonc.2023.1272788

OPEN ACCESS

EDITED BY
Alberto Traverso,
Maastro Clinic, Netherlands

REVIEWED BY
Ming Yi,
Zhejiang University, China
Barani Kumar Rajendran,
Yale University, United States

*CORRESPONDENCE
Lijian Zhang
lijian.zhang@aliyun.com
Chunhui Li
lichunhui0860312@sina.com
Chuan Fang
chuanfang@hbu.edu.cn

†These authors have contributed equally to this work

RECEIVED 19 September 2023
ACCEPTED 03 November 2023
PUBLISHED 27 November 2023

CITATION
Zhao H, Wang L, Fang C, Li C and Zhang L (2023) Factors influencing the diagnostic and prognostic values of circulating tumor cells in breast cancer: a meta-analysis of 8,935 patients. *Front. Oncol.* 13:1272788. doi: 10.3389/fonc.2023.1272788

Factors influencing the diagnostic and prognostic values of circulating tumor cells in breast cancer: a meta-analysis of 8,935 patients

Hongfang Zhao[1,2†], Luxuan Wang[3†], Chuan Fang[1,2,3,4,5*], Chunhui Li[1,2,3,5*] and Lijian Zhang[1,2,3,4,5*]

[1]Clinical Medicine College, Hebei University, Baoding, China, [2]Department of Neurosurgery, Affiliated Hospital of Hebei University, Baoding, China, [3]Department of Neurological Function Examination, Affiliated Hospital of Hebei University, Baoding, China, [4]Postdoctoral Research Station of Neurosurgery, Affiliated Hospital of Hebei University, Hebei University, Baoding, China, [5]Key Laboratory of Precise Diagnosis and Treatment of Glioma in Hebei Province, Affiliated Hospital of Hebei University, Hebei University, Baoding, China

Background: Circulating tumor cells (CTCs) could serve as a predictive biomarker in breast cancer (BC). Due to its high heterogeneity, the diagnostic and prognostic values of CTC are challenging.

Methods: We searched published studies from the databases of PubMed, Cochrane Library, Embase, and MEDLINE. The detection capability and hazard ratios (HRs) of CTCs were extracted as the clinical diagnosis and prognosis evaluation. Subgroup analyses were divided according to the detection methods, continents, treatment periods, therapeutic plans, and cancer stages.

Results: In this study, 35 publications had been retrieved with 8,935 patients enrolled. The diagnostic efficacy of CTC detection has 74% sensitivity and 98% specificity. The positive CTC detection (CTC^+) would predict worse OS and PFS/DFS in both mid-therapy and post-therapy (HR_{OS}, 3.09; 95% CI, 2.17–4.39; $HR_{PFS/DFS}$, 2.06; 95% CI, 1.72–2.47). Moreover, CTC^+ indicated poor survival irrespective of the treatment phases and sampling times (HR_{OS}, 2.43; 95% CI, 1.85–3.19; $HR_{PFS/DFS}$, 1.82; 95% CI, 1.66–1.99). The CTC^+ was associated with poor survival regardless of the continents of patients (HR_{OS} = 2.43; 95% CI, 1.85–3.19).

Conclusion: Our study suggested that CTC^+ was associated with a worse OS and PFS/DFS in the Asian population. The detection method, the threshold level of CTC^+, therapeutic approaches, and sampling times would not affect its diagnostic and prognostic values.

KEYWORDS

heterogeneity, circulating tumor cell, breast cancer, diagnosis, prognostic value

Background

Breast cancer (BC) is the most common cancer and will be the primary leading cause of cancer-related mortality for women in the future (1, 2). Imaging and clinicopathological information are the traditional methods for diagnosis and prognosis assessment (3). However, those evaluations could not reflect the BC condition in real time. Thus, it is difficult to assign optimal treatments (4, 5). Therefore, there is considerable interest in developing more accurate and convenient methods for diagnosis and prognosis assessment.

Liquid biopsy has been considered as a non-invasive approach and utilized comprehensively in cancer research (6). The common analytes of liquid biopsy include circulating tumor cells (CTCs), circulating tumor DNA (ctDNA), and extracellular vesicles (7). CTCs are tumor cells which are shed from the primary cancers or secondary tumors. It could enter into the circulation system and cause secondary cancer formations consequently (8). Previous evidence showed that CTCs could represent tumor progression (9–11). Furthermore, the positive detection of CTCs (CTC^+) in the circulation system could evaluate the survival of the patients (12). There has been an increasing number of literature emphasizing the potential of CTCs having an important role in diagnosis, prognosis, and therapeutic effect assessment in clinical settings (13–16).

Several meta-analyses have explored the relationships between CTC^+ and cancer outcomes. In their study involving 2,957 patients from 27 cohorts, Jin and his colleagues revealed that CTCs indicated poor prognoses universally in lung cancers (14). Current studies also showed similar outcomes in hepatocellular carcinoma and pancreatic cancer (15, 16). Although the prognostic and predictive values of CTCs have been verified in many studies, some results were controversial (17). Further investigations are required to identify the factors that influence the diagnostic and prognostic value of CTC^+. Additionally, there is a lack of sufficient research on the diagnostic and prognostic values of CTCs in BC, particularly in relation to the detection methods, therapeutic approaches, and cancer stages (18). Thus, the aims of our study are to investigate the factors that influence CTC^+ and to analyze their associations with overall survival (OS), progression-free survival (PFS), and disease-free survival (DFS) of BC patients.

Methods

This study was prospectively registered in PROSPERO on 08 December 2022 (CRD42022379387) (19) and was performed based on the PRISMA reporting guidelines (Supplementary Tables 1, 2).

Retrieval strategy and eligibility criteria

The systematic review of the English language articles was conducted based on the PubMed, Cochrane Library, Embase, and MEDLINE databases from 1 January 1970 to 27 April 2023. The detailed search strategies are exhibited in Supplementary Table 3. The inclusion criteria were as follows: 1) the clinical sample sources were the peripheral blood samples; 2) the studies provide data of true-positive and false-positive rates for diagnosis detection (3); OS or PFS/DFS was reported as HR of univariate Cox analysis and the 95% confidence interval (CI) was considered valid data; and 4) the patients had BC, whether it had metastasized or not. Both prospective and retrospective observational cohort studies were eligible for inclusion.

Data extraction

A standard table was constructed for information extraction. Two authors (HF and LX) conducted an independent literature review and recorded their findings. In order to control for selection bias, the authors compared their extracted data at the end of the revision process and resolved any disparities. Duplicate items were removed. If they could not solve the differences, a senior researcher (LJ) performed the data extraction again.

Main outcomes and study quality assessment

The purpose of this study was to evaluate the diagnostic efficiency of CTC detection and the prognostic value of CTCs. Firstly, we evaluated the quality of all the diagnostic test studies according to the Quality Assessment of Diagnosis Accuracy Studies-2. Secondly, the Newcastle-Ottawa Scale was used to assess the quality of the studies included in the prognosis analysis (20). This scale awarded points based on patient selection (maximum of 4 points), outcome assessment (maximum of 3 points), and comparability of the cohort (maximum of 2 points), with a maximum total of 9 points. The risk of bias was conducted using the Risk of Bias in Non-Randomized Studies of Intervention (Cochrane Bias Methods Group) (21). Publication bias was verified by funnel plot.

Statistical analysis

The statistical analysis was performed using Stata (Version 12.0). Sensitivity, specificity, and area under the curve were regarded as the gauge of diagnostic analysis. Meanwhile, outcome data were reported as HRs in the prognosis analysis. An HR that exceeds 1 indicated a worse outcome. A higher HR value indicated a poorer prognosis. We estimated study heterogeneity using I^2 statistics, where greater than 50% was considered significant heterogeneity ($I^2 > 50\%$). It was preferred to use a fixed-effects model in the absence of significant heterogeneity and a random-effects model in the presence of significant heterogeneity. The *P*-values reported were two-sided, and statistical significance was set at $P < 0.05$.

Results

Study characteristics for diagnostic and prognostic value analyses

In this study, the articles were selected according to the diagnostic and prognostic roles of CTCs. There were 1,102 articles obtained from four databases for diagnostic analysis. In order to obtain a comprehensive selection, the full texts of the initially included articles were read entirely. Eight hundred twenty-six studies were unsuitable for inclusion because of duplicate publication. Furthermore, 19 articles were excluded due to missing information, special CTC types, and multivariate Cox which might influence the entire result. Thirty-five articles (8,935 patients) were included after the selection procedure (Figure 1). The main features of the eligible studies are summarized in Tables 1, 2 (12, 22–55). The QUADAS-2 revised tool and the Newcastle-Ottawa scale were utilized to assess the biases and qualities in the meta-analysis procedure (Supplementary Tables 3-6).

The diagnostic performance of CTC detection

Among the 12 included studies, 7 studies investigated the diagnostic efficacy of CTC detection for all cancer stages, 4 studies mainly focused on the metastatic stage, and 1 study did not provide information on the cancer stage. The results showed a high diagnostic efficacy of CTC detection with 0.74 sensitivity (95% CI, 0.65–0.81) and 0.98 specificity (95% CI, 0.88–1.00). The diagnostic score and odds ratio were 4.85 and 127.17, respectively (Figure 2A). Positive and negative diagnostic likelihood ratios (DLRs) were 33.96 and 0.27 (Figure 2B). Remarkably, the Fogan diagram indicated that an individual who tested positive with a CTC test had a 97% chance of developing BC (Figure 2C). This indicated that the detection methods had good effectiveness for CTCs. The summary receiver operating characteristic curves (SROCs) showed an area under the curve of 0.89 (95% CI, 0.86–0.91). Combined with the diagnostic odds ratio, the result also provided evidence of the values of those CTC detection methods

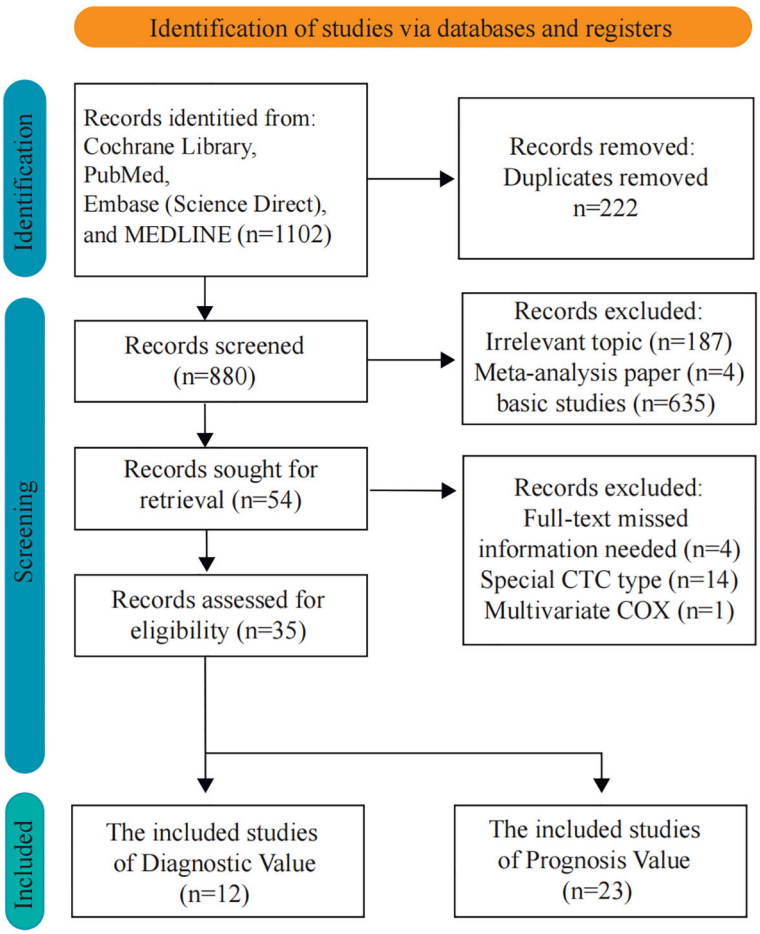

FIGURE 1
Flow diagram of the study selection for the present meta-analysis.

TABLE 1 Articles included in the diagnostic meta-analysis.

Study	First author of the study (ref.), year	Country	Cancer stage	No. of patients	Detection	TP	FP	FN	TN
1	Riethdorf et al., 2007 (22)	Germany	MBC	237	CellSearch System	53	8	29	137
2	Sawada et al., 2016 (23)	Japan	MBC	42	Fluidic cell microarray chip system	17	9	5	11
3	Sheng et al., 2017 (24)	China	N/A	55	Immunostaining-fluorescence *in-situ* hybridization	41	0	4	10
4	Li et al., 2017 (25)	China	MBC	190	CellCollector	95	0	32	63
5	Jin et al., 2020 (26)	China	ALL	157	CytoSorter system	109	1	19	28
6	Li et al., 2018 (27)	China	ALL	119	NE-FISH platform	85	7	14	13
7	Li et al., 2013 (28)	China	ALL	103	IMPs + ICC	42	0	36	25
8	Weissenstein et al., 2012 (29)	Switzerland	ALL	69	Combination of cytokeratin and EpCAM antibodies	39	0	20	10
9	Zhang et al., 2021 (30)	China	ALL	179	A label-free microfluidic chip	95	9	34	41
10	Kim et al., 2011 (31)	Japan	ALL	77	Telomerase-specific replication-selective adenovirus	21	0	29	80
11	Chen et al., 2010 (32)	China	ALL	100	A three-marker (CK19, hMAM, and CEA) RT-PCR assay	47	1	33	19
12	Zhao et al., 2013 (33)	China	MBC	158	A three-marker (CK19, hMAM, and CEA) RT-PCR assay	86	0	12	60

ICC, immunocytochemistry; IMPs, immunomagnetic nanoparticles; NE-FISH, negative enrichment-fluorescence in-situ hybridization; RT-PCR, reverse transcription-polymerase chain reaction; EpCAM, epithelial cell adhesion molecule; CK 19, cytokeratin 19; hMAM, human mammaglobin; CEA, carcinoembryonic antigen-positive.

(Supplementary Figures S1A, B). Heterogeneity was significant in these analyses ($I^2 > 50\%$). However, the funnel plot asymmetry test with linear regression indicated a non-significant publication bias in the meta-analysis ($P = 0.37$) (Supplementary Figure S1C). Thus, we performed a metaregression analysis and showed that continent was the potential source of heterogeneity. Our subgroup analysis indicated that specificity would be higher in Chinese patients (Supplementary Table 7).

Factors that influence the association between CTC and poor prognosis

In order to identify the factors that influence the CTC^+ prognosis value, the variables were examined in the metaregression, including publication year, sample size, age, continent, detection method, CTC^+ definition, tumor stage, therapeutic regimen, sampling time, and follow-up time (Supplementary Table 8). Our results showed that the detection method and continent were the major elements of the heterogeneity in the pooled HR_{OS} and $HR_{PFS/DFS}$ ($P = 0.01$). Then, we divided the subgroups and analyzed them according to the differences in the detection method and continent.

Previous studies demonstrated that the CellSearch System was the most used detection system for CTC detection (56). More recently, researchers have combined two systems/methods for detection, namely, immunomagnetic nanospheres (IMNs) and reverse transcription-polymerase chain reaction (RT-PCR), to improve the significance of the CTC prognostic value. Those studies were classified and analyzed as another subset in the subgroup analysis, which was named the Not CellSearch System subset (Figure 3). The calculated analysis revealed that CTC^+ was associated with poor survival and could be regarded as a high-risk biomarker (HR_{OS}, 2.43; 95% CI, 1.85–3.19; $HR_{PFS/DFS}$, 1.82; 95% CI, 1.66–1.99) (Figures 3A, B; Table 3). The overall heterogeneity was significant in the OS analysis ($I^2 = 75.5\%$). We suspected that heterogeneity might come from the Not CellSearch System subset ($I^2 = 89.2\%$); however, publication bias did not exist in this subset ($P_{Begg} > 0.05$; $P_{Egger} = 0.652$) (Supplementary Figures S2A, B; Table 4). The one-way sensitivity analysis considered that the exclusion of any article did not affect the entire outcome (Supplementary Figure S2C). The trim-and-fill analysis suggested that one study might be missed and that if it were published, the relationship would not be reversed (the adjusted HR, 0.99; 95% CI, 0.351–2.724, Supplementary Figure S2D; Table 3). Furthermore, the association between CTC^+ and poor OS would be obvious if the CellSearch System was utilized as the detection system in the clinical trial (HR = 2.74; 95% CI, 2.30–3.28).

The different detection methods implied that variations existed in the threshold levels. Thus, we performed a subgroup analysis for the CTC^+ definition according to the different threshold levels. The pooled results suggested that CTC^+ was a stable prognosticator in poor survival assessment (HR_{OS}, 2.43; 95% CI, 1.85–3.19; $HR_{PFS/DFS}$, 1.82; 95% CI, 1.66–1.99) (Figures 4A, B; Table 3). The overall heterogeneity was significant in the PFS/DFS subgroup ($I^2 = 75.5\%$). The publication bias, one-way sensitivity, and the trim-and-fill analysis demonstrated that the results were reliable and not reversed (the adjusted HR, 1.68) (Supplementary Figure S2E–H; Table 4). When the CTC^+ was defined as 1 CTC per 7.5 mL, the poor PFS/DFS was significantly associated with CTC^+ (HR, 2.04;

TABLE 2 Characteristics of the studies included in the meta-analysis.

Study ID	First author of the study, year	Country	Continent	No. of patients	Age	Cancer stage	Sampling time	Detection system[a]	CTC$^+$ definition[b]
1	Radovich M, 2020 (34)	Indianapolis	America	123	49.6	Early	Mid-therapy	CellSearch System	1 per 7.5 ml
2	Massimo Cristofanilli, 2004 (35)	America	America	177	58	Advanced	Post-therapy	CellSearch System	5 per 7.5 ml
3	François-Clément Bidard, 2021 (36)	France	Europe	377	64	Advanced	Mid-therapy	CellSearch System	5 per 7.5 ml
4	Halle C.F. Moore, 2021 (37)	America	America	37	N/A	Advanced	Baseline	CellSearch System and HD-SCA assay	5 per 7.5 ml
5	Jeffrey B Smerage, 2014 (38)	America	America	288	N/A	Advanced	Post-therapy	CellSearch System	5 per 7.5 ml
6	Elisabeth Trapp, 2018 (39)	Germany	Europe	1087	53	Early	Post-therapy	CellSearch System	1 per 7.5 ml
7	Shunyun Pang, 2021 (40)	China	Asian	110	52.7	ALL	Baseline	Immunomagnetic nanospheres (IMNs)	19 per 7.5 ml
8	Markus Wallwiener, 2012 (41)	Germany	Europe	486	55	Advanced	Baseline	CellSearch System	5 per 7.5 ml
9	Carolyn S Hall, 2016 (42)	America	America	509	53	Early	Baseline	CellSearch System	1 per 7.5 ml
10	Jean-Marie Ramirez, 2014 (43)	Germany	Europe	254	60	Advanced	Baseline	EPISPOT and CellSearch system	1 per 7.5 ml
11	William Jacot, 2019 (44)	France	Europe	150	N/A	Advanced	Mid-therapy	CellSearch System	5 per 7.5 ml
12	Jean-Yves Pierga, 2015 (45)	France	Europe	52	50.6	Early	Baseline	CellSearch System	1 per 7.5 ml
13	Julia Jueckstock, 2016 (46)	Germany	Europe	1221	53	Early	Baseline	Manually performed immunocytochemistry	1 per 23 ml
14	Daniel F Hayes, 2006 (47)	America	America	177	N/A	Advanced	Baseline	CellSearch System	5 per 7.5 ml
15	Zhaomei Mu, 2015 (48)	America	America	115	54.5	Advanced	Baseline	CellSearch System	5 per 7.5 ml
16	Brigitte Rack, 2014 (12)	Germany	Europe	2026	N/A	Early	Post-therapy	CellSearch System	1 per 30 ml
17	Anna-Maria Larsson, 2018 (49)	Sweden	Europe	152	65	Advanced	Baseline	CellSearch System	5 per 7.5 ml
18	Yuqin Yang, 2022 (50)	China	Asia	216	46	Early	Mid-therapy	Liquid Biopsy System	1 per 4 ml
19	Yukako Shiomi-Mouri, 2013 (51)	Japan	Asia	97	59	Advanced	Baseline	CellSearch System	1 per 7.5 ml
20	Shaheenah Dawood, 2008 (52)	America	America	185	49	Advanced	Baseline	CellSearch System	5 per 7.5 ml
21	Mandar Karhade, 2014 (53)	America	America	105	54	Early	Baseline	CellSearch System	1 per 7.5 ml
22	Morales S, 2018 (54)	Spain	Europe	67	59.6	Advanced	Mid-therapy	CellSearch System and RT-PCR methods	5 per 7.5 ml
23	Naoki Hayashi, 2011 (55)	Japan	Asia	49	54.1	Advanced	Mid-therapy	CellSearch System	5 per 7.5 ml

(Continued)

10.3389/fonc.2023.1272788

TABLE 2 Continued

Outcome[e]	CTC status[d]		HR (95% CI)		Materials		Anatomic stage	Histologic grade	Lymph node involvement
	–	+	PFS/DFS	OS	Therapy methods[e]	Follow-up time[f]	I–IV	I–III	Y/N
DFS/OS	73	50	1.68 (0.85–3.32)	2.3 (0.95–5.57)	Accepted surgery	<20 months	33/67/23/0	1/18/101	52/71
PFS/OS	60	20	2.52 (1.4532–4.3704)	6.49 (2.1303–19.7735)	Systemic therapy	<20 months	N/A	N/A	N/A
PFS	239	138	1.22 (0.97–1.54)	N/A	Chemotherapy	>20 months	N/A	N/A	N/A
PFS	27	7	1.4 (0.59–3.32)	N/A	Accepted surgery	>20 months	N/A	N/A	N/A
PFS/OS	165	123	2.13 (1.63–2.79)	1.94 (1.52–2.47)	Chemotherapy	<20 months	IV	N/A	N/A
DFS/OS	889	198	1.37 (0.86–2.17)	2.07 (1.01–4.24)	Chemotherapy	>20 months	N/A	58/528/501	365/718
PFS/OS	55	55	3.56 (1.86–6.82)	4.98 (2.06–12.02)	Accepted surgery	>20 months	19/38/18/20	N/A	N/A
PFS/OS	281	205	1.82 (1.41–2.34)	4.79 (2.95–7.79)	Systemic therapy	<20 months	IV	N/A	N/A
RFS/OS	385	124	2.72 (1.57–4.72)	2.29 (1.12–4.67)	Accepted surgery	>20 months	I-III	56/232/202	234/273
OS	132	122	N/A	0.386 (0.223–0.668)	Chemotherapy	N/A	N/A	N/A	N/A
PFS/OS	64	86	2 (1.4–2.8)	3.6 (2.3–5.8)	Chemotherapy	<20 months	IV	N/A	N/A
DFS	34	18	3.69 (1.34–10.21)	N/A	Accepted surgery	>20 months	IV	N/A	N/A
DFS/OS	970	251	1.25 (0.88–1.77)	1.47 (0.96–2.23)	Accepted surgery	>20 months	ALL	59/604/557	1122/422
PFS/OS	90	87	1.89 (1.37–2.61)	2.45 (1.64–3.65)	Systemic therapy	>20 months	IV	N/A	N/A
PFS	79	36	2.38 (1.44–3.95)	N/A	Systemic therapy	<20 months	0/0/12/103	N/A	N/A
PFS/OS	1,174	330	2.257 (1.595–3.195)	2.447 (1.491–4.015)	Chemotherapy	>20 months	N/A	N/A	N/A

(Continued)

10.3389/fonc.2023.1272788

TABLE 2 Continued

Outcome[e]	CTC status[d]		HR (95% CI)		Materials		Anatomic stage	Histologic grade	Lymph node involvement
	–	+	PFS/DFS	OS	Therapy methods[e]	Follow-up time[f]	I–IV	I–III	Y/N
PFS/OS	73	79	1.68 (1.17–2.42)	2.52 (1.58–4.01)	Systemic therapy	>20 months	N/A	13/65/46	44/92
OS	172	44	N/A	1.934 (0.607–6.168)	Chemotherapy	<20 months	52/124/40/0	N/A	N/A
OS	53	45	N/A	3.816 (1.839–7.917)	Chemotherapy	N/A	N/A	10/42/28	N/A
OS	114	71	N/A	3.1 (1.8–5.2)	Chemotherapy	N/A	22/59/43/56	N/A	71/77
PFS/OS	71	34	3.93 (1.55–9.94)	2.36 (0.84–6.65)	Accepted surgery	>20 months	N/A	4/15/92	62/51
PFS	39	38	2.18 (1.22–3.9)	N/A	Systemic therapy	N/A	N/A	N/A	N/A
PFS/OS	28	21	2.627 (1.161–5.946)	3.096 (1.313–7.302)	Systemic therapy	>20 months	N/A	N/A	N/A

ref., reference; CTC, circulating tumor cell; CTC^+, positive CTC detection; HR, hazard ratio; CI, confidence interval; OS, overall survival; PFS, progression-free survival; DFS, disease-free survival; RFS, relapse-free survival; N/A, not applicable; nMBC, non-metastatic breast cancer; MBC, metastasis breast cancer.

In order for the analysis to be successful:

[a]Except for the CellSearch System, other methods and combinations are deemed as "Not CellSearch System" in the meta-analysis.

[b]In addition to "1 per 7.5 ml" and "5 per 7.5 ml," other CTC^+ definitions are considered as "other CTC^+" in the meta-analysis.

[c]Based on the previous studies, the DFS/PFS/RFS could be regarded as the same data to calculate HR, and single data are not declared in the analysis.

[d]The number of samples detected by the detection methods was not the same as the population involved in the corresponding clinical trials; the "–" label meant that the CTC could not be detected by the detection methods, and vice versa.

[e]The detailed therapy information classified by the subgroups includes chemotherapy, accepted surgery, and systemic therapy (surgery + other treatment).

[f]The follow-up time is divided into "<20 months" and ">20 months." If the data could not be classified, it would be considered as "not applicable."

10.3389/fonc.2023.1272788

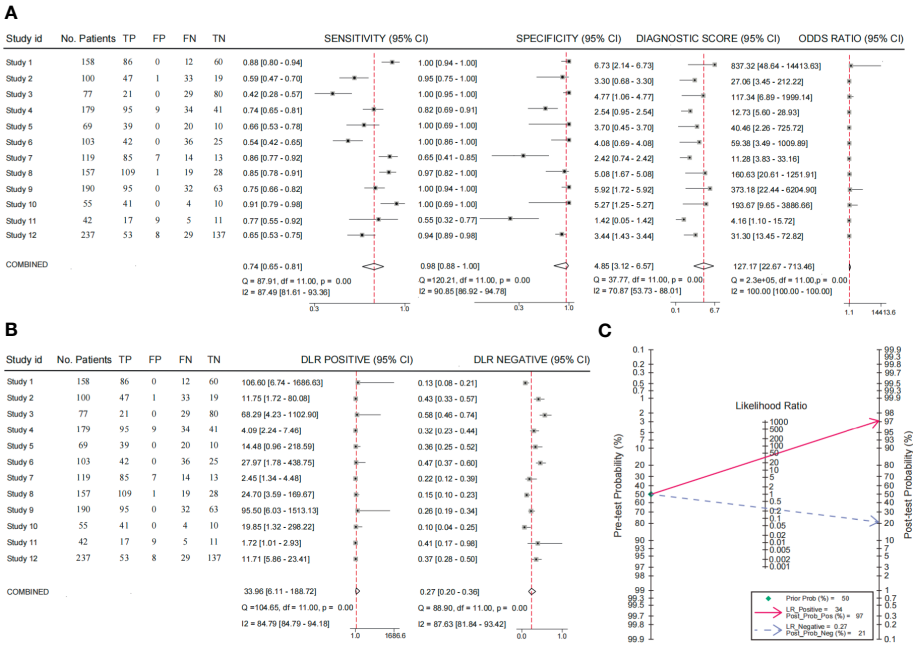

FIGURE 2
Analysis of the diagnostic values of CTC. **(A)** The sensitivity, specificity, diagnostic score, and odds ratio of CTCs for the diagnosis of BC; **(B)** the analysis of DLR positive and DLR negative; **(C)** the Fagan nomogram of the diagnostic values of CTCs.

95% CI, 1.53–2.72). Meanwhile, the CTC^+ was defined as 5 CTCs per 7.5 mL, and the poor OS was more significantly associated with CTC^+ (HR_{OS}, 2.96; 95% CI, 2.27–3.87).

Association of CTC^+ prognostic value in different continents

To identify another source of heterogeneity, we conducted a subgroup analysis, based on the difference of continents (Figure 5; Table 3). Our results showed that the relationship of CTC^+ with poor survival was not influenced by the different regions (HR_{OS} = 2.43; 95% CI, 1.85–3.19; $HR_{PFS/DFS}$ = 1.82; 95% CI, 1.66–1.99) (Figures 5A, B; Table 3). The heterogeneity was moderate in the PFS/DFS subgroup (I^2 = 49.1%). Furthermore, the heterogeneity might mainly come from the Europe subset (I^2 = 54.8%). However, publication bias did not exist (Supplementary Figures S2I, J; Table 4). The outcome was not changed in the one-way sensitivity analysis (Supplementary Figure S2K). The adjusted HR would be 1.512 after the trim-and-fill analysis (95% CI, 1.358–1.682) (Supplementary Figure S2L; Table 4). Compared with the subsets in the subgroup analyses, CTC^+ may be closely related to worse survival in Asian patients (HR_{OS}, 3.51; 95% CI, 2.27–5.42; $HR_{PFS/DFS}$, 3.16; 95% CI, 1.90–5.26).

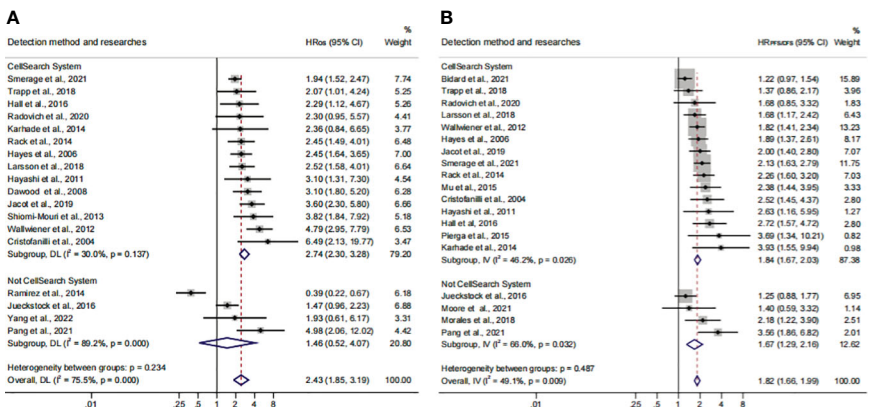

FIGURE 3
The subgroup analysis of detection methods in prognosis value. **(A)** The pooled HR_{OS} of the detection method; **(B)** the pooled $HR_{PFS/DFS}$ of the detection method.

TABLE 3 Summary of subgroup meta-analysis for CTC prognosis value evaluation.

Subgroup		HR_{OS} (95% CI)	$HR_{PFS/DFS}$ (95% CI)
Detection method and research	CellSearch System	2.74 (2.30, 3.28)	1.84 (1.67, 2.03)
	Not CellSearch System	1.46 (0.52, 4.07)	1.67 (1.29, 2.16)
CTC and research	1 per 7.5ml	1.79 (0.81, 3.93)	2.04 (1.53, 2.72)
	5 per 7.5ml	2.96 (2.27, 3.87)	1.78 (1.60, 1.98)
	Other CTC definition	2.26 (1.38, 3.71)	1.85 (1.47, 2.33)
Continent and research	Europe	2.00 (1.12, 3.58)	1.62 (1.44, 1.82)
	America	2.31 (1.90, 2.81)	2.15 (1.83, 2.52)
	Asian	3.51 (2.27, 5.42)	3.16 (1.90, 5.26)
Therapy and research	Chemotherapy	2.04 (1.27, 3.30)	1.69 (1.47, 1.93)
	Accepted surgery	2.23 (1.47, 3.40)	1.91 (1.52, 2.39)
	Systemic therapy	3.23 (2.30, 4.54)	1.95 (1.67, 2.26)
Sample time and research	Baseline	2.31 (1.46, 3.67)	1.88 (1.64, 2.16)
	Mid-therapy	3.09 (2.17, 4.39)	1.53 (1.29, 1.82)
	Post-therapy	2.29 (1.65, 3.18)	2.06 (1.72, 2.47)
Tumor stage and research	Advanced stage	2.57 (1.70, 3.88)	1.78 (1.60, 1.98)
	Early stage	1.97 (1.54, 2.52)	1.83 (1.52, 2.20)
All research studies	–	2.43 (1.85, 3.19)	1.82 (1.66, 1.99)

Relationship between CTC+ prognostic value and clinical therapeutic characteristics

Previous studies considered that some drugs, such as sorafenib and digitoxin, could limit or kill tumor cells detaching from the primary distant sites (57). Thus, we conducted a subgroup analysis to investigate the influence of different treatment methods and sampling times on the prognostic value of CTC^+. The calculated HR suggested that the relationship was not affected by different treatment methods (HR_{OS}, 2.43; 95% CI, 1.85–3.19; $HR_{PFS/DFS}$, 1.82; 95% CI, 1.66–1.99) (Figures 6A, B; Table 3). The heterogeneity was significant in the OS subgroup analysis (I^2 = 75.5%). Comparing the heterogeneity of the subsets, the results indicated that the source came from the chemotherapy subset (I^2 = 85.1%). However, publication bias was not discovered in this subset (Supplementary Figures S2M, N). The outcome was stable in the one-way sensitivity analysis (Supplementary Figure S2O). The adjusted HR would be 1.57 analyzed by the trim-and-fill analysis (Supplementary Figure S2P; Table 4). Furthermore, the subset results showed that the patients who received systemic therapy would have worse survival than other patients when the CTC was detected (HR_{OS}, 3.23; 95% CI, 2.30–4.45; $HR_{PFS/DFS}$, 1.95; 95% CI, 1.67–2.26).

The subgroup analysis of sampling times indicated that the relationship between CTC^+ and poor survival would be stable regardless of the treatment phases (HR_{OS}, 2.43; 95% CI, 1.85–3.19; $HR_{PFS/DFS}$, 1.82; 95% CI, 1.66–1.99) (Figures 7A, B; Table 3). The heterogeneity of OS analysis was significant (I^2 = 75.5%), and the heterogeneity of the subgroup might result from the baseline subset (I^2 = 84.9%). The result was reliable after the publication bias, the one-way sensitivity, and the trim-and-fill analysis (Supplementary Figures S3A–D; Table 4). Consistent with a previous study, our result showed that CTC detection at mid-therapy or post-therapy could be used for monitoring therapeutic effects and had prognostic relevance (58). For instance, the subset outcomes exhibited that patients with CTC^+ would have worse OS and PFS/DFS in both mid-therapy and post-therapy (HR_{OS}, 3.09; 95% CI, 2.17–4.39; $HR_{PFS/DFS}$, 2.06, 95% CI, 1.72–2.47).

The analysis of CTC prognosis value for all patients and cancer stages

In order to investigate the prognostic value of CTC^+ in different stages of BC, we conducted a subgroup analysis. We divided the data into subgroups according to cancer stages. The calculated analysis showed that the prognostic value of CTCs would not be affected by the cancer stages (HR_{OS}, 2.35; 95% CI, 1.78–3.10; $HR_{PFS/DFS}$, 1.79; 95% CI, 1.63–1.97) (Figures 8A, B; Table 3). The OS subgroup analysis showed a significant heterogeneity (I^2 = 75.9%), and it might come from the advanced stage subset (I^2 = 85.5%). However, the result was stable after the publication bias, the one-way sensitivity, and the trim-and-fill analysis (Supplementary Figures S4E–H; Table 4). Furthermore, the relationship between CTC and poor OS was more obvious in the advanced BC stage (HR_{OS}, 2.57; 95% CI, 1.70–3.88). However, as for the poor PFS/DFS forecast, early BC stage patients may benefit more from the relationship ($HR_{PFS/DFS}$, 1.83; 95% CI, 1.52–2.20).

Herein, 18 available trials and 6,794 individuals could be unitized in the HR_{OS} extraction. $HR_{PFS/DFS}$ was available in 19 studies, which consisted of 6,696 patients. The analyzed HR indicated that CTC^+ could represent poor survival in all BC patients (HR_{OS}, 2.43; 95% CI, 1.85–3.19; $HR_{PFS/DFS}$, 1.82; 95% CI, 1.66–1.99) (Figures 9A, B; Table 3). The heterogeneity was significant in all BC analyses; however, the metaregression and subgroup analyses showed that the result was stable and reliable. Despite the overall heterogeneity being moderate in some subgroups (I^2 < 50%) (Figures 3B, 4B, 5B, 6B, 7B, 8B), the heterogeneity analyses of the subsets in the subgroup analysis

TABLE 4 Summary of the bias analysis and trim-and-fill analysis.

Factors	OS					PFS/DFS				
	Publication bias			The adjusted HR of trim-and-fill analysis			Publication bias		The adjusted HR of trim-and-fill analysis	
	Subset	Begg's funnel	Egger's funnel	Missed studies	Adjusted HR	Subset	Begg's funnel	Egger's funnel	Missed studies	Adjusted HR
Detection system	Not CellSearch System	1	0.64	1	0.98 (0.35–2.72)	Not CellSearch System	0.50	0.40	1	1.51 (0.87–2.61)
Continent	Europe	0.45	0.66	2	1.51 (0.84–2.72)	Europe	0.35	0.60	3	1.51 (1.36–1.68)
CTC definition	1 per 7.5 m	0.85	0.11	2	1.25 (0.61–2.58)	1 per 7.5 m	0.60	0.54	1	1.68 (0.99–2.87)
	5 per 7.5 m	0.08	0.02	5	2.17 (1.64–2.88)	5 per 7.5 m				
	Other	0.50	0.42	2	1.55 (0.90–2.66)	Other				
Therapeutic plan	Chemotherapy	0.80	0.95	3	1.57 (1.02–2.41)	Chemotherapy	1	0.58	0	1.74 (1.33–2.29)
						Accepted surgery	0.65	0.09	2	1.87 (1.28–2.74)
Sample time	Baseline	0.53	0.69	3	1.78 (1.15–2.77)	Mid-therapy	0.62	0.13	2	1.50 (1.13–2.01)
Cancer stage	Advanced stage	1	0.65	1	0.98 (0.35–2.72)	Early stage	0.29	0.19	2	1.75 (1.28–2.39)

10.3389/fonc.2023.1272788

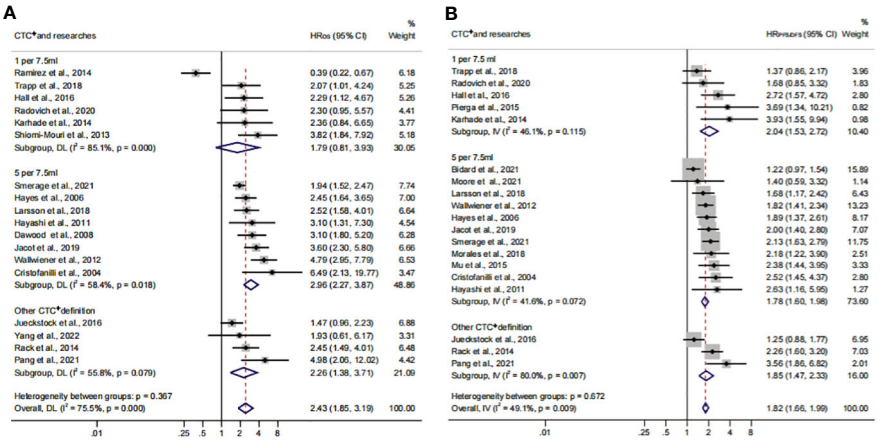

FIGURE 4
The subgroup analysis of CTC$^+$ definition in prognosis value. **(A)** The calculated HR_{OS} of CTC$^+$ definition; **(B)** the calculated $HR_{PFS/DFS}$ of CTC$^+$ definition.

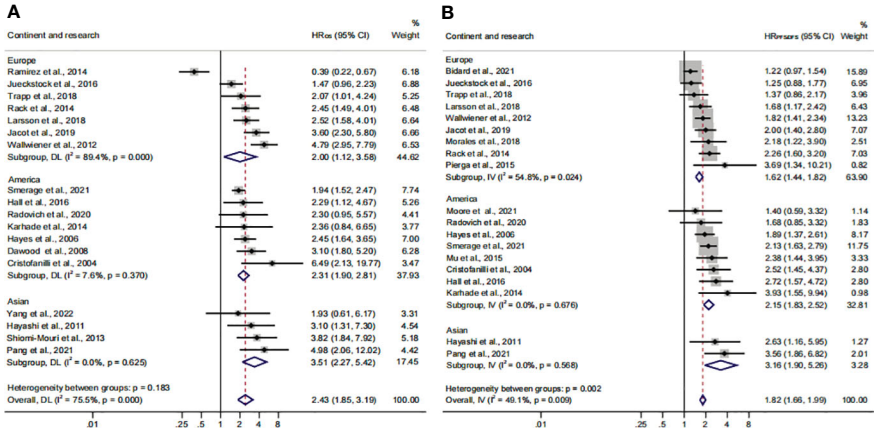

FIGURE 5
The continent subgroup analysis of prognosis assessment. **(A)** The pooled HR_{OS} of continent; **(B)** the pooled $HR_{PFS/DFS}$ of continent.

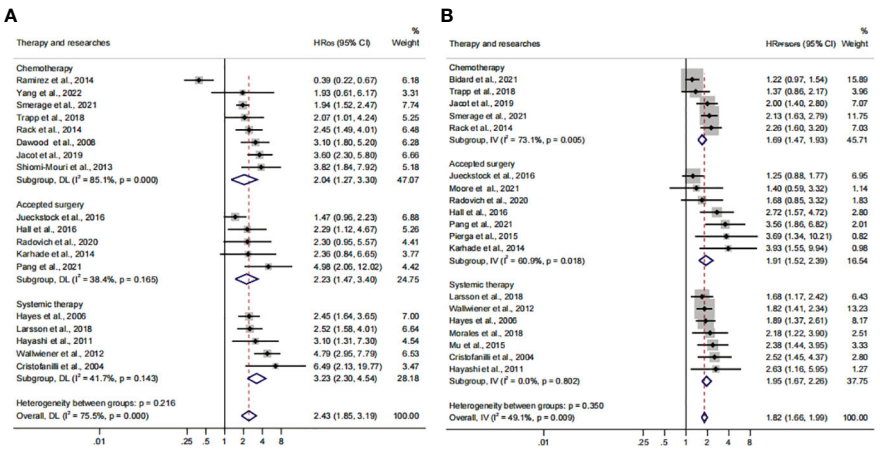

FIGURE 6
The therapy subgroup analysis of survival evaluation. **(A)** The calculated HR_{OS} of therapy; **(B)** the calculated $HR_{PFS/DFS}$ of therapy.

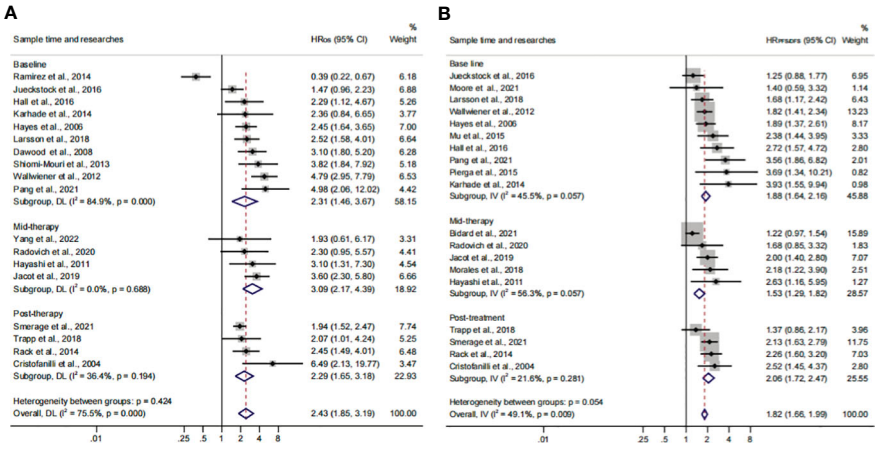

FIGURE 7
The sample time and therapy subgroup analysis of survival evaluation. **(A)** The pooled HR_{OS} of sample time; **(B)** the pooled $HR_{PFS/DFS}$ of sample time.

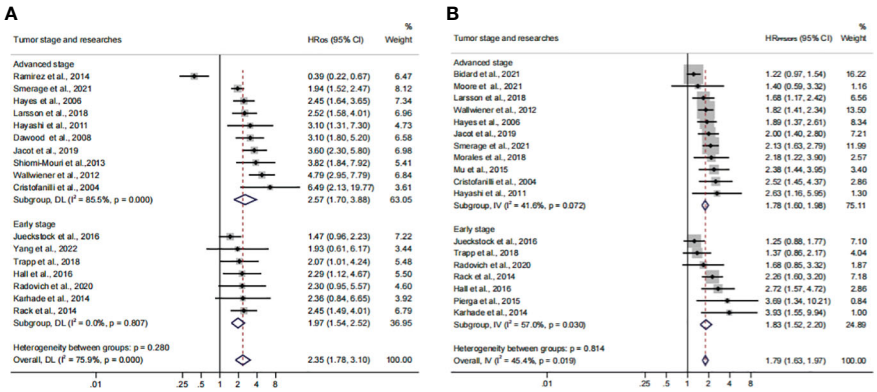

FIGURE 8
Analysis of prognosis values in different stages. **(A)** The calculated HR_{OS} of the tumor stage; **(B)** the calculated $HR_{PFS/DFS}$ of the tumor stage.

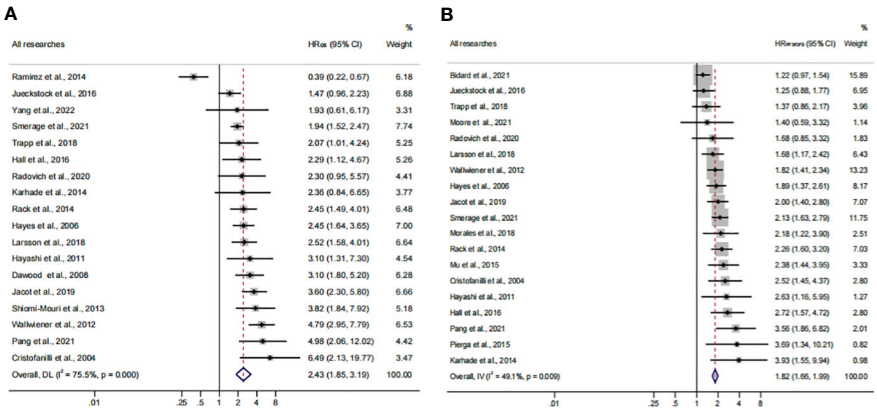

FIGURE 9
Analysis of prognosis values for all patients. **(A)** The pooled HR_{OS} of all research studies; **(B)** the pooled $HR_{PFS/DFS}$ of all research studies.

could support the stability and reliability of the analyses (I^2 > 50%) (Supplementary Figures S3E–P, S4A–D, I–P, S5; Table 4).

Discussion

In a rapidly evolving cancer prediction field, CTC detection technologies have attracted the attention of researchers. In this study, we investigated the diagnostic effectiveness of the widely used CTC detection approaches including the CellSearch System, ICC, and RT-PCR. Our results suggested that CTC detection was effective and had high diagnostic value for BC patients. The CellSearch System might have a higher diagnostic value compared with other detection methods. Moreover, the different threshold levels do not affect the relationship between CTC^+ and poor prognosis. In the prognosis subanalysis, patients detected by the CellSearch System with CTC^+ showed a worse prognosis (HR_{OS}, 2.74; 95% CI, 2.30–3.28; $HR_{PFS/DFS}$, 1.84, 95% CI, 1.67–2.03). The subgroup analysis for patients from continents indicated that CTC^+ was associated with a worse OS and PFS/DFS in the Asian population which was consistent with a previous study and could be regarded as a more obvious biomarker for patients from Asia (16, 59, 60). It may be caused by the differences between ethnic, but the specific reason is not yet clear and needs further research.

Most studies revealed that the presence of CTCs implied a worse prognosis at baseline. However, the relationships between CTCs and the therapeutic regimen were unclear. Our results demonstrated that CTC^+ at mid-/post-therapy could not only reflect the therapeutic effect but also evaluate the prognostic relevance. The prognostic ability was not influenced by the time points of sampling. Moreover, our research also showed that the relationship between CTC^+ and poor survival was changing constantly. Thus, we suggest that patients should repeat the CTC detection after the therapy to obtain a more accurate survival assessment. Comparing the three time points, the pooled HRs indicated that patients should conduct CTC detection again after treatment to obtain a more accurate evaluation of survival. Altogether, the association between CTCs and poor survival should be considered stable, regardless of the treatment methods the patient is receiving. However, the relationship between CTC^+ and different therapeutic regimens was not investigated in the subgroup analysis due to insufficient information which deserves further study in the future. Previous studies have demonstrated that the prognosis of early and advanced BC was obviously different (61, 62). In line with previous studies, our findings showed that CTC^+ could serve as an independent predictor for cancer progression (35, 63–65). To sum up, our study showed that CTCs could be utilized as a high-value marker for all BC patients. The value was stable after the heterogeneity analysis. Moreover, CTC detection should be conducted in different stages which could predict the prognosis and treatment response for BC patients.

With the development of detection techniques, novel methods such as microgels and antifouling nanofilm could facilitate in the separation and purification of CTCs, which could promote the CTCs to enter the clinic (66–68). Although the utility of CTC detection was not included in the clinical practice guidelines of BC, many studies have shown its great potential in the management of BC patients (69, 70). For instance, the results obtained from Chakraborty's group encouraged the incorporation of CTC quantification as a prognostic marker and for minimally invasive tumor burden assessment in multiple myeloma (71). In the future, the level of CTCs might be an important component of stage definition for BC patients. Moreover, investigation of the genomic/transcriptional/proteomic profiles of CTCs could provide comprehensive information in choosing therapeutic strategies. For example, some CTC measurement technologies achieved the genotyping of CTCs, including crucial gene mutations and clone heterogeneity, such as TP53, PIK3CA, ERBB2, KLK10, NUMBL, GFB1, and BSG (72, 73). Those achievements would help clinicians select personalized treatment and more effective therapeutic regimens during tumor progression. The present studies suggested the clinical value of CTCs in the diagnosis, prognosis, and treatment of BC. However, the utilization of CTCs urgently needs standard detection methods and clinical guidelines, especially for the differences in populations, therapeutic schemes, BC stages, thresholds, and the appropriate time points for blood sampling (74).

CTCs could not be the unique prognostic factor due to the complex mechanism of BC development, invasion, and metastasis. The progression of BC could be regulated by the tumor microenvironment (TME) and deeply influenced by cancer-associated fibroblasts, macrophages, neutrophils, T regulatory cells, tumor-infiltrating lymphocytes, and the related secreted molecules (75). For example, the number of $CD68^+$ macrophages, the count of tumor-infiltrating lymphocytes, and the expression of TGF-β in different genetic levels could serve as prognostic and predictive markers (76–78). Those specific cells and related secreted molecules were equally important for the evaluation of BC prognosis. The design and construct of drugs aimed at those molecules would be a promising way for BC patients. For instance, Yi and his team produced bispecific antibodies targeting TGF-β and human PD-L1 (termed YM101 and BiTP) showing antitumor activity in the TNBC. This means that CTCs, as a kind of TME-related molecule, would also have the potential possibility to be utilized by the drug design of BC (79, 80).

Some limitations exist and should be considered deliberately. First, compared with other cancers, BC was relatively general. Meanwhile, some confounding factors were not clear and discussed which are equally important including detection markers, anatomic stages, histologic grades, and the metastatic conditions of the lymph nodes/organs. These factors could not be regarded as subgroups. Second, only a fraction of the literature directly offered univariate HR, LCI, and UCI values. In order to ensure the accuracy of data, studies were not included in this analysis that do not provide original data. Some articles only exhibited survival curves. These articles were not included because extracting data from survival curves also led to measurement bias. Third, according to the funnel plot, the meta-analysis adopted a systematic retrieval strategy and did not identify significant publication bias. However, some gray publications were

not taken into analysis factually including meetings and abstracts written in other languages and inaccessible articles. Fourth, a series of data were still not detailed enough in the analysis. For example, the first follow-up time and the definition of BC stages in some articles were not clear. This could also influence the analysis outcomes. Finally, in our analysis, only one male patient was involved. This meant that the final outcome may be not valuable for men.

Conclusions

Our results provided the latest evidence to support that CTCs have a high and stable value of the diagnosis and prognosis for BC, especially for patients from Asia. We suggest that patients should have CTC detection sequentially during treatment, especially when BC progression has been identified. In the future, novel techniques should be developed to improve the efficacy of CTC detection.

Author contributions

HZ: Investigation, Methodology, Writing – original draft. LW: Investigation, Methodology, Writing – original draft. CF: Conceptualization, Writing – review & editing. CL: Conceptualization, Funding acquisition, Writing – review & editing. LZ: Conceptualization, Funding acquisition, Investigation, Writing – review & editing.

Funding

The author(s) declare financial support was received for the research, authorship, and/or publication of this article. This work was supported by the National Natural Science Foundation of China (No. 82201541), China Postdoctoral Science Foundation (No. 2022M710997), and Provincial Medical Talents Project funded by Hebei Province (No. 361007).

Conflict of interest

The authors declare that the research was conducted in the absence of any commercial or financial relationships that could be construed as a potential conflict of interest.

Publisher's note

Supplementary material

The Supplementary Material for this article can be found online at: https://www.frontiersin.org/articles/10.3389/fonc.2023.1272788/full#supplementary-material

SUPPLEMENTARY FIGURE 1
The analyses of SROC with prediction & confidence contours, diagnostic odds ratio and Deeks' funnel plot asymmetry Test in the diagnosis effect of CTC.

SUPPLEMENTARY FIGURE 2
The further identification and analysis of the heterogeneity. **(A)** the Begg's funnel plot of the 'Not CellSearch system' group analysis in HR_{OS}; **(B)** the Egger's publication bias plot of the 'Not CellSearch system' group analysis in HR_{OS}; **(C)** the one-way sensitivity analysis of the 'Not CellSearch system' group analysis in HR_{OS}; **(D)** the trim-and-fill analysis of the 'Not CellSearch system' group analysis in HR_{OS}; **(E)** the Begg's funnel plot of 'other definition of the CTC+' group analysis in $HR_{PFS/DFS}$; **(F)** the Egger's publication bias plot of the 'other definition of CTC+' group analysis in $HR_{PFS/DFS}$; **(G)**the one-way sensitivity analysis of 'other definition of the CTC+' group analysis in $HR_{PFS/DFS}$; **(H)** the trim-and-fill analysis of the 'other definition of CTC+' group analysis in $HR_{PFS/DFS}$; **(I)** the Begg's funnel plot of the 'Europe' group analysis in $HR_{PFS/DFS}$; **(G)** the Egger's publication bias plot of the 'Europe' group analysis in $HR_{PFS/DFS}$;**(K)** the one-way sensitivity analysis of the 'Europe' group analysis in $HR_{PFS/DFS}$; **(L)** the trim-and-fill analysis of the 'Europe' group analysis in $HR_{PFS/DFS}$; **(M)** the Begg's funnel plot of the 'chemotherapy' group analysis in HR_{OS}; **(N)** the Egger's publication bias plot of the 'chemotherapy' group analysis in HR_{OS}; **(O)** the one-way sensitivity analysis of the 'chemotherapy' group analysis in HR_{OS}; **(P)** the trim-and-fill analysis of the 'chemotherapy' group analysis in HR_{OS}.

SUPPLEMENTARY FIGURE 3
The further identification and analysis of the heterogeneity. **(A)** the Begg's funnel plot of the 'baseline' group analysis in HR_{OS}; **(B)** the Egger's publication bias plot of the 'baseline' group analysis in HR_{OS}; **(C)** the one-way sensitivity analysis of the 'baseline' group analysis in HR_{OS}; **(D)** the trim-and-fill analysis of the 'baseline' group analysis in HR_{OS}; **(E)** the Begg's funnel plot of the 'Europe' group analysis in HR_{OS}; **(F)** the Egger's publication bias plot of the 'Europe' group analysis in HR_{OS}; **(G)** the one-way sensitivity analysis of the 'Europe' group analysis in HR_{OS}; **(H)** the trim-and-fill analysis of the 'Europe' group analysis in HR_{OS}; **(I)** the Begg's funnel plot of the '1 per 7.5 ml' group analysis in HR_{OS}; **(G)** the Egger's publication bias plot of the '1 per 7.5 ml' group analysis in HR_{OS};**(K)** the one-way sensitivity analysis of the '1 per 7.5 ml' group analysis in HR_{OS}; **(L)** the trim-and-fill analysis of the '1 per 7.5 ml' group analysis in HR_{OS}; **(M)** the Begg's funnel plot of the '5 per 7.5 ml' group analysis in HR_{OS}; **(N)** the Egger's publication bias plot of the '5 per 7.5 ml' group analysis in HR_{OS}; **(O)** the one-way sensitivity analysis of the '5 per 7.5 ml' group analysis in HR_{OS}; **(P)** the trim-and-fill analysis of the '5 per 7.5 ml' group analysis in HR_{OS}.

SUPPLEMENTARY FIGURE 4
The further identification and analysis of the heterogeneity. **(A)** the Begg's funnel plot of the 'other definition of CTC+' group analysis in HR_{OS}; **(B)** the Egger's publication bias plot of the 'other definition of CTC+' group analysis in HR_{OS}; **(C)** the one-way sensitivity analysis of the 'other definition of CTC+' group analysis in HR_{OS}; **(D)** the trim-and-fill analysis of the 'other definition of CTC+' group analysis in HR_{OS}; **(E)** the Begg's funnel plot of the 'advanced stage' group analysis in HR_{OS}; **(F)** the Egger's publication bias plot of the 'advanced stage' group analysis in HR_{OS}; **(G)** the one-way sensitivity analysis of the 'advanced stage' group analysis in HR_{OS}; **(H)** the trim-and-fill analysis of the 'advanced stage' group analysis in HR_{OS}; **(I)** the Begg's funnel plot of the 'Not CellSearch system' group analysis in $HR_{PFS/DFS}$; **(G)** the Egger's publication bias plot of the 'Not CellSearch system' group analysis in $HR_{PFS/DFS}$; **(K)** the one-way sensitivity analysis of the 'Not CellSearch system' group analysis in $HR_{PFS/DFS}$; **(L)** the trim-and-fill analysis of the 'Not CellSearch system' group analysis in $HR_{PFS/DFS}$; **(M)** the Begg's funnel plot of the 'mid-therapy' group analysis in $HR_{PFS/DFS}$; **(N)** the Egger's publication bias plot of the 'mid-therapy' group analysis in $HR_{PFS/DFS}$; **(O)** the one-way sensitivity analysis of the 'mid-therapy' group analysis in $HR_{PFS/DFS}$; **(P)** the trim-and-fill analysis of the 'mid-therapy' group analysis in $HR_{PFS/DFS}$.

SUPPLEMENTARY FIGURE 5

The further identification and analysis of the heterogeneity. **(A)** the Begg's funnel plot of the 'chemotherapy' group analysis in $HR_{PFS/DFS}$; **(B)** the Egger's publication bias plot of the 'chemotherapy' group analysis in $HR_{PFS/DFS}$; **(C)** the one-way sensitivity analysis of the 'chemotherapy' group analysis in $HR_{PFS/DFS}$; **(D)** the trim-and-fill analysis of the 'chemotherapy' group analysis in $HR_{PFS/DFS}$; **(E)** the Begg's funnel plot of the 'accepted surgery' group analysis in $HR_{PFS/DFS}$; **(F)** the Egger's publication bias plot of the 'accepted surgery' group analysis in $HR_{PFS/DFS}$; **(G)** the one-way sensitivity analysis of the 'accepted surgery' group analysis in $HR_{PFS/DFS}$; **(H)** the trim-and-fill analysis of the 'accepted surgery' group analysis in $HR_{PFS/DFS}$; **(I)** the Begg's funnel plot of the 'early stage' group analysis in $HR_{PFS/DFS}$; **(G)** the Egger's publication bias plot of the 'early stage' group analysis in $HR_{PFS/DFS}$; **(K)** the one-way sensitivity analysis of the 'early stage' group analysis in $HR_{PFS/DFS}$; **(L)** the trim-and-fill analysis of the 'early stage' group analysis in $HR_{PFS/DFS}$.

References

1. Abbaspour M, Akbari V. Cancer vaccines as a targeted immunotherapy approach for breast cancer: an update of clinical evidence. *Expert Rev Vaccines* (2022) 21(3):337–53. doi: 10.1080/14760584.2022.2021884

2. Kong X, Li J, Li Y, Duan W, Qi Q, Wang T, et al. A novel long non-coding RNA AC073352.1 promotes metastasis and angiogenesis via interacting with YBX1 in breast cancer. *Cell Death Dis* (2021) 12(7):670. doi: 10.1038/s41419-021-03943-x

3. Shao N, Wan F, Abudurexiti M, Wang J, Zhu Y, Ye D. Causes of death and conditional survival of renal cell carcinoma. *Front Oncol* (2019) 9:591. doi: 10.3389/fonc.2019.00591

4. Rizvi S, Khan SA, Hallemeier CL, Kelley RK, Gores GJ. Cholangiocarcinoma - evolving concepts and therapeutic strategies. *Nat Rev Clin Oncol* (2018) 15(2):95–111. doi: 10.1038/nrclinonc.2017.157

5. Chen SY, Huang HY, Lin HP, Fang CY. Piperlongumine induces autophagy in biliary cancer cells via reactive oxygen species-activated Erk signaling pathway. *Int J Mol Med* (2019) 44(5):1687–96. doi: 10.3892/ijmm.2019.4324

6. Martins I, Ribeiro IP, Jorge J, Joana J, Gonçalves AC, Sarmento-Ribeiro AB, et al. Liquid biopsies: applications for cancer diagnosis and monitoring. *Genes (Basel)* (2021) 12(3):349. doi: 10.3390/genes12030349

7. Zhang W, Duan X, Zhang Z, Yang Z, Zhao C, Liang C, et al. Combination of CT and telomerase+ circulating tumor cells improves diagnosis of small pulmonary nodules. *JCI Insight* (2021) 6(11):e148182. doi: 10.1172/jci.insight.148182

8. Deng Z, Wu S, Wang Y, Shi D. Circulating tumor cell isolation for cancer diagnosis and prognosis. *EBioMedicine* (2022) 83:104237. doi: 10.1016/j.ebiom.2022.104237

9. De Giorgi U, Mego M, Scarpi E, Giordano A, Giuliano M, Valero V, et al. Association between circulating tumor cells and peripheral blood monocytes in metastatic breast cancer. *Ther Adv Med Oncol* (2019) 11:1–12. doi: 10.1177/1758835919866065

10. Dobiasova B, Mego M. Biomarkers for inflammatory breast cancer: diagnostic and therapeutic utility. *Breast Cancer (Dove Med Press)* (2020) 12:153–63. doi: 10.2147/BCTT.S231502

11. Jin F, Zhu L, Shao J, Yakoub M, Schmitt L, Reißfelder C, et al. Circulating tumour cells in patients with lung cancer universally indicate poor prognosis. *Eur Respir Rev* (2022) 31(166):220151. doi: 10.1183/16000617.0151-2022

12. Rack B, Schindlbeck C, Jückstock J, Andergassen U, Hepp P, Zwingers T, et al. Circulating tumor cells predict survival in early average-to-high risk breast cancer patients. *J Natl Cancer Inst* (2014) 106(5):dju066. doi: 10.1093/jnci/dju066

13. Meng Y, Sun J, Zheng Y, Zhang G, Yu T, Piao H. Platelets: the emerging clinical diagnostics and therapy selection of cancer liquid biopsies. *Onco Targets Ther* (2021) 14:3417–28. doi: 10.2147/OTT.S311907

14. Lu C, Han J, Sun X, Yang G. Electrochemical detection and point-of-care testing for circulating tumor cells: current techniques and future potentials. *Sensors (Basel)* (2020) 20(21):6073. doi: 10.3390/s20216073

15. Cui K, Ou Y, Shen Y, Li S, Sun Z. Clinical value of circulating tumor cells for the diagnosis and prognosis of hepatocellular carcinoma (HCC): A systematic review and meta-analysis. *Med (Baltimore)* (2020) 99(40):e22242. doi: 10.1097/MD.0000000000022242

16. Wang Y, Yu X, Hartmann D, Zhou J. Circulating tumor cells in peripheral blood of pancreatic cancer patients and their prognostic role: a systematic review and meta-analysis. *HPB (Oxford)* (2020) 22(5):660–9. doi: 10.1016/j.hpb.2019.11.003

17. Soltysova A, Sedlackova T, Dvorska D, Jasek K, Chokhachi Baradaran P, Horvathova Kajabova V, et al. Monosomy 3 influences epithelial-mesenchymal transition gene expression in uveal melanoma patients) consequences for liquid biopsy. *Int J Mol Sci* (2020) 21(24):9651. doi: 10.3390/ijms21249651

18. Piñeiro R, Martínez-Pena I, López-López R. Relevance of CTC clusters in breast cancer metastasis. *Adv Exp Med Biol* (2020) 1220:93–115. doi: 10.1007/978-3-030-35805-1_7

19. Moher D, Liberati A, Tetzlaff J, Altman DGPRISMA Group. Preferred reporting items for systematic reviews and meta-analyses: the PRISMA statement. *PloS Med* (2009) 6(7):e1000097.

20. Gong Z, Tang J, Hu W, Song X, Liu X, Mu J, et al. Serum galactose-deficient immunoglobulin A1 in recurrent immunoglobulin a nephropathy after kidney transplantation: A meta-analysis. *Transpl Immunol* (2023) 79:101850. doi: 10.1016/j.trim.2023.101850

21. Sterne JA, Hernán MA, Reeves BC, Savović J, Berkman ND, Viswanathan M, et al. ROBINS-I: a tool for assessing risk of bias in non-randomised studies of interventions. *BMJ* (2016) 355:i4919. doi: 10.1136/bmj.i4919

22. Riethdorf S, Fritsche H, Müller V, Rau T, Schindlbeck C, Rack B, et al. Detection of circulating tumor cells in peripheral blood of patients with metastatic breast cancer: a validation study of the CellSearch system. *Clin Cancer Res* (2007) 13(3):920–8. doi: 10.1158/1078-0432.CCR-06-1695

23. Sawada T, Araki J, Yamashita T, Masubuchi M, Chiyoda T, Yunokawa M, et al. Prognostic impact of circulating tumor cell detected using a novel fluidic cell microarray chip system in patients with breast cancer. *EBioMedicine* (2016) 11:173–82. doi: 10.1016/j.ebiom.2016.07.027

24. Sheng Y, Wang T, Li H, Zhang Z, Chen J, He C, et al. Comparison of analytic performances of Cellsearch and iFISH approach in detecting circulating tumor cells. *Oncotarget* (2017) 8(5):8801–6. doi: 10.18632/oncotarget.6688

25. Li JB, Geng CZ, Yan M, Wang YS, Ouyang QC, Yin YM, et al. Circulating tumor cells in patients with breast tumors were detected by a novel device: a multicenter, clinical trial in China. *Zhonghua yi xue za zhi* (2017) 97(24):1857–61. doi: 10.3760/cma.j.issn.0376-2491.2017.24.003

26. Jin L, Zhao W, Zhang J, Chen W, Xie T, Wang L, et al. Evaluation of the diagnostic value of circulating tumor cells with CytoSorter® CTC capture system in patients with breast cancer. *Cancer Med* (2020) 9(5):1638–47. doi: 10.1002/cam4.2825

27. Li Y, Ma G, Zhao P, Chen W, Xie T, Wang L, et al. Improvement of sensitive and specific detection of circulating tumor cells using negative enrichment and immunostaining-FISH. *Clin Chim Acta* (2018) 485:95–102. doi: 10.1016/j.cca.2018.06.034

28. Li FR, Li Q, Zhou HX, Qi H, Deng CY. Detection of circulating tumor cells in breast cancer with a refined immunomagnetic nanoparticle enriched assay and nested-RT-PCR. *Nanomedicine* (2013) 9(7):1106–13. doi: 10.1016/j.nano.2013.03.002

29. Weissenstein U, Schumann A, Reif M, Link S, Toffol-Schmidt UD, Heusser P. Detection of circulating tumor cells in blood of metastatic breast cancer patients using a combination of cytokeratin and EpCAM antibodies. *BMC Cancer* (2012) 12:206. doi: 10.1186/1471-2407-12-206

30. Zhang X, Lu X, Gao W, Wang Y, Jia C, Cong H. A label-free microfluidic chip for the highly selective isolation of single and cluster CTCs from breast cancer patients. *Transl Oncol* (2021) 14(1):100959. doi: 10.1016/j.tranon.2020.100959

31. Kim SJ, Masago A, Tamaki Y, Akazawa K, Tsukamoto F, Sato J, et al. A novel approach using telomerase-specific replication-selective adenovirus for detection of circulating tumor cells in breast cancer patients. *Breast Cancer Res Treat* (2011) 128(3):765–73. doi: 10.1007/s10549-011-1603-2

32. Chen Y, Zou TN, Wu ZP, Zhou YC, Gu YL, Liu X, et al. Detection of cytokeratin 19, human mammaglobin, and carcinoembryonic antigen-positive circulating tumor cells by three-marker reverse transcription-PCR assay and its relation to clinical outcome in early breast cancer. *Int J Biol Markers* (2010) 25(2):59–68. doi: 10.1177/172460081002500201

33. Zhao S, Yang H, Zhang M, Zhang D, Liu Y, Liu Y, et al. Circulating tumor cells (CTCs) detected by triple-marker EpCAM, CK19, and hMAM RT-PCR and their relation to clinical outcome in metastatic breast cancer patients. *Cell Biochem Biophys* (2013) 65(2):263–73. doi: 10.1007/s12013-012-9426-2

34. Radovich M, Jiang G, Hancock BA, Chitambar C, Nanda R, Falkson C, et al. Association of circulating tumor DNA and circulating tumor cells after neoadjuvant chemotherapy with disease recurrence in patients with triple-negative breast cancer: preplanned secondary analysis of the BRE12-158 randomized clinical trial. *JAMA Oncol* (2020) 6(9):1410–5. doi: 10.1001/jamaoncol.2020.2295

35. Cristofanilli M, Budd GT, Ellis MJ, Stopeck A, Matera J, Miller MC, et al. Circulating tumor cells, disease progression, and survival in metastatic breast cancer. *N Engl J Med* (2004) 351(8):781–91. doi: 10.1056/NEJMoa040766

36. Bidard FC, Jacot W, Kiavue N, Dureau S, Kadi A, Brain E, et al. Efficacy of circulating tumor cell count-driven vs clinician-driven first-line therapy choice in hormone receptor-positive, ERBB2-negative metastatic breast cancer: the STIC CTC randomized clinical trial. *JAMA Oncol* (2021) 7(1):34–41. doi: 10.1001/jamaoncol.2020.5660

37. Moore HCF, Barlow WE, Somlo G, Gralow JR, Schott AF, Hayes DF, et al. A randomized trial of fulvestrant, everolimus, and anastrozole for the front-line treatment of patients with advanced hormone receptor-positive breast cancer, SWOG S1222. *Clin Cancer Res* (2022) 28(4):611–7. doi: 10.1158/1078-0432.CCR-21-3131

38. Smerage JB, Barlow WE, Hortobagyi GN, Winer EP, Leyland-Jones B, Srkalovic G, et al. Circulating tumor cells and response to chemotheruregapy in metastatic breast cancer: SWOG S0500. *J Clin Oncol* (2014) 32(31):3483–9. doi: 10.1200/JCO.2014.56.2561

39. Trapp E, Janni W, Schindlbeck C, Jückstock J, Andergassen U, de Gregorio A, et al. Presence of circulating tumor cells in high-risk early breast cancer during follow-up and prognosis. *J Natl Cancer Inst* (2019) 111(4):380–7. doi: 10.1093/jnci/djy152

40. Pang S, Li H, Xu S, Feng L, Ma X, Chu Y, et al. Circulating tumour cells at baseline and late phase of treatment provide prognostic value in breast cancer. *Sci Rep* (2021) 11(1):13441. doi: 10.1038/s41598-021-92876-8

41. Wallwiener M, Hartkopf AD, Baccelli I, Riethdorf S, Schott S, Pantel K, et al. The prognostic impact of circulating tumor cells in subtypes of metastatic breast cancer. *Breast Cancer Res Treat* (2013) 137(2):503–10. doi: 10.1007/s10549-012-2382-0

42. Hall CS, Karhade MG, Bowman Bauldry JB, Valad LM, Kuerer HM, DeSnyder SM, et al. Prognostic value of circulating tumor cells identified before surgical resection in nonmetastatic breast cancer patients. *J Am Coll Surg* (2016) 223(1):20–9. doi: 10.1016/j.jamcollsurg.2016.02.021

43. Ramirez JM, Fehm T, Orsini M, Cayrefourcq L, Maudelonde T, Pantel K, et al. Prognostic relevance of viable circulating tumor cells detected by EPISPOT in metastatic breast cancer patients. *Clin Chem* (2014) 60(1):214–21. doi: 10.1373/clinchem.2013.215079

44. Jacot W, Cottu P, Berger F, Dubot C, Venat-Bouvet L, Lortholary A, et al. Actionability of HER2-amplified circulating tumor cells in HER2-negative metastatic breast cancer: the CirCe T-DM1 trial. *Breast Cancer Res* (2019) 21(1):121. doi: 10.1186/s13058-019-1215-z

45. Pierga JY, Petit T, Lévy C, Ferrero JM, Campone M, Gligorov J, et al. Pathological response and circulating tumor cell count identifies treated HER2+ inflammatory breast cancer patients with excellent prognosis: BEVERLY-2 survival data. *Clin Cancer Res* (2015) 21(6):1298–304. doi: 10.1158/1078-0432.CCR-14-1705

46. Jueckstock J, Rack B, Friedl TW, Scholz C, Steidl J, Trapp E, et al. Detection of circulating tumor cells using manually performed immunocytochemistry (MICC) does not correlate with outcome in patients with early breast cancer - Results of the German SUCCESS-A- trial. *BMC Cancer* (2016) 16:401. doi: 10.1186/s12885-016-2454-3

47. Hayes DF, Cristofanilli M, Budd GT, Ellis MJ, Stopeck A, Miller MC, et al. Circulating tumor cells at each follow-up time point during therapy of metastatic breast cancer patients predict progression-free and overall survival. *Clin Cancer Res* (2006) 12 (14 Pt 1):4218–24. doi: 10.1158/1078-0432.CCR-05-2821

48. Mu Z, Wang C, Ye Z, Austin L, Civan J, Hyslop T, et al. Prospective assessment of the prognostic value of circulating tumor cells and their clusters in patients with advanced-stage breast cancer. *Breast Cancer Res Treat* (2015) 154(3):563–71. doi: 10.1007/s10549-015-3636-4

49. Larsson AM, Jansson S, Bendahl PO, Jörgensen LT, Loman N, Graffman C, et al. Longitudinal enumeration and cluster evaluation of circulating tumor cells improve prognostication for patients with newly diagnosed metastatic breast cancer in a prospective observational trial. *Breast Cancer Res* (2018) 20(1):48. doi: 10.1186/s13058-018-0976-0

50. Yang Y, Li L, Tian W, Qiao Z, Qin Q, Su L, et al. A nomogram for predicting the HER2 status of circulating tumor cells and survival analysis in HER2-negative breast cancer. *Front Oncol* (2022) 12:943800. doi: 10.3389/fonc.2022.943800

51. Shiomi-Mouri Y, Kousaka J, Ando T, Tetsuka R, Nakano S, Yoshida M, et al. Clinical significance of circulating tumor cells (CTCs) with respect to optimal cut-off value and tumor markers in advanced/metastatic breast cancer. *Breast Cancer* (2016) 23(1):120–7. doi: 10.1007/s12282-014-0539-x

52. Dawood S, Broglio K, Valero V, Reuben J, Handy B, Islam R, et al. Circulating tumor cells in metastatic breast cancer: from prognostic stratification to modification of the staging system? *Cancer* (2008) 113(9):2422–30. doi: 10.1002/cncr.23852

53. Karhade M, Hall C, Mishra P, Anderson A, Kuerer H, Bedrosian I, et al. Circulating tumor cells in non-metastatic triple-negative breast cancer. *Breast Cancer Res Treat* (2014) 147(2):325–33. doi: 10.1007/s10549-014-3103-7

54. Morales S, Velasco A, Gasol A, Córdoba F, Vidal J, Serrate A, et al. Circulating tumor cells (CTCs) and cytokeratin 19 (CK19) mRNA as prognostic factors in heavily pretreated patients with metastatic breast cancer. *Cancer Treat Res Commun* (2018) 16:13–7. doi: 10.1016/j.ctarc.2018.04.003

55. Hayashi N, Nakamura S, Tokuda Y, Shimoda Y, Yagata H, Yoshida A, et al. Prognostic value of HER2-positive circulating tumor cells in patients with metastatic breast cancer. *Int J Clin Oncol* (2012) 17(2):96–104. doi: 10.1007/s10147-011-0260-0

56. Piñeiro R. Introduction - biology of breast cancer metastasis and importance of the analysis of CTCs. *Adv Exp Med Biol* (2020) 1220:1–10. doi: 10.1007/978-3-030-35805-1_1

57. Mu W, Chu Q, Yang H, Guan L, Fu S, Gao T, et al. Multipoint costriking nanodevice eliminates primary tumor cells and associated-circulating tumor cells for enhancing metastasis inhibition and therapeutic effect on HCC. *Adv Sci (Weinh)* (2022) 9(9):2101472. doi: 10.1002/advs.202101472

58. Zhang L, Riethdorf S, Wu G, Wang T, Yang K, Peng G, et al. Meta-analysis of the prognostic value of circulating tumor cells in breast cancer. *Clin Cancer Res* (2012) 18 (20):5701–10. doi: 10.1158/1078-0432.CCR-12-1587

59. Qiao GL, Qi WX, Jiang WH, Chen Y, Ma LJ. Prognostic significance of circulating tumor cells in esophageal carcinoma: a meta-analysis. *Onco Targets Ther* (2016) 9:1889–97. doi: 10.2147/OTT.S100005

60. Han L, Chen W, Zhao Q. Prognostic value of circulating tumor cells in patients with pancreatic cancer: a meta-analysis. *Tumour Biol* (2014) 35(3):2473–80. doi: 10.1007/s13277-013-1327-5

61. Yao Y, Zhu X, Liu W, Jiang J, Jiang H. Meta-analysis of the prognostic value of circulating tumor cells in gastrointestinal cancer. *Med (Baltimore)* (2022) 101(42): e31099. doi: 10.1097/MD.0000000000031099

62. Huang C, Lin X, He J, Liu N. Enrichment and detection method for the prognostic value of circulating tumor cells in ovarian cancer: A meta-analysis. *Gynecol Oncol* (2021) 161(2):613–20. doi: 10.1016/j.ygyno.2021.02.024

63. Mansouri S, Mokhtari-Hesari P, Naghavi-Al-Hosseini F, Majidzadeh-A K, Farahmand L. The prognostic value of circulating tumor cells in primary breast cancer prior to any systematic therapy: A systematic review. *Curr Stem Cell Res Ther* (2019) 14(6):519–29. doi: 10.2174/1574888X14666190306103759

64. Lv Q, Gong L, Zhang T, Ye J, Chai L, Ni C, et al. Prognostic value of circulating tumor cells in metastatic breast cancer: a systemic review and meta-analysis. *Clin Transl Oncol* (2016) 18(3):322–30. doi: 10.1007/s12094-015-1372-1

65. Myung JH, Eblan MJ, Caster JM, Park SJ, Poellmann MJ, Wang K, et al. Multivalent binding and biomimetic cell rolling improves the sensitivity and specificity of circulating tumor cell capture. *Clin Cancer Res* (2018) 24(11):2539–47. doi: 10.1158/1078-0432.CCR-17-3078

66. Seyfoori A, Seyyed Ebrahimi SA, Samiei E, Akbari M. Multifunctional hybrid magnetic microgel synthesis for immune-based isolation and post-isolation culture of tumor cells. *ACS Appl Mater Interfaces* (2019) 11(28):24945–58. doi: 10.1021/acsami.9b02959

67. Xiang Y, Zhang H, Lu H, Wei B, Su C, Qin X, et al. Bioorthogonal microbubbles with antifouling nanofilm for instant and suspended enrichment of circulating tumor cells. *ACS Nano* (2023) 17(10):9633–46. doi: 10.1021/acsnano.3c03194

68. Wu X, Xiao T, Luo Z, He R, Cao Y, Guo Z, et al. A micro-/nano-chip and quantum dots-based 3D cytosensor for quantitative analysis of circulating tumor cells. *J Nanobiotechnology* (2018) 16(1):65. doi: 10.1186/s12951-018-0390-x

69. Zhou J, Wu J, Hao X, Li P, Zhang H, Wu X, et al. An exploratory study on the checkout rate of circulating tumor cells and the prediction of efficacy of neoadjuvant therapy and prognosis in patients with HER-2-positive early breast cancer. *Front Oncol* (2022) 12:966624. doi: 10.3389/fonc.2022.966624

70. Wu Y, Meng Q, Yang Z, Shi L, Hu R, Zhang P, et al. Circulating HER-2 mRNA in the peripheral blood as a potential diagnostic and prognostic biomarker in females with breast cancer. *Oncol Lett* (2018) 16(3):3726–34. doi: 10.3892/ol.2018.9091

71. Chakraborty R, Lentzsch S. Circulating tumor cell burden as a component of staging in multiple myeloma: ready for prime time? *J Clin Oncol* (2022) 40(27):3099–102. doi: 10.1200/JCO.22.01040

72. Cullinane C, Fleming C, O'Leary DP, Hassan F, Kelly L, O'Sullivan MJ, et al. Association of circulating tumor DNA with disease-free survival in breast cancer: A systematic review and meta-analysis. *JAMA Netw Open* (2020) 3(11):e2026921. doi: 10.1001/jamanetworkopen.2020.26921

73. Kanwar N, Balde Z, Nair R, Dawe M, Chen S, Maganti M, et al. Heterogeneity of circulating tumor cell-associated genomic gains in breast cancer and its association with the host immune response. *Cancer Res* (2021) 81(24):6196–206. doi: 10.1158/0008-5472.CAN-21-1079

74. Lin D, Shen L, Luo M, Zhang K, Li J, Yang Q, et al. Circulating tumor cells: biology and clinical significance. *Signal Transduct Target Ther* (2021) 6(1):404. doi: 10.1038/s41392-021-00817-8

75. Mittal S, Brown NJ, Holen I. The breast tumor microenvironment: role in cancer development, progression and response to therapy. *Expert Rev Mol Diagn* (2018) 18 (3):227–43. doi: 10.1080/14737159.2018.1439382

76. Ahn J, Yoon Y, Yeu Y, Lee H, Park S. Impact of TGF-b on breast cancer from a quantitative proteomic analysis. *Comput Biol Med* (2013) 43(12):2096–102. doi: 10.1016/j.compbiomed.2013.09.022

77. Bahhnassy A, Mohanad M, Shaarawy S, Ismail MF, El-Bastawisy A, Ashmawy AM, et al. Transforming growth factor-β, insulin-like growth factor I/insulin-like growth factor I receptor and vascular endothelial growth factor-A: prognostic and predictive markers in triple-negative and non-triple-negative breast cancer. *Mol Med Rep* (2015) 12(1):851–64. doi: 10.3892/mmr.2015.3560

78. Barrett-Lee P, Travers M, Luqmani Y, Coombes RC. Transcripts for transforming growth factors in human breast cancer: clinical correlates. *Br J Cancer* (1990) 61(4):612–7. doi: 10.1038/bjc.1990.136

79. Yi M, Niu M, Wu Y, Ge H, Jiao D, Zhu S, et al. Combination of oral STING agonist MSA-2 and anti-TGF-β/PD-L1 bispecific antibody YM101: a novel immune cocktail therapy for non-inflamed tumors. *J Hematol Oncol* (2022) 15(1):142. doi: 10.1186/s13045-022-01363-8

80. Yi M, Wu Y, Niu M, Zhu S, Zhang J, Yan Y, et al. Anti-TGF-β/PD-L1 bispecific antibody promotes T cell infiltration and exhibits enhanced antitumor activity in triple-negative breast cancer. *J Immunother Cancer* (2022) 10(12):e005543. doi: 10.1136/jitc-2022-005543

frontiers | Frontiers in Immunology

TYPE Original Research
PUBLISHED 04 December 2023
DOI 10.3389/fimmu.2023.1245514

OPEN ACCESS

EDITED BY
Feifei Teng,
Shandong University Cancer Center, China

REVIEWED BY
Ming Yi,
Zhejiang University, China
Fuhao Wang,
Shandong University, China

*CORRESPONDENCE
Huiqing Lin
huiqing.lin@whu.edu.cn
Xiaofei Wu
wxf613932@163.com
Xiangpan Li
rm001227@whu.edu.cn

†These authors have contributed equally to this work

RECEIVED 23 June 2023
ACCEPTED 13 November 2023
PUBLISHED 04 December 2023

CITATION
Zhao F, Zhao C, Xu T, Lan Y, Lin H, Wu X and Li X (2023) Single-cell and bulk RNA sequencing analysis of B cell marker genes in TNBC TME landscape and immunotherapy.
Front. Immunol. 14:1245514.
doi: 10.3389/fimmu.2023.1245514

Single-cell and bulk RNA sequencing analysis of B cell marker genes in TNBC TME landscape and immunotherapy

Fangrui Zhao[1†], Chen Zhao[1†], Tangpeng Xu[1†], Yanfang Lan[1], Huiqing Lin[2*], Xiaofei Wu[3*] and Xiangpan Li[1*]

[1]Department of Oncology, Renmin Hospital of Wuhan University, Wuhan, Hubei, China, [2]Department of Thoracic Surgery, Renmin Hospital of Wuhan University, Wuhan, China, [3]Department of Neurology, Central War Zone General Hospital of the Chinese People's Liberation Army, Wuhan, Hubei, China

Objective: This study amied to investigate the prognostic characteristics of triple negative breast cancer (TNBC) patients by analyzing B cell marker genes based on single-cell and bulk RNA sequencing.

Methods: Utilizing single-cell sequencing data from TNBC patients, we examined tumor-associated B cell marker genes. Transcriptomic data from The Cancer Genome Atlas (TCGA) database were used as the foundation for predictive modeling. Independent validation set was conducted using the GSE58812 dataset. Immune cell infiltration into the tumor was assessed through various, including XCELL, TIMER, QUANTISEQ, CIBERSORT, CIBERSORT-ABS, and ssGSEA. The TIDE score was utilized to predict immunotherapy outcomes. Additional investigations were conducted on the immune checkpoint blockade gene, tumor mutational load, and the GSEA enrichment analysis.

Results: Our analysis encompassed 22,106 cells and 20,556 genes in cancerous tissue samples from four TNBC patients, resulting in the identification of 116 B cell marker genes. A B cell marker gene score (BCMG score) involving nine B cell marker genes (*ZBP1, SEL1L3, CCND2, TNFRSF13C, HSPA6, PLPP5, CXCR4, GZMB*, and *CCDC50*) was developed using TCGA transcriptomic data, revealing statistically significant differences in survival analysis ($P<0.05$). Functional analysis demonstrated that marker genes were predominantly associated with immune-related pathways. Notably, substantial differences between the higher and lower- BCMG score groups were observed in terms of immune cell infiltration, immune cell activity, tumor mutational burden, TIDE score, and the expression of immune checkpoint blockade genes.

Conclusion: This study has established a robust model based on B-cell marker genes in TNBC, which holds significant potential for predicting prognosis and response to immunotherapy in TNBC patients.

KEYWORDS

B cell marker genes, TNBC, single-cell sequencing, cancer immunotherapy, predictive score

Introduction

Triple-negative breast cancer (TNBC) is a distinct subtype of breast cancer characterized by the absence of estrogen receptor (ER), progesterone receptor (PR) and human epidermal growth factor receptor 2 (HER2) expression in immunohistochemistry (1). Accounting for approximately 15–20% of all breast cancers, TNBC exhibits aggressive clinical symptoms (2). Although chemotherapy remains a major therapeutic method for metastatic TNBC; its efficacy is limited, yielding a median overall survival time of 12-18 months (2). Consequently, there is an urgent need for innovative therapeutic strategies.

In recent years, immunotherapy has emerged as a promising intervention, demonstrating prolonged survival in various solid tumors (3–5). Notably, immune checkpoint inhibitor (ICI) monotherapy in TNBC patients has shown response rates ranging from 5% to 23% (6), while combined with chemotherapy, for early-stage TNBC patients exhibit pathologically complete response rates between 22% and 60% (7). Despite these advances, only a subset of patients benefits from immunotherapy, highlighting the need for the development of predictive models and the identification of novel biomarkers to better anticipate treatment outcomes and prognosis.

Single-cell RNA sequencing (scRNA-seq) technology and related data analysis methods has facilitated the exploration of molecular characteristics of immune cells within the tumor microenvironment (TME) (8). This unparalleled opportunity has provided insights into cancer immunity, enabling the establishment of genetic markers based on immune cell molecular characteristics to predict immunotherapy outcomes in cancer patients (9, 10).

Recent research has demonstrated that tumor-infiltrating B lymphocytes (TIL-Bs) in breast cancer, responding to B cell receptor (BCR) activation and generating immunoglobulin (Ig) *in vivo* (11–13). Thus, B cells may significantly influence the prognosis of breast cancer, particularly in patients with immunogenic TNBC. Here, our study aimed to conduct an integrated analysis of scRNA-seq data from TNBC samples, identify B cell marker genes, and subsequently develop a predictive model for accessing the prognosis of TNBC patients.

Methods

Data collection

Transcriptional RNA sequencing data from single-cell profiling datasets of four TNBC tumor tissue (GSM4909281, GSM4909282, GSM4909283 and GSM4909284; accessible at https://www.ncbi.nlm.nih.gov/geo/) were acquired for the purpose of investigating B cell marker genes. Concurrently, clinical profiles and transcriptomic data were obtained from the Cancer Genome Atlas (TCGA) and Gene Expression Omnibus (GEO) databases.

Processing single-cell sequencing data

The single-cell sequencing data obtained from patients were subjected to comprehensive analysis through the R software and related packages. Seurat objects were constructed following the parsing of single-cell sequencing data sourced from TNBC samples represented by GSM4909281, GSM4909282, GSM4909283, and GSM4909284. The DoubletFinder package was applied to eliminate the cell doublets within the sample. Exclusion criteria for cells of suboptimal quality are as follows: 1) the number of features exceeding 500 and falling below 6000, 2) the mitochondrial genes expression below 10%, 3) the expression of erythroid genes less than 5%. In order to integrate data from multiple samples, the software known as "harmony" was employed.

The Uniform Manifold Approximation and Projection (UMAP) method was adopted to reduce the number of dimensions, displaying clustered cells with only two dimensions on a map. The subpopulations of tumor-associated B cells were determined by using the "SingleR" software as previous publications indicated (14, 15). Marker genes for different cell types were ascertained through Wilcoxon-Mann-Whitney test and the "FindAllMarkers" function analysis. The criteria for filtering marker genes of various cell types included a | log2 (fold change) | > 1 and the adjusted P value less than 0.05.

Functional enrichment

The functional annotation of marker genes associated with tumor-associated B cells was augmented through enrichment analysis using the Gene Ontology (GO) and the Kyoto Encyclopedia of Genes and Genomes (KEGG). The c2.cp.v2023.2.Hs.symbols.gmt dataset from the MSigDB database (https://www.gsea-msigdb.org/gsea/msigdb) was used for Gene Set Enrichment Analysis (GSEA) to elucidate the biological processes involved in the B-cell marker gene.

A predictive model of B cell marker gene

A predictive model for B cell marker gene expression in TNBC was developed to predict TNBC prognosis. In the univariate COX regression analysis, genes identified as B-cell markers were incorporated. The least absolute shrinkage and selection operator (LASSO) regression was performed to construct a penalty function, effectively compressing the coefficients of variables and reducing overfitting of the model caused by prognosis-related genes. Subsequently, the outcomes from the multivariate COX regression analysis were used to formulate a predictive B cell marker gene score (BCMG score) model.

The formula is as follows:

$$BCMG\ \ score = \beta_1 * \ Expr_1 + \beta_2 * \ Expr_2 + \ldots + \beta_n * Expr_n$$

Here, *Expr* denotes the mRNA expression of the crucial gene, *n* denotes the number of genes included in the model, and β represents the associated regression coefficient determined in the multivariate gene COX regression analysis. The data was then classified into higher and lower- BCMG score groups based on the median value of the BCMG score.

To validate the model's robustness, an independent third-party validation set, GSE58812, was employed to assess and confirm the predictive performance of the model.

Immune infiltration analysis

Based on the gene expression dataset of patients, the CIBERSORT algorithm was conducted to determine the magnitude of immune cell proliferation in each sample. Spearman correlation analysis was performed to examine the variations in immune cell infiltration between the two groups. A single-sample GSEA was carried out to further assess the differences in immune cell activity between the higher and lower- BCMG score groups. Estimation techniques were implemented to determine the differences of immune scores, stromal scores, overall scores, and tumor purity between the two groups. Multiple tools, including XCELL, TIMER, MCP counter, CIBERSORT, and CIBERSORT-abs, were applied to establish a correlation between B cell marker genes and immune cells.

Forecasting the patient's response to immunotherapy

Spearman test was used to analyze the correlation of expression between model and immune genes. The TIDE score was incorporated to evaluate the effectiveness of immunotherapy in individual patients. Patients with lower TIDE scores indicated a decreased risk of immunological escape, which suggested a higher likelihood of effective immunotherapy. An online tool TIDE (http://tide.dfci.harvard.edu/) was used to examine the immunotherapy scores of each patient, and investigate the differences in immunotherapy results between the higher and lower- BCMG score groups.

Analysis of the tumor's mutational burden

The raw data of the patient's tumor mutations were obtained and downloaded from the TCGA database. The "maftools" package in R was used to generate waterfall graphs in accordance with predefined specifications. This study also further assessed the differences in tumor mutation burden as well as predicted discrepancies between higher and lower-BCMG score groups.

Statistics analyses

Kaplan-Meier method and the log-rank test were utilized for survival analysis. Alternately, the Wilcoxon rank-sum test was employed to compare the differences existing between the two groups. R (4.1.2, available at https://www.r-project.org/) was conducted throughout the entire data analysis process. P values of less than 0.05 on both sides were defined as statistically significant.

Results

Examination of single cells

The integration of single-cell sequencing data from four TNBC patients was achieved using the "Harmony" package. After excluding cells of suboptimal quality, the subsequent study consisted of the examination of 22,106 cells and 20,556 genes (Figure 1). The identification of potential marker genes for TNBC-associated B cells was conducted through the application of the Wilcoxon-Mann-Whitney test, revealing 116 distinct genes with significant differences (Table S1). The clinical characteristics of the training group TCGA and the testing group GSE58812 was detailed in Table S2.

Tumor-associated B-cell marker gene enrichment analysis

The investigation of genes enriched in tumors associated B cells yielded notable results. The GO and KEGG analysis revealed that marker genes of B cells predominantly influenced functional pathways specific to B cells. Significant differences were observed in cell pathway activity scoring across different cell types. Particularly, the unfolded protein response signaling pathway demonstrated notable activity in B cells. The B cell marker genes mainly participate in biological processes such as pid CD8 tcr dowstream pathway, pid IL12 pathway, WP cancer imunotherapy by PD 1 blockade, and WP T cell recpto signaling pathway. (Figure 2).

Development of a predictive model for B-Cell marker gene expression

The evaluation of the 116 genes involved a univariate COX regression to identify the 10 genes associated with prognosis. In order to prevent overfitting, a lasso regression analysis was subsequently performed. The results of the lasso regression were further subjected to a multifactor COX regression analysis to construct predictive models. The final model incorporated the following variables: *ZBP1, SEL1L3, CCND2, TNFRSF13C, HSPA6, PLPP5, CXCR4, GZMB*, and *CCDC50* (Figures 3A, B).

The predictive score was computed based on the expression levels of the selected genes using the following formula:

$$\text{BCMG score} = (-0.0390 \times ZBP1) + (-0.3450 \times SEL1L3) + (-0.0474 \times CCND2) + (-0.0716 \times TNFRSF13C) + (0.2560 \times HSPA6) + (0.5725 \times PLPP5) + (-0.1924 \times CXCR4) + (-0.1424 \times GZMB) + (-0.1246 \times CCDC50)$$

Patients from TCGA and GEO were divided into higher and lower- BCMG score groups according to the median value of the scores obtained from TCGA.

Model validation

The survival curves revealed that patients classified in the higher BCMG score group had a worse prognosis than those in the lower

10.3389/fimmu.2023.1245514

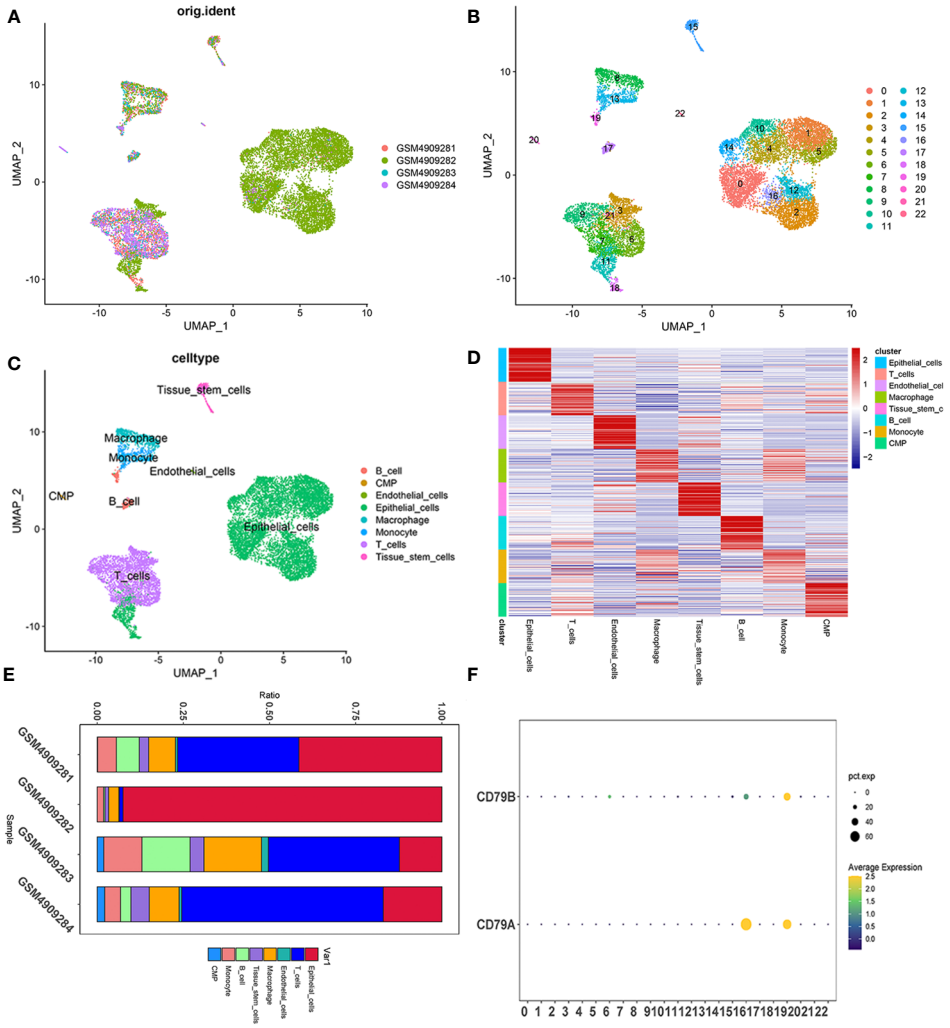

FIGURE 1
Single cell sequencing profile of 22,106 cells from human samples of TNBC. **(A–C)** UMAP plots of 22,106 tumor-associated B cells here, colored by individual samples **(A)**, 22 cell clusters identified when resolution equals 2 **(B)** and cell types **(C)**. **(D)** Heatmap displaying the top 10 marker genes in each cell cluster. **(E)** Proportions of each cell type in each sample colored by cell types. **(F)** Expression analysis of BCMGs in 22 cell clusters. The intensity of the color indicates the average expression of the gene. Dot size indicates the percentage of cells expressing the gene.

BCMG score group (Figures 3C, D). The time-dependent receiver operating characteristic (ROC) curves indicated that the predictive model had an outstanding discriminatory capability (Figures 3E, F). Importantly, these results were not only internally validated within the study group but also externally validated in an independent validation group (Figures 3E, F). According to the findings of the independent predictive study (Figures 4A, B), the predictive model was identified as a significant independent predictive factor in patients with TNBC. The correlation analysis with clinical characteristics further highlighted the close association between the predictive model and lymph node metastases (Figure 4). In-depth exploration of the correlation between the model genes and patient prognosis (Figure 5) revealed that the expression levels of *ZBP1*, *SEL1L3*, *CCND2*, *TNFRSF13C*, *CXCR4*, *GZMB*, and *CCDC50* were higher in the lower BCMG score group compared to the higher group. Conversely, the higher BCMG score group exhibited significantly higher levels of expression for *HSPA6* and *PLPP5* (Figure 6).

Analysis of tumor mutation burden

The analysis of the tumor mutation burden revealed an inverse relationship with the prognostic model. The waterfall plot visually illustrated that the mutation types were not identical between the higher and lower- BCMG score groups. The survival analysis results indicated that patients with lower tumor mutation load exhibited a more favorable prognosis (Figure 7).

10.3389/fimmu.2023.1245514

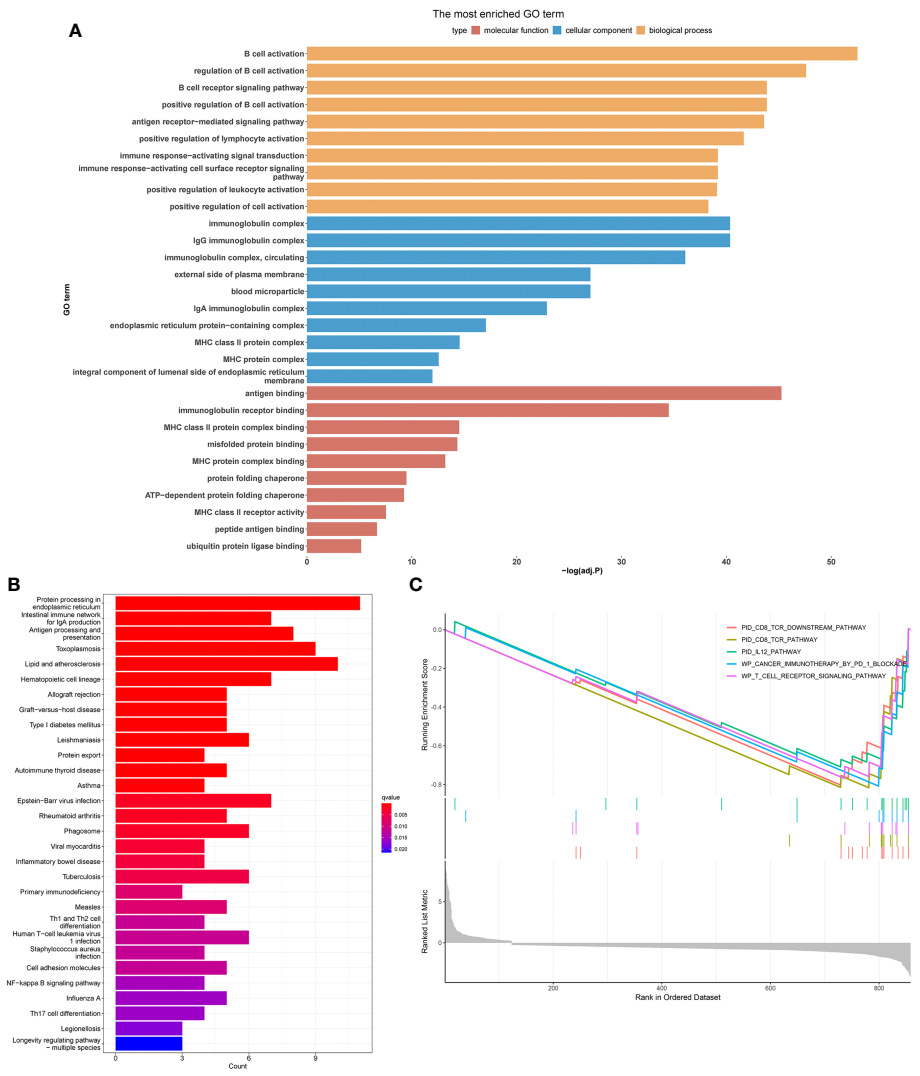

FIGURE 2
Exploring the differences in activity in different cell types by employing different enrichment analysis methods. Histogram of GO **(A)**, KEGG **(B)** and GSEA **(C)** enrichment analysis.

Analysis of TME

The CIBERSORT analysis demonstrated the differential presence and activity of various immune cell types in the TMB between the higher and lower- BCMG score groups. Specifically, $CD8^+$ T cells, activated memory $CD4^+$ T cells, M1 macrophages, M2 macrophages and eosinophils were found to serve different functions between the two groups (Figures 8A, B). The overall activity of the majority of immune cells exhibited notable changes in both groups, further emphasizing the dynamic nature of the TME (Figure 8C). The ESTIMATE algorithm indicated that the lower BCMG score group had significantly higher tumor scores, interstitial scores, total scores, and tumor purity scores than the higher BCMG score group (Figure 8D). Furthermore, correlation analysis between the predictive scores and the TME analyzed by the four methods CIBERSORT-ABS, CIBERSORT, QUANTISEQ, and XCELL, demonstrated the potential influence of B-cell marker gene model on the TME (Figure 9).

Predictions regarding immunotherapy

Correlation analysis revealed that *ZBP1, GZMB, CCND2*, and *TNFRSF13C* exhibited strong correlations with the majority of the genes that inhibit immune response (Figure 10A). Simultaneously, a significant difference was observed between the higher and lower-BCMG score groups concerning the expression of several immune blockade checkpoint genes (Figure 10C). The TIDE ratings were used to make predictions about the outcomes of immunotherapy treatment for patients classified as either high or low BCMG expression. The TIDE scores of patients in the high expressed group were significantly higher than those of patients in the low

10.3389/fimmu.2023.1245514

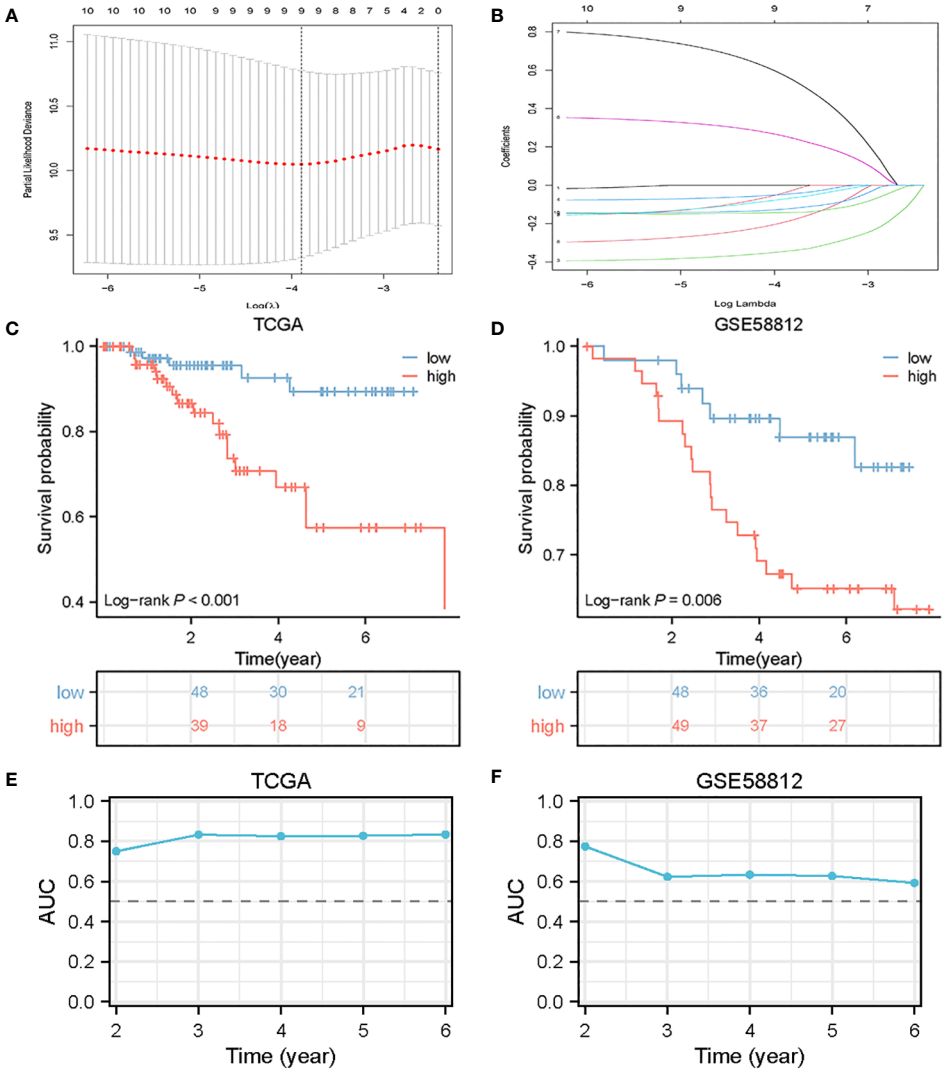

FIGURE 3
Construction of BCMG score model in the TNBC cohort. **(A)** Log (λ) change curves of regression coefficients and cross-validation for optimizing the parameter in LASSO regression. **(B)** Tenfold cross-validation of adjusted parameter choices in lasso regression. **(C, D)** Kaplan-Meier survival analysis of TCGA and GSE58812 of TNBC patients stratified by higher and lower- BCMG score. **(E, F)** ROC curve analysis for predicting the risk of death in the cohort of TCGA **(E)** and GSE58812 **(F)**.

expressed group, which indicated a higher likelihood of immune evasion in the high expressed group and immunotherapy may be less effective for patients at high expression. In addition, there were observed differences between the two groups in terms of CD8 scores, CD274 ratings, MDSC scores, T cell dysfunction scores, and T cell exclusion scores (Figure 10B).

Discussion

In this study, we investigated the role of B-cell marker genes in TNBC using scRNA-seq technology. We successfully established a novel prediction score for TNBC patients, derived from the identified B-cell marker genes within the TCGA database. This prediction score was rigorously validated for its predictive capabilities in an independent cohort of the GEO dataset. Our analysis highlighted specific genes, including *ZBP1, SEL1L3, CCND2, TNFRSF13C, CXCR4, GZMB*, and *CCDC50*, which exhibited protective characteristics. In contrast, *HSPA6* and *PLPP5* were identified as having negative implications. Subsequently, the nine gene signatures collectively contribute to a robust predictive model that emerges as a promising predictor for clinical prognosis in TNBC patients.

Patients with TNBC exhibit a significantly higher level of immune infiltration compared to other breast cancer subtypes, despite their overall poor prognosis. The higher immune infiltration is characterized by elevated tumor-infiltrating lymphocytes (TILs) (16), increased levels of PD-L1 expression in tumor cells and immune cells (17, 18), and a greater number of non-synonymous mutations, which produce tumor-specific neoantigens, activate neoantigen-specific T cells, and trigger anti-tumor immune responses (19, 20). This unique immune landscape suggests a

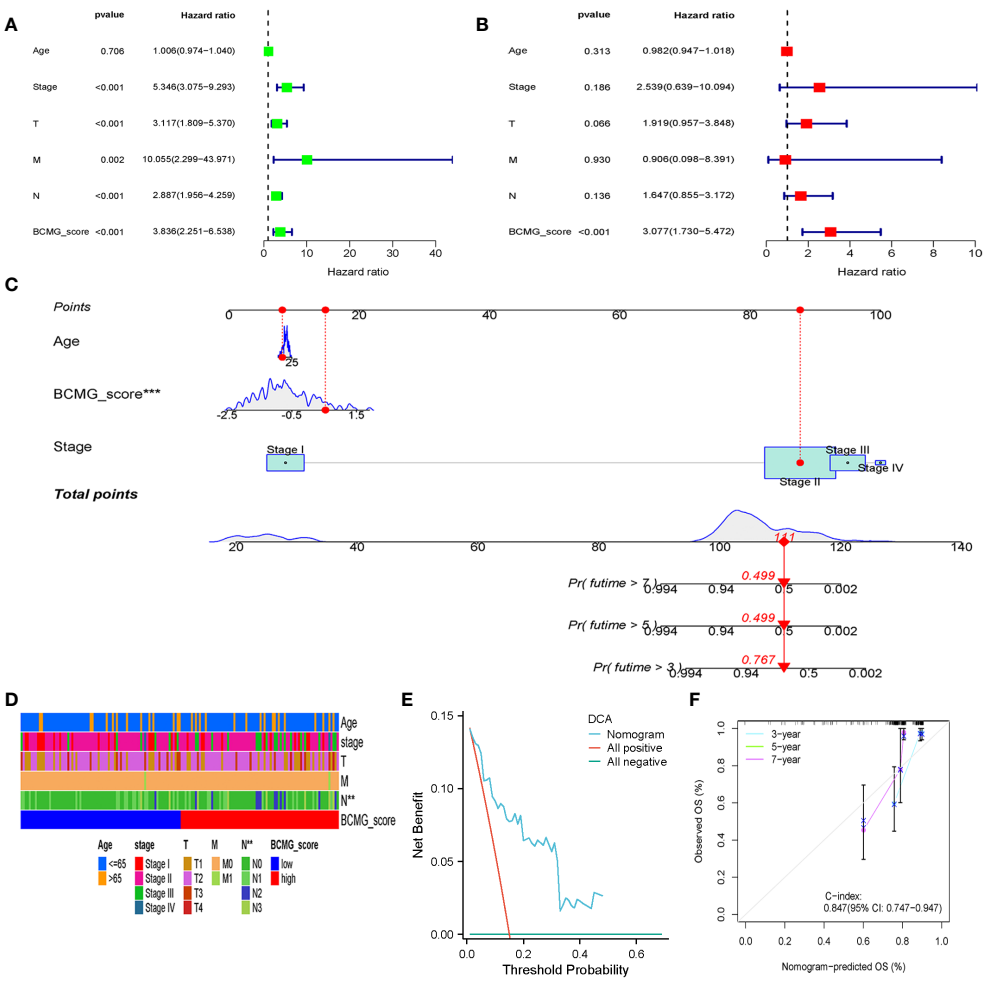

FIGURE 4
Clinical analysis in the cohort of TCGA. **(A)** Univariate Cox regression analysis revealed the association between patients' survival and clinicopathological parameters along with BCMG score. **(B)** Multivariate Cox regression analysis uncovered that only the BCMG score (P< 0.001) was an independent prognostic factor for TNBC patients. **(C)** The prediction of 3-, 5-, and 7-year survival for TNBC patients based on the prognostic nomogram derived from the BCMG score and other clinicopathologic feature. **(D)** Clinical correlation with age, stage, T, N, M and BCMG score shown in heatmap. **(E)** DCA curve analysis. **(F)** Calibration Curve illustrated the consistency between predicted and observed 3-, 5-, and 7- year survival rates in TNBC patients depending on the prognostic nomogram.

greater potential for benefit from immunotherapy in TNBC comparison to other subtypes. ICIs can block immunosuppressive receptors and increase the cellular toxicity and proliferation of TILs (3, 21, 22). According to the findings of a few studies, the effectiveness of ICI monotherapy ranges from 5% to 23% (6), whereas the effectiveness of combination therapy ranges from 22% to 60% (7). Nonetheless, some patients experienced resistance during or after treatment, leading to immune escape and tumor recurrence. Dual checkpoint blockade, which have synergistic anti-tumor effects in advanced malignancies, such as anti-CTLA-4 and anti-PD-1, could potentially serve as a more effective therapeutic strategy (23). Furthermore, recent studies have explored innovative strategies, such as bispecific antibodies targeting TGF-β and PD-L1 (BiTP), which have demonstrated potent antitumor activity in TNBC. BiTP in murine TNBC models showed higher anti-tumor activity compared with solo anti-PD-L1 or anti-TGF-β (24). The rejection and exhaustion of $CD8^+$ T cells are two key factors that contribute to the reduced tolerance of ICI therapy. When enhanced $CD8^+$ T-cell infiltration occurs, there is a shift towards heat immunity (25). BiTP has a high binding affinity to the dual targets, which reduces collagen deposition, enhances $CD8^+$ T-cell penetration and increases TILs (26).

Our study provides valuable insights into the molecular landscape of TNBC-associated B cells and their functional implications in tumor biology. These findings underscore the intricate interplay between the identified prognostic model and the immune landscape within the TME, and we also illustrate potential immunomodulatory roles of the B-cell marker genes in the context of TNBC. Moreover, the differential mutation burden observed in distinct BCMG score groups highlights the importance of considering mutational characteristics in conjunction with the prognostic model for a comprehensive understanding of the disease prognosis in TNBC patients.

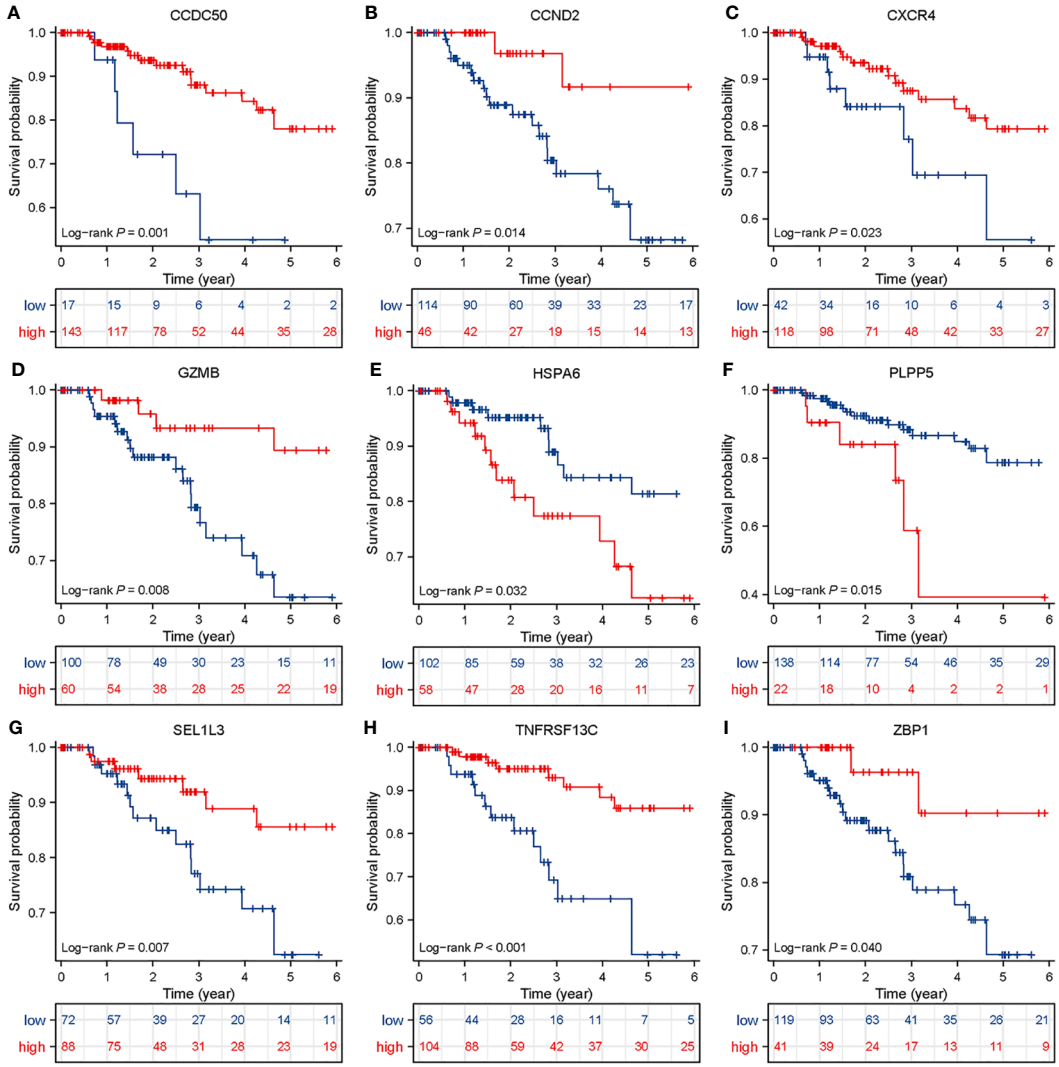

FIGURE 5
Survival analysis in TNBC patients based on BCMG score. Kaplan-Meier survival analysis of TCGA TNBC patients stratified by high and low *CCDC50, CCND2, CXCR4, GZMB, HSPA6, PLPP5, SEL1L3, TNFRSF 13C*, and *ZBP1* **(A–I)**, which were based on the best cutoff values.

Extensive investigations in the breast cancer TME have primarily focused on $CD8^+$ T lymphocytes and natural killer (NK) cells (27). In contrast, TIL-B lymphocytes (TIL-Bs) cells may exhibit antigen-induced phenotype (28), and it is hypothesized that autoantibodies play a role in initiating tumor cell clearance (29). TIL-Bs have also been identified as antigen-presenting cells, contributing to the stimulation of an immune response against tumors (30). Moreover, there is a potential for TIL-Bs to form stromal clusters with T cells, engaging in functional cross-talk in both directions. The formation of BCR-immune complexes may also be facilitated by TIL-Bs through the upregulation of BCR pathway components (1). Besides, $CD8^+$ T cells represent pivotal defense cells in TME and establish a functional cycle with dendritic cells (DCs) and NKs (31). Positive crosstalk is observed between $CD8^+$ T cells and DCs, with $CD8^+$ T cells inducing NK cell activity (32). Therefore, it is possible that B cells exert a significant influence on the prognosis of breast cancer, particularly in patients of immunogenic TNBC.

The scRNA-seq technology has allowed for a more in-depth exploration of the molecular properties of immune cells within the TME, offering potential insights into novel biomarkers (33). In this study, the investigation of B-cell marker genes provides valuable insights into the potential role of nine specific genes in influencing the prognosis of individuals diagnosed with TNBC. *ZBP1*, overexpressed in necrotic breast tumors, has been linked to the induction of interferon. In the absence of *ZBP1*, both the process of tumor necrosis and the suppression of metastasis are prevented (34). *SEL1L3*, with decreased expression in cancer cells during sustained endoplasmic reticulum stress (35), may serve as a predictive tool for survival outcomes and immunotherapy response in various cancers (36–39). The promoter of *CCND2* is hypermethylated (40–42) in solid tumors, which leads to *CCND2* hypo-expression (40, 43, 44) and promotes cell proliferation (45). *TNFRSF13C* could encode B-cell activating factor receptor, which regulates B-cell proliferation, development and maturation (46, 47). High levels of *CXCR4* levels were expressed in more than 40% of

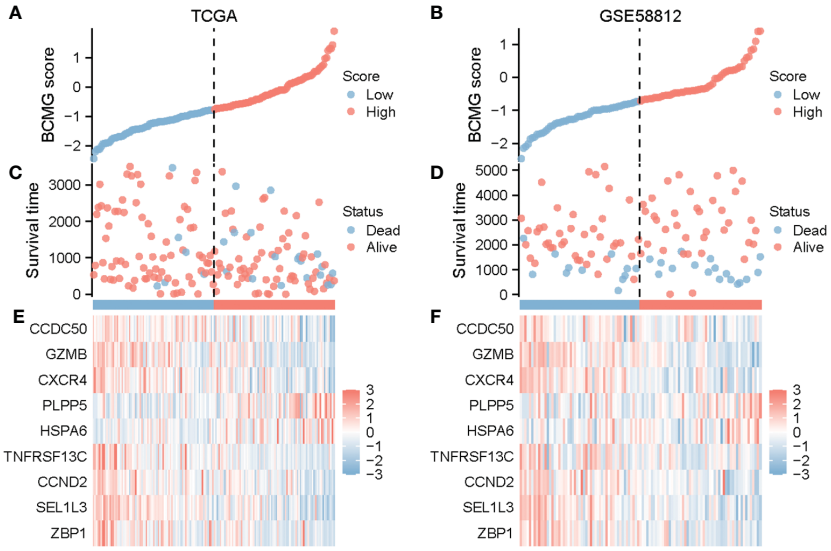

FIGURE 6
Prognostic analysis of TNBC patients on the basis of BCMG score in TCGA and GEO. BCMG score distribution in TCGA **(A)** and GSE58812 **(B)**. Scatterplot of survival status and survival time of TNBC patients in TCGA **(C)** and GSE58812 **(D)**. Heatmap generated on the basis of identified gene expression in TCGA **(E)** and GSE58812 **(F)**.

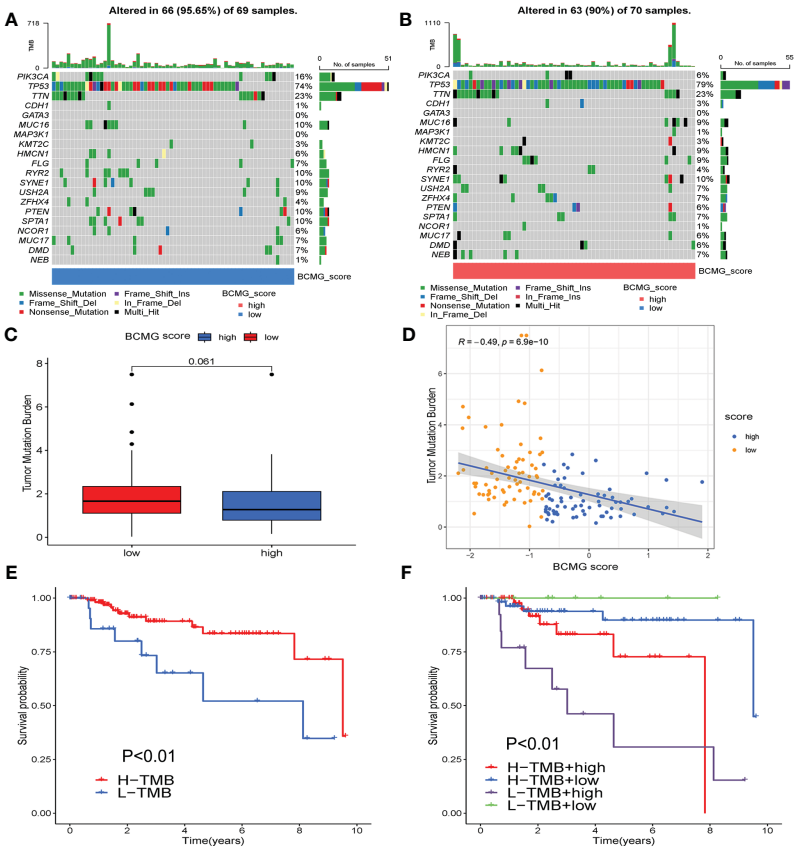

FIGURE 7
Tumor mutation burden analysis. **(A, B)** Differential counting of tumor mutation burden between higher and lower - BCMG score groups. **(C)** Tumor mutation load comparison. **(D)** Correlation analysis of BCMG score and mutation burden. **(E, F)** Prognostic analysis of tumor mutation load in higher and lower- BCMG score groups.

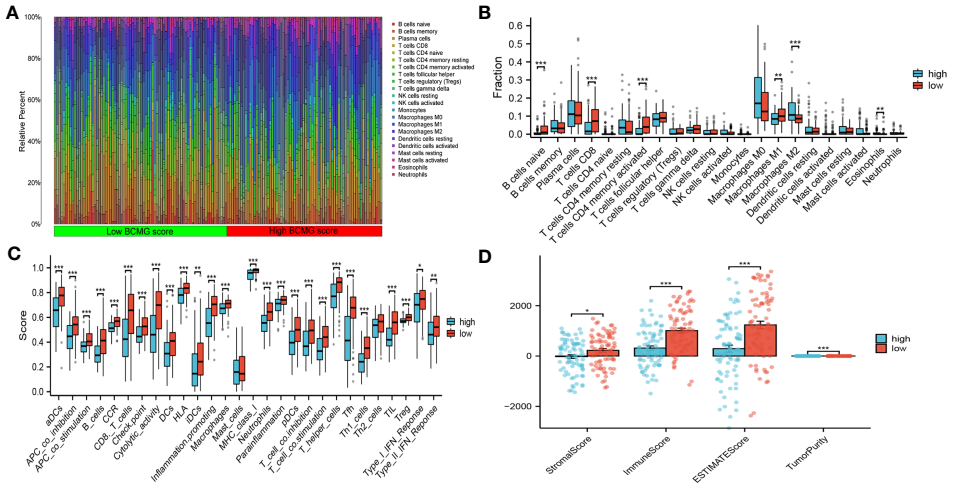

FIGURE 8
Correlation of the B cell prognostic model genes with immune cell infiltration and immune checkpoint in TCGA cohort. **(A)** Analysis of immune cell infiltration in higher and lower- BCMG score groups. **(B)** The comparison of 22 immune cells' infiltration level in higher and lower- BCMG score groups. **(C)** The comparison of 28 immune cells' infiltration level in higher and lower- BCMG score groups. **(D)** TME score differences compared based on the ESTIMATE algorithm. *P < 0.05; **P < 0.01; ***P < 0.001.

breast tumor tissues (48) and in 75% of TNBC patients (49), and overexpression of *CXCR4* in cancer cells contributes to tumor growth, invasion, metastasis, and recurrence (50). *GZMB*, known for stimulating anti-tumor immune responses and inhibit tumor growth (51), is correlated with favorable prognosis in breast cancer tissues (52, 53). *CCDC50* is known to mediate apoptosis via the NF-κB pathway (54) and had prognostic predictive value in lung adenocarcinoma (55). The two-way role of *HSPA6* in tumor,

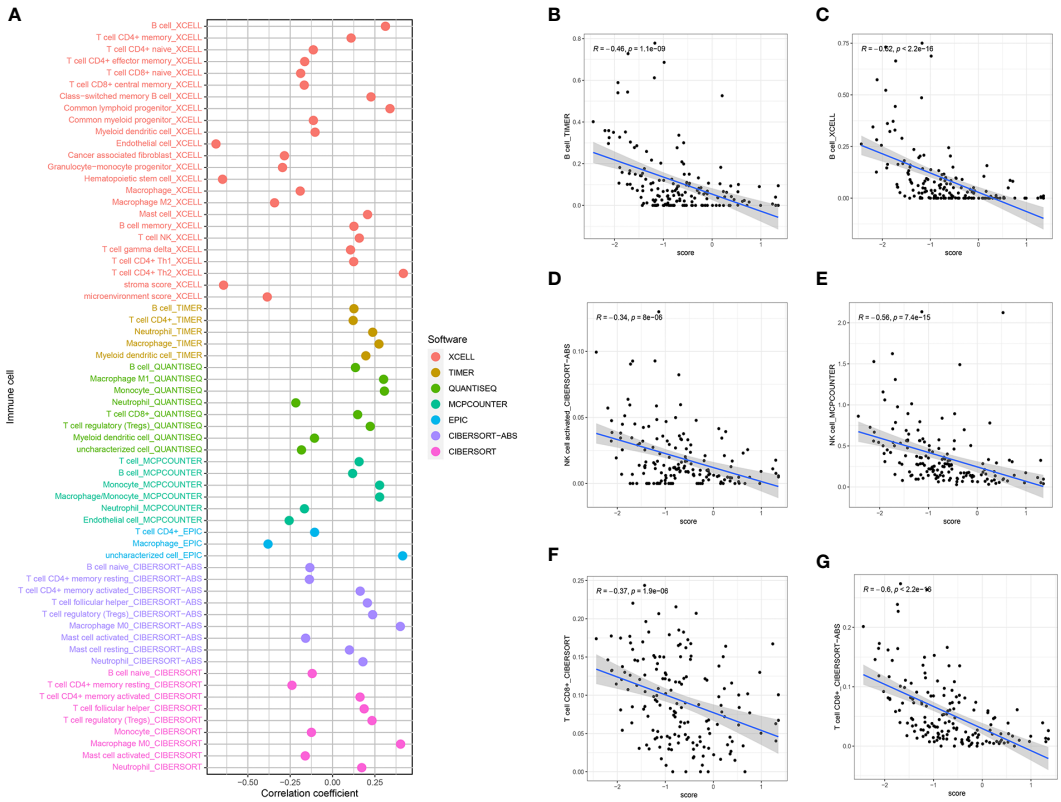

FIGURE 9
BCMG score and immune cell correlation analysis. **(A)** Spearman correlation analysis showed that BCMG scores strongly correlated with tumor-infiltrating immune cells. **(B–G)** Correlation of predictive models and immune cells based on XCELL, TIMER, QUANTISEQ, CIBERSORT, and CIBERSORT-abs.

10.3389/fimmu.2023.1245514

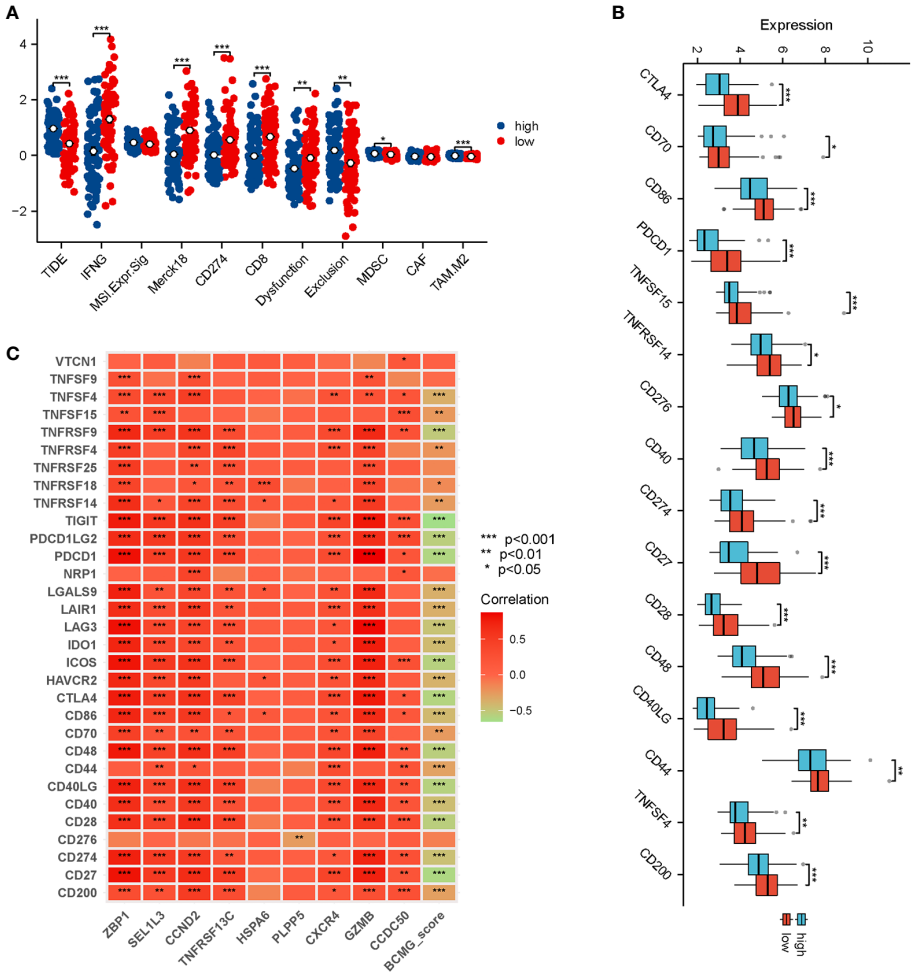

FIGURE 10
Prediction of response of TNBC patients to immunotherapy. **(A)** Analysis of differences in TIDE, IFNG, MSI Expr, Merck18, CD274, CD8, Dysfunction, Exclusion, MDSC, CAF, and TAM M2 between higher and lower- BCMG score groups. **(B)** Analysis of immune checkpoint blocking gene expression between higher and lower- BCMG score groups. **(C)** Relevance of model genes and immune checkpoint blocking gene.

acting as both a potential target for tumor inhibition and risk factor of tumor development and tumor progression, underscores the complexity of its functions in cancer biology (56). Our study suggested a negative correlation between high *HSPA6* expression and prognosis, which contradicts the findings reported by Shen et al., where high *HSPA6* expression was positively correlated with longer overall survival (57). This discrepancy may arise from the multifaceted functions of *HSPA6*, affecting different aspects of cancer biology. *PLPP5* participates in the regulation of many cancer-associated transduction pathways such as the JAK/STAT (58), and its overexpression in pancreatic and small cell lung cancer cells may promote proliferation and survival (59). However, in breast cancer cell lines, down-regulation of *PLPP5* inhibits tumor growth and increases apoptosis (60), which is consistent with our study.

Despite these intriguing findings, there are certain limitations in the current study. Additional research is needed to get a deeper understanding of molecular interactions and mechanisms underlying these gene functions. Furthermore, it is essential to verify these findings in cell lines, animal models, and tissue samples to ensure their relevance and applicability to clinical settings.

Conclusion

In conclusion, this study established a robust model utilizing B cell marker genes to predict prognosis and immunotherapy response in TNBC patients, contributing novel insights into the understanding of TNBC molecular landscape and its implications for therapeutic interventions. The discovery of these gene signatures adds to our understanding of TNBC and offers a promising avenue for improving patient outcomes and guiding therapeutic strategies in this challenging subtype of breast cancer. Further research and clinical validation may continue to refine the application of these gene signatures in the clinical management of TNBC patients.

Data availability statement

The datasets presented in this study can be found in online repositories. The names of the repository/repositories and accession number(s) can be found in the article/Supplementary Material.

Ethics statement

Ethical approval was not required for the study involving humans in accordance with the local legislation and institutional requirements. Written informed consent to participate in this study was not required from the participants or the participants' legal guardians/next of kin in accordance with the national legislation and the institutional requirements.

Author contributions

Conceptualization: CZ and HL; Data curation: TX; Methodology: XW; Formal analysis: YL; Writing-original draft: FZ; Review and editing of the manuscript: CZ and XL. All authors contributed to the article and approved the submitted version.

Funding

The author(s) declare financial support was received for the research, authorship, and/or publication of this article. The study was financed by Natural Science Foundation of Hubei Province (2023AFB165) and Renmin Hospital of Wuhan University Cross-Innovation Talent Project (JCRCWL-2022-003).

Conflict of interest

The authors declare that the research was conducted in the absence of any commercial or financial relationships that could be construed as a potential conflict of interest.

Publisher's note

All claims expressed in this article are solely those of the authors and do not necessarily represent those of their affiliated organizations, or those of the publisher, the editors and the reviewers. Any product that may be evaluated in this article, or claim that may be made by its manufacturer, is not guaranteed or endorsed by the publisher.

Supplementary material

The Supplementary Material for this article can be found online at: https://www.frontiersin.org/articles/10.3389/fimmu.2023.1245514/full#supplementary-material

References

1. Harris RJ, Cheung A, Ng JCF, Laddach R, Chenoweth AM, Crescioli S, et al. Tumor-infiltrating B lymphocyte profiling identifies IgG-biased, clonally expanded prognostic phenotypes in triple-negative breast cancer. *Cancer Res* (2021) 81(16):4290–304. doi: 10.1158/0008-5472.CAN-20-3773

2. Garrido-Castro AC, Lin NU, Polyak K. Insights into molecular classifications of triple-negative breast cancer: improving patient selection for treatment. *Cancer Discovery* (2019) 9(2):176–98. doi: 10.1158/2159-8290.CD-18-1177

3. Kim ST, Cristescu R, Bass AJ, Kim KM, Odegaard JI, Kim K, et al. Comprehensive molecular characterization of clinical responses to PD-1 inhibition in metastatic gastric cancer. *Nat Med* (2018) 24(9):1449–58. doi: 10.1038/s41591-018-0101-z

4. Motzer RJ, Rini BI, McDermott DF, Redman BG, Kuzel TM, Harrison MR, et al. Nivolumab for metastatic renal cell carcinoma: results of a randomized phase II trial. *J Clin Oncol* (2015) 33(13):1430–7. doi: 10.1200/JCO.2014.59.0703

5. El-Khoueiry AB, Sangro B, Yau T, Crocenzi TS, Kudo M, Hsu C, et al. Nivolumab in patients with advanced hepatocellular carcinoma (CheckMate 040): an open-label, non-comparative, phase 1/2 dose escalation and expansion trial. *Lancet* (2017) 389 (10088):2492–502. doi: 10.1016/S0140-6736(17)31046-2

6. Keenan TE, Tolaney SM. Role of immunotherapy in triple-negative breast cancer. *J Natl Compr Canc Netw* (2020) 18(4):479–89. doi: 10.6004/jnccn.2020.7554

7. Nanda R, Liu MC, Yau C, Shatsky R, Pusztai L, Wallace A, et al. Effect of pembrolizumab plus neoadjuvant chemotherapy on pathologic complete response in women with early-stage breast cancer: an analysis of the ongoing phase 2 adaptively randomized I-SPY2 trial. *JAMA Oncol* (2020) 6(5):676–84. doi: 10.1001/jamaoncol.2019.6650

8. Chen H, Ye F, Guo G. Revolutionizing immunology with single-cell RNA sequencing. *Cell Mol Immunol* (2019) 16(3):242–9. doi: 10.1038/s41423-019-0214-4

9. Zhong R, Chen D, Cao S, Li J, Han B, Zhong H. Immune cell infiltration features and related marker genes in lung cancer based on single-cell RNA-seq. *Clin Trans Oncol* (2021) 23(2):405–17. doi: 10.1007/s12094-020-02435-2

10. Wu T, Wu X, Wang HY, Chen L. Immune contexture defined by single cell technology for prognosis prediction and immunotherapy guidance in cancer. *Cancer Commun (Lond)* (2019) 39(1):21. doi: 10.1186/s40880-019-0365-9

11. Hu X, Zhang J, Wang J, Fu J, Li T, Zheng X, et al. Landscape of B cell immunity and related immune evasion in human cancers. *Nat Genet* (2019) 51(3):560–7. doi: 10.1038/s41588-018-0339-x

12. Helmink BA, Reddy SM, Gao J, Zhang S, Basar R, Thakur R, et al. B cells and tertiary lymphoid structures promote immunotherapy response. *Nature* (2020) 577 (7791):549–55. doi: 10.1038/s41586-019-1922-8

13. Garaud S, Buisseret L, Solinas C, Gu-Trantien C, de Wind A, Van den Eynden G, et al. Tumor infiltrating B-cells signal functional humoral immune responses in breast cancer. *JCI Insight* (2019) 5(18):e129641. doi: 10.1172/jci.insight.129641

14. Chung W, Eum HH, Lee HO, Lee KM, Lee HB, Kim KT, et al. Single-cell RNA-seq enables comprehensive tumour and immune cell profiling in primary breast cancer. *Nat Commun* (2017) 8:15081. doi: 10.1038/ncomms15081

15. Hu Q, Hong Y, Qi P, Lu G, Mai X, Xu S, et al. Atlas of breast cancer infiltrated B-lymphocytes revealed by paired single-cell RNA-sequencing and antigen receptor profiling. *Nat Commun* (2021) 12(1):2186. doi: 10.1038/s41467-021-22300-2

16. Denkert C, von Minckwitz G, Darb-Esfahani S, Lederer B, Heppner BI, Weber KE, et al. Tumour-infiltrating lymphocytes and prognosis in different subtypes of breast cancer: a pooled analysis of 3771 patients treated with neoadjuvant therapy. *Lancet Oncol* (2018) 19(1):40–50. doi: 10.1016/S1470-2045(17)30904-X

17. Mittendorf EA, Philips AV, Meric-Bernstam F, Qiao N, Wu Y, Harrington S, et al. PD-L1 expression in triple-negative breast cancer. *Cancer Immunol Res* (2014) 2 (4):361–70. doi: 10.1158/2326-6066.CIR-13-0127

18. Gatalica Z, Snyder C, Maney T, Ghazalpour A, Holterman DA, Xiao N, et al. Programmed cell death 1 (PD-1) and its ligand (PD-L1) in common cancers and their correlation with molecular cancer type. *Cancer Epidemiol Biomarkers Prev* (2014) 23 (12):2965–70. doi: 10.1158/1055-9965.EPI-14-0654

19. Luen S, Virassamy B, Savas P, Salgado R, Loi S. The genomic landscape of breast cancer and its interaction with host immunity. *Breast* (2016) 29:241–50. doi: 10.1016/j.breast.2016.07.015

20. Schumacher TN, Schreiber RD. Neoantigens in cancer immunotherapy. *Science* (2015) 348(6230):69–74. doi: 10.1126/science.aaa4971

21. Ribas A, Wolchok JD. Cancer immunotherapy using checkpoint blockade. *Science* (2018) 359(6382):1350–5. doi: 10.1126/science.aar4060

22. Topalian SL, Hodi FS, Brahmer JR, Gettinger SN, Smith DC, McDermott DF, et al. Safety, activity, and immune correlates of anti-PD-1 antibody in cancer. *N Engl J Med* (2012) 366(26):2443–54. doi: 10.1056/NEJMoa1200690

23. Nikoo M, Rabiee F, Mohebbi H, Eghbalifard N, Rajabi H, Yazdani Y, et al. Nivolumab plus ipilimumab combination therapy in cancer: Current evidence to date. *Int Immunopharmacol* (2023) 117:109881. doi: 10.1016/j.intimp.2023.109881

24. Li T, Wang X, Niu M, Wang M, Zhou J, Wu K, et al. Bispecific antibody targeting TGF-beta and PD-L1 for synergistic cancer immunotherapy. *Front Immunol* (2023) 14:1196970. doi: 10.3389/fimmu.2023.1196970

25. Mortezaee K, Majidpoor J. Mechanisms of CD8(+) T cell exclusion and dysfunction in cancer resistance to anti-PD-(L)1. *BioMed Pharmacother* (2023) 163:114824. doi: 10.1016/j.biopha.2023.114824

26. Yi M, Wu Y, Niu M, Zhu S, Zhang J, Yan Y, et al. Anti-TGF-beta/PD-L1 bispecific antibody promotes T cell infiltration and exhibits enhanced antitumor activity in triple-negative breast cancer. *J Immunother Cancer* (2022) 10(12):e005543. doi: 10.1136/jitc-2022-005543

27. Ramakrishnan R, AsSudani D, Nagaraj S, Hunter T, Cho HI, Antonia S, et al. Chemotherapy enhances tumor cell susceptibility to CTL-mediated killing during cancer immunotherapy in mice. *J Clin Invest* (2010) 120(4):1111–24. doi: 10.1172/JCI40269

28. Singh M, Al-Eryani G, Carswell S, Ferguson JM, Blackburn J, Barton K, et al. High-throughput targeted long-read single cell sequencing reveals the clonal and transcriptional landscape of lymphocytes. *Nat Commun* (2019) 10(1):3120. doi: 10.1038/s41467-019-11049-4

29. Scott AM, Wolchok JD, Old LJ. Antibody therapy of cancer. *Nat Rev Cancer* (2012) 12(4):278–87. doi: 10.1038/nrc3236

30. Rossetti RAM, Lorenzi NPC, Yokochi K, Rosa M, Benevides L, Margarido PFR, et al. B lymphocytes can be activated to act as antigen presenting cells to promote anti-tumor responses. *PLoS One* (2018) 13(7):e0199034. doi: 10.1371/journal.pone.0199034

31. Zheng X, Jiang K, Xiao W, Zeng D, Peng W, Bai J, et al. CD8(+) T cell/cancer-associated fibroblast ratio stratifies prognostic and predictive responses to immunotherapy across multiple cancer types. *Front Immunol* (2022) 13:974265. doi: 10.3389/fimmu.2022.974265

32. Uzhachenko RV, Shanker A. CD8(+) T lymphocyte and NK cell network: circuitry in the cytotoxic domain of immunity. *Front Immunol* (2019) 10:1906. doi: 10.3389/fimmu.2019.01906

33. Zhao J, Shi Y, Cao G. The application of single-cell RNA sequencing in the inflammatory tumor microenvironment. *Biomolecules* (2023) 13(2):344. doi: 10.3390/biom13020344

34. Baik JY, Liu Z, Jiao D, Kwon HJ, Yan J, Kadigamuwa C, et al. ZBP1 not RIPK1 mediates tumor necroptosis in breast cancer. *Nat Commun* (2021) 12(1):2666. doi: 10.1038/s41467-021-23004-3

35. Fridman WH, Pages F, Sautes-Fridman C, Galon J. The immune contexture in human tumours: impact on clinical outcome. *Nat Rev Cancer* (2012) 12(4):298–306. doi: 10.1038/nrc3245

36. Zhang C, Ge C. A Simple Competing Endogenous RNA Network Identifies Novel mRNA, miRNA, and lncRNA Markers in Human Cholangiocarcinoma. *BioMed Res Int* (2019) 2019:3526407. doi: 10.1155/2019/3526407

37. Uhlen M, Fagerberg L, Hallstrom BM, Lindskog C, Oksvold P, Mardinoglu A, et al. Proteomics. Tissue-based map of the human proteome. *Science* (2015) 347 (6220):1260419. doi: 10.1126/science.1260419

38. Mei Y, Chen MM, Liang H, Ma L. A four-gene signature predicts survival and anti-CTLA4 immunotherapeutic responses based on immune classification of melanoma. *Commun Biol* (2021) 4(1):383. doi: 10.1038/s42003-021-01911-x

39. Zhong H, Wang J, Zhu Y, Shen Y. Comprehensive analysis of a nine-gene signature related to tumor microenvironment in lung adenocarcinoma. *Front Cell Dev Biol* (2021) 9:700607. doi: 10.3389/fcell.2021.700607

40. Castro M, Grau L, Puerta P, Gimenez L, Venditti J, Quadrelli S, et al. Multiplexed methylation profiles of tumor suppressor genes and clinical outcome in lung cancer. *J Transl Med* (2010) 8:86. doi: 10.1186/1479-5876-8-86

41. McCullough LE, Chen J, Cho YH, Khankari NK, Bradshaw PT, White AJ, et al. Modification of the association between recreational physical activity and survival after breast cancer by promoter methylation in breast cancer-related genes. *Breast Cancer Res* (2017) 19(1):19. doi: 10.1186/s13058-017-0811-z

42. Lehmann U, Berg-Ribbe I, Wingen LU, Brakensiek K, Becker T, Klempnauer J, et al. Distinct methylation patterns of benign and Malignant liver tumors revealed by quantitative methylation profiling. *Clin Cancer Res* (2005) 11(10):3654–60. doi: 10.1158/1078-0432.CCR-04-2462

43. Evron E, Umbricht CB, Korz D, Raman V, Loeb DM, Niranjan B, et al. Loss of cyclin D2 expression in the majority of breast cancers is associated with promoter hypermethylation. *Cancer Res* (2001) 61(6):2782–7.

44. Evron E, Dooley WC, Umbricht CB, Rosenthal D, Sacchi N, Gabrielson E, et al. Detection of breast cancer cells in ductal lavage fluid by methylation-specific PCR. *Lancet* (2001) 357(9265):1335–6. doi: 10.1016/S0140-6736(00)04501-3

45. Hung CS, Wang SC, Yen YT, Lee TH, Wen WC, Lin RK. Hypermethylation of CCND2 in lung and breast cancer is a potential biomarker and drug target. *Int J Mol Sci* (2018) 19(10):3096. doi: 10.3390/ijms19103096

46. Gross JA, Dillon SR, Mudri S, Johnston J, Littau A, Roque R, et al. TACI-Ig neutralizes molecules critical for B cell development and autoimmune disease. impaired B cell maturation in mice lacking BLyS. *Immunity* (2001) 15(2):289–302. doi: 10.1016/S1074-7613(01)00183-2

47. Smulski CR, Eibel H. BAFF and BAFF-receptor in B cell selection and survival. *Front Immunol* (2018) 9:2285. doi: 10.3389/fimmu.2018.02285

48. Salvucci O, Bouchard A, Baccarelli A, Deschenes J, Sauter G, Simon R, et al. The role of CXCR4 receptor expression in breast cancer: a large tissue microarray study. *Breast Cancer Res Treat* (2006) 97(3):275–83. doi: 10.1007/s10549-005-9121-8

49. Chu QD, Panu L, Holm NT, Li BD, Johnson LW, Zhang S. High chemokine receptor CXCR4 level in triple negative breast cancer specimens predicts poor clinical outcome. *J Surg Res* (2010) 159(2):689–95. doi: 10.1016/j.jss.2008.09.020

50. Chatterjee S, Behnam Azad B, Nimmagadda S. The intricate role of CXCR4 in cancer. *Adv Cancer Res* (2014) 124:31–82. doi: 10.1016/B978-0-12-411638-2.00002-1

51. Zhang Z, Zhang Y, Xia S, Kong Q, Li S, Liu X, et al. Gasdermin E suppresses tumour growth by activating anti-tumour immunity. *Nature* (2020) 579(7799):415–20. doi: 10.1038/s41586-020-2071-9

52. Zhou Y, Zheng J, Bai M, Gao Y, Lin N. Effect of pyroptosis-related genes on the prognosis of breast cancer. *Front Oncol* (2022) 12:948169. doi: 10.3389/fonc.2022.948169

53. Zhong Y, Peng F, Luo X, Wang X, Yang B, Tang X, et al. A pyroptosis-related gene signature for prognostic and immunological evaluation in breast cancer. *Front Oncol* (2022) 12:964508. doi: 10.3389/fonc.2022.964508

54. Bohgaki M, Tsukiyama T, Nakajima A, Maruyama S, Watanabe M, Koike T, et al. Involvement of Ymer in suppression of NF-kappaB activation by regulated interaction with lysine-63-linked polyubiquitin chain. *Biochim Biophys Acta* (2008) 1783(5):826–37. doi: 10.1016/j.bbamcr.2007.09.006

55. Xu Y, Wang Y, Liang L, Song N. Single-cell RNA sequencing analysis to explore immune cell heterogeneity and novel biomarkers for the prognosis of lung adenocarcinoma. *Front Genet* (2022) 13:975542. doi: 10.3389/fgene.2022.975542

56. Song B, Shen S, Fu S, Fu J. HSPA6 and its role in cancers and other diseases. *Mol Biol Rep* (2022) 49(11):10565–77. doi: 10.1007/s11033-022-07641-5

57. Shen S, Wei C, Fu J. RNA-sequencing reveals heat shock 70-kDa protein 6 (HSPA6) as a novel thymoquinone-upregulated gene that inhibits growth, migration, and invasion of triple-negative breast cancer cells. *Front Oncol* (2021) 11:667995. doi: 10.3389/fonc.2021.667995

58. Kilbas PO, Akcay IM, Doganay GD, Arisan ED. Bag-1 silencing enhanced chemotherapeutic drug-induced apoptosis in MCF-7 breast cancer cells affecting PI3K/Akt/mTOR and MAPK signaling pathways. *Mol Biol Rep* (2019) 46(1):847–60. doi: 10.1007/s11033-018-4540-x

59. Mahmood SF, Gruel N, Nicolle R, Chapeaublanc E, Delattre O, Radvanyi F, et al. PPAPDC1B and WHSC1L1 are common drivers of the 8p11-12 amplicon, not only in breast tumors but also in pancreatic adenocarcinomas and lung tumors. *Am J Pathol* (2013) 183(5):1634–44. doi: 10.1016/j.ajpath.2013.07.028

60. Bernard-Pierrot I, Gruel N, Stransky N, Vincent-Salomon A, Reyal F, Raynal V, et al. Characterization of the recurrent 8p11-12 amplicon identifies PPAPDC1B, a phosphatase protein, as a new therapeutic target in breast cancer. *Cancer Res* (2008) 68 (17):7165–75. doi: 10.1158/0008-5472.CAN-08-1360

frontiers | Frontiers in Immunology

TYPE Original Research
PUBLISHED 08 January 2024
DOI 10.3389/fimmu.2023.1308807

OPEN ACCESS

EDITED BY
Feifei Teng,
Shandong University Cancer Center, China

REVIEWED BY
Fangfang Zhou,
Soochow University, China
Qingyu Huang,
Shandong First Medical University and Shandong Academy of Medical Sciences, China

*CORRESPONDENCE
Xiaohua Yan
yanxiaohua@ncu.edu.cn
Shuo Tu
tushuo@126.com

†These authors have contributed equally to this work

RECEIVED 07 October 2023
ACCEPTED 18 December 2023
PUBLISHED 08 January 2024

CITATION
Zhang C, Li Z, Hu K, Ren Y, Zhang H, Zhao Y, Wei W, Tu S and Yan X (2024) The prognostic implications and tumor-suppressive functions of CYR61 in estrogen receptor-positive breast cancer.
Front. Immunol. 14:1308807.
doi: 10.3389/fimmu.2023.1308807

The prognostic implications and tumor-suppressive functions of CYR61 in estrogen receptor-positive breast cancer

Cheng Zhang[1,2†], Zhihua Li[3†], Kaiheng Hu[4], Yifei Ren[4], Haoran Zhang[4], Yuankang Zhao[4], Wenjing Wei[1], Shuo Tu[1*] and Xiaohua Yan[1,3*]

[1]The MOE Basic Research and Innovation Center for the Targeted Therapeutics of Solid Tumors, School of Basic Medical Sciences, Jiangxi Medical College, Nanchang University, Nanchang, China, [2]Department of GCP, The First Affiliated Hospital, Jiangxi Medical College, Nanchang University, Nanchang, China, [3]Department of Breast Surgery of Third Hospital of Nanchang and Key Laboratory of Breast Diseases of Jiangxi, Nanchang, China, [4]Queen Mary School, Jiangxi Medical College, Nanchang University, Nanchang, China

Due to the therapeutic resistance of endocrine therapy and the limited efficacy of immune checkpoint inhibitors in estrogen receptor (ER)-positive breast cancer (BRCA), there is an urgent need to develop novel prognostic markers and understand the regulation of the tumor immune microenvironment (TIME). As a matricellular protein, CYR61 has been shown to either promote or suppress cancer progression depending on cancer types. However, how CYR61 functions in ER-positive BRCA remains elusive. In this study, we comprehensively analyzed the expression of CYR61 in BRCA based on the TCGA and METABRIC databases. Our findings showed that the expression of CYR61 is downregulated in different subtypes of BRCA, which is associated with elevated promoter methylation levels and predicts bad clinical outcomes. By comparing the high or low CYR61 expression groups of ER-positive BRCA patients, we found that CYR61 is intimately linked to the expression of genes involved in tumor-suppressive pathways, such as the TGF-β and TNF signaling pathways, and genes related to cytokine-receptor interaction that may regulate cancer immunity. Moreover, reduced CYR61 expression is associated with an altered TIME that favors cancer progression. Finally, experimental analyses ascertained that CYR61 is downregulated in clinical BRCA tissues compared to matched normal breast tissues. Furthermore, CYR61 is able to impede the proliferation and colony formation of ER-positive BRCA cells. In summary, our study reveals that CYR61 could serve as a novel prognostic marker for ER-positive BRCA, and function as an inhibitor of cancer progression by both acting on cancer cells and remodeling the TIME.

KEYWORDS

Cyr61, ER-positive breast cancer, tumor immune microenvironment (TIME), immune cell infiltration, cancer cell proliferation

1 Introduction

Breast cancer (BRCA) accounts for one-third of all female patient tumor occurrences, posing a serious threat to women's lives and health worldwide (1). Based on disparities in immunohistochemical markers, BRCA can be further classified into estrogen receptor (ER)-positive, progesterone receptor (PR)-positive, HER2-positive and triple-negative (ER-/PR-/HER2-) subtypes (2, 3). The development of both normal mammary tissue and ER-positive BRCA depend heavily on estrogen and its receptors (4). Although endocrine therapy has been shown effective in hormone-positive BRCA, drug resistance and cancer relapse remain significant challenges (5, 6). With our increasing understanding of the tumor immune microenvironment (TIME), various immunotherapies, such as immune checkpoint inhibitors (ICIs), have been developed and considered promising for triple-negative breast cancer (TNBC) (7). However, the efficacy of immunotherapy in ER-positive BRCA seems to be less satisfied (3, 5). Therefore, there is an urgent need to develop new prognostic molecular makers and to understand the regulation of the immune microenvironment of ER-positive BRCA.

The cysteine-rich angiogenesis inducer 61 (CYR61, also known as CCN1) is an extracellular secretory matrix protein. CYR61 has been appreciated for playing an important role in various biological processes, such as angiogenesis, tissue repair, inflammation response, cell migration and invasion (8, 9). The dysregulation of CYR61 has been found in different human diseases including cancer (9, 10). Previous studies have found that CYR61 expression is upregulated in gliomas and pancreatic carcinoma, whereas downregulated in prostate carcinoma and non-small cell lung carcinoma (10–12). Interestingly, CYR61 has been reported to promote or suppress cancer progression, depending on the type and stage of cancer (9, 10). As a typical transcriptional target of the YAP/TEAD signaling pathway, CYR61 was reported to be negatively correlated with the expression level of ESR1 that encodes estrogen receptor alpha, in BRCA (13, 14). However, it remains to be further elucidated whether the expression of CYR61 may serve as a prognostic marker for BRCA and whether CYR61 may regulate the TIME.

In this study, through comprehensive analyses of different cancer databases, we found that CYR61 expression was significantly downregulated in different subtypes of BRCA, including ER-positive BRCA. Reduced CYR61 expression was associated with increasing levels of its promoter methylation, and predicted reduced survival rates in cancer patients. Intriguingly, analyses of ER-positive BRCA patients in The Cancer Genome Atlas Program (TCGA) database also indicated that CYR61 was associated with some tumor-suppressor pathways and remodeling of the TIME. In addition, experimental studies verified that CYR61 was downregulated in clinical breast cancer tissues compared to matched normal tissues, and demonstrated that CYR61 can inhibit the proliferation and growth of ER-positive BRCA cells. These results reveal that CYR61 exerts an inhibitory role in ER-positive BRCA by regulating cancer cell proliferation and the TIME remodeling, and may serve as an independent prognostic marker.

2 Materials and methods

2.1 Acquisition and processing of data

The mRNA matrix, methylation matrix, and survival data of BRCA patients were obtained from TCGA. These datasets were coupled with transcriptional data from the TCGA-pancancer cohorts and the Genotype-Tissue Expression (GTEx) database. Access to these datasets was facilitated through UCSC Xena (http://xena.ucsc.edu/). The relevant clinical data of these BRCA patients were acquired utilizing the R package "TCGAbiolinks". The mRNA matrix, methylation matrix, and relevant survival data of the Molecular Taxonomy of Breast Cancer International Consortium (METABRIC) cohorts were obtained from cBioPortal (https://www.cbioportal.org/), a platform dedicated to multi-omics tumor genetics analysis. Then, all attained transcriptional data were transformed into the $\log_2$(TPM+1) format, an essential step preparing them for subsequent statistical analyses. The transformation of probe identifiers was executed utilizing the R package "tinyarray".

2.2 Inclusion criteria of patients and samples from TCGA and METABRIC databases

Breast cancer patients meeting specific eligibility criteria were selected for the subsequent data analyses. First, breast tissue samples with available mRNA expression data were considered. Second, one sample per patient was retained, with preference shown for frozen samples. Lastly, TCGA patients with both overall survival (OS) and disease-specific survival (DSS) data, and METABRIC patients with both OS and relapse-free survival (RFS) data were selected for the analyses.

2.3 Gene expression analysis by cancer databases

To clarify the correlation between CYR61 expression level and BRCA, boxplots based on CYR61 expression were plotted using the TCGA-pancancer cohorts and GTEx datasets. Additionally, CYR61 mRNA expression boxplots were plotted for normal breast tissue, ER-positive and/or PR-positive BRCA samples from the TCGA and METABRIC cohorts. Paired boxplots were also generated based on matched tumor samples and normal tissue from TCGA. BRCA samples were grouped based on various clinical features (PAM50, Stage, T stage, M stage, N stage), and boxplots were sequentially drawn according to CYR61 expression within each group.

2.4 DNA methylation analysis

All probe numbers corresponding to the CYR61 promoter were obtained from Mexpress (https://mexpress.be/). The final β value of CYR61 for each sample was calculated as the average of β values from

the relevant probes. Boxplots were plotted based on the β values of CYR61 for each sample. Dotted plots were generated based on both mRNA and β values for each sample. Similar to expression analysis, BRCA samples were divided into different groups based on clinical features (PAM50, Stage, T stage, M stage, N stage), and boxplots were drawn based on the degree of CYR61 methylation in each group.

2.5 Prognostic analysis

Kaplan-Meier curve analyses were performed using BRCA and ER-positive BRCA groups in TCGA BRCA cohorts and METABRIC cohorts. The optimal cutoff point was determined using the "surv_cutpoint" function from the R package "survminer", considering CYR61 expression. The log-rank P value was computed.

2.6 Pathway enrichment analysis

Enrichment analysis was carried out based on CYR61 expression levels in pre- and post-10% ER-positive BRCA samples. Genes expressed in at least 50% samples with a count of more than 30 were subjected to differential expression analysis with a threshold of |logFC| >1 and p <0.05 for the two groups. The resulting differential genes (DEGs) were enriched using the "clusterProfiler" package for gene ontology (GO) and KEGG analyses. Gene Set Enrichment Analysis (GSEA) was utilized to further analyze the relationships between CYR61 expression and key pathways.

2.7 Immune cell infiltration analysis

Immune cell infiltration was predicted using the R package "CIBERSORT" based on the sample's expression matrix. CIBERSORT deconvolution algorithm was used to analyze the relative fractions of 22 infiltrating immune cell types in CYR61 samples from TCGA datasets. Samples were divided into high-expression and low-expression groups according to medium CYR61 expression. Violin plots were generated to illustrate immune cell infiltration differences. For immune cells showing significant differences in infiltration, dot plots were created to visualize the correlation of CYR61 mRNA expression with cell infiltration. To further explore the association between CYR61 and immune infiltration, the "ESTIMATE" package was utilized to estimate the scores (ESTIMSTE score, stromal score, immune score) for each sample. The correlation between these scores and CYR61 expression was displayed through heatmaps.

2.8 Cell culture

Human ER-positive breast cancer cell line MCF-7 was obtained from Cell Bank/Stem Cell Bank, Chinese Academy of Sciences. MCF-7 was cultured in RPMI 1640 medium (Solarbio, Beijing), supplemented with 10% fetal bovine serum (FBS, Gibco, USA) in a humidified incubator at 37°C in 5% CO2 atmosphere.

2.9 Gene silencing and reagents

The non-specific control siRNA (NC) and those targeting human CYR61 were purchased from RiboBio (China). siRNAs were transfected with the siTranTM siRNA transfection reagent (OriGene). The sequences of siRNAs used in this study were as follow: CYR61 siRNA #1, 5'-CCACACGAGTTACCAATGA-3'; CYR61 siRNA #2, 5'-GAACCAGTCAGGTTTACTT-3'. Recombinant human CYR61 (CB98) peptides was purchased from Novoprotein (Shanghai).

2.10 Collection of clinic breast cancer samples

A total of seven ER-positive BRCA samples and the adjacent matched normal tissues were excised from inpatients at the department of breast surgery of Third Hospital of Nanchang. The tumor tissues were stored in liquid nitrogen after excising from cancer patients. Informed consent was obtained from all individuals participating in this study. The usage of clinical sections was consented by the Medical Ethics Committee of Third Hospital of Nanchang. The processes of clinical sample collection and usage were in strict accordance with the guideline. All procedures performed in this study were in accordance with the ethical standards of the Medical Ethics Committee of Third Hospital of Nanchang.

2.11 Lentivirus production and stable cell line establishment

To produce defective lentivirus, HEK293FT cells were transfected with the empty lentivirus vector pL6.3-CMV-GFP-IRES-MCS or the CYR61-expressing derivative, along with the package plasmids pCMVΔ8.9 and VSVG. The culture supernatants were collected at 48 h post-transfection, and the viral particles were concentrated by centrifugation. To establish CYR61- or vector-expressing stable cell lines, MCF-7 cells were infected with lentivirus particles at a multiplicity of infection (MOI) of 50 pfu per cell. At 48 h post-infection, the cells were washed with PBS, complemented with fresh growth medium containing 1 μg/mL of blasticidin. The drug-resistant cells were pooled as stable cells, which were further maintained with blasticidin-containing growth medium.

2.12 RNA purification and real-time quantitative PCR

RNA purification and reverse transcription were performed as previously described (15). Briefly, total RNA was extracted from ER-positive BRCA tissues and matched paracancer tissues, from 7

patients undergoing surgery in Third Hospital of Nanchang, then reverse-transcribed into cDNA. Next, the relative mRNA expression of genes was normalized to that of GAPDH, and the fold change was evaluated using the 2−ΔΔCT method. The primer sequences used for q-PCR were obtained from Sangon Biotech (Shanghai, China): CYR61, forward 5'-GGTCAAAGTT ACCGGGCAGT-3' and reverse 5'-GGAGGCATCGAATC CCAGC-3'; GAPDH forward 5'-ACAACTTTGGTATCG TGGAAGG-3' and reverse 5'-GCCATCACGCCACAGTTTC-3'.

2.13 Western blotting

For breast tissues, after homogenization, the samples were lysed with RIPA lysis buffer (R0020, Solarbio, Beijing), and the protein lysates were obtained after high-speed centrifugation. Likewise, cells were lysed with RIPA lysis buffer as above. Lysates were then separated by 10% SDS-PAGE and transferred to PVDF membranes to incubate with primary antibodies, including CYR61 (39382, CST, USA) and Tubulin (3873, CST, USA), followed by further incubation with the corresponding secondary antibodies. The bands on the membranes were finally visualized using the enhanced chemiluminescence (ECL) substrate (ECL-P-500, Yanxi Biotech, Shanghai) using the Tanon (Tanon 5200, Shanghai) Automatic Chemiluminescence Imaging System.

2.14 MTT and CCK8 assays

1×10^3 viable cells were cultivated per well on 96-well plates in a final volume of 100 µl DMEM containing 10% FBS. For MTT assays, after 1-4 days of incubation, each sample was added with 20 µL per well of MTT solution (M8180, Solarbio, Beijing) and incubated at 37°C for 4 h. After aspiration of the supernatants, cells were incubated with 150 µL of DMSO (Solarbio, Beijing) at 37°C for 30 min. The absorbance was measured at 490 nm in a SpectraMaxR ParadigmR microplate reader (Molecular Decices, USA). For CCK8 assays, after 1-4 days of incubation, each sample was added with 10 µL per well of CCK8 solution (CA1210, Solarbio, Beijing) and incubated at 37°C for 2 h. The absorbance was detected at 450 nm in a SpectraMaxR ParadigmR microplate reader (Molecular Decices, USA).

2.15 Colony formation assay

Clonogenic growth of MCF-7 cells was determined by plating 1×10^3 cells in 3 mL of growth medium in 6-well plates, and each sample was performed in triplicate. After incubation for 10-15 days, cells were fixed with methanol and stained with crystal violet solution, then the colony cells were imaged, and colony numbers were calculated by the ImageJ software.

2.16 Statistical analysis

Statistical analyses were performed using R (version 4.2.2) and GraphPad Prismversion 8.0). The significance between the means was calculated using wilcoxon rank-sum test, whereas paired t-test was conducted to compare paired tissue samples. Each experiment was performed at least in triplicate, and the values were presented as mean ± SD. The Kaplan-Meiermethod and log-rank test were used for survival analysis of cancer patients.

3 Results

3.1 Analysis of CYR61 gene expression in pan-cancer and breast cancer

To investigate the roles of CYR61 in BRCA, we first explored its expression levels in pan-cancer based on public TCGA and GTEx databases. As a result, CYR61 was downregulated in most of the cancer types, such as BRCA, adrenocortical carcinoma (ACC), bladder urothelial carcinoma (BLCA), kidney chromophobe (KICH) and liver hepatocellular carcinoma (LIHC), amongst others (Figure 1A).

Then we specifically studied the expression of CYR61 in BRCA tissues based on the TCGA database. CYR61 expression level was downregulated in BRCA tissues compared to normal breast tissues, as assessed in all available cancer and normal tissue samples, as well as in paired tissues (Figures 1B, C). The expression of CYR61 was also reduced in ER-positive or PR-positive BRCA tissues when compared to normal breast tissues (Figures 1D–G). Similar results were obtained when the HER2-positive, luminal subtypes or triple-negative breast cancer were analyzed (Figure 1H). Furthermore, we found that the expression level of CYR61 was downregulated in different stages of BRCA tissues compared with normal tissues (Figures 1I–L).

3.2 Enhanced promoter methylation levels correlate with downregulated expression levels of CYR61 in breast cancer

DNA methylation plays an important role in regulating gene expression, especially those occur in the gene promoter regions (6, 16). Therefore, we sought to explore whether the altered expression of CYR61 in BRCA is related to its promoter methylation level. Indeed, analyses of the TCGA datasets showed that CYR61 promoter methylation levels were significantly upregulated in BRCA tissues compared to normal breast tissues (Figure 2A), which closely correlated with the decreased expression level of CYR61 in BRCA (Figure 2B). Similar results were obtained in ER-positive BRCA (Figures 2C, D). In addition, the methylation level of the CYR61 promoter was also greatly upregulated in different subtypes or developmental stages of BRCA than those in normal breast tissue (Figures 2E–I). These observations were also consistent with the reduced CYR61 expression levels in BRCA (Figures 1F–M).

3.3 The prognostic value of CYR61 expression in breast cancer

Given the aberrant expression of CYR61 in BRCA, we analyzed the relationships between CYR61 expression levels and patient

10.3389/fimmu.2023.1308807

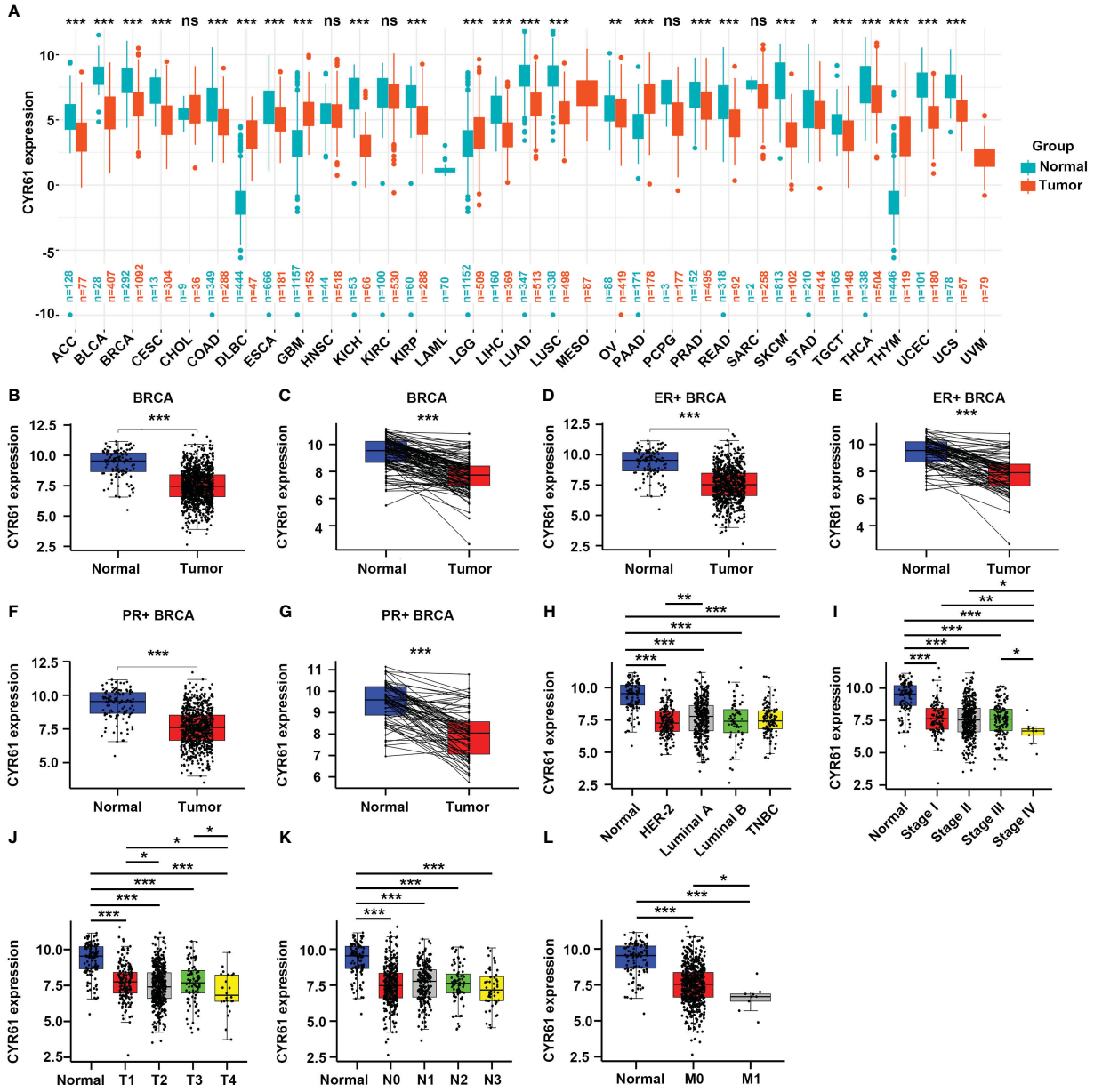

FIGURE 1
CYR61 expression is downregulated in BRCA than in the normal counterparts. **(A)** Comparation of the CYR61 mRNA expression levels between tumor samples and normal samples in different subtypes of BRCA based on TCGA and GTNx databases. **(B, C)** Comparation of the CYR61 mRNA expression levels between all available BRCA samples and normal breast samples **(B)**, or between matched BRCA samples and normal breast samples **(C)** in the TCGA database. **(D, E)** Comparation of the CYR61 mRNA expression levels between all ER+ BRCA samples and normal breast samples **(D)**, or between paired ER+ BRCA samples and normal samples **(E)** in the TCGA database. **(F, G)** Comparation of the CYR61 mRNA expression levels between all PR+ BRCA samples and normal breast samples **(F)**, or between matched PR+ BRCA samples and normal samples **(G)** in the TCGA database. **(H–L)** Comparation of the CYR61 mRNA expression levels in normal breast samples and in BRCA samples of different PAM50 status **(H)**, cancer stages (stage I, II, III and IV) **(I)**, primary tumor site stages (T1, T2, T3 and T4) **(J)**, lymph node stages (N0, N1, N2 and N3) **(K)** or metastatic spread stages (M0 and M1) **(L)** in the TCGA database. *p<0.05, **p<0.01, ***p<0.001. ns, no significance.

prognosis. Survival curve analyses based on the TCGA datasets indicated that lower CYR61 expression levels were associated with shorter overall survival (OS) and disease-specific survival (DSS) rates, in all BRCA patients (Figures 3A, B) or ER-positive BRCA patients (Figures 3C, D). Moreover, these results were confirmed by survival curve analyses based on the METABRIC data, assessed either in all BRCA patients (Figures 3E, F) or ER-positive BRCA patients (Figures 3G, H).

3.4 CYR61 is linked to remodeling of TIME in breast cancer

To further explore the role of CYR61 in BRCA, we next assessed whether CYR61 expression is associated with remodeling of the TIME using the TCGA data. As shown in Figures 4A, B, CYR61 expression positively correlates with stromal scores, immune scores and estimate scores, either in BRCA or in ER-positive BRCA. Among the 22 types of

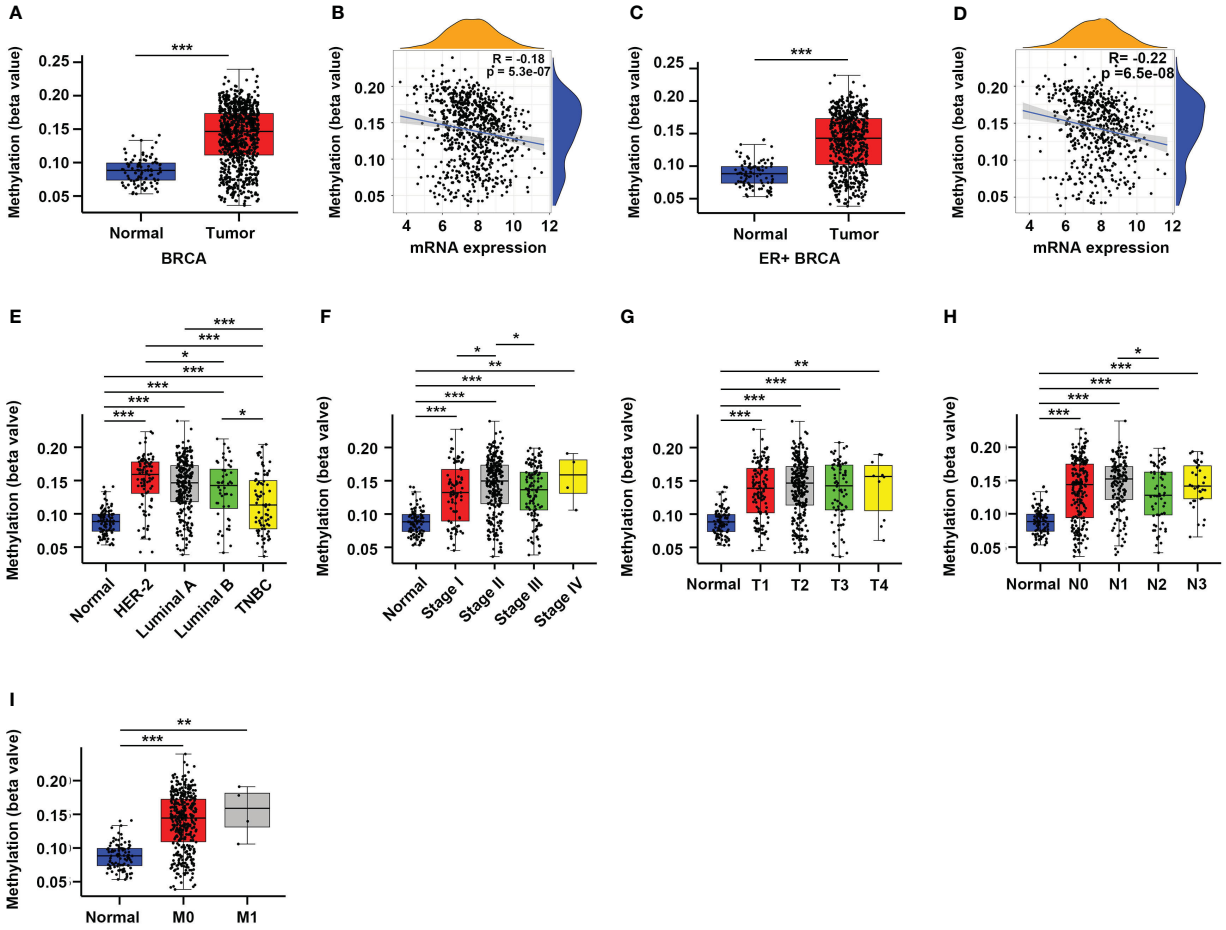

FIGURE 2
Enhanced promoter methylation level correlates with reduced CYR61 expression in BRCA patients. **(A, C)** Comparation of CYR61 gene methylation levels in normal breast samples with that in all BRCA samples **(A)** or in ER+ BRCA samples **(C)**. **(B, D)** Correlations of the methylation levels of CYR61 gene with its expression levels in all BRCA samples **(B)** or in ER+ BRCA samples **(D)**. **(E–I)** Comparation of the CYR61 gene methylation level in normal breast samples with that in BRCA samples of different PAM50 status **(E)**, cancer stages **(F)**, primary tumor site stages **(G)**, lymph node stages **(H)** or metastatic spread stages **(I)** in the TCGA database. *p<0.05, **p<0.01, ***p<0.001.

immune cells investigated, the results of violin plots showed that lower CYR61 expression correlated with reduced infiltrations of antitumor immune cells in both BRCA and ER-positive BRCA patients, including resting memory CD4 T cells and naive B cells (Figures 4C, D). On the other hand, CYR61 expression was negatively correlated with the infiltration of some protumor immune cell types, such as Treg cells and M2 type macrophages (Figures 4C, D). In addition, scatter plot analyses also confirmed the relationships between CYR61 expression and the infiltrations of these immune cells in both BRCA and ER-positive BRCA tissues (Figures 4E–L). These results suggested that downregulation of CYR61 is associated with an impaired antitumor immune microenvironment in BRCA, potentially contributing to tumor progression and immune evasion.

3.4 CYR61 expression relates to tumor-suppressive genes and pathways in ER-positive breast cancer

Next, we investigated the possible mechanisms of CYR61 in BRCA. To this end, ER-positive BRCA patients with 10 percent highest and 10 percent lowest CYR61 expression were compared (Figure 5A). Using $|\log_2(\text{fold change})| > 1.0$, $p < 0.05$, and count value >30 as the cutoff, 2408 differentially expressed genes (DEGs) were identified between the two groups, including 1629 upregulated genes and 779 downregulated genes) (Figure 5B). The top 50 genes that were positively or negatively correlated with CYR61 expression level were shown in heatmaps (Figures 5C, D). GO term and KEGG pathway enrichment analyses indicated that these DEGs were closely associated with extracellular matrix (ECM) composition and organization, and regulation of cell adhesion or integrin signaling (Figures 5E, F), which is consistent with the typical role of CYR61 as a matricellular protein. In addition, as shown in Figures 5E, F, the CYR61 DEGs were also related to the TGF-β and TNF signaling pathways, which have been reported to suppress the growth of ER-positive BRCA (17, 18), as well as genes related to cytokine-receptor interactions, which are crucial for remodeling the TIME (19). GSEA analyses showed that CYR61 DEGs were positively correlated with TGF-β and TNF signaling pathway genes (Figures 5G–I). Finally, scatter plot results showed that CYR61 expression displayed a positive correlation with the TGF-β pathway genes, such as TGFB2, TGFB3, TGFBR2, INHBA and FST in ER-positive BRCA (Figures 5J–N). However, the expression of CYR61

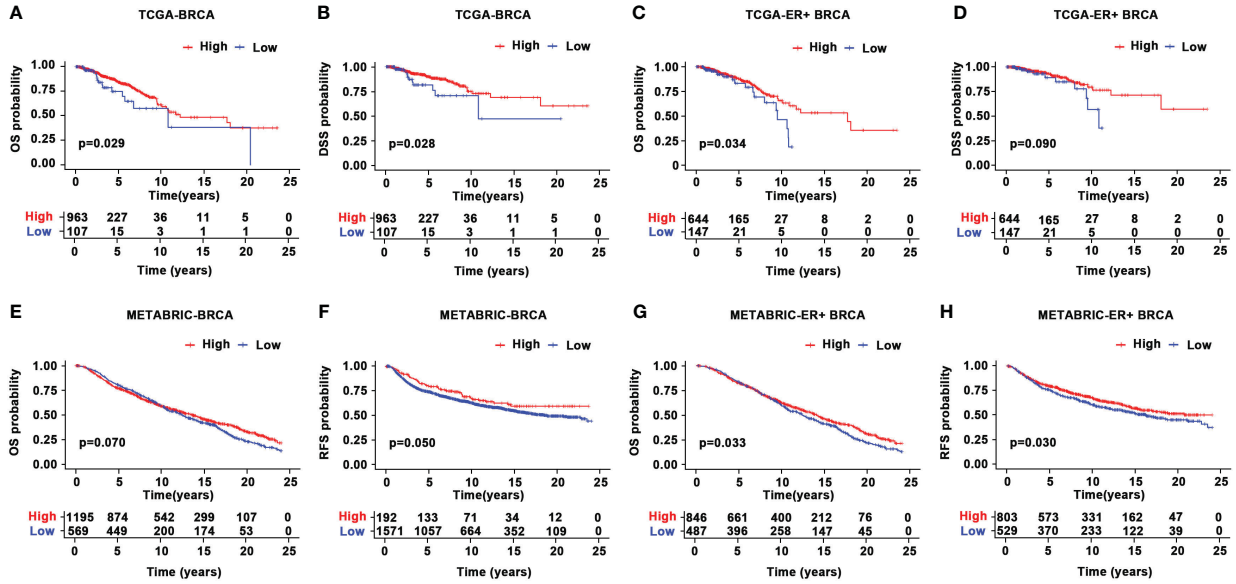

FIGURE 3
Prognostic value of CYR61 expression in BRCA. **(A, B)** Kaplan-Meier survival curve analyses illustrating the OS **(A)** and DSS **(B)** rates of high or low CYR61-expressing BRCA patients in the TCGA database. **(C, D)** Kaplan-Meier survival curve analyses illustrating the OS **(C)** or DSS **(D)** rates of high or low CYR61-expressing ER-positive BRCA patients in the TCGA database. **(E, F)** Kaplan-Meier survival curve analyses illustrating the OS **(E)** or RFS **(F)** rates of high or low CYR61-expressing BRCA patients in the METABRIC database. **(G, H)** Kaplan-Meier survival curve analyses illustrating the OS **(E)** or RFS **(F)** rates of high or low CYR61-expressing ER-positive BRCA patients in the METABRIC database.

was negatively associated with ESR1 which encodes estrogen receptor alpha (Figure 5O).

3.6 CYR61 inhibits the proliferation and colony formation of ER-positive breast cancer cells

The above results suggest that downregulation of CYR61 is an important factor contributing to the pathogenesis of BRCA, especially ER-positive BRCA. Subsequently, we verified the expression and functions of CYR61 experimentally. To support our bioinformatic data, the expression of CYR61 was dramatically downregulated in 5 out of 7 clinically obtained ER-positive BRCA tissues compared to matched paracancer normal breast tissues, at either the mRNA or protein level (Figures 6A, B). Then we established MCF-7-derived stable cell lines overexpressing CYR61 or the control vector (Figure 6C). Indeed, MTT, CCK8 and colony formation assays showed that ectopic CYR61 was able to attenuate the proliferation and growth of MCF-7 cells (Figures 6D–F). Similar results were obtained when MCF-7 cells were administered with recombinant human CYR61 protein (rhCYR61) (Figures 6G–I). Another piece of evidence was that depletion of CYR61 expression in MCF-7 cells via siRNAs enhanced the proliferation and colony formation of cancer cells (Figures 6J–M).

4 Discussion

In the present study, we firstly integrated the data from the TCGA and GTNx cancer databases and performed a pan-cancer analysis of CYR61 expression. CYR61 was found to be downregulated in the majority of the 22 cancer types, such as breast cancer (BRCA), adrenocortical cancer (ACC), bladder cancer (BLCA), and cervical cancer (CESC), whereas upregulated in glioblastoma (GBM), pancreatic carcinoma (PAAD), large B-cell lymphoma (DLBC), and thymoma (THYM) (Figure 1A). This is in accordance with previous studies showing that CYR61 is aberrantly expressed in several cancers (9, 10, 20). In addition, CYR61 has been reported to either promote or suppress cancer progression, depending on cancer types (9, 10). However, the expressional alteration and functional role of CYR61 in BRCA are less understood and controversial. While some studies implicated that CYR61 is upregulated in BRCA, one notable study reported that the expression of CYR61 is conversely associated with that of ESR1, which encodes the major estrogen receptor (13, 21–23). Furthermore, both CYR61 and ESR1 genes are regulated by Hippo/YAP signaling in BRCA. YAP signaling suppresses the development of ER-positive BRCA by inhibiting ESR1 gene expression, while simultaneously induces CYR61 expression (13, 14). Our study using updated datasets in the TCGA revealed that CYR61 expression is downregulated in different subtypes or developing stages of BRCA tissues when compared with normal breast tissues (Figure 1). Moreover, we also analyzed the methylation status of CYR61 gene promoter based on the TCGA-BRCA database. Intriguingly, reduced expression of CYR61 is well correlated with elevated methylation level of its promoter (Figure 1). These results strongly suggest that CYR61 expression in BRCA is not only controlled by upstream signaling pathways, but also influenced by epigenetic mechanisms.

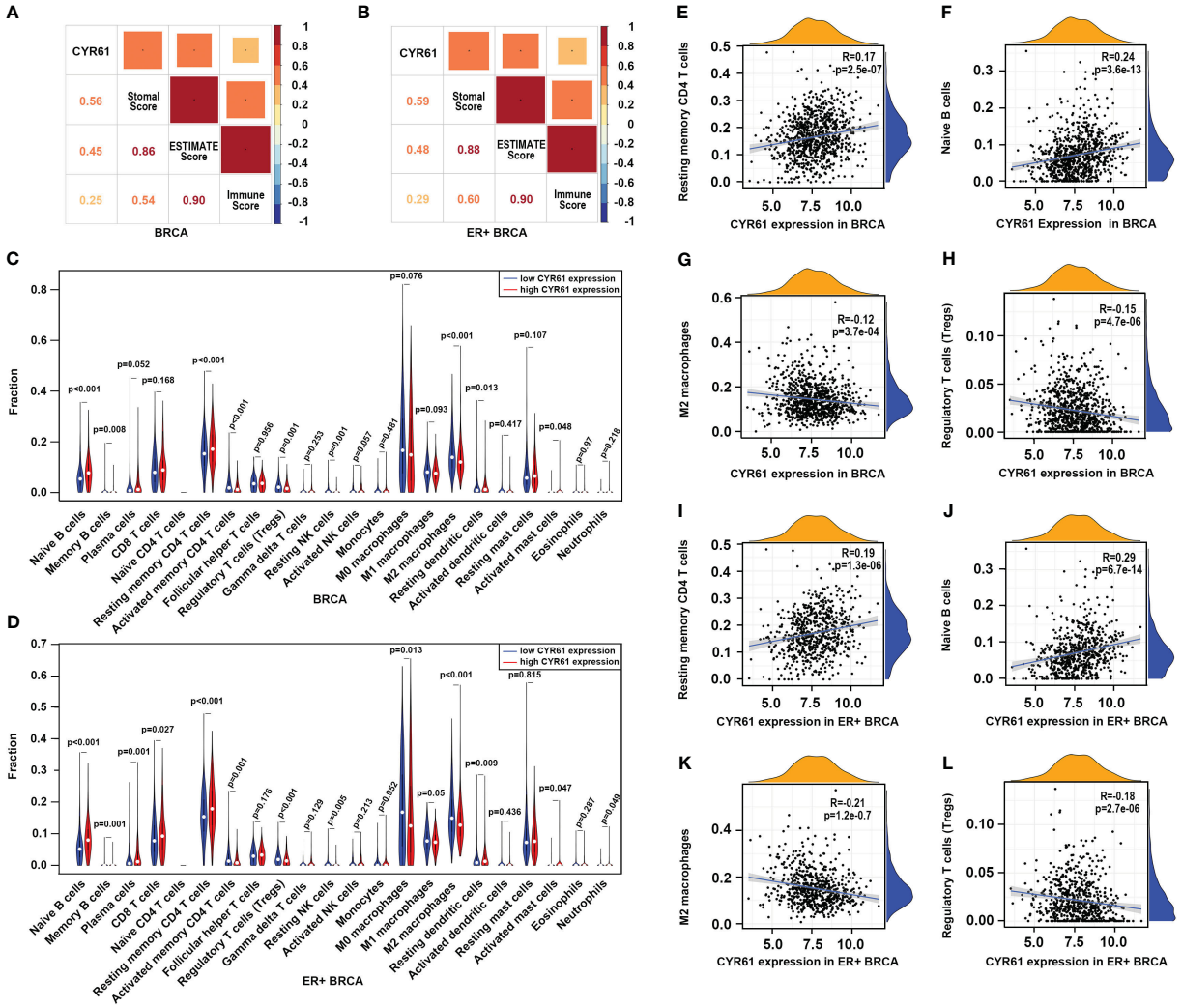

FIGURE 4
Downregulation of CYR61 is associated with a reduced antitumor immunity in the TME of BRCA patients. **(A, B)** Correlations of CYR61 expression level with the ESTIMATE scores assessed with BRCA samples **(A)** or ER+ BRCA samples **(B)** in the TCGA database. **(C, D)** Violin graphs showing the different immune cell infiltrations between low and high CYR61-expressing BRCA groups **(C)** or ER+ BRCA groups **(D)** in the TCGA database. Different groups were divided by the medium expression level of CYR61. The white dots indicate the medium levels of immune cell infiltrations. **(E–H)** Scatter plots showing the correlations of CYR61 expression with infiltrated resting memory CD4 T cells **(E)**, naive B cells **(F)**, M2 type macrophages **(G)** and Treg cells **(H)** in BRCA samples in the TCGA database. **(I–L)** Scatter plots showing the correlations of CYR61 expression with infiltrated resting memory CD4 T cells **(I)**, naive B cells **(J)**, M2 type macrophages **(K)** and Treg cells **(L)** in ER+ BRCA samples in the TCGA database.

The current classification of BRCA distinguishes three main subgroups, including hormone receptor (ER and/or PR)-positive/HER2-negative (HR+/HER2-), HER2-positive (HER2+, amplified/overexpressed) and triple-negative (ER-/PR-/HER2-) subtypes (3, 24). With the highest incidence in women, BRCA is a major health challenge globally (3). As such, different therapeutic strategies have been developed to cope with BRCA, such as hormone/endocrine therapy for HR-positive/HER2-negative BRCA, chemotherapy and targeted therapy for HER2-positive and triple-negative BRCA, in addition to surgery resection and radiotherapy (24–26). However, drug resistance usually occurs and causes cancer recurrence and relapse (3, 24). Thereafter, there is an urgent need to identify novel prognostic markers and therapeutic targets. Our results indicated that, based on the TCGA and METABRIC databases, lower CYR61 expression levels were associated with OS and DSS rates in all BRCA or ER-positive BRCA patients (Figure 3), implicating that CYR61 may serve as a new prognostic marker in BRCA.

BRCA progression depends not only on intrinsic cues in cancer cells, but also on the tumor microenvironment (TME) especially the tumor immune microenvironment (TIME), which provides a proper soil for cancer cell survival, proliferation and dissemination (7). We have compared the immune cell infiltrations between CYR61-low and -high BRCA patients using TCGA data (Figure 4). As a result, in both BRCA and ER-positive BRCA, the CYR61 expression level positively correlated with the infiltrations of some antitumor immune cell types including resting

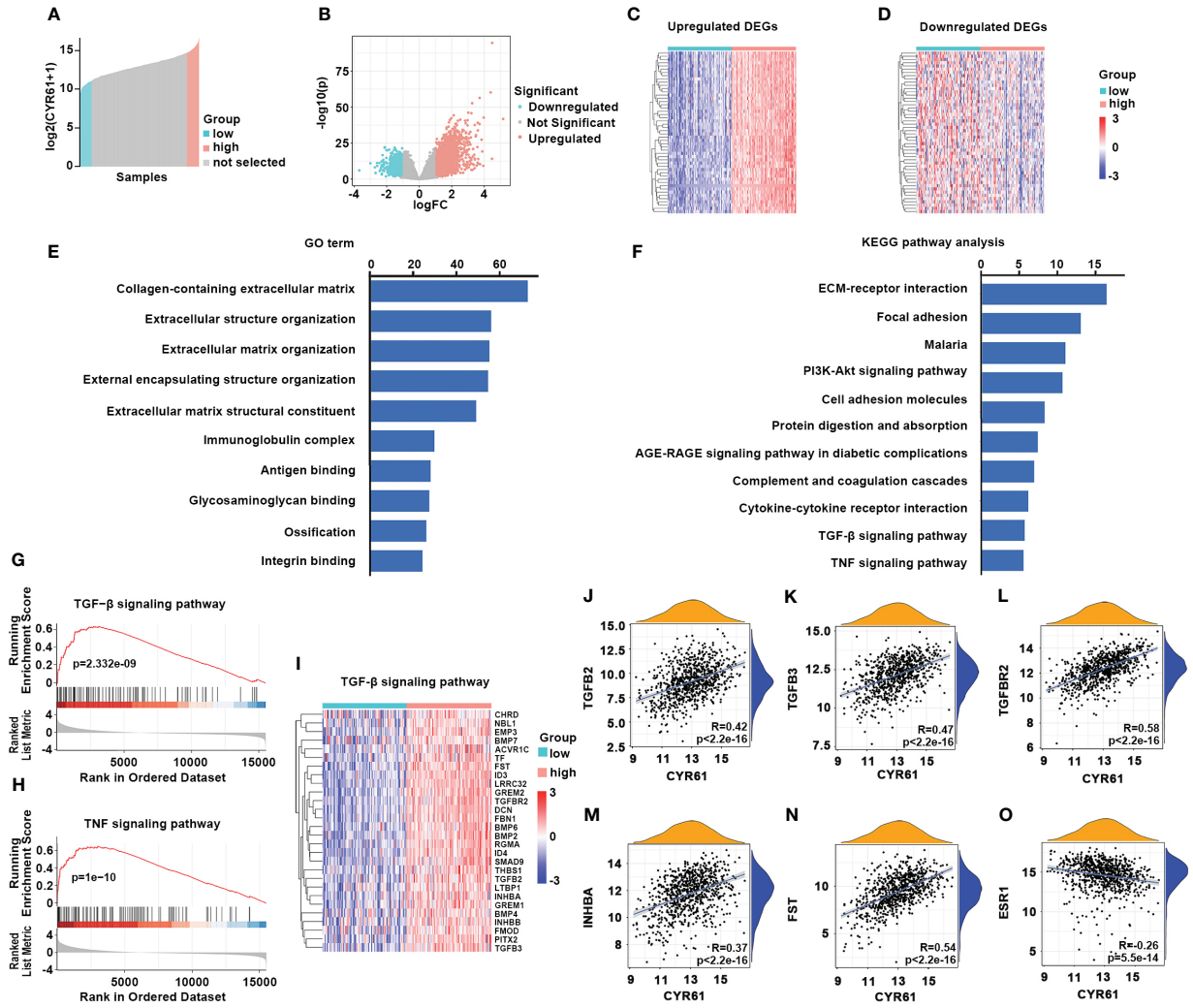

FIGURE 5
Analyses of CYR61-associated genes and pathways in ER-positive BRCA. **(A)** Comparison of 10% highest and 10% lowest CYR61 expression patients of ER+ BRCA from TCGA database. **(B)** Volcano plot showing the DEGs associated with CYR61 expression in ER+BRCA patients. **(C, D)** Heatmaps showing the DEGs that were positively **(C)** or negatively **(D)** associated with CYR61 expression. **(E, F)** GO term **(E)** and KEGG pathway **(F)** enrichment analyses of CYR61 DEGs. **(G, H)** GSEA analyses of the relationships of CYR61 DEGs to gene sets of TGF-β signaling **(G)** or TNF signaling **(H)**. **(I)** Heatmap for CYR61 DEGs linked to the TGF-β signaling pathway. **(J–O)** Scatter plots displaying the correlations of CYR61 expression to the expression levels of some typical TGF-β pathway genes **(J–N)** or to that of ESR1 **(O)**.

memory CD4 T cells and naive B cells, whereas negatively correlated with the infiltrations of Treg cells and M2 type macrophages that play a crucial role in immunosuppression. These results suggest that downregulation of CYR61 in BRCA is associated with a TIME of attenuated antitumor immunity, thereby favoring cancer progression. Our results are also in accordance with previous studies showing that CYR61 could either positively or negatively regulates the inflammatory responses in the liver and cancer immunity in pancreatic adenocarcinoma, in a context-dependent manner (27–29). In addition, in consideration that the single-cell and spatial RNA sequencing approaches have displayed a powerful capability and been widely used in elaborating the composition and function of TME/TIME (30–32), it is important to further explore the role of CYR61 in the regulation of BRCA immunity by utilizing single-cell and spatial omics approaches in the future.

Given that ER-positive BRCA is the most prevalent subtype, we further explored the underlying mechanisms and functional actions of CYR61 in ER-positive BRCA. By comparing high and low CYR61 expression patients, 2408 DEGs were found to be relevantly expressed with the CYR61 expression level (Figure 5). GO term and KEGG pathway analyses showed that these DEGs were associated with the known roles of CYR61 in regulating cell matrix formation and organization, ECM-receptor interaction, cell adhesion and integrin signaling. In addition, the CYR61 DEGs are also linked to some tumor-suppressive pathways, including TGF-β and TNF signaling, and also to gene sets of cytokine-cytokine receptor interaction, which may play a role in

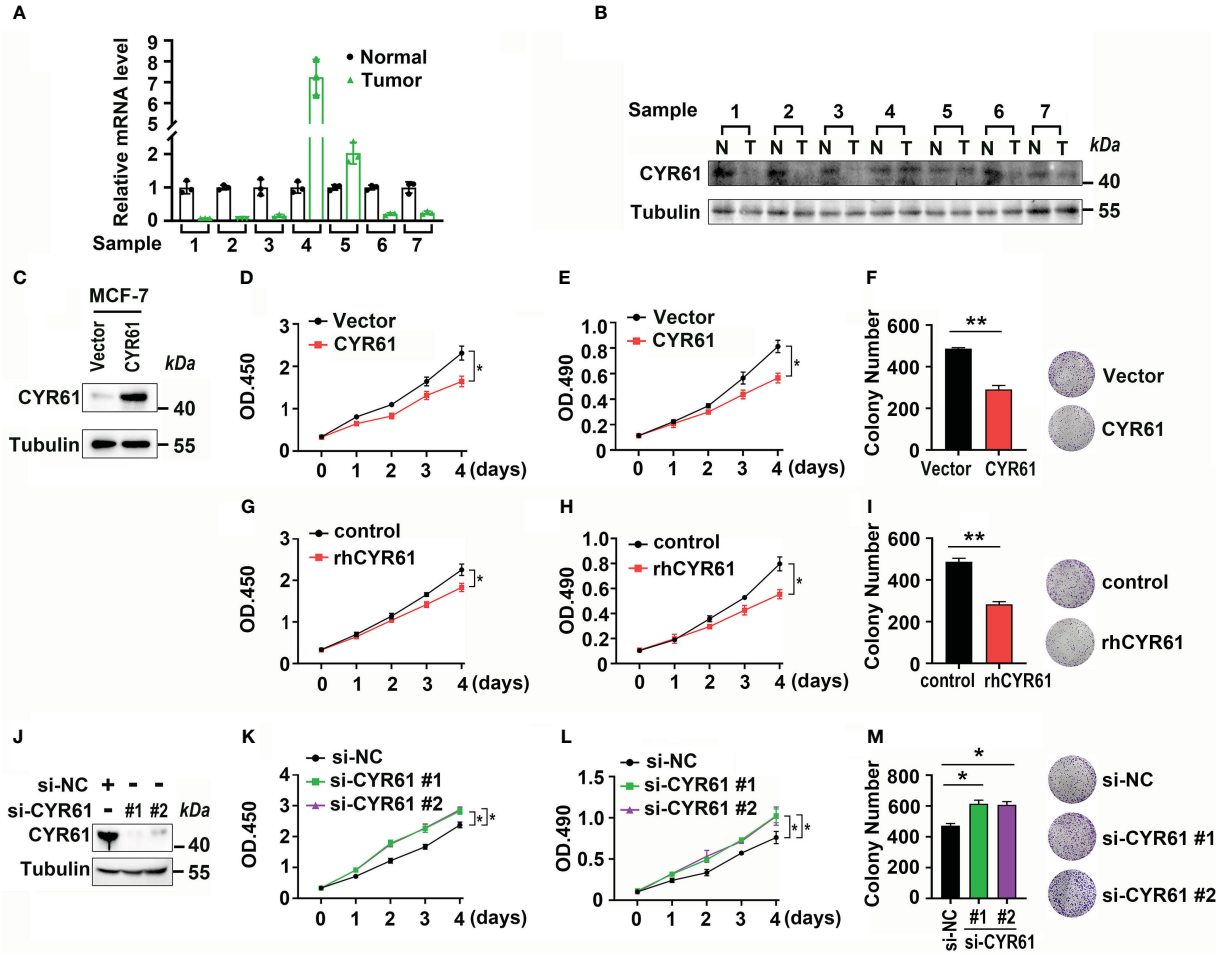

FIGURE 6
CYR61 inhibits the proliferation and colony formation of ER-positive BRCA cells. **(A, B)** q-PCR **(A)** and western blotting **(B)** analyses of CYR61 expression in 7 ER+ BRCA tissues and their matched paracancer normal breast tissues from patients. **(C)** Verification of CYR61- or the control vector-overexpressing MCF-7 stable cells by western blotting. **(D–F)** MCF-7 cells overexpressing CYR61 or the control vector were subjected to cell proliferation **(D, E)** and colony formation **(F)** examinations. **(G–I)** MCF-7 cells were treated with or without 10 ng/ml recombinant human CYR61 protein (rhCYR61) for the indicated time periods, followed by cell proliferation **(D, E)** and colony formation **(F)** examinations. **(J–M)** MCF-7 cells were transfected with a non-specific (NS) or CYR61-targeting siRNAs for 36 h, followed by western blotting **(J)**, cell proliferation **(K, L)** and colony formation **(M)** assays. *p<0.05; **p<0.01.

remodeling the TIME (17–19). Finally, experimental assays confirmed that CYR61 is downregulated in most of the clinic ER-positive BRCA tissues and acts as an inhibitor of cancer cell proliferation and colony formation (Figure 6).

In summary, by combining bioinformatic and experimental studies, we found that reduced expression level of CYR61 may serve as a new prognostic marker for ER-positive BRCA, and revealed that CYR61 acts as a tumor inhibitor by impeding cancer cell malignant transformation and remodeling the TIME.

Data availability statement

The original contributions presented in the study are included in the article/supplementary material. Further inquiries can be directed to the corresponding authors.

Ethics statement

The studies involving humans were approved by the Medical Ethics Committee of Third Hospital of Nanchang. The studies were conducted in accordance with the local legislation and institutional requirements. The participants provided their written informed consent to participate in this study.

Author contributions

CZ: Data curation, Formal analysis, Funding acquisition, Investigation, Writing – original draft, Methodology. ZL: Formal analysis, Funding acquisition, Investigation, Methodology, Resources, Writing – original draft. KH: Data curation, Investigation, Methodology, Software, Visualization, Writing –

original draft. YR: Data curation, Investigation, Methodology, Software, Writing – original draft. HZ: Data curation, Investigation, Visualization, Writing – original draft. YZ: Data curation, Methodology, Software, Writing – original draft. WW: Data curation, Methodology, Software, Writing – original draft. ST: Funding acquisition, Methodology, Supervision, Writing – review & editing, Conceptualization. XY: Conceptualization, Funding acquisition, Supervision, Writing – review & editing.

Funding

The author(s) declare financial support was received for the research, authorship, and/or publication of this article. This work was supported by grants from the National Natural Science Foundation of China (NSFC, 32370765 and 32060162), the Natural Science Foundation of Jiangxi Province of China (20224ACB206032, 20224BAB206002 and 20202BAB206046) and the Jiangxi Province Graduate Innovation Fund (YC2018-B017).

Conflict of interest

The authors declare that the research was conducted in the absence of any commercial or financial relationships that could be construed as a potential conflict of interest.

Publisher's note

References

1. Siegel RL, Miller KD, Wagle NS, Jemal A. Cancer statistics, 2023. *CA Cancer J Clin* (2023) 73:17–48. doi: 10.3322/caac.21763

2. Harbeck N, Penault-Llorca F, Cortes J, Gnant M, Houssami N, Poortmans P, et al. Breast cancer. *Nat Rev Dis Primers* (2019) 5(1):66. doi: 10.1038/s41572-019-0111-2

3. Hong RX, Xu BH. Breast cancer: an up-to-date review and future perspectives. *Cancer Commun* (2022) 42:913–36. doi: 10.1002/cac2.12358

4. Rauner G, Kuperwasser C. Microenvironmental control of cell fate decisions in mammary gland development and cancer. *Dev Cell* (2021) 56:1875–83. doi: 10.1016/j.devcel.2021.06.016

5. Huppert LA, Gumusay O, Idossa D, Rugo HS. Systemic therapy for hormone receptor-positive/human epidermal growth factor receptor 2-negative early stage and metastatic breast cancer. *CA Cancer J Clin* (2023) 73:480–515. doi: 10.3322/caac.21777

6. Garcia-Martinez L, Zhang YS, Nakata Y, Chan HL, Morey L. Epigenetic mechanisms in breast cancer therapy and resistance. *Nat Commun* (2021) 12 (1):1786. doi: 10.1038/s41467-021-22024-3

7. Onkar SS, Carleton NM, Lucas PC, Bruno TC, Lee AV, Vignali DAA, et al. The great immune escape: understanding the divergent immune response in breast cancer subtypes. *Cancer Discovery* (2023) 13:23–40. doi: 10.1158/2159-8290.CD-22-0475

8. Krupska I, Bruford EA, Chaqour B. Eyeing the Cyr61/CTGF/NOV (CCN) group of genes in development and diseases: highlights of their structural likenesses and functional dissimilarities. *Hum Genomics* (2015) 9:24. doi: 10.1186/s40246-015-0046-y

9. Kim KH, Won JH, Cheng N, Lau LF. The matricellular protein CCN1 in tissue injury repair. *J Cell Commun Signal* (2018) 12:273–9. doi: 10.1007/s12079-018-0450-x

10. Yeger H, Perbal B. The CCN axis in cancer development and progression. *J Cell Commun Signal* (2021) 15:491–517. doi: 10.1007/s12079-021-00618-2

11. Xie D, Yin D, Tong X, O'Kelly J, Mori A, Miller C, et al. Cyr61 is overexpressed in gliomas and involved in integrin-linked kinase-mediated Akt and beta-catenin-TCF/Lef signaling pathways. *Cancer Res* (2004) 64:1987–96. doi: 10.1158/0008-5472.CAN-03-0666

12. Tong X, Xie D, O'Kelly J, Miller CW, Muller-Tidow C, Koeffler HP. Cyr61, a member of CCN family, is a tumor suppressor in non-small cell lung cancer. *J Biol Chem* (2001) 276:47709–14. doi: 10.1074/jbc.M107878200

13. Li X, Zhuo S, Zhuang T, Cho YS, Wu GJ, Liu YC, et al. YAP inhibits ERα and ER^+ breast cancer growth by disrupting a TEAD-ERα signaling axis. *Nat Commun* (2022) 13 (1):3075. doi: 10.1038/s41467-022-30831-5

14. Ma SH, Tang T, Probst G, Konradi A, Jin CY, Li FL, et al. Transcriptional repression of estrogen receptor alpha by YAP reveals the Hippo pathway as therapeutic target for ER+ breast cancer. *Nat Commun* (2022) 13(1):1061. doi: 10.1038/s41467-022-28691-0

15. Luo WC, Li Y, Zeng Y, Li YN, Cheng MZ, Zhang C, et al. Tea domain transcription factor TEAD4 mitigates TGF-beta signaling and hepatocellular carcinoma progression independently of YAP. *Mol Cell Biol* (2023) 15(2):mjad010. doi: 10.1093/jmcb/mjad010

16. Liu RC, Zhao E, Yu HJ, Yuan CY, Abbas MN, Cui HJ. Methylation across the central dogma in health and diseases: new therapeutic strategies. *Signal Transduct Target Ther* (2023) 8(1):310. doi: 10.1038/s41392-023-01528-y

17. Bertazza L, Mocellin S. The dual role of tumor necrosis factor (TNF) in cancer biology. *Curr Med Chem* (2010) 17:3337–52. doi: 10.2174/092986710793176339

18. Babyshkina N, Dronova T, Erdyneeva D, Gervas P, Cherdyntseva N. Role of TGF-β signaling in the mechanisms of tamoxifen resistance. *Cytokine Growth F R* (2021) 62:62–9. doi: 10.1016/j.cytogfr.2021.09.005

19. Binnewies M, Roberts EW, Kersten K, Chan V, Fearon DF, Merad M, et al. Understanding the tumor immune microenvironment (TIME) for effective therapy. *Nat Med* (2018) 24:541–50. doi: 10.1038/s41591-018-0014-x

20. D'Antonio LSKB, Albadine R, Mondul AM, Platz EA, Netto GJ, Getzenberg RH. Decreased expression of cyr61 is associated with prostate cancer recurrence after surgical treatment. *Clin Cancer Res* (2010) 16:5908–13. doi: 10.1158/1078-0432.CCR-10-1200

21. Nguyen N, Kuliopulos A, Graham RA, Covic L. Tumor-derived Cyr61(CCN1) promotes stromal matrix metalloproteinase-1 production and protease-activated receptor 1-dependent migration of breast cancer cells. *Cancer Res* (2006) 66:2658–65. doi: 10.1158/0008-5472.CAN-05-2082

22. Bartkowiak K, Heidrich I, Kwiatkowski M, Gorges TM, Andreas A, Geffken M, et al. Cysteine-rich angiogenic inducer 61: pro-survival function and role as a biomarker for disseminating breast cancer cells. *Cancers* (2021) 13(3):563. doi: 10.3390/cancers13030563

23. Kim H, Son S, Ko Y, Lee JE, Kim S, Shin I, et al. and Cyr61 are overexpressed in tamoxifen-resistant breast cancer and induce transcriptional repression of ERα. *J Cell Sci* (2021) 134(11):jcs256503. doi: 10.1242/jcs.256503

24. Loibl S, Poortmans P, Morrow M, Denkert C, Curigliano G. Breast cancer. *Lancet* (2021) 397:1750–69. doi: 10.1016/S0140-6736(20)32381-3

25. Agostinetto E, Gligorov J, Piccart M. Systemic therapy for early-stage breast cancer: learning from the past to build the future. *Nat Rev Clin Oncol* (2022) 19:763–74. doi: 10.1038/s41571-022-00687-1

26. Will M, Liang JC, Metcalfe C, Chandarlapaty S. Therapeutic resistance to anti-oestrogen therapy in breast cancer. *Nat Rev Cancer* (2023) 23(10):673–85. doi: 10.1038/s41568-023-00604-3

27. Mooring M, Fowl BH, Lum SZC, Liu Y, Yao K, Softic S, et al. Hepatocyte stress increases expression of yes-associated protein and transcriptional coactivator with PDZ-binding motif in hepatocytes to promote parenchymal inflammation and fibrosis. *Hepatology* (2020) 71:1813–30. doi: 10.1002/hep.30928

28. Todoric J, Di Caro G, Reibe S, Henstridge DC, Green CR, Vrbanac A, et al. Fructose stimulated *de novo* lipogenesis is promoted by inflammation. *Nat Metab* (2020) 2:1034–45. doi: 10.1038/s42255-020-0261-2

29. Liu X, Chen BB, Chen JH, Su ZY, Sun SL. Deubiquitinase ubiquitin-specific peptidase 10 maintains cysteine rich angiogenic inducer 61 expression via Yes1

associated transcriptional regulator to augment immune escape and metastasis of pancreatic adenocarcinoma. *Cancer Sci* (2022) 113:1868–79. doi: 10.1111/cas.15326

30. Tan ZY, Kan C, Sun MQ, Yang F, Wong MY, Wang SY, et al. Mapping breast cancer microenvironment through single-cell omics. *Front Immunol* (2022) 13. doi: 10.3389/fimmu.2022.868813

31. Wang XY, Almet AA, Nie Q. The promising application of cell-cell interaction analysis in cancer from single-cell and spatial transcriptomics. *Semin Cancer Biol* (2023) 95:42–51. doi: 10.1016/j.semcancer.2023.07.001

32. Liu C, Li XH, Huang QY, Zhang M, Lei TY, Wang FH, et al. Single-cell RNA-sequencing reveals radiochemotherapy-induced innate immune activation and MHC-II upregulation in cervical cancer. *Signal Transduct Target Ther* (2023) 8(1):44. doi: 10.1038/s41392-022-01264-9

frontiers | Frontiers in Immunology

TYPE Original Research
PUBLISHED 02 February 2024
DOI 10.3389/fimmu.2024.1331841

OPEN ACCESS

EDITED BY
Chao Liu,
Shandong Cancer Hospital, China

REVIEWED BY
Xinpei Deng,
Sun Yat-Sen University Cancer Center (SYSUCC), China
Guichuan Lai,
Chongqing Medical University, China
Yue Shengqin,
Renmin Hospital of Wuhan University, China

*CORRESPONDENCE
You Meng
13912774015@163.com
Shengbin Pei
psb@student.pumc.edu.cn
Jiale Cheng
438586918@qq.com

†These authors have contributed equally to this work and share first authorship

RECEIVED 01 November 2023
ACCEPTED 17 January 2024
PUBLISHED 02 February 2024

CITATION
Chen W, Kang Y, Sheng W, Huang Q, Cheng J, Pei S and Meng Y (2024) A new 4-gene-based prognostic model accurately predicts breast cancer prognosis and immunotherapy response by integrating WGCNA and bioinformatics analysis. *Front. Immunol.* 15:1331841. doi: 10.3389/fimmu.2024.1331841

A new 4-gene-based prognostic model accurately predicts breast cancer prognosis and immunotherapy response by integrating WGCNA and bioinformatics analysis

Wenlong Chen[1†], Yakun Kang[2†], Wenyi Sheng[1†], Qiyan Huang[1], Jiale Cheng[1*], Shengbin Pei[2,3*] and You Meng[1*]

[1]Department of Thyroid and Breast Surgery, The Affiliated Suzhou Hospital of Nanjing Medical University, Suzhou Municipal Hospital, Gusu School, Nanjing Medical University, Suzhou, China, [2]Department of Breast Surgery, The First Affiliated Hospital of Nanjing Medical University, Nanjing, China, [3]Department of Breast Surgical Oncology, National Cancer Center/National Clinical Research Center for Cancer/Cancer Hospital, Chinese Academy of Medical Sciences and Peking Union Medical College, Beijing, China

Background: Breast cancer (BRCA) is a common malignancy in women, and its resistance to immunotherapy is a major challenge. Abnormal expression of genes is important in the occurrence and development of BRCA and may also affect the prognosis of patients. Although many BRCA prognosis model scores have been developed, they are only applicable to a limited number of disease subtypes. Our goal is to develop a new prognostic score that is more accurate and applicable to a wider range of BRCA patients.

Methods: BRCA patient data from The Cancer Genome Atlas database was used to identify breast cancer-related genes (BRGs). Differential expression analysis of BRGs was performed using the 'limma' package in R. Prognostic BRGs were identified using co-expression and univariate Cox analysis. A predictive model of four BRGs was established using Cox regression and the LASSO algorithm. Model performance was evaluated using K-M survival and receiver operating characteristic curve analysis. The predictive ability of the signature in immune microenvironment and immunotherapy was investigated. *In vitro* experiments validated POLQ function.

Results: Our study identified a four-BRG prognostic signature that outperformed conventional clinicopathological characteristics in predicting survival outcomes in BRCA patients. The signature effectively stratified BRCA patients into high- and low-risk groups and showed potential in predicting the response to immunotherapy. Notably, significant differences were observed in immune cell abundance between the two groups. *In vitro* experiments demonstrated that POLQ knockdown significantly reduced the viability, proliferation, and invasion capacity of MDA-MB-231 or HCC1806 cells.

Conclusion: Our 4-BRG signature has the potential as an independent biomarker for predicting prognosis and treatment response in BRCA patients, complementing existing clinicopathological characteristics.

KEYWORDS

breast cancer, POLQ, prognostic signature, immune landscape, drug screening

1 Introduction

Breast cancer (BRCA) has overtaken lung cancer to become the world's leading cancer and the most deadly malignancy among women (1). With the continuous progress of BRCA diagnosis and treatment technology, the 5-year survival rate of early BRCA patients can reach 95%, so early screening, diagnosis, and treatment of BRCA are the keys to a good prognosis (2). BRCA is a highly heterogeneous disease, and patients differ in their response to treatment and prognosis even if the clinical stage and pathological grade are the same. Although these molecular subtypes are widely used, the prognosis of BRCA cases of each subtype is still very different. Therefore, it is of great clinical significance to explore new prognostic features.

In cancer research, prognostic models are widely used to predict the prognosis of patients. Van De Vijver et al. first performed 70 genetic signatures that were strongly associated with survival in BRCA patients (3). Peng et al. constructed a molecular prognostic score based on 23 genes that accurately predicted the overall survival of BRCA patients (4). In addition, various prognostic models were constructed between cancer types, and these features were shown to be more accurate in predicting clinical prognosis than assessed by traditional pathological and imaging methods (5–7). In the field of BRCA research, new prognostic models are not yet fully developed. Therefore, we included breast cancer-related genes in the construction of prognostic models to estimate novel strategies for predicting outcomes in BRCA patients.

Over time, immunotherapy has made more significant progress in other cancer types, including melanoma, kidney cancer, and lung cancer (8). In the early stage, due to the weak immunogenicity of BRCA, it is regarded as a "cold tumor", and scholars believe that immunotherapy is difficult to make a big breakthrough in it. Still, in recent years, immunotherapy has made good progress in triple-negative BRCA, especially in metastatic BRCA (9–12). Therefore, finding an effective way to predict long-term survival and response to immune checkpoint inhibitor treatment in BRCA patients is critical (13).

In this study, weighted gene co-expression network analysis was used to screen out the genes associated with BRCA prognosis. The prognostic features were derived from univariate Cox regression and LASSO regression analyses performed on the TCGA BRCA training cohort. After rigorous validation in multiple cohorts, we demonstrated that the POLQ-related signature can effectively predict BRCA prognosis. By using the median risk score, we stratified the BRCA samples into high-risk and low-risk groups, which displayed distinct overall survival, progression-free survival, and disease-free interval, as well as differences in clinical characteristics, immune infiltration, response to ICI treatment, and chemotherapy drug sensitivity. To facilitate clinical application, we developed a nomogram that can guide BRCA treatment. These findings shed light on the immunological and prognostic significance of POLQ in BRCA and highlight the potential of its related biomarkers as promising targets for the diagnosis and treatment of BRCA.

2 Materials and methods

2.1 Data collection

Utilizing multiple datasets, including GSE16228, GSE20685, GSE20711, GSE42658, and GSE88770 from the Gene Expression Omnibus (GEO) database, you collected a total of 745 BRCA tumor tissue samples and 43 normal tissue samples as training sets. Additionally, 1089 BRCA tumor samples from TCGA were used as the testing cohort. To ensure accurate analysis, patients lacking important clinical information such as OS and relapse status were excluded, and data normalization was performed to mitigate batch effects.

2.2 WGCNA

By constructing a weighted gene coexpression network using the WGCNA R software package, you aimed to identify coexpression gene modules, investigate the relationship between the gene network and phenotype, and identify core genes within the network. Here's an overview of the process we followed: Calculation of Median Absolute Deviation (MAD): You calculated the MAD for each gene in the BRCA gene expression profile. Selection of genes: The top 50% of genes with the smallest MAD values were excluded. This step helped filter out less informative genes. Removal of outliers: The "goodSamplesGenes" method from the WGCNA package was used to remove outlier genes and samples from the

dataset. Construction of a scale-free co-expression network: Using WGCNA, you built a scale-free co-expression network. The Pearson correlation matrix and average linkage method were employed for pairs of genes. Weighted adjacency matrix construction: A power function (A_mn=|C_mn|^β) was applied to construct the weighted adjacency matrix. The soft threshold parameter, β was used to accentuate strong gene correlations and compensate for weaker ones. Topological overlap matrix (TOM): The weighted adjacency matrix was transformed into a TOM to estimate network connectivity. The hierarchical clustering method helped create a cluster tree structure for the TOM matrix. Module analysis: Dissimilarity of characteristic genes within the modules was computed. Tangent lines of the module tree were selected, and some modules were combined for further analysis.

2.3 Identification of DEGs and functional enrichment analysis

We identified 129 differentially expressed genes between the BRCA group and the normal control group using the "Limma" package. The selection criteria included a $|logFC| \geq 1$ and $p < 0.01$. Next, you employed the "clusterProfiler" package for conducting the Gene Ontology (GO) function and Kyoto Encyclopedia of Genes and Genomes (KEGG) pathway enrichment analysis based on these DEGs. GO function analysis categorizes genes into different functional groups, while KEGG pathway analysis explores molecular interactions and networks within cells. These analyses provide valuable insights into the biological mechanisms underlying BRCA and can reveal potential therapeutic targets and interventions.

2.4 Random survival forest variable screening

Random Survival Forest (RSF) is an ensemble method that consists of a collection of randomly growing survival trees. The tree-building rules in RSF are similar to those of random forest, which is an extended methodology used for analyzing survival data. To identify prognostic genes in the training set, univariate Cox proportional regression models were initially employed. Then, 1000 classification trees were constructed using bootstrap samples. During the tree-building process, candidate variables were randomly selected at each node, and nodes were classified based on survival criteria such as survival time and truncation information. To determine the variables entering the model, gene screening was performed using exponential sequencing or gene occurrence frequency. Each decision tree within the random survival forest is a binary survival tree, generated following the top-down recursive splitting principle. This approach involves sequentially dividing the training set from the root node, which helps prevent model overfitting. Using RSF, researchers can obtain valuable insights into the prognosis of specific diseases, including potential prognostic genes and their impact on survival outcomes.

2.5 GeneMANIA analysis

GeneMANIA (http://www.genemania.org) is an excellent resource for constructing protein-protein interaction (PPI) networks and analyzing gene function and interactions. This user-friendly database enables researchers to visualize functional networks between genes and gain insights into gene behavior. The GeneMANIA website provides the flexibility to customize the data sources of gene nodes, including physical interaction, gene coexpression, gene colocalization, gene enrichment analysis, and predictions from other sources. By incorporating these diverse data sources, researchers can obtain a comprehensive understanding of gene relationships and their functional implications. In this study, we utilized GeneMANIA to construct a core gene network specific to ovarian cancer patients. This network serves as a valuable tool to investigate the potential mechanisms underlying the action of identified genes within the context of ovarian cancer. By visualizing and analyzing these gene interactions, we can gain insights into the functional associations and pathways involved in the disease. Make sure to carefully interpret the findings from the gene network analysis and consider additional validation strategies to strengthen the conclusions.

2.6 Analysis of immune cell infiltration

To assess various aspects of the tumor microenvironment (TME) in BRCA patients, we employed several algorithms. The ESTIMATE algorithm allowed us to evaluate the Stromalscore, Immunescore, and TMEscore. These scores provide insights into the levels of stromal and immune cell infiltration within the tumor. For a detailed analysis of immune cell types in the TME, we utilized the CIBERSORT algorithm. CIBERSORT is a widely used method that employs support vector regression to deconvolute the expression matrix of immune cell subtypes. This enabled us to quantify the levels of immune cell infiltration in each patient. To further assess the TME, we employed the MCPcounter algorithm. This algorithm generates abundance scores for eight immune cell types and two stromal cell types (including T cells, CD8+ T cells, cytotoxic lymphocytes, NK cells, B lymphocytes, monocytes, bone marrow dendritic cells, neutrophils, endothelial cells, and fibroblasts) based on the gene expression matrix. Notably, MCPcounter has been verified to exhibit a high correlation between estimated scores and actual cell scores when conducting quantitative validation. By evaluating the association between the risk scores (derived from the previously constructed prognostic model), gene expression levels, and immune cell infiltration, we aim to understand the interplay between the genetic signature and the immune microenvironment in BRCA. Additionally, we examine subgroup differences in immune checkpoint expression and

immune function, providing valuable insights into potential immunotherapeutic targets and treatment strategies.

2.7 Development of the prognostic model

From a pool of 100 intersection genes, we conducted univariate Cox regression (uniCox) analysis to identify 18 genes that showed associations with prognosis. Subsequently, we employed the "glmnet" package for regression analysis, specifically utilizing LASSO-cox analysis, to construct a prognostic model. The risk scores for individual patients were calculated by summing the gene expression values multiplied by their respective gene coefficients in the model. This risk score served as an indicator of the likelihood of an adverse prognosis. To further analyze and visualize the patient data, we divided the patients into high and low-risk groups based on the median risk score. Utilizing the "stats" package (version 3.6.0), we performed Principal Component Analysis (PCA). This analysis aids in dimensionality reduction by transforming and clustering the patients' gene expression profiles. Specifically, we initially applied a z-score transformation to standardize the gene expression data and then utilized the prompt function to obtain a reduced matrix representing the principal components. It's worth mentioning that the selection of genes and the use of LASSO-cox analysis contribute to the construction of a robust prognostic model. Moreover, conducting PCA analysis allows for a comprehensive visualization of the patient data, which may reveal patterns or clusters related to prognosis.

2.8 Clinical significance analysis of the risk model

After excluding patients with missing data, we integrated their clinical information and risk score to conduct uniCox and multivariate Cox regression (multiCox) analyses. These analytical approaches allow us to assess the relationship between the risk score model and patient prognosis. To evaluate the accuracy of the risk score model as a prognostic predictor, we performed ROC analysis using the pROC package (version 1.17.0.1). The Area Under Curve (AUC) values were calculated to provide a quantitative measure of the predictive power. We also used the CI function of the package to determine the Confidence Intervals (CI) around the AUC values, providing a measure of the uncertainty associated with the predictions. By analyzing the AUC values and their corresponding CI, we can determine the final results and assess whether the risk score model can serve as an independent and reliable prognostic predictor. It's important to note that further studies may explore alternative methods or consider additional variables to enhance the predictive capabilities of the risk score model. The pROC package is a valuable resource in this process, facilitating the calculation of AUC values and their associated confidence intervals.

2.9 Establishment of a predictive nomogram

In addition to the patient's risk score and clinicopathological features, we employed the "rms" package to construct a nomogram. This nomogram combined multiple variables to visualize their relative contributions in predicting patient outcomes. To assess the prognostic predictive power of these clinical features, particularly for 1-year, 3-year, and 5-year OS, we performed ROC analysis. The ROC analysis allows us to evaluate the accuracy of the predictive models by examining the true positive rate against the false positive rate. To validate the predictive accuracy of the nomogram, we utilized calibration curves. These curves provide graphical representations of the agreement between predicted outcomes and observed outcomes. The incorporation of calibration curves allows for an assessment of the accuracy and reliability of the predictive model. It's important to note that future studies may further explore alternative methods or consider additional factors to enhance the predictive capabilities of the nomogram. The "rms" package serves as a valuable tool in this process, facilitating the creation of comprehensive and informative prediction models.

2.10 Drug sensitivity analysis

The Genomics of Drug Sensitivity in Cancer (GDSC) database, accessible at https://www.cancerrxgene.org/, serves as a valuable resource for cancer drug sensitivity genomics. In our study, we utilized the R software package called "pRRophetic" to predict the sensitivity of tumor samples to chemotherapy. By applying a filter condition of $p < 0.001$, we determined the chemotherapy sensitivity for each tumor sample. The prediction process involved regression analysis to estimate the IC50 values for specific chemotherapeutic agents. To evaluate the accuracy of regression and prediction, we conducted 10-fold cross-validation tests using the GDSC training set. For all parameters, including the removal of batch effects using "combat" and averaging repeated gene expression, we opted for the default values. These steps enable us to mitigate potential biases and enhance the reliability of the predictions. It is worth noting that future research may explore alternative parameter settings or incorporate additional validation techniques to further refine the predictions. The GDSC database and the pRRophetic package offer a powerful combination for investigating and understanding chemotherapy sensitivity in cancer samples.

2.11 Cell transfection

Two distinct small interfering RNAs (siRNAs) targeting POLQ were synthesized by Ribobio (Guangzhou, China). The transfection protocols were executed following the manufacturer's guidelines, using Lipofectamine 3000 (Invitrogen, USA). Supplementary Table 1 contains the siRNA sequences for POLQ.

2.12 RT-qPCR

Total RNA was extracted from tissues or cell lines using TRIzol reagent (15596018, Thermo) and standard protocols were followed. Subsequently, cDNAs were synthesized using the PrimeScript™RT kit (R232-01, Vazyme). The Roche LightCycler 480 platform (Roche, GER) was employed to quantify gene expression levels, utilizing SYBR qPCR Master Mix (Q111-02, Vazyme). Supplementary Table 1 contains the primer sequences, which were sourced from Tsingke Biotech (Beijing, China).

2.13 Cell counting kit-8 assay

Each well of a 96-well plate was seeded with 2000 treated cells. Following this, the cells were subjected to treatment with the CCK-8 labeling reagent (A311-01, Vazyme) and evaluated at various time points, including days 1, 2, 3, 4, and 5.

2.14 Wound healing

After achieving 95% confluency, the transfected cells were subsequently plated into 6-well plates. To produce a straight line, a sterile pipette tip with a volume of 200 μL was utilized, followed by gentle rinsing with PBS to remove any unattached cells and debris. Subsequently, the serum-free cell medium was replaced to maintain cell culture. Images were captured at 0 and 48 hours in the same location.

2.15 Transwell

A density of 2×10^4 cells per well in 200 μL of serum-free medium was used to seed the cells in the upper chamber of a transwell plate. The upper chamber was either coated or uncoated with matrix glue (BD Biosciences, USA). The lower compartment was loaded with 700 μL of complete medium supplemented with 10% serum. After 36 hours of incubation, the cells were fixed, stained, and counted by microscopy. Images were captured for analysis.

2.16 Statistical analysis

All statistical analyses were performed using R language (Version 3.6). All statistical tests were bilateral, and P <0.05 was considered statistically significant.

3 Results

3.1 Identification of DEG sets associated with BRCA patients compared to normal women

To establish our study cohort, we obtained gene expression profiles from five GEO datasets, comprising 745 tumor tissue samples and 43 normal control tissue samples, which served as the training cohort. Additionally, we utilized the TCGA-BRCA cohort, consisting of 1089 BRCA tumor tissue samples, as the validation cohort. In the training set, we identified genes that demonstrated significant differential expression (|logFC|>1 & p<0.01) (Figures 1A, B). We employed WGCNA analysis to construct a gene coexpression network for BRCA using the training set. Subsequently, we employed dynamic hybrid cutting to generate a hierarchical clustering tree, which facilitated the identification of gene modules. The tree branches represented groups of genes with similar expression patterns, with each gene represented as a leaf in the tree (Figures 1C–E). Furthermore, we successfully constructed twelve modules within the training cohort, and we identified the magenta modules as potential hub modules (Figure 1F).

3.2 Acquisition of intersection genes and molecular characteristics analysis in BRCA

To verify the reliability of the genes obtained above, we performed a Venn analysis based on the DEG set and hub gene set data (Figure 2A). A total of 100 intersection genes were screened for GO and KEGG enrichment. GO analysis showed that these intersection genes are enriched in a variety of biological processes, including cell cycle, mitotic cell cycle process, cell division, nuclear division, and chromosome segregation. KEGG analysis revealed that cell cycle, oocyte meiosis, progesterone-mediated oocyte maturation, and p53 signaling pathway were enriched by these intersection genes (Figure 2B). In addition, we constructed PPI networks using an online tool (https://cn.string-db.org) to explore the association between the intersection genes. The results showed that CDK1, BUB1B. KIF11, KIF20A, and CCNB1 were hub genes (confidence score = 0.900) (Figures 2C, D). These hub genes are highly expressed in tumor tissues compared to normal control tissues and in the ROC curve, these hub genes displayed a pretty AUC value (Figures 2E, F), implying their potentially critical roles in BRCA. Furthermore, the Genemania network also indicated that the five genes have a close interaction in multiple biological functions, including mitotic nuclear division, negative regulation of cell cycle phase transition, and cell cycle checkpoint (Figure 2G). In immune cell infiltration analysis, we found that a variety of immune cells, including $CD8^+$T cells, plasma cells, activated NK cells, and macrophages M2 were more abundant in normal tissues, while macrophages M1, T cells $CD4^+$ memory resting, and γδ T cells were more infiltrated in tumor tissues (Figures 2H, I).

3.3 Development and validation of the prognostic model

Based on 100 intersection genes, the researchers conducted a uniCox analysis and identified 18 prognostic-related genes, which were found to be highly expressed in tumor tissues (Figure 3A). They then developed a risk model to assess the prognostic predictive ability of these intersection genes specifically in BRCA patients. To establish

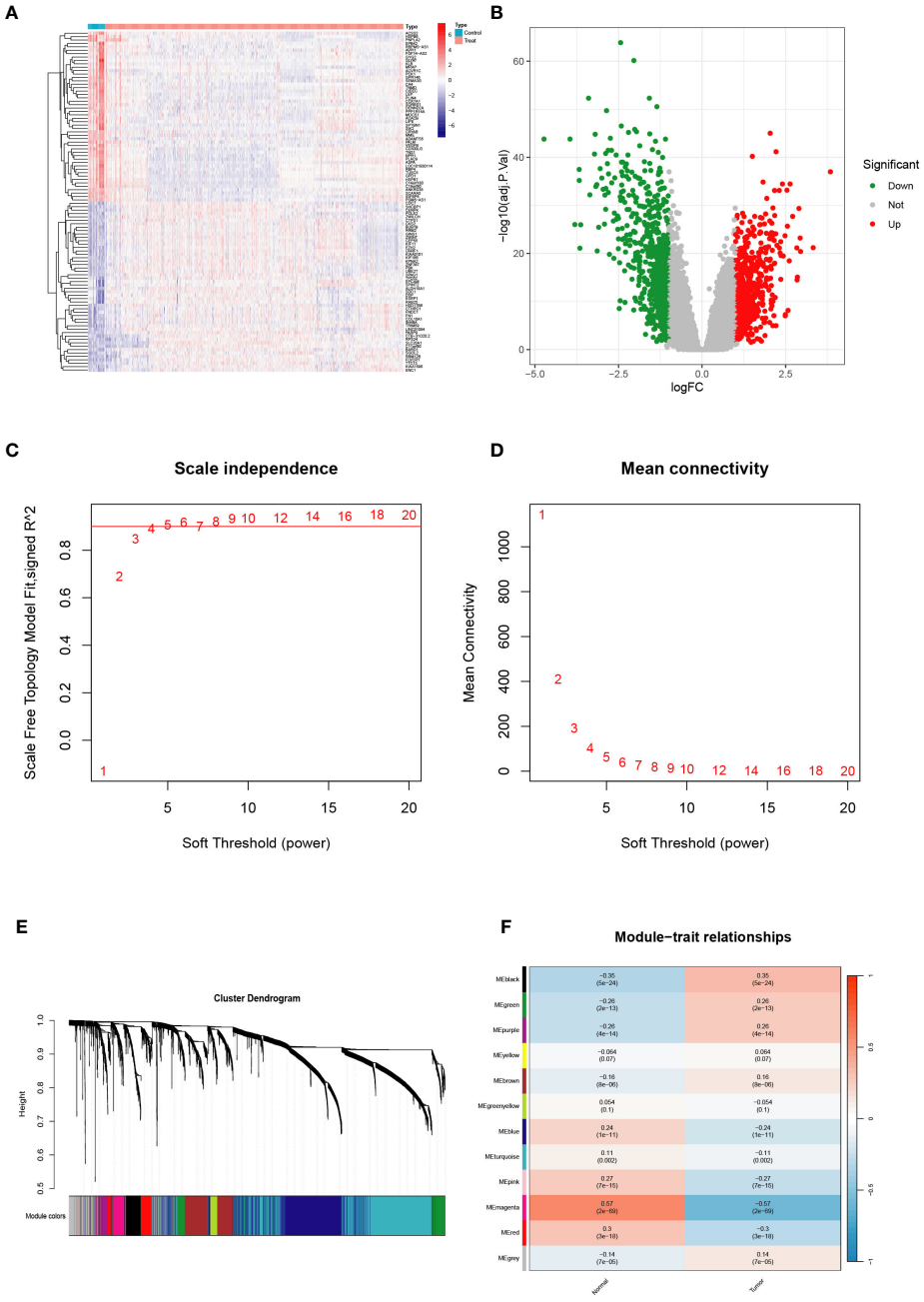

FIGURE 1
Validation of the hub module via weighted gene coexpression network analysis. **(A, B)** Differentially expressed genes are shown on the heatmap and the volcano plot for the five Gene Expression Omnibus (GEO) datasets. **(C, D)** The scale-free fit index and the average connectivity of soft threshold power and hierarchical clustering tree of genes based on topological overlap are confirmed for the five GEO datasets. **(E, F)** A total of 12 modules were obtained and the correlation of these modules between the normal group and tumor group for the five GEO datasets.

the optimal predictive model, LASSO and multiCox analysis were performed on 18 prognosis-related differentially expressed genes. Ultimately, four genes (RAD51AP1, HELLS, PLSCR4, and POLQ) were identified, and the formula for the risk score was derived as follows: risk score = (0.171787939 * expression of RAD51AP1) + (0.180159626 * expression of HELLS) + (-0.35136865 * expression of PLSCR4) + (0.35452173 * expression of POLQ). Following the risk score calculation, the patients were divided into high-risk and low-risk groups based on the median risk score. Kaplan-Meier analysis demonstrated that low-risk patients had a better OS compared to the high-risk patients (Figure 3B). Additionally, PCA analysis showed a distinct separation of patients into high-risk and low-risk groups (Figure 3C). The prognostic model exhibited promising predictive ability with AUC values of 0.76 (95% CI = 0.91-0.62), 0.68 (95% CI = 0.71-0.56), and 0.64 (95% CI = 0.68-0.56) for predicting patients' OS at 1, 3, and 5 years, respectively (Figure 3D). Moreover, there was an inverse correlation between the risk score and patient survival, as evidenced by the decreasing OS and increasing mortality rate with higher risk scores (Figures 3E, F). The expression heatmap in Figure 3G illustrates the gene expression patterns involved in

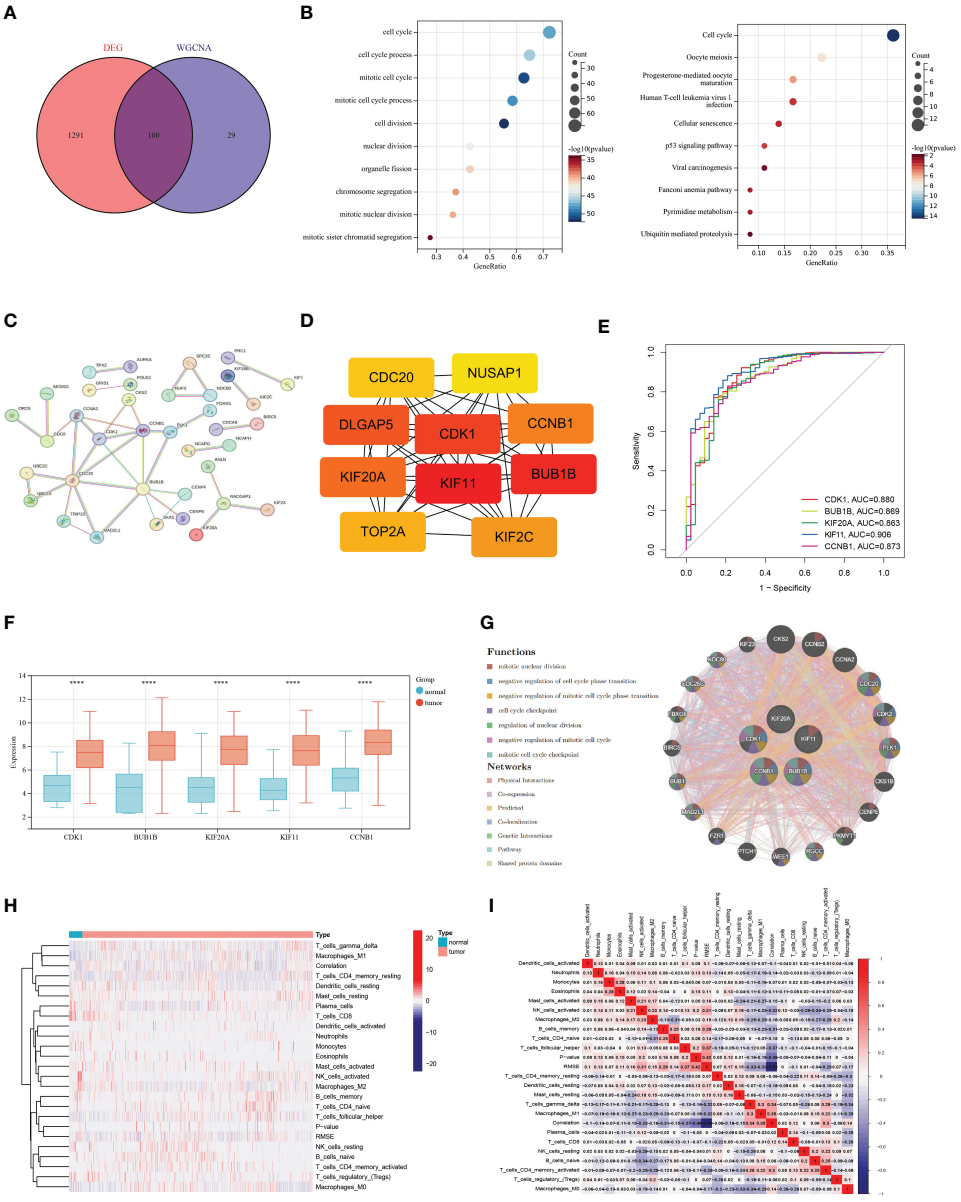

FIGURE 2
Acquisition of intersection genes and molecular characteristics analysis. **(A)** Venn diagram based on differentially expressed genes and hub gene set. **(B)** Gene Ontology and Kyoto Encyclopedia of Genes and Genomes analysis of intersection genes. (C) The protein-protein interaction network was acquired from the STRING database among intersection genes. **(D)** Hub genes in the intersection gene set. **(E)** Receiver operating characteristic curve of five hub genes. **(F)** Differential expression of hub genes in breast cancer (BRCA) and normal tissues. **(G)** The networks among five hub genes are based on the GeneMANIA database. **(H–I)** Immune cell infiltration analysis in BRCA and normal tissues. (P<0.0001 ****).

constructing the prognostic model. Importantly, the prognostic model was validated in an independent cohort and showed good predictive power (Figures 4A–F).

3.4 Clinical correlation analysis of the prognostic model and construction of a nomogram

UniCox and multiCox analyses were conducted to assess the independent prognostic value of the risk score (Figures 5A, B). The forest plot indicated that the risk score is comparable to tumor grade and tumor stage as an independent risk factor for predicting the prognosis of BRCA patients. Patients who experienced distant metastasis or tumor relapse exhibited higher risk scores (Figures 5C, D), suggesting a correlation between the risk score and increased risk of metastasis and poorer prognosis. To enhance predictability, a nomogram was developed based on clinical characteristics to estimate the 1-year, 3-year, and 5-year OS of BRCA patients (Figure 5E). The calibration curves in Figure 5F demonstrated the high accuracy of the nomogram in predicting the 3-year and 5-year OS of BRCA patients. Additionally, the receiver operating characteristic (ROC) curve in Figure 5G revealed the AUC values of the nomogram for predicting the 1-year, 3-year, and 5-year OS:

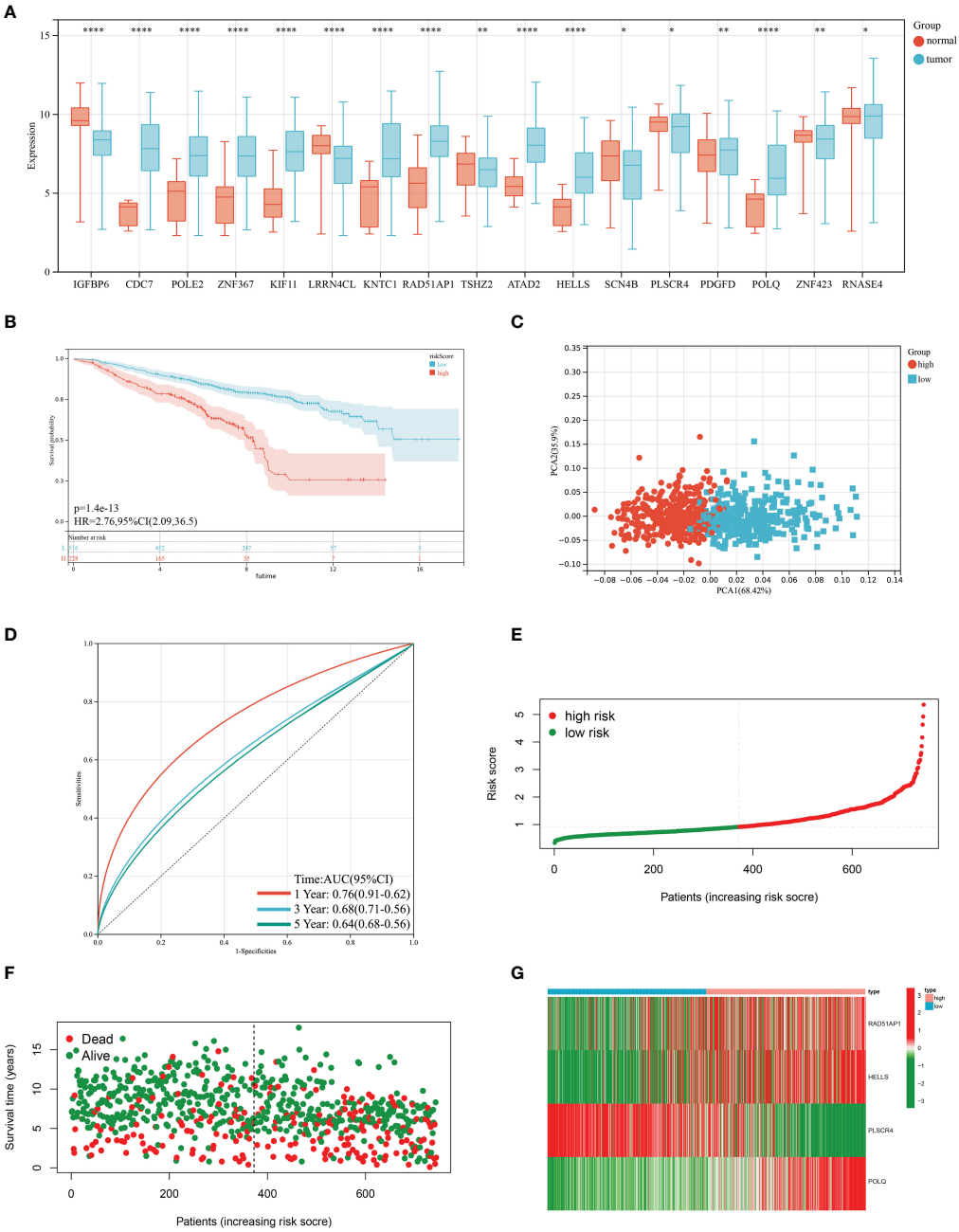

FIGURE 3
Construction of the prognostic model in the training cohort. **(A)** Differences in the expression of 17 prognostic-related genes among BRCA and normal tissues. **(B)** Kaplan–Meier analysis of the Overall Survival (OS) between high- and low-risk groups. **(C)** Principal Component Analysis based on the prognostic model. **(D)** Receiver operating characteristic curve to predict the sensitivity and specificity of 1-, 3-, and 5-year survival according to the risk score. **(E, F)** Ranked dot and scatter plots showing the risk score distribution and patient survival status. **(G)** Expression patterns of 4 selected prognostic genes in high- and low-risk groups. (*P*<0.05 *; *P*<0.01 **; *P*<0.001 ***, *P*<0.0001 ****).

0.89 (95% CI = 0.97-0.92), 0.87 (95% CI = 0.95-0.79), and 0.86 (95% CI = 0.94-0.79), respectively.

3.5 Assessment of TME, checkpoints, and immune function in distinct groups

In our study, we explored the correlation between immune cell abundance and the risk score. Our findings, as depicted in Figure 6A, revealed interesting associations between the risk score and different immune cell types. Specifically, the risk score positively correlated with memory B cells, naïve $CD4^+$ T cells, macrophages M0, and activated NK cells. Conversely, it exhibited a negative correlation with naïve B cells, resting $CD4^+$ memory T cells, resting dendritic cells, and γδ T cells. Furthermore, our analysis demonstrated that the risk score was linked to higher StromalScore, ImmuneScore, and ESTIMATEScore, as illustrated in Figure 6B. This suggests that the risk score may indicate increased stromal and immune activity within

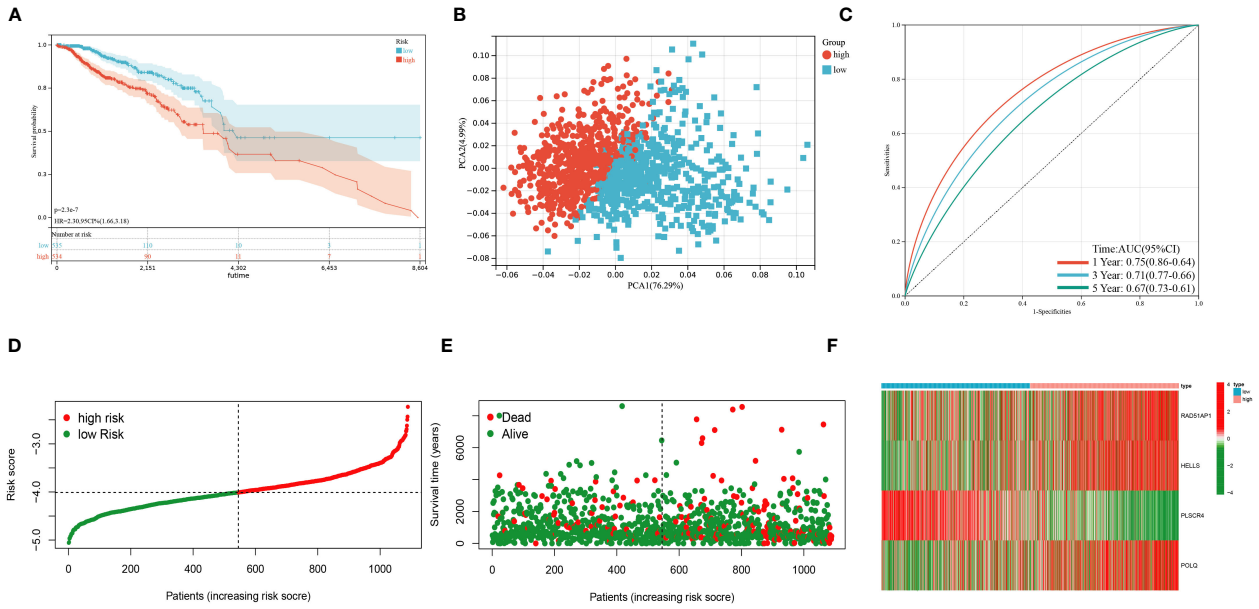

FIGURE 4
Validation of the prognostic model in the test cohort. **(A)** Kaplan–Meier analysis of the Overall Survival (OS) between high- and low-risk groups. **(B)** Principal Component Analysis based on the prognostic model. **(C)** Receiver operating characteristic curve to predict the sensitivity and specificity of 1-,3-, and 5-year survival according to the risk score. **(D–E)** Ranked dot and scatter plots showing the risk score distribution and patient survival status. **(F)** Expression patterns of 4 selected prognostic genes in high- and low-risk groups. (P<0.05*; P<0.01**; P<0.001***, P<0.0001****).

the TME. To delve deeper, we assessed the association between the genes utilized in constructing the risk score model and the infiltration levels of various immune cells. Notably, we observed significant correlations between the expression levels of certain genes, such as POLQ, and the abundance of specific immune cell types. For instance, the expression level of POLQ displayed a significant positive correlation with naïve B cell infiltration and a negative correlation with activated NK cell infiltration, as shown in Figure 6C. Figure 6D revealed significant differences in various immune functions between the high-risk and low-risk groups, such as T cell co-inhibition, immune checkpoint expression, cytolytic activity, and type I IFN response. The MCPcounter analysis in Figure 6E demonstrated that the high-risk group had decreased infiltration levels of endothelial cells, fibroblasts, and immune cells compared to the low-risk group. Moreover, by analyzing 35 common immune checkpoints including PD-1, PD-L1, CTLA-4, and LAG3 between the high and low-risk groups (Figure 6F), it was observed that the low-risk group exhibited lower levels of immune checkpoint expression.

3.6 Drug sensitivity analysis

For evaluating the predictive power of the risk score in assessing clinical drug therapy sensitivity among BRCA patients, we employed the "pRRophetic" package to calculate the IC50 values associated with 138 drugs for each patient. Our analysis yielded intriguing findings regarding potential drug responses based on the risk score. Patients with low-risk scores exhibited promising indications of positive responses to several drugs, including All-trans-retinoic acid (ATRA), bleomycin, cytarabine, doxorubicin, gemcitabine, paclitaxel, and sorafenib. On the other hand, patients with high-risk scores displayed a greater likelihood of positive responses to bicalutamide, docetaxel, as well as various targeted therapy drugs such as dasatinib, lapatinib, axitinib, and other similar medications (Figure 7). Taken together, these outcomes suggest a noteworthy correlation between the risk score and drug sensitivity. Nonetheless, it remains essential to exercise caution and further validate these observations through rigorous validation studies. May these findings contribute to the advancement of personalized medicine approaches for better management of BRCA patients!

3.7 Core genes related to genetic alterations, TMB, and targeted therapy/chemotherapy in BRCA

To determine whether four genes exist in the somatic mutation frequencies in BRCA, we extracted the oncoprint profiles based on the cBioPortal database (http://www.cbioportal.org/). The somatic mutation frequencies of RAD51AP1, HELLS, PLSCR4, and POLQ were 1.9%, 0.4%, 1.4%, and 1.7%, respectively (Figure 8A). In addition, tumor mutation burden (TMB) is a very important and identifiable clinical biomarker for immunotherapy. We calculated the TMB of each sample, and after analysis, we found that there was a significant correlation between the expression levels of RAD51AP1, HELLS, PLSCR4, POLQ, and the TMB data. Specifically, high expression of PLSCR4 was associated with lower TMB. In contrast, high expression of RAD51AP1, HELLS, and POLQ was associated with higher TMB in BRCA (Figure 8B).

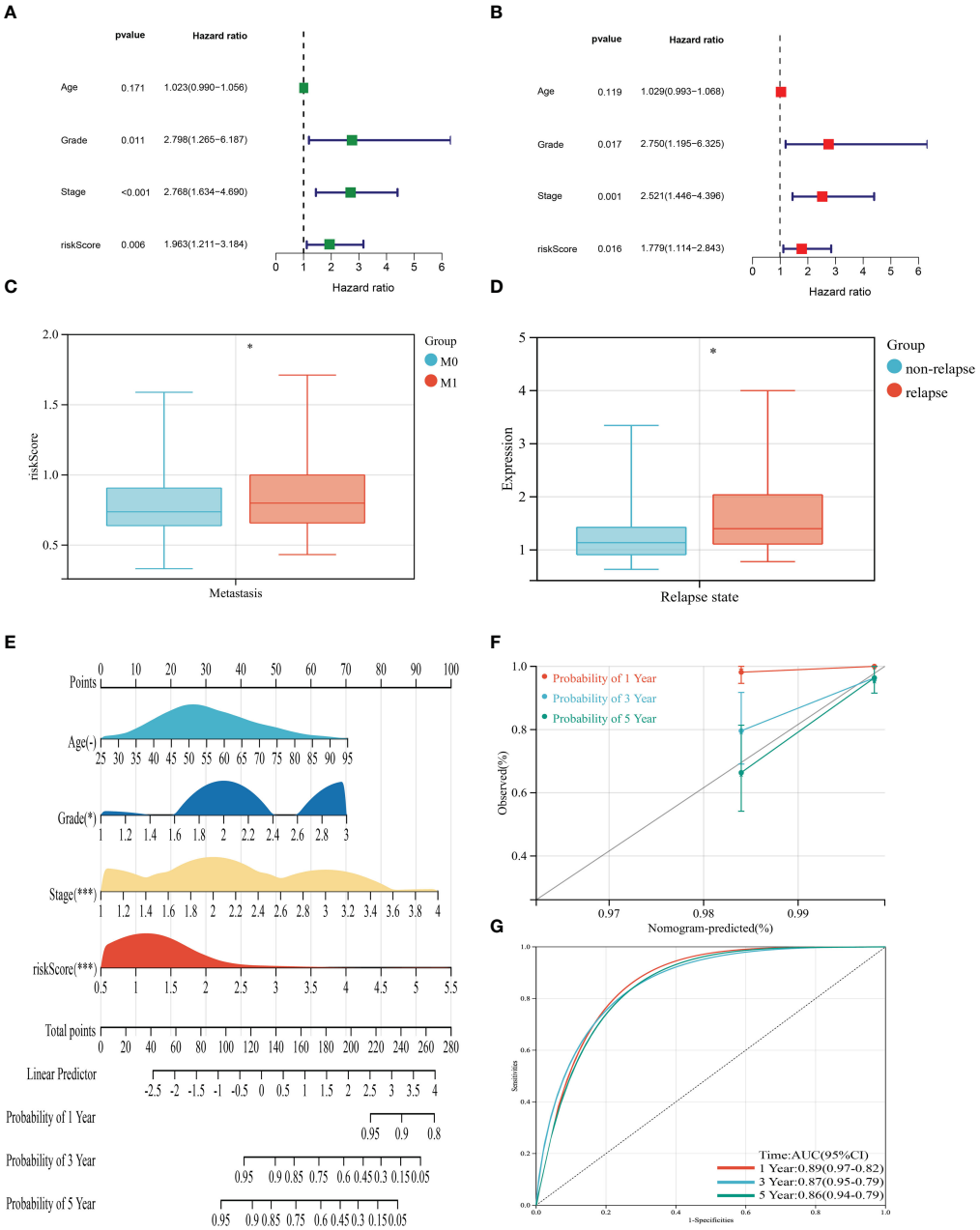

FIGURE 5
Clinical correlation analysis of the risk score and establishment of the prognostic nomogram. **(A, B)** uniCox and multiCox analysis showed the prognostic value of the risk score. **(C)** Correlation between risk score and tumor metastasis of BRCA. **(D)** Correlation between risk score and tumor relapse of BRCA. **(E)** Nomogram for predicting the 1-, 3-, and 5-year OS of BRCA patients in the entire cohort. **(F)** Calibration curve of the prognostic nomogram. **(G)** Receiver operating characteristic curves of the prognostic nomogram for 1-, 3-, and 5-year OS in BRCA. (*P*<0.05 *; *P*<0.01 **; *P*<0.001 ***).

In addition, previous studies have shown that abnormal epigenetic modifications can drive tumorigenesis and resistance to treatment. We extracted DNA methylation profiles of these core genes in BRCA based on the TCGA database and the results showed increased methylation levels in BRCA compared to normal breast tissue (Figure 8C).

Taking into account the chemotherapy used in daily work, we evaluated the response of gene expression subtypes (low or high expression levels) to five chemotherapy agents and one ErbB-2 inhibitor: Docetaxel, Doxorubicin, gemcitabine paclitaxel, and Apatinib. Interestingly, low RAD51AP1, HELLS, PLSCR4, and POLQ may be more sensitive to docetaxel, apatinib, while high RAD51AP1, HELLS, PLSCR4, and POLQ may be more sensitive to doxorubicin, gecitabine, and paclitaxel (Figure 8D).

3.8 Biological function and POLQ expression in BRCA are confirmed

By doing *in vitro* tests, we furthered our understanding of POLQ ‘s role. Firstly, the results of bioinformatics analysis showed that the expression of POLQ in BRCA tissues was higher

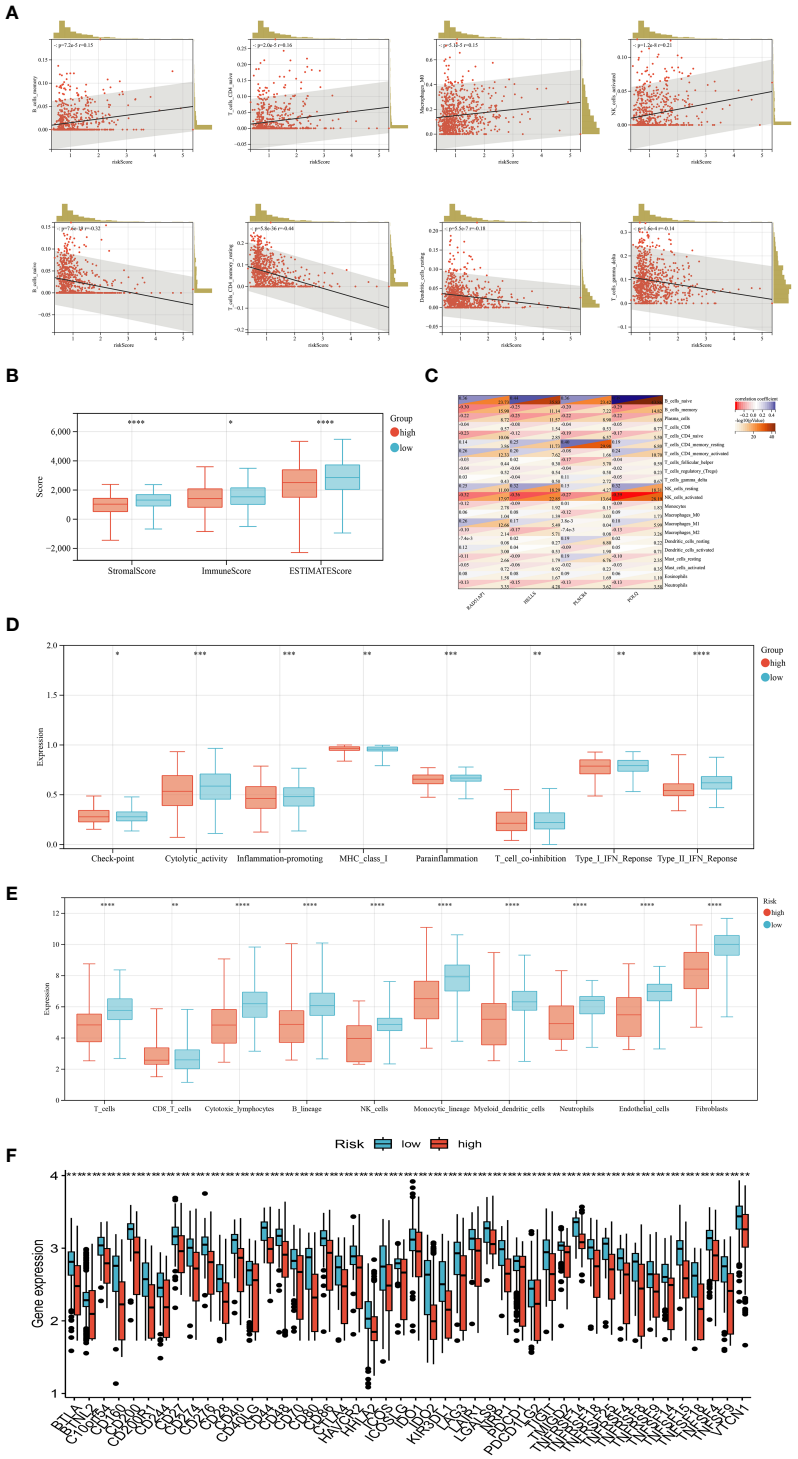

FIGURE 6
Evaluation of tumor microenvironment, checkpoints, and immune functions between the two groups. **(A)** Correlations between risk score and immune cell infiltration levels. **(B)** Correlations between risk score and tumor microenvironment scores. **(C)** Correlations between the abundance of immune cells and genes involved in the development of the prognostic model. **(D)** Assessment of differences in immune function between the two groups. **(E)** Abundance of 8 infiltrating immune cell types and 2 stromal cell types in the two groups. **(F)** Expression of 35 common immune checkpoints in the two groups. (P<0.05 *; P<0.01 **; P<0.001 ***, P<0.0001 ****).

than that in normal tissues (Figure 9A). We verified the results in 20 pairs of clinical tissue samples and obtained consistent results (Figure 9B). To select suitable BRCA cell lines for POLQ knockdown assay, we verified the expression level of POLQ in 5 cell lines, and the results showed that the expression level of HCC1806 and MDA-MB-231 cell lines was relatively high (Figure 9C). Therefore, we selected these two cell lines for POLQ knockdown experiments and verified their transfection efficiency

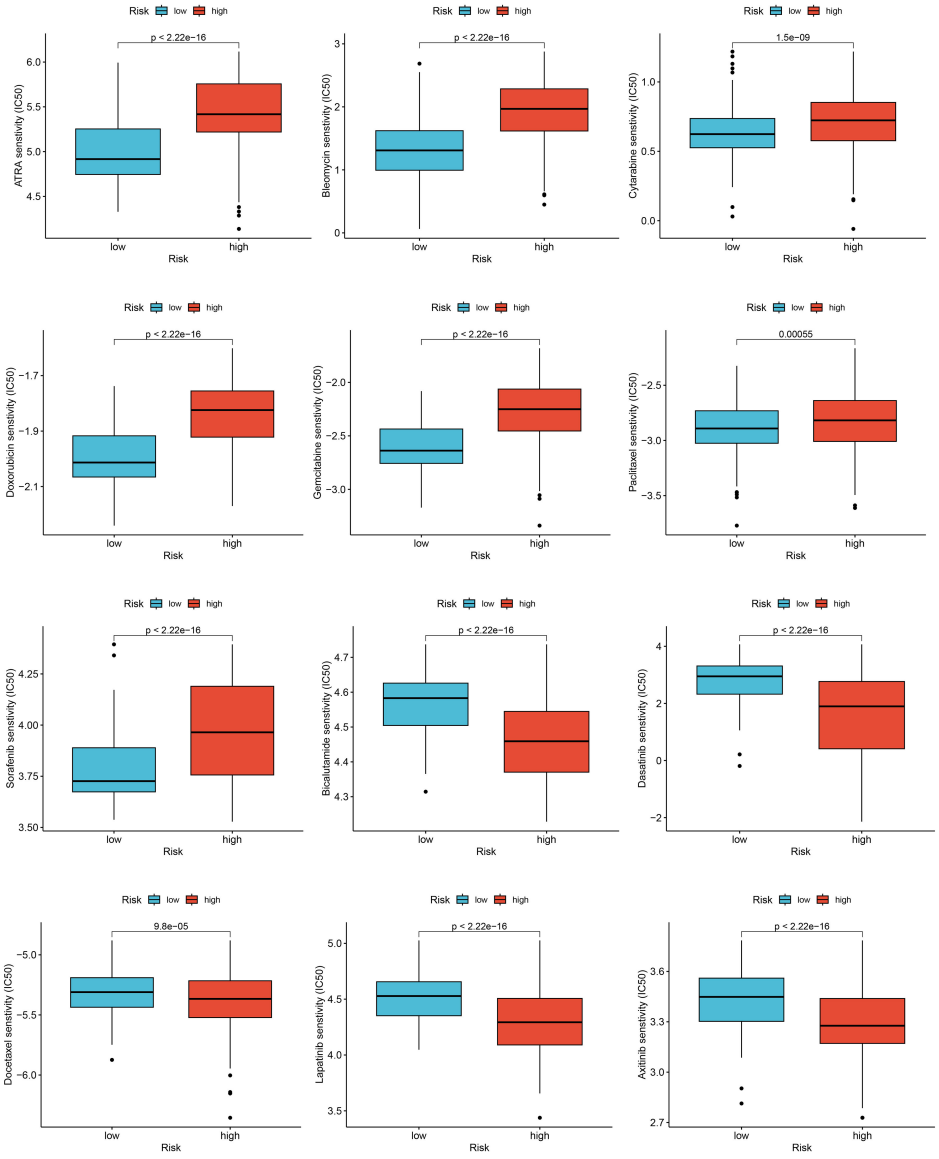

FIGURE 7
Relationships between risk score and drug sensitivity.

(Figure 9D). In CCK-8 studies, we saw that cells with POLQ knockdown displayed significantly decreased proliferative activity (Figures 9E, F). Colony-forming experiments also showed that the proliferation ability of melanoma cells was significantly reduced after POLQ knockdown (Figures 9G, J). Wound healing experiments showed that the migration ability of BRCA cells was significantly reduced after POLQ gene knockdown (Figures 9H, I). After the knockdown of POLQ, two cell lines significantly reduced their ability to heal, migration, and invasion (Figures 9K–M).

4 Discussion

Heterogeneity is one of the important characteristics of BRCA (14). Although most studies believe that BRCA is monoclonal in origin, due to multiple divisions, proliferation, and continuous evolution in the process of occurrence and development, epigenetic, genomic, and microenvironment changes lead to different phenotypes and biological characteristics of cells, resulting in heterogeneity (15). It showed different histological types, differentiation degree, cell proliferation rate, invasion and metastasis ability, and therapeutic responsiveness. Therefore, the accurate implementation of personalized medicine for BRCA requires further research and exploration (16, 17).

In our study, we used the WGCNA method to screen out BRCA-related genes that are specifically expressed in BRCA tissues. Subsequently, four genes were identified by difference analysis, univariate Cox regression, lasso regression, and multifactor Cox regression, and were further used to create a new risk profile. Patients were divided into high-risk and low-risk groups based on a median risk score. The difference in survival rate between the high-risk group and low-risk group was statistically significant, and

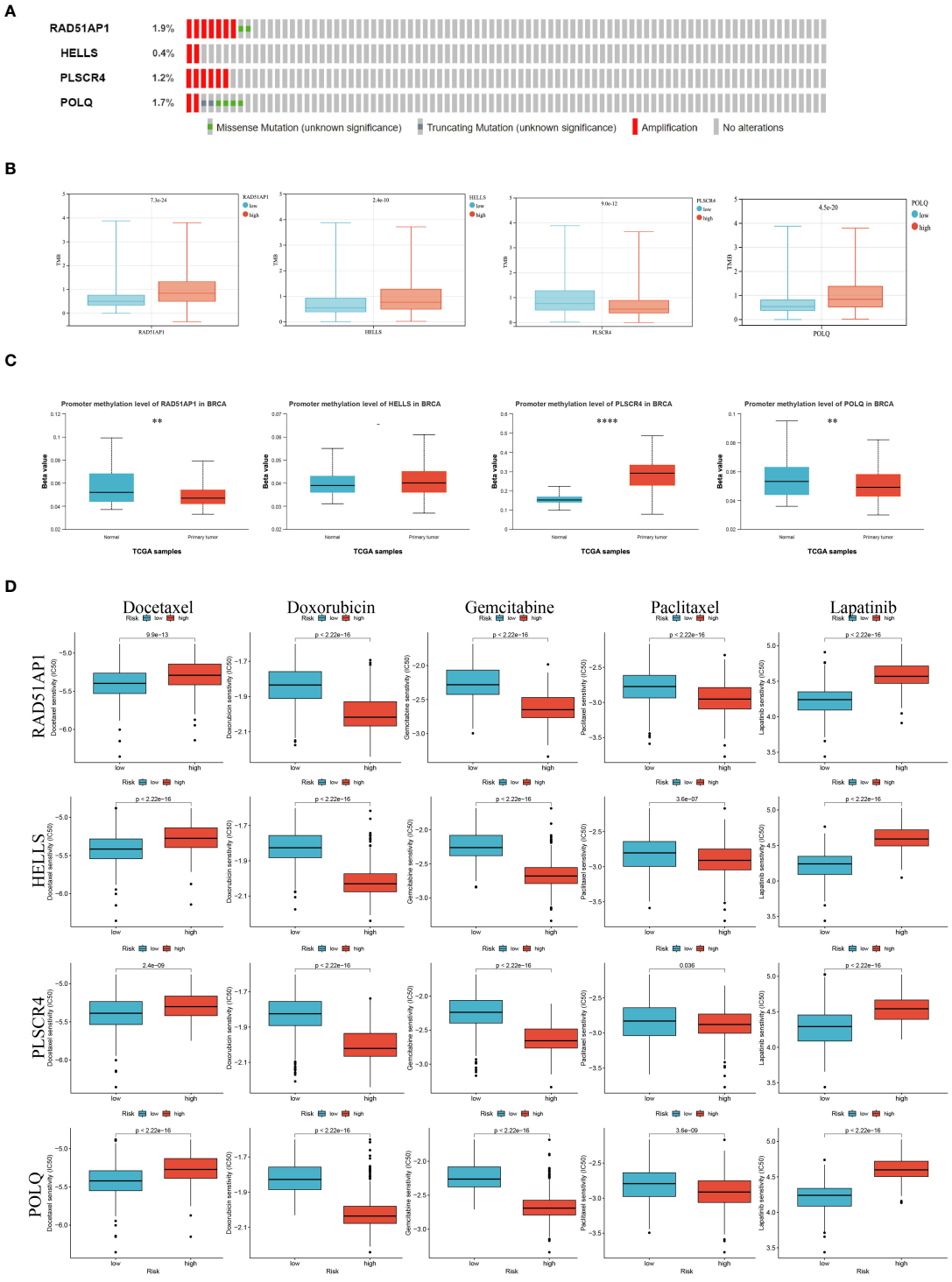

FIGURE 8
Epigenetic modification and genetic alteration of 4 key genes. **(A)**The DNA alteration of 4 key genes. **(B)** Tumor mutation burden of 4 key genes. **(C)** The DNA promoter methylation levels of 4 key genes are based on the Cancer Genome Atlas database. **(D)** The estimated IC50 values of docetaxel, doxorubicin, gemcitabine, paclitaxel, and lapatinib for 4 key genes. (*P*<0.05 *; *P*<0.01 **; *P*<0.001 ***, *P*<0.0001 ****).

the prognosis of the low-risk group was significantly better than that of the high-risk group (P<0.01). Validation analysis of TCGA and GEO databases showed that our prognostic model based on related genes could well distinguish BRCA patients. The forest map showed that risk score was an independent risk factor for predicting prognosis in patients with BRCA compared to tumor grade and tumor stage. We also found that BRCA patients who developed distant metastases or tumor recurrence had higher risk scores. Overall, based on our findings, a higher risk score implies a higher risk of metastasis and a worse prognosis. Compared to

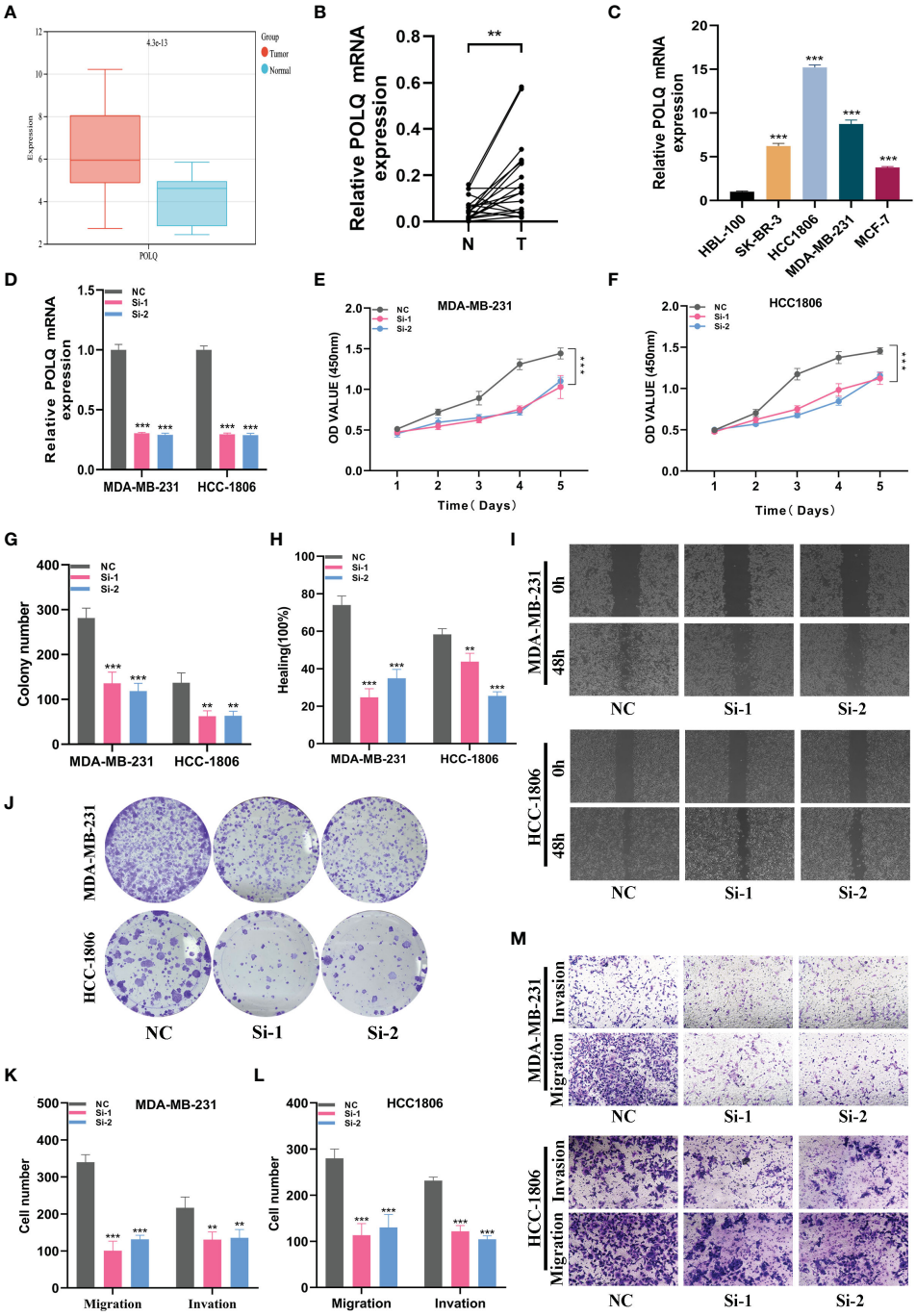

FIGURE 9
In vitro experiment about POLQ. **(A)** POLQ is highly expressed in breast cancer. **(B)** The expression level of POLQ is higher in breast cancer tissues. **(C)** The expression level of POLQ was higher in the MDA-MB-231 or HCC1806 cells. **(D)** Transfection efficiency of POLQ. **(E, F)** CCK-8. After POLQ knockdown, the proliferative ability of MDA-MB-231 or HCC1806 cell lines decreased significantly. **(G, J)** Clone formation. After POLQ knockdown, the proliferative ability of the two cell lines decreased significantly. **(H, I)** Healing test. After POLQ knockdown, the migration ability of MDA-MB-231 or HCC1806 cell lines decreased significantly. **(K–M)** Transwell assay. After POLQ knockdown, the migration and invasion abilities of MDA-MB-231 or HCC1806 cell lines were significantly decreased. (P<0.05*; P<0.01**; P<0.001***, P<0.0001****)

other existing BRCA prognostic models, such as apoptosis-related gene prognostic models (AUC at 1, 3, 5 years = 0.637, 0.701, 0.695), platelet-related prognostic models (AUC at 1, 3, 5 years = 0.639, 0.563, 0.596), and anoikis and immune-related gene prognostic models (AUC at 1, 3, 5 years = 0.521, 0.643, 0.695), our model shows more accurate predictive performance (18–20).

Immunotherapy is a new type of anti-tumor therapy that is completely different from the previous anti-tumor therapy (21). Under normal circumstances, immune cells are the protectors of our body kingdom, and the body's immune system has an immune surveillance function, which can recognize, kill, and timely eliminate abnormal cells in the body (22). As abnormal cells,

tumor cells can be recognized and eliminated by the body's immune system under normal circumstances. Immunotherapy has also been carried out in a series of studies in BRCA, although its effect is not as significant as in lung cancer, melanoma, and other tumors, it has achieved a certain effect in triple-negative BRCA (23, 24), while the results in HR-positive/HER2-negative and HER2-positive BRCA are still immature or the efficacy needs further exploration (25). At present, the immune checkpoint inhibitor used in BRCA clinics is programmed death protein-1 (PD-1) programmed death protein ligand-1 (PD-L1), and other immune checkpoint inhibitors are still being studied and explored (26). The effective rate of immune checkpoint inhibitors is low, and most of them are combined with chemotherapy drugs. The research on the combination with other drugs is still underway (27). What we know is that one of the important reasons for the low efficiency of immune checkpoint inhibitors and their use in combination with chemotherapeutic agents in clinical treatment is that the immunotherapy-sensitive population cannot be accurately screened by the available means, whereas the TMB may drive effective anti-tumor immune responses and ultimately lead to a sustained clinical response to immunotherapy. Our results showed that the expression of genes involved in the model, such as POLQ, was significantly correlated with the TMB data in the BRCA patients, and that this group of patients with high POLQ expression levels was more likely to show better therapeutic effects to immunotherapy, which may provide a certain reference value for the individualized precision treatment of BRCA patients in the clinical practice. However, this needs to be confirmed by more real-world studies. Chimeric antigen receptor T (CAR-T) cell therapy is a personalized immunotherapy approach that has made some progress in BRCA treatment (28). Car-T cell therapy works by introducing a CAR that targets a BRCA-specific antigen into a redesigned T cell in the patient's body, thereby activating and boosting the patient's immune system to attack tumor cells. Vaccine therapy is a method of using specific antigens to stimulate the patient's immune system to produce an anti-tumor immune response. In BRCA immunotherapy, researchers are developing various vaccines, including cancer vaccines, tumor polypeptide vaccines, and genetic vaccines, to activate the patient's immune system to fight BRCA (29). In addition to the strategies mentioned above, there are several other BRCA immunotherapies under investigation. Examples being explored include the combination of immune checkpoint inhibitors, tumor-associated antigen (TAA) specific T cell therapy, and the use of immune promoters (30). While there have been some encouraging advances in BRCA immunotherapy, the effectiveness and safety of these strategies are still being evaluated in research and clinical trials. Therefore, for specific patients, it is still necessary to discuss and make decisions in detail according to individual circumstances.

In our study, we further calculated the correlation between immune cell abundance and risk score. We found that risk scores were positively correlated with memory B cells, primary $CD4^+$ T cells, macrophage M0, and activated NK cells, and negatively correlated with primary B cells, resting $CD4^+$ memory T cells, resting dendritic cells, and gamma-delta T cells. Given the important role of initial $CD4^+$ T cells, macrophage M0, and other immune cells in immunotherapy, our prognostic model has a certain guiding significance for the immunotherapy response of BRCA patients. Our results also found that the genes involved in the model construction were significantly correlated with the infiltration levels of most immune cells. For example, POLQ gene expression levels were significantly positively correlated with naive B cell infiltration and negatively correlated with activated NK cell infiltration. At present, the immune checkpoint inhibitor used in BRCA clinics is programmed death protein-1 (PD-1) programmed death protein ligand-1 (PD-L1), and other immune checkpoint inhibitors are still being studied and explored. We analyzed 35 common immune checkpoints such as PD-1, PD-L1, CTLA-4, and LAG3 between the high and low-risk groups, and found that the expression level of immune checkpoints in the low-risk group was lower. This may indicate a better response to immunotherapy in the high-risk group. However, the efficacy of immune checkpoint inhibitors is low in single-drug treatment, and most of them are combined with chemotherapy drugs, and the study of combination with other drugs is still ongoing. Therefore, clinicians must identify individualized treatment at an early stage, as sensitive drugs vary from person to person. To find chemotherapy drugs that are more sensitive to high-risk populations, we perform drug sensitivity analysis to develop specific drugs for high-risk populations.

DNA repair is indeed crucial for maintaining genomic stability and preventing the development of cancer. The evolving understanding of the DNA damage response pathway has expanded the possibilities for therapeutic approaches in oncology. It is becoming increasingly clear that genomic instability in cells caused by defective DNA damage responses contributes to the development of cancer (31, 32). On the other hand, these defects can also serve as a therapeutic opportunity (33, 34). Targeting various components of the DNA Damage Repair (DDR) pathway, such as PARP, ATM, ATR, CHK1, WEE1, and DNA-PK, has led to the development of DDR-targeted drugs, some of which are currently under clinical study (35, 36). Currently, inhibitors of these DDR components, some of which are under clinical study (37, 38). It's also interesting to note the potential synergy between DDR inhibitors and conventional cancer therapies, as well as their correlation with immune checkpoint inhibitor response, which promotes the exploration of combination therapies. These advancements in DNA repair-targeting drugs are increasingly playing a significant role in the field of tumor therapy (39, 40). Drugs that target DNA repair pathways are showing an increasing role in the field of tumor therapy (33, 39, 41).

POLQ is a large protein composed of helicase (HD) and polymerase domains (PD), and deletion of either leads to synthetic lethality of HR deficiency (42). POLQ is a promising target in cancer therapy, and POLQ inhibitors are being actively developed by the scientific and industrial communities (43). On August 5, 2021, Artios Pharma published the clinical registration of the First-in-class drug ART4215 on the clinical trials website. ART4215 is the world's first highly selective oral small-molecule targeted POLQ inhibitor in the Polθ polymerase domain to enter clinical studies. On August 10, 2022, Artios Pharma announced that it has initiated a Phase II study of ART4215 in combination with the PARP inhibitor talazoparib in BRCA-deficient BRCA. POLQ helicases and POLQ polymerase

inhibitors have been developed, and these POLQ inhibitors (POLQi) have specific effects on killing BRCA-deficient cells (44), but the specific mechanism of action of POLQ is unknown. More clinical trials are needed to confirm the promise of POLQ inhibitors in BRCA patients, especially those at high risk.

The study looked for monitoring and predictors of immunotherapy in BRCA patients, such as immune-related markers or gene expression characteristics. This will help determine which patients are suitable for immunotherapy and provide individualized treatment decisions. By delving deeper into immunotherapy for BRCA, we can reveal the interaction between the immune system and the tumor, develop more accurate and effective treatments, and improve patient outcomes and survival. However, the prognostic model we constructed through bioinformatics requires further external validation on independent datasets to verify its predictive performance and generalization ability. In addition, the application of the prognostic model in clinical practice should fully consider the actual clinical environment, feasibility, and interpretability. At the same time, BRCA is a dynamically changing disease, and biomarkers and clinical characteristics of patients may change over time. Prognostic models need to be able to account for this variation and provide real-time, valid recommendations in treatment decisions.

5 Conclusions

In this study, transcriptomics and proteomics were combined to conduct a comprehensive analysis. These data are integrated to conduct in-depth research, break through the limitations of a single omics study, conduct a joint analysis of different omics data, dig for more meaningful information in the limited data, build the body regulatory network, and deeply understand the regulation and causality between various molecules. The immunological and prognostic significance of POLQ in breast cancer was explored systematically. Notably, we advocate effective prognostic signatures based on POLQ-related genes. Our findings provide a novel and accurate classification and treatment strategy for breast cancer patients.

Data availability statement

The datasets presented in this study can be found in online repositories. The names of the repository/repositories and accession number(s) can be found in the article/Supplementary Material.

Ethics statement

The studies involving humans were approved by Ethics Committee of Nanjing Medical University. The studies were conducted in accordance with the local legislation and institutional requirements. The participants provided their written informed consent to participate in this study.

Author contributions

WC: Conceptualization, Writing – original draft, Writing – review & editing. YK: Data curation, Writing – original draft, Writing – review & editing. WS: Formal analysis, Writing – original draft, Writing – review & editing. QH: Methodology, Writing – original draft, Writing – review & editing. JC: Software, Writing – original draft, Writing – review & editing. SP: Data curation, Methodology, Writing – original draft, Writing – review & editing. YM: Methodology, Software, Writing – original draft, Writing – review & editing.

Funding

The author(s) declare financial support was received for the research, authorship, and/or publication of this article. This research was funded by the 2021 Suzhou Science and Technology Bureau 550 (Medical and Health Technology Innovation) project (Grant No. SKJY2021126); the 551 2021 Project of Beijing Sisko Clinical Oncology Research Foundation (Grant No. Y552 Young2021-0087); and the 2023 Suzhou Science and Technology Bureau (Medical 553 Innovation Applied Research) project (Grant No. SKYD2023140).

Acknowledgments

We are very grateful for the data provided by databases such as TCGA, and GEO. Thanks to the reviewers and editors for their sincere comments.

Conflict of interest

The authors declare that the research was conducted in the absence of any commercial or financial relationships that could be construed as a potential conflict of interest.

Publisher's note

Supplementary material

The Supplementary Material for this article can be found online at: https://www.frontiersin.org/articles/10.3389/fimmu.2024.1331841/full#supplementary-material

References

1. Siegel RL, Miller KD, Fuchs HE, Jemal A. Cancer statistics, 2022. *CA Cancer J Clin* (2022) 72(1):7–33. doi: 10.3322/caac.21708

2. Cardoso F, Kyriakides S, Ohno S, Penault-Llorca F, Poortmans P, Rubio IT, et al. Early breast cancer: esmo clinical practice guidelines for diagnosis, treatment and follow-up†. *Ann Oncol* (2019) 30(8):1194–220. doi: 10.1093/annonc/mdz173

3. van de Vijver MJ, He YD, van't Veer LJ, Dai H, Hart AA, Voskuil DW, et al. A gene-expression signature as a predictor of survival in breast cancer. *New Engl J Med* (2002) 347(25):1999–2009. doi: 10.1056/NEJMoa021967

4. Shimizu H, Nakayama KI. A 23 gene-based molecular prognostic score precisely predicts overall survival of breast cancer patients. *EBioMedicine* (2019) 46:150–9. doi: 10.1016/j.ebiom.2019.07.046

5. Chen HY, Yu SL, Chen CH, Chang GC, Chen CY, Yuan A, et al. A five-gene signature and clinical outcome in non-small-cell lung cancer. *New Engl J Med* (2007) 356(1):11–20. doi: 10.1056/NEJMoa060096

6. Liu T, Fang P, Han C, Ma Z, Xu W, Xia W, et al. Four transcription profile-based models identify novel prognostic signatures in oesophageal cancer. *J Cell Mol Med* (2020) 24(1):711–21. doi: 10.1111/jcmm.14779

7. Steck SE, Murphy EA. Dietary patterns and cancer risk. *Nat Rev Cancer* (2020) 20 (2):125–38. doi: 10.1038/s41568-019-0227-4

8. Zhang Y, Zhang Z. The history and advances in cancer immunotherapy: understanding the characteristics of tumor-infiltrating immune cells and their therapeutic implications. *Cell Mol Immunol* (2020) 17(8):807–21. doi: 10.1038/s41423-020-0488-6

9. Adams S, Gatti-Mays ME, Kalinsky K, Korde LA, Sharon E, Amiri-Kordestani L, et al. Current landscape of immunotherapy in breast cancer: A review. *JAMA Oncol* (2019) 5(8):1205–14. doi: 10.1001/jamaoncol.2018.7147

10. Esteva FJ, Hubbard-Lucey VM, Tang J, Pusztai L. Immunotherapy and targeted therapy combinations in metastatic breast cancer. *Lancet Oncol* (2019) 20(3):e175–e86. doi: 10.1016/s1470-2045(19)30026-9

11. Loibl S, Poortmans P, Morrow M, Denkert C, Curigliano G. Breast cancer. *Lancet* (2021) 397(10286):1750–69. doi: 10.1016/s0140-6736(20)32381-3

12. Polk A, Svane IM, Andersson M, Nielsen D. Checkpoint inhibitors in breast cancer - current status. *Cancer Treat Rev* (2018) 63:122–34. doi: 10.1016/j.ctrv.2017.12.008

13. Henriques B, Mendes F, Martins D. Immunotherapy in breast cancer: when, how, and what challenges? *Biomedicines* (2021) 9(11):1687. doi: 10.3390/biomedicines9111687

14. Yeo SK, Guan JL. Breast cancer: multiple subtypes within a tumor? *Trends Cancer* (2017) 3(11):753–60. doi: 10.1016/j.trecan.2017.09.001

15. Liang Y, Zhang H, Song X, Yang Q. Metastatic heterogeneity of breast cancer: molecular mechanism and potential therapeutic targets. *Semin Cancer Biol* (2020) 60:14–27. doi: 10.1016/j.semcancer.2019.08.012

16. Choi Y, Kim EJ, Seol H, Lee HE, Jang MJ, Kim SM, et al. The hormone receptor, human epidermal growth factor receptor 2, and molecular subtype status of individual tumor foci in multifocal/multicentric invasive ductal carcinoma of breast. *Hum Pathol* (2012) 43(1):48–55. doi: 10.1016/j.humpath.2010.08.026

17. McDonald ES, Clark AS, Tchou J, Zhang P, Freedman GM. Clinical diagnosis and management of breast cancer. *J Nucl Med* (2016) 57 Suppl 1:9s–16s. doi: 10.2967/jnumed.115.157834

18. Lu X, Yuan Q, Zhang C, Wang S, Wei W. Predicting the immune microenvironment and prognosis with a anoikis - related signature in breast cancer. *Front Oncol* (2023) 13:1149193. doi: 10.3389/fonc.2023.1149193

19. Xie J, Zou Y, Ye F, Zhao W, Xie X, Ou X, et al. A novel platelet-related gene signature for predicting the prognosis of triple-negative breast cancer. *Front Cell Dev Biol* (2021) 9:795600. doi: 10.3389/fcell.2021.795600

20. Gao Y, Huang Q, Qin Y, Bao X, Pan Y, Mo J, et al. A prognostic model related to necrotizing apoptosis of breast cancer based on biorthogonal constrained depth semi-supervised nonnegative matrix decomposition and single-cell sequencing analysis. *Am J Cancer Res* (2023) 13(9):3875–97.

21. Barzaman K, Moradi-Kalbolandi S, Hosseinzadeh A, Kazemi MH, Khorramdelazad H, Safari E, et al. Breast cancer immunotherapy: current and novel approaches. *Int Immunopharmacol* (2021) 98:107886. doi: 10.1016/j.intimp.2021.107886

22. Bates JP, Derakhshandeh R, Jones L, Webb TJ. Mechanisms of immune evasion in breast cancer. *BMC Cancer* (2018) 18(1):556. doi: 10.1186/s12885-018-4441-3

23. Keenan TE, Tolaney SM. Role of immunotherapy in triple-negative breast cancer. *J Natl Compr Canc Netw* (2020) 18(4):479–89. doi: 10.6004/jnccn.2020.7554

24. Zhu Y, Zhu X, Tang C, Guan X, Zhang W. Progress and challenges of immunotherapy in triple-negative breast cancer. *Biochim Biophys Acta Rev Cancer* (2021) 1876(2):188593. doi: 10.1016/j.bbcan.2021.188593

25. Keshavarz S, Wall JR, Keshavarz S, Vojoudi E, Jafari-Shakib R. Breast cancer immunotherapy: A comprehensive review. *Clin Exp Med* (2023) 23(8):4431–47. doi: 10.1007/s10238-023-01177-z

26. Vranic S, Cyprian FS, Gatalica Z, Palazzo J. Pd-L1 status in breast cancer: current view and perspectives. *Semin Cancer Biol* (2021) 72:146–54. doi: 10.1016/j.semcancer.2019.12.003

27. Naimi A, Mohammed RN, Raji A, Chupradit S, Yumashev AV, Suksatan W, et al. Tumor immunotherapies by immune checkpoint inhibitors (Icis); the pros and cons. *Cell Commun Signal* (2022) 20(1):44. doi: 10.1186/s12964-022-00854-y

28. Jardim DL, Goodman A, de Melo Gagliato D, Kurzrock R. The challenges of tumor mutational burden as an immunotherapy biomarker. *Cancer Cell* (2021) 39 (2):154–73. doi: 10.1016/j.ccell.2020.10.001

29. Ye F, Dewanjee S, Li Y, Jha NK, Chen ZS, Kumar A, et al. Advancements in clinical aspects of targeted therapy and immunotherapy in breast cancer. *Mol Cancer* (2023) 22(1):105. doi: 10.1186/s12943-023-01805-y

30. Fan C, Zhang S, Gong Z, Li X, Xiang B, Deng H, et al. Emerging role of metabolic reprogramming in tumor immune evasion and immunotherapy. *Sci China Life Sci* (2021) 64(4):534–47. doi: 10.1007/s11427-019-1735-4

31. Huang RX, Zhou PK. DNA damage response signaling pathways and targets for radiotherapy sensitization in cancer. *Signal Transduct Target Ther* (2020) 5(1):60. doi: 10.1038/s41392-020-0150-x

32. Parekh VJ, Wien F, Grange W, De Long TA, Arluison V, Sinden RR. Crucial role of the C-terminal domain of hfq protein in genomic instability. *Microorganisms* (2020) 8(10):1598. doi: 10.3390/microorganisms8101598

33. Cleary JM, Aguirre AJ, Shapiro GI, D'Andrea AD. Biomarker-guided development of DNA repair inhibitors. *Mol Cell* (2020) 78(6):1070–85. doi: 10.1016/j.molcel.2020.04.035

34. Huang R, Zhou PK. DNA damage repair: historical perspectives, mechanistic pathways and clinical translation for targeted cancer therapy. *Signal Transduct Target Ther* (2021) 6(1):254. doi: 10.1038/s41392-021-00648-7

35. Cheng B, Pan W, Xing Y, Xiao Y, Chen J, Xu Z. Recent advances in ddr (DNA damage response) inhibitors for cancer therapy. *Eur J Med Chem* (2022) 230:114109. doi: 10.1016/j.ejmech.2022.114109

36. Groelly FJ, Fawkes M, Dagg RA, Blackford AN, Tarsounas M. Targeting DNA damage response pathways in cancer. *Nat Rev Cancer* (2023) 23(2):78–94. doi: 10.1038/s41568-022-00535-5

37. Hanna D, Chopra N, Hochhauser D, Khan K. The role of parp inhibitors in gastrointestinal cancers. *Crit Rev Oncol Hematol* (2022) 171:103621. doi: 10.1016/j.critrevonc.2022.103621

38. Raimundo L, Calheiros J, Saraiva L. Exploiting DNA damage repair in precision cancer therapy: brca1 as a prime therapeutic target. *Cancers (Basel)* (2021) 13(14):3438. doi: 10.3390/cancers13143438

39. Sheng H, Huang Y, Xiao Y, Zhu Z, Shen M, Zhou P, et al. Atr inhibitor azd6738 enhances the antitumor activity of radiotherapy and immune checkpoint inhibitors by potentiating the tumor immune microenvironment in hepatocellular carcinoma. *J Immunother Cancer* (2020) 8(1):e000340. doi: 10.1136/jitc-2019-000340

40. Shi C, Qin K, Lin A, Jiang A, Cheng Q, Liu Z, et al. The role of DNA damage repair (Ddr) system in response to immune checkpoint inhibitor (Ici) therapy. *J Exp Clin Cancer Res* (2022) 41(1):268. doi: 10.1186/s13046-022-02469-0

41. Patterson-Fortin J, Bose A, Tsai WC, Grochala C, Nguyen H, Zhou J, et al. Targeting DNA repair with combined inhibition of nhej and mmej induces synthetic lethality in tp53-mutant cancers. *Cancer Res* (2022) 82(20):3815–29. doi: 10.1158/0008-5472.Can-22-1124

42. Wood RD, Doublié S. DNA polymerase Θ (Polq), double-strand break repair, and cancer. *DNA Repair (Amst)* (2016) 44:22–32. doi: 10.1016/j.dnarep.2016.05.003

43. Patterson-Fortin J, Jadhav H, Pantelidou C, Phan T, Grochala C, Mehta AK, et al. Polymerase Θ Inhibition activates the cgas-sting pathway and cooperates with immune checkpoint blockade in models of brca-deficient cancer. *Nat Commun* (2023) 14(1):1390. doi: 10.1038/s41467-023-37096-6

44. Baxter JS, Zatreanu D, Pettitt SJ, Lord CJ. Resistance to DNA repair inhibitors in cancer. *Mol Oncol* (2022) 16(21):3811–27. doi: 10.1002/1878-0261.13224

frontiers | Frontiers in Immunology

TYPE Original Research
PUBLISHED 08 February 2024
DOI 10.3389/fimmu.2024.1302797

OPEN ACCESS

EDITED BY
Chao Liu,
Shandong Cancer Hospital, China

REVIEWED BY
Xiaohui Li,
Shandong Cancer Hospital, China
Qingyu Huang,
Shandong First Medical University and Shandong Academy of Medical Sciences, China

*CORRESPONDENCE
Jie Chen
cj2365255@126.com

RECEIVED 27 September 2023
ACCEPTED 22 January 2024
PUBLISHED 08 February 2024

CITATION
Zhou L-Z, Xiao H-Q and Chen J (2024) Mismatch repair gene *MSH6* correlates with the prognosis, immune status and immune checkpoint inhibitors response of endometrial cancer.
Front. Immunol. 15:1302797.
doi: 10.3389/fimmu.2024.1302797

Mismatch repair gene *MSH6* correlates with the prognosis, immune status and immune checkpoint inhibitors response of endometrial cancer

Lin-Zhi Zhou[1], Hong-Qi Xiao[2] and Jie Chen[1]*

[1]Department of Gynecological Oncology, Harbin Medical University Cancer Hospital, Harbin, China, [2]Department of General Surgery, The Second Affiliated Hospital of Harbin Medical University, Harbin, China

Objective: Many patients treated with immune checkpoint inhibitors (ICIs) developed primary or secondary drug resistance for unknown reasons. This study investigates whether mismatch repair (MMR) genes are responsible for this therapeutic restriction.

Methods: We obtained the transcriptional, clinical and single nucleotide polymorphism data for endometrial cancer (EC) from The Cancer Genome Atlas and the immunophenoscore data of EC from The Cancer Immunome Atlas, then analyzed in R to evaluate the relationship between MMR genes and clinicopathological features, prognosis, immune infiltration, immune checkpoint expression and responsiveness to ICIs in EC. We used differentially expressed genes in the *MSH6* high and low expression groups to conduct GO and KEGG analyses to explore the impact of *MSH6* on the biological functions of EC. Finally, we verified the bioinformatics results with *in vitro* experiments.

Results: Our analyses showed that compared with the high *MSH6* expression group, the low *MSH6* expression group had better survival outcomes and less aggressive clinicopathological features. In the multivariate Cox analysis, *MSH6* was the only independent risk factor that could predict the prognosis of EC. Besides, the low *MSH6* expression group also had a higher immune score, more active immune infiltration and higher immune checkpoint expression, resulting in better responsiveness to ICIs treatment, consistent with the enrichment of GO terms and KEGG pathways related to immune response in this group. Meanwhile, the GO and KEGG enrichment results of the *MSH6* high expression group were associated with cell cycle, DNA damage repair and tumorigenesis. To exclude the influence of *MSH6* mutations, we performed the previous analyses on the *MSH6* wild-type tumor samples and obtained consistent results. *In vitro* experiments also confirmed that after knocking down *MSH6* in endometrial cancer cells, their proliferation, migration and invasion abilities were weakened, while the expression levels of PD-L1 and PD-L2 were elevated. In comparison, overexpression of *MSH6* showed an opposite trend.

Conclusion: Reduced *MSH6* expression could serve as a potential biomarker for predicting better prognosis, active immune status, higher immune checkpoint expression level and better responsiveness to ICIs treatment in EC. *MSH6* may become a potential target for treating solid tumors.

KEYWORDS

endometrial cancer, mismatch repair, immune infiltration, immune checkpoint, immune checkpoint inhibiter, prognosis, MSH6

1 Introduction

In recent years, due to the extension of life expectancy and the increase in the obesity rate, the morbidity and mortality of endometrial cancer (EC) have continued to rise and show a younger trend (1, 2). EC is typically categorized into type I and type II according to clinical, endocrine and epidemiological features, or into endometrioid, serous and clear cell carcinoma based on histopathological characteristics (3). Many cases have demonstrated that both categorization schemes can accurately identify the nature and prognosis of most tumors. However, in some cases, the tumor morphology is vague, and the characteristics overlap, making it challenging to categorize accurately, resulting in overtreatment or insufficient treatment. In 2013, the American Cancer Genome Atlas (TCGA) divided ECs into four molecular subtypes based on multi-omics features and gradually optimized them: *POLE* ultra-mutated, microsatellite instability-high (MSI-H)/mismatch repair deficient (dMMR), *p53* abnormal and no specific molecular profile (4, 5). This classification is significant in predicting patients' prognosis and recurrence risk and can provide individualized diagnosis and treatment strategies.

Among the four molecular subtypes, the MSI-H/dMMR subtype accounts for approximately 30% of all primary ECs and 13% to 30% of all recurrent ECs (6), which is caused by mutations (germline pathogenic variants or double somatic pathogenic variants) or epigenetic changes in four MMR genes (*MLH1*, *MSH2*, *MSH6*, *PMS2*) (7, 8). This subtype is characterized by high tumor mutational burden (TMB), increased tumor-infiltrating lymphocytes and upregulated expression of immune checkpoints, making it an ideal target for immune checkpoint inhibitors (ICIs) (6, 9, 10). In May 2017, based on the findings of many clinical trials (11–13), the US Food and Drug Administration (FDA) accelerated the approval of pembrolizumab for the treatment of refractory adult and pediatric MSI-H/dMMR solid tumors, including EC (14). In 2021, this classification system was formally incorporated into the NCCN guidelines for uterine neoplasms, with precise detection and treatment protocols developed (15). By blocking programmed cell death 1 ligand (PD-L1) on tumor cells and programmed cell death receptor 1 (PD-1) or cytotoxic T lymphocyte antigen-4 (CTLA-4) on T cells, ICIs can inhibit their immunosuppressive interactions, reactivate the exhausted immune cells in the tumor microenvironment (TME), and restore the antitumor effect of effector T cells (16, 17).

ICIs have revolutionized cancer treatment, but the response of patients with MSI-H/dMMR tumors (different origins or the same origin) varies greatly. Some patients may be susceptible to ICIs and have responsiveness durably, while nearly half of the patients fail to benefit from them for unknown reasons (18). We want to explore whether different MMR gene defects are to blame for this treatment restriction from the perspective of the MMR gene itself and whether we could develop drugs that specifically target these different MMR genes to improve patients' responsiveness to ICIs in the future. Besides, effective biomarkers are required to guide patient selection. In addition to MSI-H/dMMR, other commonly used markers for predicting reactivity include PD-L1, tumor-infiltrating lymphocytes and TMB, but these markers are not entirely reliable (19, 20). To address these issues, we investigated the connections between MMR genes and clinicopathological characteristics, prognosis, immune infiltration, immune checkpoint expression and response to ICIs in EC at the gene level by bioinformatics analysis, and the results were then confirmed by *in vitro* experiments.

2 Materials and methods

2.1 Bioinformatics analysis

2.1.1 Data acquisition and processing

We obtained EC's transcriptional and clinical data from TCGA (https://portal.gdc.cancer.gov/) and the survival information on pan-cancer from the UCSC XENA database (https://xenabrowser.net/datapages/) (21). Perl scripts (https://www.perl.com/) were used to merge and preprocess the raw data to extract the gene expression matrix and clinical information. A total of 35 normal samples and 552 tumor samples were collected.

2.1.2 Survival analysis

The survival information of TCGA-UCEC was screened, including survival status, overall survival (OS), progression-free survival (PFS), disease-specific survival (DSS) and disease-free

survival (DFS). Then, they were merged with the MMR gene expression data in tumor samples and divided into high and low expression groups according to the medium FPKM value of MMR gene. "survival" (https://cran.r-project.org/web/packages/survival/index.html) and "survminer" packages (https://cran.r-project.org/web/packages/survminer/index.html) were invoked in R Version 4.1.3 (https://www.r-project.org/) to analyze the survival difference between the high and low expression groups, "timeROC" package (https://cran.r-project.org/web/packages/timeROC/index.html) was used to assess the predictive accuracy of MMR genes (22).

2.1.3 The correlation of MMR gene with clinicopathological features and prognosis

We used the "limma" package (https://bioconductor.org/packages/release/bioc/html/limma.html) in R to analyze whether there were differences in clinicopathological characters between the high and low expression groups of MMR genes. The "ggpubr" package (https://cran.r-project.org/web/packages/ggpubr/index.html) was used to analyze whether there were differences in MMR gene expression among different clinicopathological features. The "survival" package was used for univariate and multivariate Cox regression analyses to determine the independent predictors related to prognosis.

2.1.4 The correlation of MMR gene with tumor immune microenvironment and immune checkpoint inhibitor response

The "ESTIMATE" algorithm was performed to calculate the immune, stromal and ESTIMATE scores for each tumor sample (23). The Wilcoxon test was used to analyze whether there were significant differences in the three scores between the MMR gene high and low expression groups (23). The "CIBERSORT" package (https://cibersortx.stanford.edu/) was called in R to analyze whether there were differences in immune cell infiltration levels between the two groups (23). Spearman's correlation test was used to analyze the correlation of the MMR gene with immune cell infiltration and immune checkpoint related gene expression (23).

The immunophenoscore (IPS) data of EC patients was downloaded from the Cancer Immunome Atlas (TCIA) (https://tcia.at/home). Then, it was merged with the MMR gene expression data in tumor samples to compare whether there were differences in multiple IPS scores between high and low MMR gene expression groups (24).

2.1.5 Repeat analysis in *MSH6* wild-type tumor samples after excluding those with *MSH6* mutations

We downloaded the single nucleotide polymorphism data of UCEC from TCGA and obtained 432 *MSH6* wild-type tumor samples and 75 *MSH6* mutant tumor samples. R was used to screen the expression data of *MSH6* and immune checkpoint related genes, survival information, immune, stromal and ESTIMATE scores, 22 types of immune cell infiltration data and IPS data of all *MSH6* wild-type tumor samples. We also divided the *MSH6* wild-type tumor samples into high and low *MSH6* expression groups according to the median FPKM value of *MSH6* and analyzed whether there were differences in survival, immune score, immune infiltration, immune checkpoint expression and ICIs treatment responsiveness between the two groups using the same methods as before.

2.1.6 Functional enrichment analyses

We used the "limma" package in R to obtain the differentially expressed genes (DEGs) between the high and low expression groups of *MSH6*, with $|\log_2$ fold change (FC)$|>1$ and adjusted $p<0.05$ as filtering conditions. The "clusterProfiler" package (https://bioconductor.org/packages/release/bioc/html/clusterProfiler.html) was used in R to conduct Gene Ontology (GO) and Kyoto Encyclopaedia Genes and Genomes (KEGG) analyses on the DEGs that were upregulated in *MSH6* high and low expression groups. Results with a false positive rate (FDR) q value<0.05 were deemed significant and were subsequently visualized using the "ggplot2" (https://cran.r-project.org/web/packages/ggplot2/index.html) and "enrichplot" (https://bioconductor.org/packages/release/bioc/html/enrichplot.html) packages.

2.2 *In vitro* assay

2.2.1 Cell culture and transfection

Endometrial cancer cells Ishikawa and HEC-1B and 293T cells were purchased from Shanghai Fuheng Biotechnology Co., Ltd. All cells were cultured in Dulbecco's modified Eagle's medium (DMEM) containing 10% fetal bovine serum (FBS) and 1% penicillin/streptomycin at 37 °C with 5% CO2. We named the lentiviral vector that can downregulate the expression of *MSH6* and its control vector as shMSH6 and shNC, respectively, and the vector that can upregulate the expression of *MSH6* and the empty vector as OE-MSH6 and Vector, respectively, all of which were purchased from Wuhan Weizhen Biological Company (China). The vector plasmid (10 μg), the helper plasmid psPAX2 (5 μg) and the helper plasmid pMD2G (5 μg) were transfected into 293T cells with Neofect® DNA transfection reagent (Beijing Neofect Biotech Co., Ltd.) at a ratio of 2:1:1. We collected the supernatant containing virus particles 48 hours after transfection and used it to infect Ishikawa and HEC-1B cells after centrifugation and filtration. Target cells were screened with a complete medium containing 2 μg/mL puromycin for 7-14 days after infection with viral particles for 48 hours to obtain stably transfected cell lines. The transfection results were verified by western blotting (WB) and reverse transcription-quantitative polymerase chain reaction (RT-qPCR) analysis. The sequence of shMSH6 was CCG GTT CTG ACA AAG GTG GTA AAT TCT CGA GAA TTT ACC ACC TTT GTC AGA ATT TTT G; The sequence of shNC was TTC TCC GAA CGT GTC ACG TTT CAA GAG AAC GTG ACA CGT TCG GAG AAT TTT TT; The sequence of OE-MSH6 was referred to NM_000179.

2.2.2 Western blotting

Cells were lysed with RIPA buffer containing protease inhibitors, and protein concentration was then detected using the

BCA Protein Assay Kit (Beyotime, China). According to the manufacturer's recommendations, 50 μg protein samples per well were separated by 10% sodium dodecyl sulfate-polyacrylamide gel electrophoresis (SDS-PAGE, Beyotime, China) and transferred the protein on the gel to the PVDF membrane, blocked the membrane with 2.5% skimmed milk for 1 hour at room temperature, and then incubated with the primary antibody against GAPDH, MSH6, PD-L1 and PD-L2 at 4°C overnight, finally incubated with the corresponding second antibody. After washing with PBST 3 times, the bands were visualized with an ECL detection reagent (meilunbio®, China). Quantitative analysis of protein expression was performed using ImageJ.

2.2.3 RT-qPCR

According to the manufacturer's recommendation, total RNA was extracted from cells using the TRIzol regent. Using a PrimeScript™ RT reagent Kit with gDNA Eraser (Perfect Real Time) (TAKARA, RR047Q, Japan) to reverse transcribed 1 μg RNA into cDNA, followed by quantitative real-time PCR using a TB Green® Premix Ex Taq™ II (Tli RNaseH Plus) (TAKARA, RR820A, Japan). The primers used in the experiment were synthesized by Beijing Ruibo Xingke Biotechnology Co., Ltd. in China, including GAPDH forward 5'-GGTGTGAACCATGAGAAGTATGA-3'and reverse 5'-GAGTCCTTCCACGATACCAAAG-3'; MSH6 forward 5'-GGCTCGAAAGACTGGACTTATT-3'and reverse 5'-CCAGGAGGCTCTGTTCATTT-3'; CD274 forward 5'-GCTGAATTGGTCATCCCAGAA-3'and reverse 5'-CAGTGCTACACCAAGGCATAA-3'; PDCD1LG2 forward 5'-CATGTGAACCTTGGAGCAATAAC-3'and reverse 5'-CCTCACTTGGACTTGAGGTATG-3'.

2.2.4 Cell proliferation and clone formation assay

After constructing endometrial cancer cell lines with stable knockdown and overexpression of *MSH6*, changes in cell proliferation activity were detected by cell proliferation and clone formation assay.

In the cell proliferation assay, the cells were seeded into 96-well plates at a ratio of 2,000 cells per well. Subsequently, 10 μl of CCK-8 reagent (Beyotime, China) was added to each well at 24 hours, 48 hours, 72 hours, 96 hours and 120 hours, respectively, according to the recommendations of the reagent manufacturer. The absorbance at 450 nm was measured with a microplate reader after incubation at 37°C for 2 hours.

In the clone formation assay, 2,000, 1,000 and 500 cells were seeded into 6-well plates for culture, and fresh complete medium was regularly replaced for 7-14 days until visible colonies were observed. The cell colonies were fixed with methanol for 30 minutes, stained with 2.5% crystal violet (Solebol, China) for 30 minutes, washed, dried, photographed and counted the colonies formed. Cloning efficiency (%) = (number of colonies formed/number of cells inoculated) × 100%.

2.2.5 Wound healing assay and transwell

The cells were spread into the 6-well plate one day in advance to ensure the density was above 90% the next day. The wound was made with a 200 μl yellow pipette tip perpendicular to the bottom of the plate. After the medium was discarded, the wound was cleaned twice with PBS to fully wash the cells in the scratch gap, and 2ml serum-free medium was added to each well. The inverted microscope was used to take photos at 0 hours and 48 hours after wound formation; the scratch area was measured at different time points with Image J (A0, A48), and the cell migration rate was calculated as follows: (A0-A48)/A0 x 100%.

The chamber (24-well, 8um pore size) and Matrigel used for the Transwell assay were purchased from Corning (United States). According to the manufacturer's recommendation, 600 μL DMEM containing 20% FBS was added to the lower chamber, and 200 μL cell suspension with a density of 4X10^5 cells/mL was added to the upper chamber. After incubation for 36 hours, the upper chamber was taken out, the cells that migrated to the lower chamber were fixed with methanol for 30 minutes, stained with 2.5% crystal violet for 30 minutes, cleaned with deionized water and dried. Five fields were randomly photographed under an inverted microscope with a magnification of 100X for counting, and the average value was taken as the number of cells that passed through. In the invasion assay, the Matrigel was thawed at 4°C overnight in advance. When using, diluted the Matrigel 8 times with DMEM and added 50 μl to the upper chamber; the entire process was performed on ice. The chamber coated with Matrigel can be used as before mentioned after incubation at 37°C and 5% CO2 for 3 hours.

2.3 Statistical analysis

Statistics for all bioinformatic analyses were performed in R Version 4.1.3. The Wilcoxon test was used when comparing two groups, and the Kruskal-Wallis test was used when comparing three or more groups. Correlation analyses between two variables were performed using the Spearman test. In the *in vitro* assay, all experiments were repeated three times, and Student's *t*-test was performed using GraphPad Prism 9.0.0 to evaluate whether there were statistical differences between two independent groups. Unless otherwise mentioned, $P<0.05$ was considered statistically significant in all analyses.

3 Results

3.1 Prognostic value of MMR genes in EC

MMR genes maintain genomic stability and inhibit tumor formation by preventing mutation accumulation and mediating apoptotic responses of DNA damage, while mutations in MMR genes cause hereditary non-polyposis colorectal cancer, and MMR defects are associated with the formation of multiple sporadic tumors (25, 26). Multiple studies have confirmed that the overexpression of MMR proteins is associated with adverse survival outcomes in a variety of tumors, including prostate cancer (27), oral squamous cell carcinoma (28), melanoma (29), etc. To determine whether MMR genes can predict the prognosis of EC patients or not, we divided EC samples into high and low expression groups based on the median FPKM value of MMR genes and found that the survival outcomes of the *MSH2* and *MSH6* low

expression groups were significantly better than their high expression groups (*MSH2*: OS, p=0.018, Figure 1A; PFS, p=0.032, Figure 1A; DSS, p=0.033, Supplementary Figure S1A; DFS, p=0.103, Supplementary Figure S1A; *MSH6*: OS, p=0.009, Figure 1B; PFS, p=0.001, Figure 1B; DSS, p<0.001, Supplementary Figure S1B; DFS, p=0.015, Supplementary Figure S1B);, while there was no significant difference between the high and low expression groups of *MLH1* and *PMS2* (*MLH1*: OS, p=0.864, Figure 1C; PFS, p=0.450, Figure 1C; DSS, p=0.869, Supplementary Figure S1C; DFS, p=0.409, Supplementary Figure S1C; *PMS2*: OS, p=0.531, Figure 1D; PFS, p=0.625, Figure 1D; DSS, p=0.647, Supplementary Figure S1D; DFS, p=0.303, Supplementary Figure S1D);. In addition, the area under the curve (AUC) of *MSH2* (Figure 1E) and *MSH6* (Figure 1F) for 1-,3-, and 5-years OS were higher than those of *MLH1* (Figure 1G) and *PMS2* (Figure 1H). All of these indicate that *MSH2* and *MSH6*, but not *MLH1* and *PMS2*, may be related to the prognosis of EC patients.

3.2 Relationship between MMR genes and clinicopathological features of EC and cox regression analysis

By evaluating the relationship between the expression of four MMR genes and the clinicopathological features of EC, we found that *MSH2* (Figure 2A) and *MSH6* (Figure 2B) were associated with various

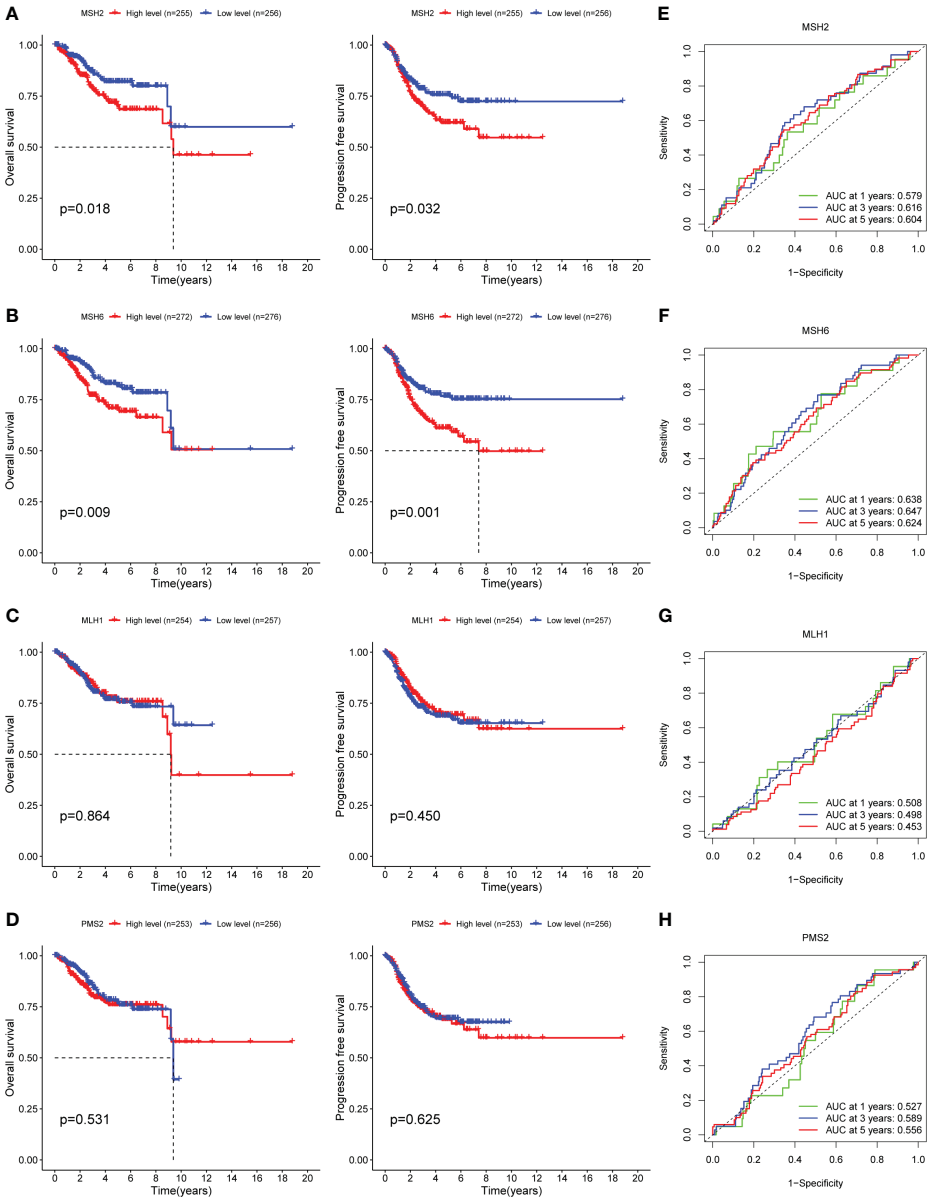

FIGURE 1
MSH2 and *MSH6*, but not *MLH1* and *PMS2*, related to the OS and PFS of EC patients. The OS and PFS curves of the low expression groups of *MSH2* **(A)** and *MSH6* **(B)** were significantly higher than those of their high expression groups, while there was no significant difference between the high and low expression groups of *MLH1* **(C)** and *PMS2* **(D)**. The area under the ROC curve of *MSH2* **(E)** and *MSH6* **(F)** was higher than that of *MLH1* **(G)** and *PMSH2* **(H)**. OS, Overall Survival; PFS, Progress Free Survival; EC, endometrial cancer.

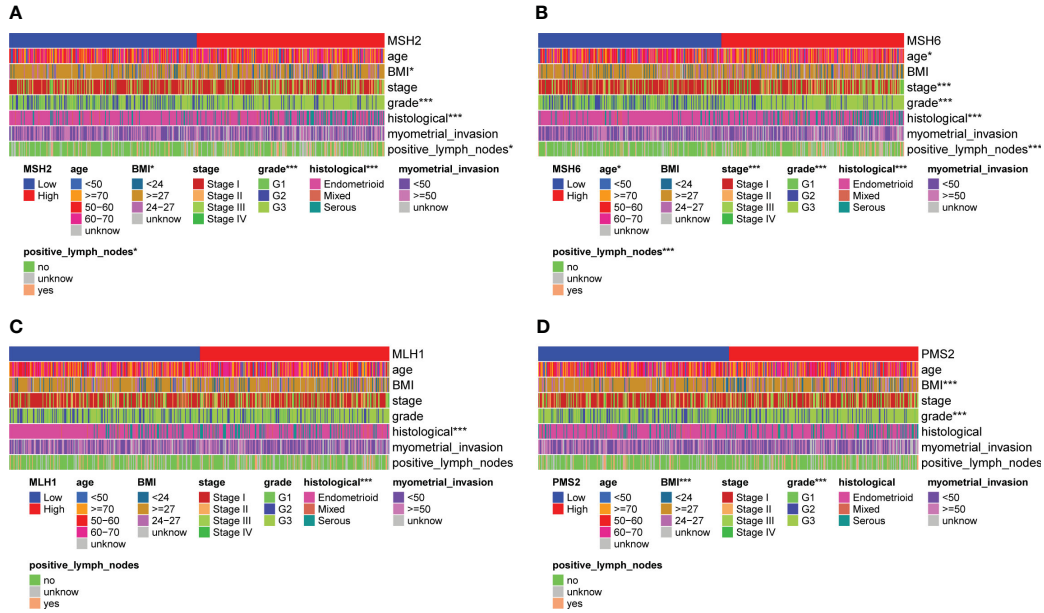

FIGURE 2
MSH2 and *MSH6*, but not *MLH1* and *PMS2*, were related to multiple crucial clinicopathological features of EC. The expression of *MSH2* **(A)** and *MSH6* **(B)** was associated with various clinicopathological features, like the age, BMI, FIGO stage and grade, histological and lymph node metastasis of EC patients, while the expression of *MLH1* **(C)** and *PMS2* **(D)** was not relevant to multiple clinicopathological features of EC. *$p < 0.05$, ***$p < 0.001$.

clinicopathological features. For example, the expression level of *MSH2* (Supplementary Figure S2A) was higher in patients with BMI<27, Federation International of Gynecology and Obstetrics (FIGO) grade III (G3), serous carcinoma and lymph node metastasis; The expression level of *MSH6* (Supplementary Figure S2B) was higher in patients with age over 60, BMI<27, FIGO stage III, G3, serous carcinoma and lymph node metastasis. These results suggested that patients with high *MSH2* and *MSH6* expression had more aggressive disease features, which were consistent with the worse survival outcomes of patients in the *MSH2* and *MSH6* high expression groups mentioned above. In comparison, the expression of *MLH1* (Figure 2C; Supplementary Figure S2C) and *PMS2* (Figure 2D; Supplementary Figure S2D) were not relevant to multiple clinicopathological features of EC.

We conducted Cox regression analysis to verify whether *MSH2* and *MSH6* can be viewed as independent prognostic factors. In univariate Cox analysis, the *p* values of the stage (p<0.001), grade (p=0.022), histological (p=0.006), lymph node metastasis (p<0.001) and *MSH6* (p=0.008) were significant, but only *MSH6* (p=0.005) remained an independent risk factor for predicting adverse outcomes in multivariate Cox regression analysis (Supplementary Table S1).

3.3 *MSH6* correlated with immune score, immune infiltration, immune checkpoint expression and ICIs Reactivity in EC

Given the high immunogenicity of dMMR EC, we tried to analyze the relationship between *MSH6* and the immune score and immune infiltration in EC. The results demonstrated that the immune, stromal and ESTIMATE scores of the low expression group of *MSH6* were significantly higher than those of the high expression group (Figure 3A). These suggest that *MSH6* is associated with immune infiltration. We next employed CIBERSORT to analyze the relationship between *MSH6* and 22 types of immune cell infiltration. We found that the expression of *MSH6* (Figure 3B) was significantly associated with the infiltration of various immune cells. For example, it was positively correlated with the infiltration of M1 macrophages, M2 macrophages, gamma delta T cells (γδT), follicular helper T cells (Tfh), naïve B cells and activated dendritic cells but negatively correlated with the infiltration of monocytes, activated NK cells, $CD8^+$T cells and regulatory T cells (Tregs). We believe that patients in the *MSH6* low expression group have a more active immune status, suggesting that they have a stronger antitumor immune response, which is also consistent with their better prognosis.

Along with immune infiltration, the expression of immune checkpoints such as PD-1 and its ligand (PD-L1) are also associated with the reactivity of dMMR ECs to ICIs. We evaluated the relationship between *MSH6* and immune checkpoint related genes in EC and found that the expression of *MSH6* was negatively correlated with the expression of multiple immune checkpoint related genes, including *CTLA-4* and *PDCD1* (Figure 3C).

In conclusion, the negative correlation between *MSH6* and active immune cell infiltration and immune checkpoint expression suggests that the expression of *MSH6* is related to the response to ICIs treatment, the lower its expression, the higher the responsiveness of patients. To verify this hypothesis, we analyzed the relationship between *MSH6* and multiple IPS scores of EC. It was found that IPS-CTLA-4 negative-PD-1 positive (p=0.0063), IPS-CTLA-4 positive-PD-1 negative (p=0.0063) and IPS-CTLA-4 positive-PD-1 positive (p=0.0005) scores were higher in the low expression group of *MSH6* (Figure 3D), suggesting that patients in

10.3389/fimmu.2024.1302797

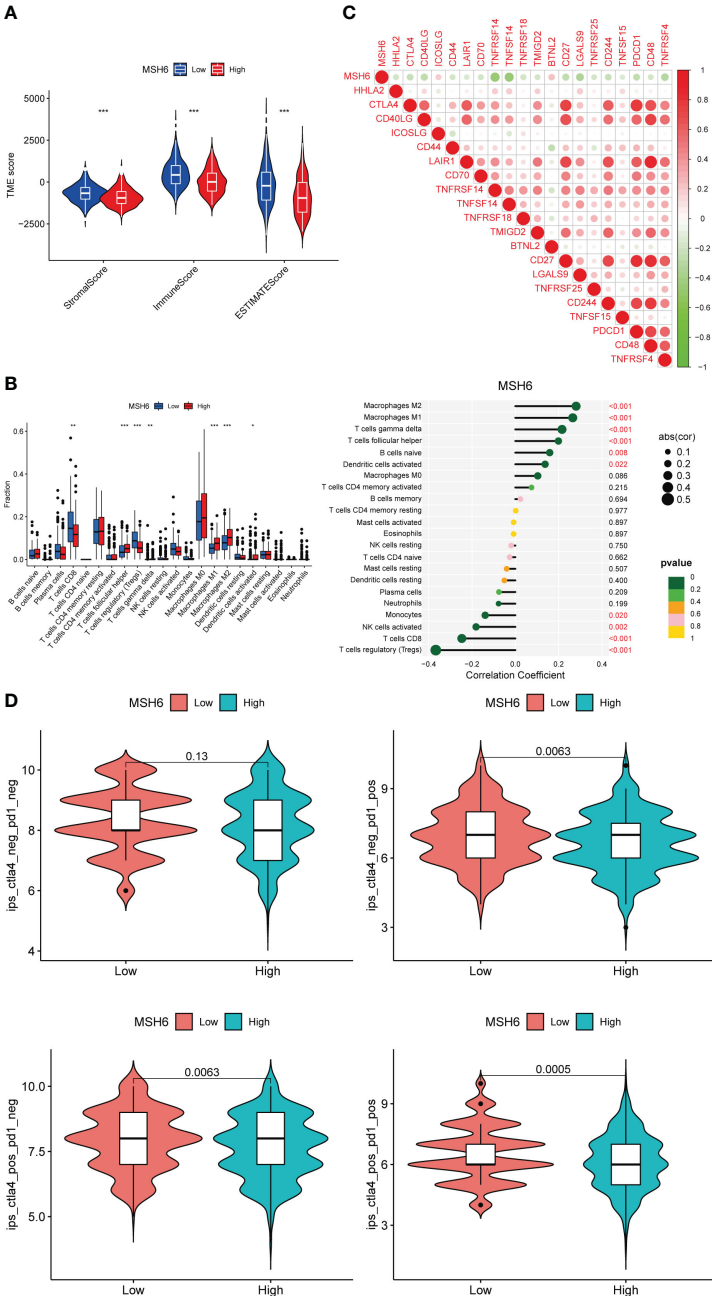

FIGURE 3
MSH6 correlated with the immune score, immune infiltration, immune checkpoint expression and ICIs reactivity in EC. The lower the expression level of *MSH6*, the higher the immune, stromal and ESTIMATE scores **(A)**, the higher the infiltration level of multiple immune cells **(B)** and the immune checkpoint expression **(C)**, and the higher the scores of multiple IPS **(D)**. *$p < 0.05$, **$p < 0.01$, ***$p < 0.001$.

the low expression group had higher reactivity against anti-CTLA-4 antibody and/or anti-PD-1 antibody.

3.4 Repeat analysis in *MSH6* wild-type tumor samples

Loss of MMR function is associated with cancer risk, progression and treatment responsiveness. Knijnenburg et al. analyzed the genomic and molecular landscape of DNA damage repair deficiency in pan-cancer using the TCGA database (30). They found that among 33 cancer types, UCEC had the most changes in the DNA damage repair gene somatic alterations, among which the incidence of MMR pathway-related gene mutations, especially *MSH6*, ranks second at 41%. The expression of *MSH6* with loss-of-function mutation differs from that of wild-type *MSH6*.

To exclude the impact of *MSH6* mutations on our results, we downloaded the single nucleotide polymorphism data of UCEC from TCGA and obtained 432 *MSH6* wild-type tumor samples and 75 *MSH6* mutant tumor samples. We performed all the previously

mentioned analyses on the remaining *MSH6* wild-type tumor samples after removing tumor samples with *MSH6* mutations and obtained results consistent with those from before. Compared with the high *MSH6* expression group, the low *MSH6* expression group had higher OS (p=0.010, Figure 4A) and PFS (p=0.020, Figure 4B), as well as higher immune, stromal and ESTIMATE scores (Figure 4C). Correlation analysis indicated that *MSH6* was negatively correlated with the infiltration of $CD8^+$T cells, activated NK cells, monocytes and Tregs, while positively correlated with the infiltration of M1 macrophages, M2 macrophages, etc (Figures 4D, E). *MSH6* was also negatively correlated with the expression of multiple immune checkpoint related genes (Figure 4F). In addition, the IPS-CTLA-4 positive-PD-1 positive (p=0.013) score in the group with low *MSH6* expression was higher than that in the group with high *MSH6* expression, suggesting a better response to anti-CTLA-4 and anti-PD-1 treatment in patients with low *MSH6* expression (Figure 4G).

3.5 Differences in biological functions between *MSH6* high and low expression groups

To explore the biological functions and pathways that may be affected by changes in *MSH6* expression in endometrial cancer, we used R to conduct GO and KEGG analyses on the DEGs upregulated in the *MSH6* high and low expression groups, respectively. GO enrichment analysis consisted of three parts: biological process (BP), cellular component (CC), and molecular function (MF). In the *MSH6* low expression group, the enriched BP terms were mainly related to immune cell migration, immune response and chemokine response, the enriched CC terms were primarily associated with the microtubule, motile cilia and dynein complex, and the enriched MF terms were mainly related to various enzyme regulator activity, cytokine activity and motor activity, etc (Figure 5A). In addition, the KEGG pathways enriched in the *MSH6* low expression group were involved in multiple immune-related diseases, such as inflammatory bowel disease and asthma, and were also related to T cell differentiation and natural killer cell-mediated cytotoxicity (Figure 5C). These results all suggested that genes enriched in the *MSH6* low expression group were mainly involved in regulating immune responses, consistent with the higher immune score (Figures 3A, 4C) and more active immune infiltration (Figures 3B, 4D, E) in the *MSH6* low expression group. In the *MSH6* high expression group, the enriched GO terms were mainly related to the regulation of mitosis, DNA replication and organism development (Figure 5B); the enriched KEGG pathways were not only associated with the cell cycle and DNA replication and DNA damage repairs related pathways such as homologous recombination, mismatch repair and base excision repair, it also involved multiple cancer-related pathways such as pancreatic cancer, renal cell carcinoma and chronic myeloid leukemia

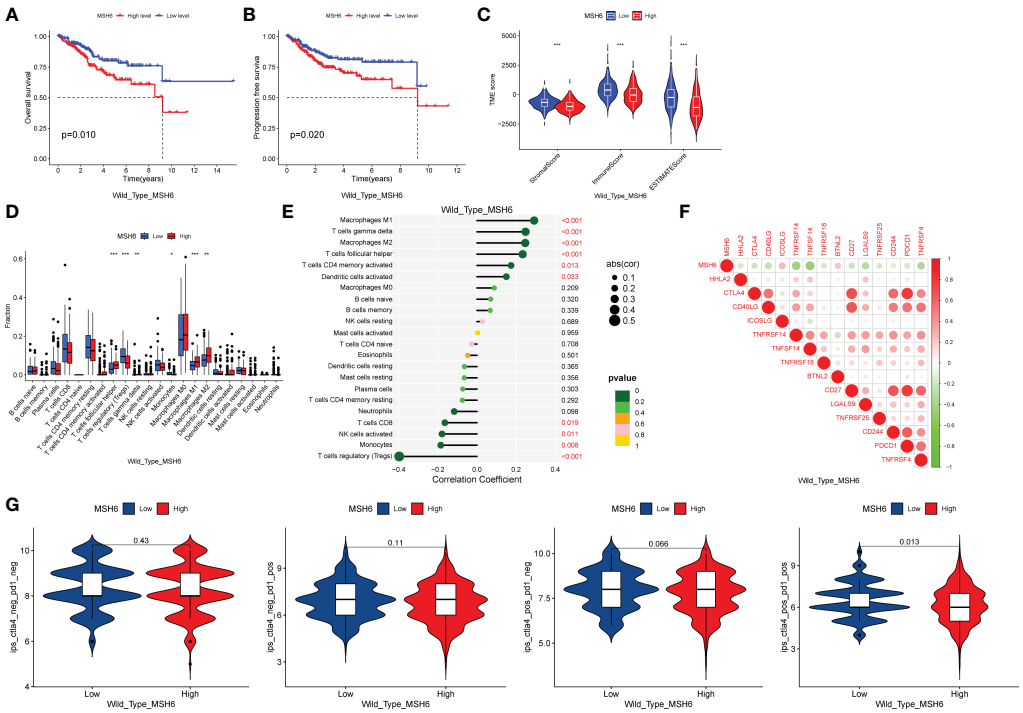

FIGURE 4
After excluding samples with *MSH6* mutations, *MSH6* was still associated with survival, immune infiltration, immune checkpoint expression and ICIs treatment responsiveness in EC. In *MSH6* wild-type endometrial cancer samples, compared with the high expression group of *MSH6*, the low expression group had higher OS **(A)** and PFS **(B)**, as well as higher immune, stromal and ESTIMATE scores **(C)**; Correlation analysis showed that *MSH6* was negatively correlated with the infiltration of multiple active immune cells **(D, E)** and the expression of immune checkpoints **(F)**; Patients with low *MSH6* expression had better response to anti-CTLA-4 and anti-PD-1 treatment **(G)**. OS, Overall Survival; PFS, Progress Free Survival; EC, endometrial cancer. *p < 0.05, **p <0.01, ***p < 0.001.

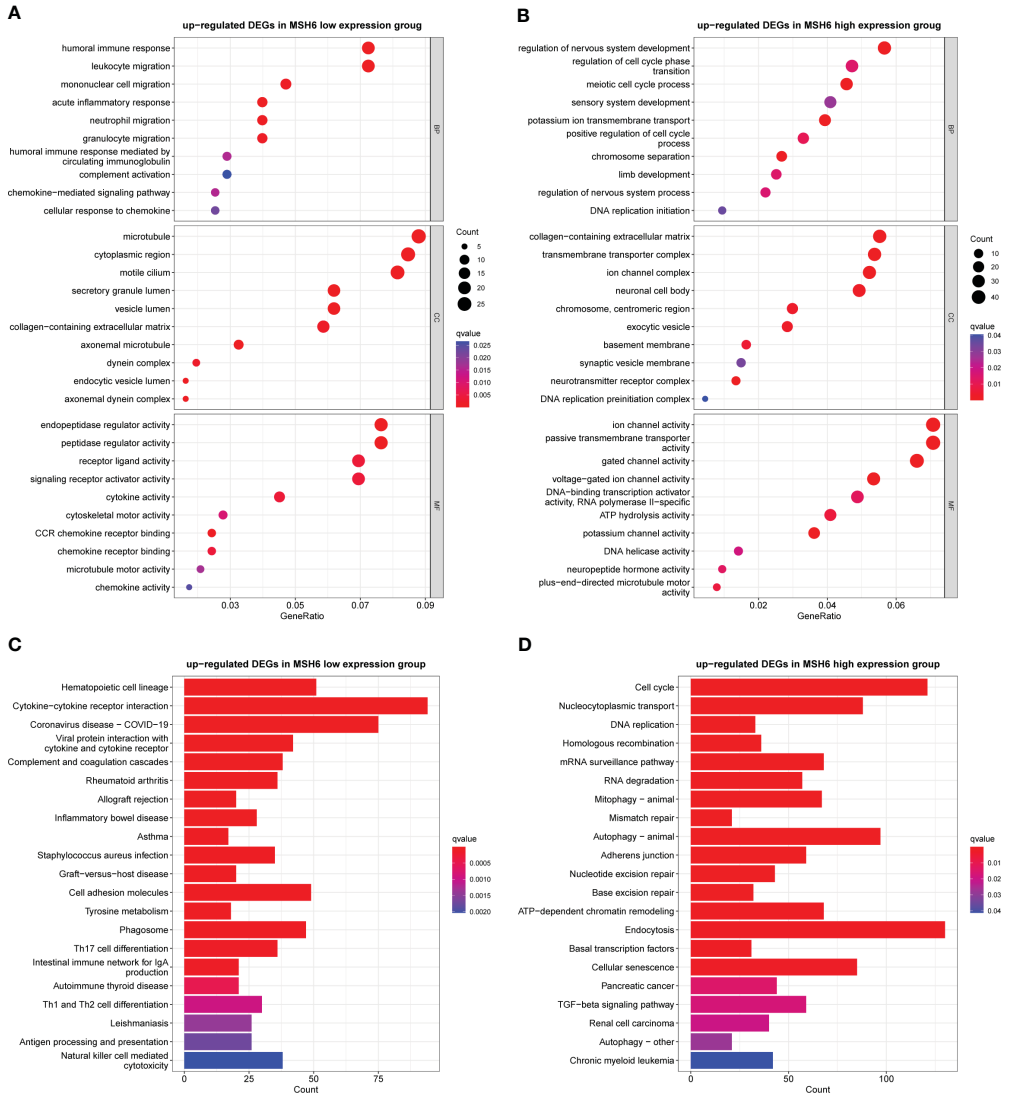

FIGURE 5
The GO and KEGG enrichment results in the *MSH6* high and low expression groups of endometrial cancer. Representative GO terms **(A)** and KEGG pathways **(C)** enriched in the *MSH6* low expression group mainly regulated immune response. Representative GO terms **(B)** and KEGG pathways **(D)** enriched in the *MSH6* high expression group were related to cell cycle regulation, DNA damage repair and tumorigenesis. GO: gene otology; KEGG: Kyoto Encyclopaedia of Genes and Genomes.

(Figure 5D). These results suggested that genes enriched in the *MSH6* high expression group were mainly related to cell proliferation, and the dysregulation of cell proliferation can lead to the occurrence of cancer, which was consistent with the previously obtained worse survival outcomes of endometrial cancer patients in the high expression group of *MSH6* (Figures 1B, 4A, B).

3.6 *MSH6* correlated with the proliferation, migration and invasion ability of endometrial cancer cells

To verify the results of the aforementioned bioinformatics analysis, we conducted *in vitro* experiments. We infected endometrial cancer cells (Ishikawa and HEC-1B) with lentivirus that can knock down or overexpress *MSH6* and confirmed its infection effect by RT-qPCR and WB (Figure 6; Supplementary Figure S3). The cell proliferation and clonal formation assay indicated that the proliferation ability of endometrial cancer cells after *MSH6* knockdown was significantly weaker than that of the control group (Figures 7A, C; Supplementary Figures S4A, C), while it was significantly stronger than that of the control group after overexpression of *MSH6* (Figures 7B, D; Supplementary Figures S4B, D). The wound healing and Transwell assay revealed that the migration and invasion ability of the *MSH6* knockdown group was significantly inferior to its control group (Figures 8A, C; Supplementary Figures S5A, C), while in the *MSH6* overexpression group, it was significantly stronger than its control group (Figures 8B, D; Supplementary Figures S5B, D).

10.3389/fimmu.2024.1302797

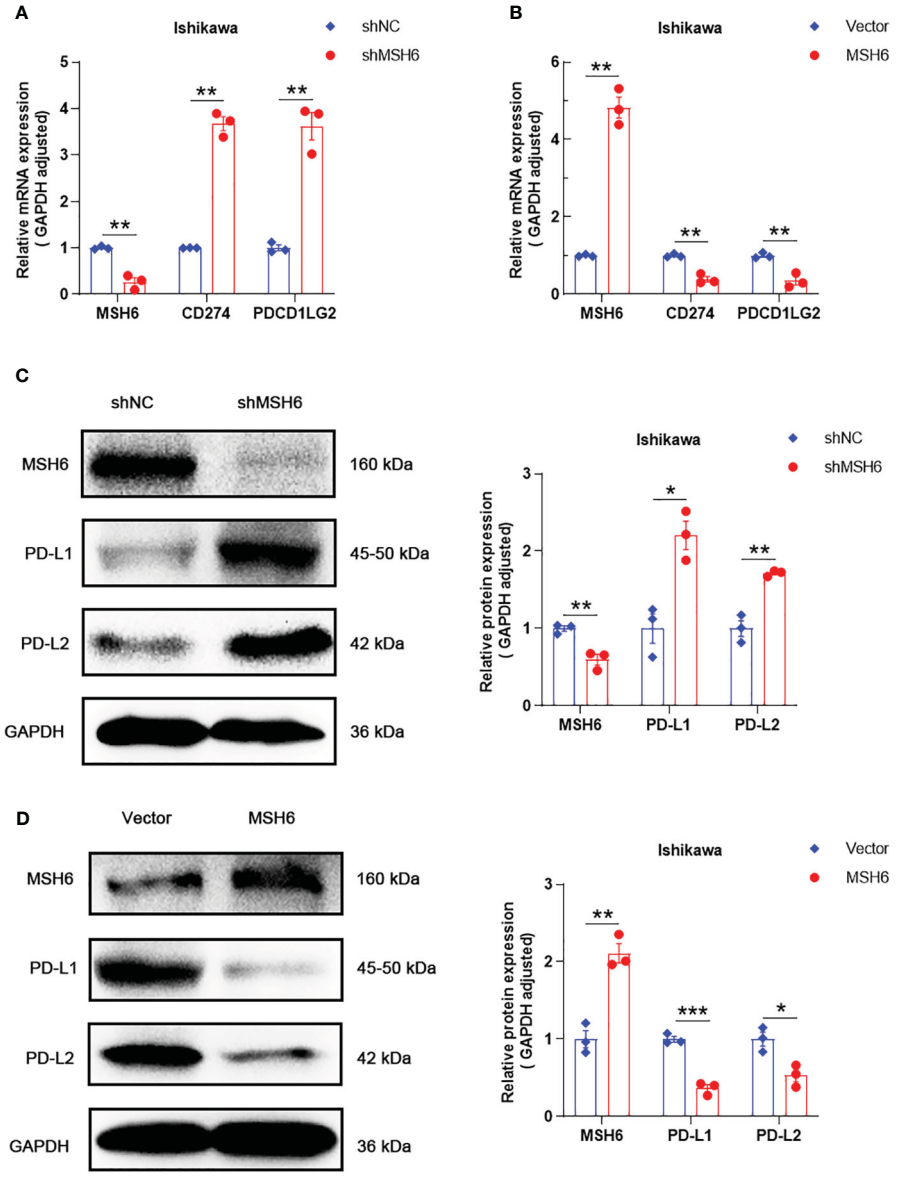

FIGURE 6
MSH6 correlated with the expression of PD-L1 and PD-L2 in Ishikawa cells. RT-qPCR and WB confirmed that after knocking down *MSH6* in Ishikawa cells, the expression levels of PD-L1 and PD-L2 were higher than those in the control group **(A, C)**, while the opposite trend was observed after overexpressing *MSH6* **(B, D)**.*$p < 0.05$, **$p < 0.01$, ***$p < 0.001$.

3.7 *MSH6* correlated with the expression of PD-L1 and PD-L2

RT-qPCR and WB also confirmed that the expression levels of PD-L1 and PD-L2 in cells after *MSH6* knockdown were significantly higher than those in the control group, while in cells after *MSH6* overexpression, they were significantly lower than those in the control group (Figure 6; Supplementary Figure S3).

4 Discussion

This study found through bioinformatics analysis that *MSH6* was associated with clinicopathological features, prognosis, immune infiltration, immune checkpoint expression and ICIs reactivity in EC. The lower expression level of *MSH6* was associated with less aggressive disease features, higher levels of immune cell infiltration (especially $CD8^+$T cells) and immune checkpoint expression in EC patients, which may be related to higher response to ICIs and better prognosis in EC patients. GO and KEGG analyses confirmed that the genes enriched in the *MSH6* low expression group were mainly involved in regulating immune response, while the genes enriched in the *MSH6* high expression group were related to tumorigenesis. *In vitro* experiments also confirmed that the proliferation, migration and invasion ability of cells in the *MSH6* knockdown group were weaker than those in the control group, but the expression levels of PD-L1 and PD-L2 were higher than those in the control group. There was an opposite trend in the overexpression group of *MSH6* and its control group.

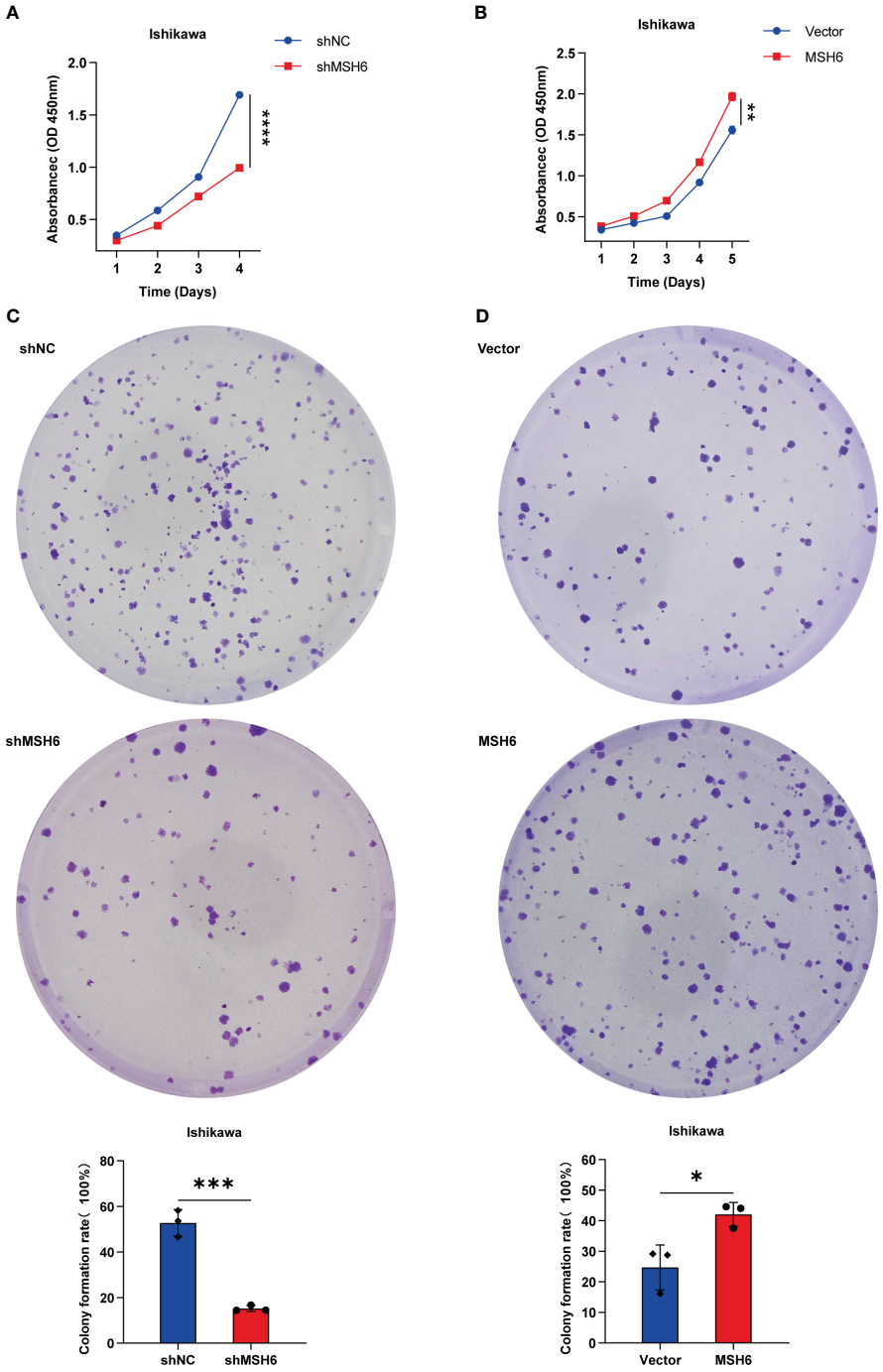

FIGURE 7
MSH6 correlated with the proliferation ability of Ishikawa cells. Cell proliferation and clone formation assay confirmed that the proliferation ability of *MSH6* knockdown Ishikawa cells was weaker than that of the control cells **(A, C)**, while in the *MSH6* overexpression Ishikawa cells, it was stronger than that of the control cells **(B, D)**. *$p < 0.05$, **$p < 0.01$, ***$p < 0.001$, ****$p < 0.0001$.

It is worth noting that when using CIBERSORT to analyze the relationship between *MSH6* and immune cell infiltration, we found that the trend of Tregs infiltration was consistent with $CD8^+$T cells but opposite to M2 macrophages. Previous studies on the immune microenvironment of various tumor types, such as nasopharyngeal cancer (31), colorectal cancer (32), and prostate cancer (33), have suggested that Tregs are positively correlated with M2 macrophages, and when they highly infiltrate tumor tissue, they usually indicate a poor prognosis. Research by Sun (34) and Tiemessen (35) also found that Tregs can promote the differentiation of monocytes into M2 macrophages. These studies typically analyzed all tumor samples uniformly without distinguishing their mismatch repair status. On the other hand, Michel et al. (36) found that the infiltrating levels of $CD8^+$T cells and $Foxp3^+$Tregs in MSI-H colorectal cancer were significantly higher than those in microsatellite stable (MSS) colorectal cancer

10.3389/fimmu.2024.1302797

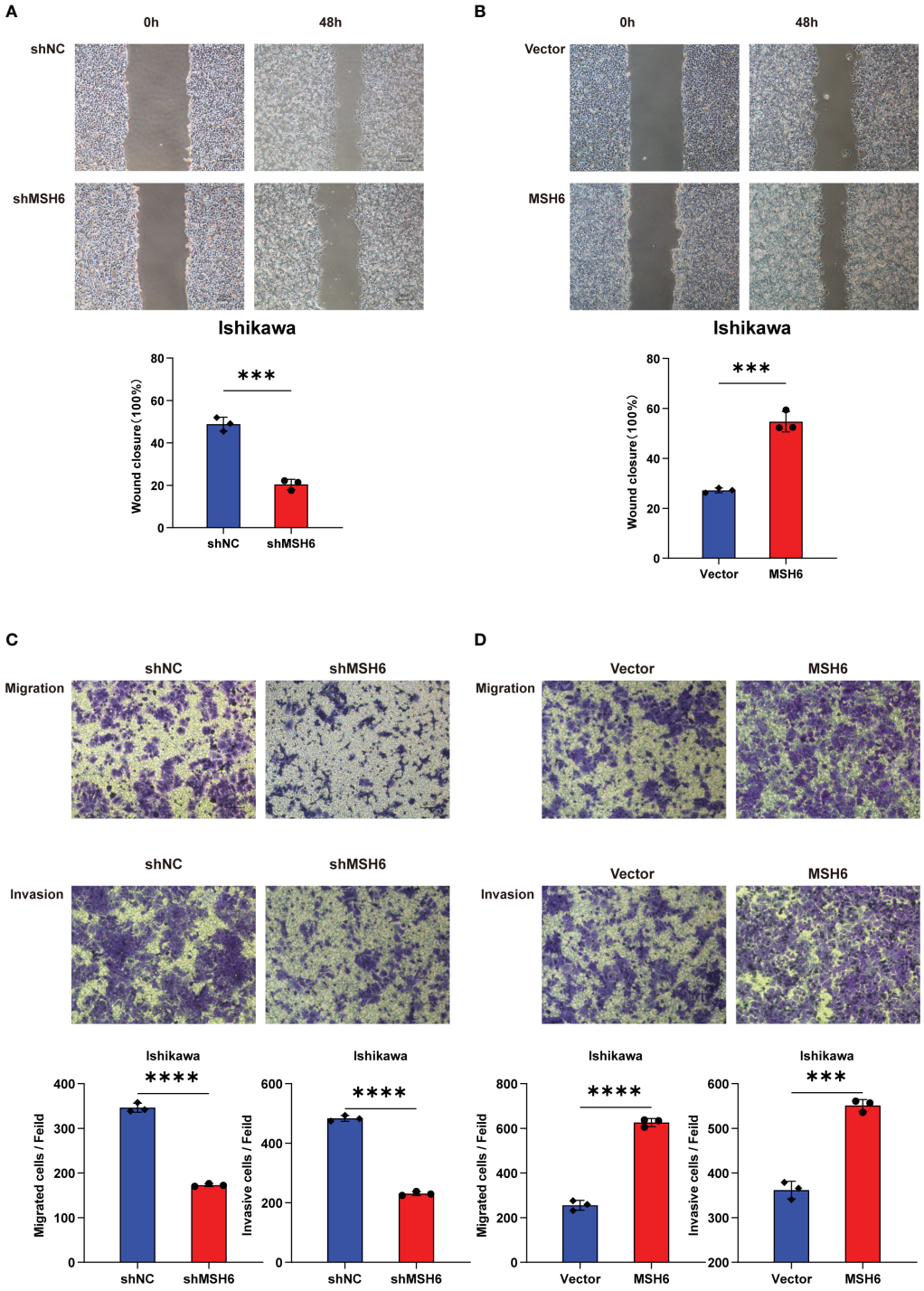

FIGURE 8
MSH6 correlated with the migration and invasion ability of Ishikawa cells. Wound healing and Transwell assay confirmed that the migration and invasion ability of *MSH6* knockdown Ishikawa cells was weaker than that of the control cells **(A, C)**, while the opposite trend was observed after overexpressing *MSH6* **(B, D)**. ***$p < 0.001$, ****$p < 0.0001$.

and the two cell types were positively correlated. They believed that microsatellite status also affects the density of infiltrating Tregs. Asaka et al. (37) also found that dMMR EC and PD-L1 positive EC had higher levels of $CD8^+$T cells, $Fxop3^+$Tregs, PD-1^+ immune cells and PD-$L1^+$ immune cells than mismatch repair proficient (pMMR) EC or PD-L1 negative EC, and they suggested that in addition to MMR status, PD-L1 was also associated with T cell-inflamed phenotype. Spranger (38) found that $CD8^+$T cells induce the expression of PD-L1 in tumor tissues by secreting IFN-r. On the other hand, $CD8^+$T cells can induce *in situ* proliferation of Tregs, which can also recruit Tregs into the tumor by secreting CCL22 and binding with CCR4 on the surface of Tregs. The two mechanisms work together to increase the infiltration level of Tregs in tumors. In conclusion, we speculated that there are three possible reasons for

the same trend of Treg infiltration as $CD8^+$T cells but opposite to M2 macrophages in our study. One is that MSH6, as a mismatch repair protein, affects the infiltration of Tregs. Second, given the inverse correlation between *MSH6* and $CD8^+$T cell infiltration, *MSH6* low-expression tumors have a high degree of $CD8^+$T cell infiltration, and these highly infiltrated $CD8^+$T cells recruit Tregs to tumors by inducing *in situ* proliferation of Tregs or by secreting cytokines. Third, PD-L1 expression was increased in tumors with low *MSH6* expression, and these highly expressed PD-L1 may also affect Tregs infiltration.

As a responder to DNA damage, the mismatch repair system plays an important role in maintaining genome stability and preventing tumorigenesis. Many studies have found that the overexpression of core genes of the mismatch repair system is related to the occurrence of various tumors. Chen et al. (39) demonstrated that *MSH6* was an overexpressed oncogene in human glioblastoma multiforme tissues that can promote gliomagenesis. In studies about prostate cancer, oral squamous cell carcinoma and melanoma, the overexpression of MMR proteins was associated with poor prognosis (27–29). Lemetre (40) and Berg (41), respectively, used the TCGA database and their own endometrial cancer samples to analyze and found that MSH6 was an independent prognostic marker, and patients with low expression of MSH6 had better survival outcomes. Our results were consistent with their findings. Given the high mutation rate of *MSH6* in endometrial cancer, we not only conducted analysis in unclassified tumor samples but also innovatively verified the results in the remaining *MSH6* wild-type tumor samples after removing those with *MSH6* mutants and obtained consistent results with them. Furthermore, to our knowledge, we are the only study that analyzed the relationship between *MSH6*, immune infiltration and ICIs treatment responsiveness in endometrial cancer. Previous studies primarily compared pMMR tumors with dMMR tumors or between dMMR tumors caused by *MLH1* promoter hypermethylation(*MLH1*-PHM) or MMR-related gene mutation. For example, Kaneko (42) suggested that dMMR ECs with *MLH1*- PHM had a worse prognosis than pMMR ECs and Lynch syndrome (LS) associated dMMR ECs (dMMR ECs without *MLH1*-PHM); Sloan (43) found that the expression of PD-L1 was the highest in LS-associated dMMR ECs, followed by dMMR ECs with *MLH1*-PHM and finally pMMR ECs. Moreover, the MMR immunohistochemical staining pattern most consistent with PD-L1 expression was MSH6 expression loss. They hypothesized which MMR protein defect was the most important variable regulating PD-L1 expression in tumors, regardless of whether it undergoes germline or somatic deficiency. We lack information on the correlation between different involved MMR genes (*MLH1*, *MSH2*, *MSH6*, or *PMS2*) and the prognosis and ICIs reactivity in EC. We supplemented this for the first time and confirmed that *MSH6* is closely associated with prognosis, immune infiltration, immune checkpoint expression and ICIs reactivity in EC. In 2021, by constructing dMLH1 tumor cells and mouse dMLH1 tumor models, Lu et al. (44). demonstrated that deletion of *MLH1* expression improves tumor infiltration of $CD8^+$ T cells and enhances ICIs reactivity by promoting cytoplasmic DNA aggregation and activating cGAS- STRING pathway. These also suggested that MMR genes themselves were related to immune infiltration and ICIs reactivity.

The limitation of this study is the lack of our own clinical samples of endometrial cancer to validate the results, especially the need to verify the relationship between *MSH6* and immune infiltration, immune checkpoint expression and ICIs treatment responsiveness. Immune checkpoint inhibitors are not routinely used in patients with endometrial cancer. Only some advanced or relapsed patients with multiple drug resistance choose to receive ICIs treatment. More time is needed to collect sufficient sample size. Understanding the communication between tumor cells and immune cells and their response to ICIs is important to guide drug administration and elucidate the mechanism of drug resistance. Single-cell NRA sequencing (sc-RNA-seq), as a powerful technique, can be used to explore the heterogeneous cellular, molecular characteristics, and intercellular communication within tumors (45). It can also be used to identify key cell types, genes, regulons and pathways with pro-tumor and antitumor potential, guiding us to explore the mechanisms related to response and resistance to ICIs treatment and biomarkers with predictive significance (46). In the future, it is necessary to collect clinical samples of endometrial cancer or construct mouse models to explore the relationship between different MMR genes, especially *MSH6*, and immune infiltration and ICIs response by using sc-RNA-seq or distinguish the cellular and molecular characteristics of different MMR deficiency patterns to find the cause for primary or secondary resistance of dMMR EC to ICIs treatment.

5 Conclusions

In conclusion, we confirmed that the expression of *MSH6* was inversely correlated with the prognosis, immune score, immune infiltration, immune checkpoint expression and ICIs response of EC. *MSH6* is anticipated to be a viable biomarker for predicting prognosis, immune status, immune checkpoint expression and perhaps the response to immunotherapy in EC patients. This study also points out new directions for potential drug development. Pharmacists can develop inhibitors that target the MMR genes, especially *MSH6*. These drugs may be used to treat refractory or metastatic advanced MSS/pMMR solid tumors, or they can be combined with ICIs to improve their reactivity in MSI-H/dMMR solid tumors. In addition, given that the infiltration trend of Tregs was similar to that of $CD8^+$ T cells, we speculated that combining Tregs-targeted therapy and ICIs may improve patient reactivity and prognosis in the presence of a preexisting T cell-inflamed tumor microenvironment.

Data availability statement

The datasets presented in this study can be found in online repositories. The names of the repository/repositories and accession number(s) can be found in the article/Supplementary Material.

Ethics statement

Ethical approval was not required for the studies on humans in accordance with the local legislation and institutional requirements because only commercially available established cell lines were used. Ethical approval was not required for the studies on animals in accordance with the local legislation and institutional requirements because only commercially available established cell lines were used.

Author contributions

L-ZZ: Writing – original draft, Conceptualization, Data curation, Formal analysis, Methodology, Software, Validation, Visualization, Writing – review & editing. H-QX: Conceptualization, Methodology, Project administration, Supervision, Writing – review & editing. JC: Conceptualization, Funding acquisition, Project administration, Resources, Supervision, Writing – review & editing.

Funding

The author(s) declare financial support was received for the research, authorship, and/or publication of this article. This work was supported by the Beijing Cancer Prevention & Treatment Society (IZXUEYANZI2019-1003).

Conflict of interest

The authors declare that the research was conducted in the absence of any commercial or financial relationships that could be construed as a potential conflict of interest.

Publisher's note

All claims expressed in this article are solely those of the authors and do not necessarily represent those of their affiliated organizations, or those of the publisher, the editors and the reviewers. Any product that may be evaluated in this article, or claim that may be made by its manufacturer, is not guaranteed or endorsed by the publisher.

Supplementary material

The Supplementary Material for this article can be found online at: https://www.frontiersin.org/articles/10.3389/fimmu.2024.1302797/full#supplementary-material

SUPPLEMENTARY FIGURE 1
MSH2 and *MSH6*, but not *MLH1* and *PMS2*, related to the DSS and DFS of EC patients. The DSS and DFS curves of the low expression groups of *MSH2* **(A)** and *MSH6* **(B)** were significantly higher than those of their high expression groups, while there was no significant difference between the high and low expression groups of *MLH1* **(C)** and *PMS2* **(D)**. DSS, Disease Specific Survival; DFS, Disease Free Survival; EC, endometrial cancer.

SUPPLEMENTARY FIGURE 2
Relationship between MMR genes and clinicopathological features of EC. Compared with patients with low expression of *MSH2* and *MSH6*, patients with high expression of *MSH2* and *MSH6* had higher stage and grade, more serous carcinoma, and higher incidence of lymph node metastasis **(A, B)**, while *MLH1* and *PMS2* expression were independent of most these clinicopathological features **(C, D)**.

SUPPLEMENTARY FIGURE 3
Validation of the relationship between *MSH6* and the expression of PD-L1 and PD-L2 in HEC-1B cells. Verify the knockdown and overexpression efficiency of *MSH6* by RT-qPCR **(A, B)** and WB in HEC-1B cells **(C, D)**, and analyze the mRNA and protein expression of immune checkpoint related genes after knockdown or overexpression of *MSH6*. *p < 0.05, **p <0.01.

SUPPLEMENTARY FIGURE 4
Validation of the relationship between *MSH6* and cell proliferation in HEC-1B cells. The effect of *MSH6* knockdown **(A, C)** or overexpression **(B, D)** on cell proliferation activity was verified in HEC-1B cells by cell proliferation and clone formation assay. *p < 0.05, **p <0.01.

SUPPLEMENTARY FIGURE 5
Validation of the relationship between *MSH6* and cell migration and invasion ability in HEC-1B cells. The effect of *MSH6* knockdown **(A, C)** or overexpression **(B, D)** on cell migration and invasion ability was verified in HEC-1B cells by wound healing and Transwell assay. **p < 0.01, ***p <0.001, ****p < 0.0001.

References

1. Lu KH, Broaddus RR. Endometrial cancer. *N Engl J Med* (2020) 383:2053–64. doi: 10.1056/NEJMra1514010

2. Lortet-Tieulent J, Ferlay J, Bray F, Jemal A. International patterns and trends in endometrial cancer incidence, 1978-2013. *J Natl Cancer Inst* (2018) 110:354–61. doi: 10.1093/jnci/djx214

3. Murali R, Soslow RA, Weigelt B. Classification of endometrial carcinoma: more than two types. *Lancet Oncol* (2014) 15:e268–278. doi: 10.1016/S1470-2045(13)70591-6

4. Cancer Genome Atlas Research N, Kandoth C, Schultz N, Cherniack AD, Akbani R, Liu Y, et al. Integrated genomic characterization of endometrial carcinoma. *Nature* (2013) 497:67–73. doi: 10.1038/nature12113

5. Talhouk A, McConechy MK, Leung S, Yang W, Lum A, Senz J, et al. Confirmation of ProMisE: A simple, genomics-based clinical classifier for endometrial cancer. *Cancer* (2017) 123:802–13. doi: 10.1002/cncr.30496

6. Green AK, Feinberg J, Makker V. A review of immune checkpoint blockade therapy in endometrial cancer. *Am Soc Clin Oncol Educ Book* (2020) 40:1–7. doi: 10.1200/EDBK_280503

7. Deshpande M, Romanski PA, Rosenwaks Z, Gerhard J. Gynecological cancers caused by deficient mismatch repair and microsatellite instability. *Cancers (Basel)* (2020) 12:3319. doi: 10.3390/cancers12113319

8. Hampel H, Pearlman R, de la Chapelle A, Pritchard CC, Zhao W, Jones D, et al. Double somatic mismatch repair gene pathogenic variants as common as Lynch syndrome among endometrial cancer patients. *Gynecol Oncol* (2021) 160:161–8. doi: 10.1016/j.ygyno.2020.10.012

9. Ding L, Chen F. Predicting tumor response to PD-1 blockade. *N Engl J Med* (2019) 381:477–9. doi: 10.1056/NEJMcibr1906340

10. Howitt BE, Shukla SA, Sholl LM, Ritterhouse LL, Watkins JC, Rodig S, et al. Association of polymerase e-mutated and microsatellite-instable endometrial cancers with neoantigen load, number of tumor-infiltrating lymphocytes, and expression of PD-1 and PD-L1. *JAMA Oncol* (2015) 1:1319–23. doi: 10.1001/jamaoncol.2015.2151

11. Le DT, Durham JN, Smith KN, Wang H, Bartlett BR, Aulakh LK, et al. Mismatch repair deficiency predicts response of solid tumors to PD-1 blockade. *Science* (2017) 357:409–13. doi: 10.1126/science.aan6733

12. Seiwert TY, Burtness B, Mehra R, Weiss J, Berger R, Eder JP, et al. Safety and clinical activity of pembrolizumab for treatment of recurrent or metastatic squamous cell carcinoma of the head and neck (KEYNOTE-012): an open-label, multicentre, phase 1b trial. *Lancet Oncol* (2016) 17:956–65. doi: 10.1016/S1470-2045(16)30066-3

13. Ott PA, Bang YJ, Berton-Rigaud D, Elez E, Pishvaian MJ, Rugo HS, et al. Safety and antitumor activity of pembrolizumab in advanced programmed death ligand 1-positive endometrial cancer: results from the KEYNOTE-028 study. *J Clin Oncol* (2017) 35:2535–41. doi: 10.1200/JCO.2017.72.5952

14. Lemery S, Keegan P, Pazdur R. First FDA approval agnostic of cancer site - when a biomarker defines the indication. *N Engl J Med* (2017) 377:1409–12. doi: 10.1056/NEJMp1709968

15. Abu-Rustum NR, Yashar CM, Bradley K, Campos SM, Chino J, Chon HS, et al. NCCN guidelines(R) insights: uterine neoplasms, version 3.2021. *J Natl Compr Canc Netw* (2021) 19:888–95. doi: 10.6004/jnccn.2021.0038

16. Muenst S, Soysal SD, Tzankov A, Hoeller S. The PD-1/PD-L1 pathway: biological background and clinical relevance of an emerging treatment target in immunotherapy. *Expert Opin Ther Targets* (2015) 19:201–11. doi: 10.1517/14728222.2014.980235

17. Zou W, Wolchok JD, Chen L. PD-L1 (B7-H1) and PD-1 pathway blockade for cancer therapy: Mechanisms, response biomarkers, and combinations. *Sci Transl Med* (2016) 8:328rv324. doi: 10.1126/scitranslmed.aad7118

18. Antill Y, Kok PS, Robledo K, Yip S, Cummins M, Smith D, et al. Clinical activity of durvalumab for patients with advanced mismatch repair-deficient and repair-proficient endometrial cancer. A nonrandomized phase 2 clinical trial. *J Immunother Cancer* (2021) 9:e002255. doi: 10.1136/jitc-2020-002255

19. Schlauc D, Fu X, Jones SF, Burris HA 3rd, Spigel DR, Reeves J, et al. Tumor-specific and tumor-agnostic molecular signatures associated with response to immune checkpoint inhibitors. *JCO Precis Oncol* (2021) 5(2021):1625–38. doi: 10.1200/PO.21

20. Lagos GG, Izar B, Rizvi NA. Beyond tumor PD-L1: emerging genomic biomarkers for checkpoint inhibitor immunotherapy. *Am Soc Clin Oncol Educ Book* (2020) 40:1–11. doi: 10.1200/EDBK_289967

21. Tomczak K, Czerwinska P, Wiznerowicz M. The Cancer Genome Atlas (TCGA): an immeasurable source of knowledge. *Contemp Oncol (Pozn)* (2015) 19:A68–77. doi: 10.5114/wo.2014.47136

22. Wang D, Peng L, Hua L, Li J, Liu Y, Zhou Y. Mapk14 is a prognostic biomarker and correlates with the clinicopathological features and immune infiltration of colorectal cancer. *Front Cell Dev Biol* (2022) 10:817800. doi: 10.3389/fcell.2022.817800

23. Xu H, Xu Q, Yin L. Prognostic value of tumor immune cell infiltration patterns in colon adenocarcinoma based on systematic bioinformatics analysis. *Cancer Cell Int* (2021) 21:344. doi: 10.1186/s12935-021-02048-x

24. Mei J, Xing Y, Lv J, Gu D, Pan J, Zhang Y, et al. Construction of an immune-related gene signature for prediction of prognosis in patients with cervical cancer. *Int Immunopharmacol* (2020) 88:106882. doi: 10.1016/j.intimp.2020.106882

25. Li GM. Mechanisms and functions of DNA mismatch repair. *Cell Res* (2008) 18:85–98. doi: 10.1038/cr.2007.115

26. Yang G, Scherer SJ, Shell SS, Yang K, Kim M, Lipkin M, et al. Dominant effects of an Msh6 missense mutation on DNA repair and cancer susceptibility. *Cancer Cell* (2004) 6:139–50. doi: 10.1016/j.ccr.2004.06.024

27. Wilczak W, Rashed S, Hube-Magg C, Kluth M, Simon R, Buscheck F, et al. Up-regulation of mismatch repair genes MSH6, PMS2 and MLH1 parallels development of genetic instability and is linked to tumor aggressiveness and early PSA recurrence in prostate cancer. *Carcinogenesis* (2017) 38:19–27. doi: 10.1093/carcin/bgw116

28. Wagner VP, Webber LP, Salvadori G, Meurer L, Fonseca FP, Castilho RM, et al. Overexpression of mutSalpha complex proteins predicts poor prognosis in oral squamous cell carcinoma. *Med (Baltimore)* (2016) 95:e3725. doi: 10.1097/MD.0000000000003725

29. Alvino E, Passarelli F, Cannavo E, Fortes C, Mastroeni S, Caporali S, et al. High expression of the mismatch repair protein MSH6 is associated with poor patient survival in melanoma. *Am J Clin Pathol* (2014) 142:121–32. doi: 10.1309/AJCPCX2D9YULBBLG

30. Knijnenburg TA, Wang L, Zimmermann MT, Chambwe N, Gao GF, Cherniack AD, et al. Genomic and molecular landscape of DNA damage repair deficiency across the cancer genome atlas. *Cell Rep* (2018) 23:239–254 e236. doi: 10.1016/j.celrep.2018.03.076

31. Aliyah SH, Ardiyan YN, Mardhiyah I, Herdini C, Dwianingsih EK, Aning S, et al. The distribution of M2 macrophage and treg in nasopharyngeal carcinoma tumor tissue and the correlation with TNM status and clinical stage. *Asian Pac J Cancer Prev* (2021) 22:3447–53. doi: 10.31557/APJCP.2021.22.11.3447

32. Chen Y, Gao Y, Ma X, Wang Y, Liu J, Yang C, et al. A study on the correlation between M2 macrophages and regulatory T cells in the progression of colorectal cancer. *Int J Biol Markers* (2022) 37:412–20. doi: 10.1177/03936155221132572

33. Erlandsson A, Carlsson J, Lundholm M, Falt A, Andersson SO, Andren O, et al. M2 macrophages and regulatory T cells in lethal prostate cancer. *Prostate* (2019) 79:363–9. doi: 10.1002/pros.23742

34. Sun W, Wei FQ, Li WJ, Wei JW, Zhong H, Wen YH, et al. A positive-feedback loop between tumour infiltrating activated Treg cells and type 2-skewed macrophages is essential for progression of laryngeal squamous cell carcinoma. *Br J Cancer* (2017) 117:1631–43. doi: 10.1038/bjc.2017.329

35. Tiemessen MM, Jagger AL, Evans HG, van Herwijnen MJ, John S, Taams LS, et al. CD4+CD25+Foxp3+ regulatory T cells induce alternative activation of human monocytes/macrophages. *Proc Natl Acad Sci USA* (2007) 104:19446–51. doi: 10.1073/pnas.0706832104

36. Michel S, Benner A, Tariverdian M, Wentzensen N, Hoefler P, Pommerenck T, et al. High density of FOXP3-positive T cells infiltrating colorectal cancers with microsatellite instability. *Br J Cancer* (2008) 99:1867–73. doi: 10.1038/sj.bjc.6604756

37. Asaka S, Yen TT, Wang TL, Shih IM, Gaillard S. T cell-inflamed phenotype and increased Foxp3 expression in infiltrating T-cells of mismatch-repair deficient endometrial cancers. *Mod Pathol* (2019) 32:576–84. doi: 10.1038/s41379-018-0172-x

38. Spranger S, Spaapen RM, Zha Y, Williams J, Meng Y, Ha TT, et al. Up-regulation of PD-L1, IDO, and T(regs) in the melanoma tumor microenvironment is driven by CD8(+) T cells. *Sci Transl Med* (2013) 5:200ra116. doi: 10.1126/scitranslmed.3006504

39. Chen Y, Liu P, Sun P, Jiang J, Zhu Y, Dong T, et al. Oncogenic MSH6-CXCR4-TGFB1 feedback loop: A novel therapeutic target of photothermal therapy in glioblastoma multiforme. *Theranostics* (2019) 9:1453–73. doi: 10.7150/thno.29987

40. Lemetre C, Vieites B, Ng CK, Piscuoglio S, Schultheis AM, Marchio C, et al. RNASeq analysis reveals biological processes governing the clinical behaviour of endometrioid and serous endometrial cancers. *Eur J Cancer* (2016) 64:149–58. doi: 10.1016/j.ejca.2016.05.028

41. Berg HF, Engerud H, Myrvold M, Lien HE, Hjelmeland ME, Halle MK, et al. Mismatch repair markers in preoperative and operative endometrial cancer samples; expression concordance and prognostic value. *Br J Cancer* (2023) 128:647–55. doi: 10.1038/s41416-022-02063-3

42. Kaneko E, Sato N, Sugawara T, Noto A, Takahashi K, Makino K, et al. MLH1 promoter hypermethylation predicts poorer prognosis in mismatch repair deficiency endometrial carcinomas. *J Gynecol Oncol* (2021) 32:e79. doi: 10.3802/jgo.2021.32.e79

43. Sloan EA, Ring KL, Willis BC, Modesitt SC, Mills AM. PD-L1 expression in mismatch repair-deficient endometrial carcinomas, including lynch syndrome-associated and MLH1 promoter hypermethylated tumors. *Am J Surg Pathol* (2017) 41:326–33. doi: 10.1097/PAS.0000000000000783

44. Lu C, Guan J, Lu S, Jin Q, Rousseau B, Lu T, et al. DNA sensing in mismatch repair-deficient tumor cells is essential for antitumor immunity. *Cancer Cell* (2021) 39:96–108 e106. doi: 10.1016/j.ccell.2020.11.006

45. Liu C, Zhang M, Yan X, Ni Y, Gong Y, Wang C, et al. Single-cell dissection of cellular and molecular features underlying human cervical squamous cell carcinoma initiation and progression. *Sci Adv* (2023) 9:eadd8977. doi: 10.1126/sciadv.add8977

46. Liu C, Li X, Huang Q, Zhang M, Lei T, Wang F, et al. Single-cell RNA-sequencing reveals radiochemotherapy-induced innate immune activation and MHC-II upregulation in cervical cancer. *Signal Transduct Target Ther* (2023) 8:44. doi: 10.1038/s41392-022-01264-9

frontiers | Frontiers in Oncology

TYPE Original Research
PUBLISHED 04 March 2024
DOI 10.3389/fonc.2024.1285511

OPEN ACCESS

EDITED BY
Alberto Traverso,
Maastro Clinic, Netherlands

REVIEWED BY
Haiyan Li,
The Sixth Affiliated Hospital of Sun Yat-sen University, China
Zekun Jiang,
Sichuan University, China

*CORRESPONDENCE
Xiaoling Leng
lengxiaoling1206@163.com;
58281431@qq.com

RECEIVED 19 September 2023
ACCEPTED 20 February 2024
PUBLISHED 04 March 2024

CITATION
Liu J, Leng X, Liu W, Ma Y, Qiu L, Zumureti T, Zhang H and Mila Y (2024) An ultrasound-based nomogram model in the assessment of pathological complete response of neoadjuvant chemotherapy in breast cancer.
Front. Oncol. 14:1285511.
doi: 10.3389/fonc.2024.1285511

An ultrasound-based nomogram model in the assessment of pathological complete response of neoadjuvant chemotherapy in breast cancer

Jinhui Liu[1], Xiaoling Leng[1]*, Wen Liu[2], Yuexin Ma[3], Lin Qiu[3], Tuerhong Zumureti[3], Haijian Zhang[3] and Yeerlan Mila[3]

[1]Department of Ultrasound, The Tenth Affiliated Hospital of Southern Medical University (Dongguan People's Hospital), Dongguan, Guangdong, China, [2]Artificial Intelligence and Smart Mine Engineering Technology Center, Xinjiang Institute of Engineering, Urumqi, China, [3]Department of Ultrasound, The Affiliated Tumor Hospital of Xinjiang Medical University, Urumqi, Xinjiang, China

Introduction: We aim to predict the pathological complete response (pCR) of neoadjuvant chemotherapy (NAC) in breast cancer patients by constructing a Nomogram based on radiomics models, clinicopathological features, and ultrasound features.

Methods: Ultrasound images of 464 breast cancer patients undergoing NAC were retrospectively analyzed. The patients were further divided into the training cohort and the validation cohort. The radiomics signatures (RS) before NAC treatment (RS1), after 2 cycles of NAC (RS2), and the different signatures between RS2 and RS1 (Delta-RS/RS1) were obtained. LASSO regression and random forest analysis were used for feature screening and model development, respectively. The independent predictors of pCR were screened from clinicopathological features, ultrasound features, and radiomics models by using univariate and multivariate analysis. The Nomogram model was constructed based on the optimal radiomics model and clinicopathological and ultrasound features. The predictive performance was evaluated with the receiver operating characteristic (ROC) curve.

Results: We found that RS2 had better predictive performance for pCR. In the validation cohort, the area under the ROC curve was 0.817 (95%CI: 0.734-0.900), which was higher than RS1 and Delta-RS/RS1. The Nomogram based on clinicopathological features, ultrasound features, and RS2 could accurately predict the pCR value, and had the area under the ROC curve of 0.897 (95%CI: 0.866-0.929) in the validation cohort. The decision curve analysis showed that the Nomogram model had certain clinical practical value.

Discussion: The Nomogram based on radiomics signatures after two cycles of NAC, and clinicopathological and ultrasound features have good performance in predicting the NAC efficacy of breast cancer.

KEYWORDS

nomogram, radiomics, breast cancer, ultrasound, neoadjuvant chemotherapy

1 Introduction

Breast cancer is the leading cause of cancer worldwide in 2020, which has become the "world's number one cancer". Highly aggressive breast cancer is difficult to treat and has a high recurrence rate and poor prognosis (1, 2). At present, neoadjuvant chemotherapy (NAC) is the standard treatment regimen for breast cancer, which can effectively reduce tumor volume and clinical stage (3). The efficacy evaluation of NAC determines the individualized treatment plan. However, the efficacy evaluation of NAC is still difficult at present.

The current efficacy evaluation methods for NAC mainly include pathological evaluation and clinical evaluation. Pathological evaluation is the gold standard for evaluating the efficacy of NAC in breast cancer (4), but it has a lag, and cannot provide timely guidance for clinical treatment. Ultrasound, as one of the main clinical evaluation methods, is more frequently used in NAC assessment than MRI and mammography (5). However, ultrasound lacks quantitative parameters compared with other imaging examinations.

In recent years, radiomics has shown potential advantages in improving the precise diagnosis of breast cancers, assessment of lymph node metastasis, and prognosis prediction (6). Ultrasound imaging combined with radiomics can achieve a timely and accurate quantitative assessment of the efficacy of NAC in breast cancer (7). For the time point to evaluate the efficacy, one study has shown that the use of pre-NAC ultrasound images of breast cancer patients can more accurately predict the efficacy of NAC (8). However, according to the Breast Cancer Diagnosis and Treatment Guidelines by the Chinese Anti-Cancer Association, the efficacy evaluation by ultrasound after two cycles of NAC has significantly improved accuracy (9, 10). Another study reported that if the efficacy was assessed as non-pathological complete response (pCR) after two cycles of NAC, and then NAC was replaced with other treatment regimens, the long-term prognosis of patients was improved (11). However, there are few reports on the use of ultrasound images after two cycles of NAC to predict its efficacy. Breast cancer before NAC often presents all malignant signs on ultrasound, while the malignant signs of breast cancer after NAC often disappear completely on ultrasound, resulting in the fact that breast cancers with different prognoses and curative effects before and after NAC treatment often have the same ultrasound signs (12, 13), and making it difficult to distinguish different prognoses using ultrasound signs. Ultrasound radiomics can extract more ultrasound signs that are invisible to the naked eye and can provide more information than conventional ultrasound (14).

Herein, we predicted the pCR of NAC in breast cancer patients. The ultrasound radiomics of breast cancer before and after NAC were extracted and their value in predicting pCR was analyzed. Furthermore, a Nomogram was constructed based on clinicopathological features, ultrasound features, and radiomics models. Our findings may help clinicians to optimize the individualized treatment for NAC patients promptly.

2 Materials and methods

2.1 Patients

This study included patients who were diagnosed with breast cancer and who were admitted to the Tumor Hospital of Xinjiang Medical University between January 2018, and April 2022. The breast cancer diagnosis was confirmed by surgery and pathology. Inclusion criteria: (I) patients who had pathologically confirmed pCR or non-pCR after NAC; (II) patients who only received complete NAC therapy; (III) patients who underwent breast ultrasonography before surgery and after two cycles of NAC. Exclusion criteria: (I) patients with unavailable pathology results; (II) patients who did not complete NAC; (III) patients with insufficient ultrasound image quality; (IV) patients who had unilateral multifocal carcinoma. The flowchart of patient enrollment is shown in Figure 1. The study was conducted following the Declaration of Helsinki and approved by the ethics committee of Tumor Hospital of Xinjiang Medical University (approval number G-2023027). The written informed consent was obtained from each patient.

We randomly assigned the finally enrolled 464 patients with breast cancer into the training cohort (n=324) and the validation cohort (n=140). In the training cohort, 84 patients had pCR and 240 patients had non-pCR. In the validation cohort, 40 patients were with pCR and 100 patients were with non-pCR.

2.2 NAC and pathological evaluation of NAC efficacy

Treatment regimens and schedules followed the National Comprehensive Cancer Network (NCCN) guidelines. The NAC regimen was based on anthracyclines and taxanes (15).

All patients underwent standard histopathological examination to assess their response to NAC. The criteria for pCR were no residual

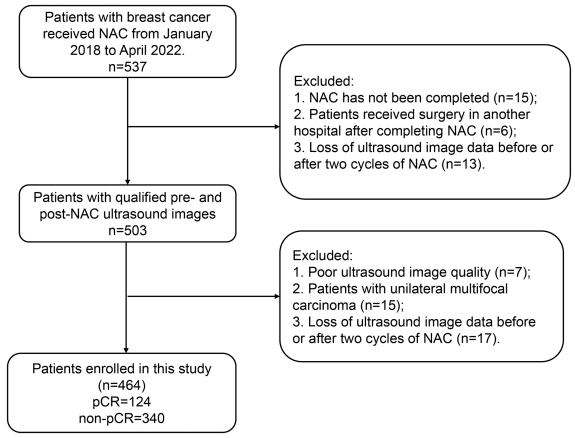

FIGURE 1
Flowchart of patient enrollment.

invasive carcinoma in the specimen (residual ductal carcinoma *in situ* may be present) and no lymph node involvement in the ipsilateral sentinel lymph node or axillary lymph node.

2.3 Data collection

Clinical data collection included patient age, tumor types (e.g., invasive ductal carcinoma, invasive lobular carcinoma), presence of vascular invasion (positive or negative), TNM staging (stages I, II, and III), T staging [stages 1-4), N staging (stages 0-3), histological grade (low grade (I, II) and high grade (III)], estrogen receptor (ER) (positive or negative), progesterone receptor (PR) (positive or negative), human epidermal growth factor receptor 2 (Her2) (positive or negative), and Ki-67 expression (< 20% or ≥ 20%). TNM staging adhered to the 2017 AJCC Eighth Edition TNM Staging Standard for breast cancer. Ultrasound data collection encompassed post-NAC tumor characteristics, such as shape (regular or irregular), position (parallel or not parallel to the skin), margins (regular or irregular), internal echo (homogeneous or non-homogeneous), posterior echo (iso-echoic or weakened-echoic), calcifications (coarse, fine, or none), distortion of surrounding structures (distorted or not distorted), blood flow (internal type, peripheral type, or none), breast background (fatty echo or fibrous echo), as well as changes in the long and anterior-posterior diameters of tumor before and after treatment (< 30% or ≥ 30%).

2.4 Ultrasound examination

Ultrasound examination was performed with GE Logic E9 with the high-frequency linear array probe L-16-5. The ultrasound images with the longest diameter were selected for analysis. Two radiologists (with at least 10 years of experience in breast ultrasound), who were blinded to the pathological findings, delineated the region of interest (ROI) in the ultrasound images by using Itk-Snap (version 3.8.0). The interclass correlation coefficient (ICC) was used to assess the agreement of the feature extraction between observers and within observers. Ratings of ICC were assigned as follows: an ICC of less than 0.40 was considered 'Poor', 0.40–0.59 was labeled 'Fair', 0.60–0.74 was categorized as 'Good', and 0.74–1.00 was deemed 'Excellent'.

2.5 Extraction of radiomics features

The flowchart of radiomics feature extraction and model establishment is shown in Figure 2. In detail, the ultrasound features were extracted from ultrasound images using the PyRadiomics open-source tool (https://pyradiomics.readthedocs.io/en/latest/index.html). The ultrasound images were processed using the Wavelet filter. A total of 7 categories of features were extracted, including 1) First Order Features; 2) Shape Features; 3) GLCM Features; 4) GLSZM Features; 5) GLRLM Features; 6) NGTDM Features; and, 7) GLDM Features. The radiomics signatures (RS) of ultrasound images before NAC (defined as RS1), and those after 2 cycles of NAC (defined as RS2) were obtained. The different signatures between RS1 and RS2 were defined as Delta-RS/RS1.

2.6 Establishment and performance evaluation of radiomics models

We used the PyRadiomics open-source tool (https://pyradiomics.readthedocs.io/en/latest/index.html) to establish radiomics models. Before the feature selection, the ICC was calculated to ensure the repeatability and stability of features with a threshold of 0.75. All signatures were normalized by the Z-score method. Student's test and Pearson correlation analysis were performed. The Least Absolute Shrinkage and Selection Operator (LASSO) was used to further screen the signatures, and according to the Minimum Squared-Error criterion, the signatures with the greatest correlation were selected. The Random Forest classifier was used to analyze the key signatures for predicting pCR, and the 10-fold cross-validation was used to optimize hyperparameters, thus improving model performance.

According to the calculation formula in the official documentation of Radiomics, the Rad-score of each patient was calculated as follows:

$$\text{Rad} - \text{score} = \beta 0 + \beta 1X1 + \beta 2X2 + \beta 3X3 + \ldots + \beta nXn\,.$$

Xn represents the RSs after screening, β0 is the constant of the Rad-score, and βn is the regression coefficient of the corresponding RS in the regression model (16).

In detail, the formula for the Rad-score of RS1 was 0.301724 + 0.018033×original_glrlm_GrayLevelNonUniformityNormalized-0.004469×original_ngtdm_Strength+0.004457×original_gldm_SmallDependenceHighGrayLevelEmphasis+0.027550×wavelet-LLH_firstorder_Mean+0.090245×wavelet-LHH_ngtdm_Coarseness+0.043016×wavelet-HLL_firstorder_MeanAbsoluteDeviation+0.045260×wavelet-HLH_glcm_DifferenceVariance-0.004468×wavelet-HLH_glszm_LargeAreaLowGrayLevelEmphasis+0.015469×wavelet-HLL_glszm_ZoneEntropy+0.002321×wavelet-HHL_ngtdm_Strength-0.005785×wavelet-LLH_glcm_ClusterShade-0.010428×wavelet-LLH_glcm_MaximumProbability.

The formula for the Rad-score of RS2 was 0.267241-0.010622×original_glcm_ClusterShade-0.022649×original_glszm_SmallAreaHighGrayLevelEmphasis+0.048624×original_ngtdm_Strength+0.010071×wavelet-LLH_firstorder_Mean+0.022298×wavelet-LLH_glcm_MaximumProbability+0.100730×wavelet-LHH_ngtdm_Coarseness-0.005865×wavelet-LHH_gldm_DependenceNonUniformityNormalized+0.005142×wavelet-HLL_firstorder_Mean+0.027327×wavelet-HHL_ngtdm_Strength+0.017414×wavelet-HHL_glszm_ZonePercentage+0.040358×wavelet-HHL_gldm_SmallDependenceEmphasis+0.020727×wavelet-LHL_firstorder_10Percentile-0.051783×wavelet-LHL_glcm_Idn-0.009552×wavelet-LLH_glrlm_LongRunLowGrayLevelEmphasis-0.001952×wavelet-LLH_glrlm_RunEntropy+0.057903×wavelet-LLL_ngtdm_Coarseness+0.001388×wavelet-LLL_ngtdm_Contrast.

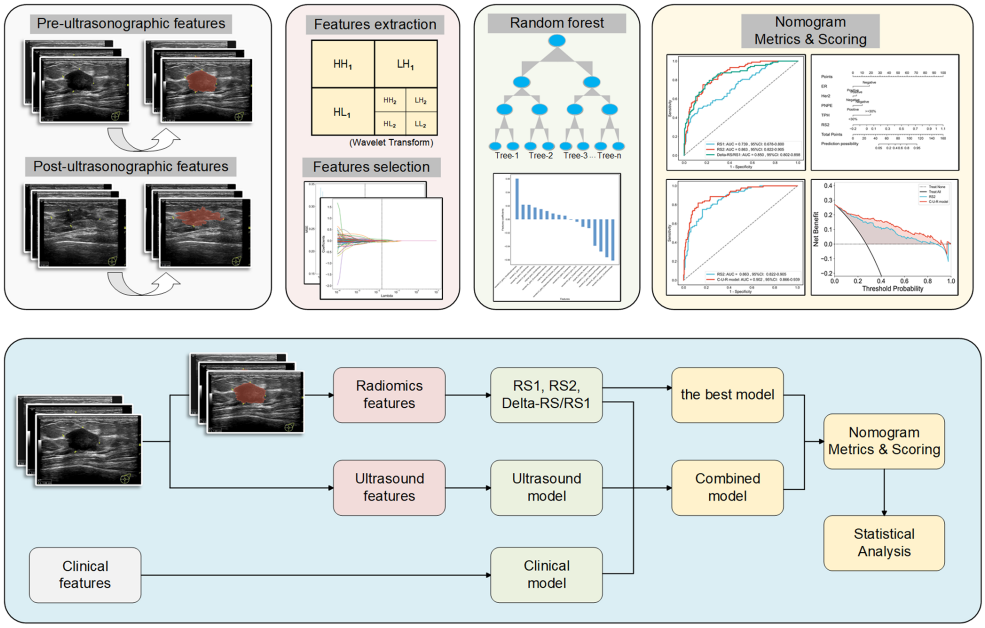

FIGURE 2
Flowchart of radiomics feature extraction and model establishment.

The formula for the Rad-score of Delta-RS/RS1 was 0.301724 + 0.012994*original_firstorder_Minimum+0.015151*original_glszm_ZoneEntropy+0.008663*original_ngtdm_Complexity-0.003557*wavelet-LHL_glcm_Imc2-0.047644*wavelet-LHL_glcm_MaximumProbability+0.060348*wavelet-LHH_glszm_SmallAreaEmphasis+0.017589*wavelet-LHH_glszm_ZoneEntropy-0.000699*wavelet-LHH_ngtdm_Coarseness+0.005423*wavelet-LLH_gldm_DependenceNonUniformityNormalized+0.021508*wavelet-LHL_glszm_ZoneEntropy-0.056111*wavelet-HLL_glszm_ZonePercentage+0.012303*wavelet-HLL_glrlm_RunLengthNonUniformity+0.006602*wavelet-HHL_firstorder_Kurtosis-0.011061*wavelet-HHL_glcm_ClusterProminence-0.061069*wavelet-HHH_glszm_ZonePercentage+0.021748*wavelet-LLH_glcm_Idmn-0.039115*wavelet-LLL_ngtdm_Coarseness.

2.7 Construction and performance evaluation of radiomics nomogram

The Nomogram was constructed based on the optimal radiomics model, and the significant clinicopathological features and ultrasound features affecting pCR. The Nomogram and the radiomics model were compared with the DeLong test. Decision curve analysis (DCA) was used to calculate and compare the net benefit at different threshold probabilities for the training and validation cohorts to assess the clinical value of the radiomics model and Nomogram.

2.8 Statistical analysis

Statistical analysis was performed using Python (version 3.7) and R language (version 4.2.0). The data of normal distribution and non-normal distribution were analyzed by t-test and Mann-Whitney U test, respectively. Enumeration data were analyzed by chi-square test. The significant clinicopathological features and ultrasound features affecting pCR were screened with univariate and multivariate analysis. The performance of each model was assessed using receiver operating characteristic (ROC) curves. The area under the ROC curve (AUC) was calculated. A two-tailed p-value <0.05 indicated statistical significance.

3 Results

3.1 Clinicopathological and ultrasound features of patients

A total of 464 patients were enrolled in this study. The clinicopathological features and ultrasound imaging features of the patients are shown in Table 1; Supplementary Table S1. In both training and validation cohorts, the ER status, Her2 status, vascular invasion, PR status, post-NAC posterior echo, percentage of ultrasound length, delta height, and percentage of ultrasound height were significantly associated with pCR ($p<0.05$). There was no significant association between pCR and other features.

The significant clinicopathological and ultrasound features were subjected to multivariate logistic regression analysis (Supplementary Tables S2, S3). The results showed that ER status, PR status, Her2 status, post-NAC posterior echo, and percentage of ultrasound height were all significantly associated with higher pCR ($p < 0.05$). Patients with negative ER and Her2 or with Post-NAC posterior echo of Weaken-Echoic and percentage of ultrasound height ≥ 30% were easier to achieve pCR.

TABLE 1 Baseline characteristics of the patients.

Characteristics	Training cohort			Validation cohort			P-value
	non-pCR (N=240)	pCR (N=84)	P-value	non-pCR (N=100)	pCR (N=40)	P-value	
Age, Mean (SD), years	48.8 (9.96)	46.9 (8.63)	0.306	47.2 (9.96)	48.8 (7.82)	0.662	0.768
NAC duration, Mean (SD), day	154 (78.9)	153 (55.5)	0.992	157 (88.8)	147 (24.1)	0.797	1
Tumor type			0.426			0.828	0.999
Invasive ductal carcinomas	214 (89.2%)	70.0 (83.3%)		87.0 (87.0%)	37.0 (92.5%)		
Invasive lobular carcinoma	6.00 (2.5%)	1.00 (1.2%)		3.00 (3.0%)	0 (0%)		
Others	20.0 (8.3%)	13.0 (15.5%)		10.0 (10.0%)	3.00 (7.5%)		
Vascular invasion			0.0034			0.0347	0.680
Positive	62.0 (25.8%)	7.00 (8.3%)		31.0 (31.0%)	4.00 (10.0%)		
Negative	178 (74.2%)	77.0 (91.7%)		69.0 (69.0%)	36.0 (90.0%)		
Nerve invasion			0.329			0.739	0.865
Positive	28.0 (11.7%)	5 (6.0%)		12.0 (12.0%)	0 (0%)		
Negative	212 (88.3%)	79.0 (94%)		88.0 (88.0%)	40.0 (100%)		
TNM stage			0.966			0.388	0.095
I	22.0 (9.2%)	10.0 (11.9%)		10.0 (10.0%)	1.00 (2.5%)		
II	88.0 (36.7%)	31.0 (36.9%)		46.0 (46.0%)	25.0 (62.5%)		
III	130 (54.2%)	43.0 (51.2%)		44.0 (44.0%)	14.0 (35.0%)		
T stage			0.552			0.478	0.912
1	53.0 (22.1%)	12.0 (14.3%)		27.0 (27.0%)	4.00 (10.0%)		
2	106 (44.2%)	48.0 (57.1%)		47.0 (47.0%)	26.0 (65.0%)		
3	45.0 (18.8%)	15.0 (17.9%)		15.0 (15.0%)	6.00 (15.0%)		
4	36.0 (15.0%)	9.00 (10.7%)		11.0 (11.0%)	4.00 (10.0%)		
N stage			0.0981			0.458	0.423
0	30.0 (12.5%)	23.0 (27.4%)		9.00 (9.0%)	7.00 (17.5%)		
1	117 (48.8%)	31.0 (36.9%)		57.0 (57.0%)	24.0 (60.0%)		
2	48.0 (20.0%)	14.0 (16.7%)		19.0 (19.0%)	2.00 (5.0%)		
3	45.0 (18.8%)	16.0 (19.0%)		15.0 (15.0%)	7.00 (17.5%)		
Histological grading			0.0023			0.719	0.298
Low grade invasive breast cancer (Grade I, II)	129 (53.8%)	51.0 (60.7%)		40.0 (40.0%)	19.0 (47.5%)		
High grade invasive breast cancer (Grade III)	111 (46.3%)	33.0 (39.3%)		60.0 (60.0%)	21.0 (52.5%)		
ER status			<0.001			<0.001	0.554
Positive	179 (74.6%)	37.0 (44.0%)		72.0 (72.0%)	14.0 (35.0%)		
Negative	61.0 (25.4%)	47.0 (56.0%)		28.0 (28.0%)	26.0 (65.0%)		
PR status			<0.001			0.0416	0.993
Positive	149 (62.1%)	25.0 (29.8%)		61.0 (61.0%)	15.0 37.5%)		
Negative	91.0 (37.9%)	59.0 (70.2%)		39.0 (39.0%)	25.0 (62.5%)		

(Continued)

TABLE 1 Continued

Characteristics	Training cohort			Validation cohort			P-value
	non-pCR (N=240)	pCR (N=84)	P-value	non-pCR (N=100)	pCR (N=40)	P-value	
Her2 status			<0.001			<0.001	0.662
Positive	49.0 (20.4%)	55.0 (65.5%)		20.0 (20.0%)	31.0 (77.5%)		
Negative	191 (79.6%)	29.0 (34.5%)		80.0 (80.0%)	9.00 (22.5%)		
Ki-67 status			0.067			0.824	0.584
< 20%	30.0 (12.5%)	3.00 (3.6%)		8.00 (8.0%)	2.00 (5.0%)		
≥ 20%	210 (87.5%)	81.0 (96.4%)		92.0 (92.0%)	38.0 (95.0%)		
Rad-score for RS1, Mean (SD)	0.229 (0.113)	0.365 (0.168)	<0.001	0.228 (0.113)	0.394 (0.216)	<0.001	0.941
Rad-score for RS2, Mean (SD)	0.188 (0.170)	0.490 (0.235)	<0.001	0.192 (0.183)	0.470 (0.247)	<0.001	0.967
Rad-score for Delta-RS/RS1, Mean (SD)	0.205 (0.137)	0.465 (0.224)	<0.001	0.196 (0.138)	0.397 (0.206)	<0.001	0.36

SD, standard deviation; ER, estrogen receptor; PR, progesterone receptor; Her2, human epidermal growth factor receptor 2; NAC, neoadjuvant chemotherapy; pCR, pathological complete response; RS, radiomics signature.
The chi-square test or Fisher's exact test was used for the nominal variable, and the Mann–Whitney test was used for the continuous variable with the abnormal distribution. A two-tailed p-value <0.05 indicated statistical significance.

3.2 Screening and modeling of radiomics features

Through radiomics feature extraction, 851 radiomics features were screened from RS1, RS2, and Delta-RS/RS1, including 216 GLCM Features, 126 GLDM Features, 144 GLRLM Features, 144 GLSZM Features, 45 NGTDM Features, 162 First Order Features, and 14 Shape Features. Before selection, the ICC for the 369 features was >0.75, ensuring the repeatability of features. After screening by LASSO regression analysis, the results showed that when λ was 0.008685 (Supplementary Figures S1A, B), 0.003393 (Supplementary Figures S1C, D), and 0.017575 (Supplementary Figures S1E, F), the optimal models of RS1, RS2, and Delta-RS/RS1 could be obtained (Supplementary Figure S1).

A total of 12, 17, and 17 radiomics features with non-zero coefficients from RS1, RS2, and Delta-RS/RS1 were obtained, respectively (Supplementary Figure S2). Among the features with positive correlation coefficients, the optimal features of Coarseness (0.090245) and Difference Variance (0.045261) in RS1, Coarseness (0.057903) in RS2, and Small Area Emphasis (0.060348) and Idmn (0.021748) in Delta-RS/RS1 had the highest weight. Among the features with negative correlation coefficients, the optimal features of RS1 had a lower weight. IDN (inverse difference normalized) (-0.051783) in RS2 had the highest weight. Additionally, among the optimal features of Delta-RS/RS1, the features with the highest weight were Zone Percentage [-0.060348 (wavelet-HH), -0.056111 (wavelet-HL)], and Maximum Probability (-0.047644).

For the comparison of Rad-Score, it was shown that there was no significant difference in the Rad-score between the training cohort and the validation cohort (p>0.05, Table 1). Further univariate analysis showed that the pCR in breast cancer patients was closely related to the Rad-score (p<0.001, Table 1).

3.3 Prediction of NAC efficacy by radiomics, clinicopathological, and ultrasound models

ROC was used to assess the role of the radiomics models in predicting the pCR status of breast cancer patients after two cycles of NAC. The Delong test showed that the performance of the RS2 (AUC_{RS2} = 0.863) was higher than the RS1 (AUC_{RS1} = 0.739, $p_{RS2\ vs\ RS1}$ = 0.002) but was no higher than Delta-RS/RS1 ($AUC_{Delta\text{-}RS/RS1}$ = 0.850, $p_{RS2\ vs\ Delta\text{-}RS/RS1}$ = 0.682) in the training cohort (Figure 3A; Table 2). In the validation cohort, the performance of the RS2 (AUC_{RS2} = 0.817) was higher than the RS1 (AUC_{RS1} = 0.799, $p_{RS2\ vs\ RS1}$ = 0.213) but was no higher than Delta-RS/RS1 ($AUC_{Delta\text{-}RS/RS1}$ = 0.748, $p_{RS2\ vs\ Delta\text{-}RS/RS1}$ = 0.689) (Figure 3B; Table 2).

The ROC curve evaluated the performance of clinicopathological and ultrasound features in predicting pCR (Figures 3C, D). In the training cohort, the AUC for clinicopathological and ultrasound features was 0.832 (95%CI: 0.779-0.884). In the validation cohort, the AUC for clinicopathological and ultrasound features was 0.862 (95%CI: 0.797-0.928).

We further evaluated the combined performance of clinicopathological features, ultrasound features, and RS2 (C-U-R model) and compared it with that of RS2 alone (Table 2). The results showed that in the training cohort, the C-U-R model ($AUC_{C\text{-}U\text{-}R\ model}$ = 0.902) had a better performance than the RS2 (AUC_{RS2} = 0.863, $p_{C\text{-}U\text{-}R\ model\ vs\ RS2}$ = 0.005) for predicting pCR (Figure 3E). In

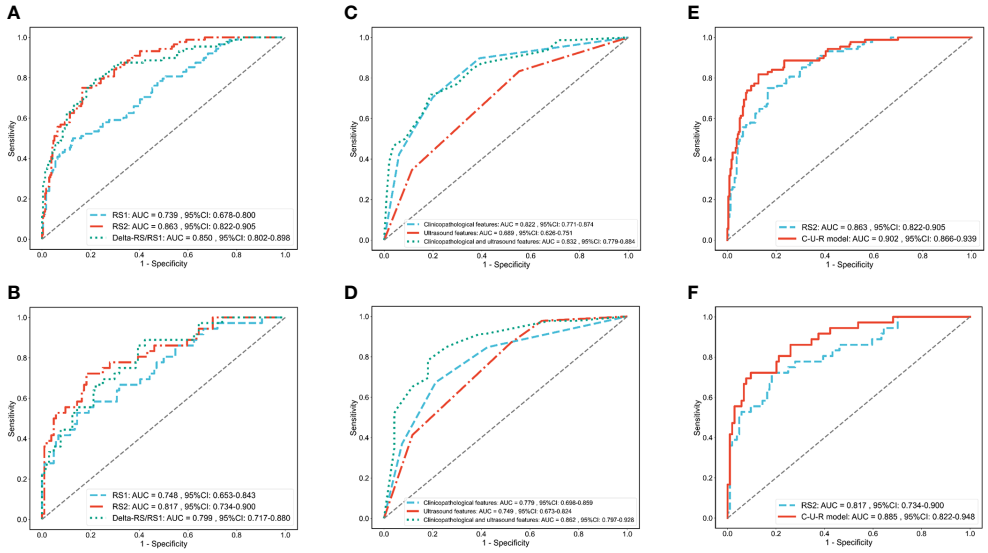

FIGURE 3
ROC analysis of each radiomics model, clinical and ultrasound model, and C-U-R model. ROC analysis of RS1, RS2, and Delta-RS/RS1 radiomics models in the training **(A)** and validation **(B)** cohorts. ROC analysis of clinicopathological features (clinical model), ultrasound features (ultrasound model), and the combination of the two (C-U model) in the training **(C)** and validation **(D)** cohorts. ROC analysis of the C-U-R model and RS2 model in the training **(E)** and validation **(F)** cohorts. C-U-R model, combined model of clinicopathological features, ultrasound features, and RS2; RS, radiomic signature; AUC, area under the ROC curve.

the validation cohort, the C-U-R model ($AUC_{C\text{-}U\text{-}R\ model}$ = 0.885) also had a better performance than the RS2 (AUC_{RS2} = 0.817, $p_{C\text{-}U\text{-}R\ model\ vs\ RS2}$ = 0.009) for predicting pCR (Figure 3F).

3.4 Construction and validation of the nomogram

We constructed a Nomogram based on the C-U-R model. As shown in Figure 4A, the item "Points" represented the corresponding score of each variable. The calculated C-statistics of the Nomogram was 0.897, indicating the model had high predictive power. In addition, we used the Hosmer-Lemesow test to verify the calibration curves of the training cohort (Figure 4B) and the validation cohort (Figure 4C), and the results showed that the difference between the training cohort (p=0.50) and the validation cohort (p=0.97) was not statistically significant. We further used the DeLong test to compare the predictive power of the Nomogram and the RS2 radiomics model, which showed that the difference between the training cohort (p=0.005) and the validation cohort (p=0.009) was statistically significant. Additionally, based on the Youden index, the optimal critical score for the Nomogram was calculated as 71.742.

3.5 Clinical application of the nomogram model

We further used the DCA to compare the Nomogram model with the RS2 radiomics model (Supplementary Figure S3). With a

TABLE 2 Performance comparison of RS1, RS2, Delta-RS/RS1, C-U-R model radiomics models.

	Training cohort				Validation cohort			
	RS1	RS2	Delta-RS/RS1	C-U-R model	RS1	RS2	Delta-RS/RS1	C-U-R model
AUC	0.739	0.863	0.850	0.902	0.748	0.817	0.799	0.885
Accuracy	0.787	0.830	0.806	0.861	0.793	0.829	0.779	0.857
Precision	0.721	0.762	0.712	0.795	0.667	0.731	0.620	0.767
Sensitivity	0.500	0.750	0.795	0.818	0.528	0.722	0.861	0.722
Specificity	0.873	0.835	0.780	0.873	0.856	0.817	0.606	0.904
Recall	0.352	0.546	0.477	0.659	0.389	0.528	0.361	0.639
F1-score	0.473	0.636	0.571	0.721	0.491	0.613	0.456	0.697
Youden Index	0.373	0.585	0.575	0.691	0.384	0.540	0.467	0.626

AUC, the area under the ROC curve; RS, radiomics signature; C-U-R, clinicopathological features, ultrasound features, and RS2.

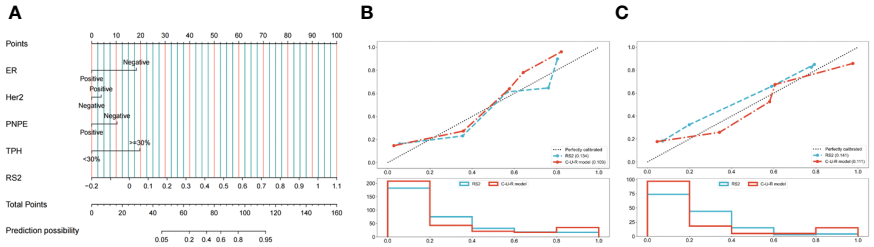

FIGURE 4
Development and performance of the nomogram. **(A)** Radiomics Nomogram was developed with vascular invasion, axillary lymph node metastasis, posterior echo delta-height/pre-height, and RS2 for the prediction of the probability of pCR. The predictors are ER, Her2, PNPE, TPH, and RS2. A vertical line was drawn from each predictor to 'Points' to get the score of the predictor. Then, the scores of each predictor were summed up. The 'Total Points' corresponded to the probability of pCR. Calibration curves of the model in the training **(B)** and validation **(C)** cohorts. The X-axis represents the predictive probability; the Y-axis denotes the observed probability. The 45° "Ideal" line represents the perfect prediction of the probability of pCR, and the "Bias-corrected" line indicates the prediction model of the nomogram. The closer the "Bias-corrected" line fits to the "Ideal" line, the better the discrimination of the nomogram is. ER, ER status; Her2, Human epidermal growth factor receptor 2; PNPE, Post-NAC posterior echo; TPH, Percentage of ultrasound length; RS, radiomic signature.

threshold probability greater than 0.3%, the Nomogram model or RS2 benefited more than the "all-treated" or the "no-treatment" regimen. When the threshold probability was greater than 26.2%, the predictive ability of the Nomogram model was better than that of the RS2 radiomics model.

4 Discussion

In this study, the performance of clinicopathological features, ultrasound features, radiomics models, and Nomogram models in predicting pCR was analyzed and compared. The results showed that the Nomogram model was superior in predicting both the energy efficiency and clinical net benefit of pCR in patients.

4.1 Predictive performance of clinicopathological and ultrasound features

We found that the clinicopathological features had better predictive value of pCR than ultrasound features. This study showed that breast cancer with posterior echo attenuation had a lower pCR rate. It is known that the pathological basis of posterior echo attenuation is that the internal tumor stroma is rich and densely arranged (17). Therefore, non-triple negative breast cancer, which has rich tumor stroma, may have lower pCR rates (18). NAC can induce necrosis and fibrosis of breast cancer cells, leading to structure collapses (19). The change of the anteroposterior diameter of the lesion is much greater than the long diameter. Therefore, the larger change rate of the tumor anteroposterior diameter after treatment also indicates that the tumor necrosis rate is high, and it is easier to achieve pCR. However, the value of conventional ultrasound in predicting pCR by macroscopic signs is limited. Then, we tried to predict pCR by combining RSs.

4.2 Predictive performance of ultrasound radiomics models

Ultrasound imaging presents several notable advantages compared to other imaging modalities, including its wide availability, cost-effectiveness, real-time nature, non-invasiveness, and superior soft tissue resolution, which facilitates the accurate capture of fine structural details (20). Li et al. (21) utilized radiomics extracted from FDG PET/CT imaging to predict pCR in 100 cases of breast cancer patients who underwent NAC. Their retrospective analysis revealed that the combined model of clinical features and PET/CT imaging radiomics achieved an AUC of 0.958 in the training set and 0.730 in the validation set, surpassing the predictive accuracy of the clinical model. In addition, Liu et al. (22) found through a multicenter study involving 586 cases of breast cancer that the combined model of clinical features and multiparametric MRI radiomics predicted the pCR of breast cancer patients after NAC with significantly higher AUC compared to the clinical model. These studies confirm that the combined model based on imaging radiomics has high accuracy in predicting the efficacy of NAC in breast cancer, indicating the significant value of imaging radiomics in predicting the efficacy of breast cancer NAC. This study, analyzing retrospectively 464 breast cancer patients undergoing NAC, confirmed that the combined model based on ultrasound imaging radiomics also had high predictive efficacy for predicting the efficacy of breast cancer NAC, markedly outperforming the clinical model and yielding greater net benefits. Furthermore, we screened the RS1 and RS2, respectively, and found that the feature with the highest weight was Coarseness (0.090245/0.100730). Coarseness reflects the grayscale difference between a central pixel or voxel and its neighbors, thereby capturing the spatial rate of grayscale intensity changes (23). The results of this study showed that for both RS1 and RS2, the ultrasound images of patients with pCR had a lower rate of spatial change and more uniform local texture, and this change

was more obvious for RS2. In addition, the weight of IDN in RS2 was -0.051783, whereas it was not present in RS1. IDN is another measure of the local homogeneity of an image. Unlike homogeneity, IDN normalizes the difference between the neighboring intensity values by dividing over the total number of discrete intensity values (24). These results suggest that patients with pCR and non-pCR have a larger difference in the local homogeneity of post-RS2 ultrasound images, which are not present in RS1. Meanwhile, the weight coefficient of the signature Difference Variance in RS1 was 0.045261, while it did not have any weight in RS2, suggesting that the effect of Difference Variance was diminished by NAC. The main reason for the above differences is the high tumor heterogeneity and disordered tumor cell arrangement before NAC treatment in breast cancer (25, 26), which is reflected in the RSs of pixel grayscale and texture inhomogeneity (27). After NAC treatment, patients with pCR will have a higher necrosis rate of tumor cells, lower tumor heterogeneity, and a uniform internal tissue structure, while patients with non-pCR will have less tumor cell necrosis and high tumor heterogeneity, which is not different than before treatment (28, 29). Consistently, we also found that the homogenization of texture feature was higher on ultrasound radiomics in patients with pCR response than in patients with non-pCR.

In this study, we used RS1 and RS2 radiomics to construct a radiomics model, and the best features selected included GLCM, NGTDM, GLSZM, GLRM, GLDM, and First Order features. Among them, GLCM and NGTDM features had the highest proportion. Studies have shown that GLCM reflects the changes in images and tumor heterogeneity by calculating the relative distance between the image and a specific pixel and by calculating the correlation coefficient of gray values in different directions (30–33). However, there are few studies on NGTDM. In this study, six types of texture features including GLCM, NGTDM, GLSZM, GLRM, GLDM, and First Order features were enrolled, and it was found that NGTDM and GLCM had similar weights. NGTDM quantifies the difference between a gray value and the average gray value of its neighbors within distance δ (30–34). Here, when we used NGTDM to evaluate the tumor ROI region, we also verified that NGTDM could accurately reflect tumor heterogeneity, thereby accurately predicting the NAC efficacy in patients.

In addition, we introduced a new radiomics model, Delta-RS/RS1, representing the magnitude of changes in ultrasound radiomics characteristics in breast cancer patients before and after NAC treatment. We found that among the positive correlation coefficients, the RSs with the highest weights were Small Area Emphasis (0.060348), Idmn (0.021748), and Zone Entropy (0.021508). Among the negative correlation coefficients, the RS with the highest weights was Zone Percentage (-0.060348 (wavelet-HH), -0.056111 (wavelet-HL)), followed by Maximum Probability (-0.047644). There were significant differences in these RSs between patients with pCR and non-pCR. In the positive correlation coefficient, the magnitude of change in patients with pCR was higher than that in patients without pCR. However, in the negative correlation coefficient, the magnitude of change in patients with pCR was lower than that in patients without pCR. The RS1, RS2, and Delta-RS/RS1 models all showed high predictive value for NAC response. However, the predictive value of RS2 and Delta-RS/RS1 was better than that of RS1. These results indicate that the radiomics model of breast cancer after two cycles of NAC can better predict the efficacy of NAC than that of before NAC. Clinicians should pay more attention to the radiomics characteristics of breast cancer after two cycles of NAC to facilitate the prediction of NAC efficacy.

4.3 Predictive performance of the C-U-R model and nomogram model

We further assessed the combined performance of the C-U-R model. We found that the C-U-R model had higher predictive performance for pCR than any single model. Then, we constructed a Nomogram model based on clinicopathological features, ultrasound features, and RS2. The Nomogram model showed accurate predictive power (C-statistics=0.897) in predicting NAC response. According to the Nomogram, after excluding RS2, the features with the highest individual scores were the percentage of ultrasound height ≥ 30% and negative ER status. We found that the optimal critical score for the Nomogram was 71.742. The breast cancer patients with a total score of > 71.742 were more likely to achieve pCR after NAC. In recent years, the Nomogram prediction model has been widely used in the clinic (33, 34). However, the indicators included in the Nomogram model for predicting the efficacy of NAC in breast cancer are confusing, and there is no conclusion on the evaluation time point of NAC. The indicators used for modeling in this study were more comprehensive, and the evaluation time point of NAC was determined to be after 2 cycles of NAC. Our results suggest that clinicians can comprehensively evaluate the efficacy of NAC according to the patients' Nomogram score, ER status, Her2 status, etc., thus making the treatment strategy with the highest benefit to the patients.

4.4 Limitations

First, due to the individual differences of patients and to obtain high-quality images, the parameters of each ultrasound instrument during the examination were not unified. Therefore, different parameters of ultrasound may affect the final performance of the model. Secondly, the Delta-RS/RS1 was relatively new, and validation on Delta-RS/RS1 is needed. Finally, this study is a single-center retrospective study. Further multicenter studies are needed to assess the reliability of the Nomogram model.

4.5 Conclusions

In summary, the Nomogram model was developed based on clinicopathological features, ultrasound features, and RS2. The Nomogram model had good prediction performance of pCR after two cycles of NAC in breast cancer patients. Therefore, conventional clinicopathological features, and breast ultrasound features before NAC treatment and in the early stage of treatment (after two cycles of NAC) combined with radiomics can provide valuable prognostic information for predicting the

efficacy of NAC in breast cancer and provide reference for making treatment strategies.

Data availability statement

The raw data supporting the conclusions of this article will be made available by the authors, without undue reservation.

Ethics statement

The studies involving humans were approved by the ethics committee of Tumor Hospital of Xinjiang Medical University. The studies were conducted in accordance with the local legislation and institutional requirements. The participants provided their written informed consent to participate in this study.

Author contributions

JL: Conceptualization, Data curation, Formal analysis, Methodology, Software, Validation, Writing – original draft. XL: Conceptualization, Funding acquisition, Project administration, Supervision, Writing – review & editing. WL: Formal analysis, Software, Writing – review & editing. YXM: Investigation, Methodology, Writing – review & editing. LQ: Investigation, Methodology, Writing – review & editing. TZ: Investigation, Methodology, Writing – review & editing. HZ: Software, Writing – review & editing. YLM: Software, Writing – review & editing.

Funding

The author(s) declare that financial support was received for the research, authorship, and/or publication of this article. This work was supported by the Project of Scientific and Technological Assistance to Xinjiang (No. 2020E0269) and the National Natural Science Foundation of China (No. 82360362).

Conflict of interest

The authors declare that the research was conducted in the absence of any commercial or financial relationships that could be construed as a potential conflict of interest.

Publisher's note

Supplementary material

The Supplementary Material for this article can be found online at: https://www.frontiersin.org/articles/10.3389/fonc.2024.1285511/full#supplementary-material

References

1. Sung H, Ferlay J, Siegel RL, Laversanne M, Soerjomataram I, Jemal A, et al. Global cancer statistics 2020: GLOBOCAN estimates of incidence and mortality worldwide for 36 cancers in 185 countries. *CA Cancer J Clin*. (2021) 71:209–49. doi: 10.3322/caac.21660

2. Xia C, Dong X, Li H, Cao M, Sun D, He S, et al. Cancer statistics in China and United States, 2022: profiles, trends, and determinants. *Chin Med J (Engl)*. (2022) 135:584–90. doi: 10.1097/CM9.0000000000002108

3. Spring LM, Fell G, Arfe A, Sharma C, Greenup R, Reynolds KL, et al. Pathologic complete response after neoadjuvant chemotherapy and impact on breast cancer recurrence and survival: A comprehensive meta-analysis. *Clin Cancer Res*. (2020) 26:2838–48. doi: 10.1158/1078-0432.CCR-19-3492

4. Wang H, Mao X. Evaluation of the efficacy of neoadjuvant chemotherapy for breast cancer. *Drug Des Devel Ther*. (2020) 14:2423–33. doi: 10.2147/DDDT.S253961

5. Dubsky P, Pinker K, Cardoso F, Montagna G, Ritter M, Denkert C, et al. Breast conservation and axillary management after primary systemic therapy in patients with early-stage breast cancer: the Lucerne toolbox. *Lancet Oncol*. (2021) 22:e18–28. doi: 10.1016/S1470-2045(20)30580-5

6. Yu Y, Tan Y, Xie C, Hu Q, Ouyang J, Chen Y, et al. Development and validation of a preoperative magnetic resonance imaging radiomics-based signature to predict axillary lymph node metastasis and disease-free survival in patients with early-stage breast cancer. *JAMA Netw Open*. (2020) 3:e2028086. doi: 10.1001/jamanetworkopen.2020.28086

7. Xu Z, Wang Y, Chen M, Zhang Q. Multi-region radiomics for artificially intelligent diagnosis of breast cancer using multimodal ultrasound. *Comput Biol Med*. (2022) 149:105920. doi: 10.1016/j.compbiomed.2022.105920

8. Gao Y, Luo Y, Zhao C, Xiao M, Ma L, Li W, et al. Nomogram based on radiomics analysis of primary breast cancer ultrasound images: prediction of axillary lymph node tumor burden in patients. *Eur Radiol*. (2021) 31:928–37. doi: 10.1007/s00330-020-07181-1

9. Breast Cancer Expert Committee of National Cancer Quality Control C, Breast Cancer Expert Committee of China Anti-Cancer A and Cancer Drug Clinical Research Committee of China Anti-Cancer A. [Guidelines for clinical diagnosis and treatment of advanced breast cancer in China (2020 Edition)]. *Zhonghua Zhong Liu Za Zhi*. (2020) 42:781–97. doi: 10.3760/cma.j.cn112152-20200817-00747

10. Jiang ZF, Li JB. [Development of guidelines and clinical practice for breast cancer]. *Zhonghua Wai Ke Za Zhi*. (2020) 58:85–90. doi: 10.3760/cma.j.issn.0529-5815.2020.02.002

11. Gradishar WJ, Moran MS, Abraham J, Aft R, Agnese D, Allison KH, et al. Breast cancer, version 3.2022, NCCN clinical practice guidelines in oncology. *J Natl Compr Canc Netw*. (2022) 20:691–722. doi: 10.6004/jnccn.2022.0030

12. Fernandes J, Sannachi L, Tran WT, Koven A, Watkins E, Hadizad F, et al. Monitoring breast cancer response to neoadjuvant chemotherapy using ultrasound strain elastography. *Transl Oncol*. (2019) 12:1177–84. doi: 10.1016/j.tranon.2019.05.004

13. Tahmassebi A, Wengert GJ, Helbich TH, Bago-Horvath Z, Alaei S, Bartsch R, et al. Impact of machine learning with multiparametric magnetic resonance imaging of the breast for early prediction of response to neoadjuvant chemotherapy and survival outcomes in breast cancer patients. *Invest Radiol*. (2019) 54:110–7. doi: 10.1097/RLI.0000000000000518

14. Bandara MS, Gurunayaka B, Lakraj G, Pallewatte A, Siribaddana S, Wansapura J. Ultrasound based radiomics features of chronic kidney disease. *Acad Radiol*. (2022) 29:229–35. doi: 10.1016/j.acra.2021.01.006

15. Gradishar WJ, Moran MS, Abraham J, Aft R, Agnese D, Allison KH, et al. NCCN guidelines(R) insights: breast cancer, version 4.2021. *J Natl Compr Canc Netw*. (2021) 19:484–93. doi: 10.6004/jnccn.2021.0023

16. Isupov I, McInnes MD, Hamstra SJ, Doherty G, Gupta A, Peddle S, et al. Development of RAD-score: A tool to assess the procedural competence of diagnostic radiology residents. *AJR Am J Roentgenol*. (2017) 208:820–6. doi: 10.2214/AJR.16.17173

17. Gan J, Zhang Z. Relationship between ultrasound values and pathology and metastasis in patients with breast cancer. *Am J Transl Res*. (2021) 13:8207–13.

18. Wang H, Wang X, Zhang Y, Cheng R, Yuan J, Zhong Z. Systemic delivery of NAC-1 siRNA by neuropilin-targeted polymersomes sensitizes antiangiogenic therapy of metastatic triple-negative breast cancer. *Biomacromolecules*. (2020) 21:5119–27. doi: 10.1021/acs.biomac.0c01253

19. Jiang M, Li CL, Luo XM, Chuan ZR, Lv WZ, Li X, et al. Ultrasound-based deep learning radiomics in the assessment of pathological complete response to neoadjuvant chemotherapy in locally advanced breast cancer. *Eur J Cancer*. (2021) 147:95–105. doi: 10.1016/j.ejca.2021.01.028

20. Jia Y, Yang J, Zhu Y, Nie F, Wu H, Duan Y, et al. Ultrasound-based radiomics: current status, challenges and future opportunities. *Med Ultrason*. (2022) 24:451–60. doi: 10.11152/mu-3248

21. Li P, Wang X, Xu C, Liu C, Zheng C, Fulham MJ, et al. ^{18}F-FDG PET/CT radiomic predictors of pathologic complete response (pCR) to neoadjuvant chemotherapy in breast cancer patients. *Eur J Nucl Med Mol Imaging*. (2020) 47:1116–26. doi: 10.1007/s00259-020-04684-3

22. Liu Z, Li Z, Qu J, Zhang R, Zhou X, Li L, et al. Radiomics of multiparametric MRI for pretreatment prediction of pathologic complete response to neoadjuvant chemotherapy in breast cancer: a multicenter study. *Clin Cancer Res*. (2019) 25:3538–47. doi: 10.1158/1078-0432.CCR-18-3190

23. Sotohidalgo JM, Martínez-Jiménez PM, Chamorromartínez J. Fuzzy Descriptors Based on Color, Coarseness, Directionality and Contrast for Image Retrieval: Proceedings of the 2015 Conference of the International Fuzzy Systems Association and the European Society for Fuzzy Logic and Technology. *Advances in Intelligent Systems Research*. Gijon, SPAIN: Atlantis Press (2015). doi: 10.2991/ifsa-eusflat-15.2015.33

24. Eilaghi A, Baig S, Zhang Y, Zhang J, Karanicolas P, Gallinger S, et al. CT texture features are associated with overall survival in pancreatic ductal adenocarcinoma - a quantitative analysis. *BMC Med Imaging*. (2017) 17:38. doi: 10.1186/s12880-017-0209-5

25. Fan M, Chen H, You C, Liu L, Gu Y, Peng W, et al. Radiomics of tumor heterogeneity in longitudinal dynamic contrast-enhanced magnetic resonance imaging for predicting response to neoadjuvant chemotherapy in breast cancer. *Front Mol Biosci*. (2021) 8:622219. doi: 10.3389/fmolb.2021.622219

26. Zheng CH, Liu ZY, Yuan CX, Dong XY, Li HM, Wang JJ, et al. Mutant allele frequency-based intra-tumoral genetic heterogeneity related to the tumor shrinkage mode after neoadjuvant chemotherapy in breast cancer patients. *Front Med (Lausanne)*. (2021) 8:651904. doi: 10.3389/fmed.2021.651904

27. Yang G, Nie P, Yan L, Zhang M, Wang Y, Zhao L, et al. The radiomics-based tumor heterogeneity adds incremental value to the existing prognostic models for predicting outcome in localized clear cell renal cell carcinoma: a multicenter study. *Eur J Nucl Med Mol Imaging*. (2022) 49:2949–59. doi: 10.1007/s00259-022-05773-1

28. Di Cosimo S, Appierto V, Silvestri M, Pruneri G, Vingiani A, Perrone F, et al. Targeted-Gene Sequencing to Catch Triple Negative Breast Cancer Heterogeneity before and after Neoadjuvant Chemotherapy. *Cancers (Basel)*. (2019) 11:1753. doi: 10.3390/cancers11111753

29. Luo Y, Huang J, Tang Y, Luo X, Ge L, Sheng X, et al. Regional methylome profiling reveals dynamic epigenetic heterogeneity and convergent hypomethylation of stem cell quiescence-associated genes in breast cancer following neoadjuvant chemotherapy. *Cell Biosci*. (2019) 9:16. doi: 10.1186/s13578-019-0278-y

30. Zwanenburg A, Vallieres M, Abdalah MA, Aerts H, Andrearczyk V, Apte A, et al. The image biomarker standardization initiative: standardized quantitative radiomics for high-throughput image-based phenotyping. *Radiology*. (2020) 295:328–38. doi: 10.1148/radiol.2020191145

31. Luo HS, Huang SF, Xu HY, Li XY, Wu SX, Wu DH. A nomogram based on pretreatment CT radiomics features for predicting complete response to chemoradiotherapy in patients with esophageal squamous cell cancer. *Radiat Oncol*. (2020) 15:249. doi: 10.1186/s13014-020-01692-3

32. Ogbonnaya CN, Zhang X, Alsaedi BSO, Pratt N, Zhang Y, Johnston L, et al. Prediction of clinically significant cancer using radiomics features of pre-biopsy of multiparametric MRI in men suspected of prostate cancer. *Cancers (Basel)*. (2021) 13:6199. doi: 10.3390/cancers13246199

33. Wang Y, Liu W, Yu Y, Liu JJ, Xue HD, Qi YF, et al. CT radiomics nomogram for the preoperative prediction of lymph node metastasis in gastric cancer. *Eur Radiol*. (2020) 30:976–86. doi: 10.1007/s00330-019-06398-z

34. Interlenghi M, Salvatore C, Magni V, Caldara G, Schiavon E, Cozzi A, et al. A machine learning ensemble based on radiomics to predict BI-RADS category and reduce the biopsy rate of ultrasound-detected suspicious breast masses. *Diagnostics (Basel)*. (2022) 12:187. doi: 10.3390/diagnostics12010187

Frontiers in Immunology

Explores novel approaches and diagnoses to treat immune disorders.

The official journal of the International Union of Immunological Societies (IUIS) and the most cited in its field, leading the way for research across basic, translational and clinical immunology.

Discover the latest Research Topics

See more →

Frontiers

Avenue du Tribunal-Fédéral 34
1005 Lausanne, Switzerland
frontiersin.org

Contact us

+41 (0)21 510 17 00
frontiersin.org/about/contact